

Alma Mater Studiorum – Università di Bologna

DOTTORATO DI RICERCA IN

Chimica

Ciclo XXVIII

Settore Concorsuale di afferenza: 03/D1

Settore Scientifico disciplinare: CHIM/08

**TOWARDS THE DEVELOPMENT OF CHEMICAL BIOLOGY PIPELINES
FOR STEM CELLS AND RECEPTOR CHARACTERIZATION**

Presentata da: Elisa Uliassi

Coordinatore Dottorato

Prof. Aldo Roda

Relatore

Prof. Maria Laura Bolognesi

Correlatore

Prof. Marinella Roberti

Esame finale anno 2016

Table of contents

Abstract

Preface

I

Part I:

TOWARDS THE DEVELOPMENT OF A CHEMICAL BIOLOGY PIPELINE FOR STEMISTRY APPLICATION

1. Introduction

1.1 The stem cell era	2
1.2 Neural stem cells (NSCs)	5
1.3 Molecular hallmarks of NSCs	7
1.4 <i>Stemistry</i> : the control of stem cells using chemistry	9
1.4.1 Maintaining pluripotent and multipotent SCs with small molecules	10
1.4.2 Identifying signaling pathways regulating NSCs fate with small molecules	11
1.4.3 Reprogramming adult stem and other differentiated cells to neural/glial lineages	12
1.5 Pathways modulating adult neurogenesis	14
1.6 New therapies for regenerative medicine: challenging and opportunities for neurodegenerative diseases	18
1.6.1 New regenerative cellular therapies for neurodegenerative diseases	19
1.6.2 New neuroregenerative therapeutic small molecules for neurodegenerative diseases	19
1.7 Target-based vs. phenotypic based approaches in NSCs	21
1.7.1 An innovative unbiased phenotypic approach toward the discovery of P7C3	22

2. Aims and objectives

3. Chemistry

3.1 Synthesis of the focused chemical library inspired by TCAs and P7C3	32
3.2 Synthesis of TCA-functionalized fluorescent congeners	35
3.3 Synthesis of TCAs-functionalized multi-target congeners	38
3.4 Synthesis of TCAs-functionalized polyamine congener	38

4. Results and discussion

4.1 A knowledge-based phenotypic approach for NSC <i>stemistry</i> application	40
4.1.1 Design rationale of the focused chemical library inspired by TCAs and P7C3	41
4.1.2 Towards the phenotypic screening for NSCs	45
4.1.2.1 Screening of molecules for neuronal and hepatic viabilities	45
4.1.2.2 Set-up of NSCs-based phenotypic screening for neurodegenerative diseases	50
4.1.3 Target identification studies	55

4.2 Design of TCAs-functionalized congeners	57
4.2.1 Design rationale of TCAs-functionalized fluorescent congeners	57
4.2.2 Design rationale of TCAs-functionalized multi-target congeners	61
4.2.3 Design rationale of TCAs- functionalized polyamine congener	64

Experimental part	67
-------------------	----

Part II:

FROM SMALL MOLECULES TO FLUORESCENT PROBES: APPLYING THE FUNCTIONALIZED CONGENER APPROACH TO P2Y₁₄ RECEPTOR

1. Introduction

1.1 G protein-coupled receptors (GPCRs) in drug discovery	2
1.2 Functionalized congener approach to explore GPCR structure and function	7
1.2.1 Adenosine A ₃ receptor and its congeners: a landmark study	9
1.3 P2Y ₁₄ receptor as drug target	13

2. Aims and objectives	18
-------------------------------	-----------

3. Chemistry

3.1 Alternative synthesis of fluorescent P2Y ₁₄ antagonist	21
3.2 Synthesis of fluorescent P2Y ₁₄ agonist	23
3.3 Synthesis of P2Y ₁₄ antagonists	24

4. Results and Discussion

4.1 Biological evaluation of P2Y ₁₄ fluorescent agonists	26
4.2 Biological evaluation of P2Y ₁₄ antagonists	28

Experimental part	39
-------------------	----

Conclusions and Perspectives	I
-------------------------------------	----------

Appendix

Representative spectra

Abstract

Chemical biology may provide useful small molecule probes that can contribute to advancing stem cells therapeutic application and the still challenging GPCR drug research field. In this context, in this thesis we focus on the development of chemical probes to the modulation of neural stem cells (NSCs) and, in parallel, to the characterization of the recently discovered P2Y₁₄ receptor (P2Y₁₄R).

Particularly, the first application deals with pursuing a knowledge-based phenotypic approach (i) and a functionalized congeners approach (ii). Strategies (i) and (ii) have been conducted in parallel with the deliberate aim of identifying critical targets/pathways involved in NSCs differentiation and starting points for the development of new drugs. Particularly, a focused library of chemical probes has been designed and synthesized. An experimental pipeline, evaluating hepato- and neuro-toxicity, neuroprotection and proliferation in cell lines and primary neurons has been used for prioritizing compounds with better chances to be further investigated in the NCS phenotypic assay (i). In parallel, the application of the functionalized congener approach has allowed to design fluorescent, multi-target and polyamine congeners of the selected chemical scaffold (ii).

Regarding the chemical biological approach towards P2Y₁₄R, we have recently achieved promising results that could aid in unveiling its pharmacological potential in diabetes and inflammation. In particular, we have used structural insights of the recently obtained structural information of P2Y₁₄R to discover a new scaffold for P2Y₁₄R antagonists. In addition, two fluorescent probes (agonist and antagonist) have been developed and their utility to detect P2Y₁₄R using fluorescence microscopy and flow cytometry has been also successfully demonstrated.

Collectively, these results provide initial clues to our understanding of stem cell biology and P2Y₁₄R pharmacology, and could inspire powerful pharmacological tools.

Preface

As elegantly discussed by Arrowsmith et al.,¹ efforts in chemical biology and drug discovery by academic medicinal chemists have increased substantially in the last ten years. These efforts occurred in part because of the availability of large numbers of uncharacterized potential drug targets emerging from genome sequencing studies, from the development of sophisticated screening technologies and from the possibility of inventing new medicines.¹ Some of these efforts, probably due to the complexity and unreliability of drug discovery, resulted in a more measured objective: to generate small molecule tools to help elucidate the roles of the targeted proteins in healthy and diseased processes. On this basis, chemical biology has matured as a scientific discipline spanning the fields of chemistry and biology and that is centered on the application of chemical tools (i.e. chemical probes), to the study and manipulation of biological systems.¹

In the years high-quality chemical probes have been developed and they have served both as powerful research tools and as seeds to spur the development of new medicines.²

A chemical probe is defined as a small-molecule modulator of protein function that allows asking mechanistic and phenotypic questions about its molecular target in biochemical, cell-based or animal studies.² Chemical probes have proven to be very impactful not only because they are complementary to genetic approaches, but also because they have unique advantages. They can rapidly and reversibly inhibit a protein in living cells or animals, can be used in almost any cell type and reveal temporal features of target inhibition.¹

Thus, chemical biology has been equally successfully used in different areas such as isolated receptor and single-cell characterization studies.³

Following this thread, in this thesis we propose and foster two different chemical biology approaches in two distinct endeavors. Particularly, we focus on the development of chemical probes to the modulation of neural stem cells (NSCs) and, in parallel, to the characterization of the recently discovered P2Y₁₄ receptor (P2Y₁₄R). Accordingly, the following two parts of this thesis deal with the two approaches.

In detail, in part I, we report on the main PhD project, conducted at the University of Bologna within the regional project Spinner-NovaMolStam, and related to the development of chemical probes for NSCs application. Stem cell research has attracted great attention and gained strong momentum in the past 15 years due to new breakthroughs in the stem cell field, availability of new and powerful techniques, and its vast potential in regeneration of tissues damaged by injury or disease.⁴ Although the modulation of NSC by small molecules is an emerging regenerative strategy for treating currently incurable neurodegenerative disorders (e.g. Alzheimer's disease), this field still presents unsurmountable challenges to medicinal chemists.⁴ Despite a variety of signaling pathways have been shown to be critically involved in NSCs self-renewal and differentiation,⁵ a validated druggable target is far from being identified. To overcome this limitation, we envisioned a chemical biology approach to the identification of novel chemical probes for NSCs. Toward this aim we exploited a knowledge-based phenotypic approach (i) and a functionalized congeners (ii) approach. As discussed in detail in Par. 4.2 of part I and Par. 1.2 of part II, the functionalized congener approach has been proposed by Dr. K.

A. Jacobson as a chemical biology platform to the study of the different proteins, in particular belonging to the GPCR superfamily.⁶ Functionalized congeners, in which a chemically functionalized chain is introduced at a structurally permissive site on a pharmacophore, have been designed from the agonist and antagonist ligands of various GPCRs.⁶ However, its versatility for other applications has been demonstrated.⁷

Strategies (i) and (ii) have been conducted in parallel with the deliberate aim of identifying critical targets/pathways in NSCs differentiation and ultimately unlocking the regenerative potential of endogenous NSCs. Particularly, a focused library of chemical probes has been developed to be tested in NSCs-based phenotypic screening assay (i). In parallel, the application of the functionalized congener approach has allowed to design fluorescent, multi-target and polyamine congeners of the selected chemical scaffold (ii).

In part II of this thesis, we report on a 7-months project conducted in the laboratory of Molecular Recognition Section, headed by Dr. Jacobson, at the National Institutes of Health (Bethesda, US).

In this second application, the exploited chemical biology approach could count on the recently obtained structural information of the P2Y₁₄ receptor (P2Y₁₄R).⁸ The P2Y₁₄R is a Gi/o-coupled receptor, which belongs to the P2Y family of purinergic receptors and it is the most recently discovered among members of P2Y family.⁹ Despite emerging as an attractive therapeutic target,¹⁰ to date, the P2Y₁₄R has not been widely explored from a medicinal chemistry perspective and its pharmacology has not been fully disclosed. Additionally, few selective radioligands are available,¹¹ thus improved and more versatile chemical probes are needed. To this end, by applying the functionalized congener approach, high-affinity antagonist and agonist fluorescent probes have been synthesized and biologically evaluated. Moreover, we have used the recently obtained structural insights of P2Y₁₄R to discover a new scaffold for developing P2Y₁₄R antagonists. Thus, the development of potent and selective agonists and antagonists of P2Y₁₄ receptor is a major achievement, given the potential critical role of this signaling protein in inflammatory, endocrine, and immune processes.¹⁰

References

- [1] Arrowsmith, C. H.; Audia, J. E.; Austin, C.; Baell, J.; Bennett, J.; Blagg, J.; Bountra, C.; Brennan, P. E.; Brown, P. J.; Bunnage, M. E.; Buser-Doepner, C.; Campbell, R. M.; Carter, A. J.; Cohen, P.; Copeland, R. A.; Cravatt, B.; Dahlin, J. L.; Dhanak, D.; Edwards, A. M.; Frederiksen, M.; Frye, S. V.; Gray, N.; Grimshaw, C. E.; Hepworth, D.; Howe, T.; Huber, K. V.; Jin, J.; Knapp, S.; Kotz, J. D.; Kruger, R. G.; Lowe, D.; Mader, M. M.; Marsden, B.; Mueller-Fahrnow, A.; Muller, S.; O'Hagan, R. C.; Overington, J. P.; Owen, D. R.; Rosenberg, S. H.; Roth, B.; Ross, R.; Schapira, M.; Schreiber, S. L.; Shoichet, B.; Sundstrom, M.; Superti-Furga, G.; Taunton, J.; Toledo-Sherman, L.; Walpole, C.; Walters, M. A.; Willson, T. M.; Workman, P.; Young, R. N.; Zuercher, W. J. The promise and peril of chemical probes. *Nat Chem Biol* **2015**, *11* (8), 536-41.
- [2] Frye, S. V. The art of the chemical probe. *Nat Chem Biol* **2010**, *6* (3), 159-161.
- [3] Hughes, J. P.; Rees, S.; Kalindjian, S. B.; Philpott, K. L. Principles of early drug discovery. *Br J Pharmacol* **2011**, *162* (6), 1239-49.
- [4] Davies, S. G.; Kennewell, P. D.; Russell, A. J.; Seden, P. T.; Westwood, R.; Wynne, G. M. Stemistry: The Control of Stem Cells in Situ Using Chemistry. *Journal of Medicinal Chemistry* **2015**, *58* (7), 2863-2894.
- [5] Bond, A. M.; Ming, G. L.; Song, H. Adult Mammalian Neural Stem Cells and Neurogenesis: Five Decades Later. *Cell Stem Cell* **2015**, *17* (4), 385-95.
- [6] Jacobson, K. A. Functionalized Congener Approach to the Design of Ligands for G Protein-Coupled Receptors (GPCRs). *Bioconjugate Chemistry* **2009**, *20* (10), 1816-1835.
- [7] Chen, W.; Ravi, R. G.; Kertesz, S. B.; Dubyak, G. R.; Jacobson, K. A. Functionalized congeners of tyrosine-based P2X(7) receptor antagonists: probing multiple sites for linking and dimerization. *Bioconjug Chem* **2002**, *13* (5), 1100-11.
- [8] Trujillo, K.; Paoletta, S.; Kiselev, E.; Jacobson, K. A. Molecular modeling of the human P2Y14 receptor: A template for structure-based design of selective agonist ligands. *Bioorg Med Chem* **2015**, *23* (14), 4056-64.
- [9] Abbracchio, M. P.; Boeynaems, J. M.; Barnard, E. A.; Boyer, J. L.; Kennedy, C.; Miras-Portugal, M. T.; King, B. F.; Gachet, C.; Jacobson, K. A.; Weisman, G. A.; Burnstock, G. Characterization of the UDP-glucose receptor (re-named here the P2Y14 receptor) adds diversity to the P2Y receptor family. *Trends Pharmacol Sci* **2003**, *24* (2), 52-5.
- [10] Jacobson, K. A.; Boeynaems, J. M. P2Y nucleotide receptors: promise of therapeutic applications. *Drug Discov Today* **2010**, *15* (13-14), 570-8.
- [11] Brunschweiler, A.; Muller, C. E. P2 receptors activated by uracil nucleotides-an update. *Curr Med Chem* **2006**, *13* (3), 289-312.

PART I

**TOWARDS THE DEVELOPMENT OF A CHEMICAL
BIOLOGY PIPELINE FOR STEMISTRY APPLICATION**

1. Introduction

1.1 The stem cell era

In 1981 the establishment of embryonic stem cells (ESCs) in culture isolated from mouse blastocysts by two independent groups,¹ initiated a flurry of studies into the stem cells (SCs) field. Then, growth of the field has been rapid, and it has been increasing steadily since about 2001. Figure 1 graphically depicts this growth rate. In fact, in the late 1990s, for the first time a method to derive ESCs from human embryos and to grow these cells in laboratory was developed.² More importantly, this raised new awareness of their therapeutic potential, which appeared to be “limitless”.³ Furthermore, in 2007, the discovery by the stem cell pioneers Yamanaka⁴ and Thomson⁵ that human somatic cells can be reprogrammed to a pluripotent state (i.e. induced pluripotent stem cells, iPSCs) has revolutionized cell biology, earning them the 2012 Nobel Prize.⁶

From that moment on, successful achievements and promises about SCs cures have been well documented in the literature. Nowadays, the remarkable potential of SCs to develop into many different cell types throughout the life and to serve as internal repair system to replenish other cells, has been widely recognized.⁶ Actually, SCs take on great importance because they are distinguished from other cell types by two important features. First, they are unspecialized cells capable of renewing themselves through cell division, even after long periods of inactivity. Second, under certain physiologic or experimental conditions, they can be induced to become tissue- or organ-specific cells with special functions.⁷

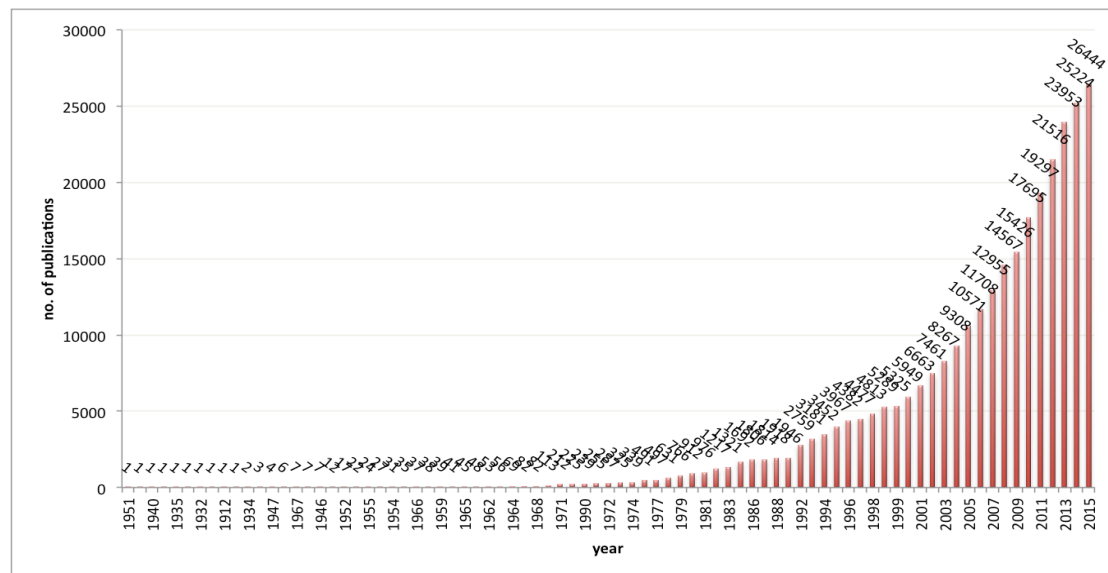


Figure 1. Number of published articles on stem cell research between 1951 and 2015. After the isolation of hESCs in 1998, the number of stem cell articles increased and has continued an upward progression (csv file downloaded from PubMed database <http://www.ncbi.nlm.nih.gov/> on Feb. 20, 2016).

Indeed, SCs are defined as cells that have clonogenic and self-renewal capabilities and that differentiate into multiple cell lineages in response to appropriate signals.

Consequently, SCs have been classified into categories according to their developmental status and their capacity to differentiate in different types of cells, or by their degree of plasticity⁷ (see Table 1). In general, adult stem cells (ASCs) are unspecialized cells found in differentiated tissues, which can self-renew for long periods of time and differentiate into specialized cell types of the tissue from which they originate (multipotent cells); ESCs are derived from mammalian embryos in the blastocyst stage and have the ability to generate any terminally differentiated cell of the body (pluripotent cells).⁷ On the other hand, cancer stem cells (CSCs) are cancer cells found within solid tumors or hematological cancers. CSCs may generate tumors through the stem cell processes of self-renewal and differentiation into multiple cell types, which reflects the heterogeneity normally associated to a particular type of cancer. CSCs are therefore tumorigenic cells and undergo to an aberrant and poorly regulated process of proliferation within a tissue, analogous to what normal SCs do.⁸ Conversely, iPSCs are a particular type of adult cells that have been genetically reprogrammed to an ESCs-like state by being forced to express genes and factors important for maintaining the defining properties of pluripotency.⁷

	CLASSIFICATION	FEATURES
Sources/types	Embryonic stem cells	are pluripotent stem cells derived from the inner cell mass of the blastocyst and can give rise to cells derived from all three germ layers (endoderm, mesoderm, and ectoderm).
	Adult stem cells	<i>endodermal origin</i> : intestinal and pulmonary epithelial SCs pancreatic SCs, mammary, thyroid and prostatic gland SCs
		<i>mesodermal origin</i> : subdivided in hematopoietic SCs and mesenchymal SCs that give rise to blood cells, urogenital system, skeletal and smooth muscles, connective tissues.
		<i>ectodermal origin</i> : neural SCs, epidermis SCs, ocular SCs.
	Cancer stem cells	identified in cancers and tumor, such as acute myeloid leukemic SCs, brain tumor SCs, breast cancer SCs etc.
Induced pluripotent stem cells	artificially derived pluripotent stem cells from a non-pluripotent cell, typically an adult somatic cell, by inducing a forced expression of specific genes.	
Degree of plasticity	Totipotent cells	zygote, spore, morula; they give rise to all the cells and tissues that make up an embryo and that support its development in utero.
	Pluripotent cells	embryonic stem cells; they give rise to cells derived from all three germ layers, but cannot give rise to an entire organism.
	Multipotent cells	progenitor cell, such as hematopoietic SCs; they give rise to a limited range of cells within a tissue type.
	Unipotent cells	precursor cells; they give rise to just one cell type.

Table 1. Classification of SCs.

Given their peculiar properties, SCs hold great promises for developmental biology, disease modeling, drug discovery, and for regenerative medicine. Accordingly, some of the applications involve the study of human development. In fact, recent reports showed how SCs form and repair tissues and organs,⁹ how aging impacts on their function, and their role in various diseases.¹⁰ In addition, the discovery of iPSCs widened the range of applications in drug discovery, and disease modeling.¹¹ By exposing a patient's skin cells to growth factors, signaling molecules, and/or genetic manipulation, it has been found a scalable and low-cost method to link human

disease to drug discovery, providing an improved model system to study disease biology. Indeed, iPSCs retain the genetic characteristics of their donors, which enables genotype-dependent pathophysiology to manifest at the cellular level and, thereby, shedding new light on phenotypic traits and cellular mechanisms of a certain disease.¹¹ Hence, this approach capitalizes on the idea of personalized medicine by using the patient's own cells to discover new drugs and thus increasing the likelihood of a favorable outcome. The search for compounds that can correct disease defects in such culture dish (the so called disease-in-a-dish)¹² is now becoming a tangible reality.

The current advances in SCs field may also make possible new regenerative approaches for the treatment of incurable diseases, such as neurodegenerative diseases.¹³ These approaches could involve cell replacement therapy (also patient-specific derived iPSCs) and/or drug treatment to stimulate the body's own regenerative capabilities by promoting survival, migration/homing, proliferation, and differentiation of endogenous stem/progenitor cells.

If stem cell replacement therapy is already in the clinics, small molecules modulating SCs are just approaching the clinical applications. Indeed, in 2012, the SCs replacement therapy field hit a milestone, reaching a total of 1 million hematopoietic stem cell/bone marrow transplants worldwide.¹⁴ In 2015, the European Medicines Agency (EMA) has approved another successful cellular therapy based on epithelial SCs (Holoclar®)¹⁵ for the treatment of limbal stem cell deficiency, a rare eye condition that can result in blindness.

However, gaps in our understanding of SCs and their maturation/engraftment into differentiated tissues have presented substantial barriers to regeneration of other tissues/organs, as in the case of spinal cord injury (SCI). SCI currently lacks therapy, although the transplantation of human central nervous system-derived SCs at 9 or 30 days post-SCI has shown some therapeutic promise in rodent models.¹⁶ However, there is no preclinical evidence supporting either the safety or efficacy of SCs transplantation in chronic SCI yet.¹⁷

Nonetheless, cell therapies showed a number of technical obstacles to their practical use. In contrast to the other cell types, SCs are particularly sensitive to soluble biochemical factors, extracellular matrixes (ECMs), and a variety of stimuli such as chemical, mechanical, optical, and electrical cues, resulting in unpredictability cell culture and generation of heterogeneous population of cells. This arises from the fact that "cocktails" of growth factors, signaling molecules, and/or genetic manipulation generally control SCs expansion and differentiation *ex vivo*.¹⁸ Clearly, there is a need for more efficient and selective methods to control the proliferation and the differentiation of SCs to produce homogenous populations of particular cell types. In fact, the ability to maintain pluripotency without compromising genomic integrity, and efficiently directing differentiation is of particular importance because undifferentiated cells can generate tumor.¹⁸ Thus, only a precise control of such relevant exogenous and micro-environmental factors may enable the regulation of cell phenotype, function, differentiation, and integration after implantation.¹⁸

Based on this, the enthusiasm surrounding the clinical potential of both ESCs and iPSCs as cell replacement therapy is hardened by key issues regarding their safety, efficacy, and genome integrity.¹⁹

By contrast, small molecules that precisely modulate SCs fate can potentially relieve

these problems, as the major convergence of SCs biology and regenerative therapy. The modulation of SCs with both naturally occurring and synthetic small molecules is being played an integral part in the advancement of SCs research and, in a certain way, is being preferred to cell-based therapy.^{19,20}

The final goal is to design compounds able to act at a particular stage of one or more pathways, leading to specific responses, which can be minutely controlled by the concentration of the compound itself. The ability to act selectively on the desired pathways, and in a controlled manner, may enable to finely regulate SCs proliferation and differentiation. This is important in the formation of new cells and tissues for use in basic research, disease modeling and drug discovery, and, ultimately in the clinic.²¹ Moreover, this is equally important for chemical biology applications. There is a compelling need not only of small molecules with regenerative potential, but also able to characterize signaling pathways involved in the regulation of SCs biology.²¹⁻²² In this context, during the last years, the rising of chemical biology as a nascent discipline of regenerative medicine is undeniable.¹⁹ And in fact, it has already demonstrated useful at dissecting the role of specific pathways in a variety of SCs processes including self-renewal, proliferation and differentiation.²³ Perhaps, the most striking improvement in our understanding of SCs biology came indeed from the application of chemical biology approaches to SCs. As its name implies, chemical biology is a multidisciplinary discipline that involves the study and perturbation of biological systems with chemical probes. Probes targeting one or several of the SCs processes can be identified either in a targeted approach based on known mechanisms and signaling pathways, or in an unbiased fashion using cell-based high-throughput screening (HTS) approaches.²⁴ The first strategy mainly includes the use of molecules that target epigenetic modifications or specific canonical signaling pathways involved in SCs biology. The target-based approach has provided several insights into the complex regulatory mechanisms of SCs fate. On the contrary, the second strategy relies on unbiased phenotypic or pathway-based cellular screens of chemical libraries with the goal of identifying small molecules agnostic for specific targets/mechanisms, but showing a desired phenotypic effect. A number of such screening strategies have been established, and among them, high-content cell-based approaches are rapidly emerging as particularly effective.²⁵ The major challenge with unbiased cell-based screens, however, is the need for subsequent identification of the specific target(s) and/or biological pathway(s) through which the small molecule exerts its effects.^{24a}

1.2 Neural stem cells (NSCs)

The application of chemical tools will be instrumental for the discoveries of novel therapies based on the knowledge and application of powerful SCs, that are neural stem cells (NSCs).²⁶

“Once the development was ended, the founts of growth and regeneration of the axons and dendrites dried up irrevocably. In the adult centers, the nerve paths are something fixed, ended, and immutable. Everything may die, nothing may be

regenerated. It is for the science of the future to change, if possible, this harsh decree" (Ramon y Cajal, 1913)

One of the longest standing dogmas in neuroscience was that the brain was a static organ lacking regenerative capacity, as suggested in 1913 by the Spanish neuro-anatomist Ramon y Cajal. Decades afterwards, investigation into anatomical changes occurring in the central nervous system (CNS) of female songbird canaries challenged this long-standing assumption.²⁷ This groundbreaking work proved that a remodeling process, which involve both cell proliferation (assessed *via* [³H]thymidine incorporation experiments) in discrete regions of the songbird brain (i.e. the ventricular zones), and cell migration/differentiation into newly grafted neurons (neurogenesis) continue throughout life.²⁸

Despite changing the scientific community's standpoint on adult neurogenesis, only in 1992 Reynolds and Weiss showed that multipotent NSCs could be isolated from the CNS of adult and embryonic mice and propagated *in vitro* in the presence of mitogens to give rise to large spheres of cells termed "neurospheres".²⁹ These neurospheres are composed of both differentiated neurons and glial cells, but also by immature SCs. Moreover, they demonstrated that a neurosphere could be produced from a single cell and that this neurosphere could be subsequently split to generate a new one, which preserves the previous cell heterogeneity. Thus, these cells, being capable to produce neurosphere, recapitulate the properties of SCs, behaving as multipotent cells able to self-renew.³⁰ Next, the identification of such cells also *in vivo* in adult brain confirmed certainly the existence of NSCs in defined regions.³¹ Indeed, it is now well-established that neurogenesis occurs throughout life in the "neurogenic niches" of the adult brain: the subventricular zone (SVZ) of the forebrain and the subgranular zone (SGZ) of the dentate gyrus (DG) within the hippocampus.³² The neurogenic niches represent a unique micro-environment that determines NSCs survival and fate by a multitude of effects, such as cell-cell contacts and interactions with specific factors.³² By definition, NSCs are undifferentiated precursor cells described by their capacity for self-renewal and multipotency. Through proliferation and division, NSCs generate clonally related progeny that differentiate to form all the major cell types of the CNS (Figure 2).³³ These cells include neurons, astrocytes and oligodendrocytes. The symmetric division of NSCs underlies their ability to self-renew and serves to maintain the NSCs population. In contrast, asymmetric mitosis produces one NSCs and one neural progenitor cell (NPCs), daughter cells with restricted differentiation capacity for neuronal or glial lineages. In addition, terminal asymmetric division generates two NPCs, but does not contribute to maintaining the NSCs pool (Figure 2). Although the gross anatomical location of proliferating immature cells has been well identified, the exact identity of the precursor cells is not well defined. They should be able to give rise to all cell types of all regions of the CNS during development, as well as reconstitute those regions following damage. Furthermore, it has been demonstrated that different subpopulations of neural precursors exist that are regionally specified to respond to certain cues related to their neighboring cells and precise anatomical location.³⁴

In fact, despite SVZ and SGZ niches share several key characteristics, a high heterogeneity of adult NSCs have been highlighted between the two neurogenic

regions. Notably, adult SVZ NSCs (also named type B cells) give rise to transient amplifying progenitors (C cells),³¹ which divide just few times before becoming neuroblasts (A cells); radial glia-like NSCs (named RGLs or type 1 cells) in the SGZ give rise to intermediate progenitor cells (IPCs) also exhibiting limited rounds of proliferation before generating neuroblasts. Then, these neuroblasts migrate tangentially along the SGZ, develop into immature neurons in the granule cell layer, and differentiate into dentate granule neurons.³⁵ While in contrast, A cells in SVZ radially migrate into the olfactory bulb where differentiate into different subtypes of interneurons.³⁶

Even though recent advances on deriving or inducing NSCs from different sources have been achieved, no direct and thorough comparison of their biological and molecular properties or of their physiological relevance and possible relationship to endogenous NSCs has yet been performed.³⁷ Indeed, NSCs are still lacking of established marker proteins, resulting in difficult characterization and isolation of *bona fide* NSCs. However, some level of consensus is recognized in terms of characterization of differentiating or differentiated cells, based on a combination of markers for immature and mature phenotypes, such as nestin and β -tubulin III, respectively (see Figure 2).³³

In the next paragraph, a general overview of molecular hallmarks characterizing NSCs will be provided.

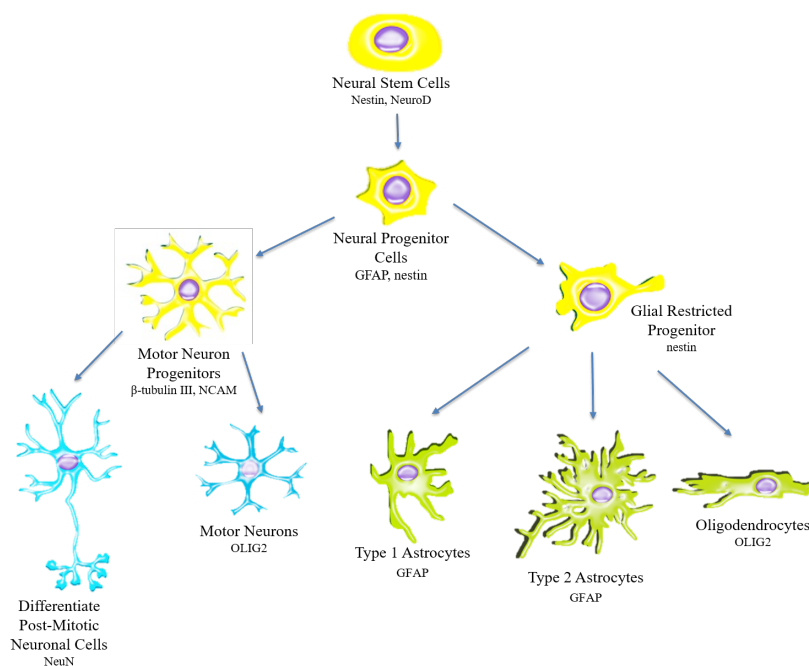


Figure 2. Graphic representation of NSCs differentiation fate and related markers.

1.3 Molecular hallmarks of NSCs

As previously anticipated, the establishment of specific markers for both mature and immature phenotypes is far to be complete.³³ Their identification would be of fundamental importance not only to detect and enable prospective isolation of *bona fide* NSCs, but also to understand how these intrinsic regulators (transcription factors, cytoskeleton proteins etc.) affect gene expression and/or cell function. To

date, only a handful of proliferation/differentiation markers have been identified and then confirmed by the recent advances in reprogramming somatic cells.³⁸ However, some of them result to be non-specific for adult NSCs and are often shared by other cell types. This problem is particularly evident in the case of distinguishing activated adult NSCs from quiescent NSCs, which do not express many unique antigens.³⁹

Following the introduction of 5-bromodeoxyuridine (BrdU),⁴⁰ a nucleotide analog that non-selectively labels proliferating cells in the adult brain, while avoiding the use of [³H]thymidine and autoradiographic techniques, the field witnessed an explosion of studies aimed at establishing specific and reliable methods to track both quiescent and proliferating cells. One of the first markers to be identified for the immature NSCs was nestin, a class VI intermediate filament protein.⁴¹ Originally described as the marker distinguishing progenitor SCs from differentiated cells both in vitro and in vivo,²⁹ nestin was also found to be expressed in CNS tumor cells.⁴² Furthermore, endothelial cells within CNS tumor have been reported to be nestin-positive, but also a variety of adult human non-CNS cells, such as newly formed human blood vessels cells, have been showed to express nestin.⁴³ Thus, even though nestin is generally recognized as a marker protein of undifferentiated NSCs at the stage that precedes the commitment of the mature progeny to a specific lineage, recent evidences suggest that nestin is also a marker for angiogenesis.⁴⁴

On the other hand, Pax6 emerged as transcription factor identified during embryonic development in precursor cells. Further studies revealed that Pax6 might represent a suitable marker for newly generated cells in the DG during the differentiation phase.⁴⁵ However, it should be noted that a small subpopulation of hilar mature neurons and certain astrocytes of the adult hippocampus also express Pax6, hence confirming its differential expression in regionally restricted areas of adult brain.⁴⁵

Another candidate for immature neuronal markers is NeuroD, which is a basic helix–loop–helix transcription factor specifically expressed in later stages of neuronal commitment.⁴⁵ In addition to NeuroD, doublecortin (DCX) is a protein that promotes microtubule polymerization and is present in migrating neuroblasts and young neurons. In general, DCX-expressing cells are temporally in-frame with polysialylated neural cell adhesion molecule (PSA-NCAM), highly expressed in neural and glial progenitor cells. However, not all newly formed neurons within the brain seem to express DCX. Its expression is known to occur in newly generated hippocampal, striatal and olfactory neurons, but within the neocortex, newly generated neurons lack DCX.⁴⁶ Thus, DCX can be used to label the post-mitotic neuronal progenitor cells and early immature neurons only in defined brain regions.³⁸

Regarding mature phenotype markers, glial fibrillar acidic protein (GFAP) is widely known as a marker for mature astrocytes in the adult brain. However, striking evidences supported the fact that it is highly expressed by radial glial cells, whose heterogeneity raises doubts about GFAP specificity.⁴⁷ Indeed, these GFAP-positive cells have been demonstrated to express not only the functional features common to astrocyte, but also the functional characteristics intermediate between astrocytes and radial glia, that may direct the migration or the formation of new neurons.⁴⁸

Conversely, neuron-specific class III beta-tubulin (Tuj-1) is used as a neuron-specific marker of newly generated cells.³⁸ It is expressed in early post-mitotic and differentiated neurons and in some mitotically active neuronal precursors. Thus, it is

considered as one of the most specific marker for labeling the neuronal lineage. Additionally, NeuN, a soluble nuclear protein, is observed in most neuronal cell types throughout the CNS, with the exception of some neuronal populations (e.g. cerebellar Purkinje cells). In this context, NeuN results to be very useful thanks to its ability to discriminate between neuronal and non-neuronal cells.⁴⁵

On the other hand, OLIG2 is a basic helix-loop-helix transcription factor that has been described in the ventral spinal cord in a subpopulation of neural progenitors that give rise first to motor neurons and then oligodendrocytes.⁴⁹ Indeed, it has been considered as suitable oligodendroglial lineage marker.⁵⁰ In this respect, it's worth to note that OLIG2 is guiltily limited to normal oligodendroglia and their progenitors in human brain. Accordingly, spatiotemporal differences in OLIG2 expression indicate that it is critical not only for initial oligodendroglial specification, but also for the development of other neural cell types.⁵⁰ Moreover, OLIG2 expression is associated with all gliomas, implying its usefulness as marker of diffuse gliomas.⁵¹

1.4 Stemistry: the control of stem cells using chemistry

Already in 2013, Angela Russell dealt with the concept of targeting resident SCs in situ using chemistry, which was elegantly defined as “regenerative medicinal chemistry”.⁵² Soon after, in 2014, Davies and Russell coined the neologism “*stemistry*” referring to the contraction of “stem cell chemistry”, which directly interfaces SCs biology and chemistry.⁵³ Since its inception, the prospect of developing new chemical entities capable of targeting the regenerative processes in vivo, represents an emerging approach in medicine and drug discovery.⁵³ Actually, the demonstration that an agent targeting the own regenerative capability of the body would have profound effects on diseases dates back to 1989, with the use of erythropoietin.⁵² This hormone is currently in clinical use for patients with severe anemia, being able to modulate the production of red blood cells from hematopoietic progenitor cells. Moreover, after the identification of the critical role played by another hormone (thrombopoietin) in the production of platelets, several thrombopoietin mimetics were developed, culminating in 2005 in the discovery of eltrombopag, marketed for the treatment of thrombocytopenia⁵⁴ and, more recently, approved for aplastic anemia.⁵⁵

In parallel, several reports retrospectively demonstrated that also existing drugs exert some of their effects by modulating SCs fate. This is the case for the antidepressant drug fluoxetine.⁵⁶

In general, small molecules are particularly attractive because can be delivered efficiently into the cell, can be targeted to specific tissues and, more importantly, their effects are reversible. The compounds doses can be changed for maximum benefit, and, from a medicinal chemistry perspective, molecules can be further modified to increase potency, selectivity, safety, or stability. Importantly, small molecules can play several roles within the SCs field, according to the following objectives:

- i. maintaining pluripotent and multipotent ESCs in an undifferentiated state while preserving self-renewal capacity;

- ii. identifying the signaling pathways implicated in regulating the different SCs types and the different SCs stages (self-renewal, proliferation, differentiation, migration, engraftment), in order to disclose their biological roles and their potential as druggable targets;
- iii. reprogramming adult stem and other differentiated cells.

Below, objective (i) applied to ESCs will be briefly discussed, whereas for objectives (ii) and (iii) significant examples in the field of NSCs will be addressed.

1.4.1 Maintaining pluripotent and multipotent SCs with small molecules

Objective (i) refers to the development of those molecules able to maintain ESCs in a continuous proliferative circle in growth and transcription factors-free conditions. This is of notable importance because it avoids genome integrity issues and the risk of tumorigenicity associated with feeder-conditioned medium. In this respect, the main contribution in this field came from the work published by Chen and colleagues in 2006.⁵⁷ The authors successfully implemented an unbiased cell-based screen of 50,000 compounds library (5 μ M) to identify small molecules able to regulate the self-renewal of ESCs. From the small (~ 30) set of compounds resulting from the primary screen, a class of 3,4-dihydropyrimido[4,5-d]pyrimidines was identified. A focused library of second-generation 3,4-dihydropyrimido[4,5-d]pyrimidines was synthesized, aiming at exploring the structure-activity-relationships (SAR). Notably, the analog SC1, also called pluripotin (Figure 3), was identified with 10-fold higher activity and relatively low cellular toxicity compared to the starting hit. To identify the cellular target(s) of SC1, affinity chromatography was performed revealing that SC1 acts simultaneously on two targets: ERK1 and Ras GTPase-activating protein. Such proteins, which have previously been shown to play a critical role in SCs differentiation,⁵⁸ could also represent targets for designing new drugs.

Thus, SC1 successfully addresses objective (i), allowing the propagation of ESCs in an undifferentiated pluripotent state under chemically defined conditions. It also addresses objective (ii), as it allowed the identification of two signaling pathways, which could themselves represent potential druggable targets.

1.4.2 Identifying signaling pathways regulating NSCs fate with small molecules

The discovery of small molecules to promote the proliferation, survival, differentiation, and/or migration of neural stem/progenitor cells (objective ii) represents an attractive strategy to tackle neurodegenerative diseases. One of the first molecules discovered to cause differentiation towards NSCs of ESCs is represented by retinoic acid (Figure 3).⁵⁹ This ability have been widely exploited to directly differentiate ESCs, even though it is relatively nonspecific in targeting specific cell lineage and its effects are hampered by chemical and metabolic instability.⁵⁹

With the aim of understanding the processes that regulate neuronal specification and identifying specific molecules, in 2003, Ding et al. set up a high-throughput

phenotypic cell-based screen with a luciferase reporter by inserting Tα1 tubulin, a specific neuronal marker.⁶⁰ Starting from the hypothesis that kinases affect the differentiation processes, a kinase-focused combinatorial library (>10⁵ compounds) was tested leading to the discovery of TWS119 (Figure 3), a 4,6-disubstituted pyrrolopyrimidine that induces neural differentiation of ESCs. By means of affinity-based and biochemical experiments, the target of TWS119 was shown to be GSK-3β. These findings provided evidence that GSK-3β is involved in mammalian neurogenesis, thereby emerging as an attractive target for clinical intervention.⁶⁰

The importance of GSK-3β in controlling neurogenesis emerged also from another recent report.⁶¹ In this case, the authors implemented a high-content screen using human NPCs to systematically characterize the effects of more than 5,000 bioactive compounds (2 μM) on both the neuronal differentiation and further the midbrain dopamine (mDA) neuron specification. From the primary screening aimed at promoting neuronal differentiation, a certain number of hits were selected for further testing. Of the promoting compounds, following experiments confirmed the effects of 21 small molecules, among which two pharmacological classes emerged: the GSK-3 inhibitors (exemplified by kenpauillone, Figure 3) and the statins (exemplified by mevastatin, Figure 3). Then, the effects of compounds on promoting the mDA neuron specification were evaluated. Re-testing of the selected hits (21 compounds) confirmed the effect on mDA specification of human NPCs by two pharmacological classes: the TGF-β receptor inhibitors (exemplified by LY364947 in Figure 3) and the statins as well (mevastatin). Thus, this study disclosed three pharmacological classes that effectively increase the rates of neuronal and/or mDA differentiation of human NPCs. It also provided molecular insights into the signaling network governing the differentiation of NPCs, which may be potentially valuable for the study/treatment of PD.⁶¹

Recently, it has been also showed the potential of natural-derived compounds to affect neurogenesis. Starting from the neurotrophic activity displayed in cell-based assays by the novel nature-inspired 2-oxa-spiro[5.5]-undecane scaffold,⁶² two compounds (comp#1 and comp#2 in Figure 3) were selected to further investigate their neurotrophic, neurogenic and neuroprotective potential in ex vivo mouse primary neurosphere, in brain slice cultures, and in vivo zebrafish and mouse models.⁶³ While from the ex vivo experiments, no significant differences among the two compounds have been observed, the results obtained from in vivo investigations

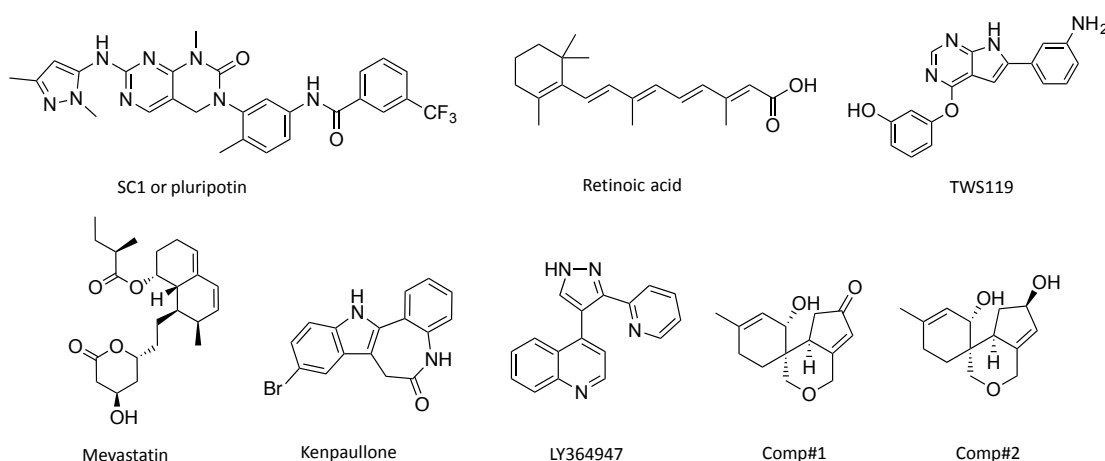


Figure 3. Small molecule probes modulating SCs fate.

suggest that comp#2 is more neurotrophic than neurogenic, whereas comp#1 exhibits the opposite profile. This difference became particularly evident in an acute ischemic stroke mouse model, revealing that comp#2 exhibits remarkable neuroprotective effects compared to the comp#1. Additionally, the molecular mechanisms of action of comp#2 appear to be linked to the modulation of the complex pathway involving TrkB-MEK-ERK-CREB-BDNF. This is because treatment with neurotrophin receptor TrkB inhibitor (ANA-12, N-[2-[[[Hexahydro-2-oxo-1H-azepin-3-yl)amino]carbonyl]phenyl]-benzo[b]thiophene-2-carboxamide) and MEK inhibitor (PD98059, 2-(2-Amino-3-methoxyphenyl)-4H-1-benzopyran-4-one) significantly reduce the neurotrophic action of the compound.⁶³

1.4.3 Reprogramming adult stem and other differentiated cells to neural/glia lineages

As mentioned above, the possibility to directly reprogramming SCs by using small molecules is particularly attractive (objective iii).⁶⁴

Accordingly, it was hypothesized that chemicals known to promote reprogramming could facilitate the cells to enter into a “plastic” state, which could allow them to be converted to NPCs under neural-specific conditions.⁶⁵

To achieve this goal, Cheng et al.⁶⁶ identified a chemical cocktail that induces NPCs from terminally differentiated cells under hypoxic condition. Particularly, the combination of Valproic acid (histone deacetylase inhibitor (HDACi), Figure 4), CHIR99021 (GSK-3 β inhibitor) and Repsox (TGF- β inhibitor), named VCR, was found to induce the transition of mouse embryonic fibroblasts to NPCs only under hypoxic conditions, and not under normoxic conditions. Thus, hypoxia, as a peculiar characteristic of in vivo SCs niches, combined with VCR cocktail that up-regulates Sox2 expression, play a major role in NPCs reprogramming. Given that, the authors further characterized the obtained chemical-induced NPCs by comparing their proliferation and self-renewal abilities in mouse brain-derived NPCs. Interestingly, they showed a high degree of similarity both in transcription profiles and their multipotency properties in vitro and in vivo, corroborating the idea that the use of lineage-specific culture conditions (VCR and hypoxia) allowed to obtain reliable NPCs from somatic cells. Moreover, the feasibility of generating chemical-induced NPCs from fibroblasts by using VCR has been significantly confirmed by the successful use of alternative inhibitors targeting HDACs, GSK-3 β and TGF- β kinases. This also supports the central role of these pathways in the direct conversion of fibroblast into NPCs.⁶⁶

Just one year later, the same group exploited a slightly modified version of the previous identified drugs cocktail VCR to directly convert mouse astrocytes into neuronal cells.⁶⁷ By optimizing the concentration of valproic acid, the authors were able to induce neurons maturation from cultured astrocytes without generating Sox2-positive NPCs. Furthermore, additional screens revealed that removal of valproic acid from the cocktail drastically abrogated the induction of neuroblasts from astrocytes, whereas excluding CHIR99021 or repsox showed minimal effects on neuroblast generation. Intriguingly, the conversion induced by VR combination

(valproic acid and repsox) displayed a similar efficiency compared to VCR cocktail. While, neuroblasts generation from astrocytes was maintained by using valproic acid alone, even displaying a lower effectiveness compared with VR, neither CHIR99021 or repsox alone nor their combination produced any neuroblast. These findings suggest that small molecules can directly convert astrocytes into neurons in vitro in a concentration- and time-dependent manner.⁶⁷ However, the practical implication of such chemical-induced conversion in vivo has not been confirmed yet, and the potential effects of these chemicals on other cells types need to be systematically and carefully evaluated. To this end, the same group tested whether VCR in combination with other small molecules known to promote neural differentiation of NPCs, might facilitate the conversion of human fibroblasts into neuronal cells.⁶⁸ Thus, they screened ~25 compounds reported to induce neural cells differentiation and they found that additional 4 small molecules [i. e. Forskolin (cAMP activator, F, in Figure 4); SP600125 (JNK inhibitor, S); GO6983 (PKC inhibitor, G) and Y-27632 (ROCK inhibitor, Y)] are required to efficiently improve the neuronal conversion. Thus, they optimized a chemicals cocktail comprising a total of 7 small molecules, defined as VCRFSGY. Such neural-promoting molecules include compounds with significantly different mechanisms of action, so that the precise regulatory mechanisms of this VCRFSGY cocktail remain to be understood. Despite that, this approach was successfully applied to generate human chemical-induced neuron from skin fibroblasts derived from familial AD patients, further supporting the feasibility to generate patient-specific neuronal cells by chemical tools.⁶⁸ Interestingly, in the same issue of Cell Stem Cell journal, another similar work has been reported by Li et al.⁶⁹ In this case, by performing two screening assays for small molecules (~ 5,000 and 1,500 compounds, respectively) able to convert mouse skin cells into neurons, the authors first identified CHIR99021, forskolin, ISX9, and SB431542 (TGF- β inhibitor, in Figure 4) for their ability to increase the number of TUJ1-positive cells and, secondly, they found an additional small molecule (i.e. I-BET151, a BET-family bromodomain inhibitor) that facilitate neuronal reprogramming and maturation. Accordingly, further experiments demonstrated

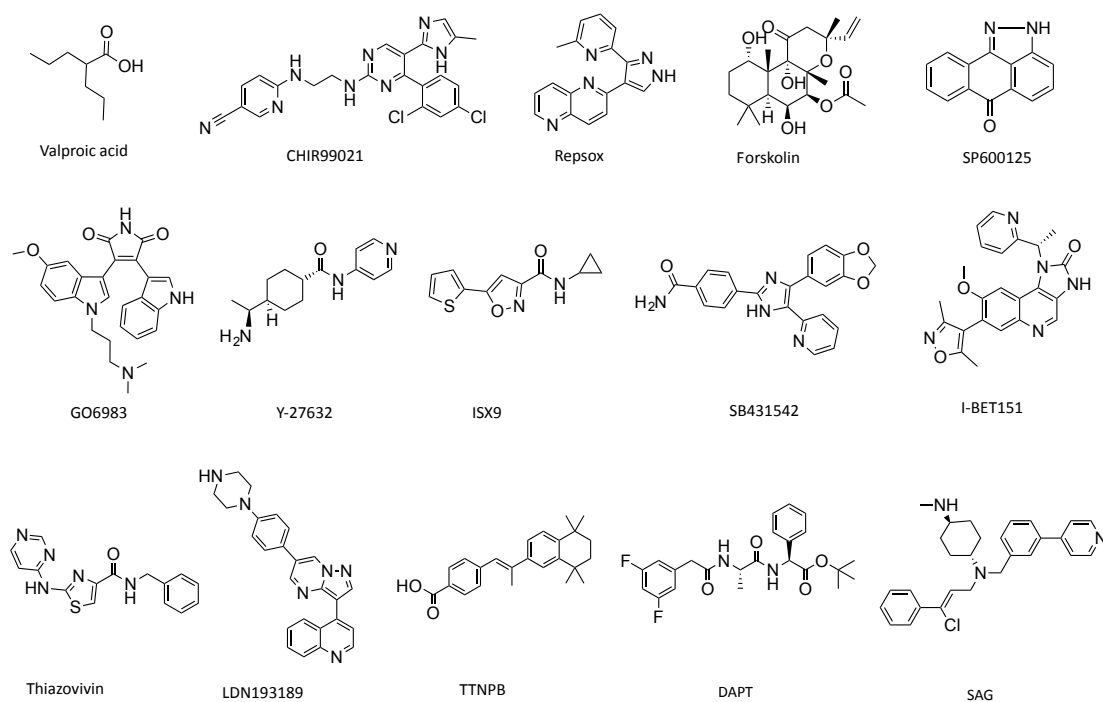


Figure 4. Small molecule probes modulating adult SCs reprogramming.

that the ISX9 molecule was essential for activating neuron-specific genes, while I-BET151 for affecting chromatin remodeling, which leads to erase the initial cell identity, while allowing the acquisition of converted fates. Moreover, co-culture assays with astrocytes or primary neurons revealed that the newly chemical-induced neurons were capable of forming functional synaptic connections reciprocally and with existing neurons.⁶⁹ Lately, one of the most recent examples of small molecules-based reprogramming provided the demonstration that the conversion of astrocytes to fully functional neurons can be achieved also with human cells.⁷⁰ Unlike the previously discussed chemical cocktail VCR used for mouse astrocytes reprogramming, the authors identified a cocktail of 9 small molecules (including, valproic acid, CHIR99021, SB431542, thiazovivin (ROCK inhibitor), LDN193189 (ROCK inhibitor), TTNPB (retinoic acid analogue), DAPT (γ -secretase inhibitor), Smoothened agonist (SAG)) able to induce human astrocytes reprogramming into neuronal cells with a specific sequence.⁷⁰

Collectively, these results indicate that direct chemical conversion may offer an alternative path for generating cell types other than neurons, providing disease models and possibilities for regenerative therapy.⁷¹

Even though small molecules probing NSCs function are highly desirable, their discovery has proven challenging because of the extremely high complexity of the mammalian neurogenesis. This raises many important questions: is there any validated target that modulate neurogenesis for druggable purposes? What is the best approach to gain information at molecular level of NSCs regulation?

In the following paragraph, we provide an overview of the intricate and complex signals orchestrating neurogenesis. Again, the chemical modulation represents one of the most suitable approaches to study such complexity.

1.5 Pathways modulating adult neurogenesis

The study of neurogenesis in the adult brain is among the most exciting and fastest moving areas of neuroscience today.⁷² However, the study of its mechanisms is still matter of intense debate, due to the lack of specific tools and markers.⁷² Several mechanisms underlying neurogenesis have been advanced and have been properly reviewed elsewhere.^{36, 73} Remarkably, what attracts our attention is that many mechanisms implicated in neurogenesis have been identified thanks to the use of chemicals or drugs. This supports the working hypothesis that small molecules can indeed play a major role as chemical probes to dissect new targets and new pathways underlying the neurogenesis and to open the way to the development of new drugs.

Among the most accredited mechanisms orchestrating neurogenesis, nuclear receptors⁷⁴ and epigenetic regulators⁷⁵ play a crucial role in intrinsically modulating neurogenesis. For example, rising evidences suggest that the activation of PPAR γ pathway promotes neuronal differentiation and axon polarity. This has been demonstrated by the fact that PPAR γ agonist pioglitazone (Figure 5), stimulated NSCs proliferation via ERK pathway by phosphorylating and up-regulating the epidermal growth factor (EGF) receptor and cyclin B protein levels.⁷⁶

Moreover, the fundamental role played by the orphan nuclear receptor Tlx in the regulation of NSCs proliferation has been recently highlighted.⁷⁷ Particularly, it has been shown that Tlx is able to maintain NSCs in a proliferative state thanks to the activation of the Wnt/ β -catenin pathway⁷⁸ and the recruitment of histone deacetylases (HDACs).⁷⁹ Importantly, the effects of HDACs activation led to the transcriptional repression of Tlx target genes, such as the cyclin-dependent kinase inhibitor, p21.⁷⁹ Additionally, the critical role of p21 was further established after chronic treatment with antidepressants imipramine, desipramine and fluoxetine (Figure 5) which decrease p21 expression, and this was associated with increased neurogenesis in vivo.⁸⁰ In addition to histone modifications, DNA methylation has emerged as an important regulator of synaptic plasticity via modulation of specific gene expression.⁸¹ The different expression of three DNA methyltransferases (DNMT1-3) in various stages and anatomical locations associated to neurogenesis, clearly demonstrate the peculiar roles of DNA methylation in this process. For instance, DNMT1 is highly expressed in proliferative cells in the adult DG and plays an important role in the survival of newly generated neurons. However, DNMT1 deletion in adult NSCs and precursor cells resulted in a decrease of newly generated mature neurons, while not influencing post-mitotic neurons survival.⁸²

In addition to nuclear receptors and epigenetic regulators mentioned above, the Hippo signaling pathway appears to be critical in maintaining NSCs quiescence.⁸³ Indeed, its transcriptional co-activator YAP protein is highly expressed in neural tubes and in the cerebellum, co-localizing with Sox2, a neural progenitor marker. Loss of downstream kinases *Mst1/2* or *Lats1/2* of Hippo pathway, corresponding with the YAP activation, leads to a marked expansion of neural progenitors, partially due to an up-regulation of stemness genes. Conversely, YAP loss-of-function results in increased cell death and precocious neural differentiation.⁸³ As confirmed in *Drosophila*, Ding and coworker showed that the Hippo pathway is modulated via inter-cellular trans-membrane proteins (crumbs and echinoid) that are both expressed in a nutrient-dependent way by niche glial cells and NSCs in order to

maintain quiescence and suppress cell growth. Indeed, their deletion resulted in the reactivation of NSCs, thus providing evidence that the Hippo pathway activity discriminates quiescent from non-quiescent NSCs in the *Drosophila* nervous system.⁸⁴ Collectively, these findings support that the Hippo pathway plays crucial roles in regulating NPCs number and suggest the possibilities for discovering useful pharmacological tools targeting specific players of this pathway.⁸⁵

In addition to these intrinsic factors, adult neurogenesis is further finely tuned by many extrinsic molecular players, including morphogens, growth factors and neurotransmitters (reviewed in ⁸⁶). Such signals form a complex network of interactions that regulate NSCs in terms of proliferation, migration, integration and plasticity maintenance. For example, bone morphogenetic proteins (BMPs) promote glia differentiation⁸⁷ and NSCs quiescence,⁸⁸ while inhibiting neural differentiation in the adult brain. Other known extrinsic regulators include Notch and Wnt pathways.^{86b} While Notch signaling is responsible for regulation of identity and self-renewal of NSCs, Wnt play a fundamental role in adult hippocampus. Notably, Wnt promotes proliferation and neuronal fate commitment of neural precursors in the adult SGZ, and its overexpression increased neurogenesis from adult progenitors both in vitro and in vivo.⁸⁹ By contrast, blockade of Wnt signaling decreases neurogenesis of adult progenitors in vitro and abrogates almost completely neurogenesis in vivo.⁸⁹ Additionally, glycogen synthase kinase-3 β (GSK-3 β), a downstream regulator of Wnt pathway, has been demonstrated to be critical in many processes during neurodevelopment. Indeed, the level of GSK-3 β activity influences NPCs proliferation/differentiation during repairing processes, as well as efficient neurotransmission in differentiated adult neurons. Understanding how GSK-3 β signaling controls neurogenesis, neuronal polarization and axon growth during brain development is particularly challenging due to the broad range of GSK-3 β substrates.⁹⁰ Indeed, recent advances suggest that GSK-3 β is a central node for multiple signaling pathways and, in this complex scenario, it orchestrates the proliferation and differentiation of neural progenitors. Moreover, the essential role of GSK-3 β signaling in neurogenesis has been confirmed by considering the involvement in neurodegenerative disorders, such as Alzheimer's disease (AD).⁹¹

Although the source of most niche signals remains to be fully characterized, it is clear that multiple morphogens are concomitantly acting on adult neural precursors to fine-tune the number of quiescent precursors and the amount of new neurons and astrocytes in the adult brain.

In addition, four neurotrophic factors have been identified, namely nerve growth factor (NGF), brain-derived neurotrophic factor (BDNF), neurotrophin 3 (NT-3), and neurotrophin 4/5 (NT-4/5) and their fundamental role in modulating neurogenesis has been widely recognized.⁹² Neurotrophins bind to receptor tyrosine kinases known as Trk receptors (TrkA-C) and their co-receptor p75NTR, displaying different binding affinities for the different neurotrophin. Interestingly, BDNF is known for its survival-promoting effects on new neuroblasts through the TrkB receptor,⁹³ whereas the proliferative effect of NGF on NSC proliferation was firstly reported by Cattaneo and McKay.⁹⁴ Soon after, following studies revealed that NGF promotes proliferation through the phosphorylation of ERK1/2 in NSCs by interacting with TrkA receptor.⁹⁵

Accumulating evidences also suggest crucial roles of neurotransmitters in regulating adult NSCs proliferation, differentiation, and synaptic integration, as well as activity-

dependent adult neurogenesis. For example, GABA, the major inhibitory neurotransmitter of the brain, promotes NSC quiescence by blocking cell-cycle progression.⁹⁶ Also the dopamine receptor D2 antagonist haloperidol (Figure 5) increases SVZ NSCs division, suggesting that dopamine promotes quiescence as well.⁹⁷ In contrast, serotonin (5HT)⁹⁸ and acetylcholine (ACh)⁹⁹ activate SVZ NSCs. Interestingly, serotonergic axons, a small set of neurons originating from the raphe, have been recently reported to critically modulate SVZ neurogenesis. Indeed, electron microscopy revealed that 5HT axons form contacts between ependymal cells/NSCs expressing the 5HT receptors 2C and 5A in the SVZ. To test this hypothesis, the authors evaluated the ability of 5HT_{2C} agonists (RO-60-0175) or antagonists (SB206553, in Figure 5) to increase or decrease SVZ proliferation, respectively.⁹⁸ Paez-Gonzalez et al. disclosed an unknown population of choline acetyltransferase (ChAT) neurons residing and regulating the SVZ neurogenic niche. In contrast to neighboring neurons, ChAT neurons appear to be functionally different as they release ACh locally in an activity-dependent manner to control neurogenic proliferation. Following experiments revealed that SVZ NSCs directly respond to local ACh release, synergizing with fibroblast growth factor receptor (FGFR) activation to

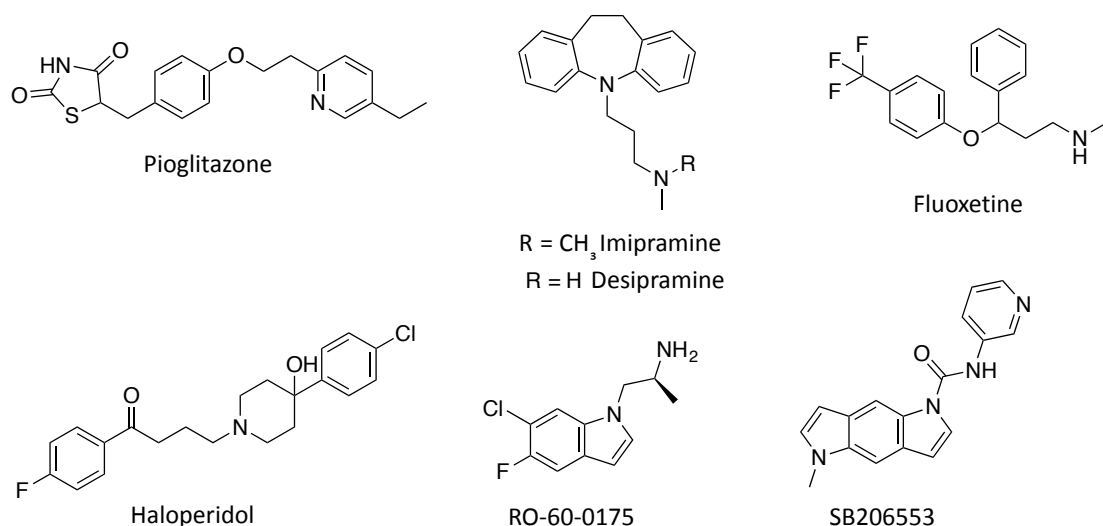


Figure 5. Small molecules modulating specific targets/pathways of NSCs.

increase neuroblast production.⁹⁹ These results suggest an unknown ChAT-mediated pathway controlling SVZ neurogenesis and thus, may open new possibilities for modulating neuroregenerative capacities in health and disease.¹⁰⁰

However, it is worth to note that it is not always clear whether pharmacological manipulations act by directly affecting neural precursors and newborn neurons or through indirect modulation of the niche.¹⁰¹ Intriguingly, antidepressants (such as imipramine and fluoxetine, in Figure 5) used in clinics, should increase neural progenitor proliferation, accelerate dendritic development, and enhance survival of newborn neurons in the adult hippocampus through changes in 5HT and norepinephrine levels.¹⁰²

In parallel to cellular players, the demonstration that stress levels negatively affected the numbers of proliferating cells in the DG¹⁰³ fueled a plethora of studies to investigate how neurogenesis can be also significantly influenced by other external stimuli. For example, van Praag et al. demonstrated that physical exercise increases

cell proliferation in DG,¹⁰⁴ while Gould and colleagues showed how learning tasks modulate adult neurogenesis in a complex and specific fashion, depending essentially on hippocampus.¹⁰⁵ Conversely, changes in neurogenesis were shown to be associated with age and pathological conditions, as in the case of AD. Particularly, the effect of neurodegeneration on adult neurogenesis is significantly very complex (reviewed in ¹⁰⁶). During neurodegeneration, activation of resident microglia, astrocytes, and infiltrating peripheral macrophages causes the release of cytokines, chemokines, neurotransmitters, and reactive oxygen species (ROS), which differently affect various aspects of neurogenesis.¹⁰⁶ For example, in animal models of AD, aberrant GABA signaling influences differentiation of neural progenitors and dendritic growth of newly neurons in the SGZ.¹⁰⁷ Another major negative regulator of adult neurogenesis is inflammation, induced by injuries, degenerative and neurological diseases.¹⁰⁸ In addition to decrease the proliferative capacity and neuronal fate commitment of neural progenitors in the adult SGZ, inflammation disrupts the niche microenvironment by increasing the number of microglia cells, that result in an impaired neurogenesis.¹⁰⁹

From the data discussed so far, it is evident that every single phase of adult neurogenesis can be regulated by different stimuli and each stimulus can have multiple targets. Furthermore, different stimuli interact with each other and impact the final outcome of adult neurogenesis. In general, regulation of adult neurogenesis by external stimuli is complex and the effect depends on timing, dose/duration, specific paradigms, animal models (age, sex, genetic background), and methods of analysis. The major challenge is to identify intrinsic cellular and molecular mechanisms underlying different stages of adult neurogenesis. What are targets of particular stimulation-quiescent putative stem cells, their specific progeny, or mature cell types from the niche? Are SGZ and SVZ niches differentially regulated by the same stimuli?

Unfortunately, we still have a lot of questions to answer about the application of NSCs in a therapeutic context. Further and concerted research is needed to fully disclose the therapeutic potential of regenerative medicine. In the following paragraph, significant examples will be described.

1.6 New therapies for regenerative medicine: challenging and opportunities for neurodegenerative diseases

Traditionally, the term “regeneration” describes the processes that properly maintain cell number (homeostasis) and replace damaged cells after injury (repair). In almost all tissues, regenerative potential is determined by the presence of a dedicated population of stem and progenitor cells, which respond to endogenous and exogenous cues to produce cells replacement as needed.¹¹⁰ Given the ability of SCs to become different cell types in the body, regenerative medicine offer great promise in treating currently incurable diseases.¹³ Particularly, the establishment that neurogenesis occurs continually throughout adults’ life hold tremendous promise for treating neurodegenerative diseases, such as AD and Parkinson’s (PD).

These and other neurodegenerative diseases share common mechanisms leading to neuronal dysfunction and, eventually, neuronal death.¹¹¹ Current therapies address the symptoms, but are yet not effective for rescuing cellular function or even halting

the neuronal death process.¹¹² As exemplified by AD clinical trials, AD drugs keep failing, having a 99.6 % failure rate. Indeed, a recent study highlighted that, between 2002 and 2012, only memantine (3,5-dimethyladamantan-1-amine) over 244 compounds in 413 clinical trials for AD, was approved in 2003.¹¹³ Reasons for these failures are numerous, ranging from insufficient understanding of mechanisms underlying such diseases to poor diagnosis techniques. For example, neurodegeneration in AD is determined by a complex and intertwined network of neurotoxic events that include oxidative stress, metals dyshomeostasis, glutamate excitotoxicity, inflammatory process, proteins (A β and tau) misfolding and aggregation. Such multifactorial nature of AD contributes in the failure of existing pharmacological approaches to alter the disease course.¹¹⁴ Furthermore, the current diagnosis relies on performing cognitive tests and looking for the presence of amyloid plaques and neurofibrillary tangles in the brain. However, it has now been recognized that the plaque stage of AD is a much-too-late phase at which to commence treatment. In addition, no single biomarker is reliable and valid for determining the true stage of AD advancement, further aggravated by the high variability of biomarker expression and disease progression in different AD patients.¹¹⁵

The depicted scenario is not different from that seen for PD¹¹⁶ or amyotrophic lateral sclerosis (ALS)¹¹⁷ (see cited review for a more detailed description). In all cases, this can be also ascribed to the models employed in vitro and in vivo, not truly representing the complexity of such diseases and lacking of clinical translation.¹¹⁵ These findings are further exacerbated by the growing incidence of ageing and consequently of neurodegenerative diseases. According to Alzheimer's Disease International, there were an estimated 46.8 million people with dementia worldwide in 2015.¹¹⁸

Against this backdrop, regenerative approaches involving both SCs replacement therapy and the modulation of SCs using small molecules have the potential to revolutionize neurodegenerative diseases treatment in the future.

1.6.1 New regenerative cellular therapies for neurodegenerative diseases

To date, the therapeutic potential of NSCs has been already demonstrated in vitro and also in vivo in various animal models of diseases, and some of them have entered the clinical trials. Starting from the outstanding paper by Blurton-Jones and coworkers,¹¹⁹ where NSCs-injection rescued the cognitive phenotype and increased synaptic density in triple transgenic mouse model of AD, the beneficial effects of NSCs transplantation in neurodegenerative states seem to be a dream becoming reality.¹²⁰ Indeed, Stemedica International recently provided the means to bring allogeneic human mesenchymal stem cells (MSCs) in clinical trial.¹²⁰ Accordingly, in 2015 the US Food and Drug Administration (FDA) granted approval for a phase 2A trial using intravenous administration of MSCs to treat patients with mild to moderate dementia caused by AD.¹²¹

An additional biopharmaceutical company, Neuralstem Inc., actively working on NSCs technology and harnessing the benefits of combining cellular and growth factor therapies, reported on the possibility to implement human cortical NSCs expressing

insulin-like growth factor-1 as a novel cellular therapy for AD.¹²² As a consequence, the observed beneficial effect arises from the synergistic actions of both cell therapy and growth factor implementation. Even though this study is still in its infancy lacking of clinical translation, Neuralstem also pioneered human fetal NSC transplants for ALS patients, already in clinical trials.¹²³ However, to date, clinical applications of NSCs based on cell replacement therapy has shown limited success due to inefficient survival, increased risk of tumorigenicity and possible immune responses¹²⁴ (as previously mentioned for SCI in Par. 1.1). In addition, the use of human ESCs or fetal SCs as SCs sources has raised numerous ethical issues.¹²⁵

1.6.2 New neuroregenerative therapeutic small molecules for neurodegenerative diseases

By contrast, adult SCs and the recently discovered iPSCs are exempted from unwanted ethical controversy, thus emerging as alternative SCs source not only for cell therapy but also for disease modeling and phenotypic drug discovery.¹¹ In fact, a recent application focused on modeling AD using both familial and sporadic patient-derived iPSCs. This study revealed stress phenotypes and differential drug responsiveness associated with intracellular amyloid beta oligomers in AD neurons and astrocytes.¹²⁶ In PD, a prominent work aimed to model disease, to identify the corresponding hallmarks, and to screen drugs has been recently reported by Chung et al.¹²⁷ Once confirmed the connection between α -Synuclein (α -Syn) and nitrosative stress in both yeast and rat models involving cortical neurons, the authors generated cortical neurons from iPSCs of PD patients with α -Syn mutations to screen for compounds that rescue α -Syn toxicity. Implementing a copper complex as a fluorescent-based sensor for the screening assay, they showed that the nitric oxide level was higher in PD-neurons compared to control. Interestingly, they found that a small molecule NAB2 (Figure 6)¹²⁸ is able to rescue yeast from α -Syn toxicity and to decrease nitric oxide level in PD-neurons.

Concerning ALS, Yang et al. performed an innovative small molecules survival screen, using motor neurons (MNs) from both wild-type and mutant SOD1 mESCs. From the screening, the multikinases (GSK-3 β and mitogen-activated protein kinase 4 (MAP4K) kinases) inhibitor kenpauillone (Figure 3) was identified. It showed an impressive ability to prolong the healthy survival of both types of MNs that can be attributed to its dual inhibition. Furthermore, kenpauillone also strongly improved the survival of human MNs derived from ALS patient-iPSCs, resulting more active than reference compounds (olesoxime and dexpramipexole).¹²⁹

Collectively, these findings clearly demonstrate that patient-derived iPSCs would enable drug evaluation in reliable models, able to recapitulate all the molecular features underlying neurodegeneration. Moreover, due to the high variability and to the lack of standardized protocol to generate iPSCs, iPSCs-based cell therapy is being blemished by reprogramming iPSCs from patient's cells. These emerge as innovative platforms for developing disease-relevant cellular phenotypes suitable for drug discovery purposes.¹¹

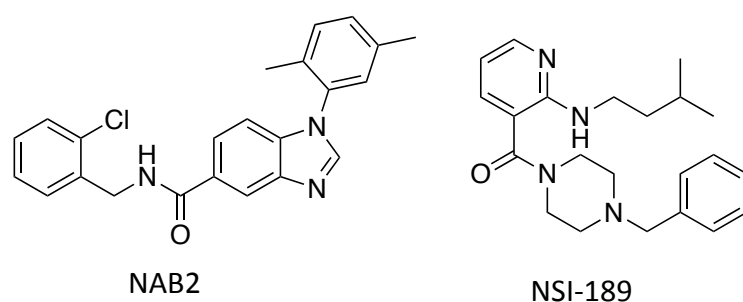


Figure 6. Small molecules with regenerative therapeutic potential.

Thus, an exciting alternative, which avoids SCs-based therapy, is rapidly emerging in the field of neuroregenerative medicine: the activation of endogenous neurogenesis and neuroprotection via chemical modulation.¹³ Small molecules triggering neurogenesis are particularly interesting not only because of their enormous therapeutic implications, but also because they can serve as tools to decipher the biological mechanisms of neurogenesis.

The chemical stimulation of endogenous SCs-based repair mechanisms has been successfully exploited to treat major depressive disorder (MDD) by Neuralstem. In this case, the company has completed Phase Ia and Ib trials evaluating safety doses and pharmacokinetic (PK) of its first neurogenic small molecule product candidate, the benzylpiperazine-aminopyridine NSI-189 (Figure 6).¹³⁰ At this time, NSI-189's mechanism of action remains elusive. As clinical trials progress, it is expected that an increasing amount of data will appear discussing how NSI-189 elicits its neurogenic effect in hippocampus and its neuroprotective/nootropic properties.

Although this paragraph reported on the first proof-of-concept of regenerative strategy, unfortunately there is not a general streamlined approach to identify small molecules with these intriguing regenerative features.

In the next paragraph, the basic strategies to discover new chemical probes and drugs targeting NSCs will be described, with a special emphasis on the peculiarities of target-based vs. phenotypic-based approaches.

1.7 Target-based vs. phenotypic based approaches in NSCs

Several target-based approaches have yielded small-molecule modulators of HSCs self-renewal, as previously mentioned in Par. 1.4.2. In the case of NSCs, the situation appears more complicated due to the lack of well-characterized pathways involved in a specific process of NSCs fate. Despite that, epigenetic alteration is an important determinant in lineage specification of NSCs,¹³¹ making epigenetic enzymes attractive targets.¹³² Among these, the HDACi have been widely studied.¹³² For example, valproic acid (Figure 4) induced neuronal differentiation of adult hippocampal neural progenitors. In addition, valproic acid inhibited astrocyte and oligodendrocyte differentiation, by up-regulating, neuron-specific genes, such as NeuroD, resulting in the induction and suppression of neuronal and glial differentiation, respectively. These results suggest that valproic acid promotes neuronal fate and inhibits glial fate simultaneously through the induction of neurogenic transcription factors including NeuroD.¹³³ Similarly, a following report

demonstrated that epigenetic mechanisms regulate timing of progenitor cell differentiation into myelin-forming oligodendrocytes *in vivo*.¹³⁴ In this context, histone deacetylation was shown to be essential during a specific temporal window of oligodendrocytes differentiation and myelin gene expression. Indeed, administration of valproic acid resulted in significant hypomyelination with delayed expression of oligodendrocytes markers, while maintaining expression of progenitor markers. Taken together, these data identify modifications of histones critical for controlling neuronal *versus* oligodendrocyte differentiation. Interestingly, another report supported the hypothesis that HDAC inhibition promotes neuronal fate and simultaneously inhibits glial fate through the direct induction of neurogenic transcription factors, such as NeuroD.¹³⁵ In detail, starting from the unexpected results that a subset of small molecules screened for cardiogenic differentiation induced a neuronal phenotype,¹³⁶ Schneider et al. counter-screened these hits for their neurogenic potential and identified five 3,5-disubstituted isoxazole hits that selectively convert NSCs into neurons expressing NeuroD.¹³⁵ In search of a more potent and soluble lead, the authors synthesized a focused library of 3,5-disubstituted isoxazoles (75 analogues) that led to the identification of ISX9 (Figure 4). Additional experiments showed that it activates CaMKII (the major HDAC kinase), which in turn led to sequestration of HDAC5 from the nucleus, thus de-repressing neurogenic transcription factors, including NeuroD. These studies provide evidence that blockade of HDAC activity plays a major role in neuronal lineage specification. Indeed, Hao et al.¹³⁷ also demonstrated that HDAC inhibition promotes neurogenesis *in vivo*; however, they suggested that the effect observed with valproic acid did not result exclusively from HDAC inhibition. It is well known that valproic acid, in addition to modulating HDAC activity, inhibits GSK-3 β and activates the mitogen-activated protein kinase (MEK)/ERK pathway. Intriguingly, the selective inhibition of GSK-3 β , HDACs, or both GSK-3 β and HDACs did not produce the same neurogenic activity as that produced by valproic acid, indicating that activation of MEK/ERK may also be proneurogenic *in vivo*. Further evidence that the inhibition of HDAC is neurogenic came from the work of Fischer et al. who demonstrated that this applies also *in vivo*. In fact, treatment of mice with the HDACi sodium butyrate (Figure 7) promoted dendrites propagation, increased synapse number, and restored learning behavior and long-term memories.¹³⁸

Collectively, these data demonstrate that HDAC mediated gene regulation is an important determinant of neural lineage progression and maintenance in the brain and that inhibition of HDACs may serve as a means to stimulate the brain's regenerative mechanisms *in vivo*.¹³⁹

Another strategy to develop small molecules for regeneration is to focus on defined molecular targets or pathways, such as Wnt-mediated signalling, which is implicated in specific regenerative processes as already shown. One potential concern about activating a regenerative pathway is the risk of causing certain genetic alterations or abnormal gene expressions that lead to the activation of some of those pathways that have been associated with cancer. Strategies such as temporal and/or synergistic activation may provide a viable solution. To discover novel compounds and pathways that interact with the canonical Wnt- β -catenin signalling pathway, Zhang et al set up a reporter based high-throughput screen for small molecules (100,000 compounds) that synergistically with Wnt3A ligand activate the reporter.¹⁴⁰

A 2,6,9-trisubstituted purine compound, QS11 (Figure 7), has been selected for its ability to synergize with canonical Wnt proteins both in vitro and in vivo. Affinity chromatography identified the GTPase activating protein of ADP-ribosylation factor 1 (ARF-GAP) as a target of QS11. Additional biochemical, genetic and functional studies have confirmed that QS11 inhibits ARF-GAP, suggesting that QS11 interacts with Wnt/ β -catenin signaling through modulating ARF activity and β -catenin localization. Although targeted modulation of known pathways and the epigenome has identified a variety of operative mechanisms in NSCs, the field still lacks a complete understanding of how to selectively control NSCs fate. Thus, designing unbiased cell-based screens to identify novel mechanisms that control NSCs fate is an emerging strategy. The promising outcomes provided by this approach led to the discovery of a 2-substituted aminothiazol (neuropathiazol, Figure 7).¹⁴¹ Warashina and colleagues used an imaging-based screen with neuronal (Tuj-1) and astroglial (GFAP) markers to identify compounds that direct the differentiation of adult NPCs into neurons or astrocytes, respectively.¹⁴¹ Notably, neuropathiazol induced up to 80% of cells to differentiate into Tuj-1-positive neurons with characteristic neuronal morphology. But also, it increased the expression of NeuroD, concomitantly decreasing the expression of Sox2. Importantly, unlike retinoic acid, neuropathiazol blocked the proliferation and BMP-induced astrocyte differentiation of NSCs.¹⁴¹ Following SAR study identified a molecule, KHS101 (Figure 7), which displayed improved neurogenic activity in vitro and brain penetration compared to neuropathiazol.¹⁴² KHS101 also increased neuronal differentiation in adult rats and affinity chromatography revealed the transforming acidic coiled-coil containing protein 3 (TACC3) as a putative target. Genetic modifications of cultured NPCs aimed at reducing TACC3 expression produced a neuronal differentiation phenotype similar to cells treated with KHS101. Interestingly, treatment with KHS101 also increased the nuclear localization of the nervous system-specific transcription factor aryl hydrocarbon receptor nuclear translocator 2 (ARNT2), whose overexpression also promotes neuronal differentiation. Altogether, these evidences indicate that KHS101 modulates neurogenesis by interacting with TACC3 and supporting the existence of a functional link between TACC3-ARNT2.¹⁵³

To discover novel signaling pathways involved in NSCs self-renewal, Diamandis et al. designed an unbiased chemical-genetic cell-based screen with the goal of identifying those that inhibit neurosphere proliferation in mouse NSCs.¹⁴³ The authors screened pharmacologically active compounds (1,267 compounds) and after filtering out cytotoxic molecules, the selected hit compounds with promising effects on NSC cultures were subjected to additional studies. These studies revealed that these hits (such as dihydrocapsaicin, an agonist of the vanilloid receptor; apomorphine, an agonist of the dopamine receptor; and PAPP (Figure 7), a serotonin agonist, as well as numerous other modulators of the serotonin, opioid and glutamate pathways¹⁴³) are neuromodulatory. In understanding the mechanisms of action of these compounds, one important question is whether they are acting on replicative NSCs or differentiated cells. Diamandis et al. addressed this point by testing whether the compounds prevented treated neurosphere cells from giving rise to new neurospheres after a period of culture without the compound. New neurosphere formation was indeed inhibited by many of the compounds, indicating that the replicative SCs capable of re-establishing neurospheres had been depleted. Notably,

many of the compounds identified as anti-proliferative for neurospheres also inhibited tumor spheroid growth in vitro, including those known as modulators of the dopamine, N-methyl-D-aspartate (NMDA), opioid, vanilloid and serotonin pathways.¹⁴³

Similarly, Kim et al. designed a chemical genomics screen with the aim of understanding genes and pathways that modulate neural stem/precursor cell differentiation.¹⁴⁴ A quantitative whole-cell immunofluorescence assay was set up to screen tool compound collections with the goal of identifying small molecules able to increase NSCs differentiation toward neuronal lineage in mouse NPCs. Notably, among the 42 proneurogenic molecules identified, 27 compounds are known GSK-3 β inhibitors. To further validate such screening by confirming the effect of GSK-3 β hit compounds on neural specification, one representative GSK-3 β inhibitor hit compound (SB627772) was confirmed in human NSCs culture. Additionally, SB627772 was also shown to promote endogenous neurogenesis in the SVZ region in vivo. This study clearly demonstrates that a phenotypic assay using immunofluorescent markers can be used for compounds screen to discover targets and pathways related to the differentiation of lineage-restricted precursor cells toward specific lineages.¹⁴⁴

Finally, the implementation of a SCs-based model of motor neurons (MNs) degeneration induced by microglial activation has been recently reported.¹⁴⁵ In contrast to the previous examples, this assay has been designed looking for neuroprotective small-molecules using SCs-derived MNs and activated microglia as a stress paradigm. From more than 10,000 small molecules tested at 10 μ M, 12 hit compounds were selected for further testing. These compounds act through diverse pathways, including the inhibition of nitric oxide production by microglia, activation of the Nrf2 pathway in microglia and astrocytes, and direct protection of neurons from nitric-oxide-induced degeneration. Hierarchical clustering of the data from expression profiling revealed a tight association of four hit compounds E5, E14, E19, and E20, whose activity was confirmed using human neurons. Considering that microglial cells are activated in many neurodegenerative disorders, the identified hit compounds could be suitable starting points for the development of new neuroprotective drugs to treat various neurodegenerative diseases.¹⁴⁵

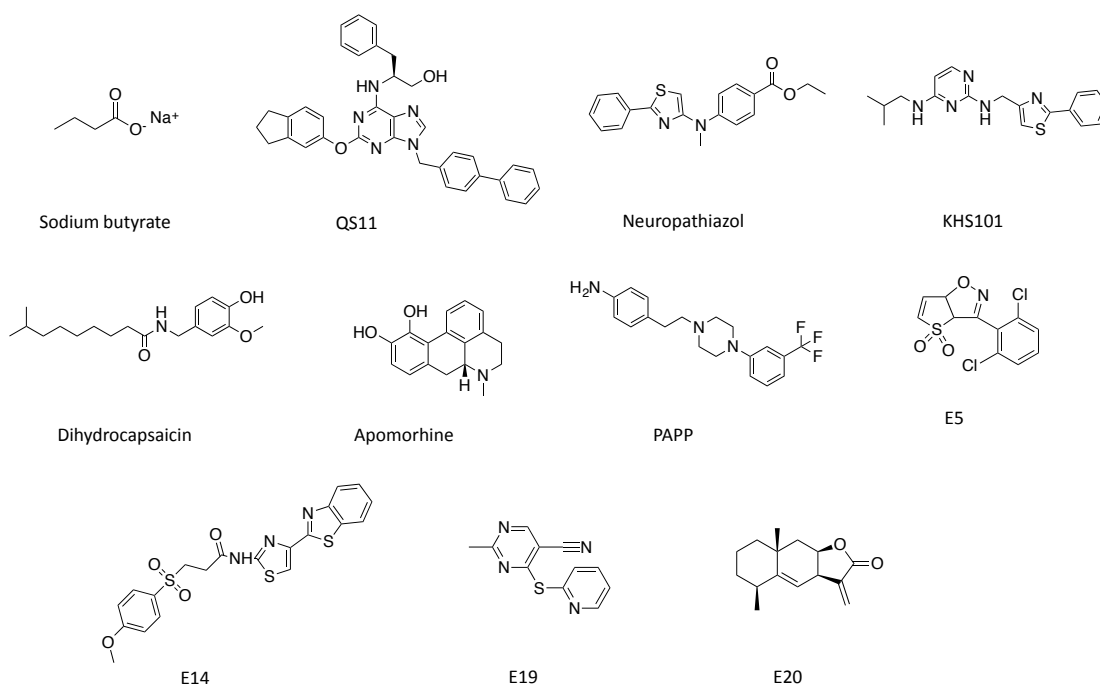


Figure 7. Small molecule probes of NSCs discovered by target-based and phenotypic based approaches.

Although these examples are only few demonstrating unique roles of small molecules in NSCs biology, systematic screens to identify previously uncovered pathways in neural precursors in an unbiased manner are being performed. For example, many of the small molecules screens designed to identify chemical regulators of SCs biology have been biased to particular pathways (i.e. Wnt) already known to be involved in SCs biology. Although these screens have helped discovering new agents that regulate NSCs biology, the screen design precludes the identification of novel pathways regulating NSCs function. Although investigations into these pathways will undoubtedly lead to new insights and potential therapies, parallel work into identifying novel pathways and targets is also necessary to move the field forward. Unbiased screening of novel pathways regulating NSCs processes will help further our understanding of the NSCs biology and of the complete network of signals regulating their self-renewal and multi-lineage differentiation potential. In the following paragraph, an exemplificative unbiased *in vivo* screening to discover molecules with neuroregenerative potential will be discussed.

1.7.1 An innovative unbiased phenotypic approach toward the discovery of P7C3

An ever-increasing number of screens for small molecules that can modulate the proliferation and differentiation of NSCs have been successfully described in the previous paragraph (and reviewed in ²⁴). However, it should be noted that such screening assays have been limited to cell lines and *ex vivo* assays, and hits in many cases display unfavorable pharmacokinetics for *in vivo* application.

A brilliant work recently published in *Cell* reported on a novel, unbiased screen to identify compounds that selectively enhance production of neurons from NSCs in living mice.¹⁴⁶ This approach proposed by Pieper et al. elegantly bypasses the

above-discussed roadblocks, leading to the discovery of a previously unknown compound with direct translational and clinical potential for neurodegenerative diseases.¹⁴⁷ First of all, the authors performed an in silico screen to identify about 1,000 compounds with favorable pharmacokinetic properties that were clustered into groups of 10. Then, the effects on cell proliferation and survival within the SGZ were detected, and re-testing individual compounds from the identified groups of molecules led to the identification of 8 proneurogenic compounds selected for the desired pharmacological profile. Particularly, an aminopropylcarbazole (P7C3, Figure 8) exhibited highly favorable pharmacological and PK profiles, being able to readily cross the BBB and to prevent the death of newborn neurons. To examine this further, the authors used a mouse model with impaired SGZ neurogenesis due to elevated apoptosis of newborn neurons. P7C3 is able to restore normal SGZ neurogenesis in this model by inhibiting apoptosis, perhaps regulated in part by maintaining mitochondrial integrity.¹⁴⁶ As a further step, a series of P7C3 derivatives were designed to explore the SAR around P7C3 scaffold with the goal of identifying compounds that promoted survival and proliferation of newborn neurons with improved potency and drug-like properties. In addition, chemical probes were purposely developed to provide insights into its mechanism of action. In the first case, the chemical optimization of P7C3 allowed the identification of two compounds, P7C3-A20 (Figure 8)¹⁴⁸ and then (-)-P7C3-S243 (Figure 8),¹⁴⁹ with improved drug-like properties, while preserving the neurogenic activity. On the basis of SAR studies, a suitable site that tolerates substitution without affecting the activity was identified. In particular, by modifying the amine function of P7C3, the probes P7C3-S324 (Figure 8)¹⁴⁷ and P7C3-S326 (Figure 8) have been developed.¹⁵⁰ Specifically, P7C3-S324 was decorated with a biotin moiety to use in affinity chromatography, while P7C3-S326 with a benzophenone photo-crosslinker modified with an alkyne functionality to use for post-crosslinking click conjugation to biotin, a fluorescent dye or a solid support. Although, the precise mechanism(s) of action is still undisclosed, P7C3-S326 allowed to identify nicotinamide phosphoribosyltransferase (NAMPT), as putative target. Interestingly, P7C3 seems to act by enhancing the activity of this protein, which represents the rate-limiting enzyme involved in the conversion of nicotinamide into nicotinamide adenine dinucleotide (NAD). These results are in line with the initial hypothesis that P7C3 class of proneurogenic compounds affects mitochondrial integrity or signaling.¹⁴⁷ Based on these encouraging findings and having established the structural requirements underlying the neurogenic activity, the authors also assessed the P7C3 neurogenic and neuroprotective efficacy in different mouse models of neurological disorders. Consistently, it has been showed that P7C3 is effective in a mouse model of PD protecting against 1-methyl-4-phenyl-1,2,3,6-tetrahydropyridine (MPTP)-mediated cell death of dopaminergic neurons in the substantia nigra.¹⁵¹ Furthermore, derivative (-)-P7C3-S243 was also evaluated in the rat 6-hydroxydopamine model of PD, showing a promising neuroprotective profile.¹⁵² Similarly, P7C3-A20 has been showed to protect ventral horn spinal cord motor neurons from cell death in the G93A-SOD1 mutant mouse model of ALS.¹⁵³ Additionally, P7C3 derivatives preserve axonal integrity after injury in a rodent model of blast-mediated traumatic brain injury (TBI)¹⁵⁴ and also rescue neurons and improve functional outcomes following peripheral nerve injury.¹⁵⁵ Furthermore, it

has been reported on the ability of P7C3 to restore the neurogenic deficits observed in the Ts65Dn mouse model of Down syndrome.¹⁵⁶ Finally, considering the convergence of evidence linking neurogenesis with depressive-like behavior, P7C3-A20 demonstrated greater proneurogenic efficacy than a wide spectrum of currently marketed antidepressant drugs in depression-prone Ghsr-null mice.¹⁵⁷

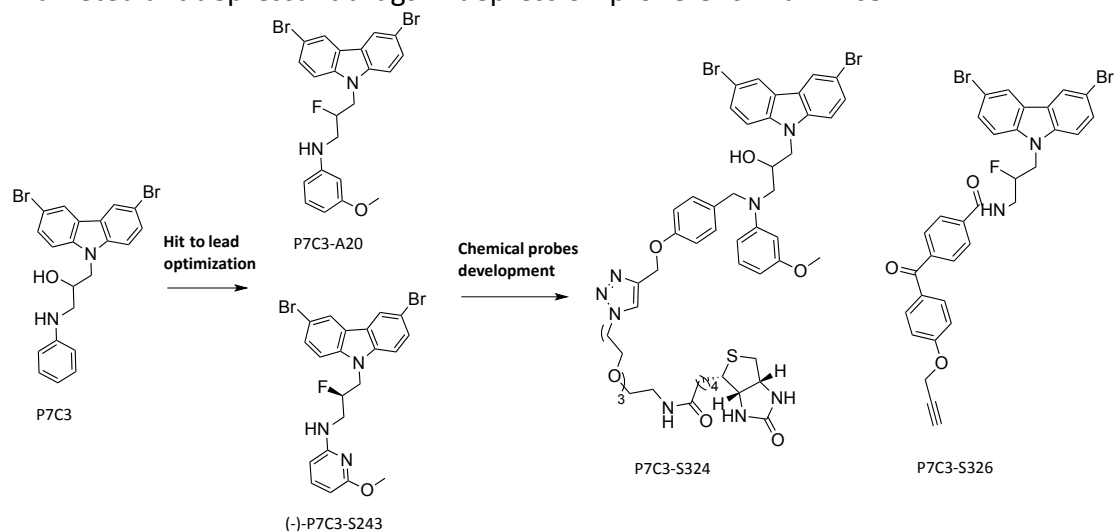


Figure 8. P7C3-based development of lead compounds and chemical probes.

All in all, this is a truly landmark study, providing several important advances: a formidable new screening approach in living mice and the related biological, biochemical and animal studies. Indeed, it offers benchmarks and methods for future *in vivo* small-molecule screening in mammals, incomparable to previous whole-organism screening in invertebrates and non-mammalian vertebrates such as zebrafish.¹⁵⁸ In this *in vivo* “target-agnostic” screen, hits are biased toward desired phenotypic and pharmacological profiles, thereby permitting to *ad hoc* filter out compounds with unfavorable PK. Moreover, the *in vivo* setting allows the modulation of SCs in their natural microenvironment, thus avoiding false positives, possibly arising from *ex vivo* SCs culture or from SCs lines. To note, P7C3 has favorable pharmacokinetics, low toxicity and no teratogenicity. Thus, as P7C3 is highly promising in promoting survival of newborn neurons and maintaining mitochondrial integrity, P7C3 derivatives may be very effective in the clinical setting of neurodegenerative disease.

Of note, this approach, which aims at discovering new neuroregenerative drugs, also represents a valuable example of chemical biology platform within academia (i.e. University of Texas Southwestern Medical Center).¹⁵⁹ Indeed, this brilliant study would not take place without the remarkable integration of a high-throughput screening facility, a medicinal chemistry laboratory, and a structural biology core, all supporting the mission of understanding and harnessing interactions between small molecules and biology.¹⁵⁹

2. Aims and objectives

The power of small molecules to address questions in cell biology has fueled an explosion of interest in chemical biology during the last two decades.¹⁶⁰ The development of chemical probes – i.e. small molecules that specifically and potently modulate the activities of cellular targets - is an established strength of chemical biology.¹⁶⁰ Indeed, such chemical probes represent valuable tools for the study of biological systems at the molecular level and also contribute to drug discovery. Particularly, chemical biology has already tackled challenges in several incurable diseases, especially in the field of neurodegeneration.¹⁶¹ In this context, chemical probes offer significant potential as tools for perturbing and understanding relatively unexplained targets and pathways involved in the neurodegenerative processes.¹⁶¹ For example, the main chemical biology approach towards understanding the causes of Alzheimer's disease (AD) was and still is largely directed to the development of chemical probes for amyloid β (A β).¹⁶¹ This has allowed to gain significant insights on its formation, structure, and interactions with metals, membranes, proteins and to develop potential drug and imaging agent candidates.¹⁶² Despite the significant advances, however the development of chemical tools and drugs for AD is an urgent need.¹¹³ Indeed, the absence of effective treatments in general against the neurodegenerative diseases provides an opportunity for innovative approaches, especially within academia.¹⁶³ In this respect, an emerging strategy relies on the activation of endogenous neural stem cells (NSCs) within our brain, as well neurogenesis and neuroprotection mechanisms, via chemical modulation.⁵³ Although it is a relatively young approach, the so-called "neuregenerative approach" has already proven useful at dissecting the role of specific pathways in a variety of NSCs processes including self-renewal, proliferation and differentiation¹⁹ that can be useful for the treatment of neurodegenerative diseases. In fact, the examples illustrated in Chapter 1 account for the significant role played by chemical biology to discovery and develop small molecules able to modulate NSCs fate in the field of neurodegeneration. Davies, the pioneer of the "stemistry" approach^{24b} clearly states that *"This emerging area of stemistry has unbelievable potential, through the stimulation of endogenous stem cell based repair mechanisms, to revolutionise human therapies. As always Chemistry is the key"*.¹⁶⁴ However, the use of chemical probes is not exempt from fundamental risks, and objective guidelines to the appropriate development of high-quality probes continue to be a matter of much concern and discussion.¹⁶⁵ At this point, a question arises: how to discover new chemical probes for NSCs? As anticipated in the previous chapter, the main approaches to generating small molecules that control NSCs fate involves the use of target-based or cell-based phenotypic screens of small molecules libraries. In general, the target-based approach begins with a druggable target that is a protein or pathway considered to be relevant for the disease or process under investigation.¹⁶⁶ An in vitro assay is then established against a purified target protein. Target-based strategy ideally identifies high-affinity compounds with a known target and mechanism of action.¹⁶⁶ Nevertheless, the limitations and drawbacks of this strategy are numerous. First, targets must be identified and validated, and validated targets for NSCs, especially for neurodegenerative diseases, have been elusive.¹⁶⁶

Second, the approach is unable to identify new targets and the available druggable target space for NSCs has been constrained to certain classes, such as kinases and epigenetic enzymes.^{24a} Third, compounds identified through in vitro assays can have chemical liabilities (for example, solubility or reactivity), and insurmountable off-target effects. Finally, compounds in target-based assays are selected for their ability to inhibit or activate an individual biological target. However, when the hit compounds from target-based approaches are tested in a cellular context, the capacity of cells to re-route signaling pathways and to activate other compensatory mechanisms is huge, and remains highly unpredictable.¹⁶⁶

In contrast, cell-based phenotypic screening involves the unbiased identification of compounds that modify a specific phenotype within the physiological context of an intact cell or organism.¹⁶⁶ In the context of neurodegenerative diseases, large chemical libraries (in the order of a million compounds) are screened on cellular models with relevant phenotypes such as overt cell death, altered localization of a disease-relevant protein and modification of specific cellular stress responses that have been linked to neurodegeneration.¹⁶⁶ The key to any unbiased phenotypic screen is a robust and consistent phenotype that can be modulated and scored for an effect that is directly connected to disease pathology. The main advantage of the phenotypic screen is that it takes place within a living cell, and accesses the complexity of in vivo biology. The screen itself filters out compounds that fail due to various chemical liabilities, such as toxicity, lack of permeation and efficacy. Moreover, various features that influence the function of a protein target within the cell, including binding partners, subcellular localization, contribute to the success of phenotypic versus target-based approaches.¹⁶⁷ Despite these advantages, phenotypic screens also have limitations, which can be overcome by the use of NSCs. In the context of neurodegenerative disease, where established in vitro models are limited by weak and variable phenotypes, NSCs provide a valuable model to screen chemical libraries.¹¹ Indeed, with the inception of induced pluripotent stem cells (iPSCs) cells derived from living patients, new relevant in vitro models can be obtained, which retain the genetic characteristics of their donors, enabling to recapitulate pathological features of a certain disease.¹¹

Furthermore, NSCs-based chemical-biological phenotypic approaches are particularly suitable for studying the complex network of intertwined molecular targets and pathways orchestrating the functional ground state of NSCs.²⁶ Indeed, such complexity limited our understanding in the field and greatly hampered the use of target-based approaches to identify small molecules modulating NSCs. Indeed, no single validated target with neuroregenerative potential has been identified, thus a phenotypic approach emerges as particularly promising.

On these premises, this part of my PhD project aims to identify new chemical probes for modulating NSCs, with a focus in the field of neuroregeneration. To achieve this goal, we exploit, in parallel, knowledge-based phenotypic (i) and functionalized congener (ii) chemical biology approaches. As depicted in Figure 9, the knowledge-based phenotypic approach (i) can be outlined as follows: designing and synthesizing a focused-chemical library (a), testing this library in a phenotypic screen (b), and identifying the target(s) of the identified hit compounds (c). Toward objective (a), we focus on a priori knowledge that some existing drugs and P7C3 drug candidate have been shown to display neuroregenerative effects. Hence, looking for suitable

scaffolds amenable to chemical manipulation, we realized that both tricyclic antidepressants (TCAs, e.g. imipramine see Par. 4.1.1 for a detailed discussion)¹⁶⁸ and P7C3 (see Par. 1.7.1)¹⁶³ share intriguing structural features, i.e. a tricyclic moiety linked to an amino function *via* a propyl alkyl chain (Figure 9). Accordingly, these two compounds may be considered as suitable starting points to develop chemical libraries with neurogenic potential. Additionally, being these molecules already characterized for their pharmacokinetic profiles, a chemical library inspired by these compounds may have the chance to identify compounds with high drug-likeness.¹⁶⁹ Thus, building on these strong premises, we aim to synthesize a focused chemical library inspired by TCAs and P7C3 (a), which would allow to explore the neurogenic- and neuroprotective-structure activity relationships around the selected scaffolds. Once the focused chemical library have been developed, before submitting to the full-scale compounds screening in the NSCs assay, the preliminary evaluation of their safety profiles in different cell lines will be performed as primary screening (b). This would improve the drug-likeness of synthesized compounds, filtering out the toxic ones. As a second step, the evaluation of neuroprotective and proliferation (neurogenesis) capabilities of the most promising compounds, will be performed in primary neurons. As illustrated in Figure 9, those that show no sign of toxicity and a neuroprotective/neurogenic profile will be progressed to the phenotypic NSCs-based assay, in order to evaluate their neurogenic potential, in terms of differentiation ability to modulate NSCs toward a given lineage (i.e. neurons, astrocytes and oligodendrocytes) (b). The last step of this knowledge-based approach relies on target identification studies (c), perhaps the most problematic issue in the proposed pipeline.

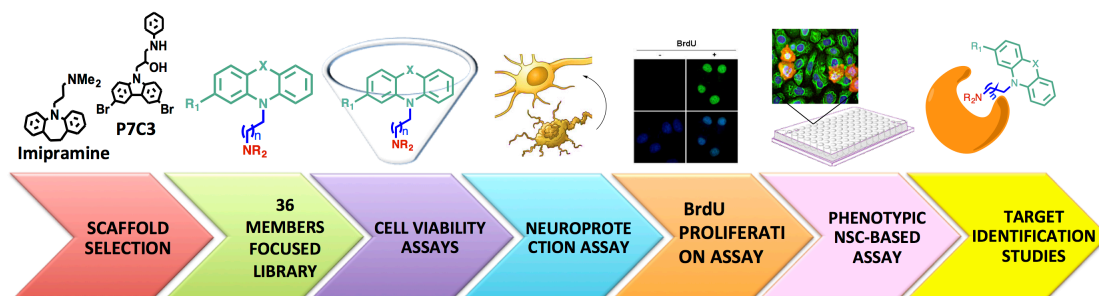


Figure 9. Knowledge-based chemical biology phenotypic pipeline.

In parallel, different sets of functionalized congeners (ii) inspired by TCAs will be developed. As medicinal chemists, the possibility to conjugate a selected compound to functionalized chains with different chemical and biological properties (i.e. functionalized congener approach) is particularly attractive.¹⁷⁰ To this end, as depicted in Figure 10, we synthesized appropriate functionalized congeners inspired by TCAs that, depending on the strategy of functionalization, have provided: fluorescent (a), dual-acting (multi-target) (b), polyamine congeners (c).

Among them, a small set of fluorescent probes inspired to TCAs will be synthesized by conjugating the imipramine pharmacophore to a fluorescent dye through different linkers (a). This will be used to potentially identify the subcellular localization of the targets whereby the selected hit compounds elicit the desired effects. On the other hand, given the complexity of NSCs landscape, the possibility to modulate such intricate signaling network by combining in a single chemical entities

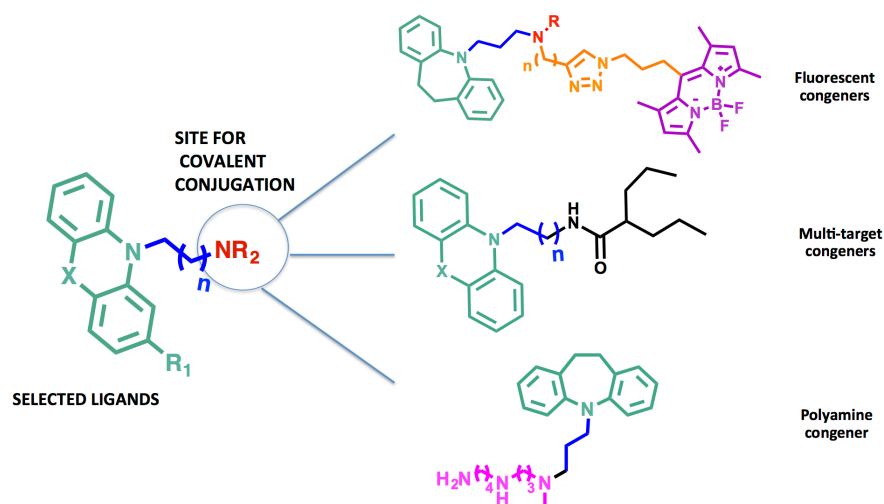


Figure 10. Design of functionalized congeners of TCAs.

two pharmacophoric fragments belonging to two molecules with different neurogenic mechanisms of action (i.e. multi-target compound)¹⁷¹ may be particularly promising. To this goal, we aim to conjugate some of the compounds of the focused library with compounds able to modulate NSCs (i.e. valproic acid). The last strategy relies on conjugation of TCA imipramine with a polyamine carrier (Figure 9). As polyamine conjugation has already showed to increase the cationic character of the starting molecule and to promote its accumulation directly into the mitochondrion, additional neuroprotective effects can be achieved following this functionalization strategy.¹⁷² Moreover, since putrescine in neurosphere stimulates neural progenitor proliferation, the appended polyamine to imipramine may also provide secondary favorable interactions underlying the neurogenic effects.¹⁷³

Collectively, this strategy may provide new insights into the regulation of neurogenesis by the use of TCAs- and P7C3-inspired focused library and functionalized congeners for discovering chemical probes of key signaling pathways implicated in NSCs proliferation/differentiation.

3. Chemistry

3.1 Synthesis of the focused chemical library inspired by TCAs and P7C3

The TCAs chemical syntheses present in the literature were obsolete and hazardous procedures, and, moreover, optimized as industrial process more than half a century ago.¹⁷⁴ Thus, they result of limited applicability to establish the SAR within a given targeted library. In fact, the reported route for the synthesis of imipramine started with the alkylation of 10,11-dihydro-5H-dibenz[b,f]azepine **1a** with 3-dimethylaminopropylchloride in presence of NaNH₂ as strong base in refluxing xylene (Figure 1).¹⁷⁵ Hence, the main synthetic challenge to obtain the TCAs-focused chemical library relies on finding a procedure, with the required following features: characterized by a simplified work-up, amenable to a parallel synthesis application, while avoiding the use of hazardous substances.

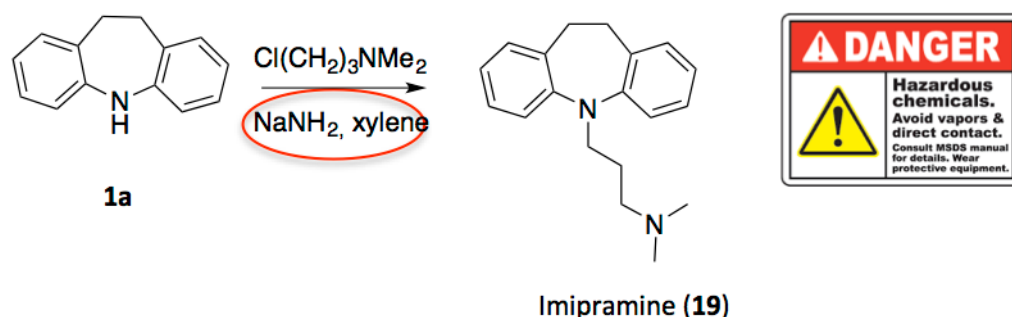
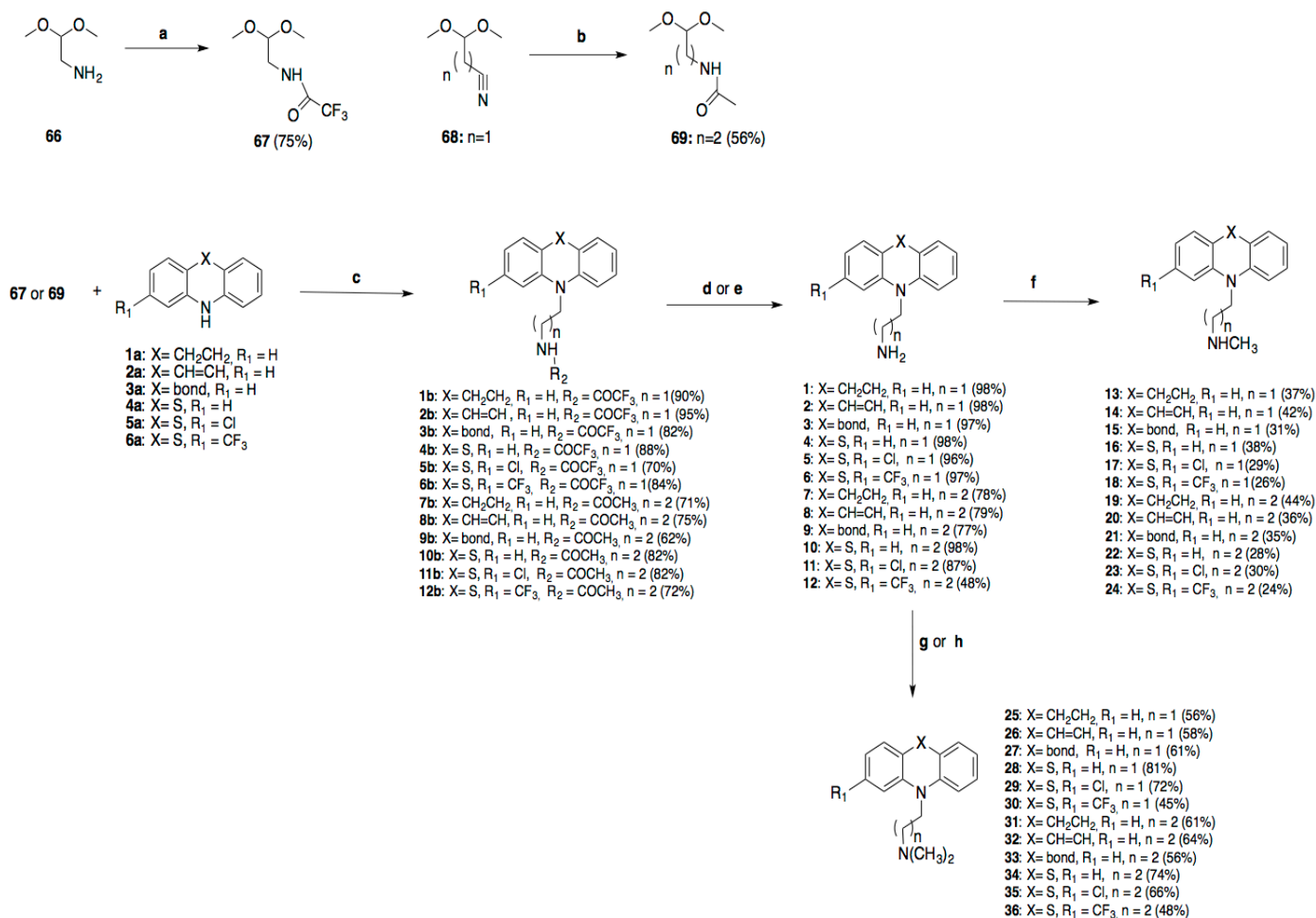


Figure 11. Reported route for the synthesis of drug imipramine **31**.

In an effort to find out a general synthetic method, which would involve a common intermediate for obtaining the primary, secondary, and tertiary amines of the selected tricyclic rings, we followed a procedure previously reported by Righi et al for similar scaffold.¹⁷⁶ It involves a direct one-pot reductive N-alkylation reaction of tricyclic aromatic amines **1a-6a** with acetals **67** and **69**, in the presence of triethylsilane (TES) as nontoxic and stable reducing agent (Scheme 1).¹⁷⁷ Thus, the synthetic route started with the synthesis of the proper acetal intermediates **67** and **69**. In detail, the synthesis of **67** has been accomplished by using trifluoroacetic anhydride (TFAA) to protect the amino functionality of compound **66** as trifluoroacetamide derivative.

For the reduction of the nitrile group of **68**, several reaction conditions have been tested before obtaining **69** (Table 2). Particularly, the first attempts involved the use of LiAlH₄ as reducing agent (conditions A-C). However, if condition A did not lead to the desired compound and allow to recover almost 60% of the starting material **68**, condition B appeared to be too drastic, not allowing either to afford **69** and to recover **68**. Looking for a compromise between the two above conditions, we tested if an increase of number of equivalents of LiAlH₄ and a reduction of reaction time (condition C), could work. Also in this case, we did not get **69**, leading to a very complex mixture of several products, extremely difficult to purify.



Scheme 1. Reagents and conditions:

a. TFAA, TEA, THF, N₂, r.t.; **b.** NaBH₄, NiSO₄, Ac₂O, MeOH, r.t.; **c.** TES, TFA, DCM, N₂, r.t., **d.** K₂CO₃, MeOH/H₂O, r.t.; **e.** KOH, MeOH/H₂O, MW, 150W, 160°C; **f.** HCOH, K10-clay, NaBH₄, MeOH, MW 30', 80°C; **g.** HCOOH, HCOH, H₂O, MW, 50W, 100°C; **h.** HCOOH, HCOH, H₂O, 80°C.

Table 2. Reaction conditions explored to target compound **69**.

Condi tions	R	Reducin g agent (eq.)	Amine trapping agent (eq.)	Catalyst (eq.)	Solven t	Reaction conditions	Results
A	H	LiAlH ₄ (3 eq.)	-	-	THF	rt, 3 h	No reaction
B	H	LiAlH ₄ (3 eq.)	-	-	THF	rt, 12 h	No reaction
C	H	LiAlH ₄ (5 eq.)	-	-	THF	rt, 2 h	No reaction
D	-COCH ₃	NaBH ₄ (7 eq.)	O(COCH ₃) ₂ (2 eq.)	NiCO ₃ (1 eq.)	MeOH	rt, 12 h	No reaction
E	-COCH ₃	NaBH ₄ (7 eq.)	O(COCH ₃) ₂ (2 eq.)	NiSO ₄ (1 eq.)	MeOH	rt, 7 h	≈50% yield
F	-COCF ₃	NaBH ₄ (7 eq.)	O(COCF ₃) ₂ (2 eq.)	NiSO ₄ (1 eq.)	MeOH	rt, 7 h	Traces of desired compound

Once experienced that LiAlH₄ was not effective, we turned our attention to a different reducing agent, i.e. NaBH₄. To overcome its limited reducing ability toward the nitrile group, we have modified the procedure proposed by Caddick et al.¹⁷⁸ In particular, it involves the use of a large excess of NaBH₄ (7 eq.) and Ni²⁺ as catalyst, which dramatically improves the reactivity of hydride donors. Moreover, to prevent dimerization reaction, a well-known side reaction that often occurs during the reduction of nitriles to primary amine, the use of a trapping agent (acetic anhydride or di-tert-butyl dicarbonate) was required. Thus, we initially tested different Ni²⁺ salts (NiCO₃ and NiSO₄), and acetic anhydride as trapping agent (corresponding to conditions D and E, respectively). Surprisingly, only NiSO₄ (conditions E) affords the target compound **69** in 50% yield. A following attempt (condition F) to obtain the trifluoroacetamide (in homology to **67**), involved the use of trifluoroacetic anhydride as trapping agent, while maintaining NiSO₄ as catalyst. Nevertheless, in this case just traces of **69** were observed, due to the instability of trifluoroacetamide derivatives under strong reducing conditions.

With the acetals **67** and **69** in hands, the reductive N-alkylation reaction of tricyclic aromatic amines **1a-6a** with **67** or **69** was performed.¹⁷⁶ This provided the tricyclic scaffolds 6,5,6 or 6,6,6 or 6,7,6 (carbazole, 10,11-dihydro-dibenzazepine, dibenzazepine and differently substituted phenothiazines) as alkyl-amide derivatives **1b-12b** in very good yields (62%-95%). Probably, the trend of yields for **7b-12b** (62%-82%) reflects the lower reactivity of acetamide derivative **69**, compared to yield for **1b-6b** (70%-95%), obtained starting from trifluoroacetamide **67**. The subsequent cleavage of the amide-protecting group to afford primary amines **1-12** involved two different procedures. In the first route, the removal of trifluoroacetamide protecting group of **1b-6b** under mild reaction conditions (K₂CO₃ in H₂O/MeOH) led to primary amine derivatives **1-6** in quantitative yield. Conversely, the cleavage of acetamide protecting group of **7b-12b** under microwave (MW) irradiation with a strong base (KOH in H₂O/MeOH) gave the primary amines **7-12** only in good yield (72%-98%). For comparison purposes, we also carried out the above-mentioned reaction under conventional reflux conditions (see Table 3). Dramatic differences have been observed in terms of both yields (45%-67% with the conventional method) and decreased reaction time (from 2 days to 90 min).

Table 3. Comparison between conventional and MW procedures.

Compounds	Reaction type	Conventional conditions (reaction time and yield)		MW conditions (reaction time and yield)	
7b-12b	Amide hydrolysis	2 days	45%-67%	90 min	72%-98%
1-3 and 7-9	Reductive alkylation	10 h	40%-58%	30 min	63%-74%

Then, compounds **1-12** were converted to their corresponding secondary amines **13-24**. Our first attempt was based on a one-pot procedure involving the N-methylation of amides **1b-12b** with NaH (as base), and MeI (as methylating agent) and the subsequent removal of the amide-protecting group using the same procedures described for **1-12**. However, searching for an alternative and greener procedure to obtain the secondary amines **13-24**, while avoiding the use of highly toxic MeI, we developed a modified version of a MW-assisted reductive amination reaction

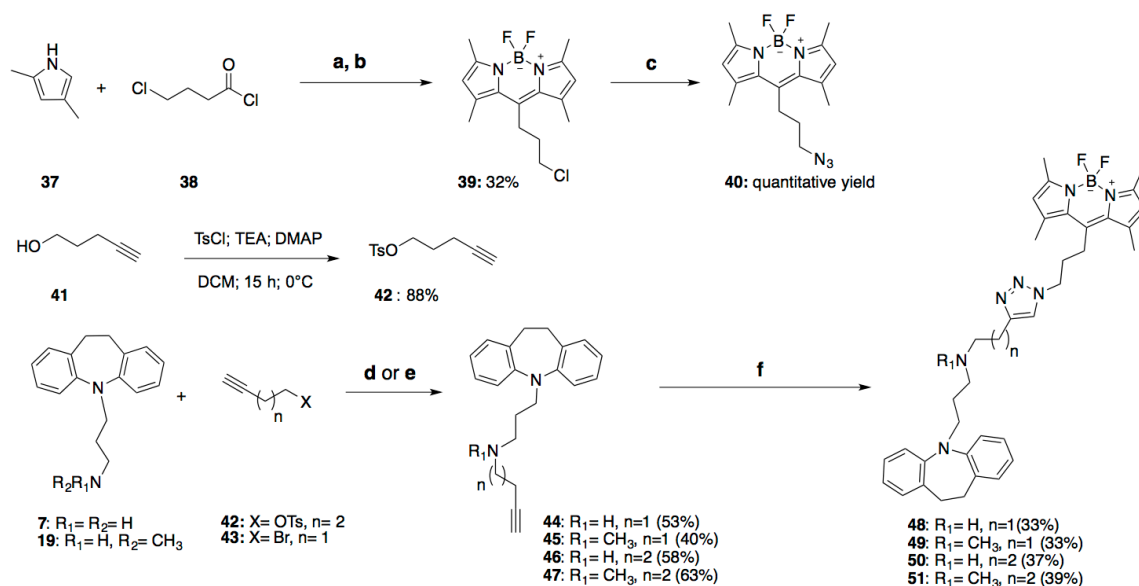
proposed by Varma.¹⁷⁹ This contemplates the use of paraformaldehyde and acidic clay montmorillonite K-10 as green catalyst, under solvent-free conditions. However, reproducing the solvent-free conditions with our derivatives did not yield any product, maybe due to the formation of a non-homogeneous the reaction mixture. This has been overcome by adding MeOH as solvent and by harnessing the capability of K-10 to act as solid acid catalyst. It determines the protonation of the carbonyl oxygen of paraformaldehyde in order to facilitate the nucleophilic attack by the primary amines **1-12** and, additionally, as supporting agent for NaBH₄, increasing its reducing ability of *in situ* generated Schiff bases. In detail, this reaction involves two steps. The first is based on the activation of paraformaldehyde with K-10 catalyst, followed by the addition of the primary amine that leads to the formation of the imine intermediate using microwave irradiation at 80°C for 30 min. Then, the addition of a mixture of K-10 catalyst and NaBH₄ and further microwave irradiation at 80°C for 10 min led to **13-24** in acceptable yield (24%-44%).

To achieve the tertiary amines **25-36**, the Eschweiler–Clarke reaction was exploited. This reductive amination involved the use of formaldehyde and formic acid, which acts as hydride donor to reduce the imine generated by reaction of primary amines with the formaldehyde.¹⁸⁰ Despite the wide synthetic utility of this reaction, it has received only limited critical investigation. An improved methodology¹⁸¹ exploited the thermal decomposition in solvent-free conditions of oxalic acid under MW irradiation into the intermediate formic acid as the actual reducing agent. However, efforts to obtain the desired compounds by using these conditions (both conventional and microwave synthesis) did not work with our derivatives. On the other hand, it is worth to note that conventional heating procedures for the same transformation required reflux for more than 10 h, affording **1-3** and **7-9** in 40%-58% yields (Table 3). On the other hand, the MW-assisted procedure developed by us revealed consistent increases in yields (ranging from 63% to 74%) and shortening of reaction time (from 10 h to 30 min). However, the choice of microwave irradiation failed in the case of phenothiazines derivatives **4-6** and **10-12**. Indeed, such compounds displayed an excessive reactivity under these microwave conditions that provided the poly-methylated (both –N and –S atoms) analogue as only reaction product. Thus, a conventional procedure was used at controlled temperature (80°C) for 8-10 h, leading to compounds **28-30** and **34-36** in satisfactory yield (45%-84%).

3.2 Synthesis of TCA-functionalized fluorescent congeners

To obtain TCA-functionalized fluorescent congeners **48-51**, we exploited a click reaction protocol (Scheme 2).

We started with the synthesis of the 10-(3-Azidopropyl)-5,5-difluoro-1,3,7,9-tetramethyl-5H-4λ⁴,5λ⁴-dipyrrrolo[1,2-c:2',1'-f][1,3,2]diazaborinine, i.e. the core of BODIPY azide **40**. Particularly, its synthesis was rapidly achieved by the condensation of 2,4-dimethylpyrrole **37** with two equivalents of acyl chloride **38** (Scheme 2). The resulting intermediate dipyrin was not isolated, as application of base and boron



Scheme 2. Reagents and conditions:

a. DCM, r.t., 30 min; **b.** TEA, $\text{BF}_3 \cdot \text{OEt}_2$, r.t., 14 h; **c.** NaN_3 , DMF, 50 °C, 36 h; **d.** NaOH, CHCl_3 : H_2O , MW, 200W, 140 °C, 10'; **e.** K_2CO_3 , DMF, 70 °C, 72 h; **f.** **40**, $\text{CuSO}_4 \cdot 5 \text{H}_2\text{O}$ (15 mol%), Na ascorbate (45 mol%), DCM: t-BuOH: H_2O , r.t., 1-2 h

trifluoride etherate yields the BODIPY chloride **39**. Next, nucleophilic substitution with NaN_3 provided the clickable azide **40**.

The introduction of the linker bearing the alkyne group on desipramine **19** and on its corresponding primary amine **7** has been performed using two different procedures. In the case of secondary amine **19**, a nucleophilic substitution with **42** or **43** has been performed. This reaction, conducted under conventional heating condition, resulted to proceed very slowly, requiring 72 h to appreciate significant amount (40%-63%) of target compounds **45** and **47**. However, the increase of the temperature, as well microwave conditions did not improve both the reaction time and the yield.

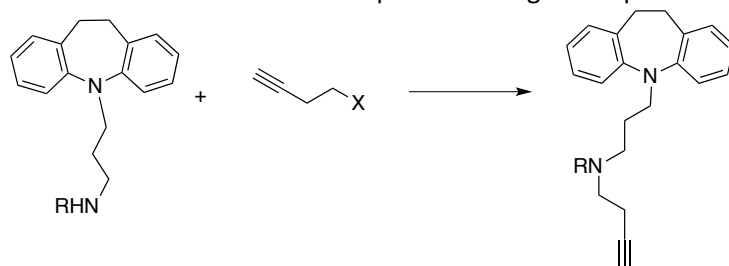
Regarding the primary amine **7**, several attempted have been accomplished to obtain the corresponding functionalized secondary amine **44** (Table 4).

First, we tried to obtain **44** starting from the corresponding trifluoroacetamide derivative of **7** (conditions A-F). Following a classic protocol (condition A), involving a weak base (K_2CO_3) to deprotonate the amide, followed by the addition of the alkynyl linker chain bearing a good leaving group (-Br), did not lead to any product and the starting material was recovered. Thus, supposing that K_2CO_3 was not sufficiently strong base to deprotonate the amide, we tried with a stronger base (NaH, condition B). However, also in this case, we did not observe any product. Then, we tested if the addition of a catalyst could be successful (conditions C-E). Although we tried three catalysts with different mechanisms, such as KI (condition C), benzyltriethylammonium chloride (TEBA, condition D) and 18-crown-6 ether (condition E), we again did not get any product. The last attempt involved the use of a different halogen derivative, bearing an iodide as leaving group (condition F). In this case, we observed only traces of the desired compound.

As a second strategy, we tried if we could obtain the desired functionalized secondary amine **44** by directly reacting the primary amine **7** with **43** (condition G). Employing a similar protocol seen for **45** and **47**, this nucleophilic substitution afforded only traces of **44**. Finally, as reported in Scheme 2, we successfully achieved

44 and **46**, by exploiting a procedure involving a biphasic solvent system (CHCl₃/H₂O 3:7) and microwave irradiation at high temperature and potency (140 °C and 200 W, respectively), which led to the titles compounds in satisfying yield (53%-58%). This procedure allows to “activate” the nucleophile by forming organic micelles in water that favors the nucleophilic attack towards poor reactive electrophiles, like **42** and **43**.

Table 4. Reaction conditions explored to target compound **44**.



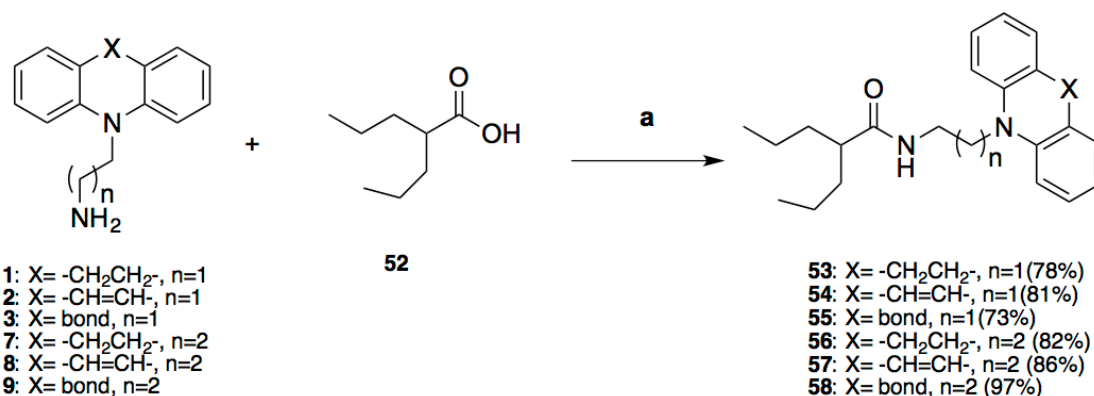
Condi tions	R	X	Base	Catalyst	Solve nt	Reaction conditions	Results
A	-COCF ₃	-Br	K ₂ CO ₃	-	DMF	MW 110°C, 1 h*	No reaction
B	-COCF ₃	-Br	NaH	-	DMF	MW 110°C, 1 h*	No reaction
C	-COCF ₃	-Br	K ₂ CO ₃	KI	DMF	MW 110°C, 1 h*	No reaction
D	-COCF ₃	-Br	K ₂ CO ₃	TEBA	CH ₃ C N	MW 80°C, 1 h*	No reaction
E	-COCF ₃	-Br	K ₂ CO ₃	18- crown-6	THF	MW 70°C, 1 h*	No reaction
F	-COCF ₃	-I	K ₂ CO ₃	-	DMF	MW 70°C, 1 h	Traces of desired compound
G	-H	-Br	NEt ₃	-	DMF	110°C, 72 h	Traces of desired compound

*then conventional heating at 80°C for 12 h

Next, copper(I)-catalyzed [3+2] cycloaddition between the terminal azide **40** and the alkynes **44-47** afforded the TCAs-related fluorescent probes **48-51** only in acceptable yield (33%-39%) due to the formation of several side-products. Efforts to minimize the excessive reactivity under these reaction conditions, by shortening the reaction time, by using an ice bath and by producing an inert nitrogen atmosphere, unfortunately failed to improve the reaction yield.

3.3 Synthesis of TCAs-functionalized multi-target congeners

As depicted in Scheme 3, to obtain TCAs-functionalized multi-target congeners **53-58**, we have exploited an amide coupling reaction. It involves the primary amines **1-3** and **7-9**, and the carboxylic function of valproic acid **52**, which were coupled using EDCI and HOBT, and NEt_3 (as base). This procedure provided the compounds **23-28** in very good yield (73%-97%), without need to further improve the reaction conditions.

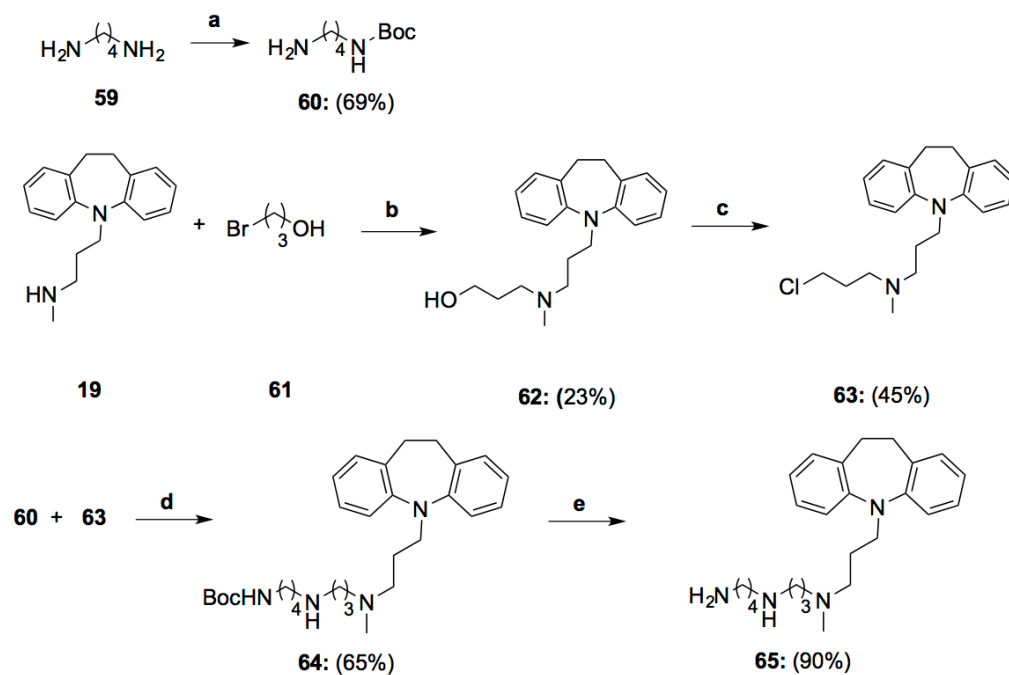


Scheme 3. Reagents and conditions:

a. EDCI, OHBT, NEt_3 , DCM, rt, overnight.

3.4 Synthesis of TCAs-functionalized polyamine congener

The synthesis of TCAs-functionalized polyamine congener has been accomplished as showed in Scheme 4. Particularly, before incorporating the polyamine backbone into the structure of desipramine **19**, it has been functionalized with 3-bromopropan-1-ol **61** through the nucleophilic substitution in the biphasic system ($\text{CHCl}_3/\text{H}_2\text{O}$ 3:7) previously developed (140 °C and 200 W, respectively). Then, the conversion of the hydroxyl group of **62** to a good leaving group was first attempted by introducing a tosyl functionality. However, this procedure failed, even employing pyridine as solvent. Thus, we decided to convert the hydroxyl group of **62** by using thionyl chloride, which afforded **63**, bearing a chloride as leaving group. This was essential to the next substitution reaction, which involved the mono-Boc-protected putrescine **60** and **63**. To achieve **64**, we developed a MW-assisted procedure that led after 1 h at 110 °C the title compound in good yield (65%). The following deprotection of the Boc-protected amino function of **64** was performed under classical conditions (10 equivalents of TFA in DCM), leading to the TCAs-functionalized polyamine congener **65** as trifluoroacetate salt, in quantitative yield.



Scheme 4. Reagents and conditions:

a. Boc_2O , CHCl_3 , $0\text{ }^\circ\text{C}$, 3 h; **b.** NaOH , CHCl_3 : H_2O , MW, 200W , $140\text{ }^\circ\text{C}$, 10'; **c.** SOCl_2 , CHCl_3 , rt, 4h; **d.** CH_3CN , MW, 50W , $110\text{ }^\circ\text{C}$, 1h; **e.** TFA, DCM, 3 h.

4. Results and discussion

In this part of thesis, we advocated a chemical biology approach to develop new chemical probes for NSCs. In particular, we followed two parallel strategies, i.e. a knowledge-based phenotypic approach and a functionalized congener strategy. In both approaches, we obtained interesting, albeit preliminary, results, which will be discussed in the following.

4.1 A knowledge-based phenotypic approach for NSC *stemistry* application

Despite recent medicinal chemistry strategy relies on target-based approach, we already pointed out that the knowledge in NSCs field is still incomplete and, according to the recent literature, validated targets/pathways are far from being identified.¹⁸² Thus, for the reasons highlighted in Chapter 2, we decided to follow a phenotypic approach. However, phenotypic approaches in big pharma mostly rely on huge collection of compounds (in some cases >400.000),¹⁸³ exploiting facilities not available in academic environment. In our case, the project should be tailored to academic settings where cost-effectiveness is a major consideration. Our attention was therefore drawn to a strategy that can yield molecules with high hit rates and a concomitant reduced library size.¹⁶⁹ We reasoned that starting from compounds biologically pre-validated and with established physicochemical properties to design a focused-chemical libraries may be particularly suitable in an academic environment.¹⁶⁹

In this respect, we envisioned to follow a knowledge-based approach. On this basis, we looked for chemotypes already reported to modulate NSCs and, at the same time, amenable for further chemical development. Herein, we discuss the design rationale underlying the focused chemical library.

4.1.1 Design rationale of the focused chemical library inspired by TCAs and P7C3

It is an intriguingly postulated that existing drugs might exert their effects by promoting neurogenesis. Specifically, the relationships between neurogenesis and the effect of antidepressants have been widely recognized since 1999.¹⁸⁴ Duman et al showed that the atrophy and death of stress-vulnerable neurons in the hippocampus, as well as decreased neurogenesis of hippocampal neurons are reversed following antidepressant treatment in animal models of depression.¹⁸⁴ Later studies, in 2009, confirmed these results showing that subjects with major depressive disorder (MDD) treated with antidepressants (imipramine and fluoxetine), displayed an increase of both neural progenitor and dividing cells in the DG.¹⁸⁵ Importantly, antidepressants from different classes have all been shown to induce neurogenesis *in vivo*, including the non-selective monoamine reuptake inhibitors (NSRI) imipramine¹⁸⁵ and amitriptyline¹⁸⁶ (belonging to the class of tricyclic antidepressants, TCAs); the selective serotonin reuptake inhibitors (SSRI) fluoxetine¹⁶⁸ and citalopram;¹⁸⁷ and the mood-stabilizers lithium,¹⁸⁸ carbamazepine¹⁸⁹ and valproic acid (Figure 12).¹³⁷ Starting from the 2000s, the

mechanisms underlying the neurogenic effect of antidepressants have attracted the interest of several researchers, and advances that have been made in the field have been exhaustively reviewed in ¹⁰².

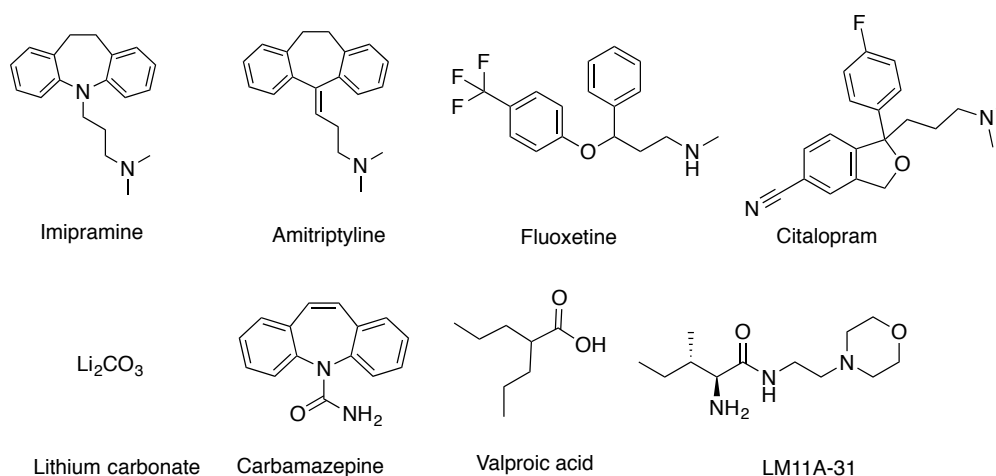


Figure 12. Antidepressant drugs with neuroregenerative/neuroprotective effects.

However, it should be noted that the association between neurogenesis and antidepressant action remains still controversial. Several mechanistic hypotheses have been advanced supporting the neurogenic effects of antidepressants. These proposed mechanisms include those directly mediated by NSCs and the astrocytes/oligodendrocytes-mechanisms that indirectly affect their fate. For example, Santarelli et al. in 2003 published a groundbreaking paper showing that fluoxetine and imipramine exert neurogenic effects by acting at ventral hippocampus and require 5HT_{1A} receptor for their effect.¹⁶⁸

It has been advanced that blocking the inhibitory control of GSK-3 β on Wnt pathways potentiates neurogenesis. Accordingly, a recent study reported on the enhanced neurogenesis promoted by chronic exposure of valproic acid (VPA) in the DG of the hippocampus. Particularly, similar to neurotrophic factors, VPA enhanced ERK pathway-dependent cortical neuronal growth. Although VPA affects the functions of GSK-3 β and HDAC, its effects on the ERK pathway were not fully mimicked by selective inhibitors of GSK-3 β or HDAC. Together, these data demonstrate that VPA activates the ERK pathway and induces ERK pathway-mediated neurotrophic actions.¹³⁷

In accordance with what suggested by the previous study, it has been proposed that the neurogenic effect of antidepressants is mediated by neurotrophic activities. Intriguingly, impaired progenitor proliferation and neurogenesis were observed in transgenic mice lacking TrkB in hippocampal NPCs, even when exposed to chronic antidepressants (fluoxetine and imipramine) treatment.¹⁹⁰ Conversely, mice lacking TrkB only in differentiated DG neurons display typical neurogenesis and respond normally to chronic antidepressants. The authors suggest that chronic exposure to antidepressants increase BDNF level implicating the subsequent TrkB activation as an indirect downstream event from the acute accumulation of monoamine, such as serotonin and noradrenaline.¹⁹⁰ Interestingly, in another study, the TCA amitriptyline was shown to bind the extracellular domains of TrkA and TrkB and induce TrkA/TrkB heterodimerization, which does not occur with imipramine.¹⁸⁶ Such ability of tricyclic

antidepressants to bind Trk receptors and, in the case of amitriptyline to induce heterodimerization, is encouraging for the development of small molecule ligands targeting these receptors for the treatment of neurodegenerative disorders.¹⁹¹ Indeed, this approach proposed by Longo led to the development of the first small molecule, referred to as LM11A-31 (Figure 12), targeting the p75 neurotrophin receptor that is just now in phase II clinical trials for patients with Alzheimer's disease (AD).¹⁹²

Regarding the indirect mechanisms controlling the neurogenic effect of antidepressant, it has recently proposed that amitriptyline significantly increased the expression of fibroblast growth factor-2, brain-derived neurotrophic factor, vascular endothelial growth factor and glial cell line-derived neurotrophic factor mRNA with a different time course in astrocyte cultures, but not in neuron-enriched cultures.¹⁹³

Another intriguing indirect mechanism has been proposed, which involves the effect of antidepressant on microglia with both pro- and anti-inflammatory properties.¹⁹⁴

Particularly, one group recently demonstrated that fluoxetine at 10 μ M inhibited microglial tumour necrosis factor- α (TNF- α) and nitric oxide (NO) production in LPS treated-microglial cells. They also found that exposure over 24 h at concentrations < 5 μ M actually created a pro-inflammatory environment.¹⁹⁵ Interestingly, another study showed that fluoxetine can significantly inhibit the synaptotoxicity, as well as reduced dendritic complexity and axonal branching of hippocampal neurons induced by astrocytes from APP/PS1 mice. These astrocytes produced high levels of soluble β -amyloid (A β), which could be significantly inhibited by fluoxetine via activation of serotonin 5-HT₂ receptors. Indeed, fluoxetine inhibited activation of astrocytes, decreased A β level, ameliorated neurotoxicity, and improved behavioral performance. These findings may provide a basis for the clinical application of fluoxetine in AD patients, and may also lay the foundation for novel astrocyte-based therapies of AD.¹⁹⁶

On the basis of all the reports showing that antidepressants increase neurogenesis and exert neuroprotective/neurotrophic effects, it has been suggested that they may be effective in the treatment of AD.¹⁹⁷ Since antidepressants are already in the market, the costs of new drug development for AD will be dramatically reduced if they can be used as prevention or treatment tools. Some preclinical and clinical studies have shown that antidepressants treatment improved the cognitive skills and clinical symptoms of AD pathology. Interestingly, a recent article showed that antidepressants, such as amitriptyline, can completely reverse the symptoms of AD in a triple-transgenic mouse model of AD (3xTg AD).¹⁹⁸ Not only treating AD mice with amitriptyline significantly reversed AD pathology by reducing reduction toxic A β amyloid aggregates, but also improved their cognitive skills in behavioral tests. Remarkably, amitriptyline treatment was able of forming new neurons in the hippocampus and cortical regions as shown by a variety biochemical assays.¹⁹⁸

This has further been confirmed by another study using SSRI citalopram.¹⁸⁷ Rather than increasing neurogenesis, citalopram is suggested to function to reduce A β accumulation in mice and human.¹⁸⁷ Indeed, citalopram reduced brain interstitial fluid A β levels in a mouse model of AD. Infusion of serotonin into the hippocampus also reduced A β levels and this effect was blocked by administration of ERK inhibitors, suggesting an important role of ERK in A β metabolism.¹⁸⁷ To validate the effects of antidepressants on AD treatment in human, the same research group

performed a retrospective comparison analysis and identified that healthy individuals who were treated with antidepressants showed significantly reduced levels of A β than those who took no antidepressants.¹⁹⁹ Therefore, there is indication that antidepressants can be used to prevent or limit plaque accumulation to reduce the risk of developing AD.

In addition, another recently discovered small molecule, P7C3 (widely discussed in Par. 1.7.1), attracted our attention for its outstanding proneurogenic and neuroprotective profile in various neurodegenerative conditions.¹⁴⁷ Moreover, looking at its structure (aminopropylcarbazole) and comparing it with that of TCAs (shown in Figure 13), we realized that these molecules, not only possess the same effect on neurogenesis, but also contain common structural features. Indeed, both the compounds share similar chemical motifs: a tricyclic moiety connected to an amino functionality through an alkyl linker. Thus, both TCAs and P7C3 may be considered as validated starting points for the design of focused libraries with neuroregenerative potential.

The idea of designing such focused library either starting from FDA-approved drugs or those (i.e. P7C3) for which the drug-like properties have been already established, aims to increasing the library's hit rate.^{169, 200} Furthermore, our scaffold selection is reinforced by the fact that these structures are highly recurrent in CNS-directed drugs and can be considered "privileged" for the synthesis of CNS-focused libraries.

To this end, recent screening of 140 FDA-approved CNS drugs suggested the effectiveness of the tricyclic group of antidepressants against three major AD targets: acetylcholinesterase (AChE), β -secretase (BACE-1), and A β aggregation, with one member, protriptyline, showing highest inhibitory activity.¹⁷¹ This finding prompted us to consider the tricyclic scaffold as prototypical structure for constructing our focused-chemical library that, in principle, should have good physicochemical properties to act at the CNS level. Furthermore, given the additional activities displayed as disease-modifying agents against AD, we strongly believed that TCAs can be considered optimal starting point for library generation.

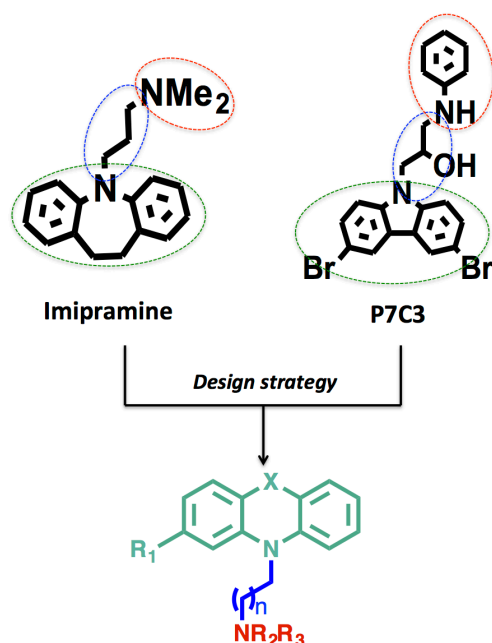
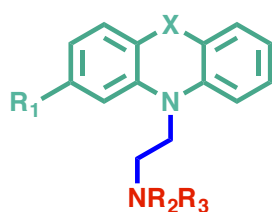


Figure 13. Design of the focused-chemical library inspired by TCAs and P7C3.

Once the general scaffold has been selected, (Figure 13), to explore structure-activity relationships (SAR) a focused-chemical library of 36 entries has been created: (1) by varying the tricyclic core, (2) by changing the number of the linker's methylene units, (3) by replacing the amino group with a primary, secondary, or tertiary amine.

As illustrated in Table 5, we selected different tricyclic scaffolds carrying 6,5,6 or 6,6,6 or 6,7,6 structures. They include the 6,5,6 carbazole moiety, which not only is present in the structure of P7C3, but its utility against AD has been widely demonstrated.²⁰¹ The choice of the 10,11-dihydro-dibenzazepine and dibenzazepine as 6,7,6 structures has been motivated by the fact these two moieties belong to the widely used antidepressants imipramine and mood stabilizer carbamazepine, respectively. Lastly, we also included differently substituted 6,6,6 phenothiazines (phenothiazine, 2-(trifluoromethyl)phenothiazine and 2-chlorophenothiazine respectively). Despite phenothiazines are not classified as antidepressants, but as antipsychotics, a recent patent claimed that phenothiazine-based compounds promote regeneration and survival of neurons, and could be useful to treat neurodegenerative diseases.²⁰² Interestingly, phenothiazine derivatives have been showed to inhibit butyrylcholinesterase, a co-regulator of cholinergic neurotransmission, whose activity is increased in AD.²⁰³

Table 5. Chemical structure of compounds 1-36 of the focused chemical library.



Compound number	X	R ₁	R ₂	R ₃	n
1	CH ₂ CH ₂	H	H	H	1
2	CH=CH	H	H	H	1
3	bond	H	H	H	1
4	S	H	H	H	1
5	S	Cl	H	H	1
6	S	CF ₃	H	H	1
7	CH ₂ CH ₂	H	H	H	2
8	CH=CH	H	H	H	2
9	bond	H	H	H	2
10	S	H	H	H	2
11	S	Cl	H	H	2
12	S	CF ₃	H	H	2
13	CH ₂ CH ₂	H	CH ₃	H	1
14	CH=CH	H	CH ₃	H	1

15	bond	H	CH ₃	H	1
16	S	H	CH ₃	H	1
17	S	Cl	CH ₃	H	1
18	S	CF ₃	CH ₃	H	1
19	CH ₂ CH ₂	H	CH ₃	H	2
20	CH=CH	H	CH ₃	H	2
21	bond	H	CH ₃	H	2
22	S	H	CH ₃	H	2
23	S	Cl	CH ₃	H	2
24	S	CF ₃	CH ₃	H	2
25	CH ₂ CH ₂	H	CH ₃	CH ₃	1
26	CH=CH	H	CH ₃	CH ₃	1
27	bond	H	CH ₃	CH ₃	1
28	S	H	CH ₃	CH ₃	1
29	S	Cl	CH ₃	CH ₃	1
30	S	CF ₃	CH ₃	CH ₃	1
31	CH ₂ CH ₂	H	CH ₃	CH ₃	2
32	CH=CH	H	CH ₃	CH ₃	2
33	bond	H	CH ₃	CH ₃	2
34	S	H	CH ₃	CH ₃	2
35	S	Cl	CH ₃	CH ₃	2
36	S	CF ₃	CH ₃	CH ₃	2

With the aim to explore the impact of linker length, we also generated two different alkyl linkers constituted by two and three methylenes, respectively. Thus, two sub-sets of functionalized tricycles, carrying 2- or 3-methylenes chains, have been developed. Furthermore, to assess the influence of amine substitution, each sub-set is composed by primary, secondary and tertiary amines, leading to **1-12**, **13-24** and **25-36**, respectively.

As already showed in Chapter 3, the developed synthetic strategy allowed to obtain compounds **1-36** (Table 5).

The obtained focused chemical library has been submitted to the screening assay, which will be described in the following.

4.1.2 Towards the phenotypic approach for NSCs

Small molecules screening using NSCs is an important research area whose objective it is to identify molecules either capable of maintaining self-renewal of NSCs, or of driving their differentiation toward specific fates. This emerging approach is also propelled by the lack of understanding of NSCs biology.²⁵ In this respect, high-content screening (HCS) is particularly well suited for NSCs-based phenotypic

approaches.²⁵ When a defined molecular target is unavailable, the simultaneous analysis of morphology and biomarker expressions in such highly heterogeneous cultures as NSCs after compounds treatment, may allow to identify hits.

Generally, in the identification of early hits, the major goal relies on the identification of potent compounds underlying the desired phenotype (i.e. NSCs proliferation/differentiation). However, hit selection based on potency often leads to molecules from which it proves very difficult to eliminate toxicity or other unfavorable properties, such as lack of cell membrane permeability and chemical reactivity.²⁰⁴ In fact, many good drugs are not very potent against their targets, but rather show very low toxicity and good pharmacokinetic properties. For example, the benzodiazepine clonazepam displays an IC_{50} of 23 μ M against its target, GABA_A receptor,²⁰⁵ which would most likely not be considered a hit in compounds screening. Nonetheless, this drug is very effective and is on the market since many years. Such discrepancy between selecting the most potent molecule that induces the desired phenotype and the actual clinical endpoint, suggests considering other parameters over the selection of more effective compounds when choosing the hits from library screening. Accordingly, the development of in vitro screens to facilitate prioritization of compounds for further testing was recently cited as a critical need for toxicity testing by the National Research Council's.²⁰⁶ In this respect, before assessing the activity of small molecules in phenotypic screening program, the determination of cytotoxicity leads to a significant improvement in the effectiveness of hit compounds in a timely and cost-effective manner. Indeed, although the HCS allows to analyze cells with a simultaneous readout of multiple phenotypic parameters,²⁰⁷ several factors limit the extensive use of cellular imaging in primary screening, such as the high cost of reagents, complex assay development and data-management issues.²⁰⁸ This is of especially importance in an academic environment where, due to the limited resources, only a limited number of hit structures can be monitored.²⁰⁴

On these bases, before embarking in full-scale NSCs-based screening of the focused chemical library, we envisioned to preliminary evaluate cytotoxicity of the compounds as a primary screening.

In particular, to potentially highlight hits from the focused chemical library with optimized physicochemical properties, a screening pipeline has been defined (see Figure XX), whose main goals are: (i) to make a preliminary screening of molecules for neuronal and hepatic viabilities; (ii) to evaluate neuroprotection (low-serum assay) in rat primary neurons; (iii) to assess the most promising compounds for their neurogenic activity (proliferation, BrdU assay) in rat primary neurons; (iv) to evaluate the differentiation of the best phenotypic compounds in a NSCs-based assays by using HCS.

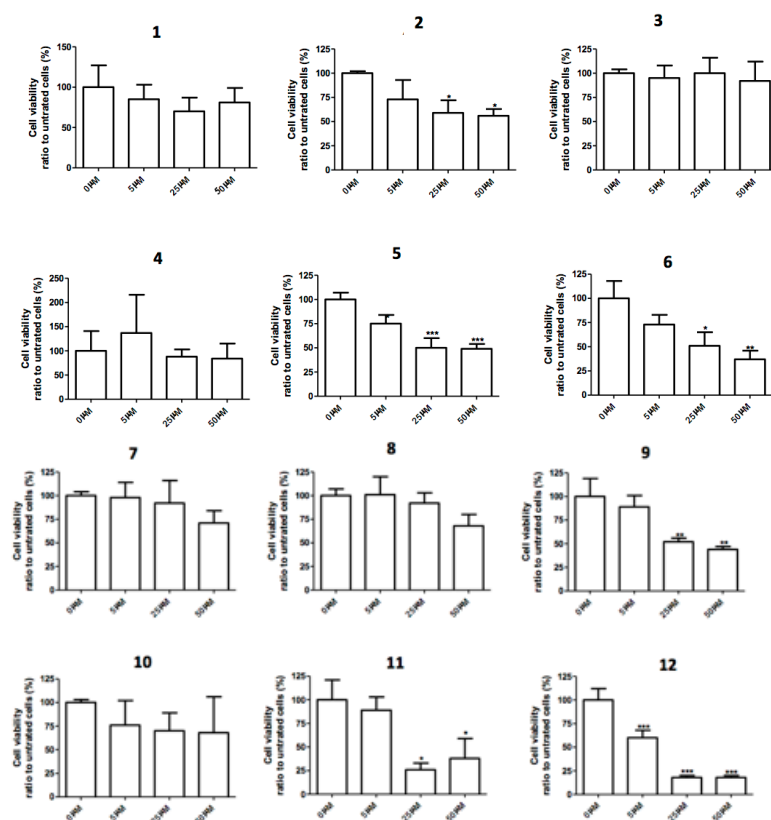
While the objectives (ii) and (iii) are still ongoing, in the following paragraphs we will focus on discussing the screening of the focused chemical library for assessing neuronal and hepatic viabilities (i) and the set-up of NSCs-based phenotypic screening (iv).

4.1.2.1 Screening of molecules for neuronal and hepatic viabilities

With the aim to identify small molecules with an optimal drug-like profile, we decided in collaboration with the laboratory of Prof. Monti (University of Bologna) to first filter out the potential cytotoxic compounds by evaluating cell viability in different cell lines.

As first screening, we tested compounds on primary rat cerebellar granule neuron (CGNs), in order to proceed only with those molecules that do not show signs of neurotoxicity. Since cerebellum is also engaged in cognition and learning and affects AD patients' bodily control, CGNs have been used as model for studying neuronal death and apoptosis in AD.²⁰⁹ To examine cell toxicity, CGNs primary neurons were exposed to compounds **1-36** for 24 h at concentrations ranging from 0 to 50 μ M, and cell viability was measured by MTT assay (Figure 14). As expected, being these compounds inspired by FDA-approved drugs, only at the higher concentrations (25-50 μ M), the compounds started to show signs of toxicity, whereas at concentrations below to 25 μ M, only some phenothiazines, including **5-6** and **12**, reduced cell viability.

Intriguingly, It should be noted that CGNs primary neurons treated with **7-8, 15-16, 19-20, 29** and **33** at the range of concentrations tested showed a slight increment in cell viability compared to untreated cells, potentially suggesting a proliferative effect.



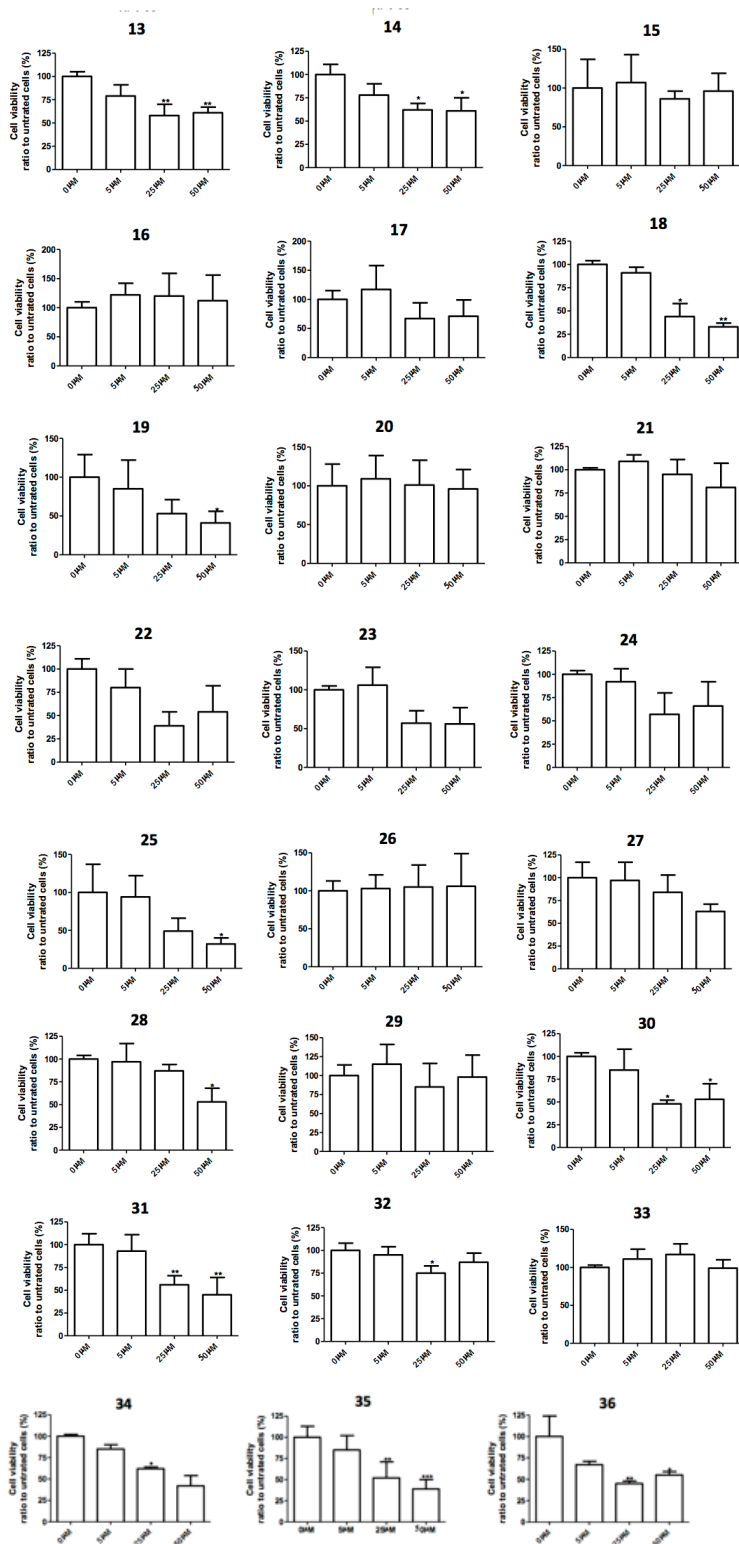


Figure 14. Toxicity of 1–36 to differentiated CGNs after 24 h treatment. Results are expressed as percentage of controls and are the mean \pm SE of four different experiments run at least in quadruplicate.

In addition to neurotoxicity, the assessment of hepatotoxicity would be of critical importance for the drug-likeness of library compounds. Indeed, although data on

antidepressant-induced liver injury are scarce, antidepressants can induce hepatotoxicity in elderly patients.²¹⁰

To this end, preliminary experiments were performed in a human hepatoma cell line (HepG2) using those compounds that show no sign of neurotoxicity from the previous screening (Figure 15). Compounds **3-4**, **7-8**, **10**, **15-21**, **23-24**, **26**, **29-31**, and **33-34** were incubated at 0–50 μ M for 24 h. A decrease in the cell viability was observed for compound **3-4**, **7**, **15**, **17-18**, **23-24**, **26** and **34** whereas no dramatic variation was found for **8**, **10**, **16**, **19-21**, **29**, **31** and **33**, even at high concentrations (25–50 μ M).

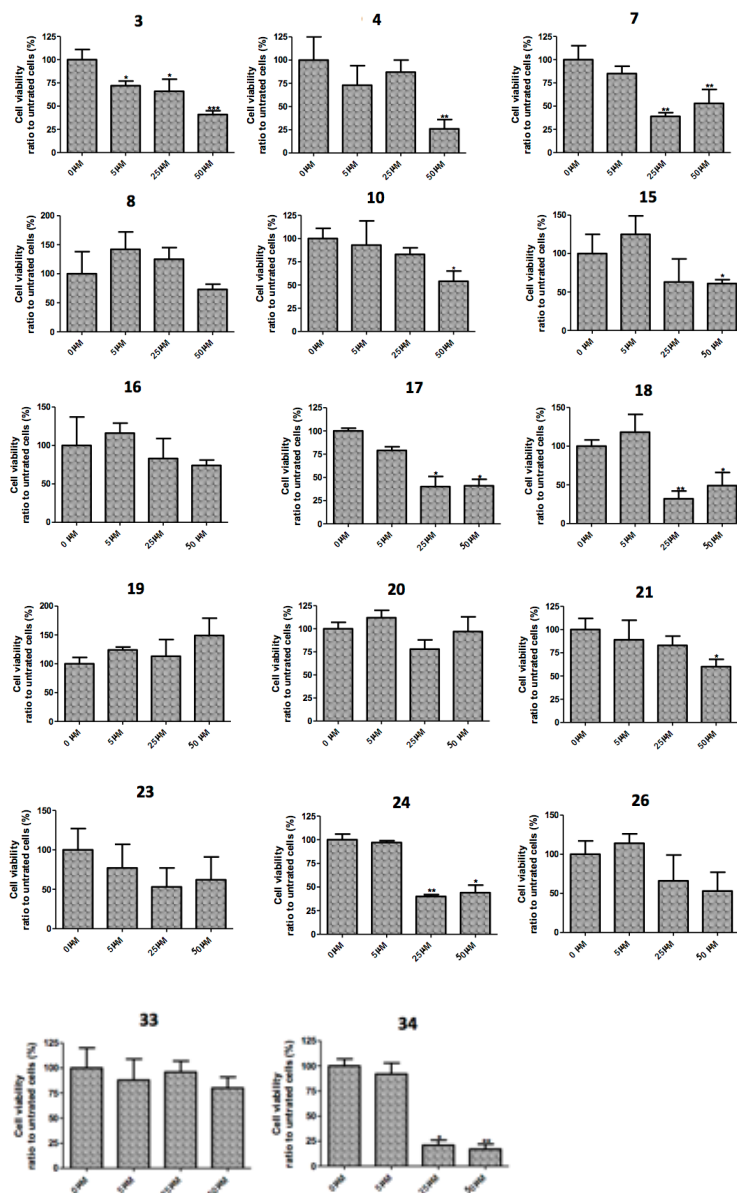


Figure 15. Toxicity of **3-4**, **7-8**, **10**, **15-21**, **23-24**, **26**, **29-31**, and **33-34** to HepG2 cells after 24 h treatment. Results are expressed as percentage of controls and are the mean \pm SE of three different experiments run at least in quadruplicate.

Considering both in vitro neurotoxicity and hepatotoxicity assays as a primary screenings of the series, we have selected **16**, **19-21**, **29** and **33**, which are the less

neurotoxic and hepatotoxic derivatives, to investigate in the further neuroprotection assay.

Particularly, a low-serum assay is being performed in CGNs. Since this test induces substantial oxidative stress leading to partial ATP depletion, K^+ loss, and the apoptotic cascade in neurons, it represents a useful model of neuronal cell death, as well as neuronal senescence.²¹¹ Thus, screening such compounds in this in vitro model may highlight potential neuroprotective molecules that will be progressed to the BrdU-based proliferation assay and then, to the NSCs-based assay.

4.1.2.2 Set-up of NSCs-based phenotypic screening for neurodegenerative diseases

In parallel, we started the set up of the NSCs (neural stem/precursor cells)-based phenotypic screening, in collaboration with the CIRI-SDV laboratory of Prof. Laura Calzà (University of Bologna). Despite the high potential, this step is particularly challenging especially for NSCs, because often cellular phenotypes differentiation caused by small molecules result in a continuum of responses, and a clear definition of a relatively narrow phenotype, is difficult to reach.²¹² Indeed, factors such as cellular heterogeneity of cells culture (e.g. neurospheres), the inability to easily expand or freeze down such cells, and the complex generation protocols introduce prohibitive constraints.²¹³ Additionally, the culture might be in a state of chronic stress owing to the in vitro environment — for example, as a result of higher oxygen tension and passaging. Furthermore, differentiated NSCs might be developmentally immature and might not represent the true physiological situation.²¹³ Accordingly, as in vitro model, the functional connectivity between the neurogenic niches within the brain is lost in NSCs, precluding detailed analysis of the phenotype within a neural network.²¹³ As a consequence, despite the potential of NSCs, most physiologically relevant cellular assays exploit oxidative stressors (such as 1-methyl-4-phenylpyridinium (MPP⁺)) or proteins overexpression (such β -amyloid for AD and γ -synuclein for PD) to mimic disease.²¹⁴

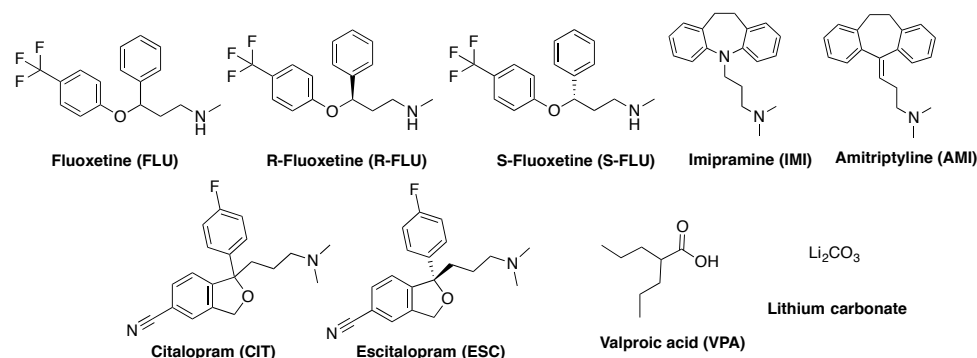
Among the available NSCs systems, the neurosphere cultures, which are identified as floating multicellular clusters that proliferate in the presence of growth factors, have been demonstrated valuable in compounds screening.¹⁴³ However, some of the characteristics of the neurospheres make them not the elective method. In fact, their composition is highly heterogeneous, being the growing cell population characterized by progenitor cells, glioblasts, neuroblasts and differentiated progeny.¹⁹³ In this respect, an alternative source of NSCs for drug screening studies is represented by NSCs derived from mouse SVZ.²¹⁵ Indeed, these NSCs can be efficiently cultured as both neurosphere and adherent monolayer, and, when grown as monolayers, these cells better recapitulate neurogenesis in vitro than neurospheres culture.²¹⁵ Because of the neurospheres's ability to expand both stem and non-stem cell populations, NSCs derived from SVZ preserved all the in vivo features of NSCs, being able to proliferate giving rise to other neural stem cells or/and to differentiate into different lineages (neurons, astrocytes and oligodendrocytes). Thus, the availability of a relevant NSCs culture system, together with the ability to maintain multipotency without producing non-stem cells population, make this germinal zone particularly suitable for compounds

screening.²¹⁶ Moreover, the wide use of mouse NSCs derived from SVZ in high-throughput screening programs prompted us to consider NSCs from mouse SVZ as a well-characterized in vitro model to perform our phenotypic screening.^{192, 217}

Once the cell source has been selected and before embarking in full-scale screening of the chemical library, another critical step relies on validating the phenotypic assay. To this end, screening programs suggest that a small set of compounds with known activities should be screened first. Screens of these compounds can indeed validate the strategy by identifying positive control compounds with the desired phenotypes.²¹²

In our case, as positive control compounds, we have focused on those for which the desired phenotypic effects have been already demonstrated both in vivo and in vitro (Figure 16a).^{80, 185, 218} They included antidepressant drugs with different mechanisms of action: the non-selective monoamine reuptake inhibitors (NSRI) imipramine¹⁸⁵ and amitriptyline;¹⁸⁶ the selective serotonin reuptake inhibitors (SSRI) fluoxetine¹⁶⁸ and citalopram;¹⁸⁷ and the mood-stabilizers lithium¹⁸⁸ and valproic acid.¹³⁷ The molecular mechanisms underlying NSCs modulation of these drugs are still unclear. In addition, a direct comparison among them in a single cellular system has not been made yet. To assess whether the observed NSC-effects may be ascribed to the antidepressant molecular mechanism of action (e.g. inhibition of monoamine transporters), we also added the enantiomers of citalopram and fluoxetine. In detail, we chose the S-enantiomer of citalopram (escitalopram), which has been recognized as the most selective marketed serotonin transporter (SERT) inhibitor.²¹⁹ In addition, we included both the R- and S- enantiomers of fluoxetine, which display similar potency at human SERT, whereas the resulting nor-metabolites display in vivo different profiles, being R-norfluoxetine basically inactive.²¹⁹

a.



b.

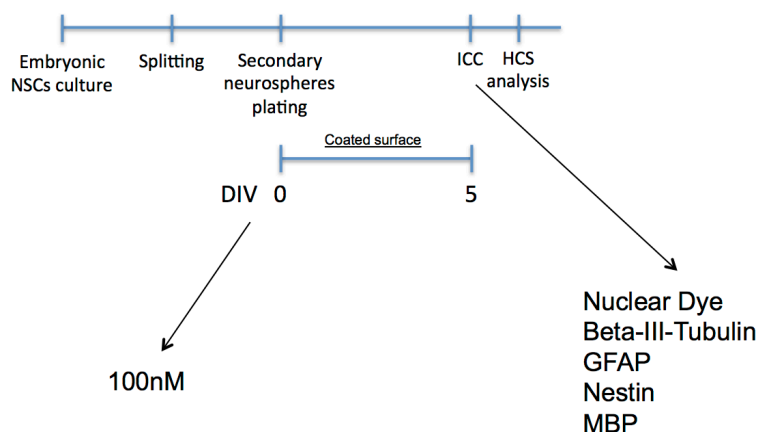


Figure 16. Antidepressants compounds tested on NSCs assay (a) and NSCs-based assay design (b).

Then, we set up our screening assay based on NSCs derived from the forebrain of mouse embryos at 14-15 days (Figure 16b). In detail, the NSCs have been treated for 5 days in vitro (5 DIV) with 100 nM of the selected antidepressant and mood stabilizer compounds (depicted in Figure 16a).

Specifically, using a high-content screening apparatus, we first evaluated the proliferative status of NSCs by counting the number of cells *versus* the apoptotic ones using the nuclear dye DAPI (2-(4-amidinophenyl)-1H-indole-6-carboxamide). As illustrated in Figure 17, all the compounds showed a profile very similar to the control, suggesting that proliferation doesn't take place under these conditions. Only for valproic acid, as the number of cells decreased, a concomitant slight increase of apoptosis has been observed.

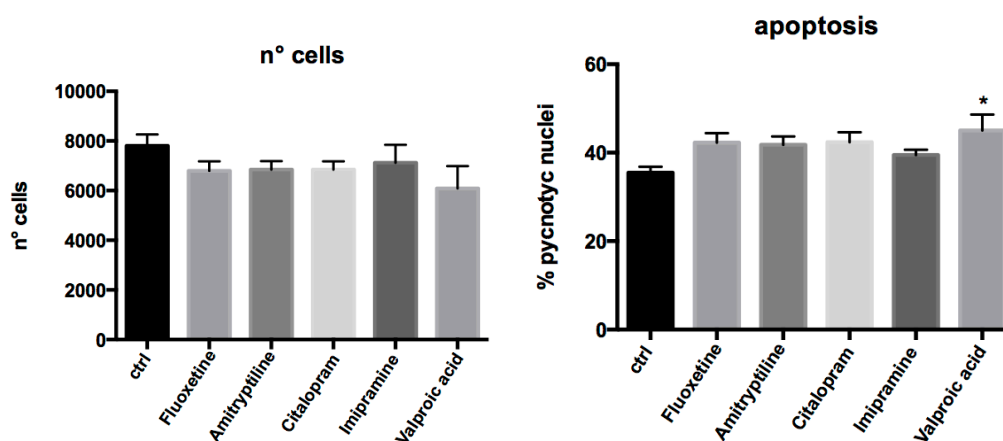


Figure 17. Evaluation of the total number of NSCs (left panel) versus the apoptotic ones (right panel).

Additionally, we evaluated the differentiation of NSCs, by assessing the percentage of neurons, astrocytes and mature oligodendrocytes (using β -III-tubulin, GFAP, and MBP markers, respectively). Analysis of the data reported in Figure 18 showed no significant increase of the β -III-tubulin positive cells after treating with 100 nM of all the tested compounds. Interestingly, SSRI S-fluoxetine displayed an increase of astrocyte differentiation (Figure 19 right panel). This is in line with previous findings, showing that fluoxetine treatment enhanced the expression of glial marker genes following neural differentiation in cultured embryonic stem cells.²²⁰ By contrast, an

in vivo study showed that fluoxetine treatment counteracted the stress-induced numerical decrease of astrocytes, but had no effect on the astrocyte cell number in control animals.²²¹ Thus, astroglial structural plasticity in response to stress and

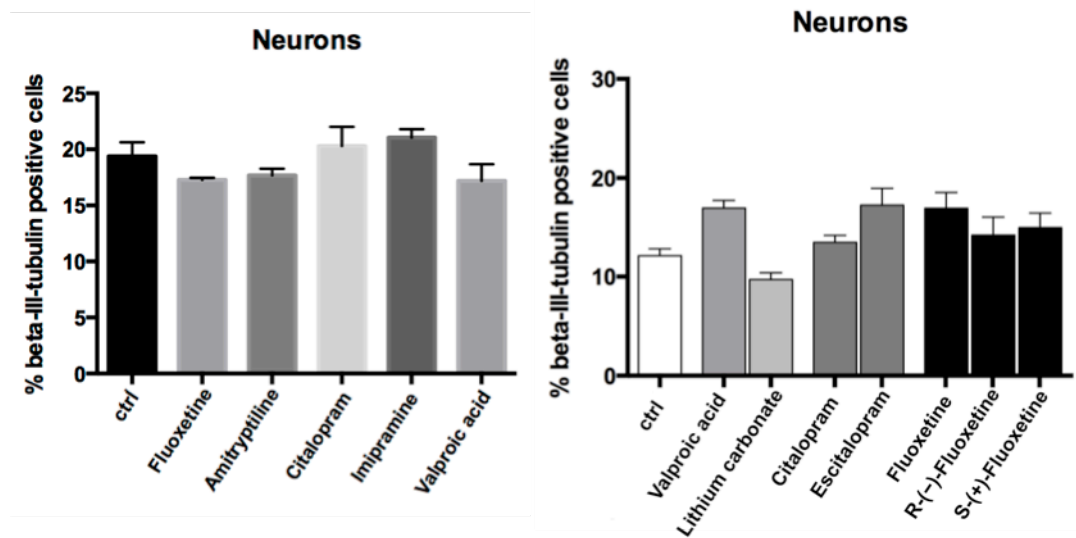


Figure 18. Differentiation of NSCs towards the neural lineage.

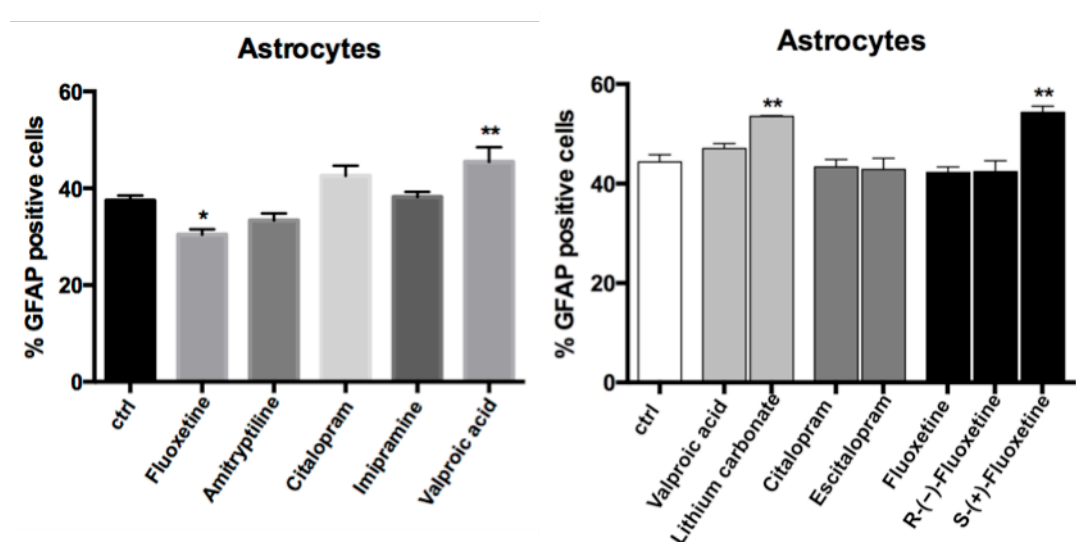


Figure 19. Differentiation of NSCs towards the astrocyte lineage.

antidepressant treatment support the hypothesis that glial changes may contribute to the cellular actions of antidepressants. Remarkably, in our model, the observed effect of S-fluoxetine on astrocyte resulted slightly different to that obtained for the racemic mixture or its R-enantiomer, suggesting a putative enantioselective mechanism of action (Figure 19, right panel).

Regarding oligodendrocyte differentiation, it's worth to note the effect shown by fluoxetine racemic mixture (Figure 20, left panel). This is consistent with a recent study showing that adult mice treated with 10 mg/kg of racemic fluoxetine reduced cell death of oligodendrocytes at 5 days after spinal cord injury (SCI).²²² Indeed, the observed effect appeared to be greater than the sum of effects displayed by the two enantiomers singularly. This might point out to a mechanism of action independent from the SERT inhibition.

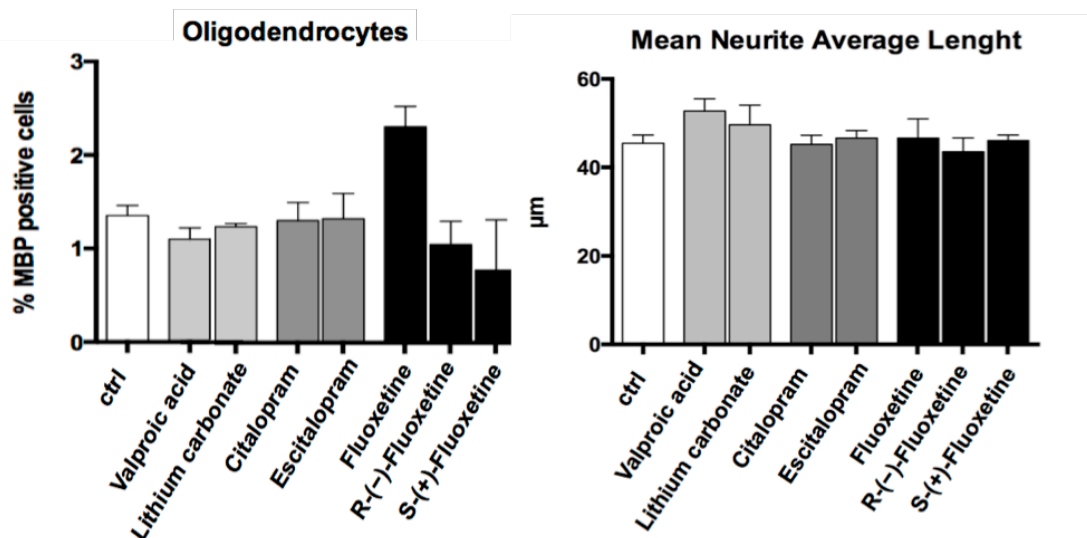


Figure 20. Differentiation of NSCs towards the oligodendrocyte lineage (left panel) and evaluation of dendritic arborization (right panel).

Lastly, we have studied the neuronal maturation in terms of neuronal morphology and dendritic arborization of cultured neurons. Also in this case, all the compounds showed a behavior similar to the control, and striking evidences could not be appreciated (Figure 20, right panel).

Regarding the lack of marked effects, we have to consider that the studied cellular system is highly complex and several crucial factors might be involved. First, as noted in Par. 4.1.2, previous studies have shown that only chronic, and not acute, antidepressants treatment increase neural cell proliferation and enhance differentiation *in vivo*,^{56, 223} and in neural precursors derived from human or mouse embryonic NSCs.²²⁴

Second, the ability of such molecules to modulate neurogenesis *in vitro* has been mainly observed at higher concentration.^{172, 225} Particularly, Kusakawa et al. reported that 8 days (but not 6 days) of treatment with 1 µM fluoxetine resulted in a significant increase of the mRNA expression levels of glial marker genes.²²⁰

Conversely, another recent report showed that 1 µM fluoxetine (which is comparable to therapeutic plasma concentrations),²²⁶ significantly enhanced the proliferation of embryonic NPCs, without affecting the differentiation.²²⁷ However, at higher concentration (20 µM), fluoxetine significantly decreased cell proliferation, as a consequence of cytotoxic effects. This is in agreement with previous findings obtained in primary rat cerebellar granule cells²²⁸ and hippocampal neural stem cells.²²⁹ Thus, the concentration used in such experiments is of critical importance due to the differences observed among *in vitro* studies.

In addition, it has been shown that although the NSCs isolated from different species and gender, or from different CNS areas at several embryonic and postnatal stages share common features (self-renewal and multipotency), but they also show significant differences in relation to their culture requirements and drug responsiveness, or to their plasticity and differentiation repertoire.²³⁰ For example, to determine whether the antidepressant-induced up-regulation of cell proliferation is specific to the hippocampus, another brain region known to contain progenitor cells in adulthood, the SVZ, was examined. Notably, chronic fluoxetine treatment did

not influence the number of BrdU-labeled cells of this brain region, demonstrating that antidepressants specifically increase cell proliferation in the hippocampus.⁵⁶ This has been further confirmed by Santarelli et al.¹⁶⁸

Furthermore, as already discussed at the beginning of this paragraph, it should be noted that, when comparing the main characteristics of NSCs in vivo and in vitro, significant differences occur. Accordingly, while in vivo the presence of a niche stringently controls NSCs activity, in vitro NSCs can divide and differentiate in the absence of a niche. Likewise, it is evident that NSCs identity in vivo evolves through developmental stages; in contrast, in vitro NSCs that have undergone long-term expansion, mainly have a single radial glia-like identity. Lastly, authentic neuronal functional phenotypes are acquired in vivo, while only partial functional maturation can be achieved in vitro.³⁷

Collectively, the obtained results and those reported in the literature, might suggest: (i) to repeat such experiments at higher compound concentration (similar to the brain therapeutic concentration); (ii) to extend the temporal frame of treatment mimicking the antidepressants chronic exposure; (iii) to perform dose-response studies.

4.1.3 Target identification studies

Despite their key roles in therapy and as biological probes, 7% of approved drugs are claimed to have no known primary target, and up to 18% lack a well-defined mechanism of action.²¹⁰ Furthermore, 37% of first-in-class drugs derive from phenotypic screens,¹⁶⁷ and consequently, the targets for some of these drugs remain largely unknown.²¹⁰

Although target identification is seen as an important and almost indispensable component of the phenotypic screening strategy, it is, however, not a critical step, in the sense that a project could advance to lead optimization and in principle even to clinical trials and market approval without target knowledge.

Nevertheless, the target identification represents a bold step in a phenotypic screening pipeline as already pointed out for P7C3 in Par 1.7.1.

Generally, three distinct and complementary approaches have been proposed for discovering the protein target of a small molecule: direct biochemical methods (i), genetic interaction methods (ii) and computational inference methods (iii).²³¹

Direct methods (i) involve labeling the protein or small molecule of interest, incubation of the two populations and direct detection of binding, usually following some type of wash procedure.²³² Genetic manipulation (ii) can also be used to identify protein targets by modulating presumed targets in cells, thereby changing small-molecule sensitivity.²³³ Target hypotheses, in contrast, can be generated by computational inference (iii), using pattern recognition to compare small molecule effects to those of known reference molecules or genetic perturbations.²⁰⁹

It should be noted that mechanistic hypotheses, rather than targets per se, for new compounds emerge from such strategies. The target pathway or protein of a new small molecule is identified, but remains to be confirmed.²³¹

Here, we discussed opportunities for medicinal chemists to make a direct impact in addressing target identification studies by using direct methods (i).

Among them, biochemical affinity purification provides the most direct approach to finding target proteins that bind small molecules of interest.²³¹ Because they are based on physical interactions involving usually proteins, biochemical methods can lead to information about molecular mechanisms of efficacy or toxicity. Moreover, unbiased protein identification, especially from lysates containing intact protein complexes, potentially allows evaluation of polypharmacological profile.²³⁴

One of the best known direct methods is the affinity purification, which involved monitoring chromatographic fractions for enzyme activity after exposure of extracts to compound immobilized on a column, followed by elution. In general, such approach requires large amounts of extract and stringent wash conditions. Such approach has been used with success to identify certain protein targets.²³⁴ However, these methods seem best suited for situations where a high-affinity ligand binds a relatively abundant target protein. Following washes can indeed bias proteins identified to those with the highest-affinity interactions, decreasing the likelihood of finding additional targets that might be important in cellular contexts.²¹⁰

Affinity purification experiments also involve the challenge of preparing immobilized affinity compounds that retain cellular activity, so that target proteins will still interact with the small molecule while it is bound to a solid support. A related issue is the identification of appropriate controls and tethers. These controls mostly rely on the availability of related inactive compounds. The inactive analog must be sufficiently different from the compound of interest to fail to bind the target, raising the possibility that it will have different physicochemical properties and therefore different nonspecific interactions with proteins. The choice of tether, influencing the type of background proteins identified, also becomes a critical parameter.²³¹

Recent affinity-based methods have attempted to overcome one or more of these challenges. Approaches based on chemical or ultraviolet light-induced cross-linking use covalent modification of the protein target or small molecule to increase the likelihood of capturing low-abundance proteins or those with low affinity for the small molecule.²¹³ If the first method requires prior knowledge of the protein being targeted, making it a slightly biased approach, the second one is still completely unbiased, but even suffers from limitations. Some small-molecule libraries are prepared for making affinity matrices after an activity is identified.²¹⁴ Because this method relies on modification of the compound structure, it requires additional studies, as the physicochemical properties of the starting molecule have been significantly modified. For example, if a small molecule can be fluorescently labeled, it can be used to probe proteins, however it should be kept in mind that it can establish different nonspecific interactions with other proteins or, even worst, it can lose the activity. Indeed, we already discussed in Par. 1.7.1 the case of P7C3 exemplified the above-mentioned limitations. Accordingly, all the newly synthesized probes for target deconvolution studies failed to identify the putative targets of P7C3.

Despite these limitations, this approach has been successfully applied to small molecules discovered to inhibit cancer cell proliferation through a phenotypic screening. Particularly, the functionalization of the identified hit with a photoreactive group for UV light-induced covalent cross-linking to interacting proteins, and, at the same time, with an alkyne group for reporter tag conjugation

for cross-linking, allowed to identify an integral mitochondrial membrane protein as target of the starting hit.²¹⁴

Although the potential of phenotypic screens for the discovery and characterization of active compounds is high, target identification remains a major challenge and only the integration of target identification strategies, including chemical labeling, proteomics, genomics and computational methods, may help in overcoming this critical step.

4.2 Design of TCAs-functionalized congeners

As at the core of such chemical biology approach is developing chemical tools to understand the mechanisms and the neuroregenerative potential of NSCs, we envisioned developing different set of functionalized congeners inspired by TCAs. Indeed, the functionalized congener approach has been already demonstrated its applicability towards different types of congeners and a wide range of GPCRs, as proposed by Jacobson.²³⁵ Such strategy was originally defined as the approach that allows the functionalization of a certain lead compound with known activity against GPCRs. Particularly, it referred to a derivative presenting a chemical reactive functional group, such as an amine or carboxylic acid that can be covalently conjugated through a spacer linker to a position structurally permissive on the pharmacophore. This means that the insensitivity to structural modification of the attachment site is an essential and indispensable condition for the synthesis of covalent conjugates that retain the activity. Thus, the goals of this approach focused on both developing potential new pharmaceutical agents in which the activity of the pharmacophore may be modulated through distal modifications, and on synthesizing molecular probes useful to explore the drug evoked response given by its interaction with the target.²³⁵ Moreover, an additional advantage of this approach is that the new congener may improve the pharmacological profile of the starting molecule by establishing secondary favorable interactions with the target(s). Accordingly, tethering different types of functionalized chain to a pharmacophore can provide a wide variety of chemical probes depending on the strategy of functionalization that includes fluorescent probes, dual-acting (multi-target) probes, conjugation to carrier/dendrimer, and so forth.¹⁷⁰

Given the success of this approach towards understanding of the structural and functional significance of GPCRs (discussed in the 2nd part of this thesis), we aim to apply this strategy to develop different set of functionalized congeners inspired by TCAs. In particular, in the following paragraphs, the design of fluorescent-, multi-target-, and polyamine-functionalized congeners inspired to TCAs have been described.

4.2.1 Design rationale of TCAs-functionalized fluorescent congeners

As already pointed out, unfortunately, there is not a general streamlined approach to target identification, and it often remains a major bottleneck in phenotypic approach. Although a great number of systematic approaches capitalizing on

proteomic and genomic technologies have been developed, from a medicinal chemistry perspective, developing properly tagged-molecules able to gain insights on the underlying mechanisms is particularly attractive.²⁰⁰

On these bases, we have developed a purposely-functionalized congeners library **48-51** by conjugating desipramine **19** and its corresponding primary amine **7** from the focused chemical library with a fluorescent dye in order to generate a selected set of fluorescent probes to potentially be used for further target identification studies (Figure 21).¹²

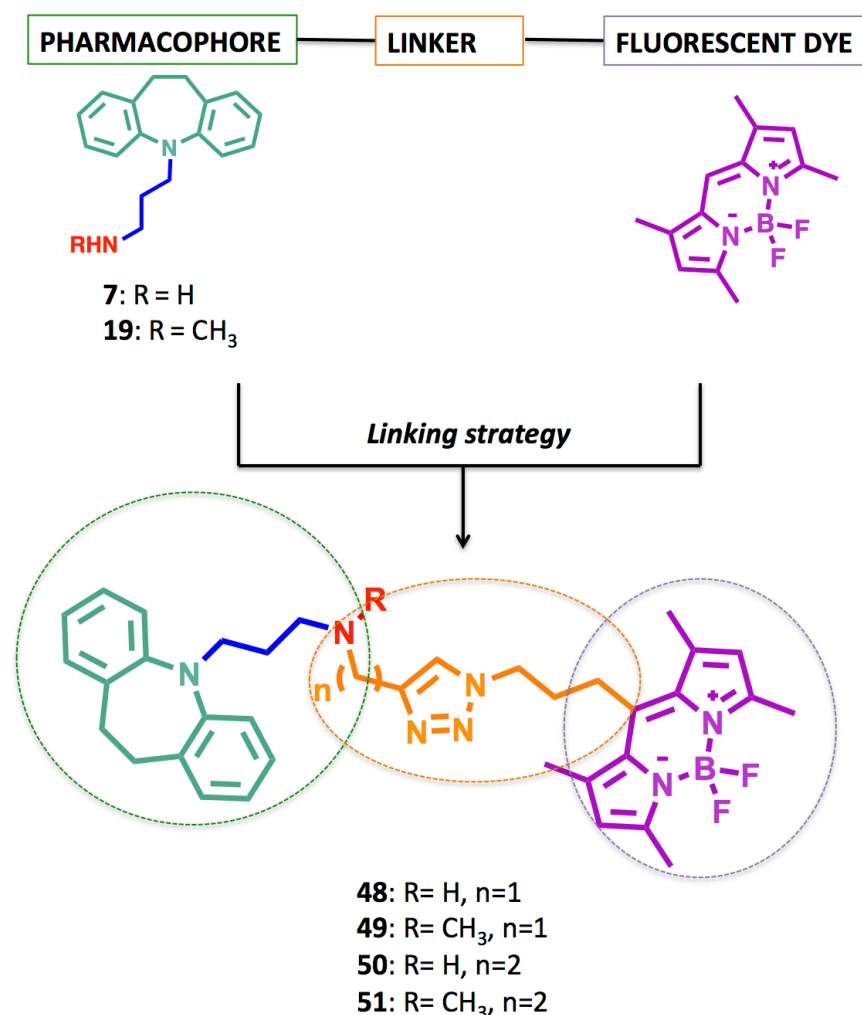


Figure 21. Design of TCA-inspired fluorescent congeners **48-51**.

Indeed, small molecules fluorescent probes have been widely used as sensors and probes in the analysis of a variety of molecules with a great potential for live cell imaging.²³⁶ An emerging field, involving the use of small molecules with fluorescent properties, is also the theranostic – i.e. a single chemical entity that integrates imaging and therapy. Even if this approach is still at its infancy, several examples validated this strategy against neurodegenerative diseases.²¹⁵ Notably, the group of Moore brilliantly exemplified as the curcumin-BODIPY analogue CRANAD-44 (Figure 22) can be effective not only to monitor A β in an AD mouse model, but also with the chelating pirazole moiety, it can significantly inhibited Cu²⁺-induced crosslinking of A β .²¹⁶

Importantly, the value of fluorescence-based imaging grows in parallel to the development of sophisticated fluorescent techniques²³⁷ and more efficient fluorescent dyes as well.²³⁸ Indeed, the advancement of fluorescence reagents, not only offer a wide range of new fluorophores with different physiochemical and spectroscopic properties (such as excitation and emission wavelengths, photobleaching, fluorescence quantum yield, stability, etc.), but has also resulted in a multitude of more complex fluorescence technologies such as fluorescence resonance energy transfer (FRET), fluorescence activated cell sorting (FACS) and fluorescence correlation spectroscopy (FCS), etc.²³⁷

The “conventional” fluorescent probe design has been performed by following hypothesis-driven approach. It implies to know the target in advance and the derived fluorescent probes is usually constituted by the recognition motif (pharmacophore), a linker and a fluorophore. Hence, the functional significance of such probes is intrinsically limited by the available knowledge of the target. An alternative approach is diversity-driven approach, in which a broad range of fluorescence molecules are constructed by diversity oriented fluorescence library approach (DOFLA), as a toolbox for unbiased screening.²³⁹

Remarkably, the second approach has already contributed to identify the fatty acid binding protein 7 (FABP7) as potential intracellular marker expressed in both human and mouse NSCs, by screening a DOFLA library on NSCs.²¹⁷ The identified BODIPY-based fluorescent probe (CDr3, in Figure 22) was confirmed to specifically label NSCs in a mixed primary mouse brain cell culture, as well as human cells differentiated from ESCs; and now is sold as chemical probe to be used in the biological studies of NSCs.¹⁹²

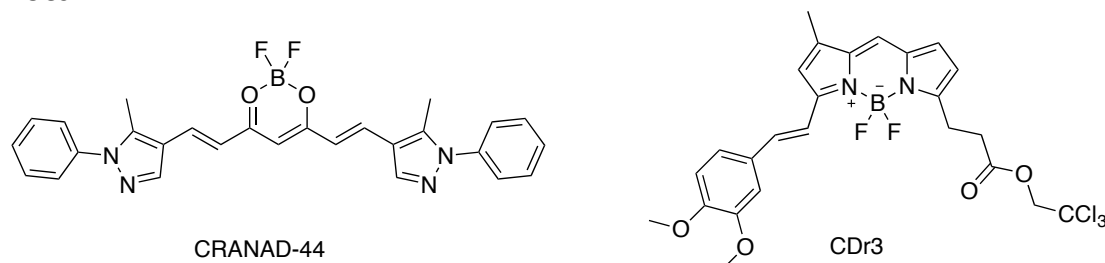


Figure 22. BODIPY-based fluorescent probes.

Since its inception, several other fluorescent probes have been reported as potential tool for cell-type-specific labeling.²⁴⁰ On the other hand, the deliberate development of fluorescent probes to gain insights of the signaling pathway(s) modulated by the selected compound in the cellular environment (i.e. NSCs) has not been reported yet. Furthermore, in such complex scenario where an exact molecular target cannot be identified, the development of such probes cannot even be started by the conventional method, as there is no available validated target.

Furthermore, in our case, little is known about the underlying mechanism by which TCAs enhance adult neurogenesis and neuroplasticity.²⁴¹ These observations support the hypothesis that the observed proneurogenic effect is mediated by mechanisms that do not only rely on inhibition of the monoamine reuptake transporters.²⁴¹ Thus, complex and oppositely directed interactions between neurotransmitter systems and other signaling pathways/proteins, including Wnt/ β -catenin, or neurotrophic factors, may be involved in the net effects displayed by TCAs.²⁴¹

Nonetheless, the profiling of TCAs revealed a complex polypharmacological multi-target profile, spanning from the interactions with amine transporters to related pre- and post- synaptic receptors.²³³

On this basis, the design of a selected set of TCAs fluorescent congener probes has been performed, as fluorescent ligands have proven to be useful tools also in a cellular context, offering a wealth of information about the mapping or identification of ligand binding sites, the movement and internalization of molecular targets and the sub-cellular localization and visualization.²⁴² Particularly, desipramine **19** and its corresponding primary amine **7** have been conjugated with a BODIPY fluorescent dye through two different linkers to give the TCA-inspired fluorescent congeners **48-51** (Figure 21), as already described in Chapter 3.

BOBIPY dye has been selected because of its distinctive and useful features, including hydrophobicity, photochemical stability, efficient uptake into cell membranes, high extinction coefficient and fluorescence quantum yield.²⁴³ Moreover the BODIPY core has been widely used as fluorescent imaging agent for A β , reinforcing our dye selection in terms of cellular permeability, stability and low toxicity.²⁴⁴

To assess if the conjugation modifies the spectroscopic features of the BODIPY dye, we investigated the native fluorescence of TCA-inspired fluorescent congeners **48-51** in two different solvents: ethanol and dichloromethane. Notably, no significant changes have been observed between the excitation and emission maxima in the different solvents (Table 6) and the identified wavelengths are similar to those already reported for this dye,¹⁹² suggesting that the conjugation did not influence its fluorescent profile. As shown in Figure 23, the excitation and emission spectra of **48-51** in dichloromethane (A, C, E, G) and in ethanol (B, D, F, H) display a small Stokes shift, but sharp excitation and emission peaks. This latter factor contributes to overall their brightness. Additional studies in different environments, including phosphate buffered saline at physiological pH, will be also performed to assess potential different behavior of **48-51**.

Table 6. Excitation and emission maxima of compounds **48-51** in different solvents.

	Dichloromethane		EtOH	
	$\lambda_{(exc)}$ (nm)	$\lambda_{(em)}$ (nm)	$\lambda_{(exc)}$ (nm)	$\lambda_{(em)}$ (nm)
48	504	507	501	503
49	502	503	500	503
50	505	507	501	503
51	505	507	505	506

Collectively, the TCA-inspired fluorescent probes **48-51** might act as invaluable tools for getting initial clues toward identifying the target(s) and for consequent unraveling the mechanism by which TCAs exert neurogenic effects.

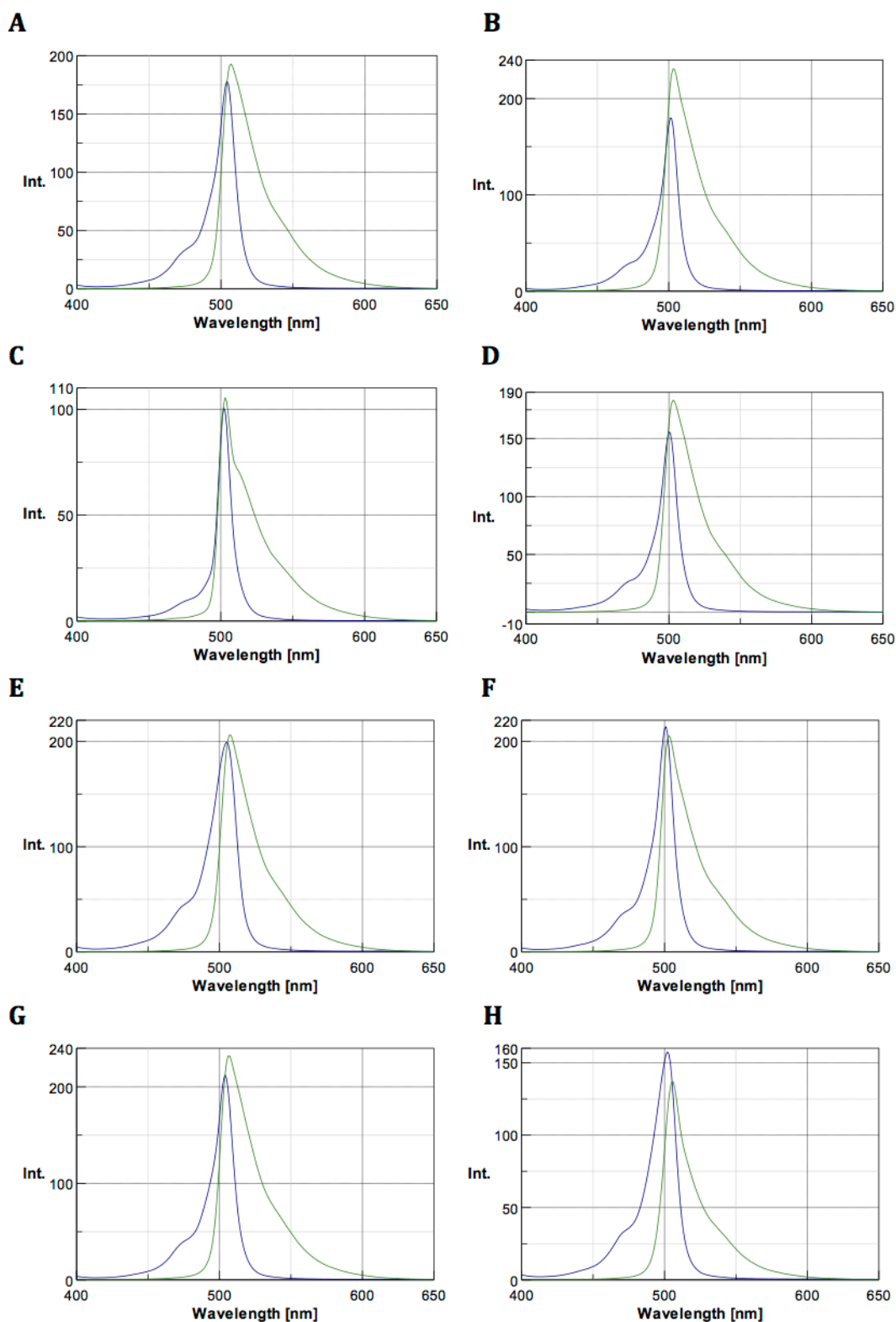


Figure 23. Fluorescent spectra of **48-51** registered at 0.5 μ M in dichloromethane (A, C, E, G) and in ethanol (B, D, F, H).

4.2.2 Design rationale of TCA-functionalized multi-target congeners

Based on the success of multi-target drug design strategy for neurodegenerative diseases,²⁴⁵ we have also designed potential multi-target ligands towards NSCs by

combining in a single chemical entities two pharmacophoric fragments belonging to two molecules with different neurogenic mechanisms of action.

Indeed, due to the resilient architecture of the complex cellular system, the modulation of networks of targets through a well-concerted polypharmacological approach²⁴⁶ may represent an innovative approach to perturb the combination of different interconnected biochemical networks orchestrating the NSCs proliferation and differentiation.

In addition, as previously discussed in Chapter 1, the ability of defined “cocktail” of small molecules to modulate specific stages of NSCs or to reprogram somatic cells into specific lineages suggest that the partial inhibition of a carefully selected small number of targets can be more efficient than complete inhibition of a single target.

In principle, these goals can be attained by either combination of compounds or by the use of equivalent multi-target ligands.²⁴⁶

In the first case, the combination of buspirone and melatonin (Figure 24), which has already completed the trial as a potential mood and cognitive agent for MDD,²⁰¹ demonstrated that both enhanced neurogenesis in the pre-clinical neurogenesis-based in vitro assays and antidepressant responses in the in vivo behavioral tests that were equivalent to fluoxetine.²⁰³ Intriguingly, buspirone increased not only the number of neuronal-positive cells, but also the number of non-neuronal (GFAP positive) cells. Melatonin repressed buspirone-induced GFAP-positive cell formation, without eliminating the ability of buspirone to promote neuronal differentiation. Melatonin had no effect alone suggesting that melatonin works synergistically with buspirone.

On the other hand, the development of multi-target ligands has provided a set of brilliant examples to support this concept. One of the most appealing examples came from the group of Youdim.²⁴⁷ They designed and synthesized a multi-target compound, (M30 in Figure 24), possessing the neuroprotective N-propargyl moiety of the anti-Parkinsonian drug, monoamine oxidase-B inhibitor, rasagiline and the antioxidant-iron chelator moiety of the 8-hydroxyquinoline derivative of the iron chelator, VK28. The authors also demonstrated the neuroprotective and the neurorestorative activity of M30, acting against multiple brain targets, including regulation on amyloid β , neurogenesis, and activation of hypoxia inducible factor signaling pathways. The diverse pharmacological properties of M30 make this compound potential valuable for treating AD.²⁴⁷

Given the crucial property played by neurogenesis for new AD-modifying drugs and considering that GSK-3 β inhibition has been reported to regulate and increase neurogenesis,²⁴⁸ novel BACE-1/GSK-3 β dual triazinone inhibitors (Figure 24) have been recently showed to exert remarkable neuroprotective and neurogenic activities and no neurotoxicity in cell-based assays. Moreover, displaying good brain permeability and pharmacokinetic properties in mice, these multi-target triazinone derivatives might emerge as suitable candidates for the development of effective multi-target drugs against AD.²⁴⁹

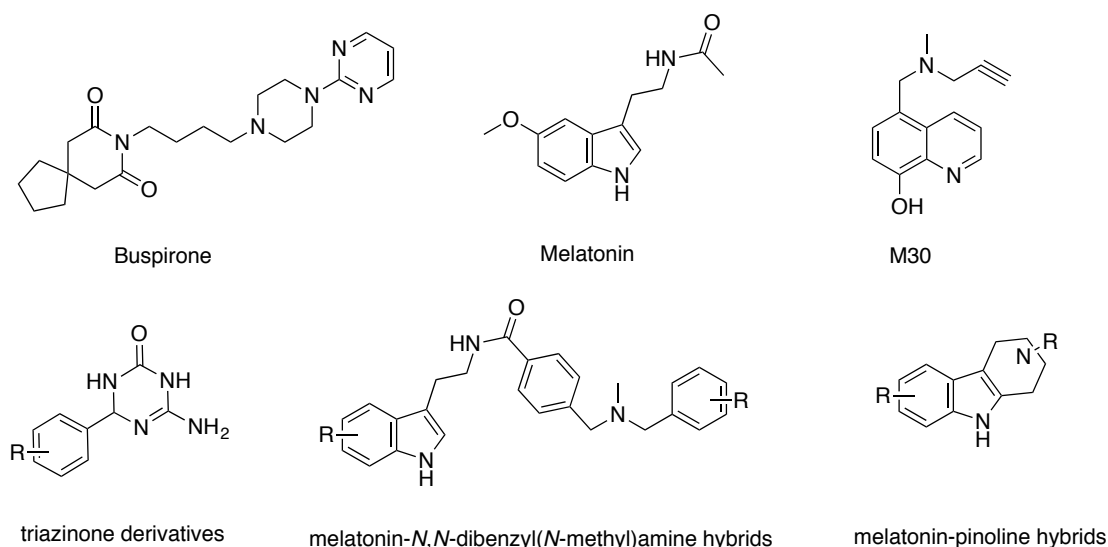


Figure 24. Multi-target with neurogenic properties.

Conversely, Rodríguez-Franco et al. exploited the neuroregenerative properties of melatonin by combining it with fragments showing interesting and complementary features to provide hybrid compounds. In 2014, the melatonin framework was combined to a selected protonable (*N,N*-dibenzyl(*N*-methyl)amine) fragment, present in the AChE inhibitor AP2238, leading to new melatonin-*N,N*-dibenzyl(*N*-methyl)amine hybrids (Figure 24). These new hybrids show a balanced multi-target profile spanning from AChE inhibitory activity to antioxidant and neuroprotective properties. Importantly, they promote maturation of NSCs into a neuronal phenotype and thus, they could contribute to CNS repair. In addition, given the low cell toxicity and efficient BBB permeability, this multi-target profile highlights these melatonin-*N,N*-dibenzyl(*N*-methyl)amine hybrids as useful prototypes in the research of innovative drugs for AD.²⁵⁰

In a following paper, the intriguing effect of melatonin has been exploited by the same author to design merged melatonin-pinoline hybrids (Figure 24). In this case, the 6-methoxy-1,2,3,4-tetrahydro- β -carboline (pinoline) is combined with melatonin, and both are structurally related to serotonin. Their multi-target profile has been evaluated and included serotonergic and melatonergic receptors, metabolic enzymes (monoamine oxidases), and antioxidant activity. Both, pinoline and 2-acetyl-6-methoxy-1,2,3,4-tetrahydro- β -carboline were able to stimulate early neurogenesis and neuronal maturation in an *in vitro* model of NSCs isolated from the adult rat SVZ. Such effects are presumably mediated via serotonergic and melatonergic stimulations.²⁵¹

On these bases, we developed multi-target ligands towards NSCs. The most common rational strategy to generate multi-target compounds is the framework combination,²²⁰ which starts with the selection of two structures or sub-structures interfering with two distinct targets relevant for the biological process under investigation.²²⁰ In fact, multi-target ligands arising from framework combination can be viewed as linked, fused, or merged depending upon the degree to which the frameworks have been integrated. In linked multi-target compounds, the molecular fragments are joined by a chemical linker (either cleavable or metabolically stable). Fused multi-target ligands are referred to compounds where the two frameworks

are connected without a discernable linker, meanwhile merged multi-target ligands indicates an overlap of a common chemical moiety present in both starting fragments.²²⁰ We turned our attention to the fusing strategy, by amalgamating into a new single molecule starting fragments as much as possible to limit the molecular weight increase.²¹⁹ To this respect, as shown in Figure 25, we conjugated the primary amines **1-3** and **17-19** of focused chemical library with other small molecules active on NSCs (i.e. valproic acid, **52**).¹⁰

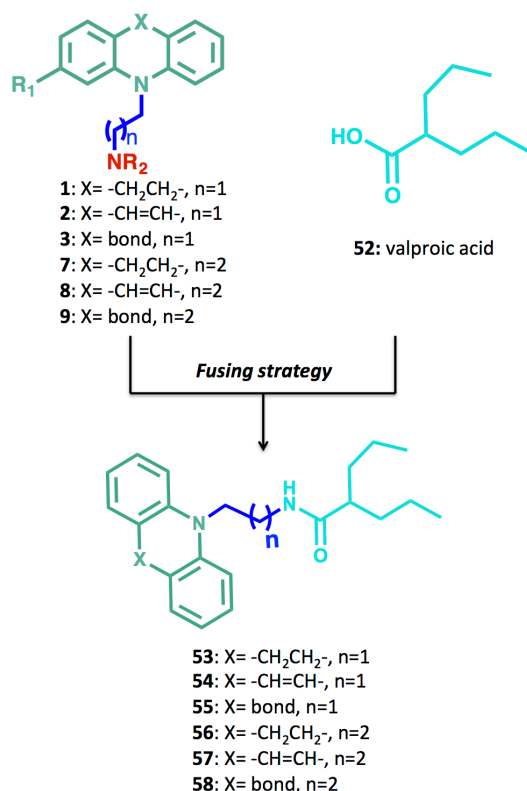


Figure 25. Design of multi-target congeners **53-58**.

As already noted in Chapter 1, the modulation of neurogenesis by targeting epigenetic enzymes using small molecules is particularly attractive.¹³² Among the HDAC inhibitors, valproic acid **52** emerged to modulate neuronal differentiation and hippocampal neurogenesis.¹³⁷ Moreover, by also interacting with GSK3, valproic acid enhanced neurogenesis by activating ERK pathway-dependent cortical neuronal growth.¹³⁷

Given the intrinsic ability of the starting molecules to simultaneously interact with multiple targets, these multi-target ligands **53-58** may provide an innovative approach to perturb the combination of different interconnected biochemical networks orchestrating the NSCs proliferation and differentiation.

4.2.3 Design rationale of TCAs-polyamine congener

Since polyamines have been considered as "privileged structures",²⁵² the last conjugation strategy of this functionalized congener approach, relies on developing polyamine-based functionalized congener inspired by TCA.

The most common natural polyamines, such as putrescine, spermidine, and spermine (Figure 26), are aliphatic molecules with amine groups distributed along their structure. These polyamines are present in all organism cells, where they play a fundamental role in cell proliferation and have both pro- and antiapoptotic effects.
252

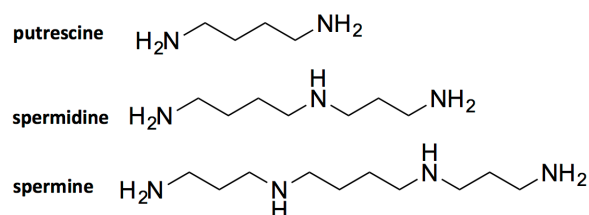


Figure 26. Some naturally occurring polyamines.

Additionally, polyamines are involved in many signaling pathways through their effects on G proteins, protein kinases, nucleotide cyclases, and receptors and through their regulation of the expression of proteins involved in a variety of processes.²⁵³ For example, spermine is also released from synaptic vesicles on depolarization, indicating that polyamines may function as neuromodulators.²⁵⁴ Moreover, polyamines influence the properties of several neurotransmitter pathways known to be involved in mental disorders, including catecholamines, γ -aminobutyric acid, nitric oxide, and glutamate.²⁵⁵

The wide range of activities displayed by polyamines is clear evidence of how nature exploits them for different roles at different targets, supporting the viability of polyamine skeletons as privileged structures. And indeed, polyaminoquinones emerged as readily accessible and easily diversified scaffolds for anticancer lead discovery,²⁵⁶ whereas tetraamine-based hybrids produced novel inhibitors of muscular nicotinic acetylcholine receptors²⁵⁷ or acetylcholinesterase enzyme.²⁵⁸ However, the polyamine roles in neurogenesis have not been widely explored. Recent evidences suggest that putrescine in neurosphere stimulates neural progenitor proliferation.⁷² Furthermore, in vivo depletion of putrescine by specific and irreversible inhibition of ornithine decarboxylase, the first key enzyme of the polyamine synthesis pathway, induces a consistent decrease in neural progenitor cell proliferation in the two neurogenic areas, the DG and the SVZ.⁷² Based on these intriguing findings, the authors proposed, as a working hypothesis for further studies, that putrescine could be the intracellular link between hormonal and growth factor signaling pathways acting on neural progenitor cell. However, no additional studies have so far been reported yet.

Nevertheless, the demonstration that the conjugation with polyamine not only increases the cationic character of the starting molecule, but also may promote accumulation directly into the mitochondrion,¹⁷² attracted our attention. Accordingly, additional neuroprotective effects may be achieved following this functionalization strategy.¹⁷² This is of particular importance, as we searched for compounds able to modulate neurogenesis and to exert neuroprotective effects.

Thus, as depicted in Figure 27, the combination of desipramine with spermidine has been envisioned leading to polyamine congener **65**.

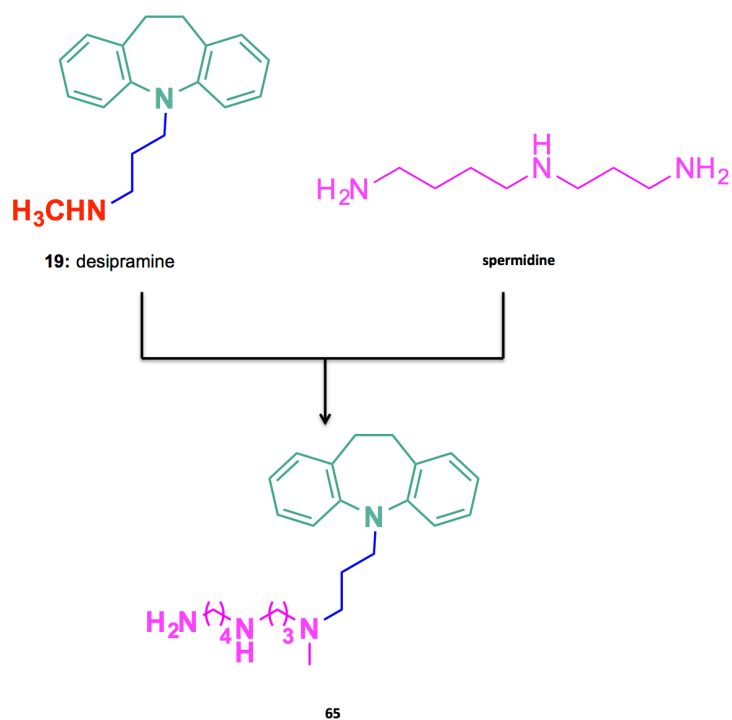


Figure 27. Design of polyamine congener **65**.

To the best of our knowledge, this represents the first example of direct conjugation of a known compound with neurogenic activity (i.e. desipramine **19**) to a polyamine carrier molecule (spermidine) that may provide further insights in the roles played by polyamine in neurogenesis and, hopefully, to compounds endowed with a promising neurogenic and neuroprotective profile.

Experimental part

General information. All the commercial available reagents and solvents were used purchased from Sigma-Aldrich (Italy), TCI chemicals (Europe) and Alfa Aesar (Germany) without purification. Column chromatography purifications were performed under "flash conditions" using Sigma-Aldrich silica gel grade 9385, 60 Å, 230-400 mesh. CEM Discover SP focused microwave reactor was used for microwave-mediated reactions. Thin layer chromatography (TLC) separations were performed on 0.20 mm silica gel 60 F254 plates (Merck, Germany), which were visualized by exposure to ultraviolet light (254 and 366 nm), iodine and potassium permanganate stains. Reactions involving generation or consumption of amine were visualized by using bromocresol green (0.04% in EtOH made blue by NaOH) following heating of the plate. Compounds were named following IUPAC rules as applied by ChemBioDraw Ultra (version 13.0). NMR experiments were run on Varian VXR 400 (401 MHz for ^1H ; 101 MHz for ^{13}C). Spectra were acquired at 300 K, using CDCl_3 and CD_3OD as solvents. Chemical shifts for ^1H and ^{13}C spectra were recorded parts per million (ppm) using the residual non-deuterated solvent as the internal standard. Data are reported as follows: chemical shift (ppm), multiplicity (indicated as: s, singlet; br s, broad singlet; exch, exchangeable proton with D_2O ; d, doublet; t, triplet; q, quartet; p, pentet; m, multiplet and combinations thereof), coupling constants (J) in Hertz (Hz) and integrated intensity.

Procedure for the preparation of N-functionalized acetals **67** and **69**:

N-(2,2-dimethoxyethyl)-2,2,2-trifluoroacetamide (**67**):

To a solution of 2,2-dimethoxyethanamine (**66**) (4.75 mmol, 0.52 mL) in THF (8 mL) were added trifluoroacetic anhydride (TFAA, 5.70 mmol, 0.79 mL) and triethylamine (5.70 mmol, 0.79 mL) and the mixture was stirred at room temperature for 4 hours. After evaporation of the solvent under vacuum the reaction mixture was neutralized with saturated solution of NaHCO_3 and diluted with DCM. The layers were separated and the aqueous phase extracted with DCM (3 x 15 mL). The organic phases were reunited, washed with brine, dried over Na_2SO_4 , filtered and evaporated at rotary evaporator. The resulting residue was purified by flash chromatography (6:4 petroleum ether/EtOAc) affording **67** as pale yellow oil. Yield 75%.

^1H NMR (401 MHz, CDCl_3) δ 6.58 (br s, 1H), 4.42 (t, $J = 5$ Hz, 1H), 3.49 (t, $J = 5$ Hz, 2H), 3.41 (s, 6H).

^{13}C NMR (101 MHz, CDCl_3) δ 41.2, 54.7, 101.7, 115.8 (q, $J = 285$ Hz), 157.4 (q, $J = 37$ Hz).

N-(3,3-dimethoxypropyl)acetamide (**69**):

To a solution of 3,3-dimethoxypropionitrile **68** (8.7 mmol, 0.98 mL) and acetic anhydride (17.4 mmol, 1.65 mL) in dry MeOH (60 mL), NiSO_4 (1.3 g, 8.7 mmol) was added. To the resulting suspension NaBH_4 (2.3 g, 60.1 mmol) was cautiously added over 30 min at 0°C . A vigorous reaction with the formation of a black precipitate takes place. After 6 h, the reaction was quenched by adding saturated solution of

NaHCO₃ (5 mL) at 0°C. Then, the obtain mixture was repeatedly filtered on celite, until removal of the black solid residue. Then, the filtrate was concentrated under reduced pressure to give the residue that was purified by flash chromatography (9:1 DCM/MeOH) to give the title compound **69 as** yellow oil. Yield 56%.

¹H NMR (401 MHz, CDCl₃) δ 6.10 (br s, 1H), 4.42 (t, J = 5.5 Hz, 1H), 3.32 (m, 8H), 1.96 (s, 3H), 1.81 (q, J = 5.5, 13 Hz, 2H).

¹³C NMR (101 MHz, CDCl₃) δ 169.9, 104.0, 53.4, 35.4, 31.9, 23.2.

General procedure for the preparation of N-functionalized tricyclic scaffolds (1b-12b):

To a solution of suitable tricyclic scaffold **1a-6a** (1 mmol) and acetal **67** or **69** (1.1-1.4 mmol) in DCM (2 mL) under nitrogen, were added trifluoroacetic acid (TFA, 13 mmol) and triethylsilane (TES, 2.5 mmol) and the resulting mixture was stirred at room temperature for 2-16 hours. The reaction was cooled at 0°C and carefully neutralized with saturated solution of NaHCO₃ and diluted with DCM. The aqueous layer was extracted with DCM (3 x) and the combined organic phases were washed with brine, dried over Na₂SO₄ and concentrated under reduce pressure. The resulting residue was purified by flash chromatography on silica gel using different eluent mixtures to give the title compounds **1b-12b**.

N-(2-(10,11-dihydro-5*H*-dibenzo[*b,f*]azepin-5-yl)ethyl)-2,2,2-trifluoroacetamide (**1b**):

The resulting residue was purified by flash chromatography (8:1.5:0.5 DCM/Tol/EtOAc) affording **1b** as white solid. Yield 90%.

¹H NMR (401 MHz, CDCl₃) δ 7.20 – 7.09 (m, 6H), 7.04-6.96 (m, 2H), 6.50 (s, 1H, exch), 3.95 (t, J = 5.9 Hz, 2H), 3.55 (q, J = 5.8 Hz, 2H), 3.15 (s, 4H).

N-(2-(5*H*-dibenzo[*b,f*]azepin-5-yl)ethyl)-2,2,2-trifluoroacetamide (**2b**):

The resulting residue was purified by flash chromatography (8:2 petroleum ether/EtOAc) affording **2b** as yellow solid. Yield 95%.

¹H NMR (401 MHz, CDCl₃) δ 7.05-7.35 (m, 9H), 6.81 (s, 2H), 3.98 (t, J = 5.5 Hz, 2H), 3.48 (m, 2H).

N-(2-(9*H*-carbazol-9-yl)ethyl)-2,2,2-trifluoroacetamide (**3b**):

The resulting residue was purified by flash chromatography (7:2:1 petroleum ether/DCM/EtOAc) affording **3b** as white solid. Yield 82%.

¹H NMR (401 MHz, CDCl₃) δ 8.09 (d, J = 7.8 Hz, 2H), 7.47 (m, 2H), 7.45 – 7.34 (m, 1H), 7.28 - 7.24 (m, 3H), 6.28 (s, 1H, exch), 4.56 (t, J = 5.9 Hz, 2H), 3.83 (q, J = 6.0 Hz, 2H).

2-(10*H*-phenothiazin-10-yl)-*N*-(trifluoromethyl)ethan-1-amine (**4b**):

The resulting residue was purified by flash chromatography (7:3 petroleum ether/EtOAc) affording **4b** as pale yellow oil. Yield 88%.

¹H NMR (401 MHz, CDCl₃) δ 7.21 (m, 4H), 7.00 (t, J = 8.0 Hz, 2H), 6.94 (d, J = 7.8 Hz, 2H), 4.16 (t, J = 5.8 Hz, 2H), 3.73 (d, J = 5.8 Hz, 2H).

2-(2-chloro-10*H*-phenothiazin-10-yl)-*N*-(trifluoromethyl)ethan-1-amine (**5b**):

The resulting residue was purified by flash chromatography (8.5:1.5 petroleum ether/ EtOAc) affording **5b** as pale yellow oil. Yield 70%.

¹H NMR (401 MHz, CDCl₃) δ 7.20 - 7.12 (m, 2H), 7.04 (d, *J* = 8.2 Hz, 1H), 6.98 - 6.79 (m, 4H), 4.07 - 4.02 (m, 2H), 3.66 (t, *J* = 6.4 Hz, 2H).

N-(trifluoromethyl)-2-(2-(trifluoromethyl)-10*H*-phenothiazin-10-yl)ethan-1-amine (**6b**):

The resulting residue was purified by flash chromatography (8.5:1.5 petroleum ether/ EtOAc) affording **6b** as pale yellow oil. Yield 84%.

¹H NMR (401 MHz, CDCl₃) δ 7.28 - 7.16 (m, 4H), 7.10 (s, 1H), 7.04 - 6.96 (m, 2H), 6.74 (s, 1H, exch), 4.16 (t, *J* = 6.0 Hz, 2H), 3.72 (q, *J* = 5.9 Hz, 2H).

N-(3-(10,11-dihydro-5*H*-dibenzo[*b,f*]azepin-5-yl)propyl)acetamide (**7b**):

The resulting residue was purified by flash chromatography (7:2:1 petroleum ether/ EtOAc/ EtOH) affording **7b** as white solid. Yield 71%.

¹H NMR (401 MHz, CDCl₃) δ 7.17 - 7.01 (m, 6H), 6.92 (t, *J* = 7.3, 2H), 5.57 (br s, 1H, exch), 3.75 (t, *J* = 6.7 Hz, 2H), 3.24 (t, *J* = 6.9 Hz, 2H), 3.14 (s, 4H), 1.87 (s, 3H), 1.85 - 1.72 (m, 2H).

N-(3-(5*H*-dibenzo[*b,f*]azepin-5-yl)propyl)acetamide (**8b**):

The resulting residue was purified by flash chromatography (6:3:1 petroleum ether/ EtOAc/ EtOH) affording **8b** as pale yellow solid. Yield 75%.

¹H NMR (CDCl₃) δ 7.33 - 7.29 (m, 2H), 7.11 - 7.07 (m, 2H), 7.05 - 6.98 (m, 4H), 6.84 (s, 2H), 6.66 (br s, 1H, exch), 3.84 (m, 2H), 3.29 (m, 2H), 1.87 (s, 3H), 1.73 (m, 2H).

N-(3-(9*H*-carbazol-9-yl)propyl)acetamide (**9b**):

The resulting residue was purified by flash chromatography (6:3:1 petroleum ether/ EtOAc/ EtOH) affording **9b** as pale pink solid. Yield 62%.

¹H NMR (401 MHz, CDCl₃) δ 8.10 (d, *J* = 7.8 Hz, 2H), 7.49 - 7.42 (m, 4H), 7.23 (t, *J* = 4.0 Hz, 2H), 4.39 (t, *J* = 6.8 Hz, 2H), 2.61 (t, *J* = 6.9 Hz, 2H), 2.40 (s, 3H), 2.05 (p, *J* = 6.9 Hz, 2H).

N-(3-(10*H*-phenothiazin-10-yl)propyl)acetamide (**10b**):

The resulting residue was purified by flash chromatography (6:3:1 petroleum ether/ EtOAc/ EtOH) affording **10b** as pale yellow oil. Yield 82%.

¹H NMR (401 MHz, CDCl₃) δ 7.21 - 7.14 (m, 4H), 6.96 - 6.85 (m, 4H), 6.24 (br s, 1H, exch), 3.31 (q, *J* = 6.1 Hz, 2H), 1.98 (q, *J* = 6.1 Hz, 2H), 1.75 (s, 3H).

N-(3-(2-chloro-10*H*-phenothiazin-10-yl)propyl)acetamide (**11b**):

The resulting residue was purified by flash chromatography (6:3:1 petroleum ether/ EtOAc/ EtOH) affording **11b** as pale yellow oil. Yield 82%.

¹H NMR (401 MHz, CD₃OD) δ 7.11 (t, *J* = 7.9 Hz, 1H), 7.05 - 7.05 (m, 1H), 6.93 (d, *J* = 8.0 Hz, 1H), 6.90 - 6.79 (m, 4H), 3.81 (t, *J* = 6.7 Hz, 2H), 3.19 (t, *J* = 6.9 Hz, 2H), 1.90 - 1.83 (m, 5H).

N-(3-(2-(trifluoromethyl)-10*H*-phenothiazin-10-yl)propyl)acetamide (**12b**):

The resulting residue was purified by flash chromatography (6:3:1 petroleum ether/EtOAc/ EtOH) affording **12b** as pale yellow oil. Yield 72%.

^1H NMR (401 MHz, CD_3OD) δ 7.17 – 7.03 (m, 5H), 6.92 – 6.85 (m, 2H), 3.89 (t, J = 6.8 Hz, 2H), 3.27 – 3.17 (m, 2H), 1.95 – 1.81 (m, 5H).

General procedure for the preparation of primary amines (1-12):

Method A: To a solution of trifluoroacetamides **1b-6b** (1 mmol) in a mixture of MeOH: H_2O (2:1, 3.5 mL), K_2CO_3 (7.88 mmol) was added and the resulting mixture is stirred at rt for 4-6 h. After evaporation of MeOH under vacuum the resulting aqueous residues was diluted with H_2O (10 mL) and extracted with DCM (3 x 15 mL). The organic phases were reunited, washed with brine, dried over Na_2SO_4 , filtered and evaporated at rotary evaporator to give the title compounds **1-6**, without any further purification.

Method B: To a solution of acetamides **7b-12b** (1 mmol) in a mixture of MeOH: H_2O (2:1, 5 mL), KOH (7.5 mmol) was added in a pressure-tight microwave tube. The resulting mixture was submitted to microwave irradiation for 90 min at 160°C , with an irradiation power of 150 W. After evaporation of the solvents under vacuum, the resulting mixture was purified by flash chromatography using as eluent a mixture of DCM: MeOH: 33% aq. NH_3 solution (9:1:0.1) to give the title compounds **7-12**.

2-(10,11-dihydro-5H-dibenzo[*b,f*]azepin-5-yl)ethan-1-amine (1):

The title compound **1** was obtained as colorless oil by using Method A. Yield 98%.

^1H NMR (401 MHz, CDCl_3) δ 7.11 (m, 6H), 6.93 (t, J = 7.3 Hz, 2H), 3.81 (t, J = 6.0 Hz, 2H), 3.18 (s, 4H), 2.86 (s, 2H).

^{13}C NMR (101 MHz, CDCl_3) δ 148.04, 134.23, 129.91, 126.43, 122.70, 120.02, 53.98, 39.82, 32.27.

MS(ESI): m/z $\text{C}_{16}\text{H}_{18}\text{N}_2$; calcd. [M]: 238.33, found [M + 1]: 239, [M + Na^+]: 261.

2-(5H-dibenzo[*b,f*]azepin-5-yl)ethan-1-amine (2):

The title compound **2** was obtained as yellow solid by using Method A. Yield 98%.

^1H NMR (401 MHz, CDCl_3) δ 7.28 – 7.19 (m, 2H), 7.11 – 6.92 (m, 6H), 6.73 (s, 2H), 3.81 (t, J = 1.5 Hz, 2H), 2.81 (m, 2H).

^{13}C NMR (101 MHz, CDCl_3) δ 150.42, 134.13, 132.12, 129.19, 128.84, 123.52, 120.70, 53.84, 39.31.

MS(ESI): m/z $\text{C}_{16}\text{H}_{16}\text{N}_2$; calcd. [M]: 236.32, found [M + 1]: 237, [M + Na^+]: 259.

2-(9H-carbazol-9-yl)ethan-1-amine (3):

The title compound **3** was obtained as pale yellow oil by using Method A. Yield 97%.

^1H NMR (401 MHz, CDCl_3) δ 8.13 (dt, J = 7.8, 1.1 Hz, 2H), 7.53 – 7.41 (m, 4H), 7.27 (m, 2H), 4.35 (t, J = 6.2 Hz, 2H), 3.18 (t, J = 6.1 Hz, 2H).

^{13}C NMR (101 MHz, CDCl_3) δ 140.65, 125.77, 122.92, 120.41, 119.07, 108.76, 46.21, 41.33.

MS(ESI): m/z $\text{C}_{14}\text{H}_{14}\text{N}_2$; calcd. [M]: 210.28, found [M + 1]: 211, [M + Na^+]: 243.

2-(10H-phenothiazin-10-yl)ethan-1-amine (4):

The title compound **4** was obtained as colorless oil by using Method A. Yield 98%.

^1H NMR (401 MHz, CDCl_3) δ 7.17 – 7.10 (m, 4H), 6.96 – 6.84 (m, 4H), 3.96 (t, J = 5.9 Hz, 2H), 3.03 (t, J = 5.9 Hz, 2H).

^{13}C NMR (101 MHz, CDCl_3) δ 145.21, 127.59, 127.24, 125.87, 122.70, 115.78, 109.98, 50.51, 38.82.

MS(ESI): m/z $\text{C}_{14}\text{H}_{14}\text{N}_2\text{S}$; calcd. [M]: 242.34, found [M + 1]: 243, [M + Na^+]: 265.

2-(2-chloro-10H-phenothiazin-10-yl)ethan-1-amine (5):

The title compound **5** was obtained as yellow oil by using Method A. Yield 96%.

^1H NMR (401 MHz, CDCl_3) δ 7.17 – 7.12 (m, 2H), 7.02 (d, J = 8.2 Hz, 1H), 6.96 – 6.82 (m, 4H), 3.92 (t, J = 5.9 Hz, 2H), 3.03 (t, J = 5.9 Hz, 2H).

^{13}C NMR (101 MHz, CDCl_3) δ 145.22, 127.61, 127.27, 125.88, 122.73, 115.80, 50.46, 38.81.

MS(ESI): m/z $\text{C}_{14}\text{H}_{13}\text{ClN}_2\text{S}$; calcd. [M]: 276.78, found [M + 1]: 277, [M + Na^+]: 299.

2-(2-(trifluoromethyl)-10H-phenothiazin-10-yl)ethan-1-amine (6):

The title compound **6** was obtained as yellow oil by using Method A. Yield 97%.

^1H NMR (401 MHz, CDCl_3) δ 7.29 – 7.13 (m, 4H), 7.10 – 7.05 (m, 1H), 7.02 – 6.88 (m, 2H), 4.02 (t, J = 5.9 Hz, 2H), 3.08 (t, J = 5.9 Hz, 2H).

^{13}C NMR (101 MHz, CDCl_3) δ 145.76, 144.26, 127.72, 127.67, 127.63, 124.87, 123.38, 119.36, 119.33, 116.15, 112.27, 112.24, 50.66, 38.65.

MS(ESI): m/z $\text{C}_{15}\text{H}_{13}\text{F}_3\text{N}_2\text{S}$; calcd. [M]: 310.34, found [M + 1]: 311, [M + Na^+]: 333.

3-(10,11-dihydro-5H-dibenzo[*b,f*]azepin-5-yl)propan-1-amine (7):

The title compound **7** was obtained as colorless oil by using Method B. Yield 78%.

^1H NMR (401 MHz, CDCl_3) δ 7.15 – 7.07 (m, 6H), 6.98 – 6.87 (m, 2H), 3.79 (t, J = 6.7 Hz, 2H), 3.16 (s, 4H), 2.71 (t, J = 7.0 Hz, 2H), 1.71 (p, J = 6.8 Hz, 2H).

^{13}C NMR (101 MHz, CDCl_3) δ 148.27, 134.23, 129.82, 126.34, 122.47, 119.91, 47.94, 39.90, 32.18, 31.69.

MS(ESI): m/z $\text{C}_{17}\text{H}_{20}\text{N}_2$; calcd. [M]: 252.36, found [M + 1]: 253, [M + Na^+]: 275.

3-(5H-dibenzo[*b,f*]azepin-5-yl)propan-1-amine (8):

The title compound **8** was obtained as yellow solid by using Method B. Yield 79%.

^1H NMR (401 MHz, CDCl_3) δ 7.24 (t, J = 7.7 Hz, 2H), 7.07 – 6.92 (m, 6H), 6.71 (s, 2H), 3.78 (t, J = 6.5, 2H), 2.74 (t, J = 6.7 Hz, 2H), 1.69 (t, J = 6.6 Hz, 2H).

^{13}C NMR (101 MHz, CDCl_3) δ 188.54, 150.76, 133.85, 132.14, 129.14, 128.80, 123.31, 120.26, 48.20, 40.05, 30.68.

MS(ESI): m/z $\text{C}_{17}\text{H}_{18}\text{N}_2$; calcd. [M]: 250.35, found [M + 1]: 251, [M + Na^+]: 273.

3-(9H-carbazol-9-yl)propan-1-amine (9):

The title compound **9** was obtained as yellow oil by using Method B. Yield 77%.

^1H NMR (401 MHz, CDCl_3) δ 8.08 (d, J = 7.8 Hz, 2H), 7.49 – 7.38 (m, 4H), 7.27 – 7.17 (m, 2H), 4.40 (t, J = 6.8 Hz, 2H), 2.74 (t, J = 6.9 Hz, 2H), 2.01 (p, J = 6.9 Hz, 2H), 1.67 (s, 1H).

^{13}C NMR (101 MHz, CDCl_3) δ 140.37, 125.60, 120.32, 118.78, 108.59, 40.44, 39.58, 32.44.

MS(ESI): m/z $\text{C}_{15}\text{H}_{16}\text{N}_2$; calcd. [M]: 224.31, found [M + 1]: 225, [M + Na^+]: 247.

3-(10H-phenothiazin-10-yl)propan-1-amine (10):

The title compound **10** was obtained as yellowish oil by using Method B. Yield 98%.

¹H NMR (401 MHz, CDCl₃) δ 7.14 - 7.18 (m, 4H), 6.96 - 6.86 (m, 4H), 3.95 (t, *J* = 6.7 Hz, 2H), 2.82 (t, *J* = 6.8 Hz, 2H), 1.95 (q, *J* = 6.7 Hz, 2H).

¹³C NMR (101 MHz, CDCl₃) δ 145.26, 127.53, 127.25, 125.37, 122.53, 115.58, 53.45, 44.79, 39.63, 30.09.

MS(ESI): *m/z* C₁₅H₁₆N₂S; calcd. [M]: 256.37, found [M + 1]: 257, [M + Na⁺]: 279.

3-(2-chloro-10H-phenothiazin-10-yl)propan-1-amine (11):

The title compound **11** was obtained as yellow oil by using Method B. Yield 87%.

¹H NMR (401 MHz, CD₃OD) δ 7.13 (t, *J* = 8.0 Hz, 1H), 7.04 (d, *J* = 8.1 Hz, 1H), 6.97 - 6.84 (m, 4H), 6.82 (d, *J* = 8.3 Hz, 1H), 3.82 (t, *J* = 6.7 Hz, 2H), 2.67 (t, *J* = 7.1 Hz, 2H), 1.82 (m, 2H).

¹³C NMR (101 MHz, CD₃OD) δ 146.64, 144.45, 133.00, 127.58, 127.31, 127.02, 124.86, 123.89, 122.76, 121.98, 115.94, 115.63, 44.64, 38.80, 29.27.

MS(ESI): *m/z* C₁₅H₁₅ClN₂S; calcd. [M]: 290.81, found [M + 1]: 291, [M + Na⁺]: 323.

3-(2-(trifluoromethyl)-10H-phenothiazin-10-yl)propan-1-amine (12):

The title compound **12** was obtained as yellowish oil by using Method B. Yield 48%.

¹H NMR (401 MHz, CDCl₃) δ 7.20 - 7.03 (m, 4H), 6.93 - 6.87 (m, 3H), 3.94 (t, *J* = 6.7 Hz, 2H), 2.80 (t, *J* = 6.7 Hz, 2H), 1.89 (t, *J* = 6.7 Hz, 2H).

¹³C NMR (101 MHz, CDCl₃) δ 145.69, 144.38, 130.16, 130.02, 129.70, 129.38, 129.06, 128.21, 127.65, 127.59, 127.51, 125.51, 124.25, 123.13, 122.81, 120.11, 119.16, 119.12, 119.08, 119.04, 115.93, 111.98, 111.94, 111.90, 111.87, 44.93, 39.51, 30.11.

MS(ESI): *m/z* C₁₆H₁₅F₃N₂S; calcd. [M]: 324.37, found [M + 1]: 325, [M + Na⁺]: 347.

General procedure for the preparation of secondary amines (13-24):

To a solution of formaldehyde (1 mmol) in MeOH (5 mL), 20 mg of clay K10 was added and left stirred at rt for 15 min in a pressured-microwave tube. Then, the appropriate primary amine **1-12** (1.5 mmol) was added to the reaction mixture and was submitted to irradiation for 30 min at 80 °C. A mixture of 10 mg of clay K10 with sodium borohydride (1.5 mmol) was then added to the reaction after cooling down to 0°C. It was allowed to reach rt and was irradiated again for 10 min at 80 °C. It was then diluted with MeOH, filtered, concentrated to dryness and purified by flash chromatography on silica gel using a gradient of DCM/MeOH/33% aq. NH₃ solution (from 9.5: 0.5: 0.05 to 9: 1: 0.1) to give secondary amines **13-24**.

2-(10,11-dihydro-5H-dibenzo[*b,f*]azepin-5-yl)-N-methylethan-1-amine (13):

The title compound **13** was obtained as yellow oil. Yield 37%.

¹H NMR (401 MHz, CDCl₃) δ 7.15 - 7.07 (m, 6H), 6.91 (m, 2H), 3.87 (t, *J* = 6.3 Hz, 2H), 3.15 (s, 4H), 2.75 (t, *J* = 6.3 Hz, 2H), 2.35 (s, 3H).

¹³C NMR (101 MHz, CD₃OD) δ 147.44, 134.50, 129.82, 126.42, 123.32, 119.00, 46.72, 46.42, 32.69, 31.52.

MS(ESI): *m/z* C₁₇H₂₀N₂; calcd. [M]: 252.36, found [M + 1]: 253, [M + Na⁺]: 275.

2-(5H-dibenzo[*b,f*]azepin-5-yl)-N-methylethan-1-amine (14):

The title compound **14** was obtained as yellow oil. Yield 42%.

^1H NMR (401 MHz, CDCl_3) δ 7.08 – 6.95 (m, 6H), 6.73 (s, 2H), 3.87 (t, $J = 5.9$ Hz, 2H), 2.70 (s, 3H).

^{13}C NMR (101 MHz, CDCl_3) δ 150.18, 134.02, 132.05, 129.18, 128.92, 123.63, 120.67, 49.78, 48.64, 35.82.

MS(ESI): m/z $\text{C}_{17}\text{H}_{18}\text{N}_2$; calcd. [M]: 250.35, found [M + 1]: 251, [M + Na^+]: 272.

2-(9H-carbazol-9-yl)-N-methylethan-1-amine (15):

The title compound **15** was obtained as yellow oil. Yield 31%.

^1H NMR (401 MHz, CDCl_3) δ 8.10 (d, $J = 7.8$ Hz, 2H), 7.47 (d, $J = 4.0$ Hz, 4H), 7.25 (q, $J = 3.8$ Hz, 2H), 4.47 (t, $J = 6.1$ Hz, 2H), 3.08 (m, 2H), 2.42 (s, 3H).

^{13}C NMR (101 MHz, CDCl_3) δ 140.52, 125.76, 122.91, 120.36, 119.05, 108.70, 43.15, 41.33, 29.71.

MS(ESI): m/z $\text{C}_{17}\text{H}_{18}\text{N}_2$; calcd. [M]: 224.31, found [M + 1]: 225, [M + Na^+]: 247.

N-methyl-2-(10H-phenothiazin-10-yl)ethan-1-amine (16):

The title compound **16** was obtained as yellow oil. Yield 38%.

^1H NMR (401 MHz, CDCl_3) δ 7.19 – 7.11 (m, 4H), 6.98 – 6.85 (m, 4H), 4.13 (t, $J = 6.0$ Hz, 2H), 3.04 (t, $J = 5.9$ Hz, 2H), 2.45 (s, 3H), 2.00 (br s, 1H, exch).

^{13}C NMR (101 MHz, CDCl_3) δ 145.01, 127.41, 127.29, 124.67, 122.50, 115.25, 56.59, 46.37, 45.83.

MS(ESI): m/z $\text{C}_{16}\text{H}_{16}\text{N}_2\text{S}$; calcd. [M]: 256.37, found [M + 1]: 257, [M + Na^+]: 279.

2-(2-chloro-10H-phenothiazin-10-yl)-N-methylethan-1-amine (17):

The title compound **17** was obtained as yellow oil. Yield 29%.

^1H NMR (401 MHz, CDCl_3) δ 7.21 – 7.10 (m, 4H), 6.95 – 6.85 (m, 4H), 4.01 – 3.92 (m, 2H), 2.75 – 2.67 (m, 2H), 2.34 (s, 3H).

^{13}C NMR (101 MHz, CDCl_3) δ 128.75, 128.38, 123.87, 123.22, 116.60, 116.48, 57.43, 46.78, 31.81.

MS(ESI): m/z $\text{C}_{16}\text{H}_{15}\text{ClN}_2\text{S}$; calcd. [M]: 290.81, found [M + 1]: 291, [M + Na^+]: 313.

N-methyl-2-(2-(trifluoromethyl)-10H-phenothiazin-10-yl)ethan-1-amine (18):

The title compound **18** was obtained as yellow oil. Yield 26%.

^1H NMR (401 MHz, CDCl_3) δ 7.24 – 7.09 (m, 5H), 7.01 – 6.91 (m, 2H), 4.06 – 3.98 (m, 2H), 2.76 – 2.67 (m, 2H), 2.34 (s, 3H).

^{13}C NMR (101 MHz, CDCl_3) δ 145.96, 144.75, 130.40, 128.29, 128.06, 127.93, 126.01, 124.11, 123.70, 123.32, 119.70, 119.67, 116.12, 112.42, 112.38, 110.56, 57.03, 47.32, 46.40.

MS(ESI): m/z $\text{C}_{16}\text{H}_{15}\text{F}_3\text{N}_2\text{S}$; calcd. [M]: 324.37, found [M + 1]: 325, [M + Na^+]: 347.

3-(10,11-dihydro-5H-dibenzo[*b,f*]azepin-5-yl)-N-methylpropan-1-amine (19):

The title compound **19** was obtained as pale yellow oil. Yield 44%.

^1H NMR (401 MHz, CDCl_3) δ 7.13 – 7.03 (m, 3H), 6.90 (t, $J = 8.0$ Hz, 1H), 3.78 (t, $J = 6.7$ Hz, 2H), 3.27 (s, 1H, exch), 3.14 (s, 3H), 2.64 (t, $J = 7.1$ Hz, 1H), 1.84 – 1.76 (m, 2H).

^{13}C NMR (101 MHz, CDCl_3) δ 148.29, 134.23, 129.85, 126.39, 122.49, 119.96, 49.74, 48.50, 36.35, 32.23, 27.94.

MS(ESI): m/z $\text{C}_{18}\text{H}_{22}\text{N}_2$; calcd. [M]: 266.39, found [M + 1]: 267, [M + Na^+]: 289.

3-(5*H*-dibenzo[*b,f*]azepin-5-yl)-*N*-methylpropan-1-amine (**20**):

The title compound **20** was obtained as yellow oil. Yield 36%.

¹H NMR (401 MHz, CDCl₃) δ 7.24 (t, *J* = 7.8 Hz, 2H), 7.07 - 6.96 (m, 4H), 6.74 (s, 2H), 3.80 (t, *J* = 6.4 Hz, 2H), 2.70 (t, *J* = 6.7 Hz, 2H), 2.32 (s, 3H), 1.78 (t, *J* = 6.6 Hz, 2H).

¹³C NMR (101 MHz, CDCl₃) δ 150.40, 133.72, 132.09, 129.17, 128.93, 123.51, 120.17, 49.61, 48.66, 35.54, 26.03.

MS(ESI): *m/z* C₁₈H₂₀N₂; calcd. [M]: 264.37, found [M + 1]: 265, [M + Na⁺]: 287.

3-(9*H*-carbazol-9-yl)-*N*-methylpropan-1-amine (**21**):

The title compound **21** was obtained as yellowish oil. Yield 35%.

¹H NMR (401 MHz, CDCl₃) δ 8.10 (d, *J* = 7.8 Hz, 2H), 7.45 (m, 4H), 7.23 (t, *J* = 7.9 Hz, 2H), 4.39 (t, *J* = 6.8 Hz, 2H), 2.61 (t, *J* = 6.9 Hz, 2H), 2.40 (s, 3H), 2.05 (p, *J* = 6.9 Hz, 2H).

¹³C NMR (101 MHz, CDCl₃) δ 140.48, 125.73, 122.89, 120.40, 118.89, 108.72, 49.16, 40.76, 36.27, 29.01.

MS(ESI): *m/z* C₁₆H₁₈N₂; calcd. [M]: 238.33, found [M + 1]: 239, [M + Na⁺]: 261.

N-methyl-3-(10*H*-phenothiazin-10-yl)propan-1-amine (**22**):

The title compound **22** was obtained as yellow oil. Yield 28%.

¹H NMR (401 MHz, CDCl₃) δ 7.17 - 7.13 (m, 4H), 6.96 - 6.85 (m, 4H), 3.91 (t, *J* = 7.0 Hz, 2H), 2.41 (t, *J* = 7.1 Hz, 2H), 2.20 (s, 3H), 2.00 - 1.92 (m, 2H).

¹³C NMR (101 MHz, CDCl₃) δ 150.90, 145.79, 127.97, 127.73, 125.68, 122.93, 116.05, 57.70, 46.09, 45.91, 25.76.

MS(ESI): *m/z* C₁₆H₁₈N₂S; calcd. [M]: 270.39, found [M + 1]: 271, [M + Na⁺]: 293.

3-(2-chloro-10*H*-phenothiazin-10-yl)-*N*-methylpropan-1-amine (**23**):

The title compound **23** was obtained as yellow oil. Yield 30%.

¹H NMR (401 MHz, CDCl₃) δ 7.19 - 7.10 (m, 2H), 7.03 (d, *J* = 8.7 Hz, 1H), 6.98 - 6.86 (m, 4H), 3.89 (dd, *J* = 7.7, 6.3 Hz, 2H), 2.41 (t, *J* = 7.0 Hz, 2H), 2.23 (s, 3H), 1.99 - 1.90 (m, 2H).

¹³C NMR (101 MHz, CDCl₃) δ 127.84, 127.47, 127.37, 122.83, 122.20, 115.85, 115.78, 57.00, 45.56, 45.45, 25.06.

MS(ESI): *m/z* C₁₆H₁₇ClN₂S; calcd. [M]: 304.84, found [M + 1]: 305, [M + Na⁺]: 327.

N-methyl-3-(2-(trifluoromethyl)-10*H*-phenothiazin-10-yl)propan-1-amine (**24**):

The title compound **24** was obtained as yellow oil. Yield 24%.

¹H NMR (401 MHz, CD₃OD) δ 7.26 - 7.12 (m, 5H), 7.04 (s, 1H), 6.97 (s, 1H), 4.04 - 3.97 (m, 2H), 2.68 (m, 2H), 2.31 (s, 3H), 1.95 (m, 2H).

¹³C NMR (101 MHz, CD₃OD) δ 145.64, 144.39, 127.61, 127.51, 127.42, 123.04, 119.03, 118.99, 115.84, 111.90, 111.87, 56.99, 45.54, 45.52, 24.99.

MS(ESI): *m/z* C₁₇H₁₇F₃N₂S; calcd. [M]: 338.39, found [M + 1]: 339, [M + Na⁺]: 361.

General procedure for the preparation of tertiary amines (25-36):

Method C To a suspension of primary amines **1-3** and **7-9** (1 mmol) in H₂O (4 mL), 37% aq. formaldehyde (10 mmol) and 90% aq. formic acid (5 mmol) solutions were

sequentially added in a pressure-tight microwave tube cooled to 0 °C. After 5 min, the reaction was allowed to reach rt, and then was submitted to microwave irradiation for 1 h at 100°C, with an irradiation power of 50 W. The reaction mixture was neutralized with NaHCO₃, followed by extraction with DCM (3x). The collected organic extracts were dried over Na₂SO₄, and evaporated in vacuum to give crude products, which were purified by column chromatography on silica gel with an eluent of DCM/MeOH/33% aq. NH₃ solution.

Method D To a suspension of primary amines **4-6** and **10-12** (1 mmol) in H₂O (4 mL), 37% aq. formaldehyde (10 mmol) and 90% aq. formic acid (5 mmol) solutions were sequentially added in a pressure tube cooled to 0 °C. After 5 min, the reaction was allowed to reach rt, and then was warmed at 80°C for 8 h. The reaction mixture was neutralized with NaHCO₃, followed by extraction with DCM (3x). The collected organic extracts were dried over Na₂SO₄, and evaporated in vacuum to give crude products, which were purified by column chromatography on silica gel with an eluent of DCM/MeOH/33% aq. NH₃ solution.

2-(10,11-dihydro-5H-dibenzo[*b,f*]azepin-5-yl)-*N,N*-dimethylethan-1-amine (**25**):

The title compound **25** was obtained as colorless oil by using Method C. Yield 56%.

¹H NMR (401 MHz, CDCl₃) δ 7.14 – 7.02 (m, 6H), 6.94 – 6.85 (m, 2H), 3.91 – 3.83 (m, 2H), 3.13 (s, 4H), 2.49 – 2.38 (m, 2H) 2.20 (s, 6H).

¹³C NMR (101 MHz, CDCl₃) δ 146.93, 145.31, 131.47, 129.20, 127.03, 124.85, 53.40, 40.15, 34.63, 31.89.

MS(ESI): *m/z* C₁₈H₂₀N₂; calcd. [M]: 266.39, found [M + 1]: 267, [M + Na⁺]: 289.

2-(5H-dibenzo[*b,f*]azepin-5-yl)-*N,N*-dimethylethan-1-amine (**26**):

The title compound **26** was obtained as yellow oil by using Method C. Yield 58%.

¹H NMR (401 MHz, CDCl₃) δ 7.22 (t, *J* = 7.8 Hz, 2H), 7.04 (m, *J* = 7.1 Hz, 4H), 6.98 (t, *J* = 7.3 Hz, 2H), 6.71 (s, 2H), 3.89 (t, *J* = 8.1 Hz, 2H), 2.55 (t, *J* = 8.1 Hz, 2H), 2.29 (s, 6H).

¹³C NMR (101 MHz, CDCl₃) δ 150.74, 133.81, 132.08, 129.11, 128.90, 123.37, 120.18, 57.22, 49.29, 45.79.

MS(ESI): *m/z* C₁₈H₂₀N₂; calcd. [M]: 264.37, found [M + 1]: 265, [M + Na⁺]: 287.

2-(9H-carbazol-9-yl)-*N,N*-dimethylethan-1-amine (**27**):

The title compound **27** was obtained as colorless oil by using Method C. Yield 56%.

¹H NMR (401 MHz, CDCl₃) δ 8.09 (t, *J* = 7.8 Hz, 1H), 7.52 – 7.35 (m, 4H), 7.30 – 7.13 (m, 2H), 4.43 (t, *J* = 7.8 Hz, 2H), 2.76 – 2.67 (m, 2H), 2.37 (s, 6H).

¹³C NMR (101 MHz, CDCl₃) δ 125.93, 125.71, 120.59, 119.47, 109.75, 108.64, 57.32, 46.07, 45.91.

MS(ESI): *m/z* C₁₆H₁₈N₂; calcd. [M]: 238.33, found [M + 1]: 239, [M + Na⁺]: 261.

N,N-dimethyl-2-(10H-phenothiazin-10-yl)ethan-1-amine (**28**):

The title compound **28** was obtained as colorless oil by using Method D. Yield 81%.

¹H NMR (401 MHz, CDCl₃) δ 7.20 – 7.09 (m, 4H), 6.93 - 6.90 (m, 4H), 4.01 (t, *J* = 7.0 Hz, 2H), 2.73 (t, *J* = 7.0 Hz, 2H), 2.34 (s, 6H).

¹³C NMR (101 MHz, CDCl₃) δ 145.01, 127.45, 127.33, 124.70, 122.55, 115.27, 105.58, 56.55, 46.29, 45.82.

MS(ESI): m/z $C_{16}H_{18}N_2S$; calcd. [M]: 270.39, found [M + 1]: 271, [M + Na⁺]: 293.

2-(2-chloro-10H-phenothiazin-10-yl)-N,N-dimethylethan-1-amine (29):

The title compound **29** was obtained as colorless oil by using Method D. Yield 72%.

¹H NMR (401 MHz, CDCl₃) δ 7.26 (s, 1H), 7.21 – 7.08 (m, 2H), 7.01 (d, J = 8.1 Hz, 1H), 6.98 – 6.85 (m, 4H), 4.01 – 3.92 (m, 2H), 2.75 – 2.62 (m, 2H), 2.33 (s, 6H).

¹³C NMR (101 MHz, CDCl₃) δ 128.76, 128.38, 123.87, 123.22, 116.60, 116.48, 57.43, 47.60, 46.78, 31.81.

MS(ESI): m/z $C_{16}H_{17}ClN_2S$; calcd. [M]: 304.84, found [M + 1]: 305, [M + Na⁺]: 327.

N,N-dimethyl-2-(2-(trifluoromethyl)-10H-phenothiazin-10-yl)ethan-1-amine (30):

The title compound **30** was obtained as yellowish oil by using Method D. Yield 45%.

¹H NMR (401 MHz, CDCl₃) δ 7.19 – 7.08 (m, 4H), 6.96 – 6.90 (m, 3H), 4.03 – 3.95 (m, 2H), 2.73 – 2.65 (m, 2H) 2.30 (s, 6H).

¹³C NMR (101 MHz, CDCl₃) δ 145.39, 144.18, 129.83, 127.72, 127.49, 127.36, 125.44, 123.54, 123.13, 122.75, 119.13, 119.10, 115.55, 111.85, 111.81, 109.99, 56.46, 46.75, 45.83.

MS(ESI): m/z $C_{16}H_{17}F_3N_2S$; calcd. [M]: 338.39, found [M + 1]: 339, [M + Na⁺]: 361.

3-(10,11-dihydro-5H-dibenzo[b,f]azepin-5-yl)-N,N-dimethylpropan-1-amine (31):

The title compound **31** was obtained as pale yellow oil by using Method C. Yield 61%.

¹H NMR (401 MHz, CDCl₃) δ 7.19 – 6.93 (m, 6H), 6.97 – 6.85 (m, 2H), 3.76 (t, J = 6.9 Hz, 3H), 3.15 (s, 4H), 2.30 (t, J = 7.8 Hz, 2H), 2.14 (s, 6H), 1.72 (p, J = 7.1 Hz, 2H).

¹³C NMR (101 MHz, CDCl₃) δ 148.28, 134.19, 129.74, 126.32, 122.36, 119.97, 57.63, 48.82, 45.45, 32.20, 26.11.

MS(ESI): m/z $C_{19}H_{24}N_2$; calcd. [M]: 280.42, found [M + 1]: 281, [M + Na⁺]: 303.

3-(5H-dibenzo[b,f]azepin-5-yl)-N,N-dimethylpropan-1-amine (32):

The title compound **32** was obtained as yellow oil by using Method C. Yield 64%.

¹H NMR (401 MHz, CDCl₃) δ 7.19 (t, J = 8.0 Hz, 2H), 7.03 – 6.87 (m, 6H), 6.67 (s, 2H), 3.70 (t, J = 6.9 Hz, 2H), 2.31 (t, J = 7.3 Hz, 2H), 2.09 (s, 6H), 1.71 – 1.62 (m, 2H).

¹³C NMR (101 MHz, CDCl₃) δ 150.89, 133.91, 132.11, 129.11, 128.79, 123.22, 120.40, 57.35, 48.65, 45.51, 25.71.

MS(ESI): m/z $C_{19}H_{22}N_2$; calcd. [M]: 278.40, found [M + 1]: 279, [M + Na⁺]: 301.

3-(9H-carbazol-9-yl)-N,N-dimethylpropan-1-amine (33):

The title compound **33** was obtained as yellow oil by using Method C. Yield 56%.

¹H NMR (401 MHz, CDCl₃) δ 8.12 – 8.05 (m, 2H), 7.46 – 7.44 (m, 4H), 7.21 (t, J = 4.0 Hz, 2H), 4.43 – 4.34 (t, J = 7.0 Hz, 2H), 2.29 (t, J = 6.8 Hz, 2H), 2.22 (s, 6H), 2.06 – 1.97 (m, 2H).

¹³C NMR (101 MHz, CDCl₃) δ 140.44, 125.56, 122.78, 120.25, 118.71, 108.71, 56.61, 45.38, 40.65, 26.90.

MS(ESI): m/z $C_{17}H_{20}N_2$; calcd. [M]: 252.36, found [M + 1]: 253, [M + Na⁺]: 275.

N,N-dimethyl-3-(10H-phenothiazin-10-yl)propan-1-amine (34):

The title compound **34** was obtained as yellow oil by using Method D. Yield 74%.

^1H NMR (401 MHz, CDCl_3) δ 7.17 – 7.08 (m, 4H), 6.94 – 6.84 (m, 4H), 3.94 – 3.86 (m, 2H), 2.40 (t, $J = 7.1$ Hz, 2H), 2.19 (s, 6H), 1.94 (p, $J = 7.0$ Hz, 2H).

^{13}C NMR (101 MHz, CDCl_3) δ 150.35, 145.24, 127.42, 127.17, 125.13, 122.38, 115.49, 57.14, 45.54, 45.36, 25.21.

MS(ESI): m/z $\text{C}_{17}\text{H}_{20}\text{N}_2\text{S}$; calcd. [M]: 284.42, found [M + 1]: 285, [M + Na^+]: 307.

3-(2-chloro-10H-phenothiazin-10-yl)-N,N-dimethylpropan-1-amine (35):

The title compound **35** was obtained as yellow oil by using Method D. Yield 66%.

^1H NMR (401 MHz, CDCl_3) δ 7.20 – 7.09 (m, 2H), 7.05 – 6.98 (m, 1H), 6.97 – 6.85 (m, 4H), 3.88 (t, $J = 7.7$ Hz, 2H), 2.40 (t, $J = 7.0$ Hz, 2H), 2.22 (s, 6H), 2.00 – 1.88 (m, 2H).

^{13}C NMR (101 MHz, CDCl_3) δ 146.52, 144.51, 133.21, 127.84, 127.47, 124.82, 123.53, 122.83, 122.20, 115.85, 115.78, 57.00, 45.56, 45.45, 25.06.

MS(ESI): m/z $\text{C}_{17}\text{H}_{19}\text{ClN}_2\text{S}$; calcd. [M]: 318.86, found [M + 1]: 319, [M + Na^+]: 341.

N,N-dimethyl-3-(2-(trifluoromethyl)-10H-phenothiazin-10-yl)propan-1-amine (36):

The title compound **36** was obtained as yellow oil by using Method D. Yield 48%.

^1H NMR (401 MHz, CDCl_3) δ 7.18 – 7.05 (m, 5H), 6.95 – 6.89 (m, 2H), 3.92 (t, $J = 7.0$ Hz, 2H), 2.39 (t, $J = 7.0$ Hz, 2H), 2.19 (s, 6H), 1.96 – 1.88 (m, 2H).

^{13}C NMR (101 MHz, CDCl_3) δ 145.64, 144.39, 129.93, 129.40, 127.61, 127.51, 127.42, 124.05, 123.04, 119.03, 118.99, 115.84, 111.90, 111.87, 56.99, 45.54, 45.52, 24.99.

MS(ESI): m/z $\text{C}_{18}\text{H}_{19}\text{F}_3\text{N}_2\text{S}$; calcd. [M]: 352.42, found [M + 1]: 353, [M + Na^+]: 375.

Procedures for the preparation of TCA-functionalized fluorescent congeners (44-47):

10-(3-Chloropropyl)-5,5-difluoro-1,3,7,9-tetramethyl-5H-4 λ^4 ,5 λ^4 -dipyrrolo[1,2-c:2',1'-f][1,3,2]diazaborinine (39):

2,4-Dimethylpyrrole **37** (2.0 mL, 19 mmol) was added to a solution of 4-chlorobutanoyl chloride **38** (0.99 mL, 8.8 mmol) in dry DCM (20 mL) over 10 min at 0 °C. The reaction was stirred at 0 °C for 30 min, then warmed up to rt and stirred for an additional 30 min. Et_3N (3.7 mL, 26 mmol) was then added in small portions at 0 °C and the mixture was stirred at rt for 10 min. $\text{BF}_3 \cdot \text{OEt}_2$ (5.5 mL, 44 mmol) was then added in portions and the mixture was stirred at rt for 14 h. The reaction was quenched with careful addition of H_2O (20 mL) and the system was stirred vigorously for 15 min. The aqueous layer was extracted with DCM (3 \times 10 mL). The organic layers were combined and washed with brine (10 mL). The organic layer was dried over Na_2SO_4 , filtered, and the solvent was removed under reduced pressure, taking care not to heat the crude mixture. The brown residue was purified by chromatography on silica gel using as eluent (DCM/petroleum ether/Tol 6:3:1). The resulting residue was further purified by recrystallization from toluene to yield 0.90 g (32 %) of **39** as a red needles. ^1H -NMR (401 MHz, CDCl_3) δ 6.04 (s, 2H), 3.68 (t, $J = 6.0$ Hz, 2H), 3.11 (t, $J = 8.0$ Hz, 2H), 2.50 (s, 6H), 2.42 (s, 6H), 2.09 - 2.04 (q, $J = 6.4$ Hz, 2H). ^{13}C -NMR (101 MHz, CDCl_3) δ 154.13, 144.40, 140.30, 131.39, 121.84, 44.70, 34.00, 16.55, 14.44.

10-(3-Azidopropyl)-5,5-difluoro-1,3,7,9-tetramethyl-5H-4 λ ⁴,5 λ ⁴-dipyrrolo[1,2-c:2',1'-f][1,3,2]diazaborinine (**40**):

Sodium azide (240 mg, 3.6 mmol) was added to a solution of **39** (600 mg, 1.9 mmol) in dry DMF (36 mL). The mixture was stirred at 40 °C for 36 h. H₂O (20 mL) was then added and the suspension was extracted with DCM (3 x 20 mL). The combined organic layers were washed with brine (20 mL). The organic layer was dried over Na₂SO₄, filtered and the solvent was removed under reduced pressure to afford 600 mg (99 %) of **40** as an orange solid. ¹H-NMR (401 MHz, CDCl₃) δ 6.02 (s, 2H), 3.43 (t, *J* = 6.4 Hz, 2H), 2.95 (t, *J* = 8.4 Hz, 2H), 2.49 (s, 6H), 2.36 (s, 6H), 1.87 - 1.82 (q, *J* = 6.4 Hz, 2H). ¹³C-NMR (101 MHz, CDCl₃) δ 154.20, 144.69, 140.35, 131.32, 121.81, 51.46, 30.95, 25.52, 16.26, 14.40.

pent-4-yn-1-yl 4-methylbenzenesulfonate (**42**):

To a solution of pent-4-yn-1-ol **41** (0.31 mL, 3.34 mmol), Et₃N (0.56 mL, 4.01 mmol), and 4-(dimethylamino)pyridine (0.008 mg, 3.07 mmol) in DCM (10 mL) at 0 °C was added *p*-toluenesulfonyl chloride (0.67 g, 3.51 mmol) portion wise. The reaction mixture was brought to rt and stirred for 15 h. Aqueous NaOH (1 N, 6 mL) was added, and the mixture was vigorously stirred for 15 min at rt. The usual workup (DCM, brine), followed by flash chromatography (petroleum ether/EtOAc 7:3) gave the title compound **42** as yellow oil (88% yield). ¹H-NMR (401 MHz, CDCl₃) δ 7.58 (d, *J* = 8.0 Hz, 2H), 7.17 (d, *J* = 8.0 Hz, 2H), 3.94 (t, *J* = 6.0 Hz, 2H), 2.22 (s, 3H), 2.05 - 2.01 (td, *J*₁ = 6.8 Hz, *J*₂ = 2.8 Hz, 2H), 1.81 (t, *J* = 2.4 Hz, 1H), 1.63 (q, *J* = 6.0 Hz, 2H). ¹³C-NMR (101 MHz, CDCl₃) δ 144.85, 132.71, 129.88, 127.67, 82.14, 69.73, 68.85, 27.54, 21.32, 14.44.

N-(3-(10,11-dihydro-5H-dibenzo[b,f]azepin-5-yl)propyl)but-3-yn-1-amine (**44**):

A mixture of **7** (0.15 g, 0.61 mmol), 4-bromobut-1-yne **43** (28 μ L, 0.30 mmol) in a mixture of H₂O/CHCl₃ (70:30, 3 mL) and 10% aq. NaOH (0.9 mL) was placed in a microwave tube. The tube was subjected to MW irradiation at 140 °C for 10 min, with an irradiation power of 200 W. Removal of the solvent under reduced pressure, followed by column chromatography on silica gel using DCM/MeOH/33% aq. NH₃ solution (9.6: 0.4: 0.02) afforded final compound **44** as colorless oil (53%). ¹H-NMR (401 MHz, CDCl₃) δ 7.15 - 7.08 (m, 6H), 6.93 - 6.90 (m, 2H), 3.81 (t, *J* = 6.8 Hz, 2H), 3.16 (s, 4H), 2.72 (t, *J* = 6.8 Hz, 2H), 2.66 (t, *J* = 6.8 Hz, 2H), 2.35 - 2.32 (m, *J*₁ = 6.4 Hz, *J*₂ = 2.4 Hz, 2H), 1.90 (t, *J* = 2.8 Hz, 1H), 1.77 (q, *J* = 6.8 Hz, 2H). ¹³C-NMR (101 MHz, CDCl₃) δ 145.70, 131.67, 127.23, 123.77, 119.87, 117.36, 79.83, 66.92, 45.83, 45.28, 44.44, 29.62, 25.65, 16.91.

N-(3-(10,11-dihydro-5H-dibenzo[b,f]azepin-5-yl)propyl)-N-methylbut-3-yn-1-amine (**45**):

To a solution of **19** (0.07 g, 0.26 mmol) in acetone (8 mL), Et₃N (0.11 mL, 0.79 mmol), 4-bromobut-1-yne **43** (0.12 g, 0.52 mmol) and DMAP (0.01 g, 0.08 mmol) were sequentially added in a pressure tube and resulting mixture was refluxed for 72 h. Then, the solvent was evaporated and the crude residue chromatographed with DCM/MeOH/33% aq. NH₃ solution (9.6: 0.4: 0.02) to afford **45** as yellow oil (40%).

¹H-NMR (401 MHz, CDCl₃) δ 7.14 - 7.07 (m, 6H), 6.92 - 6.89 (m, 2H), 3.77 (t, *J* = 6.4 Hz, 2H), 3.16 (s, 4H), 2.52 (t, *J* = 7.2 Hz, 2H), 2.42 (t, *J* = 6.8 Hz, 2H), 2.26 (dd, *J*₁ = 6.8 Hz, *J*₂ = 1.6 Hz, 2H), 2.17 (s, 3H), 1.91 (s, 1H), 1.72 (q, *J* = 7.2 Hz, 2H).

¹³C-NMR (100MHz, CDCl₃) δ 148.28, 134.20, 129.77, 126.33, 122.38, 119.97, 68.90, 55.98, 55.01, 48.69, 41.98, 32.22, 25.61, 16.87.

N-(3-(10,11-dihydro-5H-dibenzo[b,f]azepin-5-yl)propyl)pent-4-yn-1-amine (46):

A mixture of **7** (0.15 g, 0.61 mmol), **42** (0.07 mg, 0.30 mmol) in a mixture of H₂O/CHCl₃ (70:30, 3 mL) and 10% aq. NaOH (0.9 mL) was placed in a microwave tube. The tube was subjected to MW irradiation at 140 °C for 10 min, with an irradiation power of 200 W. Removal of the solvents under reduced pressure, followed by column chromatography on silica gel using DCM/MeOH/33% aq. NH₃ solution (9.6: 0.4: 0.02) afforded final compound **46** as colorless oil (53%).

¹H-NMR (401 MHz, CDCl₃) δ 7.13 - 7.05 (m, 6H), 6.91 - 6.87 (m, 2H), 3.78 (t, *J* = 6.8 Hz, 2H), 3.14 (s, 4H), 2.64 (t, *J* = 6.8 Hz, 4H), 2.19 (td, *J*₁ = 7 Hz, *J*₂ = 2.8 Hz, 2H), 1.89 (t, *J* = 2.8 Hz, 1H), 1.74 (q, *J* = 7.2 Hz, 2H), 1.63 (q, *J* = 6.8 Hz, 2H).

¹³C-NMR (101 MHz, CDCl₃) δ 148.26, 134.21, 129.79, 126.32, 122.43, 119.92, 84.02, 68.49, 48.65, 48.49, 47.50, 32.17, 28.52, 28.24, 16.28.

N-(3-(10,11-dihydro-5H-dibenzo[b,f]azepin-5-yl)propyl)-N-methylpent-4-yn-1-amine (47):

To a solution of **19** (0.07 g, 0.26 mmol) in acetone (8 mL), Et₃N (0.11 mL, 0.79 mmol), **42** (0.12 g, 0.52 mmol) and DMAP (0.01 g, 0.08 mmol) were sequentially added in a pressure tube and resulting mixture was refluxed for 72 h. Then, the solvent was evaporated and the crude residue chromatographed with DCM/MeOH/33% aq. NH₃ solution (9.6: 0.4: 0.02) to afford **47** as yellow oil (63%).

¹H-NMR (401 MHz, CDCl₃) δ 7.12 - 7.07 (m, 6H), 6.92 - 6.88 (m, 2H), 3.76 (t, *J* = 6.8 Hz, 2H), 3.16 (s, 4H), 2.35 (q, *J* = 6.8 Hz, 4H), 2.15 - 2.13 (td, *J*₁ = 7Hz, *J*₂ = 2,4 Hz, 2H), 2.12 (s, 3H), 1.89 (t, *J* = 2.8 Hz, 1H), 1.71 (q, *J* = 6.8 Hz, 2H), 1.60 (q, *J* = 7.2 Hz, 2H).

¹³C-NMR (101 MHz, CDCl₃) δ 148.31, 134.18, 129.75, 126.32, 122.33, 119.99, 84.32, 68.28, 56.33, 55.39, 48.74, 42.24, 32.25, 26.15, 25.71, 16.21.

General click procedure for the preparation of TCA-functionalized fluorescent congeners (48-51):

The alkyne congener **44-47** (1.0 mmol) was dissolved in a 1:1:1 mixture of *t*-BuOH, H₂O and DCM (10 mL). To this solution, the azide **40** (1.2 mmol) was added while stirring vigorously at rt. Copper (II) sulfate pentahydrate (15 mol%) and sodium ascorbate (45 mol%) were then added sequentially to the reaction mixture, which was left stirring for 1-2 h under nitrogen. The solvents were then removed under vacuum and the resulting residue was purified by column chromatography on silica gel and, when needed, recrystallized to afford compounds **48-51**.

N-(2-(1-(3-(5,5-difluoro-1,3,7,9-tetramethyl-5H-4λ⁴,5λ⁴-dipyrrolo[1,2-c:2',1'-f][1,3,2]diazaborinin-10-yl)propyl)-1H-1,2,3-triazol-4-yl)ethyl)-3-(10,11-dihydro-5H-dibenzo[b,f]azepin-5-yl)propan-1-amine (48):

The resulting residue was purified by flash chromatography, using as eluent $\text{CHCl}_3/\text{EtOH}/33\% \text{ aq. NH}_3$ solution (9.5: 0.5: 0.05), and then recrystallized from EtOH and H_2O to afford **48** as orange needles (33% yield).

$^1\text{H-NMR}$ (401 MHz, CDCl_3) δ 7.15 (s, 1H), 7.12 - 7.03 (m, 6H), 6.89 - 6.86 (m, 2H), 6.01 (s, 2H), 4.35 (t, $J = 5.6$ Hz, 2H), 3.73 (t, $J = 6.4$ Hz, 2H), 3.12 (s, 4H), 2.93 (t, $J = 8.4$ Hz, 2H), 2.80 (t, $J = 7.2$ Hz, 2H), 2.57 (t, $J = 7.2$ Hz, 2H), 2.49 (s, 6H) 2.42 (t, $J = 6.4$ Hz, 2H), 2.16 (m, 9H), 2.08 (q, 2H), 1.71 (q, $J = 6.4$ Hz, 2H).

$^{13}\text{C-NMR}$ (101 MHz, CDCl_3) δ 154.48, 148.29, 146.69, 143.78, 140.09, 134.20, 131.25, 129.81, 126.31, 122.41, 121.92, 121.47, 119.90, 57.09, 54.98, 49.78, 48.41, 42.07, 32.30, 32.15, 25.61, 25.54, 23.65, 16.07, 14.45.

$^{11}\text{B-NMR}$ (128 MHz, CDCl_3) δ 1.18 (t, $J = 32.64$ Hz, B-F).

$^{19}\text{F-NMR}$ (377 MHz, CDCl_3) δ -146.60 (m).

MS(ESI): m/z $\text{C}_{38}\text{H}_{46}\text{BF}_2\text{N}_7$; calcd. [M]: 649.64, found [M + 1]: 650, [M + Na⁺]: 672, [M + K⁺]: 688.

N-(2-(1-(3-(5,5-difluoro-1,3,7,9-tetramethyl-5H-4 λ^4 ,5 λ^4 -dipyrrolo[1,2-c:2',1'-f][1,3,2]diazaborinin-10-yl)propyl)-1H-1,2,3-triazol-4-yl)ethyl)-3-(10,11-dihydro-5H-dibenzo[b,f]azepin-5-yl)-N-methylpropan-1-amine (**49**):

The resulting residue was purified by flash chromatography, using as eluent DCM/petroleum ether/Tol/MeOH/33% aq. NH_3 solution (7.5: 0.5: 1: 1: 0.1), and then recrystallized from toluene to afford **49** as orange needles (33% yield).

$^1\text{H-NMR}$ (401 MHz, CDCl_3) δ 7.18 (s, 1H), 7.11 - 7.04 (m, 6H), 6.90 - 6.86 (m, 2H), 6.00 (s, 2H), 4.40 (t, $J = 6$ Hz, 2H), 3.76 (t, $J = 6.8$ Hz, 2H), 3.12 (s, 4H), 2.94 (td, $J_1 = 8.4$ Hz, $J_2 = 3.2$ Hz, 2H), 2.84 (m, $J = 6.4$ Hz, 4H), 2.65 (t, $J = 6.8$ Hz, 2H), 2.48 (s, 6H), 2.16 (s, 6H), 2.10 (q, $J = 8.8$ Hz, 2H), 1.17 (q, $J = 6.8$ Hz, 2H).

$^{13}\text{C-NMR}$ (101 MHz, CDCl_3) δ 154.51, 148.22, 146.43, 143.68, 140.05, 134.20, 131.22, 129.81, 126.33, 122.46, 121.93, 121.55, 119.89, 49.85, 48.98, 48.33, 47.28, 32.25, 32.13, 28.23, 26.02, 25.51, 16.07, 14.44.

$^{11}\text{B-NMR}$ (128.5MHz, CDCl_3) δ 1.19 (t, $J = 32.6$ Hz, B-F).

$^{19}\text{F-NMR}$ (377MHz, CDCl_3) δ -146.56 (m).

MS (ESI): m/z $\text{C}_{37}\text{H}_{44}\text{BF}_2\text{N}_7$; calcd. [M]: 635.61, found [M + 1]: 636, [M + Na⁺]: 658, [M + K⁺]: 675.

3-(1-(3-(5,5-difluoro-1,3,7,9-tetramethyl-5H-4 λ^4 ,5 λ^4 -dipyrrolo[1,2-c:2',1'-f][1,3,2]diazaborinin-10-yl)propyl)-1H-1,2,3-triazol-4-yl)-N-(3-(10,11-dihydro-5H-dibenzo[b,f]azepin-5-yl)propyl)propan-1-amine (**50**):

The resulting residue was purified by flash chromatography, using as eluent DCM/petroleum ether/Tol/MeOH/33% aq. NH_3 solution (7.5: 0.5: 1: 1: 0.1) to afford **50** as orange waxy solid (38% yield).

$^1\text{H-NMR}$ (401 MHz, CDCl_3) δ 7.19 (s, 1H), 7.11 - 7.06 (m, 6H), 6.90 - 6.87 (m, 2H), 6.00 (s, 2H), 4.43 (t, $J = 6.4$ Hz, 2H), 3.77 (t, $J = 6.4$ Hz, 2H), 3.12 (s, 4H), 2.95 (m, $J = 8.4$ Hz, 2H), 2.70 (t, $J = 7.2$ Hz, 2H), 2.63 (m, 4H), 2.48 (s, 6H), 2.16 (s, 6H), 2.12 (q, $J = 6.4$ Hz, 2H), 1.80 (m, 4H).

$^{13}\text{C-NMR}$ (101 MHz, CDCl_3) δ 154.48, 148.22, 148.04, 143.70, 140.08, 134.19, 131.24, 129.79, 126.35, 122.46, 121.93, 120.95, 119.90, 49.86, 49.03, 48.46, 47.50, 32.27, 32.15, 29.54, 28.06, 25.52, 23.29, 16.06, 14.44.

$^{11}\text{B-NMR}$ (128.5Hz, CDCl_3) δ 1.19 (t, $J = 32.64$ Hz, B-F).

¹⁹F-NMR (400MHz, CDCl₃) δ -146.53 (m).

MS (ESI): m/z C₃₈H₄₆BF₂N₇; calcd. [M]: 649.64, found [M + 1]: 650, [M + Na⁺]: 672.

3-(1-(3-(5,5-difluoro-1,3,7,9-tetramethyl-5H-4λ⁴,5λ⁴-dipyrrolo[1,2-c:2',1'-f][1,3,2]diazaborinin-10-yl)propyl)-1H-1,2,3-triazol-4-yl)-N-(3-(10,11-dihydro-5H-dibenzo[b,f]azepin-5-yl)propyl)-N-methylpropan-1-amine (51):

The resulting residue was purified twice by flash chromatography, using as eluent DCM/petroleum ether/Tol/MeOH/33% aq. NH₃ solution (7.5: 0.5: 1: 1: 0.1) to afford **51** as orange waxy solid (39% yield).

¹H-NMR (401 MHz, CDCl₃) δ 7.18 (s, 1H), 7.12 - 7.05 (m, 6H), 6.89 - 6.86 (m, 2H), 6.01 (s, 2H), 4.43 (t, *J* = 6 Hz, 2H), 3.75 (t, *J* = 6.8 Hz, 2H), 3.13 (s, 4H), 2.96 (m, *J*₁ = 8.4 Hz, *J*₂ = 2.8 Hz, 2H), 2.65 (t, *J* = 7.6 Hz, 2H), 2.49 (s, 6H), 2.37 (t, *J* = 6.8 Hz, 2H), 2.31 (t, *J* = 7.2 Hz, 2H), 2.17 (s, 6H), 2.12 (m, 5H), 1.75 (q, *J* = 6.8 Hz, 2H), 1.70 (q, *J* = 6.8 Hz, 2H).

¹³C-NMR (101 MHz, CDCl₃) δ 154.48, 148.31, 143.73, 140.09, 134.18, 131.25, 129.75, 126.32, 122.34, 121.93, 120.85, 119.96, 57.07, 55.42, 49.83, 48.71, 42.25, 32.32, 32.21, 27.26, 25.70, 25.54, 23.39, 16.08, 14.44.

¹¹B-NMR (128 MHz, CDCl₃) δ 1.20 (t, *J* = 32.64 Hz, B-F).

¹⁹F-NMR (377MHz, CDCl₃) δ -146.55 (m).

MS (ESI): m/z C₃₉H₄₈BF₂N₇; calcd. [M]: 663.67, found [M + 1]: 664, [M + Na⁺]: 686.

General procedure for the preparation of hybrids (53-58):

A solution of valproic acid **52** (1.07 mmol) in DCM (7 mL), Et₃N (2.92 mmol), hydroxybenzotriazole (HOBT; 1.70 mmol), 1-ethyl-3-[3-(dimethylamino)propyl]carbodiimide hydrochloride (EDCI; 2.92 mmol) was cooled to 0 °C and stirred for 30 min. A solution of the appropriate amine (**1-3** and **7-9**, 1 mmol) and Et₃N (2.92 mmol) in DCM (2 mL) was subsequently added, and the mixture was stirred overnight at rt under nitrogen. The solvent was removed under vacuum, and the obtained residue was purified by flash chromatography on silica gel using as eluent a mixture of DCM/MeOH.

N-(2-(10,11-dihydro-5H-dibenzo[b,f]azepin-5-yl)ethyl)-2-propylpentanamide (53):

The resulting residue was purified twice by flash chromatography, using as eluent DCM/MeOH (10: 0.05) and then petroleum ether/EtOAc (6: 4), to afford **53** as white solid (78% yield).

¹H NMR (401 MHz, CDCl₃) δ 7.17 – 7.03 (m, 6H), 6.92 (t, *J* = 7.3 Hz, 2H), 5.57 (br s, 1H, exch), 3.88 (t, *J* = 5.8 Hz, 2H), 3.41 (q, *J* = 5.7 Hz, 2H), 3.15 (s, 4H), 1.96 – 1.88 (m, 1H), 1.54 – 1.42 (m, 2H), 1.35 – 1.21 (m, 2H), 1.21 – 1.07 (m, 4H), 0.78 (t, *J* = 7.3 Hz, 3H).

¹³C NMR (101 MHz, CDCl₃) δ 176.06, 147.55, 134.00, 129.92, 126.65, 122.98, 119.89, 49.74, 47.87, 37.44, 35.25, 32.29, 20.79, 14.03.

N-(2-(5H-dibenzo[b,f]azepin-5-yl)ethyl)-2-propylpentanamide (54):

The resulting residue was purified by flash chromatography (6: 4 petroleum ether/EtOAc), to afford **54** as pale yellow solid. Yield 81%.

¹H NMR (401 MHz, CDCl₃) δ 7.30 – 7.21 (m, 2H), 7.11 – 6.96 (m, 6H), 6.76 (s, 2H), 6.02 (br s, 1H, exch), 3.90 – 3.82 (m, 2H), 3.37 (t, *J* = 5.4 Hz, 2H), 1.95 – 1.90 (m, 1H), 1.52 – 1.39 (m, 2H), 1.33 – 1.20 (m, 2H), 1.18 – 1.03 (m, 4H), 0.76 (t, *J* = 7.3 Hz, 3H).

^{13}C NMR (101 MHz, CDCl_3) δ 176.10, 149.63, 133.92, 132.10, 129.22, 129.17, 123.92, 120.71, 49.73, 47.75, 36.31, 35.21, 20.74, 14.03.

N-(2-(9*H*-carbazol-9-yl)ethyl)-2-propylpentanamide (55):

The resulting residue was purified by flash chromatography (10: 0.05 DCM/MeOH) affording **55** as white solid. Yield 73%.

^1H NMR (401 MHz, CDCl_3) δ 8.08 (d, $J = 7.8$ Hz, 2H), 7.48 – 7.41 (m, 4H), 7.28 – 7.19 (m, 2H), 5.48 (br s, 1H, exch), 4.47 (t, $J = 6.2$ Hz, 2H), 3.72 (q, $J = 6.2$ Hz, 2H), 1.53 – 1.44 (m, 2H), 1.88 – 1.81 (m, 1H), 1.35 – 1.11 (m, 6H), 0.82 (t, $J = 7.2$ Hz, 3H).

^{13}C NMR (101 MHz, CDCl_3) δ 176.60, 140.29, 125.84, 122.93, 120.37, 119.22, 108.68, 47.42, 42.41, 38.32, 34.90, 20.76, 14.08.

N-(3-(10,11-dihydro-5*H*-dibenzo[*b,f*]azepin-5-yl)propyl)-2-propylpentanamide (56):

The resulting residue was purified by flash chromatography (9.8:0.2 DCM/MeOH) affording **56** as white solid. Yield 77%.

^1H NMR (401 MHz, CDCl_3) δ 7.16 – 7.01 (m, 6H), 6.91 (t, $J = 7.3$ Hz, 2H), 3.77 (t, $J = 6.7$ Hz, 2H), 3.28 (q, $J = 6.7$ Hz, 2H), 3.15 (s, 4H), 1.90 (m, 1H), 1.78 (q, $J = 6.7$ Hz, 2H), 1.59 – 1.43 (m, 2H), 1.36 – 1.07 (m, 6H), 0.82 (t, $J = 7.1$ Hz, 3H).

^{13}C NMR (101 MHz, CDCl_3) δ 175.92, 148.05, 134.17, 129.89, 126.41, 122.62, 120.29, 119.80, 48.01, 37.03, 35.22, 32.16, 27.87, 20.81, 14.08.

N-(3-(5*H*-dibenzo[*b,f*]azepin-5-yl)propyl)-2-propylpentanamide (57):

The resulting residue was purified by flash chromatography (9.6:0.4 DCM/MeOH) affording **57** as white solid. Yield 86%.

^1H NMR (401 MHz, CDCl_3) δ 7.31 – 7.22 (m, 2H), 7.08 (m, 2H), 7.00 (m, 4H), 6.78 (s, 2H), 6.14 (br s, 1H, exch), 3.81 (t, $J = 5.9$ Hz, 1H), 3.30 (q, $J = 5.9$ Hz, 1H), 1.95 – 1.87 (m, 1H), 1.76 (p, $J = 7.1$ Hz, 2H), 1.45 (m, 2H), 1.32 – 1.03 (m, 6H), 0.78 (t, $J = 7.2$ Hz, 3H).

^{13}C NMR (101 MHz, CDCl_3) δ 175.96, 150.26, 133.45, 132.29, 129.20, 129.13, 123.64, 120.10, 49.02, 47.52, 38.17, 35.15, 26.06, 20.75, 14.10.

N-(3-(9*H*-carbazol-9-yl)propyl)-2-propylpentanamide (58):

The resulting residue was purified by flash chromatography (9.8:0.2 DCM/MeOH) affording **58** as white solid. Yield 97%.

^1H NMR (401 MHz, CDCl_3) δ 8.09 (d, $J = 8.0$ Hz, 2H), 7.45 (t, $J = 7.1$, 2H), 7.38 (d, $J = 8.2$ Hz, 2H), 7.24 – 7.21 (m, 2H), 5.30 (br s, 1H, exch), 4.36 (t, $J = 6.8$ Hz, 2H), 3.27 (q, $J = 6.6$ Hz, 2H), 2.08 (p, $J = 6.9$ Hz, 2H), 1.84 – 1.77 (m, 1H), 1.51 – 1.36 (m, 2H), 1.32 – 1.04 (m, 6H), 0.82 (m, 3H).

^{13}C NMR (101 MHz, CDCl_3) δ 176.05, 140.08, 125.80, 122.88, 120.47, 119.06, 108.44, 47.68, 40.90, 37.33, 35.11, 29.03, 20.78, 14.05.

Procedures for the preparation of TCA-functionalized polyamine congener (65):

4-[3-Amino-propyl)-tert-butoxycarbonyl-amino]- butyl}-carbamic acid tert-Butyl Ester (60):

To a solution of 1,4-diaminobutane **59** (0.34 mL, 0.67 mmol) in CHCl₃ (5 mL) was added tert-butyl dicarbonate (0.24 mL, 1.03 mmol) portion wise at 0 °C. The reaction was stirred at 0 °C for 3 h, and then the solvents were removed in vacuo. The resulting residue was washed with H₂O (10 mL) for 30 min, and then the insoluble bis-substituted product was removed by filtration. The filtrate was extracted with DCM (3 × 10 mL), and the organic layers were combined, washed with brine (30 mL), and dried over Na₂SO₄. The solvents were removed in vacuo to afford a pale yellow oil **60** (69% yield).

¹H-NMR (401 MHz, CDCl₃) δ 4.74 (s, 1H), 3.07 (m, 2H), 2.67 (t, *J* = 7.2 Hz, 2H), 1.43 (m, 4H), 1.38 (s, 9H) 1.33 (s, 2H).

¹³C-NMR (101 MHz, CDCl₃) δ 155.98, 78.93, 41.73, 40.36, 30.79, 28.37, 27.43.

3-((3-(10,11-dihydro-5H-dibenzo[*b,f*]azepin-5-yl)propyl)(methylamino)propan-1-ol (**62**):

A mixture of **19** (0.14 g, 0.54 mmol), 3-bromopropan-1-ol **61** (0.07 mg, 0.54 mmol) in a mixture of H₂O/CHCl₃ (70:30, 2 mL) and 10% aq. NaOH (0.5 mL) was placed in a microwave tube. The tube was subjected to MW irradiation at 140 °C for 10 min, with an irradiation power of 200 W. Removal of the solvents under reduced pressure, followed by column chromatography on silica gel using DCM/MeOH/33% aq. NH₃ solution (9.6: 0.4: 0.02) afforded final compound **62** as colorless oil (23%).

¹H NMR (401 MHz, CDCl₃) δ 7.18 – 7.05 (m, 6H), 6.92 (t, *J* = 7.2 Hz, 2H), 3.81 – 3.69 (m, 4H), 3.16 (s, 4H), 2.50 (t, *J* = 5.7 Hz, 2H), 2.46 – 2.36 (m, 2H), 2.15 (s, 3H), 1.74 (q, *J* = 7.1 Hz, 2H), 1.69 – 1.58 (m, 2H).

¹³C NMR (101 MHz, CDCl₃) δ 148.17, 134.17, 129.79, 126.42, 122.46, 119.95, 64.50, 58.26, 56.04, 48.76, 41.98, 32.23, 27.79, 25.59.

3-chloro-*N*-(3-(10,11-dihydro-5H-dibenzo[*b,f*]azepin-5-yl)propyl)-*N*-methylpropan-1-amine (**63**):

To a solution of **62** (0.87 g, 0.27 mmol) in CHCl₃ (3 mL) was added SOCl₂ (0.04 mL, 0.53 mmol) dropwise at 0 °C. The resulting mixture was stirred at rt for 4 h under nitrogen and then was quenched by adding NaHCO₃ saturated solution (15 mL). The aqueous phase was extracted with DCM (3 x 10 mL) and the organic layers were combined, washed with brine (30 mL), and dried over Na₂SO₄. The resulting residue was purified by column chromatography to give the title compound **63** as colorless oil (45% yield).

¹H NMR (401 MHz, CDCl₃) δ 7.13 – 7.05 (m, 6H), 6.90 (t, *J* = 7.2 Hz, 2H), 3.76 (t, *J* = 6.7 Hz, 2H), 3.47 (t, *J* = 6.5 Hz, 2H), 3.15 (s, 4H), 2.37 (q, *J* = 7.0, 5.0 Hz, 2H), 2.11 (s, 3H), 1.82 (m, 2H), 1.70 (p, *J* = 6.9, 12 Hz, 2H).

¹³C NMR (101 MHz, CDCl₃) δ 148.22, 134.15, 129.76, 126.33, 122.34, 119.94, 55.30, 54.50, 48.54, 43.17, 42.23, 32.23, 30.25, 25.59.

tert-butyl (4-(((3-(10,11-dihydro-5H-dibenzo[*b,f*]azepin-5-yl)propyl)(methylamino)propyl)amino)butyl)carbamate (**64**):

A mixture of **63** (0.04 g, 0.12 mmol), **60** (0.04 mg, 0.24 mmol) in CH₃CN (1.2 mL) was placed in a microwave tube. The tube was subjected to MW irradiation at 110 °C for 1 h, with an irradiation power of 50 W. Removal of the solvents under reduced

pressure, followed by column chromatography on silica gel using a gradient of DCM/MeOH/33% aq. NH₃ solution (from 9: 1: 0.1 to 8.5: 1.5: 0.15) afforded final compound **64** as yellow oil (65%).

¹H NMR (401 MHz, CDCl₃) δ 7.11 – 7.04 (m, 6H), 6.88 (t, *J* = 7.4 Hz, 2H), 4.87 (br s, 1H, exch), 3.73 (t, *J* = 6.6 Hz, 2H), 3.13 (s, 4H), 3.06 (m, 2H), 2.76 (t, *J* = 6.5 Hz, 2H), 2.60 (t, *J* = 7.3 Hz, 2H), 2.39 (m, 4H), 2.13 (s, 3H), 1.72 (dt, *J* = 27.8, 6.8 Hz, 4H), 1.56 (t, *J* = 7.4 Hz, 2H), 1.45 (m, 11H).

¹³C NMR (101 MHz, CDCl₃) δ 156.06, 148.07, 134.10, 129.80, 126.40, 122.51, 119.91, 56.67, 55.51, 48.61, 48.27, 48.00, 41.73, 39.85, 32.16, 28.41, 27.35, 25.51, 24.90.

*N*¹-(3-((3-(10,11-dihydro-5*H*-dibenzo[*b,f*]azepin-5-yl)propyl)(methyl)amino)propyl)-*N*⁴-methylbutane-1,4-diamine (**65**):

To a solution of the protected amine **64** (0.04 g, 0.08 mmol) in DCM (2 mL), TFA (93 μL, 1.21 mmol) was added dropwise at 0°C. The resulting solution was left to stir at room temperature for 3 h. The solvent was then evaporated under vacuum washing with heptane (3 times) to remove the excess of TFA. The solid residues were repeatedly triturated with diethyl ether and filtered to afford the title compound **65** as pale yellow solid (90%).

¹H NMR (401 MHz, CD₃OD) δ 7.25 – 7.14 (m, 6H), 7.05 – 6.94 (m, 2H), 3.93 (t, *J* = 6.5 Hz, 2H), 3.38 - 3.11 (m, 7H), 3.1 – 3.09 (m, 4H), 3.03 (t, *J* = 7.1 Hz, 2H), 2.80 (s, 3H), 2.21 – 2.02 (m, 4H), 1.91 – 1.73 (m, 4H).

¹³C NMR (101 MHz, CD₃OD) δ 147.70, 134.12, 129.59, 126.27, 122.75, 119.31, 54.52, 52.57, 46.85, 46.81, 44.22, 39.00, 38.52, 31.71, 24.07, 22.73, 22.18, 20.87.

Native fluorescence study of 48-51

General information

All the spectra were recorded using a Jasco FP-750 spectrofluorometer, equipped with the control and data acquisition software FP-750. Both excitation and emission slits were set up at 5 nm bandwidth, and 1 cm quartz cells were employed.

General procedure

Accurately weighed amounts of the studied compounds were dissolved using ethanol or DCM to obtain 1 mM stock solutions. From these stocks, intermediate dilutions were prepared as required. The final concentration of the compounds was 0.5 μM.

References

- [1] (a) Martin, G. R. Isolation of a pluripotent cell line from early mouse embryos cultured in medium conditioned by teratocarcinoma stem cells. *Proc Natl Acad Sci USA* **1981**, *78* (12), 7634-8; (b) Evans, M. J.; Kaufman, M. H. Establishment in culture of pluripotential cells from mouse embryos. *Nature* **1981**, *292* (5819), 154-6.
- [2] Thomson, J. A.; Itskovitz-Eldor, J.; Shapiro, S. S.; Waknitz, M. A.; Swiergiel, J. J.; Marshall, V. S.; Jones, J. M. Embryonic stem cell lines derived from human blastocysts. *Science* **1998**, *282* (5391), 1145-7.
- [3] Have We Entered the Stem Cell Era? <http://discovermagazine.com/2009/nov/14-have-we-entered-the-stem-cell-era> (accessed Feb. 20, 2016).
- [4] Takahashi, K.; Tanabe, K.; Ohnuki, M.; Narita, M.; Ichisaka, T.; Tomoda, K.; Yamanaka, S. Induction of pluripotent stem cells from adult human fibroblasts by defined factors. *Cell* **2007**, *131* (5), 861-72.
- [5] Yu, J.; Vodyanik, M. A.; Smuga-Otto, K.; Antosiewicz-Bourget, J.; Frane, J. L.; Tian, S.; Nie, J.; Jonsdottir, G. A.; Ruotti, V.; Stewart, R.; Slukvin, I.; Thomson, J. A. Induced pluripotent stem cell lines derived from human somatic cells. *Science* **2007**, *318* (5858), 1917-20.
- [6] Lensch, M. W.; Mummery, C. L. From stealing fire to cellular reprogramming: a scientific history leading to the 2012 Nobel Prize. *Stem Cell Reports* **2013**, *1* (1), 5-17.
- [7] Stem Cell Basics. <http://stemcells.nih.gov/staticresources/info/basics/SCprimer2009.pdf> (accessed Feb. 20, 2016).
- [8] Reya, T.; Morrison, S. J.; Clarke, M. F.; Weissman, I. L. Stem cells, cancer, and cancer stem cells. *Nature* **2001**, *414* (6859), 105-11.
- [9] Liu, Y.; Yang, R.; He, Z.; Gao, W. Q. Generation of functional organs from stem cells. *Cell Regen* **2013**, *2* (1), 1.
- [10] Raveh-Amit, H.; Berzsenyi, S.; Vas, V.; Ye, D.; Dinnyes, A. Tissue resident stem cells: till death do us part. *Biogerontology* **2013**, *14* (6), 573-590.
- [11] Tang, S.; Xie, M.; Cao, N.; Ding, S. Patient-Specific Induced Pluripotent Stem Cells for Disease Modeling and Phenotypic Drug Discovery. *J Med Chem* **2016**, *59* (1), 2-15.
- [12] Mack, D. L.; Guan, X.; Wagoner, A.; Walker, S. J.; Childers, M. K. Disease-in-a-dish: the contribution of patient-specific induced pluripotent stem cell technology to regenerative rehabilitation. *Am J Phys Med Rehabil* **2014**, *93* (11 Suppl 3), S155-68.
- [13] Zhao, C.; Deng, W.; Gage, F. H. Mechanisms and functional implications of adult neurogenesis. *Cell* **2008**, *132* (4), 645-60.
- [14] Global number of HSCTs hits 1 million. http://www.hematologytimes.com/p_article.do?id=2979 (accessed Feb. 16, 2016).
- [15] Holoclar ex vivo expanded autologous human corneal epithelial cells containing stem cells. http://www.ema.europa.eu/ema/index.jsp?curl=pages/medicines/human/medicines/002450/human_med_001844.jsp&mid=WC0b01ac058001d124 (accessed Feb. 20, 2016).
- [16] Piltti, K. M.; Salazar, D. L.; Uchida, N.; Cummings, B. J.; Anderson, A. J. Safety of human neural stem cell transplantation in chronic spinal cord injury. *Stem Cells Transl Med* **2013**, *2* (12), 961-74.
- [17] Portal, T. S. C. Neural Stem Cells Safe for Chronic Spinal Cord Injury Therapy - See more at: <http://stemcellportal.com/content/neural-stem-cells-safe-chronic-spinal-cord-injury-therapy> - sthash.1RslWUIG.LXeA02hQ.dpuf. <http://stemcellportal.com/content/neural-stem-cells-safe-chronic-spinal-cord-injury-therapy> - sthash.1RslWUIG.dpuf (accessed Feb 20, 2016).
- [18] Chen, K. G.; Mallon, B. S.; McKay, R. D.; Robey, P. G. Human pluripotent stem cell culture: considerations for maintenance, expansion, and therapeutics. *Cell Stem Cell* **2014**, *14* (1), 13-26.
- [19] Ao, A.; Hao, J.; Hong, C. C. Regenerative chemical biology: current challenges and future potential. *Chem Biol* **2011**, *18* (4), 413-24.
- [20] Zhu, S.; Wei, W.; Ding, S. Chemical strategies for stem cell biology and regenerative medicine. *Annu Rev Biomed Eng* **2011**, *13*, 73-90.
- [21] Li, W.; Li, K.; Wei, W.; Ding, S. Chemical approaches to stem cell biology and therapeutics. *Cell Stem Cell* **2013**, *13* (3), 270-83.

- [22] Xu, Y.; Shi, Y.; Ding, S. A chemical approach to stem-cell biology and regenerative medicine. *Nature* **2008**, *453* (7193), 338-44.
- [23] Zhang, Y.; Li, W.; Laurent, T.; Ding, S. Small molecules, big roles -- the chemical manipulation of stem cell fate and somatic cell reprogramming. *J Cell Sci* **2012**, *125* (Pt 23), 5609-20.
- [24] (a) Lairson, L. L.; Lyssiotis, C. A.; Zhu, S.; Schultz, P. G. Small molecule-based approaches to adult stem cell therapies. *Annu Rev Pharmacol Toxicol* **2013**, *53*, 107-25; (b) Davies, S. G.; Kennewell, P. D.; Russell, A. J.; Seden, P. T.; Westwood, R.; Wynne, G. M. Stemistry: The Control of Stem Cells in Situ Using Chemistry. *Journal of Medicinal Chemistry* **2015**, *58* (7), 2863-2894.
- [25] Xia, X.; Wong, S. T. Concise review: a high-content screening approach to stem cell research and drug discovery. *Stem Cells* **2012**, *30* (9), 1800-7.
- [26] Gage, F. H.; Temple, S. Neural stem cells: generating and regenerating the brain. *Neuron* **2013**, *80* (3), 588-601.
- [27] Colucci-D'Amato, L.; Bonavita, V.; di Porzio, U. The end of the central dogma of neurobiology: stem cells and neurogenesis in adult CNS. *Neurol Sci* **2006**, *27* (4), 266-70.
- [28] Goldman, S. A.; Nottebohm, F. Neuronal production, migration, and differentiation in a vocal control nucleus of the adult female canary brain. *Proc Natl Acad Sci U S A* **1983**, *80* (8), 2390-4.
- [29] Reynolds, B. A.; Weiss, S. Generation of neurons and astrocytes from isolated cells of the adult mammalian central nervous system. *Science* **1992**, *255* (5052), 1707-10.
- [30] Kornblum, H. I. Introduction to neural stem cells. *Stroke* **2007**, *38* (2 Suppl), 810-6.
- [31] Doetsch, F.; Caille, I.; Lim, D. A.; Garcia-Verdugo, J. M.; Alvarez-Buylla, A. Subventricular zone astrocytes are neural stem cells in the adult mammalian brain. *Cell* **1999**, *97* (6), 703-16.
- [32] Fuentealba, L. C.; Obernier, K.; Alvarez-Buylla, A. Adult neural stem cells bridge their niche. *Cell Stem Cell* **2012**, *10* (6), 698-708.
- [33] Reekmans, K.; Praet, J.; Daans, J.; Reumers, V.; Pauwels, P.; Van der Linden, A.; Berneman, Z. N.; Ponsaerts, P. Current challenges for the advancement of neural stem cell biology and transplantation research. *Stem Cell Rev* **2012**, *8* (1), 262-78.
- [34] Bonaguidi, M. A.; Wheeler, M. A.; Shapiro, J. S.; Stadel, R. P.; Sun, G. J.; Ming, G. L.; Song, H. In vivo clonal analysis reveals self-renewing and multipotent adult neural stem cell characteristics. *Cell* **2011**, *145* (7), 1142-55.
- [35] (a) Sun, G. J.; Zhou, Y.; Stadel, R. P.; Moss, J.; Yong, J. H.; Ito, S.; Kawasaki, N. K.; Phan, A. T.; Oh, J. H.; Modak, N.; Reed, R. R.; Toni, N.; Song, H.; Ming, G. L. Tangential migration of neuronal precursors of glutamatergic neurons in the adult mammalian brain. *Proc Natl Acad Sci U S A* **2015**, *112* (30), 9484-9; (b) Seri, B.; Garcia-Verdugo, J. M.; McEwen, B. S.; Alvarez-Buylla, A. Astrocytes give rise to new neurons in the adult mammalian hippocampus. *J Neurosci* **2001**, *21* (18), 7153-60.
- [36] Bond, A. M.; Ming, G. L.; Song, H. Adult Mammalian Neural Stem Cells and Neurogenesis: Five Decades Later. *Cell Stem Cell* **2015**, *17* (4), 385-95.
- [37] Conti, L.; Cattaneo, E. Neural stem cell systems: physiological players or in vitro entities? *Nat Rev Neurosci* **2010**, *11* (3), 176-87.
- [38] Zhang, J.; Jiao, J. Molecular Biomarkers for Embryonic and Adult Neural Stem Cell and Neurogenesis. *Biomed Res Int* **2015**, *2015*, 727542.
- [39] Urban, N.; Guillemot, F. Neurogenesis in the embryonic and adult brain: same regulators, different roles. *Front Cell Neurosci* **2014**, *8*, 396.
- [40] Gratzner, H. G. Monoclonal antibody to 5-bromo- and 5-iododeoxyuridine: A new reagent for detection of DNA replication. *Science* **1982**, *218* (4571), 474-5.
- [41] Lendahl, U.; Zimmerman, L. B.; McKay, R. D. CNS stem cells express a new class of intermediate filament protein. *Cell* **1990**, *60* (4), 585-95.
- [42] Sugawara, K.; Kurihara, H.; Negishi, M.; Saito, N.; Nakazato, Y.; Sasaki, T.; Takeuchi, T. Nestin as a marker for proliferative endothelium in gliomas. *Lab Invest* **2002**, *82* (3), 345-51.
- [43] Mokry, J.; Cizkova, D.; Filip, S.; Ehrmann, J.; Osterreicher, J.; Kolar, Z.; English, D. Nestin expression by newly formed human blood vessels. *Stem Cells Dev* **2004**, *13* (6), 658-64.
- [44] Suzuki, S.; Namiki, J.; Shibata, S.; Mastuzaki, Y.; Okano, H. The neural stem/progenitor cell marker nestin is expressed in proliferative endothelial cells, but not in mature vasculature. *J Histochem Cytochem* **2010**, *58* (8), 721-30.
- [45] von Bohlen Und Halbach, O. Immunohistological markers for staging neurogenesis in adult hippocampus. *Cell Tissue Res* **2007**, *329* (3), 409-20.

- [46] Verwer, R. W.; Sluiter, A. A.; Balesar, R. A.; Baayen, J. C.; Noske, D. P.; Dirven, C. M.; Wouda, J.; van Dam, A. M.; Lucassen, P. J.; Swaab, D. F. Mature astrocytes in the adult human neocortex express the early neuronal marker doublecortin. *Brain* **2007**, *130* (Pt 12), 3321-35.
- [47] Pinto, L.; Gotz, M. Radial glial cell heterogeneity--the source of diverse progeny in the CNS. *Prog Neurobiol* **2007**, *83* (1), 2-23.
- [48] Seki, T.; Sato, T.; Toda, K.; Osumi, N.; Imura, T.; Shioda, S. Distinctive population of Gfap-expressing neural progenitors arising around the dentate notch migrate and form the granule cell layer in the developing hippocampus. *J Comp Neurol* **2014**, *522* (2), 261-83.
- [49] Novitsch, B. G.; Chen, A. I.; Jessell, T. M. Coordinate regulation of motor neuron subtype identity and pan-neuronal properties by the bHLH repressor Olig2. *Neuron* **2001**, *31* (5), 773-89.
- [50] Jakovcevski, I.; Zecevic, N. Olig transcription factors are expressed in oligodendrocyte and neuronal cells in human fetal CNS. *J Neurosci* **2005**, *25* (44), 10064-73.
- [51] Ligon, K. L.; Alberta, J. A.; Kho, A. T.; Weiss, J.; Kwaan, M. R.; Nutt, C. L.; Louis, D. N.; Stiles, C. D.; Rowitch, D. H. The oligodendroglial lineage marker OLIG2 is universally expressed in diffuse gliomas. *J Neuropathol Exp Neurol* **2004**, *63* (5), 499-509.
- [52] Russell, A. J. Regenerative medicinal chemistry: the in situ control of stem cells. *ACS Med Chem Lett* **2013**, *4* (4), 365-8.
- [53] Davies, S. G.; Kennewell, P. D.; Russell, A. J.; Seden, P. T.; Westwood, R.; Wynne, G. M. Stemistry: the control of stem cells in situ using chemistry. *J Med Chem* **2015**, *58* (7), 2863-94.
- [54] Erickson-Miller, C. L.; DeLorme, E.; Tian, S. S.; Hopson, C. B.; Stark, K.; Giampa, L.; Valoret, E. I.; Duffy, K. J.; Luengo, J. L.; Rosen, J.; Miller, S. G.; Dillon, S. B.; Lamb, P. Discovery and characterization of a selective, nonpeptidyl thrombopoietin receptor agonist. *Exp Hematol* **2005**, *33* (1), 85-93.
- [55] GSK. GSK gains FDA Breakthrough Therapy designation for Promacta®/Revolade® (eltrombopag) for severe aplastic anaemia. <https://http://www.gsk.com/en-gb/media/press-releases/2014/gsk-gains-fda-breakthrough-therapy-designation-for-promactarevolade-eltrombopag-for-severe-aplastic-anaemia/> (accessed Feb 20, 2016).
- [56] Malberg, J. E.; Eisch, A. J.; Nestler, E. J.; Duman, R. S. Chronic antidepressant treatment increases neurogenesis in adult rat hippocampus. *J Neurosci* **2000**, *20* (24), 9104-10.
- [57] Chen, S.; Do, J. T.; Zhang, Q.; Yao, S.; Yan, F.; Peters, E. C.; Scholer, H. R.; Schultz, P. G.; Ding, S. Self-renewal of embryonic stem cells by a small molecule. *Proc Natl Acad Sci U S A* **2006**, *103* (46), 17266-71.
- [58] Thisse, B.; Thisse, C. Functions and regulations of fibroblast growth factor signaling during embryonic development. *Dev Biol* **2005**, *287* (2), 390-402.
- [59] Strickland, S.; Mahdavi, V. The induction of differentiation in teratocarcinoma stem cells by retinoic acid. *Cell* **1978**, *15* (2), 393-403.
- [60] Ding, S.; Wu, T. Y.; Brinker, A.; Peters, E. C.; Hur, W.; Gray, N. S.; Schultz, P. G. Synthetic small molecules that control stem cell fate. *Proc Natl Acad Sci U S A* **2003**, *100* (13), 7632-7.
- [61] Rhim, J. H.; Luo, X.; Xu, X.; Gao, D.; Zhou, T.; Li, F.; Qin, L.; Wang, P.; Xia, X.; Wong, S. T. A High-content screen identifies compounds promoting the neuronal differentiation and the midbrain dopamine neuron specification of human neural progenitor cells. *Sci Rep* **2015**, *5*, 16237.
- [62] Mehta, G.; Samineni, R.; Srihari, P.; Reddy, R. G.; Chakravarty, S. Diverted organic synthesis (DOS): accessing a new, natural product inspired, neurotrophically active scaffold through an intramolecular Pauson-Khand reaction. *Org Biomol Chem* **2012**, *10* (34), 6830-3.
- [63] Chakravarty, S.; Maitra, S.; Reddy, R. G.; Das, T.; Jhelum, P.; Kootar, S.; Rajan, W. D.; Samanta, A.; Samineni, R.; Pabbaraja, S.; Kernie, S. G.; Mehta, G.; Kumar, A. A novel natural product inspired scaffold with robust neurotrophic, neurogenic and neuroprotective action. *Sci Rep* **2015**, *5*, 14134.
- [64] Jung, D. W.; Kim, W. H.; Williams, D. R. Reprogram or reboot: small molecule approaches for the production of induced pluripotent stem cells and direct cell reprogramming. *ACS Chem Biol* **2014**, *9* (1), 80-95.
- [65] Wu, M. Z.; Li, M.; Liu, G. H.; Izpisua Belmonte, J. C. A chemical approach to "rewire" neural progenitor cells. *Cell Res* **2014**, *24* (6), 641-2.
- [66] Cheng, L.; Hu, W.; Qiu, B.; Zhao, J.; Yu, Y.; Guan, W.; Wang, M.; Yang, W.; Pei, G. Generation of neural progenitor cells by chemical cocktails and hypoxia. *Cell Res* **2014**, *24* (6), 665-79.
- [67] Cheng, L.; Gao, L.; Guan, W.; Mao, J.; Hu, W.; Qiu, B.; Zhao, J.; Yu, Y.; Pei, G. Direct conversion of astrocytes into neuronal cells by drug cocktail. *Cell Res* **2015**, *25* (11), 1269-72.

- [68] Hu, W.; Qiu, B.; Guan, W.; Wang, Q.; Wang, M.; Li, W.; Gao, L.; Shen, L.; Huang, Y.; Xie, G.; Zhao, H.; Jin, Y.; Tang, B.; Yu, Y.; Zhao, J.; Pei, G. Direct Conversion of Normal and Alzheimer's Disease Human Fibroblasts into Neuronal Cells by Small Molecules. *Cell Stem Cell* **2015**, *17* (2), 204-12.
- [69] Li, X.; Zuo, X.; Jing, J.; Ma, Y.; Wang, J.; Liu, D.; Zhu, J.; Du, X.; Xiong, L.; Du, Y.; Xu, J.; Xiao, X.; Wang, J.; Chai, Z.; Zhao, Y.; Deng, H. Small-Molecule-Driven Direct Reprogramming of Mouse Fibroblasts into Functional Neurons. *Cell Stem Cell* **2015**, *17* (2), 195-203.
- [70] Zhang, L.; Yin, J. C.; Yeh, H.; Ma, N. X.; Lee, G.; Chen, X. A.; Wang, Y.; Lin, L.; Chen, L.; Jin, P.; Wu, G. Y.; Chen, G. Small Molecules Efficiently Reprogram Human Astroglial Cells into Functional Neurons. *Cell Stem Cell* **2015**, *17* (6), 735-47.
- [71] Nawy, T. Stem cells: fast track to neurons. *Nat Methods* **2015**, *12* (10), 915.
- [72] Rakic, P. Adult neurogenesis in mammals: an identity crisis. *J Neurosci* **2002**, *22* (3), 614-8.
- [73] Ming, G. L.; Song, H. Adult neurogenesis in the mammalian central nervous system. *Annu Rev Neurosci* **2005**, *28*, 223-50.
- [74] Jeong, Y.; Mangelsdorf, D. J. Nuclear receptor regulation of stemness and stem cell differentiation. *Exp Mol Med* **2009**, *41* (8), 525-37.
- [75] Ma, D. K.; Marchetto, M. C.; Guo, J. U.; Ming, G. L.; Gage, F. H.; Song, H. Epigenetic choreographers of neurogenesis in the adult mammalian brain. *Nat Neurosci* **2010**, *13* (11), 1338-44.
- [76] Wada, K.; Nakajima, A.; Katayama, K.; Kudo, C.; Shibuya, A.; Kubota, N.; Terauchi, Y.; Tachibana, M.; Miyoshi, H.; Kamisaki, Y.; Mayumi, T.; Kadowaki, T.; Blumberg, R. S. Peroxisome proliferator-activated receptor gamma-mediated regulation of neural stem cell proliferation and differentiation. *J Biol Chem* **2006**, *281* (18), 12673-81.
- [77] Islam, M. M.; Zhang, C. L. TLX: A master regulator for neural stem cell maintenance and neurogenesis. *Biochim Biophys Acta* **2015**, *1849* (2), 210-6.
- [78] Qu, Q.; Sun, G.; Li, W.; Yang, S.; Ye, P.; Zhao, C.; Yu, R. T.; Gage, F. H.; Evans, R. M.; Shi, Y. Orphan nuclear receptor TLX activates Wnt/beta-catenin signalling to stimulate neural stem cell proliferation and self-renewal. *Nat Cell Biol* **2010**, *12* (1), 31-40; sup pp 1-9.
- [79] Sun, G.; Yu, R. T.; Evans, R. M.; Shi, Y. Orphan nuclear receptor TLX recruits histone deacetylases to repress transcription and regulate neural stem cell proliferation. *Proc Natl Acad Sci U S A* **2007**, *104* (39), 15282-7.
- [80] Pechnick, R. N.; Zonis, S.; Wawrowsky, K.; Cosgayon, R.; Farrokhi, C.; Lacayo, L.; Chesnokova, V. Antidepressants Stimulate Hippocampal Neurogenesis by Inhibiting p21 Expression in the Subgranular Zone of the Hippocampus. *PLoS ONE* **2011**, *6* (11), e27290.
- [81] Feng, J.; Zhou, Y.; Campbell, S. L.; Le, T.; Li, E.; Sweatt, J. D.; Silva, A. J.; Fan, G. Dnmt1 and Dnmt3a maintain DNA methylation and regulate synaptic function in adult forebrain neurons. *Nat Neurosci* **2010**, *13* (4), 423-30.
- [82] Noguchi, H.; Kimura, A.; Murao, N.; Matsuda, T.; Namihira, M.; Nakashima, K. Expression of DNMT1 in neural stem/precursor cells is critical for survival of newly generated neurons in the adult hippocampus. *Neurosci Res* **2015**, *95*, 1-11.
- [83] Cao, X.; Pfaff, S. L.; Gage, F. H. YAP regulates neural progenitor cell number via the TEA domain transcription factor. *Genes Dev* **2008**, *22* (23), 3320-34.
- [84] Ding, R.; Weynans, K.; Bossing, T.; Barros, C. S.; Berger, C. The Hippo signalling pathway maintains quiescence in Drosophila neural stem cells. *Nat Commun* **2016**, *7*, 10510.
- [85] Santucci, M.; Vignudelli, T.; Ferrari, S.; Mor, M.; Scalvini, L.; Bolognesi, M. L.; Uliassi, E.; Costi, M. P. The Hippo Pathway and YAP/TAZ-TEAD Protein-Protein Interaction as Targets for Regenerative Medicine and Cancer Treatment. *J Med Chem* **2015**, *58* (12), 4857-73.
- [86] (a) Suh, H.; Deng, W.; Gage, F. H. Signaling in adult neurogenesis. *Annu Rev Cell Dev Biol* **2009**, *25*, 253-75; (b) Faigle, R.; Song, H. Signaling mechanisms regulating adult neural stem cells and neurogenesis. *Biochim Biophys Acta* **2013**, *1830* (2), 2435-48.
- [87] Bonaguidi, M. A.; McGuire, T.; Hu, M.; Kan, L.; Samanta, J.; Kessler, J. A. LIF and BMP signaling generate separate and discrete types of GFAP-expressing cells. *Development* **2005**, *132* (24), 5503-14.
- [88] Mira, H.; Andreu, Z.; Suh, H.; Lie, D. C.; Jessberger, S.; Consiglio, A.; San Emeterio, J.; Hortiguera, R.; Marques-Torres, M. A.; Nakashima, K.; Colak, D.; Gotz, M.; Farinas, I.; Gage, F. H. Signaling through BMP-IA regulates quiescence and long-term activity of neural stem cells in the adult hippocampus. *Cell Stem Cell* **2010**, *7* (1), 78-89.

- [89] Lie, D. C.; Colamarino, S. A.; Song, H. J.; Desire, L.; Mira, H.; Consiglio, A.; Lein, E. S.; Jessberger, S.; Lansford, H.; Dearie, A. R.; Gage, F. H. Wnt signalling regulates adult hippocampal neurogenesis. *Nature* **2005**, *437* (7063), 1370-5.
- [90] Hur, E. M.; Zhou, F. Q. GSK3 signalling in neural development. *Nat Rev Neurosci* **2010**, *11* (8), 539-51.
- [91] Avila, J.; Insausti, R.; Del Rio, J. Memory and neurogenesis in aging and Alzheimer's disease. *Aging Dis* **2010**, *1* (1), 30-6.
- [92] Oliveira, S. L.; Pillat, M. M.; Cheffer, A.; Lameu, C.; Schwindt, T. T.; Ulrich, H. Functions of neurotrophins and growth factors in neurogenesis and brain repair. *Cytometry A* **2013**, *83* (1), 76-89.
- [93] Bath, K. G.; Mandairon, N.; Jing, D.; Rajagopal, R.; Kapoor, R.; Chen, Z. Y.; Khan, T.; Proenca, C. C.; Kraemer, R.; Cleland, T. A.; Hempstead, B. L.; Chao, M. V.; Lee, F. S. Variant brain-derived neurotrophic factor (Val66Met) alters adult olfactory bulb neurogenesis and spontaneous olfactory discrimination. *J Neurosci* **2008**, *28* (10), 2383-93.
- [94] Cattaneo, E.; McKay, R. Proliferation and differentiation of neuronal stem cells regulated by nerve growth factor. *Nature* **1990**, *347* (6295), 762-5.
- [95] Wang, B.; Gao, Y.; Xiao, Z.; Chen, B.; Han, J.; Zhang, J.; Wang, X.; Dai, J. Erk1/2 promotes proliferation and inhibits neuronal differentiation of neural stem cells. *Neurosci Lett* **2009**, *461* (3), 252-7.
- [96] Fernando, R. N.; Eleuteri, B.; Abdelhady, S.; Nussenzweig, A.; Andang, M.; Ernfors, P. Cell cycle restriction by histone H2AX limits proliferation of adult neural stem cells. *Proc Natl Acad Sci USA* **2011**, *108* (14), 5837-42.
- [97] Kippin, T. E.; Kapur, S.; van der Kooy, D. Dopamine specifically inhibits forebrain neural stem cell proliferation, suggesting a novel effect of antipsychotic drugs. *J Neurosci* **2005**, *25* (24), 5815-23.
- [98] Tong, C. K.; Chen, J.; Cebrian-Silla, A.; Mirzadeh, Z.; Obernier, K.; Guinto, C. D.; Tecott, L. H.; Garcia-Verdugo, J. M.; Kriegstein, A.; Alvarez-Buylla, A. Axonal control of the adult neural stem cell niche. *Cell Stem Cell* **2014**, *14* (4), 500-11.
- [99] Paez-Gonzalez, P.; Asrican, B.; Rodriguez, E.; Kuo, C. T. Identification of distinct ChAT(+) neurons and activity-dependent control of postnatal SVZ neurogenesis. *Nat Neurosci* **2014**, *17* (7), 934-42.
- [100] Pilz, G. A.; Jessberger, S. ChAT me up: how neurons control stem cells. *Nat Neurosci* **2014**, *17* (7), 897-8.
- [101] Berg, D. A.; Belnoue, L.; Song, H.; Simon, A. Neurotransmitter-mediated control of neurogenesis in the adult vertebrate brain. *Development* **2013**, *140* (12), 2548-61.
- [102] (a) Pascual-Brazo, J.; Baekelandt, V.; Encinas, J. M. Neurogenesis as a new target for the development of antidepressant drugs. *Curr Pharm Des* **2014**, *20* (23), 3763-75; (b) Pilar-Cuellar, F.; Vidal, R.; Diaz, A.; Castro, E.; dos Anjos, S.; Vargas, V.; Romero, B.; Valdizan, E. M. Signaling pathways involved in antidepressant-induced cell proliferation and synaptic plasticity. *Curr Pharm Des* **2014**, *20* (23), 3776-94.
- [103] Gould, E.; Cameron, H. A.; Daniels, D. C.; Woolley, C. S.; McEwen, B. S. Adrenal hormones suppress cell division in the adult rat dentate gyrus. *J Neurosci* **1992**, *12* (9), 3642-50.
- [104] van Praag, H.; Kempermann, G.; Gage, F. H. Running increases cell proliferation and neurogenesis in the adult mouse dentate gyrus. *Nat Neurosci* **1999**, *2* (3), 266-70.
- [105] Gould, E.; Beylin, A.; Tanapat, P.; Reeves, A.; Shors, T. J. Learning enhances adult neurogenesis in the hippocampal formation. *Nat Neurosci* **1999**, *2* (3), 260-5.
- [106] Winner, B.; Kohl, Z.; Gage, F. H. Neurodegenerative disease and adult neurogenesis. *Eur J Neurosci* **2011**, *33* (6), 1139-51.
- [107] Li, L.; Xie, T. Stem cell niche: structure and function. *Annu Rev Cell Dev Biol* **2005**, *21*, 605-31.
- [108] Kohman, R. A.; Rhodes, J. S. Neurogenesis, inflammation and behavior. *Brain Behav Immun* **2013**, *27* (1), 22-32.
- [109] Luo, X. G.; Chen, S. D. The changing phenotype of microglia from homeostasis to disease. *Transl Neurodegener* **2012**, *1* (1), 9.
- [110] Wagers, A. J. The stem cell niche in regenerative medicine. *Cell Stem Cell* **2012**, *10* (4), 362-9.
- [111] Palop, J. J.; Chin, J.; Mucke, L. A network dysfunction perspective on neurodegenerative diseases. *Nature* **2006**, *443* (7113), 768-73.

- [112] Young, A. B. Four decades of neurodegenerative disease research: how far we have come! *J Neurosci* **2009**, *29* (41), 12722-8.
- [113] Cummings, J. L.; Morstorf, T.; Zhong, K. Alzheimer's disease drug-development pipeline: few candidates, frequent failures. *Alzheimers Res. Ther.* **2014**, *6* (4), 37.
- [114] Huang, Y.; Mucke, L. Alzheimer mechanisms and therapeutic strategies. *Cell* **2012**, *148* (6), 1204-22.
- [115] Banik, A.; Brown, R. E.; Bamburg, J.; Lahiri, D. K.; Khurana, D.; Friedland, R. P.; Chen, W.; Ding, Y.; Mudher, A.; Padjen, A. L.; Mukaetova-Ladinska, E.; Ihara, M.; Srivastava, S.; Padma Srivastava, M. V.; Masters, C. L.; Kalaria, R. N.; Anand, A. Translation of Pre-Clinical Studies into Successful Clinical Trials for Alzheimer's Disease: What are the Roadblocks and How Can They Be Overcome? *J Alzheimers Dis* **2015**, *47* (4), 815-43.
- [116] Valadas, J. S.; Vos, M.; Verstreken, P. Therapeutic strategies in Parkinson's disease: what we have learned from animal models. *Ann N Y Acad Sci* **2015**, *1338*, 16-37.
- [117] Vucic, S.; Rothstein, J. D.; Kiernan, M. C. Advances in treating amyotrophic lateral sclerosis: insights from pathophysiological studies. *Trends Neurosci* **2014**, *37* (8), 433-42.
- [118] World Alzheimer Report 2015: The Global Impact of Dementia, Alzheimer's Disease International 2015. <http://www.alz.co.uk/research/statistics> (accessed Jan 20, 2016).
- [119] Blurton-Jones, M.; Kitazawa, M.; Martinez-Coria, H.; Castello, N. A.; Muller, F. J.; Loring, J. F.; Yamasaki, T. R.; Poon, W. W.; Green, K. N.; LaFerla, F. M. Neural stem cells improve cognition via BDNF in a transgenic model of Alzheimer disease. *Proc Natl Acad Sci U S A* **2009**, *106* (32), 13594-9.
- [120] Ready or Not: Stem Cell Therapies Poised to Enter Trials for Alzheimer's. <http://www.alzforum.org/news/conference-coverage/ready-or-not-stem-cell-therapies-poised-enter-trials-alzheimers> (accessed Feb 20, 2016).
- [121] FDA GRANTS IND APPROVAL FOR PHASE IIA CLINICAL TRIAL USING STEMEDICA'S ITMSC THERAPY TO TREAT ALZHEIMER'S DISEASE <http://www.stemmedica.com/info/allogeneic-adult-stem-cells/alzheimer-clinical-trial/2015-06-09-FDA-Grants-IND-Approval-for-Phase-IIa-Clinical-Trial-Using-Stemmedica-itMSC-Therapy-to-Treat-Alzheimers.asp> (accessed Feb 20, 2016).
- [122] McGinley, L. M.; Sims, E.; Lunn, J. S.; Kashlan, O. N.; Chen, K. S.; Bruno, E. S.; Pacut, C. M.; Hazel, T.; Johe, K.; Sakowski, S. A.; Feldman, E. L. Human Cortical Neural Stem Cells Expressing Insulin-Like Growth Factor-I: A Novel Cellular Therapy for Alzheimer's Disease. *Stem Cells Transl Med* **2016**, *5* (3), 379-91.
- [123] Mazzini, L.; Gelati, M.; Profico, D. C.; Sgaravizzi, G.; Progetti Pensi, M.; Muzi, G.; Ricciolini, C.; Rota Nodari, L.; Carletti, S.; Giorgi, C.; Spera, C.; Domenico, F.; Bersano, E.; Petruzzelli, F.; Cisari, C.; Maglione, A.; Sarnelli, M. F.; Stecco, A.; Querin, G.; Masiero, S.; Cantello, R.; Ferrari, D.; Zalfa, C.; Binda, E.; Visioli, A.; Trombetta, D.; Novelli, A.; Torres, B.; Bernardini, L.; Carriero, A.; Prandi, P.; Servo, S.; Cerino, A.; Cima, V.; Gaiani, A.; Nasuelli, N.; Massara, M.; Glass, J.; Soraru, G.; Boulis, N. M.; Vescovi, A. L. Human neural stem cell transplantation in ALS: initial results from a phase I trial. *J Transl Med* **2015**, *13*, 17.
- [124] Wray, S.; Fox, N. C. Stem cell therapy for Alzheimer's disease: hope or hype? *Lancet Neurol* **2015**.
- [125] Dunnett, S. B.; Rosser, A. E. Challenges for taking primary and stem cells into clinical neurotransplantation trials for neurodegenerative disease. *Neurobiol Dis* **2014**, *61*, 79-89.
- [126] Kondo, T.; Asai, M.; Tsukita, K.; Kutoku, Y.; Ohsawa, Y.; Sunada, Y.; Imamura, K.; Egawa, N.; Yahata, N.; Okita, K.; Takahashi, K.; Asaka, I.; Aoi, T.; Watanabe, A.; Watanabe, K.; Kadoya, C.; Nakano, R.; Watanabe, D.; Maruyama, K.; Hori, O.; Hibino, S.; Choshi, T.; Nakahata, T.; Hioki, H.; Kaneko, T.; Naitoh, M.; Yoshikawa, K.; Yamawaki, S.; Suzuki, S.; Hata, R.; Ueno, S.; Seki, T.; Kobayashi, K.; Toda, T.; Murakami, K.; Irie, K.; Klein, W. L.; Mori, H.; Asada, T.; Takahashi, R.; Iwata, N.; Yamanaka, S.; Inoue, H. Modeling Alzheimer's disease with iPSCs reveals stress phenotypes associated with intracellular Abeta and differential drug responsiveness. *Cell Stem Cell* **2013**, *12* (4), 487-96.
- [127] Chung, C. Y.; Khurana, V.; Auluck, P. K.; Tardiff, D. F.; Mazzulli, J. R.; Soldner, F.; Baru, V.; Lou, Y.; Freyzon, Y.; Cho, S.; Mungenast, A. E.; Muffat, J.; Mitalipova, M.; Pluth, M. D.; Jui, N. T.; Schule, B.; Lippard, S. J.; Tsai, L. H.; Krainc, D.; Buchwald, S. L.; Jaenisch, R.; Lindquist, S. Identification and rescue of alpha-synuclein toxicity in Parkinson patient-derived neurons. *Science* **2013**, *342* (6161), 983-7.
- [128] Tardiff, D. F.; Jui, N. T.; Khurana, V.; Tambe, M. A.; Thompson, M. L.; Chung, C. Y.; Kamadurai, H. B.; Kim, H. T.; Lancaster, A. K.; Caldwell, K. A.; Caldwell, G. A.; Rochet, J. C.

- Buchwald, S. L.; Lindquist, S. Yeast reveal a "druggable" Rsp5/Nedd4 network that ameliorates alpha-synuclein toxicity in neurons. *Science* **2013**, *342* (6161), 979-83.
- [129] Yang, Y. M.; Gupta, S. K.; Kim, K. J.; Powers, B. E.; Cerqueira, A.; Wainger, B. J.; Ngo, H. D.; Rosowski, K. A.; Schein, P. A.; Ackeifi, C. A.; Arvanites, A. C.; Davidow, L. S.; Woolf, C. J.; Rubin, L. L. A small molecule screen in stem-cell-derived motor neurons identifies a kinase inhibitor as a candidate therapeutic for ALS. *Cell Stem Cell* **2013**, *12* (6), 713-26.
- [130] Fava, M.; Johe, K.; Ereshefsky, L.; Gertsik, L. G.; English, B. A.; Bilello, J. A.; Thurmond, L. M.; Johnstone, J.; Dickerson, B. C.; Makris, N.; Hoepfner, B. B.; Flynn, M.; Mischoulon, D.; Kinrys, G.; Freeman, M. P. A Phase 1B, randomized, double blind, placebo controlled, multiple-dose escalation study of NSI-189 phosphate, a neurogenic compound, in depressed patients. *Mol Psychiatry* **2015**.
- [131] Lilja, T.; Heldring, N.; Hermanson, O. Like a rolling histone: epigenetic regulation of neural stem cells and brain development by factors controlling histone acetylation and methylation. *Biochim Biophys Acta* **2013**, *1830* (2), 2354-60.
- [132] Swaminathan, A.; Kumar, M.; Halder Sinha, S.; Schneider-Anthony, A.; Boutillier, A. L.; Kundu, T. K. Modulation of neurogenesis by targeting epigenetic enzymes using small molecules: an overview. *ACS Chem Neurosci* **2014**, *5* (12), 1164-77.
- [133] Hsieh, J.; Nakashima, K.; Kuwabara, T.; Mejia, E.; Gage, F. H. Histone deacetylase inhibition-mediated neuronal differentiation of multipotent adult neural progenitor cells. *Proc Natl Acad Sci U S A* **2004**, *101* (47), 16659-64.
- [134] Shen, S.; Li, J.; Casaccia-Bonnel, P. Histone modifications affect timing of oligodendrocyte progenitor differentiation in the developing rat brain. *J Cell Biol* **2005**, *169* (4), 577-89.
- [135] Schneider, J. W.; Gao, Z.; Li, S.; Farooqi, M.; Tang, T. S.; Bezprozvanny, I.; Frantz, D. E.; Hsieh, J. Small-molecule activation of neuronal cell fate. *Nat Chem Biol* **2008**, *4* (7), 408-10.
- [136] Sadek, H.; Hannack, B.; Choe, E.; Wang, J.; Latif, S.; Garry, M. G.; Garry, D. J.; Longgood, J.; Frantz, D. E.; Olson, E. N.; Hsieh, J.; Schneider, J. W. Cardiogenic small molecules that enhance myocardial repair by stem cells. *Proc Natl Acad Sci U S A* **2008**, *105* (16), 6063-8.
- [137] Hao, Y.; Creson, T.; Zhang, L.; Li, P.; Du, F.; Yuan, P.; Gould, T. D.; Manji, H. K.; Chen, G. Mood stabilizer valproate promotes ERK pathway-dependent cortical neuronal growth and neurogenesis. *J Neurosci* **2004**, *24* (29), 6590-9.
- [138] Fischer, A.; Sananbenesi, F.; Wang, X.; Dobbin, M.; Tsai, L. H. Recovery of learning and memory is associated with chromatin remodelling. *Nature* **2007**, *447* (7141), 178-82.
- [139] Lyssiotis, C. A.; Lairson, L. L.; Boitano, A. E.; Wurdak, H.; Zhu, S.; Schultz, P. G. Chemical control of stem cell fate and developmental potential. *Angew Chem Int Ed Engl* **2011**, *50* (1), 200-42.
- [140] Zhang, Q.; Major, M. B.; Takanashi, S.; Camp, N. D.; Nishiya, N.; Peters, E. C.; Ginsberg, M. H.; Jian, X.; Randazzo, P. A.; Schultz, P. G.; Moon, R. T.; Ding, S. Small-molecule synergist of the Wnt/beta-catenin signaling pathway. *Proc Natl Acad Sci U S A* **2007**, *104* (18), 7444-8.
- [141] Warashina, M.; Min, K. H.; Kuwabara, T.; Huynh, A.; Gage, F. H.; Schultz, P. G.; Ding, S. A synthetic small molecule that induces neuronal differentiation of adult hippocampal neural progenitor cells. *Angew Chem Int Ed Engl* **2006**, *45* (4), 591-3.
- [142] Wurdak, H.; Zhu, S.; Min, K. H.; Aimone, L.; Lairson, L. L.; Watson, J.; Chopiuk, G.; Demas, J.; Charette, B.; Halder, R.; Weerapana, E.; Cravatt, B. F.; Cline, H. T.; Peters, E. C.; Zhang, J.; Walker, J. R.; Wu, C.; Chang, J.; Tuntland, T.; Cho, C. Y.; Schultz, P. G. A small molecule accelerates neuronal differentiation in the adult rat. *Proc Natl Acad Sci U S A* **2010**, *107* (38), 16542-7.
- [143] Diamandis, P.; Wildenhain, J.; Clarke, I. D.; Sacher, A. G.; Graham, J.; Bellows, D. S.; Ling, E. K.; Ward, R. J.; Jamieson, L. G.; Tyers, M.; Dirks, P. B. Chemical genetics reveals a complex functional ground state of neural stem cells. *Nat Chem Biol* **2007**, *3* (5), 268-73.
- [144] Kim, K. J.; Wang, J.; Xu, X.; Wu, S.; Zhang, W.; Qin, Z.; Wu, F.; Liu, A.; Zhao, Y.; Fang, H.; Zhu, M.; Zhao, J.; Zhong, Z. A chemical genomics screen to discover genes that modulate neural stem cell differentiation. *J Biomol Screen* **2012**, *17* (2), 129-39.
- [145] Hoing, S.; Rudhard, Y.; Reinhardt, P.; Glatza, M.; Stehling, M.; Wu, G.; Peiker, C.; Bocker, A.; Parga, J. A.; Bunk, E.; Schwamborn, J. C.; Slack, M.; Sterneckert, J.; Scholer, H. R. Discovery of inhibitors of microglial neurotoxicity acting through multiple mechanisms using a stem-cell-based phenotypic assay. *Cell Stem Cell* **2012**, *11* (5), 620-32.
- [146] Pieper, A. A.; Xie, S.; Capota, E.; Estill, S. J.; Zhong, J.; Long, J. M.; Becker, G. L.; Huntington, P.; Goldman, S. E.; Shen, C. H.; Capota, M.; Britt, J. K.; Kotti, T.; Ure, K.; Brat, D. J.; Williams, N. S.;

- MacMillan, K. S.; Naidoo, J.; Melito, L.; Hsieh, J.; De Brabander, J.; Ready, J. M.; McKnight, S. L. Discovery of a proneurogenic, neuroprotective chemical. *Cell* **2010**, *142* (1), 39-51.
- [147] Pieper, A. A.; McKnight, S. L.; Ready, J. M. P7C3 and an unbiased approach to drug discovery for neurodegenerative diseases. *Chem Soc Rev* **2014**, *43* (19), 6716-26.
- [148] MacMillan, K. S.; Naidoo, J.; Liang, J.; Melito, L.; Williams, N. S.; Morlock, L.; Huntington, P. J.; Estill, S. J.; Longgood, J.; Becker, G. L.; McKnight, S. L.; Pieper, A. A.; De Brabander, J. K.; Ready, J. M. Development of proneurogenic, neuroprotective small molecules. *J Am Chem Soc* **2011**, *133* (5), 1428-37.
- [149] Naidoo, J.; De Jesus-Cortes, H.; Huntington, P.; Estill, S.; Morlock, L. K.; Starwalt, R.; Mangano, T. J.; Williams, N. S.; Pieper, A. A.; Ready, J. M. Discovery of a neuroprotective chemical, (S)-N-(3-(3,6-dibromo-9H-carbazol-9-yl)-2-fluoropropyl)-6-methoxyppyridin-2-amine [(-)-P7C3-S243], with improved druglike properties. *J Med Chem* **2014**, *57* (9), 3746-54.
- [150] Wang, G.; Han, T.; Nijhawan, D.; Theodoropoulos, P.; Naidoo, J.; Yadavalli, S.; Mirzaei, H.; Pieper, A. A.; Ready, J. M.; McKnight, S. L. P7C3 neuroprotective chemicals function by activating the rate-limiting enzyme in NAD salvage. *Cell* **2014**, *158* (6), 1324-34.
- [151] De Jesus-Cortes, H.; Xu, P.; Drawbridge, J.; Estill, S. J.; Huntington, P.; Tran, S.; Britt, J.; Tesla, R.; Morlock, L.; Naidoo, J.; Melito, L. M.; Wang, G.; Williams, N. S.; Ready, J. M.; McKnight, S. L.; Pieper, A. A. Neuroprotective efficacy of aminopropyl carbazoles in a mouse model of Parkinson disease. *Proc Natl Acad Sci U S A* **2012**, *109* (42), 17010-5.
- [152] De Jesús-Cortés, H.; Miller, A. D.; Britt, J. K.; DeMarco, A. J.; De Jesús-Cortés, M.; Stuebing, E.; Naidoo, J.; Vázquez-Rosa, E.; Morlock, L.; Williams, N. S.; Ready, J. M.; Narayanan, N. S.; Pieper, A. A. Protective efficacy of P7C3-S243 in the 6-hydroxydopamine model of Parkinson's disease. *Npj Parkinson's Disease* **2015**, *1*, 15010.
- [153] Tesla, R.; Wolf, H. P.; Xu, P.; Drawbridge, J.; Estill, S. J.; Huntington, P.; McDaniel, L.; Knobbe, W.; Burket, A.; Tran, S.; Starwalt, R.; Morlock, L.; Naidoo, J.; Williams, N. S.; Ready, J. M.; McKnight, S. L.; Pieper, A. A. Neuroprotective efficacy of aminopropyl carbazoles in a mouse model of amyotrophic lateral sclerosis. *Proc Natl Acad Sci U S A* **2012**, *109* (42), 17016-21.
- [154] Yin, T. C.; Britt, J. K.; De Jesus-Cortes, H.; Lu, Y.; Genova, R. M.; Khan, M. Z.; Voorhees, J. R.; Shao, J.; Katzman, A. C.; Huntington, P. J.; Wassink, C.; McDaniel, L.; Newell, E. A.; Dutca, L. M.; Naidoo, J.; Cui, H.; Bassuk, A. G.; Harper, M. M.; McKnight, S. L.; Ready, J. M.; Pieper, A. A. P7C3 neuroprotective chemicals block axonal degeneration and preserve function after traumatic brain injury. *Cell Rep* **2014**, *8* (6), 1731-40.
- [155] Kemp, S. W.; Szykaruk, M.; Stanoulis, K. N.; Wood, M. D.; Liu, E. H.; Willand, M. P.; Morlock, L.; Naidoo, J.; Williams, N. S.; Ready, J. M.; Mangano, T. J.; Beggs, S.; Salter, M. W.; Gordon, T.; Pieper, A. A.; Borschel, G. H. Pharmacologic rescue of motor and sensory function by the neuroprotective compound P7C3 following neonatal nerve injury. *Neuroscience* **2015**, *284*, 202-16.
- [156] Latchney, S. E.; Jaramillo, T. C.; Rivera, P. D.; Eisch, A. J.; Powell, C. M. Chronic P7C3 treatment restores hippocampal neurogenesis in the Ts65Dn mouse model of Down Syndrome. *Neurosci Lett* **2015**, *591*, 86-92.
- [157] Walker, A. K.; Rivera, P. D.; Wang, Q.; Chuang, J. C.; Tran, S.; Osborne-Lawrence, S.; Estill, S. J.; Starwalt, R.; Huntington, P.; Morlock, L.; Naidoo, J.; Williams, N. S.; Ready, J. M.; Eisch, A. J.; Pieper, A. A.; Zigman, J. M. The P7C3 class of neuroprotective compounds exerts antidepressant efficacy in mice by increasing hippocampal neurogenesis. *Mol Psychiatry* **2015**, *20* (4), 500-8.
- [158] Saxe, J. P. Screening: Your brain on drugs. *Nat Chem Biol* **2010**, *6* (9), 639-40.
- [159] Ready, J. M.; Lynch, K. W. Science at the interface of chemistry and biology at the University of Texas Southwestern Medical Center. *ACS Chem Biol* **2007**, *2* (8), 512-4.
- [160] Arrowsmith, C. H.; Audia, J. E.; Austin, C.; Baell, J.; Bennett, J.; Blagg, J.; Bountra, C.; Brennan, P. E.; Brown, P. J.; Bunnage, M. E.; Buser-Doepner, C.; Campbell, R. M.; Carter, A. J.; Cohen, P.; Copeland, R. A.; Cravatt, B.; Dahlin, J. L.; Dhanak, D.; Edwards, A. M.; Frederiksen, M.; Frye, S. V.; Gray, N.; Grimshaw, C. E.; Hepworth, D.; Howe, T.; Huber, K. V.; Jin, J.; Knapp, S.; Kotz, J. D.; Kruger, R. G.; Lowe, D.; Mader, M. M.; Marsden, B.; Mueller-Farnow, A.; Muller, S.; O'Hagan, R. C.; Overington, J. P.; Owen, D. R.; Rosenberg, S. H.; Roth, B.; Ross, R.; Schapira, M.; Schreiber, S. L.; Shoichet, B.; Sundstrom, M.; Superti-Furga, G.; Taunton, J.; Toledo-Sherman, L.; Walpole, C.; Walters, M. A.; Willson, T. M.; Workman, P.; Young, R. N.; Zuercher, W. J. The promise and peril of chemical probes. *Nat Chem Biol* **2015**, *11* (8), 536-41.
- [161] Narayan, P.; Ehsani, S.; Lindquist, S. Combating neurodegenerative disease with chemical probes and model systems. *Nat Chem Biol* **2014**, *10* (11), 911-20.

- [162] Reinke, A. A.; Gestwicki, J. E. Insight into amyloid structure using chemical probes. *Chem Biol Drug Des* **2011**, *77* (6), 399-411.
- [163] Pieper, A. A.; McKnight, S. L.; Ready, J. M. P7C3 and an unbiased approach to drug discovery for neurodegenerative diseases. *Chemical Society Reviews* **2014**, *43* (19), 6716-6726.
- [164] Davies, S. Interview with Steve Davies. *Chem Commun (Camb)* **2012**, *48* (81), 10068.
- [165] Workman, P.; Collins, I. Probing the probes: fitness factors for small molecule tools. *Chem Biol* **2010**, *17* (6), 561-77.
- [166] Khurana, V.; Tardiff, D. F.; Chung, C. Y.; Lindquist, S. Toward stem cell-based phenotypic screens for neurodegenerative diseases. *Nat Rev Neurol* **2015**, *11* (6), 339-50.
- [167] Swinney, D. C.; Anthony, J. How were new medicines discovered? *Nat Rev Drug Discov* **2011**, *10* (7), 507-19.
- [168] Santarelli, L.; Saxe, M.; Gross, C.; Surget, A.; Battaglia, F.; Dulawa, S.; Weisstaub, N.; Lee, J.; Duman, R.; Arancio, O.; Belzung, C.; Hen, R. Requirement of Hippocampal Neurogenesis for the Behavioral Effects of Antidepressants. *Science* **2003**, *301* (5634), 805-809.
- [169] Wassermann, A. M.; Camargo, L. M.; Auld, D. S. Composition and applications of focus libraries to phenotypic assays. *Front Pharmacol* **2014**, *5*, 164.
- [170] Jacobson, K. A. Functionalized congener approach to the design of ligands for G protein-coupled receptors (GPCRs). *Bioconjug Chem* **2009**, *20* (10), 1816-35.
- [171] Bansode, S. B.; Jana, A. K.; Batkulwar, K. B.; Warkad, S. D.; Joshi, R. S.; Sengupta, N.; Kulkarni, M. J. Molecular investigations of protriptyline as a multi-target directed ligand in Alzheimer's disease. *PLoS One* **2014**, *9* (8), e105196.
- [172] Simoni, E.; Bergamini, C.; Fato, R.; Tarozzi, A.; Bains, S.; Motterlini, R.; Cavalli, A.; Bolognesi, M. L.; Minarini, A.; Hrelia, P.; Lenaz, G.; Rosini, M.; Melchiorre, C. Polyamine conjugation of curcumin analogues toward the discovery of mitochondria-directed neuroprotective agents. *J Med Chem* **2010**, *53* (19), 7264-8.
- [173] Malaterre, J.; Strambi, C.; Aouane, A.; Strambi, A.; Rougon, G.; Cayre, M. A novel role for polyamines in adult neurogenesis in rodent brain. *Eur J Neurosci* **2004**, *20* (2), 317-30.
- [174] F. Haefliger; Schindler, W. Tertiary aminoalkyl-aminodibenzyls US 2554736. 1951.
- [175] Vardanyan, R. S.; Hruby, V. J. -32- - Antibiotics. In *Synthesis of Essential Drugs*, Vardanyan, R. S.; Hruby, V. J., Eds. Elsevier: Amsterdam, 2006; pp 425-498.
- [176] Righi, M.; Bedini, A.; Piersanti, G.; Romagnoli, F.; Spadoni, G. Direct, One-Pot Reductive Alkylation of Anilines with Functionalized Acetals Mediated by Triethylsilane and TFA. Straightforward Route for Unsymmetrically Substituted Ethylenediamine. *The Journal of Organic Chemistry* **2010**, *76* (2), 704-707.
- [177] Suresh C. Ameta, P. B. P., Rakshit Ameta, Chetna Ameta. *Microwave-Assisted Organic Synthesis: A Green Chemical Approach*. Apple Academic Press ed.; 2014.
- [178] Caddick, S.; de K. Haynes, A. K.; Judd, D. B.; Williams, M. R. V. Convenient synthesis of protected primary amines from nitriles. *Tetrahedron Letters* **2000**, *41* (18), 3513-3516.
- [179] Varma, R. S.; Dahiya, R. Sodium borohydride on wet clay: Solvent-free reductive amination of carbonyl compounds using microwaves. *Tetrahedron* **1998**, *54* (23), 6293-6298.
- [180] Pine, S. H.; Sanchez, B. L. Formic acid-formaldehyde methylation of amines. *The Journal of Organic Chemistry* **1971**, *36* (6), 829-832.
- [181] Rosenau, T.; Potthast, A.; Rohrling, J.; Hofinger, A.; Sixta, H.; Kosma, P. A solvent-free and formalin-free Eschweiler-Clarke methylation for amines. *Synthetic Communications* **2002**, *32* (3), 457-466.
- [182] Scadden, D. T. The stem-cell niche as an entity of action. *Nature* **2006**, *441* (7097), 1075-1079.
- [183] Zheng, W.; Thorne, N.; McKew, J. C. Phenotypic screens as a renewed approach for drug discovery. *Drug Discovery Today* **2013**, *18* (21-22), 1067-1073.
- [184] Duman, R. S.; Malberg, J.; Thome, J. Neural plasticity to stress and antidepressant treatment. *Biol Psychiatry* **1999**, *46* (9), 1181-91.
- [185] Boldrini, M.; Underwood, M. D.; Hen, R.; Rosoklija, G. B.; Dwork, A. J.; John Mann, J.; Arango, V. Antidepressants increase neural progenitor cells in the human hippocampus. *Neuropsychopharmacology* **2009**, *34* (11), 2376-89.
- [186] Jang, S. W.; Liu, X.; Chan, C. B.; Weinshenker, D.; Hall, R. A.; Xiao, G.; Ye, K. Amitriptyline is a TrkA and TrkB receptor agonist that promotes TrkA/TrkB heterodimerization and has potent neurotrophic activity. *Chem Biol* **2009**, *16* (6), 644-56.
- [187] Cirrito, J. R.; Disabato, B. M.; Restivo, J. L.; Verges, D. K.; Goebel, W. D.; Sathyan, A.; Hayreh, D.; D'Angelo, G.; Benzinger, T.; Yoon, H.; Kim, J.; Morris, J. C.; Mintun, M. A.; Sheline, Y. I. Serotonin

- signaling is associated with lower amyloid-beta levels and plaques in transgenic mice and humans. *Proc Natl Acad Sci U S A* **2011**, *108* (36), 14968-73.
- [188] Eom, T. Y.; Jope, R. S. Blocked inhibitory serine-phosphorylation of glycogen synthase kinase-3alpha/beta impairs in vivo neural precursor cell proliferation. *Biol Psychiatry* **2009**, *66* (5), 494-502.
- [189] Boku, S.; Nakagawa, S.; Masuda, T.; Nishikawa, H.; Kato, A.; Toda, H.; Song, N.; Kitaichi, Y.; Inoue, T.; Koyama, T. Effects of mood stabilizers on adult dentate gyrus-derived neural precursor cells. *Prog Neuropsychopharmacol Biol Psychiatry* **2011**, *35* (1), 111-7.
- [190] Li, Y.; Luikart, B. W.; Birnbaum, S.; Chen, J.; Kwon, C. H.; Kernie, S. G.; Bassel-Duby, R.; Parada, L. F. TrkB regulates hippocampal neurogenesis and governs sensitivity to antidepressant treatment. *Neuron* **2008**, *59* (3), 399-412.
- [191] Longo, F. M.; Massa, S. M. Small-molecule modulation of neurotrophin receptors: a strategy for the treatment of neurological disease. *Nat Rev Drug Discov* **2013**, *12* (7), 507-25.
- [192] <http://www.stemcell.com/en/Products/All-Products/NeuroFluor-CDr3.aspx> (accessed Feb 20, 2016).
- [193] Kajitani, N.; Hisaoka-Nakashima, K.; Morioka, N.; Okada-Tsuchioka, M.; Kaneko, M.; Kasai, M.; Shibasaki, C.; Nakata, Y.; Takebayashi, M. Antidepressant acts on astrocytes leading to an increase in the expression of neurotrophic/growth factors: differential regulation of FGF-2 by noradrenaline. *PLoS One* **2012**, *7* (12), e51197.
- [194] Watkins, C. C.; Sawa, A.; Pomper, M. G. Glia and immune cell signaling in bipolar disorder: insights from neuropharmacology and molecular imaging to clinical application. *Transl Psychiatry* **2014**, *4*, e350.
- [195] Tynan, R. J.; Weidenhofer, J.; Hinwood, M.; Cairns, M. J.; Day, T. A.; Walker, F. R. A comparative examination of the anti-inflammatory effects of SSRI and SNRI antidepressants on LPS stimulated microglia. *Brain Behav Immun* **2012**, *26* (3), 469-79.
- [196] Qiao, J.; Wang, J.; Wang, H.; Zhang, Y.; Zhu, S.; Adilijiang, A.; Guo, H.; Zhang, R.; Guo, W.; Luo, G.; Qiu, Y.; Xu, H.; Kong, J.; Huang, Q.; Li, X. M. Regulation of astrocyte pathology by fluoxetine prevents the deterioration of Alzheimer phenotypes in an APP/PS1 mouse model. *Glia* **2016**, *64* (2), 240-54.
- [197] Kim, H. J.; Kim, W.; Kong, S. Y. Antidepressants for neuro-regeneration: from depression to Alzheimer's disease. *Arch Pharm Res* **2013**, *36* (11), 1279-90.
- [198] Chadwick, W.; Mitchell, N.; Carroll, J.; Zhou, Y.; Park, S. S.; Wang, L.; Becker, K. G.; Zhang, Y.; Lehrmann, E.; Wood, W. H., 3rd; Martin, B.; Maudsley, S. Amitriptyline-mediated cognitive enhancement in aged 3xTg Alzheimer's disease mice is associated with neurogenesis and neurotrophic activity. *PLoS One* **2011**, *6* (6), e21660.
- [199] Sheline, Y. I.; West, T.; Yarasheski, K.; Swarm, R.; Jasieliec, M. S.; Fisher, J. R.; Ficker, W. D.; Yan, P.; Xiong, C.; Frederiksen, C.; Grzelak, M. V.; Chott, R.; Bateman, R. J.; Morris, J. C.; Mintun, M. A.; Lee, J. M.; Cirrito, J. R. An antidepressant decreases CSF Abeta production in healthy individuals and in transgenic AD mice. *Sci Transl Med* **2014**, *6* (236), 236re4.
- [200] Clark, J.; Xu, Y.; Hilcove, S.; Ding, S. Exploring Stem Cell Biology with Small Molecules and Functional Genomics. In *Chemical and Functional Genomic Approaches to Stem Cell Biology and Regenerative Medicine*, John Wiley & Sons, Inc.: 2007; pp 187-206.
- [201] Saturnino, C.; Iacopetta, D.; Sinicropi, M. S.; Rosano, C.; Caruso, A.; Caporale, A.; Marra, N.; Marengo, B.; Pronzato, M. A.; Parisi, O. I.; Longo, P.; Ricciarelli, R. N-alkyl carbazole derivatives as new tools for Alzheimer's disease: preliminary studies. *Molecules* **2014**, *19* (7), 9307-17.
- [202] Chen, A. C. Y.; Scott, J. M.; Stearns, B. A.; Stock, N. S.; Truong, Y. P. Tricyclic compounds useful as neurogenic and neuroprotective agents. WO 2013043744 A2: 2013.
- [203] Darvesh, S.; McDonald, R. S.; Darvesh, K. V.; Mataija, D.; Conrad, S.; Gomez, G.; Walsh, R.; Martin, E. Selective reversible inhibition of human butyrylcholinesterase by aryl amide derivatives of phenothiazine. *Bioorg Med Chem* **2007**, *15* (19), 6367-78.
- [204] Hughes, J. P.; Rees, S.; Kalindjian, S. B.; Philpott, K. L. Principles of early drug discovery. *Br J Pharmacol* **2011**, *162* (6), 1239-49.
- [205] Spero, L. Modulation of specific [3H]phenytoin binding by benzodiazepines. *Neurochem Res* **1985**, *10* (6), 755-65.
- [206] (a) Breier, J. M.; Radio, N. M.; Mundy, W. R.; Shafer, T. J. Development of a high-throughput screening assay for chemical effects on proliferation and viability of immortalized human neural progenitor cells. *Toxicol Sci* **2008**, *105* (1), 119-33; (b) Toxicity Testing in the Twenty-first Century: A Vision and a Strategy Washington, D.C: The National Academies Press; 2007.

- [207] Gasparri, F. An overview of cell phenotypes in HCS: limitations and advantages. *Expert Opin Drug Discov* **2009**, *4* (6), 643-57.
- [208] Zanella, F.; Lorens, J. B.; Link, W. High content screening: seeing is believing. *Trends Biotechnol* **2010**, *28* (5), 237-45.
- [209] Young, D. W.; Bender, A.; Hoyt, J.; McWhinnie, E.; Chirn, G. W.; Tao, C. Y.; Tallarico, J. A.; Labow, M.; Jenkins, J. L.; Mitchison, T. J.; Feng, Y. Integrating high-content screening and ligand-target prediction to identify mechanism of action. *Nat Chem Biol* **2008**, *4* (1), 59-68.
- [210] Gregori-Puigjane, E.; Setola, V.; Hert, J.; Crews, B. A.; Irwin, J. J.; Lounkine, E.; Marnett, L.; Roth, B. L.; Shoichet, B. K. Identifying mechanism-of-action targets for drugs and probes. *Proc Natl Acad Sci U S A* **2012**, *109* (28), 11178-83.
- [211] Miller, T. M.; Johnson, E. M., Jr. Metabolic and genetic analyses of apoptosis in potassium/serum-deprived rat cerebellar granule cells. *J Neurosci* **1996**, *16* (23), 7487-95.
- [212] Eggert, U. S. The why and how of phenotypic small-molecule screens. *Nat Chem Biol* **2013**, *9* (4), 206-9.
- [213] Evans, M. J.; Saghatelian, A.; Sorensen, E. J.; Cravatt, B. F. Target discovery in small-molecule cell-based screens by in situ proteome reactivity profiling. *Nat Biotechnol* **2005**, *23* (10), 1303-7.
- [214] Cisar, J. S.; Cravatt, B. F. Fully functionalized small-molecule probes for integrated phenotypic screening and target identification. *J Am Chem Soc* **2012**, *134* (25), 10385-8.
- [215] Bolognesi, M. L. G., A.; Prati, F.; Uliassi, E. From companion diagnostics to theranostics: a new avenue for Alzheimer's disease? *J Med Chem under revision*.
- [216] Zhang, X.; Tian, Y.; Yuan, P.; Li, Y.; Yaseen, M. A.; Grutzendler, J.; Moore, A.; Ran, C. A bifunctional curcumin analogue for two-photon imaging and inhibiting crosslinking of amyloid beta in Alzheimer's disease. *Chem Commun (Camb)* **2014**, *50* (78), 11550-3.
- [217] Yun, S. W.; Leong, C.; Zhai, D.; Tan, Y. L.; Lim, L.; Bi, X.; Lee, J. J.; Kim, H. J.; Kang, N. Y.; Ng, S. H.; Stanton, L. W.; Chang, Y. T. Neural stem cell specific fluorescent chemical probe binding to FABP7. *Proc Natl Acad Sci U S A* **2012**, *109* (26), 10214-7.
- [218] (a) Epp, J. R.; Beasley, C. L.; Galea, L. A. Increased hippocampal neurogenesis and p21 expression in depression: dependent on antidepressants, sex, age, and antipsychotic exposure. *Neuropsychopharmacology* **2013**, *38* (11), 2297-306; (b) Wang, Y. X.; Zhang, X. R.; Zhang, Z. J.; Li, L.; Xi, G. J.; Wu, D.; Wang, Y. J. Protein kinase Mzeta is involved in the modulatory effect of fluoxetine on hippocampal neurogenesis in vitro. *Int J Neuropsychopharmacol* **2014**, *17* (9), 1429-41.
- [219] Morphy, R.; Rankovic, Z. The physicochemical challenges of designing multiple ligands. *J Med Chem* **2006**, *49* (16), 4961-70.
- [220] Morphy, R.; Rankovic, Z. Designed multiple ligands. An emerging drug discovery paradigm. *J Med Chem* **2005**, *48* (21), 6523-43.
- [221] Czeh, B.; Simon, M.; Schmelting, B.; Hiemke, C.; Fuchs, E. Astroglial plasticity in the hippocampus is affected by chronic psychosocial stress and concomitant fluoxetine treatment. *Neuropsychopharmacology* **2006**, *31* (8), 1616-26.
- [222] Lee, J. Y.; Kang, S. R.; Yune, T. Y. Fluoxetine prevents oligodendrocyte cell death by inhibiting microglia activation after spinal cord injury. *J Neurotrauma* **2015**, *32* (9), 633-44.
- [223] Kodama, M.; Fujioka, T.; Duman, R. S. Chronic olanzapine or fluoxetine administration increases cell proliferation in hippocampus and prefrontal cortex of adult rat. *Biol Psychiatry* **2004**, *56* (8), 570-80.
- [224] (a) Chang, E. A.; Beyhan, Z.; Yoo, M. S.; Siripattarapavat, K.; Ko, T.; Lookingland, K. J.; Madhukar, B. V.; Cibelli, J. B. Increased cellular turnover in response to fluoxetine in neuronal precursors derived from human embryonic stem cells. *Int J Dev Biol* **2010**, *54* (4), 707-15; (b) Chang, K. A.; Kim, J. A.; Kim, S.; Joo, Y.; Shin, K. Y.; Kim, S.; Kim, H. S.; Suh, Y. H. Therapeutic potentials of neural stem cells treated with fluoxetine in Alzheimer's disease. *Neurochem Int* **2012**, *61* (6), 885-91.
- [225] Manev, H.; Uz, T.; Smalheiser, N. R.; Manev, R. Antidepressants alter cell proliferation in the adult brain in vivo and in neural cultures in vitro. *Eur J Pharmacol* **2001**, *411* (1-2), 67-70.
- [226] (a) Karson, C. N.; Newton, J. E.; Livingston, R.; Jolly, J. B.; Cooper, T. B.; Sprigg, J.; Komoroski, R. A. Human brain fluoxetine concentrations. *J Neuropsychiatry Clin Neurosci* **1993**, *5* (3), 322-9; (b) Komoroski, R. A.; Newton, J. E.; Cardwell, D.; Sprigg, J.; Pearce, J.; Karson, C. N. In vivo ¹⁹F spin relaxation and localized spectroscopy of fluoxetine in human brain. *Magn Reson Med* **1994**, *31* (2), 204-11.

- [227] Hui, J.; Zhang, J.; Kim, H.; Tong, C.; Ying, Q.; Li, Z.; Mao, X.; Shi, G.; Yan, J.; Zhang, Z.; Xi, G. Fluoxetine regulates neurogenesis in vitro through modulation of GSK-3 β /beta-catenin signaling. *Int J Neuropsychopharmacol* **2015**, *18* (5).
- [228] Zusso, M.; Debetto, P.; Guidolin, D.; Barbierato, M.; Manev, H.; Giusti, P. Fluoxetine-induced proliferation and differentiation of neural progenitor cells isolated from rat postnatal cerebellum. *Biochem Pharmacol* **2008**, *76* (3), 391-403.
- [229] Chiou, S. H.; Chen, S. J.; Peng, C. H.; Chang, Y. L.; Ku, H. H.; Hsu, W. M.; Ho, L. L.; Lee, C. H. Fluoxetine up-regulates expression of cellular FLICE-inhibitory protein and inhibits LPS-induced apoptosis in hippocampus-derived neural stem cell. *Biochem Biophys Res Commun* **2006**, *343* (2), 391-400.
- [230] Bazan, E.; Alonso, F. J.; Redondo, C.; Lopez-Toledano, M. A.; Alfaro, J. M.; Reimers, D.; Herranz, A. S.; Paino, C. L.; Serrano, A. B.; Cobacho, N.; Caso, E.; Lobo, M. V. In vitro and in vivo characterization of neural stem cells. *Histol Histopathol* **2004**, *19* (4), 1261-75.
- [231] Schenone, M.; Dancik, V.; Wagner, B. K.; Clemons, P. A. Target identification and mechanism of action in chemical biology and drug discovery. *Nat Chem Biol* **2013**, *9* (4), 232-40.
- [232] Burdine, L.; Kodadek, T. Target identification in chemical genetics: the (often) missing link. *Chem Biol* **2004**, *11* (5), 593-7.
- [233] Zheng, X. S.; Chan, T. F.; Zhou, H. H. Genetic and genomic approaches to identify and study the targets of bioactive small molecules. *Chem Biol* **2004**, *11* (5), 609-18.
- [234] Pieretti, S.; Haanstra, J. R.; Mazet, M.; Perozzo, R.; Bergamini, C.; Prati, F.; Fato, R.; Lenaz, G.; Capranico, G.; Brun, R.; Bakker, B. M.; Michels, P. A.; Scapozza, L.; Bolognesi, M. L.; Cavalli, A. Naphthoquinone derivatives exert their antitrypanosomal activity via a multi-target mechanism. *PLoS Negl Trop Dis* **2013**, *7* (1), e2012.
- [235] Jacobson, K. A.; Ukena, D.; Padgett, W.; Kirk, K. L.; Daly, J. W. Molecular probes for extracellular adenosine receptors. *Biochem Pharmacol* **1987**, *36* (10), 1697-707.
- [236] Kang, N. Y.; Ha, H. H.; Yun, S. W.; Yu, Y. H.; Chang, Y. T. Diversity-driven chemical probe development for biomolecules: beyond hypothesis-driven approach. *Chem Soc Rev* **2011**, *40* (7), 3613-26.
- [237] Sridharan, R.; Zuber, J.; Connelly, S. M.; Mathew, E.; Dumont, M. E. Fluorescent approaches for understanding interactions of ligands with G protein coupled receptors. *Biochim Biophys Acta* **2014**, *1838* (1 Pt A), 15-33.
- [238] Lavis, L. D.; Raines, R. T. Bright ideas for chemical biology. *ACS Chem Biol* **2008**, *3* (3), 142-55.
- [239] Yun, S. W.; Kang, N. Y.; Park, S. J.; Ha, H. H.; Kim, Y. K.; Lee, J. S.; Chang, Y. T. Diversity oriented fluorescence library approach (DOFLA) for live cell imaging probe development. *Acc Chem Res* **2014**, *47* (4), 1277-86.
- [240] (a) Er, J. C.; Leong, C.; Teoh, C. L.; Yuan, Q.; Merchant, P.; Dunn, M.; Sulzer, D.; Sames, D.; Bhinghe, A.; Kim, D.; Kim, S. M.; Yoon, M. H.; Stanton, L. W.; Je, S. H.; Yun, S. W.; Chang, Y. T. NeuO: a fluorescent chemical probe for live neuron labeling. *Angew Chem Int Ed Engl* **2015**, *54* (8), 2442-6; (b) Leong, C.; Lee, S. C.; Ock, J.; Li, X.; See, P.; Park, S. J.; Ginhoux, F.; Yun, S. W.; Chang, Y. T. Microglia specific fluorescent probes for live cell imaging. *Chem Commun (Camb)* **2014**, *50* (9), 1089-91; (c) Yun, S. W.; Leong, C.; Bi, X.; Ha, H. H.; Yu, Y. H.; Tan, Y. L.; Narayanan, G.; Sankaran, S.; Kim, J. Y.; Hariharan, S.; Ahmed, S.; Chang, Y. T. A fluorescent probe for imaging symmetric and asymmetric cell division in neurosphere formation. *Chem Commun (Camb)* **2014**, *50* (56), 7492-4.
- [241] Pilar-Cuellar, F.; Vidal, R.; Diaz, A.; Castro, E.; dos Anjos, S.; Vargas, V.; Romero, B.; Valdizan, E. M. Signaling pathways involved in antidepressant-induced cell proliferation and synaptic plasticity. *Current Pharmaceutical Design* **2014**, *20* (23), 3776-94.
- [242] Ma, Z.; Du, L.; Li, M. Toward fluorescent probes for G-protein-coupled receptors (GPCRs). *J Med Chem* **2014**, *57* (20), 8187-203.
- [243] Kowada, T.; Maeda, H.; Kikuchi, K. BODIPY-based probes for the fluorescence imaging of biomolecules in living cells. *Chemical Society Reviews* **2015**, *44* (14), 4953-4972.
- [244] Ono, M.; Watanabe, H.; Kimura, H.; Saji, H. BODIPY-based molecular probe for imaging of cerebral beta-amyloid plaques. *ACS Chem Neurosci* **2012**, *3* (4), 319-24.
- [245] Cavalli, A.; Bolognesi, M. L.; Minarini, A.; Rosini, M.; Tumiatti, V.; Recanatini, M.; Melchiorre, C. Multi-target-directed ligands to combat neurodegenerative diseases. *J Med Chem* **2008**, *51* (3), 347-72.
- [246] Bolognesi, M. L. Polypharmacology in a single drug: multitarget drugs. *Curr Med Chem* **2013**, *20* (13), 1639-45.

- [247] Gal, S.; Fridkin, M.; Amit, T.; Zheng, H.; Youdim, M. B. M30, a novel multifunctional neuroprotective drug with potent iron chelating and brain selective monoamine oxidase-ab inhibitory activity for Parkinson's disease. *J Neural Transm Suppl* **2006**, (70), 447-56.
- [248] Morales-Garcia, J. A.; Luna-Medina, R.; Alonso-Gil, S.; Sanz-Sancristobal, M.; Palomo, V.; Gil, C.; Santos, A.; Martinez, A.; Perez-Castillo, A. Glycogen synthase kinase 3 inhibition promotes adult hippocampal neurogenesis in vitro and in vivo. *ACS Chem Neurosci* **2012**, 3 (11), 963-71.
- [249] (a) Prati, F.; De Simone, A.; Armirotti, A.; Summa, M.; Pizzirani, D.; Scarpelli, R.; Bertozzi, S. M.; Perez, D. I.; Andrisano, V.; Perez-Castillo, A.; Monti, B.; Massenzio, F.; Polito, L.; Racchi, M.; Sabatino, P.; Bottegoni, G.; Martinez, A.; Cavalli, A.; Bolognesi, M. L. 3,4-Dihydro-1,3,5-triazin-2(1H)-ones as the First Dual BACE-1/GSK-3beta Fragment Hits against Alzheimer's Disease. *ACS Chem Neurosci* **2015**, 6 (10), 1665-82; (b) Prati, F.; De Simone, A.; Bisignano, P.; Armirotti, A.; Summa, M.; Pizzirani, D.; Scarpelli, R.; Perez, D. I.; Andrisano, V.; Perez-Castillo, A.; Monti, B.; Massenzio, F.; Polito, L.; Racchi, M.; Favia, A. D.; Bottegoni, G.; Martinez, A.; Bolognesi, M. L.; Cavalli, A. Multitarget drug discovery for Alzheimer's disease: triazinones as BACE-1 and GSK-3beta inhibitors. *Angew Chem Int Ed Engl* **2015**, 54 (5), 1578-82.
- [250] Lopez-Iglesias, B.; Perez, C.; Morales-Garcia, J. A.; Alonso-Gil, S.; Perez-Castillo, A.; Romero, A.; Lopez, M. G.; Villarroya, M.; Conde, S.; Rodriguez-Franco, M. I. New melatonin-N,N-dibenzyl(N-methyl)amine hybrids: potent neurogenic agents with antioxidant, cholinergic, and neuroprotective properties as innovative drugs for Alzheimer's disease. *J Med Chem* **2014**, 57 (9), 3773-85.
- [251] de la Fuente Revenga, M.; Perez, C.; Morales-Garcia, J. A.; Alonso-Gil, S.; Perez-Castillo, A.; Caignard, D. H.; Yanez, M.; Gamo, A. M.; Rodriguez-Franco, M. I. Neurogenic Potential Assessment and Pharmacological Characterization of 6-Methoxy-1,2,3,4-tetrahydro-beta-carboline (Pinoline) and Melatonin-Pinoline Hybrids. *ACS Chem Neurosci* **2015**, 6 (5), 800-10.
- [252] Melchiorre, C.; Bolognesi, M. L.; Minarini, A.; Rosini, M.; Tumiatti, V. Polyamines in drug discovery: from the universal template approach to the multitarget-directed ligand design strategy. *J Med Chem* **2010**, 53 (16), 5906-14.
- [253] Igarashi, K.; Kashiwagi, K. Modulation of cellular function by polyamines. *Int J Biochem Cell Biol* **2010**, 42 (1), 39-51.
- [254] Masuko, T.; Kusama-Eguchi, K.; Sakata, K.; Kusama, T.; Chaki, S.; Okuyama, S.; Williams, K.; Kashiwagi, K.; Igarashi, K. Polyamine transport, accumulation, and release in brain. *J Neurochem* **2003**, 84 (3), 610-7.
- [255] Fiori, L. M.; Turecki, G. Implication of the polyamine system in mental disorders. *J Psychiatry Neurosci* **2008**, 33 (2), 102-10.
- [256] Bolognesi, M. L.; Calonghi, N.; Mangano, C.; Masotti, L.; Melchiorre, C. Parallel synthesis and cytotoxicity evaluation of a polyamine-quinone conjugates library. *J Med Chem* **2008**, 51 (17), 5463-7.
- [257] Rosini, M.; Budriesi, R.; Bixel, M. G.; Bolognesi, M. L.; Chiarini, A.; Hucho, F.; Krogsgaard-Larsen, P.; Mellor, I. R.; Minarini, A.; Tumiatti, V.; Usherwood, P. N.; Melchiorre, C. Design, synthesis, and biological evaluation of symmetrically and unsymmetrically substituted methocramine-related polyamines as muscular nicotinic receptor noncompetitive antagonists. *J Med Chem* **1999**, 42 (25), 5212-23.
- [258] Tumiatti, V.; Milelli, A.; Minarini, A.; Rosini, M.; Bolognesi, M. L.; Micco, M.; Andrisano, V.; Bartolini, M.; Mancini, F.; Recanatini, M.; Cavalli, A.; Melchiorre, C. Structure-activity relationships of acetylcholinesterase noncovalent inhibitors based on a polyamine backbone. 4. Further investigation on the inner spacer. *J Med Chem* **2008**, 51 (22), 7308-12.

PART II

FROM SMALL MOLECULES TO FLUORESCENT PROBES: APPLYING THE FUNCTIONALIZED CONGENER APPROACH TO P2Y₁₄ RECEPTOR

1. Introduction

1.1 G protein-coupled receptors (GPCRs) in drug discovery

Seven-transmembrane (7TM) domain G protein-coupled receptors (GPCRs) constitute the largest integral membrane protein family in the human genome, with almost 1000 members.¹ All GPCRs share the canonical fold of 7TM helices embedded in the membrane and linked by alternating intracellular (I-III) and extracellular loops (II-IV). The extracellular loops and the N-termini constitute the ligand-binding domain for the class A GPCRs, while the intracellular loops and the C-termini are involved in G-protein binding and activation. Despite these similarities, several differences have been reported between the members within class A GPCRs. According to the nature of ligand, the conformational rearrangements of helices produce different binding pockets (in size, shape and amino acid interactions network), so that, for example, the binding pocket of acetylcholine in M2 muscarinic receptor is more deeply embedded within the 7TM segment compared to that of more polar nucleosides in A_{2A} receptor (see detailed review² on this argument). Striking differences have also been observed between the binding pocket of an agonist and antagonist in the same GPCR.² Thus, the size, shape and interactions network made by amino acids of these binding pockets explain the ability of GPCRs to discriminate between diverse chemical signals, that can be translated into the multiple conformations adopted by GPCR, each of which is associated with a specific physiological response. And in fact, given these peculiar properties, the GPCR superfamily represents the major transducers of the information (including responses to hormones, neurotransmitters and extracellular stimuli) flow into the cells. As such, GPCRs are associated with a multitude of diseases that make members of this family, important pharmacological targets. Indeed, GPCRs encompass the largest family of proteins targeted by drug discovery and their high tractability and profitability reflect the fact that GPCRs continue to be one of the most important target classes (30-50% of the marketed drugs) in the portfolio of the majority of pharma companies.³

As in 2004 Filmore pointed out “It’s a GPCR world”,⁴ and undoubtedly it is still right today, even though the GPCR drug discovery is moving towards new paradigms.⁵ If for a long time, it was not possible to understand the “GPCR world”, because their multi-membrane spanning structure makes them difficult to isolate and crystallize, the beginning of 1980s provided a series of breakthroughs that eventually allowed the detailed structural characterization of these proteins.⁶

Starting from the crucial observation made by Lefkowitz that the cloning and sequencing of β_2 -adrenergic receptor (β_2 AR) gene have revealed significant similarities to rhodopsins (the well-characterized model of GPCRs),⁶ in 2000, Palczewski was able to get the first x-ray structure of rhodopsin.⁷ However, this structure provided only limited details of GPCR functioning, due to the relatively low resolution and low sequence homology to most druggable GPCRs. Since then, a plethora of mutagenesis, biophysical and biochemical studies with the goal of characterizing GPCR structures and functions have been developed. But, only in 2007, Kobilka obtained the crystal structure of the β_2 AR in its inactive state thanks to the manipulation and stabilization of GPCR structure with an antibody protruding out of the membrane.⁸ This structure shed light on how antagonists bind within the

7TM hydrophobic core of the receptor and stabilize the inactive conformation. This opens new possibilities and new collaborations in the field,⁹ culminating in the establishment of the first structure of the β_2 AR with the partial inverse agonist carazolol at 2.4 Å resolution in the active state, a state that had previously considered being too unstable to be isolated.¹⁰ Indeed, by using T4 lysozyme (a highly crystallizable protein at the N-terminus of the receptor) to stabilize the highly dynamic structure of β_2 AR and the development of a new detergent to enable the purification of the complex, the crystal structure in the active state was obtained and was compared to the inactive one. This provided valuable insights into the activation process, including the identity of the specific helices that move and affect G protein binding. Finally, in 2011 Kobilka's group published the first ever structure of a GPCR in the active state with the high affinity agonist BI-167107 at 3.5 Å resolution¹¹ and then bound to the G_s protein at 3.2 Å resolution.¹² The stabilization of its active state with a nanobody has again led to unprecedented, atomic-level understanding of GPCR function including the movement of the crucial helices and loops.

Kobilka's work was also accompanied by pioneering work from the Stevens group at Scripps Research Institute (currently at University of Southern California), which also developed special techniques to crystallize GPCRs. Indeed, in the same year, the crystal structure of A_{2A} adenosine receptor was also solved in complex with the agonist UK-432097.¹³

The new developments achieved in the GPCR field led to Lefkowitz and Kobilka being awarded the 2012 Nobel Prize in Chemistry and, from that moment on, the GPCR research area¹⁴ seemed to be on the cusp of a new era for GPCR drug discovery. In addition, the new improvements obtained in X-ray crystallography have provided tremendous insights into the molecular mechanisms underlying ligand recognition, GPCR activation and constitutive activity.³ In fact, these breakthroughs have opened the way to not only a detailed dissection of the mechanism of GPCR function, but also to structure-based drug design, substantiating how the GPCR structural revolution is impacting current drug discovery.¹⁵ Indeed, until that moment, the design of selective ligand that is able to discriminate among the receptor subtypes within a GPCR subfamily resulted to be particularly difficult, if not impossible. Indeed, when comparing members within a subfamily (i.e. muscarinic receptors), the high sequence similarity in the orthosteric pocket makes the development of such selective ligand extremely problematic to accomplish. Instead, the diversity shown within the cytoplasmic loops and C terminus open new possibilities in this context.

As a consequence, the first insights into the challenges of developing subtype selective drugs came from the recently solved GPCR crystal structures. These include the structure of the human M_2 muscarinic acetylcholine receptor bound to the antagonist 3-quinuclidinyl-benzilate,¹⁶ as well as the structure of M_3 receptor bound to the bronchodilator drug tiotropium.¹⁷ These works revealed the structural and functional diversity among the muscarinic receptor subtypes that can be exploited to design selective ligands, which would avoid the side effects associated with the lack of selectivity of the currently used muscarinic ligands. Also the crystal structures of key opioid receptors μ ¹⁸ and δ ¹⁹ have been successfully obtained in complex with a morphinan antagonist and naltrindole, respectively. This would be of fundamental importance due to the wide clinical use of opioid ligands to relieve severe pain. Current opioid drugs indeed display remarkable side effects (depression of respiratory and intestinal activity, addiction, etc.), and these crystal structures

together with structure-based approaches may lead to design more selective opioid drugs with a better pharmacological profile.

Recently, the solved crystal structures of P2Y₁₂ receptor (P2Y₁₂R) in complex with antagonist AZD1283 (antithrombotic drug),²⁰ and different agonists 2MeSATP (partial) and 2MeSADP (full)²¹ reveal striking conformational differences between agonist and antagonist complexes especially in the extracellular regions resulting in different orientations of the ligands and partially overlapped binding sites. Moreover, by analyzing in detail the extracellular interface, an additional pocket adjacent to ligand-binding region was also identified, suggesting that these structure may represent invaluable starting points for designing P2Y₁₂R ligands with improved pharmacological properties and allosteric modulators as well, with potential clinical application as antithrombotic drugs. However, the possibility to rationally design an allosteric ligand for GPCR became a tangible reality since the x-ray structures of another P2Y₁ receptor (P2Y₁R) in complex with a nucleotide antagonist MRS2500 and a non-nucleotide antagonist BPTU were obtained.²² Remarkably, the crystal structure in complex with BPTU is particularly significant as highlighted an allosteric pocket on the external receptor interface with the lipid bilayer, making BPTU the first structurally characterized selective GPCR ligand located entirely outside of the orthosteric binding site. Moreover, recent reports showed that in addition to P2Y₁₂R, also P2Y₁ is involved in platelet aggregation, thus, suggesting it as a new promising antithrombotic target, which may offer a better pharmacological profile than P2Y₁₂R inhibitors.²³

Despite these tremendous advances, GPCR have always been and still remain a complex target class. The above discussed x-ray structures indeed show previously unobtainable details of interactions between GPCRs and ligands, including the roles of lipophilic regions and water molecules as driving forces of binding. In addition, the structures have revealed several surprising ligand-binding modes, including sites outside the orthosteric pocket. In addition to the structural information about the ligand-GPCR complexes, such structures have provided insights into the structural basis of the superfamily's biochemical functions. GPCRs can concomitantly interact with a vast array of endogenous and exogenous ligands and adopt multiple conformational states that couple to different signaling pathways. Several innovative paradigms of drug action arise as a consequence of these properties of GPCRs, and include biased ligands, allosteric modulators, oligomerization, GPCR regulation, polypharmacology and off-targets evaluation, and deorphanisation.⁵

Perhaps, one of the most significant discoveries in this context has been the observation that ligand binding produces conformational changes in GPCR structure that is associated to differential interaction with G proteins, arrestins and other proteins inside the cell, thereby leading to different physiological responses, a phenomenon called "functional selectivity" or "biased agonism".²⁴ This concept arises from the fact that GPCR exist as an ensemble of conformations, each of which is preferentially linked to specific signaling effectors and, once ligand binds to the receptor in a certain conformation, this can produce different biochemical effects. As recently proposed, several endogenous peptides that activate the μ -opioid receptor display particularly distinct bias profiles.²⁵ Nonetheless, this peculiar ability of ligands interacting with GPCR has been exploited to develop GPCR biased agonists already in the clinical trials. For example, μ -opioid receptor G_i-biased ligand, namely TRV130, has already launched Phase 3 clinical program for postoperative pain.²⁶ The typical

side effects associated to the opioid drugs, such as the unbiased morphine, are avoided by eliminating the arrestin pathway responsible for those adverse effects. Another significant and related approach to selectively target GPCR relies on allosteric modulation. As discussed above for P2Y₁R, the allosteric modulators do not bind to the orthosteric ligand binding pocket, but instead act at an alternatively located binding site (allosteric site), structurally distinct from the orthosteric site, to either potentiate (positive allosteric modulator) or inhibit (negative allosteric modulator) activation of the receptor by its natural ligand. Compounds with an allosteric mode of action may have, in principle, a number of theoretical advantages over orthosteric ligands. For example, if allosteric modulators do not display any agonism, they are quiescent in the absence of endogenous agonist and only exert their effect in the presence of a released orthosteric agonist. Thus, such allosteric modulators have the potential to maintain activity dependence and both temporal and spatial aspects of endogenous physiological signaling. Additionally, as previously anticipated, allosteric ligands offer the potential advantage of greater receptor selectivity, as allosteric pocket across receptor subtypes are less conserved than the orthosteric site. Conversely, selectivity may be also achieved by combining both orthosteric and allosteric pharmacophores within the same molecule to yield a novel class of 'bitopic' GPCR ligand.²⁷ The promising profile of allosteric ligand has been employed by AstraZeneca to develop a novel metabotropic glutamate receptor 2 (mGluR₂) positive allosteric modulator, AZD8529. It is able to potentiate the effects of glutamate on mGluR₂ with a good selectivity over the other glutamate receptor sub-types and is currently in clinical trials indicated for addiction treatment.²⁸ Moreover, there is a growing appreciation that GPCR regulation and signaling is much more complex than originally envisioned, and includes signaling through G protein independent pathways, signaling activated after agonist-mediated GPCR internalization, and GPCR oligomerization. If the first point is well recognized since the establishment that β -arrestins can also function as molecular mediators of G-protein independent signaling by acting to a variety of signaling proteins (i.e. ERK-mitogen-activated protein kinase pathway),²⁹ the second point is still under intense investigation and will be not discussed herein (see cited review³⁰ for details). On the other hand, the role of GPCR oligomerization is not completely clear. GPCRs do indeed form dimers (or higher order oligomers), and that dimerization can occur between the same GPCRs, close family members, or distinct families of GPCRs. It has been proposed that GPCR dimerization affects ligand binding, receptor activation, desensitization and trafficking, as well as receptor signaling. Moreover, the interface between monomers can cooperatively transmit allosteric effects. For example, the heteromeric assembly of mGluR₂ and 5-HT_{2A} receptors enhances glutamate-elicited Gi signaling and reduces 5-HT-elicited Gq signaling. Interestingly, antipsychotic drugs invert this signaling balance through the complex (Gi signaling decreases, whereas Gq signaling increases), modifying the balance from being in favor of Gi signaling (normal complex) to being in favor of Gq signaling (propsychotic). This arises from the modulation of the interaction between significant TM residues (TM4-5) at the interface of heteromer, induced by the ligand binding. Accordingly, disease states involving psychosis, such as schizophrenia, are associated with a variable disruption of the Gi-Gq balance (i.e. decrease in Gi and increase in Gq), consistent with the mGluR₂ down-regulation and 5-HT_{2A} receptor up-regulation observed in untreated schizophrenic patients. Further in vivo experiments corroborate this finding, suggesting the potential benefits of combination therapy involving mGluR₂ agonist

and 5-HT_{2A} receptor inverse agonist in the treatment of schizophrenia, especially in resistant cases.³¹

Mechanistic insights in this process would be of pivotal importance because some GPCRs are active only in the dimeric state (i.e. mGluRs). Thus, compounds specifically targeting the heteromeric interface are particularly promising not only to serve as powerful tools to explore the significance of GPCR heteromers, but also may serve for the development of highly selective drugs for the treatment of a variety of disorders.³²

Additionally, the design of multitarget ligands deliberately targeting GPCRs has been recently emerged as suitable alternative in GPCR drug discovery. In this case, the authors exploited the multitarget profile of new hybrid molecules, designed by combining elements of a known agonist of the 5-HT₄ serotonin receptor (RS67333) and an inhibitor of the enzyme acetylcholinesterase (donepezil). The identified lead compound, namely Donecopride, displayed both acetylcholinesterase inhibitory effects and partial 5-HT₄ receptor agonist activity in vitro in nanomolar ranges and exhibited in vivo pro-cognitive and anti-amnesic effects, resulting particularly promising as multitarget ligand for the treatment of Alzheimer's disease.³³

If drugs with multiple mechanisms of action are particularly attractive and effective, often the observed polypharmacological profile of such drugs can be also detrimental. Especially, when searching for new small molecules that act at GPCRs, the so-called off-targets effect of a candidate molecule should be carefully determined in broad screening at other receptors, ion channels, enzymes, and transporters.³⁴ This would be of particular importance in the de-risking process, when that activity is considered undesirable. To achieve this goal different approaches have been developed. For example, Paoletta et al. systematically examined the promiscuity of a set of adenosine/adenine congeners, previously designed for the treatment of neuropathic pain, to reveal unexpected interactions of these ligands with numerous off-target sites of Psychoactive Drug Screening Program (PDSP).³⁵ This revealed an association of structures and substructures of the nucleosides with specific interactions with other GPCRs, ion channels and a transporter in the CNS. Interestingly, the results obtained showed specific interactions with biogenic amine receptors, such as adrenergic receptors and serotonergic receptors. Moreover, after selecting compounds with a $K_i < 1 \mu\text{M}$ or showing a recognition pattern within this series of compounds, molecular modeling studies have been performed based on x-ray structures and homology models. This allowed an improved understanding of the structural requirements for these off-target interactions with other Family A GPCRs. This systematic analysis of structural features of the ligands with amino acid residues of the binding site of the receptors is aimed at predicting promiscuity of new analogues within a ligand family and designing more selective ligands.³⁵

In a recent work, a chemoproteomic platform to explore the polypharmacological profile of 5-HT_{1A} and 5-HT₆ receptor ligands has been developed. This relied on synthesizing a new set of probes suitable for the nonbiased study of off-targets activities. Starting from high-affinity ligands of these receptors, proper modifications with appropriate tag(s) for covalent binding (such as benzophenone and biotin) have been introduced. The resulting probes allow subsequent enrichment of the bound proteins of the cell homogenate to enable protein profiling by using mass spectrometry. In addition to bind their cognate receptor, several additional targets have been identified in proteomic experiments. In particular, HSP60 and prohibitin

proteins have been recognized as off-targets of 5-HT_{1A} and 5-HT₆ receptor ligands, respectively. This approach could be extended to other drugs of interest to study the targeted proteome in disease-relevant systems.³⁶

Lastly, despite the remarkable progress in the field of GPCR biology during the past two decades, a number of GPCRs have not yet been linked to endogenous ligands. These “orphan” receptors represent a large part (> 140 GPCRs) of the genes encoding for GPCRs.³⁷ In this respect, Pfizer created a novel chemical probe identification platform with the aim of discovering chemical probes for members of orphan GPCR. GPCR-focused libraries were screened against a set of orphan GPCR targets, providing the identification of the first small molecule agonist for GPR39 receptor. It is thought that this receptor is involved in the regulation of insulin secretion and preservation of β -cells in the pancreas. As confirmed by functional and biochemical assays, this compound stimulated intracellular Ca²⁺ mobilization and cAMP signal transduction pathways in recombinant cells overexpressing GPR39, but not in parental cells. However, it did not potentiate glucose-stimulated insulin secretion in human islet preparations, possibly because the compound was not sufficiently potent or efficacious, GPR39 signaling through the Ca²⁺ pathway might not be coupled to insulin secretion, or GPR39 was not involved in insulin signaling.³⁸ Thus, the deorphanization of orphan GPCRs is one of the most important missions in GPCR research. Searching for ligands of orphan GPCRs and elucidating their structure, signaling, and physiological and pathophysiological roles shall offer new opportunities for discovering next-generation medicines.

These key issues sit at the forefront of GPCR research and are considered critical to the future successful development of new therapeutic modalities and drugs.

1.2 Functionalized congener approach to explore GPCR structure and function

In the early 1980s, the first reports appeared on the development of “functionalized congeners”, which were introduced by Jacobson and coworker.³⁹ Actually, two papers were reported on the same issue of *Journal of Medicinal Chemistry*,⁴⁰ which dealt with the development of functionalized congeners of adenosine as agonists and xanthines as antagonists of adenosine receptors. The approach was conceptually expanded in 1987, when Jacobson et al proposed its applicability towards different types of congeners and a wide range of GPCR.⁴¹ The functionalized congener approach was originally defined as the approach that allows the functionalization of a certain drug with known activity against GPCR (Figure 1). Particularly, it referred to a derivative presenting a chemical reactive functional group, such as an amine or carboxylic acid that can be covalently conjugated through a spacer linker to a position structurally permissive on the pharmacophore. This means that the insensitivity to structural modification of the attachment site is an essential and indispensable condition for the synthesis of covalent conjugates that retain binding affinities at the binding site. Thus, the goals of this approach focused on both developing potential new pharmaceutical agents in which the activity of the pharmacophore may be modulated through distal modifications, and on synthesizing molecular probes useful to explore the drug binding site and evoked response given by its interaction with the receptor.⁴¹ Moreover, an additional advantage of this approach is that the new congener may improve the pharmacological profile of the starting molecule by establishing secondary favorable interactions with the receptor.

Indeed, tethering different types of functionalized chain to a pharmacophore can provide a wide variety of chemical probes depending on the strategy of functionalization that includes spectroscopic probes, conjugation to carrier/dendrimer, dual-acting probes and so forth.⁴²

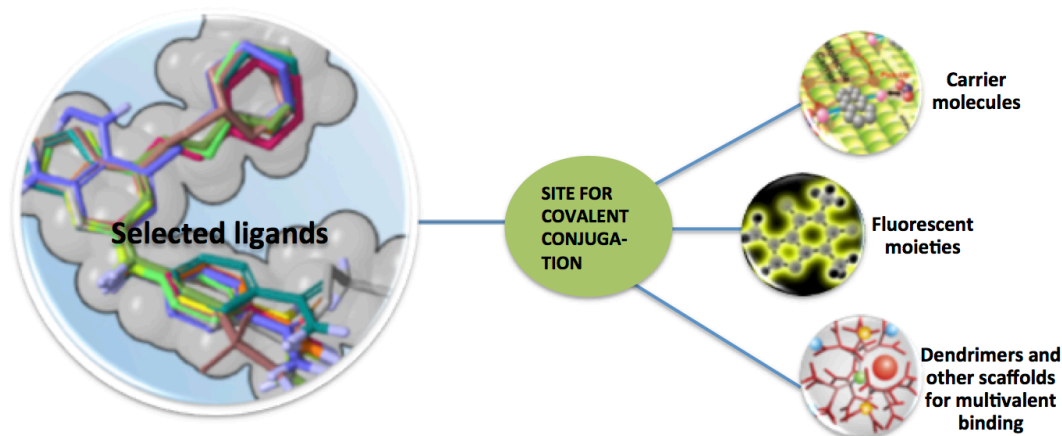


Figure 1. General representation of the functionalized congener approach.

Since that moment, this approach was particularly productive in elucidating the subtle differences among adenosine receptor (AR) subtypes, long before the first x-ray structure of A_{2A} AR was available.

And as confirmed by Wikström in a report named “Chemical Biology in the USA”, the brilliant work developed by Jacobson was indeed regarded as “a typical example of chemical biology research in the study of the different subtypes of a GPCR subfamily”.⁴³

Indeed, by applying this approach, Jacobson and coworkers successfully characterized the adenosine receptors and their agonists and antagonists, suggesting them as potential druggable targets.⁴⁴ At that time, adenosine receptors were just discovered and nothing or little was known about the physiological roles mediated by these receptors. Adenosine was considered a depressant neuromodulator and its involvement in multiple diseases and conditions including inflammation, endocrine disorders, cancer, cerebral and cardiac ischaemia has been only successively demonstrated.⁴⁴

Of note, this approach has been successfully applied to a wide range of GPCRs, including all the adenosine, P2Y, muscarinic acetylcholine and adrenergic receptors. To provide an exemplificative application of this approach, the A_3 AR and its congeners will be selected to further discussion in the following paragraph.

1.2.1 Adenosine A_3 receptor and its congeners: a landmark study

Adenosine A_3 receptors (A_3 ARs) are G protein-coupled receptors coupled to G_i/G_q and are involved in a variety of intracellular signaling pathways and physiological functions. A_3 ARs mediate a sustained cardioprotective function during cardiac ischemia, it is involved in the inhibition of neutrophil degranulation in neutrophil-mediated tissue injury, it has been implicated in both neuroprotective and neurodegenerative effects, and it may also mediate both cell proliferation and cell death.⁴⁵

The main approach to develop adenosine receptor agonists basically relied on modifications of endogenous ligand (adenosine) and can be schematically outlined as follows: modification of adenine by substituting N⁶-, C²-positions and modification of ribose moiety by C5'- and 4'-substitutions, and ribose ring constraint. On the other hand, adenosine constituted also the starting point to design A₃AR antagonists, having established the boundaries of structural requirements to switch from agonists to antagonists.⁴⁶ It should be mentioned that chemically diverse antagonists have been already developed, but they will not be described at this time (see cited review⁴⁷ for details).

Indeed, the prototypical A₃Rs agonist IB-MECA (CF101, **1** in Figure 2) and the more selective agonist Cl-IB-MECA (CF102, **2**) have been discovered in 1994 by introducing a 3-iodobenzyl group at N⁶ position and a chlorine at C² (only for Cl-IB-MECA) of adenine, and modifying the C5' position of the ribose moiety with a small amide group.⁴⁸

Once the structural requirements for obtaining A₃AR selective agonists have been confirmed,⁴⁹ these compounds have been widely used, as pharmacological probes in the elucidation of the physiological role of A₃AR and IB-MECA have been also radioiodinated, giving rise to [¹²⁵I]-I-AB-MECA, as a high-affinity radioligand for A₃AR.⁵⁰ Of note, IB-MECA (CF101) and Cl-IB-MECA (CF102), sponsored by Can-Fite BioPharma, are currently in clinical trials for the treatment of rheumatoid arthritis⁵¹ and hepatocellular carcinoma,⁵¹ respectively.

Modifications at the ribose moiety first regarded the 4'-thio substitution that affects AR selectivity, producing several highly potent and selective A₃AR agonists even varying the size of substituent at N⁶-position, such as compound **3**.⁵² This can be easily converted into selective antagonist **4**, by truncating 4'-thioadenosine derivatives at the 5' position.⁵³

Additionally, conformational studies of the ribose moiety and its equivalents indicate that the ring oxygen is not required for A₃AR selectivity and that the North (N) ring conformation is favored in binding to the A₃AR. The conformation constrain of the ribose-like ring is achieved by using the bicyclo[3.1.0]hexane ring system, which assumes an (N)-envelope conformation affording highly selective A₃AR agonists such as MRS3558 (**5**) (K_i = 0.29 nM at human A₃AR).⁵⁴ By contrast, the opposite isomer, which maintains a South (S) conformation of the ribose-like ring, was >100-fold less potent at the A₃R. A further conformational locking of ribose-like moiety can be obtained by modifying the 5' positions with a spiro lactam that produces a highly selective antagonist **6** toward A₃AR, suggesting that the A₃AR is not so strictly dependent on the 5' region for ligand recognition.⁴⁶

Substitutions at the C² position encompass the introduction of rigid arylalkynyl group in full agonist MRS5698 (**7**), a 3,4- difluorophenyl derivative, that appeared to be better tolerated by the receptor both in terms of affinity and selectivity (K_i = 3 nM at A₃AR).⁵⁵ To further extend the SAR studies, while keeping this last modification at C², the N⁶ position substitutions with both small and large hydrophobic groups at N⁶ maintained the activity as A₃R selective agonist.⁵⁵ On the other hand, truncation the 5' position of ribose-like ring provided also in this case selective antagonists, but only with small hydrophobic groups at N⁶ position, such as **8**.⁵⁶

Moreover, docking studies allowed to identify additional substitutions on C²-phenylethynyl and particularly sulfonate group substituent provided N⁶-3-

chlorobenzyl-2-(3-sulfophenylethynyl) derivative **9** (MRS5841) that bound selectively to human A₃R (K_i = 1.9 nM) as agonist.⁵⁷

Agonist analogues with greater in vivo efficacy were selected using a phenotypic screen in a Bennett mouse model of chronic neuropathic pain. This identified derivatives containing different C²-arylethynyl groups, such as 5-chloro-thien-2-yl in MRS5980 (**10**, K_i = 0.7 nM), that were particularly effective in vivo compared to **7**.⁵⁸

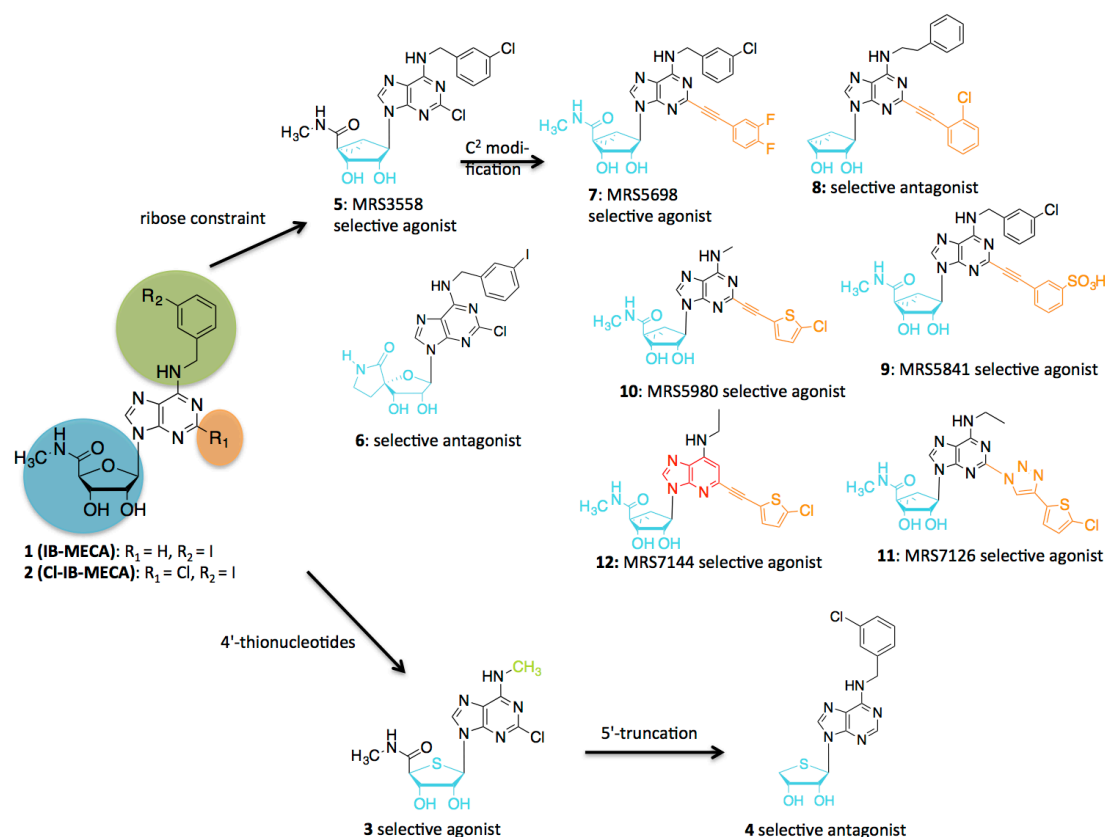


Figure 2. Development of A₃R congeners.

By combining molecular modeling and phenotypic screening to identify additional nucleoside derivatives with translational potential, the linear ethynyl group at C² has been substituted with a 1,2,3-triazol-1-yl linker. This modification would avoid potential in vivo liabilities of the alkyne group as a Michael acceptor for nucleophiles such as glutathione, although this risk was later shown to be minimal in a metabolomics study.⁵⁹ This modification successfully provided several N⁶-methyl derivatives, among which N⁶-ethyl 5-chlorothien-2-yl analogue (**11**, MRS7126) preserved in vivo efficacy (85% protection at 1 h) with short duration.⁶⁰

In addition, N⁶-small alkyl derivatives were newly optimized for A₃AR affinity and the effects of a 1-deaza-adenine modification probed. 1-Deaza-N⁶-ethyl alkyne **12** (MRS7144, K_i = 1.7 nM) was highly efficacious in vivo. Thus, the presence of N¹ is not required for nanomolar binding affinity or potent functional activity. Docking of 1-deaza compounds to a receptor homology model confirmed a similar binding mode as previously reported 1-aza derivatives. This is the first demonstration in non-ribose adenosine analogues that the 1-deaza modification can maintain high A₃AR affinity, selectivity, and efficacy.⁶¹

Collectively, the iterative optimization process of adenosine-based A₃ ligands showed that there is a pronounced interrelationship of substitution at various sites

on the adenosine structure with respect to their effects on A₃AR affinity, selectivity, and efficacy.

Another alternative of functionalized congener approach is the development of fluorescent ligands for characterization of adenosine receptors (ARs), which hold promise in drug discovery. The size of a strategically labeled AR ligand can be greatly increased after the attachment of a fluorophore, with the possibility of improving the pharmacological profile of the parent molecule via secondary interactions given by the fluorophore. Indeed, the choice of fluorophore (e.g. Alexa Fluor 488), attachment point and linker length can significantly alter the selectivity and potency of the starting molecule. Fluorescent derivatives of adenosine agonists and antagonists (e.g. XAC and other heterocyclic antagonist scaffolds) have been successfully synthesized and characterized.⁶²

In particular, several previously developed A₃ agonist and newly synthesized congeners have been conjugate to a fluorophore linked through the C² or N⁶ position of adenosine-based ligands presenting the (N)-methanocarba structural motif for enhancing A₃R selectivity. Such fluorescent derivatives were compared in radioligand binding affinity and selectivity at the human A₃R in membranes of Chinese hamster ovary (CHO) cells expressing the receptor. Two derivatives namely MRS5218 (**13** in Figure 3) and MRS5704 (**14**) were the most promising derivatives and were selected for further studies in subsequent experiments using whole cells. In particular, **13** was tethered to the Cy5 fluorophore (a cyanine dye that absorbs in the orange region and fluoresces in the red region), by a flexible amide chain at the C² position. In contrast, **14** was conjugated to the rigid polycyclic 1-pyrenyl fluorophore moiety through an ethynyl group extending from the C² position. By flow cytometry

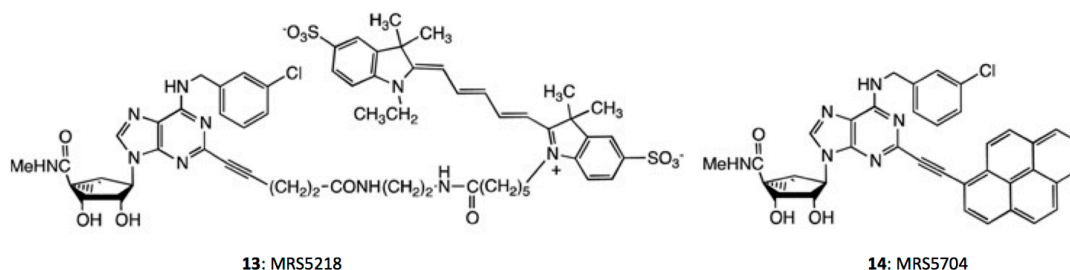


Figure 3. Fluorescent A₃R ligands.

experiments, the hydrophobic C²-(1-pyrenyl) derivative **14** has been showed to bind non-selectively, whereas C²-tethered cyanine5-dye labeled **13** bound selectively to human A₃R expressed in whole CHO cells. The same behavior of **13** was observed in a native cell line expressing A₃R (human promyelocytic leukemic HL-60 cell line). These findings suggested that **13** might be a useful tool for characterizing the A₃AR.⁶³ The functionalized congener approach has been demonstrated to be feasible for modulating and even enhancing the pharmacological profile of a ligand of a GPCR based on conjugation to a biocompatible polyamidoamine (PAMAM) dendrimers designed to interact with distal extracellular regions of a 7TM-spanning receptor without drug release unlike nanocarrier.⁶⁴

Jacobson and coworker have reported on the feasibility of potent and selective activation of specific subtypes of ARs using multivalent conjugates and the ability to modulate the selectivity based on the linkage between the pharmacophore and the polymeric carrier. Particularly, N⁶-chain elongated functionalized congener ADAC (N6-[4-[[[4-[[[(2-aminoethyl)amino]carbonyl]methyl]anilino]carbonyl]methyl]-

phenyl]-adenosine), A₁ congener has been covalently conjugated to polyamidoamine (PAMAM) dendrimers of both generations 2.5 (G2.5) and 3 (G3) and further linked to AlexaFluor 488 (AF488) moiety for fluorescent detection. Depending on the nature of the linker moiety, the G2.5 multivalent conjugates led to unexpected high selectivity in binding to the human A₃AR with the most selective G2.5 **15** showing > 100-fold selectivity in both radiobinding ($K_{i\text{ app}} = 2.4$ nM) and functional assays ($EC_{50} = 1.6$ nM in inhibition of adenylate cyclase) compared to A₁ and A_{2A} receptors. Moreover, since residual amino groups on dendrimers are associated with cytotoxicity, the G2.5 dendrimer **15** carrying an unreacted terminal carboxylate groups was selected for fluorescent microscopy studies. Intriguingly, the A₃R selective G2.5 dendrimer **15** was able to bind CHO cells expressing the A₃AR but did not bind cells that did not express the receptor. However, the fluorescent signal was not uniform on the membrane, suggesting the potential existence of higher-order receptor oligomers of A₃AR. Thus, this A₃AR selective conjugate **15** could be useful in pharmacological models of tissue rescue from ischemia and as a fluorescent conjugate tool to characterize the A₃R in situ and to probe the existence of A₃AR oligomers.⁶⁵

In a following example, again the N⁶-chain elongated functionalized congener ADAC was conjugated to higher generation (G5.5) PAMAM dendrimers, generating high molecular weight (60 amide-linked nucleoside moieties), multivalent AR agonist acting at the A₃AR. Additionally, an amine-functionalized derivative of AF488 was introduced to the dendrimer, as seen previously. The resulting dendrimer **16** was only slightly selective for the A₃AR in radiobinding assay and non-selective in an assay of adenylate cyclase inhibition. Despite that, it displayed to protect A₃-transfected HL-1 cells using both an LDH assay and an apoptosis assay with greater potency ($IC_{50} = 35$ nM) than the corresponding monomeric nucleosides, which protected in the μ molar range. Thus, a multivalent conjugate not only has been demonstrated to preserve binding affinity at the ARs, but also it displayed greatly enhanced functional potency in an in vitro model of cardioprotection.⁶⁶

In the search of different linker moieties to use for dendrimers-nucleosides covalent coupling, Cu(I)-catalyzed “click” chemistry reaction was exploited to conjugate the distal alkyne of a 2-octadiynyl nucleoside previously synthesized with the azide-derivatized G4 (fourth-generation) PAMAM dendrimers to form triazoles. The newly synthesized triazole-linked conjugates retained A₃AR activation with apparent K_i of 0.1–0.3 nM, displaying selectivity and enhanced A₃AR affinity in comparison with various amide-linked dendrimers. Furthermore, a bifunctional conjugate **17** was also prepared by linking both A₃ (via triazole-linked conjugates) and P2Y₁₄ receptors (via amide-linked uridine-5'-diphosphoglucuronic acid) pharmacophores. **17** represents the first example of multivalent dendrimer conjugate able to simultaneously targeting two different GPCRs with selectivity over other ARs and P2Y receptors that can be useful to evaluate the formation of heteromeric GPCR aggregates. Moreover, this polypharmacological profile may exert synergistic effects useful in disease treatment.⁶⁷

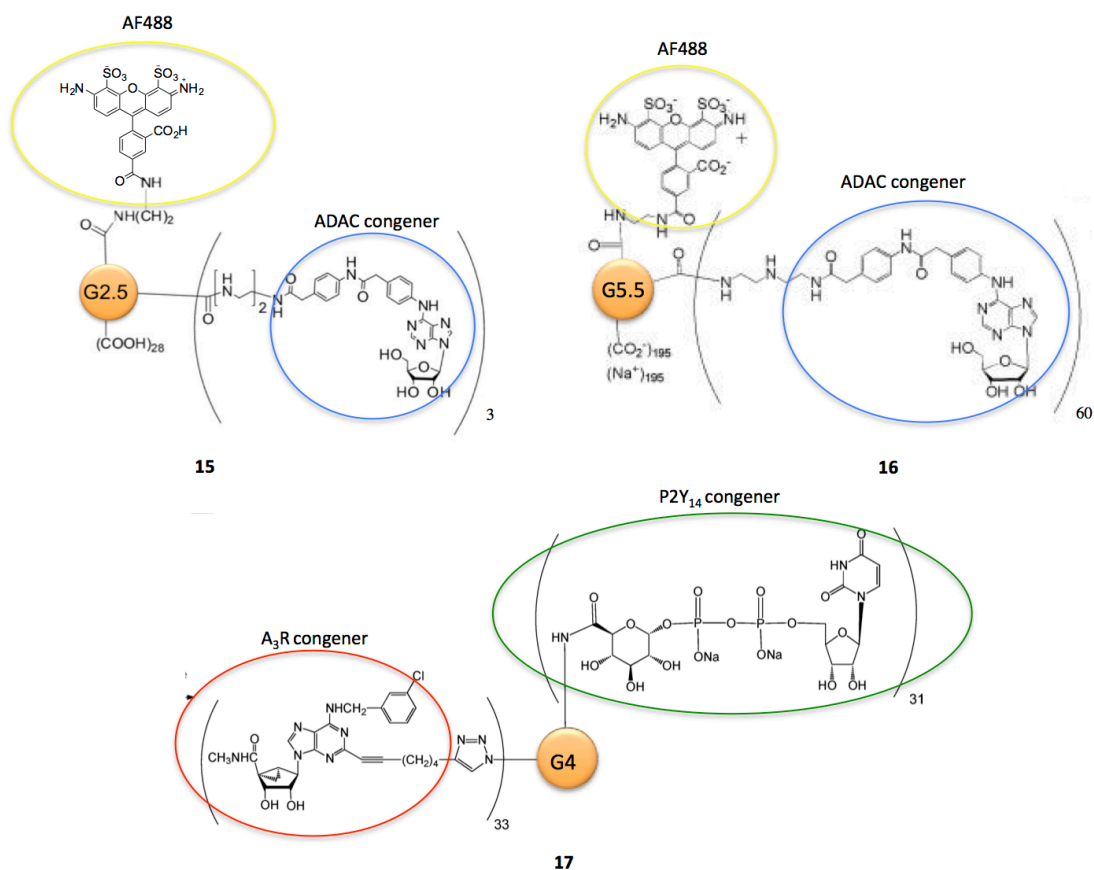


Figure 4. Functionalized A₃R congeners conjugated to PAMAM dendrimers.

Hence, the functionalized congener approach, including both small molecules and macromolecular conjugates development, has been brilliantly applied for studying the chemical and biological properties of GPCRs, thus having the potential to provide useful tools in GPCRs research and also in some cases useful therapeutics.

1.3 P2Y₁₄ receptor as drug target

Despite the well-characterized adenosine and purinergic receptors discussed earlier, only about fifteen years have elapsed since the first characterization of the orphan gene GPR105,⁶⁸ subsequently named P2Y₁₄ receptor (P2Y₁₄R).⁶⁹ This receptor is a G_i-coupled receptor potently activated by UDP-glucose (UDPG, **18** in Figure 5) that, even sharing important structural similarities with members of the P2Y receptor family, displays a significantly different pharmacological response profile.

The P2Y receptors (P2YR) are a group of eight molecularly defined GPCRs that can be divided in two subfamilies, according to the primary sequence identity and to the G-coupled protein. The P2Y₁R, P2Y₂R, P2Y₄R and P2Y₆R activate G_q/phospholipase C-β and can be grouped into a P2Y₁R-like subfamily of P2YR. The P2Y₁₂R, P2Y₁₃R and P2Y₁₄R exhibit 45–50% homology and comprise a second group of P2YR, the so-called P2Y₁₂R-like subfamily that activate the G protein of the G_{αi/o} and inhibit adenylyl cyclase activity.⁷⁰

P2Y₁₄R identified as the most recently discovered receptor among the other members of P2Y family, is now well known that is activated not only by UDPG, but also other nucleotide sugars with a relative potency order (in a concentration range

0.1-1.0 μ M): UDP-glucose (**18**) > UDP-galactose (**19**) > UDP-glucuronic acid (UDPGA, **20**) > UDP-N-acetylglucosamine (**21**).⁷¹ Moreover, following studies revealed that also UDP is a potent agonist of P2Y₁₄R.⁷²

Given its peculiar feature to be the only known P2Y subtype to be activated by UDP-glucose, P2Y₁₄R adds diversity to the P2Y family⁶⁹ and stimulated a flurry of studies not only concerning its role in health and diseases, but also regarding the physiological functions of UDP-sugars, which have long been considered exclusively as activated carriers of sugar moieties in the metabolism of carbohydrates.⁷¹

The widespread distribution of P2Y₁₄R was observed in adipose tissue, stomach, intestine, some brain regions, skeletal muscles, spleen, lung, and heart and it is associated with immune and inflammatory cells as well as many epithelia suggesting a pivotal role in immune and inflammatory responses.⁷³

Indeed, P2Y₁₄R expression and UDP-glucose were up-regulated following inflammatory injury in mast cell-like cell lines, suggesting that the P2Y₁₄R is a mediator of degranulation in these cells. Accordingly, the potent P2Y₁₄R agonist, 2-thio-UDP-glucose, enhanced the release of β -hexosaminidase, an indicator of granule secretion.⁷⁴ Using siRNA to knock down the P2Y₁₄R also reduced hexosaminidase secretion. Similar results were reported using the human bone marrow-derived mast cell line LAD2, and incubation of these cells with the selective antagonist PPTN (10 μ M) resulted in reduced UDP-sugar-potentiated C3a-promoted hexaminidase secretion.⁷⁵

UDP-glucose also promoted Rho kinase-dependent chemotaxis of human neutrophils,⁷⁶ and adding the P2Y₁₄R antagonist PPTN to a polymorphonuclear neutrophils suspension abolished this effect.⁷⁷

In addition to promoting recruitment of circulating neutrophils, UDP-glucose induced the mobilization and enhanced re-location of bone marrow stem cells.⁷⁸ Particularly P2Y₁₄R-mediated hematopoietic stem cell mobilization provides a potential tool to improve the efficiency and outcome of hematopoietic peripheral stem cell transplantation. Furthermore, primitive hematopoietic stem cells lacking P2Y₁₄R displayed impaired ability to restore hematopoiesis in irradiated mice, suggesting that the P2Y₁₄R on progenitor stem cells promotes regenerative responses after injury.⁷⁹

Functional studies regarding the high expression levels in the gastrointestinal tract revealed an influence of P2Y₁₄ in gastric motility function; however Bassil et al. demonstrated that some effects of UDP-glucose were independent of P2Y₁₄R signaling.⁸⁰ P2Y₁₄R has also been identified as one of the 293 GPCRs expressed in human pancreatic islets.⁸¹ It is known that GPCRs play a critical role in regulation of hormones secretion from pancreatic islets. Depending on their presence in different islet cells (α -, β -, or δ - cells), a certain GPCR have a different impact on the release of glucagon, insulin or somatostatin. Interestingly, a recent study suggests contribution of the P2Y₁₄R to this process.⁸² Particularly, it pointed out that UDP-glucose released from liver cells in obese states, acts as a chemo-attractant to recruit monocytes/macrophages, leading to liver inflammation and insulin resistance. Indeed, P2Y₁₄R knockout mice were protected from high fat diet (HFD)-induced glucose intolerance, and exhibited improved systemic insulin sensitivity and enhanced insulin action in adipose tissue, liver and skeletal muscles. Furthermore, P2Y₁₄R knockout mice exhibited a reduced number of macrophages in the liver compared to wild type and the plasma levels of UDP-glucose were 4-fold elevated in HFD-fed animals compared to controls.⁸²

Notably, a recent report that is in apparent conflict with the results described above showed no differences in insulin sensitivity between western diet (rich in fat and cholesterol)-fed wild type and P2Y₁₄R-deficient mice.⁸³ Meister and coworkers also found that insulin immunostaining of pancreatic tissue was similar in both genotypes, but glucose-promoted insulin secretion and serum insulin levels in perfused islets were markedly reduced in P2Y₁₄R-deficient mice. Perfusion of wild type islets with UDP-glucose did not increase insulin secretion, supporting the fact that the P2Y₁₄R regulates functions necessary, but not sufficient to promote insulin granule exocytosis. Additionally, transcriptome analysis of pancreatic islets demonstrated that P2Y₁₄R deletion led to the down regulation of >300 genes, including the glucose transporter SLC2A2 and several GPCR-modulated insulin release pathways.⁸³

The discrepancy highlighted by these two studies may be ascribed to the different contributions of liver inflammation in insulin sensitivity between the two mouse models; but also suggest that the physiological relevance of P2Y₁₄R still remains to be defined in more detail.

Taken together these experimental evidences support the idea that P2Y₁₄R may be an attractive target for the treatment of diabetes and other inflammatory diseases. However, to date, the P2Y₁₄R has not been widely explored from a medicinal chemistry perspective. Concerning the agonists, the structure-activity relationships (SAR) of analogues of the native ligands have been evaluated by Jacobson's group. The P2Y₁₄R receptor seems to be the most structurally restrictive member of the P2Y family, at least with respect to modification of the nucleobase, ribose and phosphate moieties of agonist ligands. Nonetheless, the demonstration that also UDP activates P2Y₁₄R, suggest that the glucose moiety is amenable to modification and is not required for activation of the P2Y₁₄R. Indeed, following studies support the initial hypothesis that the glucose moiety of UDPG can be modified.

The first SAR study was directed to explore modifications of the nucleobase, which led to the identification of 2-thio-UDP-glucose (MRS2690, **22** in Figure 5) displaying 7-fold greater potency for the P2Y₁₄R than does UDP-glucose.⁸⁴ Several analogues of UDP also have been developed that exhibit high potency and selectivity at the P2Y₁₄R, by replacing glucose with other sugars, substitution of hydroxyl groups of glucose with fluorine, and chain extension. Indeed, docking studies based on the previously developed model of P2Y₁₄R,⁸⁵ suggest that the hexose moiety of UDPG interacts with multiple H-bonding and charged residues and therefore may provide a suitable region for agonist modification.⁸⁶ Indeed, the carboxylate group of UDPGA can be extended via an amide linkage to a flexible chain (i.e. 2-acylaminoethylamides derivatives), without loosing P2Y₁₄R activity. Molecular modeling explained that retain the activity because of predicting the close proximity of this chain to the second extracellular loop of the receptor. In addition, replacement of glucose with other sugars did not significantly affect P2Y₁₄R potency. Accordingly, elective monofluorination of the glucose moiety highlighted the importance for the 2''- and 6''-hydroxyl groups in receptor recognition. All the other attempts to modify ribose such as abolished the activity.⁸⁶

Based on these findings, the structural permissive site was further modified by removing or substituting with smaller phosphoester groups, which were tolerated at this receptor. Simple alkyl esters at this position and analogues of UDP displayed highly potent agonist activity at the P2Y₁₄R. The effects of these modifications to preserve and enhance potency at the P2Y₁₄R were additive with the previously

identified 2-thio substitution of the uracil moiety, affording compounds with nanomolar and subnanomolar potency. These include α,β -difluoromethylene-UDP

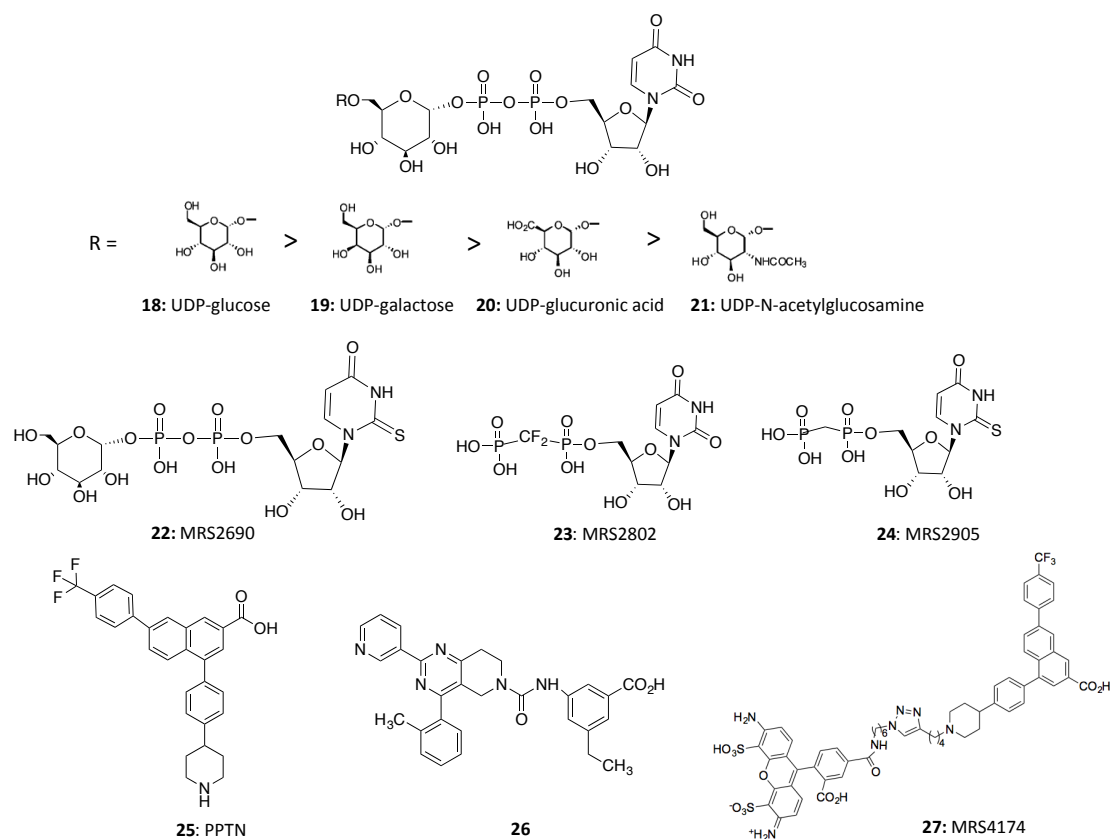


Figure 5. P2Y₁₄R agonists, antagonists and fluorescent antagonist probe.

(MRS2802, **23**) and α,β -methylene-2-thio-UDP (MRS2905, **24**). Notably, these molecules also displayed high selectivity for activation of the P2Y₁₄R at concentrations that are inactive at the UDP-activated P2Y₆ receptor as well as at other P2Y receptors.⁸⁷

On the other hand, non-nucleotide antagonists of the P2Y₁₄R have been discovered through high-throughput screens by the Merck Frosst company, leading to the identification of Black and coworkers applied high-throughput screens to identify naphthoic acid (**25**)⁸⁸ and dihydropyridopyrimidine (**26**)⁸⁹ compounds as potential P2Y₁₄R antagonists with pIC₅₀ values of 2.2 and 8.4, respectively. Analogs of each type of molecule subsequently were synthesized. Whereas dihydropyridopyrimidine derivatives (**26**) appeared to be noncompetitive antagonists of the P2Y₁₄R, the 4,7-disubstituted naphthoic acid derivative (PPTN, **25** in Figure 5) inhibited [³H]-UDP binding suggesting antagonist of the orthosteric site of the receptor. Even though PPTN shows a promising pharmacological profile, not inhibiting up to 10 μ M PPTN the other G_{q/i}-linked P2YRs, but unfortunately, it displays low oral bioavailability, and additional P2Y₁₄R antagonists will be needed.

Additionally, few selective radioligands for P2YRs are available, thus improved and more versatile affinity probes are needed.⁹⁰

To this end, Kiselev et al. designed the first fluorescent ligand of the P2Y₁₄R, i.e. the AF488-labeled antagonist MRS4174 (**27**).⁹¹ This compound contained a functionalized chain at the secondary nitrogen of the piperidine ring, selected as suitable for tethering fluorophore on the basis of docking studies at a P2Y₁₄R

homology model. An azide-bearing AF488 was conjugated to the alkyne congener of **25** by [2 + 3] click cycloaddition reaction. Flow cytometry showed high specific P2Y₁₄R binding of MRS4174 (**27**) with exceptionally high affinity ($K_i = 80$ pM) in antagonizing UDPG-induced cAMP inhibition in P2Y₁₄R-expressing CHO cells. Collectively, the development of P2Y₁₄R fluorescent probes and small molecules agonists and antagonists both as pharmacological tools and as potential therapeutic agents may lead to considerable progress for further supporting and expanding the previous pharmacological investigations.

2. Aims and objectives

Since the introduction of fluorescent ligands in the mid 1970s,⁹² they have been widely applied as powerful tools to monitor the structure and dynamics of GPCRs. The success of such approach lies on the fact that, in comparison to isotope-labeled methods, fluorescence-based technology represents a safe and inexpensive way to “watch” receptors in living cells because of its biocompatibility, affordability, and feasibility in a variety of strategies.⁹³

Notably, the value of fluorescent probes for receptors grows in parallel to the development of sophisticated fluorescent techniques⁹⁴ and more efficient fluorescent dyes as well.⁹⁵ Indeed, the advancement of fluorescence reagents, not only offer a wide range of new fluorophores with different physicochemical and spectroscopic properties (such as excitation and emission wavelengths, photobleaching, fluorescence quantum yield, stability, etc.), but has also resulted in a multitude of more complex fluorescence technologies such as fluorescence resonance energy transfer (FRET), fluorescence activated cell sorting (FACS) and fluorescence correlation spectroscopy (FCS), etc.⁹⁴

Moreover, as already discussed, the versatility of this approach allows its application to a wide range of molecules including small molecules, antibodies, proteins, and dendrimers. Among these probes, fluorescent ligands efficiently consent the real-time monitoring of ligand–receptor interactions, the visualization and localization of GPCRs, their internalization and trafficking. On the other hand, fluorescent antibodies, proteins, and amino acids mostly contribute to receptor-based studies, such as receptors oligomerization.⁹⁶ Importantly, fluorescent probes play also a pivotal role in studying orphan GPCRs.

Currently, the main strategy to rationally design fluorescent ligands relies on conjugating an agonist or antagonist of the GPCRs to various fluorophores. By using this strategy, GPCR fluorescent ligands with high affinity and selectivity have been reported, as seen for A₃R receptor.⁶² However, some key issues must be addressed in probe design, especially including physicochemical properties and pharmacological activities of the final probes. Because of the large mass of fluorophores, their conjugation to ligands or pharmacophores targeted at GPCRs may have a big impact on the properties of the final conjugate, especially the affinity and selectivity to the receptor. Thus, the choice of a fluorophore is perhaps the most critical step in the rational design of fluorescent probes.⁹³ Accordingly, numerous factors are implicated in its biological functionality, and these include excitation and emission wavelengths, fluorescence quantum yield, fluorescence life-time, photostability and size. This latter factor is of fundamental importance because significantly impacts on the physicochemical properties of fluorescent conjugates, especially in the case of small molecule-based probes, often causing nonspecific binding.⁹⁵

Another important aspect to consider is the positional attachment of a fluorophore to the ligand structure. It must be particularly suitable to minimize the influence on receptor binding affinity.

Furthermore, the linker should provide the proper spacing between the pharmacophore and fluorophore in order to maintain the pharmacological activity and hopefully improved solubility, stability and affinity. Usually, the linker is a carbon chain that ends with heteroatoms such as nitrogen atoms. The terminal heteroatom groups are used to couple with the fluorophores or pharmacophores. It has been

reported that the high lipophilicity would increase the nonspecific binding of a fluoroligand. Therefore, polyamide, polyethylene glycol, and peptide hydrophilic linkers are being preferred.⁹³

Compared with peptide, antibodies, proteins, and amino acids -based probes, small-molecule probes have become more promising tools for the study of GPCRs, owing to their tremendous advantages in stability, solubility, reasonable cell permeability, subtype selectivity, and application in high-throughput screening.

The development of such probes started with the selection of a known ligand or drug. This ligand must have a high affinity and selectivity to the receptor, as well as a structurally permissive site for further modification in its chemical structure.⁶² A reactive group, such as amine, hydroxyl, alkynyl, or carboxyl group, is generally introduced into the ligand molecules and following condensation and click reactions at this site are performed to conjugate the pharmacophores and linkers or fluorophores.

In light of these considerations, the functionalized congener approach aimed at developing fluorescent probes targeting P2Y₁₄ is particularly attractive because of the limited knowledge of its structure and physiological responses.

As previously mentioned, in a recent paper, Jacobson and coworker have reported on the structure of the first P2Y₁₄ fluorescent antagonist probe structurally derived from the potent and highly selective PPTN antagonist (**25**).⁹⁷ This molecule selectively labeled the P2Y₁₄R in live cells as quantified by flow cytometry. It has been designed based on the docking studies performed with **25** showing that the piperidine moiety is suitable for tethering fluorophores. Click chemistry has been used to conjugate functionalized an alkyne derivative of **25** and the azide bearing AlexaFluor488. However, the previously reported synthesis of fluorescent antagonist MRS4174⁹⁷ (**27**) suffered from a low yield in the final click cycloaddition step to link the azide-functionalized fluorophore and the alkyne-functionalized pharmacophore. Given the remarkably high affinity of **27** and its low nonspecific character, we explored an alternate synthesis of this compound. This was necessary to provide a sufficient supply of this fluorescent probe to be use in displacement assay.⁹⁸

In parallel, the design of fluorescent agonist probes has been envisioned based on previous SAR studies of UDP analogues. Particularly, the terminal sugar moiety of UDPG has been identified as structurally permissive for further modification without losing the activity. In particular, the amide derivatives at the glucose C6 position have been found to retain the activity toward P2Y₁₄R. Thus, for designing fluorescent-agonist probes at P2Y₁₄R, the UDPGA has been selected as suitable starting point. Particularly, UDPGA has been conjugated to different boron-dipyrromethene (BODIPY) dyes with the reactive amine linkers of varying length. Importantly, the longer chain analogue MRS4183 retains the activity and served as a tracer for microscopy and flow cytometry, displaying minimal nonspecific binding.⁹⁹

Additionally, thanks to the recent human P2Y₁₄R homology model based on human P2Y₁₂R X-ray structures¹⁰⁰ as template to conduct docking and molecular dynamics simulations, the development of non-nucleotide based antagonists has been envisaged starting from the structure of **25**. The immediate goal was to suggest bioisosteric substitutions to the hydrophobic and bulky naphthalene ring of **25** that would maintain a similar orientation of the piperidine and 4-(trifluoromethyl)-phenyl substituents when bound to the receptor and therefore preserve receptor affinity. Along this line, we aim at simultaneously reducing both the molecular weight and the high lipophilicity of **25** that contributes to its low solubility and

difficulty of purification. On these bases, the design and synthesis of structural analogues of **25** have been developed by replacing one phenyl ring of naphthoic acid core of **25** with an alkyne or a triazole. In particular, I was involved in the first part of the development of triazolyl derivatives, enabling to set up the synthetic route for achieving 3 of the overall 40 triazole compounds.^{98, 101}

To sum up, given the increasing interest in developing fluorescent ligand probes as pharmacological tools for characterizing GPCRs, a new synthetic route to obtain the previously synthesized fluorescent antagonist probe **27** has been reported. The main goal consists of improving the reaction yield as **27**, which has proved to be a highly potent and selective in situ tracer of P2Y₁₄R in whole-cell binding assays. In parallel, the development of P2Y₁₄R fluorescent congeners has provided the opportunity to get additional insights to further study the role and distribution, as well the structural feature of the binding site of this receptor.

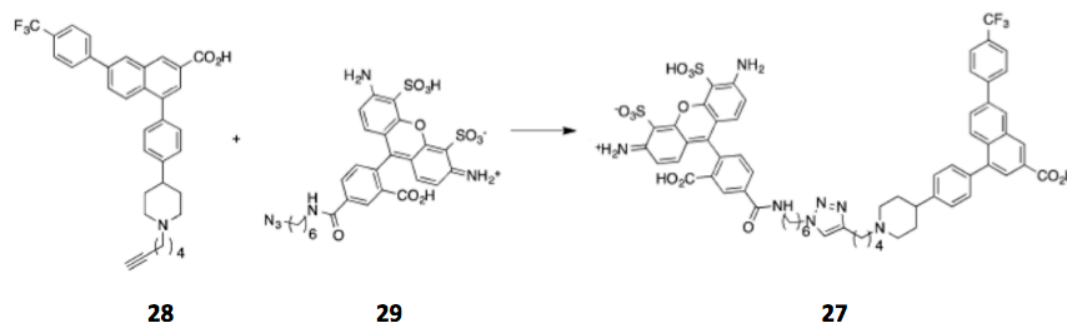
As a further step, the development of non-nucleotide antagonists makes possible to achieve compounds with better physicochemical properties compared to the liabilities of nucleotide-based ligands and the low bioavailability of **25**.

Collectively, such fluorescent congeners and non-nucleotide antagonists may be powerful tools in expanding the SAR of P2Y₁₄R, which still lacks chemical diversity in its collective ligands.

3. Chemistry

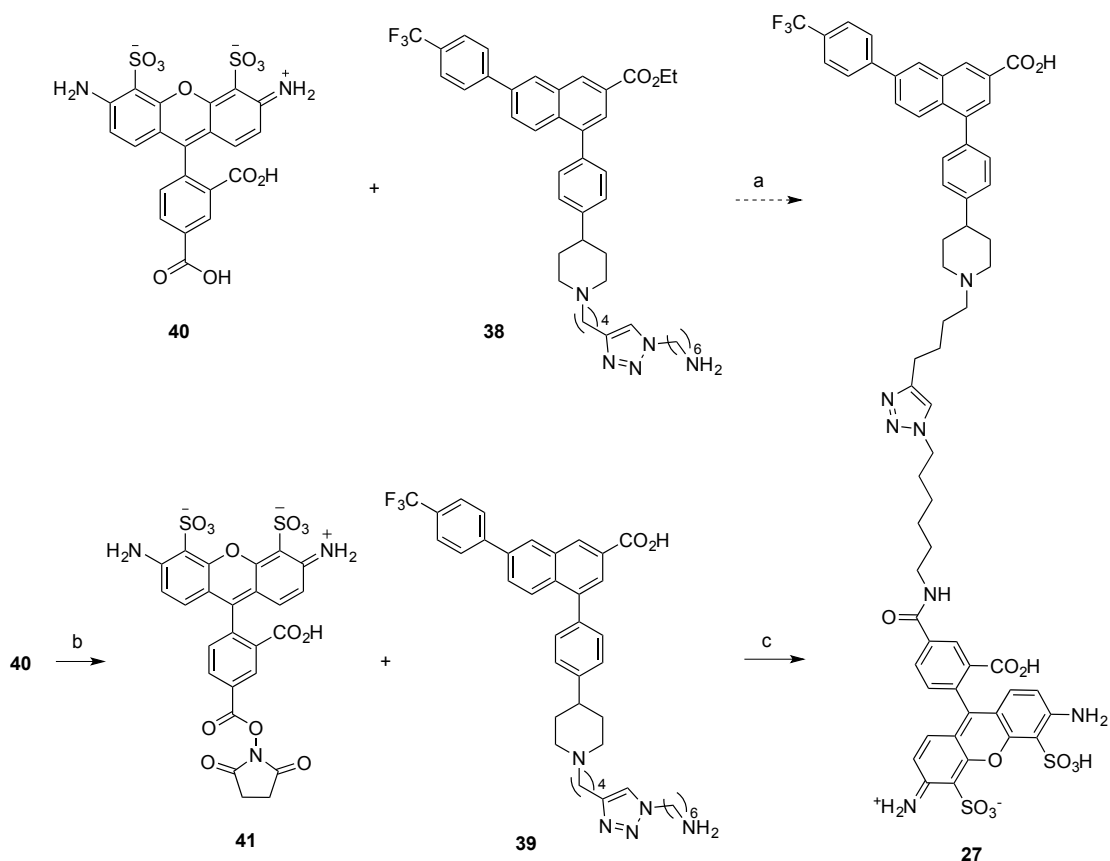
3.1 Alternative synthesis of fluorescent P2Y₁₄ antagonist

The previously developed synthesis of **27** suffered from a low reaction yield (4%) in the final click cycloaddition step to link the azide-functionalized fluorophore **29** and the alkyne-functionalized pharmacophore **28** (Scheme 1).⁹⁷



Scheme 1. Reagents and conditions: CuSO₄ (7.5% aqueous solution), sodium ascorbate (1 M aqueous solution), tBuOH, H₂O, 25°C (4%).

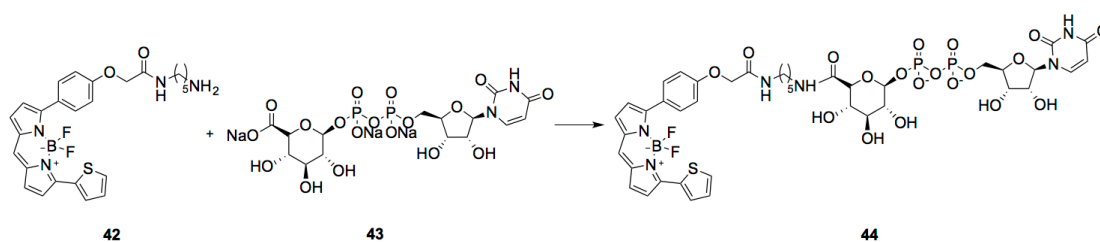
Thus, we explore a more efficient route that consisted of forming an amide as the ultimate step (Schemes 2A and 2B).⁹⁸ In details, to provide the functionalized congener **28**, the synthetic pathway started with the formation of the two parts composing the triazole linker chain. In particular, the functionalized alkyne chain **32** has been synthesized from compound hex-5-yn-1-ol **30**, which was subjected to two substitution reactions, involving first the formation of the tosylate **31** and its following replacement with a bromine. Next, 6-amino-1-hexanol **33** was reacted with HBr to afford its bromine derivative **34**, substituted again to afford the chain bearing the azide functionality **35**. Once formed the key intermediates **32** and **35**, **32** was conjugated to the pharmacophore of **25**, previously protected at carboxylic function as ethyl ester **36**, yielding functionalized congener **37**. To provide the triazole **38**, click chemistry reaction was exploited involving the azide **35** and the alkyne functionalized congener **37** (Scheme 3A).¹⁰² The functionalized congener **38**, containing the preformed triazole chain with a terminal amino function, was then converted to the corresponding carboxylic acid derivative **39** by using LiOH to hydrolyze the ester.



Scheme 2B. Reagents and conditions: **b.** TSTU, DIPEA, DMF, 0 °C for 1 h then r.t. for 2h; **c.** **39**, DIPEA, DMF, overnight.

3.2 Synthesis of fluorescent P2Y₁₄ agonist

As depicted in Scheme 3, the synthesis of derivative **44** (MRS4183) was accomplished using standard coupling conditions involving the commercially available primary amine of the BODIPY dyes (**42**) and the carboxylate group of UDP-glucuronic acid **43**.⁹⁹



Scheme 3. Reagents and conditions: COMU (1.5 equiv), DIPEA (2 equiv), DMF, 0 °C, 0.3% yield.

Before establishing this synthetic protocol, different conditions were tried (Table 1) to increase the reaction yield and simplify the purification process. Indeed, the first attempt (condition A) to synthesize **44** resulted in an impure product even after several successive purification attempts, due to an impurity co-eluting with the desired product. The higher reactivity of a different coupling agent, [[(Z)-(1-cyano-2-ethoxy-2-oxoethylidene)amino]oxy-morpholin-4-ylmethylidene]-dimethylazanium hexafluorophosphate (COMU, conditions B and C), compared to HATU led to the

formation of numerous side products during the reaction that complicated the purification process (2 or 3 purifications) without leading to a significant detectable amount of title compound. Nevertheless, the best performing procedure (condition D), using excess of **43** (1.5 equiv), COMU (1.5 equiv) as coupling agent and DIPEA (2 equiv) as base, provided the desired, pure product after one purification step using a C18 HPLC column, however, in a very low yield (0.3%).⁹⁹

Table 1. Different conditions used for obtaining derivative **44**. The solvent used was dry DMF. Condition D gave the best results.

Condition	Bodipy TR-cadaverine.HCl (42)	UDP-glucuronic acid.Na ⁺ ₃ (43)	Coupling agent	Base
A	1 eq	1.5 eq	HATU 1.5 eq	NEt ₃ 1 eq
B	1.2 eq	1 eq	COMU 1.5 eq	DIPEA 1.5 eq
C	1 eq	1.5 eq	COMU 1.5 eq	DIPEA 1.5 eq
D	1 eq	1.5 eq	COMU 1.5 eq	DIPEA 2 eq

Abbreviations: COMU, [[(Z)-(1-cyano-2-ethoxy-2-oxoethylidene)amino]oxy-morpholin-4-ylmethylidene]-dimethylazanium hexafluorophosphate; HATU, 1-[bis(dimethylamino)methylene]-1H-1,2,3-triazolo[4,5-b]pyridinium 3-oxid hexafluorophosphate; DIPEA, diisopropylethylamine.

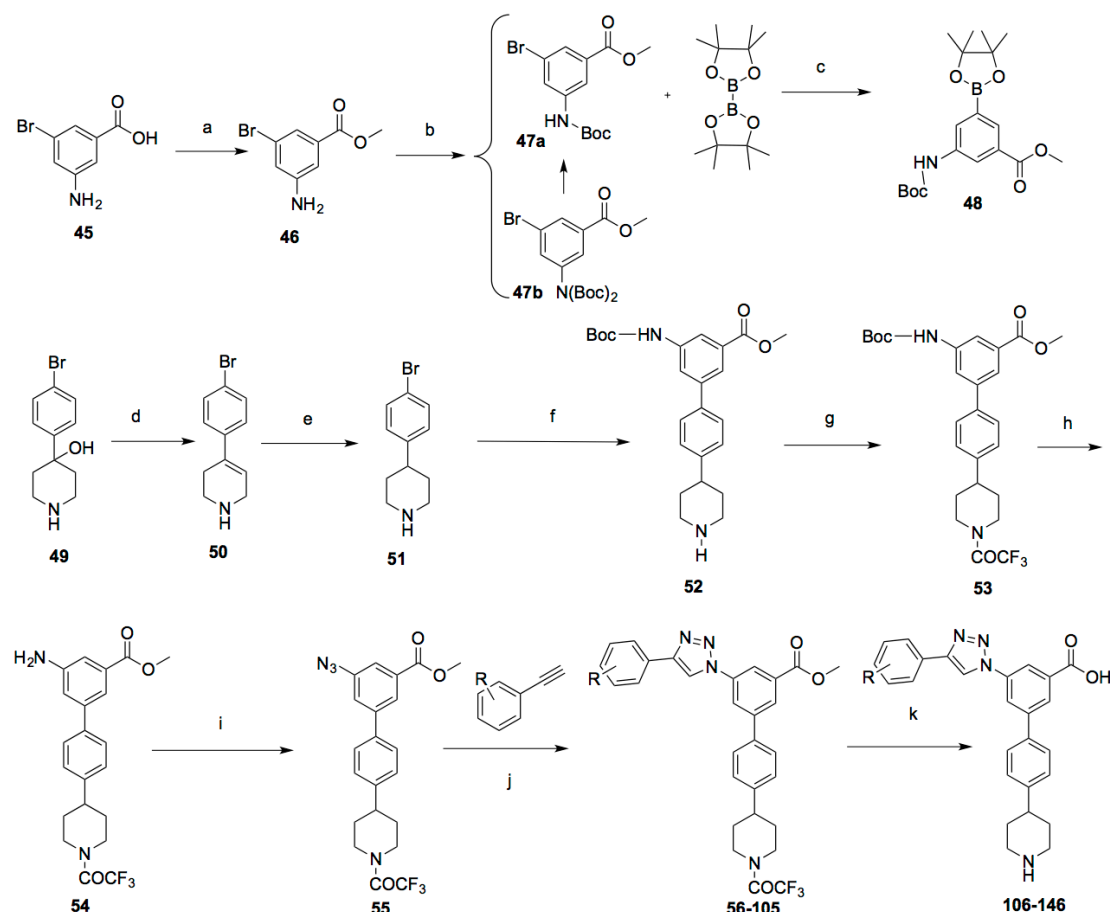
3.3 Synthesis of P2Y₁₄ antagonists

Based on the recently developed hP2Y₁₄R homology model built on the agonist-bound hP2Y₁₂R X-ray structure and refined by molecular dynamics,¹⁰⁰ the docking pose of PPTN **25** suggested two bioisosteric alternatives to the naphthoic acid core. The first relies on replacing one phenyl ring of naphthoic acid core of **25** with an alkyne group (synthesis not showed, see Results and Discussion). However, this modification provided derivative **148** displaying moderate potency and it was not selected as lead compound. On the other hand, the second alternative proposed to replace one phenyl ring of naphthoic acid core of **25** with a triazole, that can interact favorably with the amino acid residues in P2Y₁₄R binding site, almost overlapping the binding pose of **25**.

Thus, a versatile synthetic approach was used for introducing arylacetylene moieties in the form of 1,2,3-triazoles^{98, 101} by click coupling with an azido group present on the core of the molecule by copper-catalyzed [2+3] cycloaddition.¹⁰²

As depicted in Scheme 4, the triazolyl derivative **106** and its analogues were synthesized starting from the 3-amino-5-bromobenzoic acid **45** and 4-(4-bromophenyl)piperidin-4-ol **49**. The carboxylic group of **45** was first converted to the methyl ester **46**, and then the amine function was protected to give Boc-derivative **47a**. A di-Boc side product **47b** accompanied the product that was initially isolated, and this impurity reverted to the desired mono-Boc product **47a** upon heating the mixture in refluxing MeOH in the presence of dilute K₂CO₃. The palladium-catalyzed condensation of arylbromide **47a** with bis(pinacolato)-diboron under basic conditions afforded dioxaborolane **48**. The acid-catalyzed dehydration of **49** yielded derivative **50**, which was reduced to provide compound **51**. Derivative **52** was obtained by coupling **48** with compound **51** under Suzuki conditions.¹⁰³ Then, the

conversion of the amino group of **52** to a trifluoroacetamide derivative **53** was accomplished by using trifluoroacetamide anhydride in the presence of base. After removing the *N*-Boc protecting group of **53** to give compound **54**, aryl azide **55** was formed from an arenediazonium tosylate that was generated in situ and subsequent addition of sodium azide.¹⁰⁴ The 1,2,3-triazolyl derivative **57** was synthesized via a click reaction involving aryl azide **55**, 4-(trifluoromethyl)phenylacetylene, Cu(II) salt and sodium ascorbate,¹⁰² followed by the one-pot hydrolysis of the trifluoroacetamide and the ester in the presence of potassium hydroxide to yield **107**.



Scheme 4. Regents and conditions:

a. CH₃OH, SOCl₂, 0 to 23 °C (98%); **b.** 1) Boc₂O, NEt₃, DMAP, CH₂Cl₂; 2) K₂CO₃, MeOH, reflux (70%); **c.** PdCl₂(dppf), AcOK, DMF, 95 °C (74%); **d.** F₃CCO₂H, 90 °C (97%); **e.** H₂, Rh/C, 100 psi (98%); **f.** Pd(Ph₃P)₄, K₂CO₃, DME, 85 °C (71%); **g.** (CF₃CO)₂O, NEt₃, Et₂O; **h.** F₃CCO₂H, CH₂Cl₂ (70%); **i.** 1) Ts-OH, NaNO₂, H₂O/acetonitrile; 2) NaN₃, (83%); **j.** CuSO₄, sodium ascorbate (1M aq.) **k.** KOH (1M aq.). R defined in Tables 3 in Results and discussion section.

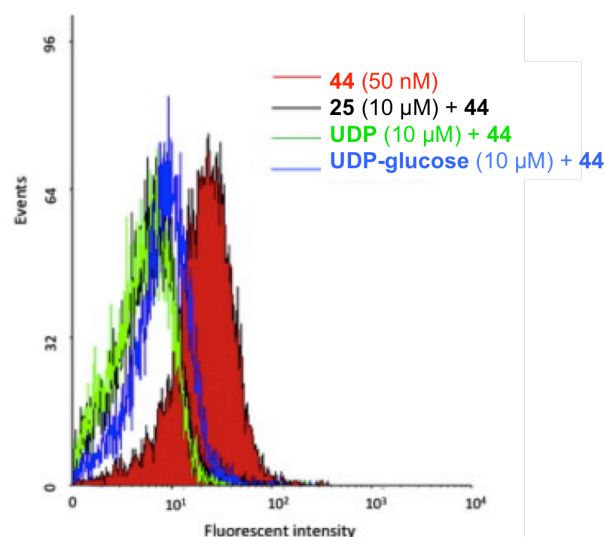


Figure 7. Inhibition of binding of **44** in P2Y₁₄R-CHO cells by antagonist PPTN **25** and agonists UDP and UDP-glucose (10 μM), analyzed by flow cytometry. Incubation of cells for 30 min with antagonist **25** or agonist UDP and UDP-glucose (all at 10 μM) followed by incubation with **44** (50 nM) for 30 min was performed.

44 to P2Y₁₄R-expressing cells by using FCM, which provided an apparent binding constant of 21.4 ± 1.1 nM, and the kinetics of binding as well, showing a $t_{1/2} = 23.9$ min at 50 nM of **44**. Competition experiments for fluorescent binding with known P2Y₁₄R ligands have been also reported. As showed in Table 2, the obtained results followed the expected rank order of P2Y₁₄R potency (**25** \gg MRS2690 > UDP > UDPG > UDPGA).

The specific labeling of P2Y₁₄R-CHO cells by **44** has been also confirmed by confocal fluorescence microscopy studies (Figure 8). As expected, the fluorescent labeling was inhibited in the presence of antagonist **25** and it is irregularly distributed on the surface of the cells and partially internalized. This is in line with previous reports showing the internalization of fluorescent agonists of other P2YRs and GPCRs.¹⁰⁵

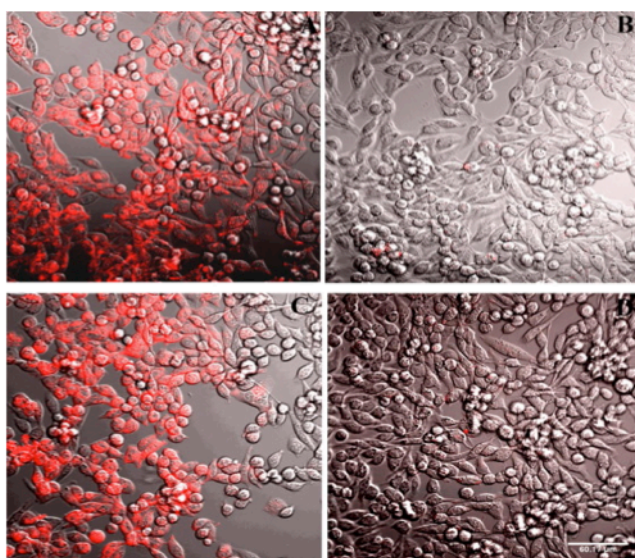


Figure 8. Fluorescence confocal microscopy. Cells were incubated using a fixed concentration of **44** (200 nM) at different times 30 min (A, B) or 120 min (C, D) of incubation in the absence (A, C) or presence (B, D) of antagonist **25** (10 μM).

Herein, a useful fluorescent probe **44**, pharmacologically complementary to the previously reported non-nucleotide fluorescent antagonist **27**, has been developed.

The utility of this probe to specifically label P2Y₁₄R using flow cytometry and fluorescence microscopy was also demonstrated. It may allow to further study the role and distribution of this receptor, and its structural requirements to design a more potent P2Y₁₄R ligands.

4.2 Biological evaluation of P2Y₁₄ antagonists

As already pointed out, only few non-nucleotide P2Y₁₄R antagonists are currently known. Black and coworkers applied high-throughput screens to identify dihydropyridopyrimidine⁸⁹ and naphthoic acid⁸⁸ compounds as potential P2Y₁₄R antagonists. Analogs of each type of molecule subsequently were synthesized. Whereas dihydropyridopyrimidine derivatives appeared to be noncompetitive antagonists of the P2Y₁₄R, the naphthoic acid derivatives inhibited [³H]-UDP binding suggesting antagonism of the orthosteric ligand binding site of the receptor. Problems with high affinity binding to serum proteins observed with several of these naphthoic acid analogs were partially circumvented in the analogue PPTN **25** that is able to retain the activity, even showing low oral bioavailability. A prodrug based on PPTN also was developed to improve its pharmacological profile.¹⁰⁶

To date, **25** is the most potent and selective P2Y₁₄R non-nucleotide antagonist, but its liabilities precluded to further develop a drug candidate.

Motivated by these findings, we searched for different scaffolds, which may resemble the structural features and the activity profile of **25** toward the P2Y₁₄R.

To this end, a computational pipeline was implemented based on a human P2Y₁₄R homology model¹⁰⁰ built on the recently reported structures of the hP2Y₁₂R,²¹ in order to suggest alternatives to the hydrophobic and bulky naphthalene ring of **25**. Thus, by means of docking and molecular dynamics simulations, the suitable alternatives relied on replacing one of the phenyl ring of naphthalene core of **25** with groups able to maintain the interactions pattern with this receptor and hopefully to improve the physicochemical properties as well. In particular, as shown in Figure 9,

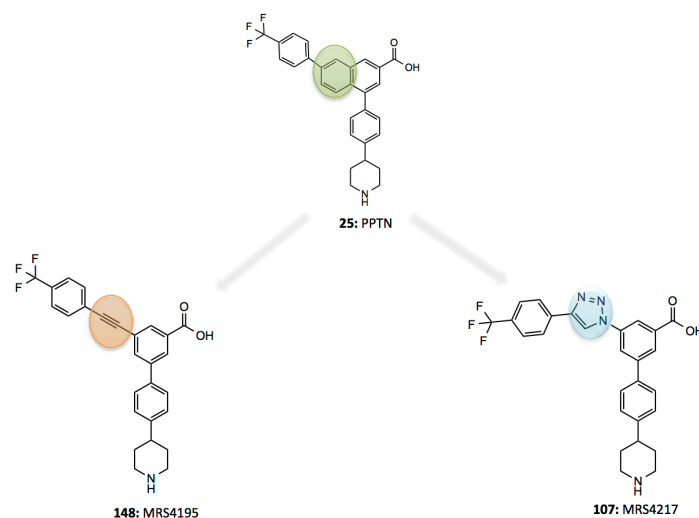


Figure 9. Design strategy to analogues of PPTN **25**.

through isosteric replacement of the phenyl ring of naphthoic acid core with an alkyne and a triazole, we developed compounds **148** and **107**, respectively.⁹⁸

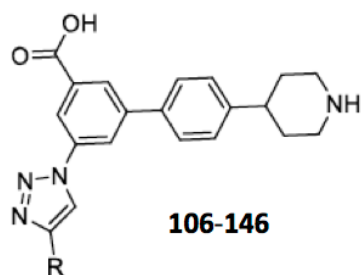
These compounds were then evaluated for the binding profile at P2Y₁₄R using flow cytometry. Particularly, thanks to the improved synthetic route for obtaining **27**,

which provide a sufficient supply of this fluorescent probe to be use in displacement assay, a novel flow cytometry competition assay using whole cells expressing P2Y₁₄ receptor and fluorescent antagonist **27** as a tracer was developed. The p-F₃C-phenyl-triazole derivative (**107**, MRS4217, IC₅₀ = 32 nM) was more potent than a corresponding alkyne **148** and was further selected as lead compound. Thus, employing different substituted alkynes to obtain the triazole core led to the development of a focused library (~40 members). The synthesized compounds were first prioritized thanks to docking studies and then assayed in the flow cytometry competition assay (Table 3). Interestingly, the compounds that at 3 μM displayed inhibition of >80% of fluorescent PPTN analogue **27** were also evaluated in the fluorescent assay with full concentration-response curves (results not shown). With these data in hand, we can conclude that the IC₅₀ values for the selected triazoles ranged from 31.7 nM (**107**) to 481 nM (**120**) compared to the IC₅₀ 6.0 nM of the reference of PPTN antagonist **25**; and the potencies were in the rank order of: **25** > **107** > **119** > **117** > **113**, **124**, **126** > **121**, **132**, **112** > **120**. Importantly, as clearly emerged from the SAR analysis, P2Y₁₄R allowed to accommodate in its binding site compounds para-substituted on the aromatic ring with hydrophobic group (such as **121** contains a tert-butyl group, whereas **117** presents a 5-bromothiophen-2-yl group). The only compounds showing a 3,4-difluorophenyl group is derivative **132**, that may give the opportunity of developing metabolically stable compounds.

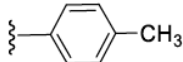
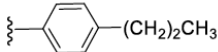
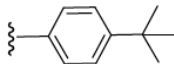
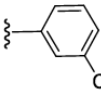
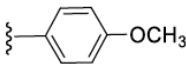
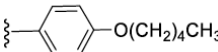
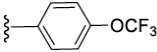
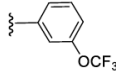
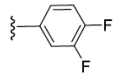
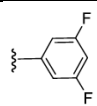
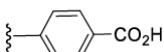
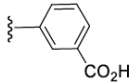
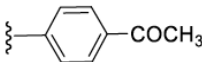
To reveal unexpected interactions of these ligands with numerous off-target sites, the Psychoactive Drug Screening Program (PDSP) has been used to test specific interactions with other GPCRs, ion channels and a transporter in the CNS. Interestingly, both compounds **25** and **148** showed only a few off-target interactions at <10 μM. In particular, the measured K_i values (μM) of **25** were 6.79 (D3 dopamine receptor) and 2.75 (δ-opioid receptor), whereas the K_i values (μM) of **148** were 1.46 (σ₁ receptor) and 3.60 (σ₂ receptor). Notably, a representative triazole derivative (**116**) showed no off-target interactions at the same concentration.

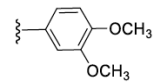
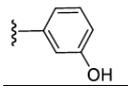
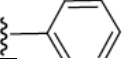
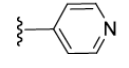
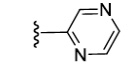
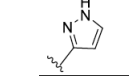
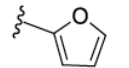
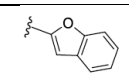
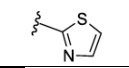
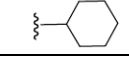
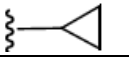
Despite the lack of information about the P2Y₁₄R X-ray structure, the predictive power of the P2Y₁₄R homology model herein demonstrates to enable GPCR drug discovery. Indeed, the high affinity derivatives together with the lack of off-target interactions in these chemical series offers powerful tools to improve our understanding of P2Y₁₄R pharmacology and potentially could lead to clinically useful drug candidates for inflammatory and endocrine diseases.

Table 3. Chemical structures of compounds **106-146** and % inhibition of P2Y₁₄R.



Compound	R =	P2Y ₁₄ R affinity, % inhibition at 3 μM ^a
25		92.6±1.2%
106		30.1±2.1%
107		92.3±0.5%
108		67.2±2.2%
109		14.5±2.1%
110		21.1±2.9%
111		26.5±5.2%
112		82.7±1.5%
113		88.8±0.8%
114		67.3±2.5%
115		44.2±1.9%
116		66.2±2.0%

117		93.1±0.8%
118		75.1±2.8%
119		91.5±0.3%
120		87.1±0.5%
121		88.9±4.6%
122		79.0±2.2%
123		39.6±7.4%
124		85.2±0.8%
125		13.7±3.1%
126		86.7±1.0%
127		65.3±4.5
128		49.9±2.2%
129		65.2±1.2%
130		37.3±4.6%
131		42.2±4.3%
132		85.0±0.6%
133		76.2±1.7%
134		33.4±1.3%
135		35.7±0.7%

136		$69.3 \pm 3.8\%$
137		$33.6 \pm 3.5\%$
138		$11.6 \pm 1.2\%$
139		$14.0 \pm 5.1\%$
140		$13.1 \pm 2.6\%$
141		$18.1 \pm 5.8\%$
142		$32.4 \pm 2.7\%$
143		$73.4 \pm 3.1\%$
144		$6.0 \pm 1.3\%$
145		$53.1 \pm 2.0\%$
146		$50.1 \pm 1.9\%$

References

- [1] Fredriksson, R.; Lagerstrom, M. C.; Lundin, L. G.; Schiöth, H. B. The G-protein-coupled receptors in the human genome form five main families. Phylogenetic analysis, paralogon groups, and fingerprints. *Mol Pharmacol* **2003**, *63* (6), 1256-72.
- [2] Lebon, G.; Warne, T.; Tate, C. G. Agonist-bound structures of G protein-coupled receptors. *Curr Opin Struct Biol* **2012**, *22* (4), 482-90.
- [3] Salon, J. A.; Lodowski, D. T.; Palczewski, K. The significance of G protein-coupled receptor crystallography for drug discovery. *Pharmacol Rev* **2011**, *63* (4), 901-37.
- [4] Filmore, D. It's a GPCR world *Modern Drug Discovery* **2004**, *7* (11), 24-28.
- [5] Jacobson, K. A. New paradigms in GPCR drug discovery. *Biochem Pharmacol* **2015**, *98* (4), 541-55.
- [6] Kobilka, B. The structural basis of G-protein-coupled receptor signaling (Nobel Lecture). *Angew Chem Int Ed Engl* **2013**, *52* (25), 6380-8.
- [7] Palczewski, K.; Kumasaka, T.; Hori, T.; Behnke, C. A.; Motoshima, H.; Fox, B. A.; Le Trong, I.; Teller, D. C.; Okada, T.; Stenkamp, R. E.; Yamamoto, M.; Miyano, M. Crystal structure of rhodopsin: A G protein-coupled receptor. *Science* **2000**, *289* (5480), 739-45.
- [8] Day, P. W.; Rasmussen, S. G.; Parnot, C.; Fung, J. J.; Masood, A.; Kobilka, T. S.; Yao, X. J.; Choi, H. J.; Weis, W. I.; Rohrer, D. K.; Kobilka, B. K. A monoclonal antibody for G protein-coupled receptor crystallography. *Nat Methods* **2007**, *4* (11), 927-9.
- [9] Stevens, R. C.; Cherezov, V.; Katritch, V.; Abagyan, R.; Kuhn, P.; Rosen, H.; Wuthrich, K. The GPCR Network: a large-scale collaboration to determine human GPCR structure and function. *Nat Rev Drug Discov* **2013**, *12* (1), 25-34.
- [10] Cherezov, V.; Rosenbaum, D. M.; Hanson, M. A.; Rasmussen, S. G.; Thian, F. S.; Kobilka, T. S.; Choi, H. J.; Kuhn, P.; Weis, W. I.; Kobilka, B. K.; Stevens, R. C. High-resolution crystal structure of an engineered human beta2-adrenergic G protein-coupled receptor. *Science* **2007**, *318* (5854), 1258-65.
- [11] Rasmussen, S. G.; Choi, H. J.; Fung, J. J.; Pardon, E.; Casarosa, P.; Chae, P. S.; Devree, B. T.; Rosenbaum, D. M.; Thian, F. S.; Kobilka, T. S.; Schnapp, A.; Konetzki, I.; Sunahara, R. K.; Gellman, S. H.; Pautsch, A.; Steyaert, J.; Weis, W. I.; Kobilka, B. K. Structure of a nanobody-stabilized active state of the beta(2) adrenoceptor. *Nature* **2011**, *469* (7329), 175-80.
- [12] Rasmussen, S. G.; DeVree, B. T.; Zou, Y.; Kruse, A. C.; Chung, K. Y.; Kobilka, T. S.; Thian, F. S.; Chae, P. S.; Pardon, E.; Calinski, D.; Mathiesen, J. M.; Shah, S. T.; Lyons, J. A.; Caffrey, M.; Gellman, S. H.; Steyaert, J.; Skiniotis, G.; Weis, W. I.; Sunahara, R. K.; Kobilka, B. K. Crystal structure of the beta2 adrenergic receptor-Gs protein complex. *Nature* **2011**, *477* (7366), 549-55.
- [13] Xu, F.; Wu, H.; Katritch, V.; Han, G. W.; Jacobson, K. A.; Gao, Z. G.; Cherezov, V.; Stevens, R. C. Structure of an agonist-bound human A2A adenosine receptor. *Science* **2011**, *332* (6027), 322-7.
- [14] Ghosh, E.; Kumari, P.; Jaiman, D.; Shukla, A. K. Methodological advances: the unsung heroes of the GPCR structural revolution. *Nat Rev Mol Cell Biol* **2015**, *16* (2), 69-81.
- [15] Cooke, R. M.; Brown, A. J.; Marshall, F. H.; Mason, J. S. Structures of G protein-coupled receptors reveal new opportunities for drug discovery. *Drug Discov Today* **2015**, *20* (11), 1355-64.
- [16] Haga, K.; Kruse, A. C.; Asada, H.; Yurugi-Kobayashi, T.; Shiroishi, M.; Zhang, C.; Weis, W. I.; Okada, T.; Kobilka, B. K.; Haga, T.; Kobayashi, T. Structure of the human M2 muscarinic acetylcholine receptor bound to an antagonist. *Nature* **2012**, *482* (7386), 547-51.
- [17] Kruse, A. C.; Hu, J.; Pan, A. C.; Arlow, D. H.; Rosenbaum, D. M.; Rosemond, E.; Green, H. F.; Liu, T.; Chae, P. S.; Dror, R. O.; Shaw, D. E.; Weis, W. I.; Wess, J.; Kobilka, B. K. Structure and dynamics of the M3 muscarinic acetylcholine receptor. *Nature* **2012**, *482* (7386), 552-6.
- [18] Manglik, A.; Kruse, A. C.; Kobilka, T. S.; Thian, F. S.; Mathiesen, J. M.; Sunahara, R. K.; Pardo, L.; Weis, W. I.; Kobilka, B. K.; Granier, S. Crystal structure of the micro-opioid receptor bound to a morphinan antagonist. *Nature* **2012**, *485* (7398), 321-6.
- [19] Granier, S.; Manglik, A.; Kruse, A. C.; Kobilka, T. S.; Thian, F. S.; Weis, W. I.; Kobilka, B. K. Structure of the delta-opioid receptor bound to naltrindole. *Nature* **2012**, *485* (7398), 400-4.
- [20] Zhang, K.; Zhang, J.; Gao, Z. G.; Zhang, D.; Zhu, L.; Han, G. W.; Moss, S. M.; Paoletta, S.; Kiselev, E.; Lu, W.; Fenalti, G.; Zhang, W.; Muller, C. E.; Yang, H.; Jiang, H.; Cherezov, V.; Katritch, V.; Jacobson, K. A.; Stevens, R. C.; Wu, B.; Zhao, Q. Structure of the human P2Y12 receptor in complex with an antithrombotic drug. *Nature* **2014**, *509* (7498), 115-8.
- [21] Zhang, J.; Zhang, K.; Gao, Z. G.; Paoletta, S.; Zhang, D.; Han, G. W.; Li, T.; Ma, L.; Zhang, W.; Muller, C. E.; Yang, H.; Jiang, H.; Cherezov, V.; Katritch, V.; Jacobson, K. A.; Stevens, R. C.; Wu, B.; Zhao, Q. Agonist-bound structure of the human P2Y12 receptor. *Nature* **2014**, *509* (7498), 119-22.

- [22] Zhang, D.; Gao, Z. G.; Zhang, K.; Kiselev, E.; Crane, S.; Wang, J.; Paoletta, S.; Yi, C.; Ma, L.; Zhang, W.; Han, G. W.; Liu, H.; Cherezov, V.; Katritch, V.; Jiang, H.; Stevens, R. C.; Jacobson, K. A.; Zhao, Q.; Wu, B. Two disparate ligand-binding sites in the human P2Y1 receptor. *Nature* **2015**, *520* (7547), 317-21.
- [23] Gachet, C. P2 receptors, platelet function and pharmacological implications. *Thromb Haemost* **2008**, *99* (3), 466-72.
- [24] Gao, Z. G.; Jacobson, K. A. Allosteric modulation and functional selectivity of G protein-coupled receptors. *Drug Discov Today Technol* **2013**, *10* (2), e237-43.
- [25] Thompson, G. L.; Lane, J. R.; Coudrat, T.; Sexton, P. M.; Christopoulos, A.; Canals, M. Biased Agonism of Endogenous Opioid Peptides at the mu-Opioid Receptor. *Mol Pharmacol* **2015**, *88* (2), 335-46.
- [26] Vardanyan, R. S.; Hruby, V. J. -5- - Anxiolytics (Tranquilizers). In *Synthesis of Essential Drugs*, Vardanyan, R. S.; Hruby, V. J., Eds. Elsevier: Amsterdam, 2006; pp 69-82.
- [27] Wootten, D.; Christopoulos, A.; Sexton, P. M. Emerging paradigms in GPCR allostery: implications for drug discovery. *Nat Rev Drug Discov* **2013**, *12* (8), 630-44.
- [28] Vardanyan, R. S.; Hruby, V. J. -9- - Antiepileptic Drugs. In *Synthesis of Essential Drugs*, Vardanyan, R. S.; Hruby, V. J., Eds. Elsevier: Amsterdam, 2006; pp 125-133.
- [29] Shenoy, S. K.; Drake, M. T.; Nelson, C. D.; Houtz, D. A.; Xiao, K.; Madabushi, S.; Reiter, E.; Premont, R. T.; Lichtarge, O.; Lefkowitz, R. J. beta-arrestin-dependent, G protein-independent ERK1/2 activation by the beta2 adrenergic receptor. *J Biol Chem* **2006**, *281* (2), 1261-73.
- [30] Irannejad, R.; von Zastrow, M. GPCR signaling along the endocytic pathway. *Curr Opin Cell Biol* **2014**, *27*, 109-16.
- [31] Fribourg, M.; Moreno, J. L.; Holloway, T.; Provasi, D.; Baki, L.; Mahajan, R.; Park, G.; Adney, S. K.; Hatcher, C.; Eltit, J. M.; Ruta, J. D.; Albizu, L.; Li, Z.; Umali, A.; Shim, J.; Fabiato, A.; MacKerell, A. D., Jr.; Brezina, V.; Sealfon, S. C.; Filizola, M.; Gonzalez-Maeso, J.; Logothetis, D. E. Decoding the signaling of a GPCR heteromeric complex reveals a unifying mechanism of action of antipsychotic drugs. *Cell* **2011**, *147* (5), 1011-23.
- [32] Ferre, S.; Casado, V.; Devi, L. A.; Filizola, M.; Jockers, R.; Lohse, M. J.; Milligan, G.; Pin, J. P.; Guitart, X. G protein-coupled receptor oligomerization revisited: functional and pharmacological perspectives. *Pharmacol Rev* **2014**, *66* (2), 413-34.
- [33] Rochais, C.; Lecoutey, C.; Gaven, F.; Giannoni, P.; Hamidouche, K.; Hedou, D.; Dubost, E.; Genest, D.; Yahiaoui, S.; Freret, T.; Bouet, V.; Dauphin, F.; Sopkova de Oliveira Santos, J.; Ballandonne, C.; Corvaisier, S.; Malzert-Freon, A.; Legay, R.; Boulouard, M.; Claeysen, S.; Dallemagne, P. Novel multitarget-directed ligands (MTDLs) with acetylcholinesterase (AChE) inhibitory and serotonergic subtype 4 receptor (5-HT4R) agonist activities as potential agents against Alzheimer's disease: the design of donecopride. *J Med Chem* **2015**, *58* (7), 3172-87.
- [34] Jacobson, K. A.; Costanzi, S.; Paoletta, S. Computational studies to predict or explain G protein coupled receptor polypharmacology. *Trends Pharmacol Sci* **2014**, *35* (12), 658-63.
- [35] Paoletta, S.; Tosh, D. K.; Salvemini, D.; Jacobson, K. A. Structural probing of off-target G protein-coupled receptor activities within a series of adenosine/adenine congeners. *PLoS One* **2014**, *9* (5), e97858.
- [36] Gamo, A. M.; Gonzalez-Vera, J. A.; Rueda-Zubiaurre, A.; Alonso, D.; Vazquez-Villa, H.; Martin-Couce, L.; Palomares, O.; Lopez, J. A.; Martin-Fontecha, M.; Benhamu, B.; Lopez-Rodriguez, M. L.; Ortega-Gutierrez, S. Chemoproteomic Approach to Explore the Target Profile of GPCR ligands: Application to 5-HT1A and 5-HT6 Receptors. *Chemistry* **2016**, *22* (4), 1313-21.
- [37] Tang, X. L.; Wang, Y.; Li, D. L.; Luo, J.; Liu, M. Y. Orphan G protein-coupled receptors (GPCRs): biological functions and potential drug targets. *Acta Pharmacol Sin* **2012**, *33* (3), 363-71.
- [38] Boehm, M.; Hepworth, D.; Loria, P. M.; Norquay, L. D.; Filipinski, K. J.; Chin, J. E.; Cameron, K. O.; Brenner, M.; Bonnette, P.; Cabral, S.; Conn, E.; Ebner, D. C.; Gautreau, D.; Hadcock, J.; Lee, E. C.; Mathiowetz, A. M.; Morin, M.; Rogers, L.; Smith, A.; VanVolkenburg, M.; Carpino, P. A. Chemical Probe Identification Platform for Orphan GPCRs Using Focused Compound Screening: GPR39 as a Case Example. *ACS Med Chem Lett* **2013**, *4* (11), 1079-84.
- [39] Jacobson, K. A.; Kirk, K. L.; Padgett, W. L.; Daly, J. W. Functionalized congeners of 1,3-dialkylxanthines: preparation of analogues with high affinity for adenosine receptors. *J Med Chem* **1985**, *28* (9), 1334-40.
- [40] Jacobson, K. A.; Kirk, K. L.; Padgett, W. L.; Daly, J. W. Functionalized congeners of adenosine: preparation of analogues with high affinity for A1-adenosine receptors. *J Med Chem* **1985**, *28* (9), 1341-6.

- [41] Jacobson, K. A.; Ukena, D.; Padgett, W.; Kirk, K. L.; Daly, J. W. Molecular probes for extracellular adenosine receptors. *Biochem Pharmacol* **1987**, *36* (10), 1697-707.
- [42] Jacobson, K. A. Functionalized congener approach to the design of ligands for G protein-coupled receptors (GPCRs). *Bioconjug Chem* **2009**, *20* (10), 1816-35.
- [43] Wikström, M. A. Chemical Biology in the USA. http://www.vinnova.se/upload/dokument/Verksamhet/Bioteknik/Rapporter_Life_Science/Chemical_Biology.pdf (accessed Mar 10, 2016).
- [44] Jacobson, K. A.; Gao, Z. G. Adenosine receptors as therapeutic targets. *Nat Rev Drug Discov* **2006**, *5* (3), 247-64.
- [45] Borea, P. A.; Varani, K.; Vincenzi, F.; Baraldi, P. G.; Tabrizi, M. A.; Merighi, S.; Gessi, S. The A3 adenosine receptor: history and perspectives. *Pharmacol Rev* **2015**, *67* (1), 74-102.
- [46] Gao, Z. G.; Kim, S. K.; Biadatti, T.; Chen, W.; Lee, K.; Barak, D.; Kim, S. G.; Johnson, C. R.; Jacobson, K. A. Structural determinants of A(3) adenosine receptor activation: nucleoside ligands at the agonist/antagonist boundary. *J Med Chem* **2002**, *45* (20), 4471-84.
- [47] Jacobson, K. A. Structure-based approaches to ligands for G-protein-coupled adenosine and P2Y receptors, from small molecules to nanoconjugates. *J Med Chem* **2013**, *56* (10), 3749-67.
- [48] Gallo-Rodriguez, C.; Ji, X. D.; Melman, N.; Siegman, B. D.; Sanders, L. H.; Orlina, J.; Fischer, B.; Pu, Q.; Olah, M. E.; van Galen, P. J.; et al. Structure-activity relationships of N6-benzyladenosine-5'-uronamides as A3-selective adenosine agonists. *J Med Chem* **1994**, *37* (5), 636-46.
- [49] Kim, H. O.; Ji, X. D.; Siddiqi, S. M.; Olah, M. E.; Stiles, G. L.; Jacobson, K. A. 2-Substitution of N6-benzyladenosine-5'-uronamides enhances selectivity for A3 adenosine receptors. *J Med Chem* **1994**, *37* (21), 3614-21.
- [50] Olah, M. E.; Gallo-Rodriguez, C.; Jacobson, K. A.; Stiles, G. L. 125I-4-aminobenzyl-5'-N-methylcarboxamidoadenosine, a high affinity radioligand for the rat A3 adenosine receptor. *Mol Pharmacol* **1994**, *45* (5), 978-82.
- [51] Baeyens, J. M. Pharmacology. In *Antidepressants, Antipsychotics, Anxiolytics*, Wiley-VCH Verlag GmbH: 2008; pp 895-922.
- [52] Jeong, L. S.; Lee, H. W.; Jacobson, K. A.; Kim, H. O.; Shin, D. H.; Lee, J. A.; Gao, Z. G.; Lu, C.; Duong, H. T.; Gunaga, P.; Lee, S. K.; Jin, D. Z.; Chun, M. W.; Moon, H. R. Structure-activity relationships of 2-chloro-N6-substituted-4'-thioadenosine-5'-uronamides as highly potent and selective agonists at the human A3 adenosine receptor. *J Med Chem* **2006**, *49* (1), 273-81.
- [53] Jeong, L. S.; Pal, S.; Choe, S. A.; Choi, W. J.; Jacobson, K. A.; Gao, Z. G.; Klutz, A. M.; Hou, X.; Kim, H. O.; Lee, H. W.; Lee, S. K.; Tosh, D. K.; Moon, H. R. Structure-activity relationships of truncated D- and L-4'-thioadenosine derivatives as species-independent A3 adenosine receptor antagonists. *J Med Chem* **2008**, *51* (20), 6609-13.
- [54] Tchilibon, S.; Joshi, B. V.; Kim, S. K.; Duong, H. T.; Gao, Z. G.; Jacobson, K. A. (N)-methanocarpa 2,N6-disubstituted adenine nucleosides as highly potent and selective A3 adenosine receptor agonists. *J Med Chem* **2005**, *48* (6), 1745-58.
- [55] Tosh, D. K.; Deflorian, F.; Phan, K.; Gao, Z. G.; Wan, T. C.; Gizewski, E.; Auchampach, J. A.; Jacobson, K. A. Structure-guided design of A(3) adenosine receptor-selective nucleosides: combination of 2-arylethynyl and bicyclo[3.1.0]hexane substitutions. *J Med Chem* **2012**, *55* (10), 4847-60.
- [56] Tosh, D. K.; Paoletta, S.; Phan, K.; Gao, Z. G.; Jacobson, K. A. Truncated Nucleosides as A(3) Adenosine Receptor Ligands: Combined 2-Arylethynyl and Bicyclohexane Substitutions. *ACS Med Chem Lett* **2012**, *3* (7), 596-601.
- [57] Paoletta, S.; Tosh, D. K.; Finley, A.; Gizewski, E. T.; Moss, S. M.; Gao, Z. G.; Auchampach, J. A.; Salvemini, D.; Jacobson, K. A. Rational design of sulfonated A3 adenosine receptor-selective nucleosides as pharmacological tools to study chronic neuropathic pain. *J Med Chem* **2013**, *56* (14), 5949-63.
- [58] Tosh, D. K.; Finley, A.; Paoletta, S.; Moss, S. M.; Gao, Z. G.; Gizewski, E. T.; Auchampach, J. A.; Salvemini, D.; Jacobson, K. A. In vivo phenotypic screening for treating chronic neuropathic pain: modification of C2-arylethynyl group of conformationally constrained A3 adenosine receptor agonists. *J Med Chem* **2014**, *57* (23), 9901-14.
- [59] Fang, Z. Z.; Tosh, D. K.; Tanaka, N.; Wang, H.; Krausz, K. W.; O'Connor, R.; Jacobson, K. A.; Gonzalez, F. J. Metabolic mapping of A3 adenosine receptor agonist MRS5980. *Biochem Pharmacol* **2015**, *97* (2), 215-23.
- [60] Tosh, D. K.; Paoletta, S.; Chen, Z.; Crane, S.; Lloyd, J.; Gao, Z. G.; Gizewski, E. T.; Auchampach, J. A.; Salvemini, D.; Jacobson, K. A. Structure-Based Design, Synthesis by Click Chemistry and Activity of Highly Selective A Adenosine Receptor Agonists. *Medchemcomm* **2015**, *6*, 555-563.

- [61] Tosh, D. K.; Crane, S.; Chen, Z.; Paoletta, S.; Gao, Z. G.; Gizewski, E.; Auchampach, J. A.; Salvemini, D.; Jacobson, K. A. Rigidified A3 Adenosine Receptor Agonists: 1-Deazaadenine Modification Maintains High in Vivo Efficacy. *ACS Med Chem Lett* **2015**, *6* (7), 804-8.
- [62] Kozma, E.; Jayasekara, P. S.; Squarcialupi, L.; Paoletta, S.; Moro, S.; Federico, S.; Spalluto, G.; Jacobson, K. A. Fluorescent ligands for adenosine receptors. *Bioorg Med Chem Lett* **2013**, *23* (1), 26-36.
- [63] Kozma, E.; Gizewski, E. T.; Tosh, D. K.; Squarcialupi, L.; Auchampach, J. A.; Jacobson, K. A. Characterization by flow cytometry of fluorescent, selective agonist probes of the A(3) adenosine receptor. *Biochem Pharmacol* **2013**, *85* (8), 1171-81.
- [64] Jacobson, K. A. GPCR ligand-dendrimer (GLiDe) conjugates: future smart drugs? *Trends Pharmacol Sci* **2010**, *31* (12), 575-9.
- [65] Klutz, A. M.; Gao, Z. G.; Lloyd, J.; Shainberg, A.; Jacobson, K. A. Enhanced A3 adenosine receptor selectivity of multivalent nucleoside-dendrimer conjugates. *J Nanobiotechnology* **2008**, *6*, 12.
- [66] Keene, A. M.; Balasubramanian, R.; Lloyd, J.; Shainberg, A.; Jacobson, K. A. Multivalent dendrimeric and monomeric adenosine agonists attenuate cell death in HL-1 mouse cardiomyocytes expressing the A(3) receptor. *Biochem Pharmacol* **2010**, *80* (2), 188-96.
- [67] Tosh, D. K.; Yoo, L. S.; Chinn, M.; Hong, K.; Kilbey, S. M., 2nd; Barrett, M. O.; Fricks, I. P.; Harden, T. K.; Gao, Z. G.; Jacobson, K. A. Polyamidoamine (PAMAM) dendrimer conjugates of "clickable" agonists of the A3 adenosine receptor and coactivation of the P2Y14 receptor by a tethered nucleotide. *Bioconjug Chem* **2010**, *21* (2), 372-84.
- [68] Chambers, J. K.; Macdonald, L. E.; Sarau, H. M.; Ames, R. S.; Freeman, K.; Foley, J. J.; Zhu, Y.; McLaughlin, M. M.; Murdock, P.; McMillan, L.; Trill, J.; Swift, A.; Aiyar, N.; Taylor, P.; Vawter, L.; Naheed, S.; Szekeres, P.; Hervieu, G.; Scott, C.; Watson, J. M.; Murphy, A. J.; Duzic, E.; Klein, C.; Bergsma, D. J.; Wilson, S.; Livi, G. P. A G protein-coupled receptor for UDP-glucose. *J Biol Chem* **2000**, *275* (15), 10767-71.
- [69] Abbracchio, M. P.; Boeynaems, J. M.; Barnard, E. A.; Boyer, J. L.; Kennedy, C.; Miras-Portugal, M. T.; King, B. F.; Gachet, C.; Jacobson, K. A.; Weisman, G. A.; Burnstock, G. Characterization of the UDP-glucose receptor (re-named here the P2Y14 receptor) adds diversity to the P2Y receptor family. *Trends Pharmacol Sci* **2003**, *24* (2), 52-5.
- [70] Abbracchio, M. P.; Burnstock, G.; Boeynaems, J. M.; Barnard, E. A.; Boyer, J. L.; Kennedy, C.; Knight, G. E.; Fumagalli, M.; Gachet, C.; Jacobson, K. A.; Weisman, G. A. International Union of Pharmacology LVIII: update on the P2Y G protein-coupled nucleotide receptors: from molecular mechanisms and pathophysiology to therapy. *Pharmacol Rev* **2006**, *58* (3), 281-341.
- [71] Lazarowski, E. R.; Harden, T. K. UDP-Sugars as Extracellular Signaling Molecules: Cellular and Physiologic Consequences of P2Y14 Receptor Activation. *Mol Pharmacol* **2015**, *88* (1), 151-60.
- [72] (a) Fricks, I. P.; Maddileti, S.; Carter, R. L.; Lazarowski, E. R.; Nicholas, R. A.; Jacobson, K. A.; Harden, T. K. UDP is a competitive antagonist at the human P2Y14 receptor. *J Pharmacol Exp Ther* **2008**, *325* (2), 588-94; (b) Carter, R. L.; Fricks, I. P.; Barrett, M. O.; Burianek, L. E.; Zhou, Y.; Ko, H.; Das, A.; Jacobson, K. A.; Lazarowski, E. R.; Harden, T. K. Quantification of Gi-mediated inhibition of adenylyl cyclase activity reveals that UDP is a potent agonist of the human P2Y14 receptor. *Mol Pharmacol* **2009**, *76* (6), 1341-8.
- [73] Harden, T. K.; Sesma, J. I.; Fricks, I. P.; Lazarowski, E. R. Signalling and pharmacological properties of the P2Y receptor. *Acta Physiol (Oxf)* **2010**, *199* (2), 149-60.
- [74] Gao, Z. G.; Ding, Y.; Jacobson, K. A. UDP-glucose acting at P2Y14 receptors is a mediator of mast cell degranulation. *Biochem Pharmacol* **2010**, *79* (6), 873-9.
- [75] Gao, Z. G.; Wei, Q.; Jayasekara, M. P.; Jacobson, K. A. The role of P2Y(14) and other P2Y receptors in degranulation of human LAD2 mast cells. *Purinergic Signal* **2013**, *9* (1), 31-40.
- [76] Sesma, J. I.; Kreda, S. M.; Steinckwich-Besancon, N.; Dang, H.; Garcia-Mata, R.; Harden, T. K.; Lazarowski, E. R. The UDP-sugar-sensing P2Y(14) receptor promotes Rho-mediated signaling and chemotaxis in human neutrophils. *Am J Physiol Cell Physiol* **2012**, *303* (5), C490-8.
- [77] Barrett, M. O.; Sesma, J. I.; Ball, C. B.; Jayasekara, P. S.; Jacobson, K. A.; Lazarowski, E. R.; Harden, T. K. A selective high-affinity antagonist of the P2Y14 receptor inhibits UDP-glucose-stimulated chemotaxis of human neutrophils. *Mol Pharmacol* **2013**, *84* (1), 41-9.
- [78] Kook, S.; Cho, J.; Lee, S. B.; Lee, B. C. The nucleotide sugar UDP-glucose mobilizes long-term repopulating primitive hematopoietic cells. *J Clin Invest* **2013**, *123* (8), 3420-35.
- [79] Cho, J.; Yusuf, R.; Kook, S.; Attar, E.; Lee, D.; Park, B.; Cheng, T.; Scadden, D. T.; Lee, B. C. Purinergic P2Y(1)(4) receptor modulates stress-induced hematopoietic stem/progenitor cell senescence. *J Clin Invest* **2014**, *124* (7), 3159-71.

- [80] Bassil, A. K.; Bourdu, S.; Townson, K. A.; Wheeldon, A.; Jarvie, E. M.; Zebda, N.; Abuin, A.; Grau, E.; Livi, G. P.; Punter, L.; Latcham, J.; Grimes, A. M.; Hurp, D. P.; Downham, K. M.; Sanger, G. J.; Winchester, W. J.; Morrison, A. D.; Moore, G. B. UDP-glucose modulates gastric function through P2Y₁₄ receptor-dependent and -independent mechanisms. *Am J Physiol Gastrointest Liver Physiol* **2009**, *296* (4), G923-30.
- [81] Amisten, S.; Salehi, A.; Rorsman, P.; Jones, P. M.; Persaud, S. J. An atlas and functional analysis of G-protein coupled receptors in human islets of Langerhans. *Pharmacol Ther* **2013**, *139* (3), 359-91.
- [82] Xu, J.; Morinaga, H.; Oh, D.; Li, P.; Chen, A.; Talukdar, S.; Mamane, Y.; Mancini, J. A.; Nawrocki, A. R.; Lazarowski, E.; Olefsky, J. M.; Kim, J. J. GPR105 ablation prevents inflammation and improves insulin sensitivity in mice with diet-induced obesity. *J Immunol* **2012**, *189* (4), 1992-9.
- [83] Meister, J.; Le Duc, D.; Ricken, A.; Burkhardt, R.; Thiery, J.; Pfannkuche, H.; Polte, T.; Grosse, J.; Schoneberg, T.; Schulz, A. The G protein-coupled receptor P2Y₁₄ influences insulin release and smooth muscle function in mice. *J Biol Chem* **2014**, *289* (34), 23353-66.
- [84] Ko, H.; Fricks, I.; Ivanov, A. A.; Harden, T. K.; Jacobson, K. A. Structure-activity relationship of uridine 5'-diphosphoglucose analogues as agonists of the human P2Y(14) receptor. *Journal of Medicinal Chemistry* **2007**, *50* (9), 2030-2039.
- [85] Ivanov, A. A.; Fricks, I.; Kendall Harden, T.; Jacobson, K. A. Molecular dynamics simulation of the P2Y₁₄ receptor. Ligand docking and identification of a putative binding site of the distal hexose moiety. *Bioorg Med Chem Lett* **2007**, *17* (3), 761-6.
- [86] Ko, H.; Das, A.; Carter, R. L.; Fricks, I. P.; Zhou, Y.; Ivanov, A. A.; Melman, A.; Joshi, B. V.; Kovac, P.; Hajdudch, J.; Kirk, K. L.; Harden, T. K.; Jacobson, K. A. Molecular recognition in the P2Y(14) receptor: Probing the structurally permissive terminal sugar moiety of uridine-5'-diphosphoglucose. *Bioorg Med Chem* **2009**, *17* (14), 5298-311.
- [87] Das, A.; Ko, H.; Buriánek, L. E.; Barrett, M. O.; Harden, T. K.; Jacobson, K. A. Human P2Y(14) receptor agonists: truncation of the hexose moiety of uridine-5'-diphosphoglucose and its replacement with alkyl and aryl groups. *J Med Chem* **2010**, *53* (1), 471-80.
- [88] Gauthier, J. Y.; Belley, M.; Deschenes, D.; Fournier, J. F.; Gagne, S.; Gareau, Y.; Hamel, M.; Henault, M.; Hyjazie, H.; Kargman, S.; Lavallee, G.; Levesque, J. F.; Li, L. H.; Mamane, Y.; Mancini, J.; Morin, N.; Mulrooney, E.; Robichaud, J.; Therien, M.; Tranmer, G.; Wang, Z. Y.; Wu, J.; Black, W. C. The identification of 4,7-disubstituted naphthoic acid derivatives as UDP-competitive antagonists of P2Y(14). *Bioorganic & Medicinal Chemistry Letters* **2011**, *21* (10), 2836-2839.
- [89] Guay, D.; Beaulieu, C.; Belley, M.; Crane, S. N.; DeLuca, J.; Gareau, Y.; Hamel, M.; Henault, M.; Hyjazie, H.; Kargman, S.; Chan, C. C.; Xu, L.; Gordon, R.; Li, L.; Mamane, Y.; Morin, N.; Mancini, J.; Therien, M.; Tranmer, G.; Truong, V. L.; Wang, Z.; Black, W. C. Synthesis and SAR of pyrimidine-based, non-nucleotide P2Y₁₄ receptor antagonists. *Bioorg Med Chem Lett* **2011**, *21* (10), 2832-5.
- [90] Brunschweiler, A.; Muller, C. E. P2 receptors activated by uracil nucleotides--an update. *Curr Med Chem* **2006**, *13* (3), 289-312.
- [91] Kiselev, E.; Barrett, M. O.; Katritch, V.; Paoletta, S.; Weitzer, C. D.; Brown, K. A.; Hammes, E.; Yin, A. L.; Zhao, Q.; Stevens, R. C.; Harden, T. K.; Jacobson, K. A. Exploring a 2-naphthoic acid template for the structure-based design of P2Y₁₄ receptor antagonist molecular probes. *ACS Chem Biol* **2014**, *9* (12), 2833-42.
- [92] McGrath, J. C.; Arribas, S.; Daly, C. J. Fluorescent ligands for the study of receptors. *Trends Pharmacol Sci* **1996**, *17* (11), 393-9.
- [93] Ma, Z.; Du, L.; Li, M. Toward fluorescent probes for G-protein-coupled receptors (GPCRs). *J Med Chem* **2014**, *57* (20), 8187-203.
- [94] Sridharan, R.; Zuber, J.; Connelly, S. M.; Mathew, E.; Dumont, M. E. Fluorescent approaches for understanding interactions of ligands with G protein coupled receptors. *Biochim Biophys Acta* **2014**, *1838* (1 Pt A), 15-33.
- [95] Lavis, L. D.; Raines, R. T. Bright ideas for chemical biology. *ACS Chem Biol* **2008**, *3* (3), 142-55.
- [96] Ciruela, F.; Jacobson, K. A.; Fernandez-Duenas, V. Portraying G protein-coupled receptors with fluorescent ligands. *ACS Chem Biol* **2014**, *9* (9), 1918-28.
- [97] Kiselev, E.; Barrett, M. O.; Katritch, V.; Paoletta, S.; Weitzer, C. D.; Brown, K. A.; Hammes, E.; Yin, A. L.; Zhao, Q.; Stevens, R. C.; Harden, T. K.; Jacobson, K. A. Exploring a 2-Naphthoic Acid Template for the Structure-Based Design of P2Y(14) Receptor Antagonist Molecular Probes. *ACS Chemical Biology* **2014**, *9* (12), 2833-2842.
- [98] Junker, A.; Balasubramanian, R.; Ciancetta, A.; Uliassi, E.; Kiselev, E.; Martiriggiano, C.; Trujillo, K.; Mtchedlidze, G.; Harden, T. K.; Jacobson, K. A. Structure-Based Design of 3-(4-Aryl-1H-1,2,3-Triazol-1-yl)-Biphenyl Derivatives as

P2Y₁₄ Receptor Antagonists. *J Med Chem under revision*.

[99] Kiselev, E.; Balasubramanian, R.; Uliassi, E.; Brown, K. A.; Trujillo, K.; Katritch, V.; Hammes, E.; Stevens, R. C.; Harden, T. K.; Jacobson, K. A. Design, synthesis, pharmacological characterization of a fluorescent agonist of the P2Y₁(4) receptor. *Bioorg Med Chem Lett* **2015**, *25* (21), 4733-9.

[100] Trujillo, K.; Paoletta, S.; Kiselev, E.; Jacobson, K. A. Molecular modeling of the human P2Y₁₄ receptor: A template for structure-based design of selective agonist ligands. *Bioorg Med Chem* **2015**, *23* (14), 4056-64.

[101] Jacobson, K. A. J. A. U., E.; Kiselev, E. . Triazole derivatives as P2Y₁₄ receptor antagonists U.S. Patent Application No. 62/233,162 filed September 25, 2015.

[102] Rostovtsev, V. V.; Green, L. G.; Fokin, V. V.; Sharpless, K. B. A stepwise Huisgen cycloaddition process: Copper(I)-catalyzed regioselective "ligation" of azides and terminal alkynes. *Angewandte Chemie-International Edition* **2002**, *41* (14), 2596-+.

[103] Suzuki, A. Cross-Coupling Reactions Of Organoboranes: An Easy Way To Construct C-C Bonds (Nobel Lecture). *Angewandte Chemie-International Edition* **2011**, *50* (30), 6722-6737.

[104] Kutonova, K. V.; Trusova, M. E.; Postnikov, P. S.; Filimonov, V. D.; Parello, J. A Simple and Effective Synthesis of Aryl Azides via Arenediazonium Tosylates. *Synthesis-Stuttgart* **2013**, *45* (19), 2706-2710.

[105] Jayasekara, P. S.; Barrett, M. O.; Ball, C. B.; Brown, K. A.; Hammes, E.; Balasubramanian, R.; Harden, T. K.; Jacobson, K. A. 4-Alkyloxyimino derivatives of uridine-5'-triphosphate: distal modification of potent agonists as a strategy for molecular probes of P2Y₂, P2Y₄, and P2Y₆ receptors. *J Med Chem* **2014**, *57* (9), 3874-83.

[106] Robichaud, J.; Fournier, J. F.; Gagne, S.; Gauthier, J. Y.; Hamel, M.; Han, Y.; Henault, M.; Kargman, S.; Levesque, J. F.; Mamane, Y.; Mancini, J.; Morin, N.; Mulrooney, E.; Wu, J.; Black, W. C. Applying the pro-drug approach to afford highly bioavailable antagonists of P2Y₁₄. *Bioorg Med Chem Lett* **2011**, *21* (14), 4366-8.

Experimental part

Reagents and instrumentation.

The proton and carbon nuclear magnetic resonance spectra were recorded using a Bruker 400 MHz NMR spectrometer. Purification of final compounds was performed by preparative HPLC (Column: Luna 5 μm C18(2) 100 Å, LC Column 250 x 4.6 mm). Method A Eluent: 0.1% TFA in water-CH₃CN from 100:0 to 70:30 in 45 min with a flow rate of 5 mL/min. Method B Eluent: 10 mM TEAA buffer-CH₃CN from 80:20 to 20:80 in 40 min with a flow rate of 4 mL/min. Purities of all tested compounds were $\geq 95\%$, as estimated by analytical HPLC (Column: Zorbax Eclipse 5 μm XDB-C18 analytical column, 150 X 4.6 mm; Agilent Technologies, Inc). Peaks were detected by UV absorption (254 nm) using a diode array detector. All derivatives tested for biological activity showed $>95\%$ purity in the HPLC systems. Analytical thin-layer chromatography was carried out on Sigma-Aldrich® TLC plates and compounds were visualized with UV light at 254 nm. Silica gel flash chromatography was performed using 230-400 mesh silica gel. Unless noted otherwise, reagents and solvents were purchased from Sigma-Aldrich. Low-resolution mass spectrometry was performed with a JEOL SX102 spectrometer with 6-kV Xe atoms following desorption from a glycerol matrix or on an Agilent LC/MS 1100 MSD, with a Waters (Milford, MA) Atlantis C18 column. High-resolution mass spectroscopic (HRMS) measurements were performed on a proteomics optimized Q-TOF-2 (Micromass-Waters) using external calibration with polyalanine.

Hex-5-yn-1-yl 4-methylbenzenesulfonate (31). To a solution of hex-5-yn-1-ol **30** (0.84 mL, 7.64 mmol), triethylamine (1.28 mL, 9.17 mmol), and 4-(dimethylamino)pyridine (20 mg, 0.15 mmol) in DCM (25 mL) at 0 °C was added *p*-toluenesulfonyl chloride (1.53 g, 8.02 mmol) in three portions. The reaction mixture was brought to r.t. and stirred for 15 h. Aqueous NaOH (1 N, 15 mL) was added, and the mixture was vigorously stirred for 15 min at r.t. The usual workup (DCM, brine) gave the title compound (1.68 g, 88%) as a yellowish oil. ¹H NMR (400 MHz, CDCl₃) δ : 1.42-1.48 (2H, m), 1.65-1.68 (2H, m), 1.84 (1H, J = 4, t), 2.05-2.09 (2H, m), 2.31 (3H, s), 3.96 (2H, J = 6, t), 7.26 (2H, J = 8.0, d), 7.69 (2H, J = 8.0, d). ¹³C NMR (100 MHz, CDCl₃) δ : 17.7, 21.6, 24.2, 27.7, 69.0, 69.9, 83.4, 127.0, 129.9, 133.0, 144.8.

6-Bromohex-1-yne (32). LiBr (1.7 g, 19.6 mmol) was added to a stirred solution of **31** (1.64 g, 6.52 mmol) in dry DMF (20 mL). After the exothermic reaction, the mixture was stirred at room temperature for 24 h. Then, water (25 mL) was added and the aqueous phase extracted with Et₂O (3 x 25 mL). The collected organic fractions were dried over Na₂SO₄, filtered and concentrated in vacuo. The residue was purified by flash chromatography using as eluent Hex: EtOAc (5:1) to afford a colorless oil (0.86 g, 82%). ¹H NMR (400 MHz, CDCl₃) δ : 1.66-1.70 (2H, m), 1.90-1.98 (3H, m), 2.24 (2H, m), 3.59 (2H, J = 6.4, t). ¹³C NMR (100 MHz, CDCl₃) δ : 19.7, 29.4, 29.7, 45.6, 69.2, 83.8.

6-Bromohexan-1-amine hydrochloride (34). 6-Aminohexanol **33** (0.5 g, 4.27 mmol) was slowly added to a stirring 48% hydrogen bromide solution (5.1 mL) at 0 °C and the resulting mixture was stirred at 80 °C for 20 h. The mixture was neutralized by adding NaOH 2N (20 mL) and extracted with EtOAc (3 x 20 mL). The combined organic fraction was washed with water (50 mL) followed by brine (50 mL) and then dried over Na₂SO₄, filtered and concentrated in vacuo. The obtained viscous oil was then dissolved in 4M hydrogen chloride solution in dioxane to give a sticky solid that is washed with Et₂O and then filtered for affording to a yellowish solid (0.55 g, 61%).

¹H NMR (400 MHz, MeOD) δ : 1.42–1.46 (4H, m), 1.59–1.70 (2H, m), 1.74–1.82 (2H, m), 2.86 (2H, J = 8, t), 3.39 (2H, J = 4, t). ¹³C NMR (100 MHz, MeOD) δ : 25.2, 27.0, 27.2, 32.2, 32.8, 44.2.

6-Azidohexan-1-amine (35). To a solution of **34** (0.55 g, 2.54 mmol) in water (25 mL), NaN₃ (0.49 g, 7.69 mmol) was added and the resulting mixture was heated at 100°C for 12 h. After cooling, 37% ammonia solution was added until a basic pH was reached, and the aqueous phase was extracted with Et₂O (3 x 20 mL). The organic fractions were collected, dried over Na₂SO₄ and filtered, and the solvent removed under vacuum to give a yellow oil (0.29 g, 80%). ¹H NMR (400 MHz, CDCl₃) δ : 1.29–1.34 (4H, m), 1.35–1.40 (2H, m), 1.50–1.54 (2H, m), 2.15 (2H, br s), 2.62 (2H, J = 4, t), 3.18 (2H, J = 8.0, t). ¹³C NMR (100 MHz, CDCl₃) δ : 26.4, 26.6, 28.8, 33.1, 41.8, 51.4

Ethyl 4-(4-(piperidin-4-yl)phenyl)-7-(4-(trifluoromethyl)phenyl)-2-naphthoate (36). To a solution of **25** (0.50 g, 1.57 mmol) in EtOH (50 mL), thionyl chloride (1.37 mL, 18.84 mmol) was carefully added over 30 min at 0°C. The reaction was allowed to warm up at rt and stirred overnight. The resulting mixture was quenched by adding 5% solution NaOH (25 mL) until basic pH. Then, the solvent was evaporated under vacuum and the aqueous residue extracted with EtOAc (3 x 20 mL). The collected organic fractions were dried over Na₂SO₄, filtered and the solvent removed under reduced pressure. The residue was purified by chromatography using as eluent DCM/MeOH/NH₄OH (7: 3: 0.3). The title compound was obtained as a white solid (0.61 g, 78%). ¹H NMR (400 MHz, MeOD) δ : 1.35 (3H, J = 4 Hz, t), 1.65–1.69 (2H, m), 1.81–1.84 (2H, m), 2.73–2.79 (3H, m), 3.15–3.19 (2H, m), 4.35 (2H, J = 8 Hz, q), 7.33–7.37 (4H, m), 7.69 (2H, J = 8 Hz, d), 7.76–7.79 (1H, m), 7.83–7.90 (4H, m), 8.26 (1H, s), 8.58 (1H, s). *m/z* (ESI, MH⁺) 504; ESI-HRMS (MH⁺) calcd. for C₃₁H₂₉F₃NO₂ 504.2150, found 504.2150.

Ethyl 4-(4-(1-(hex-5-yn-1-yl)piperidin-4-yl)phenyl)-7-(4-(trifluoromethyl)phenyl)-2-naphthoate (37). K₂CO₃ (0.12 g, 0.9 mmol) was added to a stirring solution of **36** (0.15 g, 0.3 mmol) in dry DMF (15 mL) and the resulting mixture left stirring for 20 min. Compound **32** (0.06 g, 0.6 mmol) was subsequently added and the reaction mixture was firstly stirred at rt for 2h and then at 50°C for 2.5h. After cooling at rt, NaHCO₃ saturated solution (15 mL) was added and the aqueous phase extracted with EtOAc (3 x 20 mL). The collected organic fractions were dried over Na₂SO₄, filtered and the solvent removed under reduced pressure. The residue was purified by chromatography using as eluent DCM/MeOH/NH₄OH (9.5: 0.5: 0.05). The desired compound was obtained as a colorless oil (0.16 g, 92%). *m/z* ¹H NMR (400 MHz, CDCl₃) δ : 1.38 (3H, J = 4 Hz, t), 1.51–1.55 (2H, m), 1.65–1.69 (2H, m), 1.90–1.99 (4H, m), 2.06–2.17 (5H, m), 2.40–2.44 (2H, m), 2.56–2.59 (1H, m), 3.10–3.13 (2H, m), 4.38 (2H, J = 8 Hz, q), 7.33 (2H, J = 8 Hz, d), 7.38 (2H, J = 8 Hz, d), 7.67–7.70 (3H, m), 7.71–7.76 (2H, m), 7.91–7.95 (2H, m), 8.15 (1H, s), 8.60 (1H, s) (ESI, MH⁺) 584. ¹³C NMR (101 MHz, CDCl₃) δ 14.42, 18.35, 25.69, 25.77, 26.49, 29.71, 32.99, 42.33, 54.27, 58.31, 61.26, 68.58, 84.31, 125.89, 126.65, 126.99, 127.11, 127.44, 127.94, 128.03, 129.55, 130.07, 130.61, 133.30, 137.61, 140.47, 143.91, 166.56. (ESI, MH⁺) 584; ESI-HRMS (MH⁺) calcd. for C₃₇H₃₇F₃NO₂ 584.2783, found 584.2776

Ethyl 4-(4-(1-(4-(1-(6-aminohexyl)-1H-1,2,3-triazol-4-yl)butyl)piperidin-4-yl)phenyl)-7-(4-(trifluoromethyl)phenyl)-2-naphthoate (38). To a solution of **37** (50 mg, 0.09 mmol) in DCM: *t*-BuOH: H₂O (1:1:1) (2 mL), compound **35** was added, followed by copper (II) sulfate pentahydrate (15 mol%) and sodium ascorbate (45 mol%). The reaction mixture was stirred for 24h at rt. The solvents were removed under vacuum and the residue rinsed with 37% ammonia solution (5 mL) and extracted with EtOAc

(3 x 8 mL). The collected organic fractions were dried over Na₂SO₄, filtered and the solvent removed under reduced pressure. The residue was purified by chromatography using as eluent a gradient of DCM/MeOH/NH₄OH (from 9.5: 0.5: 0.05 to 7: 3: 0.3). The title product was obtained as a white solid (32 mg, 51%).¹H NMR (400 MHz, CDCl₃) δ: 1.35-1.39 (7H, m), 1.58-1.65 (6H, m), 1.83-1.88 (6H, m), 2.04-2.07 (2H, m), 2.39-2.42 (3H, m), 2.65-2.71 (6H, m) 3.09-3.17 (2H, m), 4.23-4.26 (2H, m), 4.38 (2H, J = 8 Hz, q), 7.21-7.23 (1H, m), 7.30-7.33 (2H, m), 7.38-7.40 (2H, m), 7.66-7.70 (3H, m), 7.73-7.76 (2H, m), 7.96-7.99 (2H, m), 8.15 (1H, s), 8.62 (1H, s). (ESI, MH⁺) 726; ESI-HRMS (MH⁺) calcd. for C₄₃H₅₁F₃N₅O₂ 726.3984, found 726.3995.

4-(4-(1-(4-(1-(6-Aminohexyl)-1H-1,2,3-triazol-4-yl)butyl)piperidin-4-yl)phenyl)-7-(4-(trifluoromethyl)phenyl)-2-naphthoic acid (39). To a solution of **38** (32 mg, 44 μmol) in MeOH (1 mL), a solution of 0.5 M LiOH (1 mL) was added and the resulting mixture was heated at 60°C and stirred overnight. After cooling, the solvents were evaporated and the residue purified by preparative HPLC (R_t = 31.08 min). The product was obtained as a white solid by freeze drying (6.5 mg, 21%).¹H NMR (400 MHz, MeOD) δ: 1.26-1.33 (4H, m), 1.52-1.64 (6H, m), 1.81-1.86 (6H, m), 2.19-2.25 (2H, m), 2.46-2.50 (2H, m), 2.66-2.70 (3H, m), 2.79 (2H, J = 8 Hz, t), 3.09-3.12 (2H, m), 4.30 (2H, J = 8 Hz, t), 7.32 (2H, J = 8 Hz, d), 7.38 (2H, J = 8 Hz, d), 7.66-7.70 (3H, m), 7.70-7.72 (4H, m), 7.89-7.94 (4H, m), 8.27 (1H, s), 8.49 (1H, s). (ESI, MH⁺) 698; ESI-HRMS (MH⁺) calcd. for C₄₁H₄₇F₃N₅O₂ 698.3690, found 698.3682.

6-Amino-9-(2-carboxy-4-((6-(4-(4-(4-(3-carboxy-6-(4-(trifluoromethyl)phenyl)-naphthalen-1-yl)phenyl)piperidin-1-yl)butyl)-1H-1,2,3-triazol-1-yl)hexyl)carbamoyl)-phenyl)-3-iminio-5-sulfo-3H-xanthene-4-sulfonate (27). To a solution of AlexaFluor 488 **40** (4.44 mg, 7.08 μmol) and *N,N*-diisopropylethylamine (1.34 μL, 7.72 μmol) in dry DMF (400 μL), TSTU (2.42 mg, 7.72 μmol) was added at 0 °C. The resulting mixture was allowed to warm up at rt and stirred for 2-3 h. Then, a solution of **39** (4.5 mg, 6.44 μmol) and *N,N*-diisopropylethylamine (1.30 μL, 7.08 μmol) in dry DMF (300 μL) was added, and the reaction was stirred overnight at r.t. After removal of the solvent, the residue was purified by preparative HPLC (Method A, R_t = 24.9 min). The product **27** was obtained as an orange solid after lyophilization (0.8 mg, 10 %). MS (ESI, m/z) 1212 [M-H]⁻; ESI-HRMS calcd. m/z for C₆₂H₅₇F₃N₂O₁₂S₂ 1212.3462, found 1212.3459 [M-H]⁻. HPLC purity 96.1% (R_t = 5.7 min).

6-amino-9-(2-carboxy-4-((6-(4-(4-(4-(3-(ethoxycarbonyl)-6-(4-(trifluoromethyl)phenyl)naphthalen-1-yl)phenyl)piperidin-1-yl)butyl)-1H-1,2,3-triazol-1-yl)hexyl)carbamoyl)phenyl)-3-iminio-5-sulfo-3H-xanthene-4-sulfonate.

To a solution of AlexaFluor 488 **40** (1.2 mg, 1.93 μmol) and *N,N*-diisopropylethylamine (0.4 μL, 2.12 μmol) in dry DMF (100 μL), TSTU (0.7 mg, 2.12 μmol) was added at 0 °C. The resulting mixture was allowed to warm up at rt and stirred for 30 min. Then, a solution of **38** (1.2 mg, 1.6 μmol) and *N,N*-diisopropylethylamine (0.4 μL, 2.12 μmol) in dry DMF (100 μL) was added, and the reaction was monitored by LC/MS, showing only traces of desired compound after 5 h.

Preparation of **44** (MRS4183):

Uridine 5'-diphosphoglucuronic acid trisodium salt (8.9 mg, 13.8 μmol) was stirred in dry DMF (300 μL) with ice cooling before the sequential addition of DIPEA (9.3 μL, 9.2 μmol) and (1-cyano-2-ethoxy-2-oxoethylideneaminoxy)dimethylamino-morpholino-carbenium hexafluorophosphate (COMU, Sigma Aldrich, St. Louis, MO, 5.9 mg, 13.8 μmol). After 20 min, a solution of 5-(((4-(4,4-difluoro-5-(2-thienyl)-4-

bora-3a,4a-diaza-s-indacene-3-yl)phenoxy)acetyl)amino)-pentylamine, hydrochloride (BODIPY TR cadaverine, Life Technologies, Grand Island, NY, 5 mg, 9.2 μmol) and DIPEA (9.3 μL , 9.2 μmol) in dry DMF (300 μL) was added. The resulting mixture was allowed to warm up and stirring continued at room temperature for 6 h in the dark. After evaporation of the solvent under vacuum, the residue was purified by preparative HPLC (Column: Luna[®] 5 μm C18(2) 100 Å, LC Column 250 x 4.6 mm, Phenomenex, Inc., Torrance, CA); Eluent: 10 mM TEAA buffer-CH₃CN from 90:10 to 40:60 in 35 min and then from 40:60 to 30:70 in 5 min with a flow rate of 5 mL/min., R_t 33.7 min). The product **11** was obtained after lyophilization as a dark blue solid (di-triethylammonium salt, 35 μg , determined using the extinction coefficient at 590 nm of 64,000, 0.3% yield). ESI-HRMS (M+H⁺)⁻ calcd. for C₄₁H₄₆BF₂N₆O₁₉P₂S²⁻ 1069.2078, found C₄₁H₄₆BF₂N₆O₁₉P₂S²⁻ 1069.2075; HPLC purity (Column: Zorbax Eclipse 5 μm XDB-C18 analytical column, 150 X 4.6 mm, Agilent Technologies, Santa Clara, CA); Eluent: 10 mM TEAA buffer-CH₃CN from 80:20 to 40:60 in 15 min with a flow rate of 1 mL/min, retention time 5.6 min) was determined to be 95.7%.

Smiles notation for **44** (MRS4183):

```
O[C@@H]1[C@H](O)[C@@H](COP(OP(O)[C@H]2O[C@H](C(NCCCCNC(COC3=CC=C(C=C3)C4=[N+]5[B](F)(F)N6C(C7=CC=CS7)=CC=C6C=C5C=C4)=O)=O)[C@@H](O)[C@H](O)[C@H]2O)=O)(O)=O)[C@H]1N(C=CC(N8)=O)C8=O
```

Methyl 3-amino-5-bromobenzoate (46). 3-Bromo-5-aminobenzoic acid **45** (1.0 g, 4.62 mmol) was stirred in methanol (15 mL) with ice cooling before addition of thionyl chloride (4.00 mL, 55.0 mmol) dropwise over 20'. The resulting mixture was allowed to warm up at r.t. and left stirring overnight. The solvent was then removed under vacuum and the residue was suspended in ethyl acetate (200 mL), before washing with 0.2M NaOH (2x100 mL) and brine (100 mL), drying (Na₂SO₄) and concentrating to afford the title compound as a white solid (1.08 g, 98%). ¹H NMR (400 MHz, CDCl₃) δ : 3.85 (2H, br s), 3.90 (3H, s), 7.00 (1H, s), 7.27 (1H, s), 7.53 (1H, s). ¹³C NMR (100 MHz, CDCl₃) δ : 52.3, 114.6, 121.6, 122.3, 122.9, 132.6, 147.7, 166.0. m/z (ESI, MH⁺) 231.

Methyl 3-bromo-5-((tert-butoxycarbonyl)amino)benzoate (47a). To a solution of **46** (0.85 g, 3.7 mmol) and trimethylamine (1.87 mL, 11.1 mmol) in DCM (35 mL), Boc₂O (0.97 g, 4.44 mmol) and DMAP (0.37 g, 3.7 mmol) were sequentially added with ice cooling bath. The resulting mixture was allowed to warm up at r.t. and left stirring overnight. The solvent was removed under reduced pressure and the resulting residue was purified by silica gel chromatography using as eluent Hex/EtOAc (8: 2) to afford the title compound as a yellow solid (0.96 g, 70%). ¹H NMR (400 MHz, MeOD) δ : 1.45 (9H, s), 3.83 (3H, s), 7.64 (1H, s), 7.84 (1H, s), 7.93 (1H, s). ¹³C NMR (100 MHz, MeOD) δ : 27.2, 51.5, 117.5, 121.9, 124.7, 125.4, 132.1, 141.3, 153.3, 165.6. m/z (ESI, MH⁺) 331.

Methyl 3-((tert-butoxycarbonyl)amino)-5-(4,4,5,5-tetramethyl-1,3,2-dioxaborolan-2-yl)benzoate (48). A solution of **47a** (0.25 g, 0.76 mmol), bis(pinacolato)diboron (0.21 g, 0.84 mmol), KOAc (0.21 g, 2.20 mmol) in dry DMF (8 mL) was degassed with N₂ for 30'. Then, PdCl₂(dppf) (0.06 g, 0.1 mmol) was added while continuing degassing for additional 5'. The reaction mixture was heated at 95 °C and left stirring overnight. After cooling down, the resulting mixture was diluted with H₂O (15 mL)

and extracted with EtOAc (3x15 mL). The organic fractions were collected, dried over Na₂SO₄ and filtered. The solvent was removed under reduced pressure to give a brown residue which was purified by silica gel chromatography using a gradient of Hex: EtOAc (from 90: 10 to 50: 50). The title compound was obtained as a white solid (0.16 g, 56%). ¹H NMR (400 MHz, CDCl₃) δ: 1.25 (12H, s), 1.44 (9H, s), 3.82 (3H, s), 6.57 (1H, br s), 7.85 (1H, s), 8.05 (1H, s), 8.06 (1H, s). ¹³C NMR (100 MHz, CDCl₃) δ: 24.9, 28.3, 52.1, 84.1, 122.2, 128.9, 130.0, 138.2, 152.6, 166.9. m/z (ESI, MH⁺) 378.

4-(4-Bromophenyl)-1,2,3,6-tetrahydropyridine (50). 4-(4-Bromophenyl)piperidin-4-ol **49** (1.0 g, 3.90 mmol) was carefully added to CF₃COOH (2.99 mL, 39 mmol) and the resulting mixture was heated at 90 °C for 3 h. After cooling down, the solvent was removed under vacuum to give the title product as a white solid (0.90 g, 97%). ¹H NMR (400 MHz, MeOD) δ: 2.68-2.72 (2H, m), 3.38 (2H, t, J = 6.1), 3.76-3.77 (2H, m), 6.10 (1H, s), 7.31 (2H, J = 8.0, d), 7.44 (2H, J = 8.0, d). ¹³C NMR (100 MHz, MeOD) δ: 23.3, 40.7, 42.0, 116.4, 121.7, 126.6, 131.4, 134.6, 138.1. m/z (ESI, MH⁺) 239.

4-(4-Bromophenyl)piperidine (51). To a solution of 4-(4-bromophenyl)-1,2,3,6-tetrahydropyridine **50** (0.90 g, 3.78 mmol) in dry MeOH (20 mL) was added a spatula of Rh/C catalyst. The resulting reaction mixture was stirred at r.t. in a hydrogen atmosphere (100 psi) for 17 h. The mixture was filtered through a cake of celite and the filtrate was concentrated to give the title compound as a pale yellow solid (0.91 g, 98%). ¹H NMR (400 MHz, MeOD) δ: 1.55-1.59 (2H, m), 1.61-1.70 (2H, m), 2.55-2.56 (1H, m), 2.64-2.70 (2H, m), 3.09-3.06 (2H, m), 7.13 (2H, J = 8.0, d), 7.31 (2H, J = 8.0, d). ¹³C NMR (100 MHz, MeOD) δ: 32.7, 41.4, 45.6, 119.4, 126.4, 128.2, 128.5, 131.2, 145.3. m/z (ESI, MH⁺) 241.

Methyl 5-((tert-butoxycarbonyl)amino)-4'-(piperidin-4-yl)-[1,1'-biphenyl]-3-carboxylate (52). A solution of **52** (0.11 g, 0.29 mmol), **48** (0.09 g, 0.32 mmol), K₂CO₃ (0.12 g, 0.87 mmol) in dry DMF (4.5 mL) was degassed with N₂ for 30'. Then, Pd(Ph₃P)₄ (0.017 g, 0.015 mmol) was added to the resulting mixture while flushing N₂ for additional 5'. The reaction was heated at 85°C for 6 h. after cooling down, H₂O (10 mL) was added and the aqueous phase was extracted with EtOAc (3 x 15 mL). The collected organic fractions were dried over Na₂SO₄, filtered and the solvent was removed under reduced pressure. The residue was purified by silica gel chromatography using a gradient of DCM: MeOH: NH₄OH (from 9: 10: 0.1 to 8: 2: 0.2) to afford the title compound as a yellowish solid (0.07 g, 71%). ¹H NMR (400 MHz, CDCl₃) δ: 1.47 (9H, s), 1.85-1.90 (4H, m), 2.65-2.68 (1H, m), 2.78-2.83 (2H, m), 3.28-3.37 (2H, m), 3.85 (3H, s), 6.67 (1H, br s), 7.04-7.06 (1H, m), 7.24 (2H, J = 8, d), 7.52 (2H, J = 8, d), 7.84 (2H, m). ¹³C NMR (100 MHz, CDCl₃) δ: 28.4, 29.7, 33.8, 42.3, 42.7, 46.7, 52.2, 61.1, 118.0, 122.6, 126.2, 126.8, 127.3, 128.4, 128.6, 131.5, 137.9, 139.3, 142.1, 146.0, 152.8, 166.9. m/z (ESI, MH⁺) 411.

Methyl 5-((tert-butoxycarbonyl)amino)-4'-(1-(2,2,2-trifluoroacetyl)piperidin-4-yl)-[1,1'-biphenyl]-3-carboxylate (53). To a suspension of **52** (0.04 g, 0.11 mmol) in THF (2.5 mL), NEt₃ (45 μL, 0.32 mmol) and TFAA (22 μL, 0.16 mmol) were added and the resulting mixture was stirred for 3 h. A saturated solution of NaHCO₃ (2 mL) was gradually added and then the organic solvent was removed under reduced pressure. The aqueous layer was extracted with DCM (3 x 5 mL). The collected organic fractions were dried over Na₂SO₄, filtered and the solvent was removed under

reduced pressure to give a yellow oil that is used in the next step without any further purification. m/z (ESI, MH^+) 507.

Methyl 5-amino-4'-(1-(2,2,2-trifluoroacetyl)piperidin-4-yl)-[1,1'-biphenyl]-3-carboxylate (54). To a solution of **53** (0.06 g, 0.11 mmol) in DCM (2 mL), TFA (170 μ L, 2.28 mmol) was added and the resulting mixture was stirred overnight. A saturated solution of $NaHCO_3$ (2 mL) was gradually added and the aqueous layer was extracted with DCM (3 x 5 mL). The collected organic fractions were dried over Na_2SO_4 , filtered and the solvent was removed under reduced pressure. The residue was purified by silica gel chromatography with 40% of EtOAc in Hex to give a yellow oil (0.27 g, 65%). (ESI, MH^+) 407. 1H NMR (400 MHz, $CDCl_3$) δ : 1.63-1.72 (2H, m), 1.93-1.97 (1H, m), 2.78-2.83 (2H, m), 3.16-3.22 (1H, m), 3.81 (3H, s), 6.99 (1H, s), 7.1-7.20 (2H, m), 7.27 (1H, s), 7.47 (2H, $J = 8$, d), 7.58 (1H, s). ^{13}C NMR (100 MHz, $CDCl_3$) δ : 32.6, 33.6, 42.1, 44.2, 46.4, 52.1, 61.0, 76.7, 77.0, 77.3, 114.8, 117.8, 118.7, 127.1, 127.4, 131.6, 138.9, 142.1, 143.7, 146.7, 167.1.

Methyl 5-azido-4'-(1-(2,2,2-trifluoroacetyl)piperidin-4-yl)-[1,1'-biphenyl]-3-carboxylate (55). To a solution of **54** (0.121 g, 0.29 mmol) in a 3:7 mixture of H_2O and acetonitrile (10 mL), *p*-toluenesulfonic acid (0.509 g, 2.6 mmol) was added, and the mixture was stirred for 5 min. $NaNO_2$ (0.184 g, 2.6 mmol) was then added, and the yellow solution was stirred at room temperature. The course of the reaction was followed by TLC (hexane: ethyl acetate =60:40), and the reaction was allowed to continue until the starting material disappeared. NaN_3 (0.030 g, 0.47 mmol) was added at room temperature, and the reaction mixture was stirred overnight. Et_2O was added, and the phases were separated. The organic phase was dried over Na_2SO_4 , filtered and concentrated under reduced pressure to give an orange oil that was purified by silica gel chromatography using as eluent hexane : ethyl acetate (70:30) to afford the title compound as a yellow oil (0.11 g, 83%). 1H NMR (400 MHz, $CDCl_3$): δ (ppm) = 8.03 (t, $J = 1.6$ Hz, 1H), 7.68 (t, $J = 1.6$ Hz, 1H), 7.56 (d, $J = 8.3$ Hz, 2H), 7.37 (t, $J = 1.6$ Hz, 1H), 7.30 (d, $J = 8.3$ Hz, 2H), 4.80 – 4.63 (m, 1H), 4.17 (dd, $J = 3.1, 14.2$ Hz, 1H), 3.96 (s, 3H), 3.27 (td, $J = 2.4, 13.3, 13.7$ Hz, 1H), 2.90 (td, $J = 4.2, 12.5$ Hz, 2H), 2.02 (d, $J = 14.2$ Hz, 2H), 1.76 (qd, $J = 4.2, 12.5$ Hz, 2H). ^{13}C NMR (100 MHz, $CDCl_3$): δ (ppm) = 166.6, 155.9, 144.9, 143.2, 141.5, 138.1, 132.7, 127.8, 125.1, 122.1, 118.7, 52.9, 46.8, 44.6, 42.5, 34.0, 33.0.

General procedure for the click cycloaddition reaction:

To a solution of aryl azide **55**, 1 eq) and aryl alkyne (1.5 eq) in 2 mL of THF: water (1:1), sodium ascorbate (freshly prepared 1 M aqueous solution) and $CuSO_4$ (0.5 eq) were sequentially added. The resulting reaction was vigorously stirred for 12 h at r.t. The reaction mixture was then concentrated *in vacuo* and purified by flash chromatography (hexane: ethyl acetate = 6 : 4).

Methyl 5-(4-phenyl-1H-1,2,3-triazol-1-yl)-4'-(1-(2,2,2-trifluoroacetyl)piperidin-4-yl)- [1,1'-biphenyl]-3-carboxylate (56). Yellow solid. MS (ESI, m/z) 535 [$M+H$] $^+$; ESI-HRMS calcd. for $C_{29}H_{26}F_3N_4O_3$ 535.1952, found 535.1957 [$M+H$] $^+$.

Methyl 5-(4-(4-(trifluoromethyl)phenyl)-1H-1,2,3-triazol-1-yl)-4'-(1-(2,2,2-trifluoroacetyl)piperidin-4-yl)- [1,1'-biphenyl]-3-carboxylate (57). Orange solid 6.9 mg (99 %). MS (ESI, m/z) 603 [$M+H$] $^+$; ESI-HRMS calcd. for $C_{30}H_{25}F_6N_4O_3$ 603.1825, found 603.1831 [$M+H$] $^+$.

Methyl 5-(4-(5-chlorothiophen-2-yl)-1H-1,2,3-triazol-1-yl)-4'-(1-(2,2,2-trifluoroacetyl)-piperidin-4-yl)-[1,1'-biphenyl]-3-carboxylate (95). Brown solid. MS (ESI, m/z) 575 [M+H]⁺; ESI-HRMS calcd. for C₂₇H₂₃F₃N₄O₃SCl 575.1131, found 575.1132 [M+H]⁺.

Methyl 5-(4-cyclohexyl-1H-1,2,3-triazol-1-yl)-4'-(1-(2,2,2-trifluoroacetyl)piperidin-4-yl)-[1,1'-biphenyl]-3-carboxylate (62). Yellow solid 5.4 mg (87 %). MS (ESI, m/z) 541.2 [M+H]⁺; ESI-HRMS calcd. for C₂₉H₃₂F₃N₄O₃ 541.2427, found 541.2419 [M+H]⁺.

5-(4-Phenyl-1H-1,2,3-triazol-1-yl)-4'-(piperidin-4-yl)-[1,1'-biphenyl]-3-carboxylic acid (106). To a solution of **56** (9 mg, 17 μmol) in 2 mL of MeOH: H₂O (1:1), KOH (9.5 mg, 170 μmol) was added, and the resulting mixture was heated at 50 °C for 12 h. After removing the solvents under reduced pressure, the mixture was purified by preparative HPLC (Method B, R_t = 25.7 min). The product was obtained as a white solid by lyophilization (1.9 mg, 26 %). MS (ESI, m/z) 425 [M+H]⁺; ESI-HRMS calcd. for C₂₆H₂₅N₄O₂ 425.1978, found 425.1980 [M+H]⁺. HPLC purity 97 % (R_t = 8.9 min). ¹H NMR (400 MHz, MeOD): δ (ppm) = 8.94 (s, 1H), 8.29 (d, J = 8 Hz, 2H), 7.88 (d, J = 8 Hz, 2H), 7.68 (d, J = 8 Hz, 2H), 7.39-7.43 (m, 2H), 7.31-7.35 (m, 3H), 2.90-2.96 (m, 5H), 1.94-1.97 (m, 2H), 1.77-1.80 (m, 2H).

5-(4-(4-(Trifluoromethyl)phenyl)-1H-1,2,3-triazol-1-yl)-4'-(piperidin-4-yl)-[1,1'-biphenyl]-3-carboxylic acid (107). To a solution of **57** (6.3 mg, 10 μmol) in 2 mL of MeOH: H₂O (1:1), KOH (5.6 mg, 100 μmol) was added, and the resulting mixture was heated at 50°C for 12 h. After removing the solvents under reduced pressure, the mixture was purified by preparative HPLC (Method B, R_t = 30.2 min). The product was obtained as a white salt by lyophilization (0.5 eq CH₃CO₂H-salt, 6.01 mg, 99 %). MS (ESI, m/z) 493.1 [M+H]⁺; ESI- HRMS calcd. for C₂₇H₂₄F₃N₄O₂ 493.1851, found 493.1853 [M+H]⁺. HPLC purity 99 % (R_t = 12.6 min). ¹H NMR (600 MHz, DMSO-*d*₆): δ (ppm) = 9.66 (s, 1H), 8.39 (t, J = 1.6 Hz, 1H), 8.28 (t, J = 1.6 Hz, 1H), 8.22 (d, J = 8.1 Hz, 2H), 8.15 (t, J = 1.6 Hz, 1H), 7.88 (d, J = 8.1 Hz, 2H), 7.75 (d, J = 8.3 Hz, 2H), 7.41 (d, J = 8.3 Hz, 2H), 3.20 – 3.15 (m, 2H), 2.76 (td, J = 3.2, 12.1 Hz, 3H), 1.88 (s, 1.5 H acetate), 1.77 (qd, J = 4.2, 12.9 Hz, 4H). ¹³C NMR (150 MHz, DMSO-*d*₆): δ (ppm) = 167.1, 146.5, 145.9, 143.9, 140.7, 137.1, 136.5, 134.4, 128.4, 128.2, 127.4 (2C), 127.2, 126.9 (2C), 126.0 (2C), 125.9 (2C), 125.2, 121.1, 119.2, 117.9, 55.0, 46.1 (2C), 41.7, 40.0, 33.4 (2C).

5-(4-(5-Chlorothiophen-2-yl)-1H-1,2,3-triazol-1-yl)-4'-(piperidin-4-yl)-[1,1'-biphenyl]-3-carboxylic acid (116). To a solution of **95** (8.3 mg, 14 μmol) in 2 mL of MeOH: H₂O (1:1), KOH (7.9 mg, 140 μmol) was added, and the resulting mixture was heated at 60 °C for 6 h. After removing the solvents under reduced pressure, the mixture was purified by preparative HPLC (Method B, R_t = 28.6 min). The product was obtained as a white solid by lyophilization (0.5 eq CH₃CO₂H-salt, 2.8 mg, 38%). MS (ESI, m/z) 465 [M+H]⁺; ESI-HRMS calcd. for C₂₄H₂₂N₄O₂SCl 465.1152, found 465.1151 [M+H]⁺. HPLC purity 98 % (R_t = 10.6 min). ¹H NMR (400 MHz, DMSO-*d*₆): δ (ppm) = 9.34 (s, 1H), 8.25 (d, J = 2.4 Hz, 1H), 8.19 (s, 1H), 8.02 (d, J = 2.4 Hz, 1H), 7.65 (d, J = 8.1 Hz, 2H), 7.36 – 7.29 (m, 3H), 7.13 (d, J = 3.8 Hz, 1H), 3.12 (d, J = 12.0 Hz, 2H), 2.76 – 2.63 (m, 3H), 1.83 – 1.61 (m, 5H).

Conclusions and Perspectives

Chemical probes -i.e. small molecules that specifically bind and modulate the activity of a cellular target- are powerful tools that allow the precise molecular-level interrogation of biological targets and their associated pathways.¹ Furthermore, chemical probes provide small molecule tools for validating clinical target candidates and, at the same time, offering chemical starting points that can be further optimized by medicinal chemistry for drug development.²

Chemical biology efforts over the past decade have targeted numerous protein classes and biological pathways.¹ However, there is still a compelling need to develop valuable strategies to discovery high-quality chemical probes.

In this thesis, we advocated two chemical biology approaches in two distinct endeavors. The first part of this thesis dealt with the development of chemical probes for modulating neural stem cells (NSCs) biology and its neuroregenerative potential for the treatment of neurodegenerative diseases. In the second part, the recently discovered P2Y₁₄ receptor was deeply investigated by designing new chemical probes, useful in dissecting the structure and function of this receptor, which has been found to be involved in inflammatory, endocrine and other pathological conditions.

As highlighted in part I of this thesis, the initial isolation of NSCs has led to large, systematic efforts to identify and manipulate molecular mechanisms of NSCs proliferation, cell fate determination, and differentiation. While many of the genetic and biochemical pathways underlying these processes are beginning to be disclosed, currently there are no validated targets to finely control NSCs fate. Moreover, few small molecule probes for specifically studying and controlling these mechanisms are available. Potentially, NSC-based chemical assays, which can be used to identify compounds that produce a phenotype of interest, provide suitable strategy for identifying such small molecules. Accordingly, in part I, we fostered two parallel and complementary approaches to identify small molecule probes for NSCs. Particularly, we were drawn to knowledge-based phenotypic (i) and functionalized congeners (ii) strategies. The first approach (i) is based on a priori knowledge that some known drugs and drug candidates (i.e. tricyclic antidepressants, TCAs and P7C3) have already been shown to display neuroregenerative effects. Thus, a focused chemical library (**1-36**) inspired by TCAs and P7C3 has been designed and synthesized. This focused library has been then preliminarily evaluated for its safety profiles in neuronal and hepatic cell models (CGNs and HepG2 cells, respectively). Notably, all the compounds resulted particularly promising from this primary screening, displaying low toxicity only at high concentrations (25-50 μ M). This is not surprising, because our library design relies on approved drugs (TCAs). With the aim to use these cell cultures as a preliminary screening to filter out compounds with toxicity liabilities, we identified **16**, **19-21**, **29** and **33** with optimal safety profiles, which were selected for further studies. These involved the assessment of their neuroprotective effects in a low-serum neuronal model of cell death and the evaluation of their potential neurogenic effects in a proliferation BrdU-based assay in primary neurons. While these experiments are still ongoing, in parallel, we started to set up the phenotypic NSCs-based assay that will be used to test the differentiation ability of

such compounds toward specific lineages (i.e. neurons, astrocytes and oligodendrocytes). Preliminary data regarding selected reference compounds have been generated.

At the same time, the exploitation of functionalized congener approach to TCAs has allowed the development of: (a) fluorescent, (b) multi-target, and (c) polyamine-based congeners. Among them, the small set of novel fluorescent probes inspired to TCAs imipramine and desimipramine (**48-51**) may be used to potentially identify the subcellular localization of these known neuroregenerative drugs in NSC. The multi-target (**53-58**) and polyamine (**65**) congeners may interfere with two or more targets of the complex NSCs signaling network, thereby in principle providing a novel set of chemical probes. In particular, polyamine congener **65** could also exploit the polyamine transporter for a facilitated entry to the CNS and accumulation in the mitochondria.

Collectively, these results represent the starting point of a phenotypic approach aimed at identifying small molecule probes that can contribute to elucidate NSCs biology. Further, they may inspire the design of neuroregenerative drugs against neurodegenerative diseases.

In part II of this thesis, the functionalized congener approach was applied to develop fluorescent probes and antagonists to characterize the P2Y₁₄ receptor. This receptor has been found to be involved in a variety of inflammatory and endocrine processes, emerging as an attractive drug target.³ Despite that, to date, the P2Y₁₄ receptor has not been widely explored from a medicinal chemistry perspective. Additionally, few selective radioligands are available,⁴ thus improved and more versatile chemical probes are needed.

Over the past decades, fluorescent probes that target GPCR have provided significant advances in exploring their functions and structures.⁵ Although many GPCR crystal structures have been resolved during the last decade,⁶ information acquired at molecular level by fluorescent probes still offered an undeniable potential. Not only they allow to study receptor–ligand interactions, but also, such fluorescent probes enable to monitor and visualize the dynamic processes of GPCR at cellular level (e.g. oligomerization and internalization). Further, these probes are also successfully used in high-throughput screening, searching for novel GPCR agonists or antagonists.⁵

In light of this considerations, based on the structural template of P2Y₁₄ receptor, Dr. Jacobson and coworkers, starting from the previously characterized antagonist **25** (PPTN), developed the first high-affinity antagonist-based fluorescent congener **27** (MRS4174).⁷ MRS4174 displayed highly favorable properties when employed as a tracer in whole-cell binding assays of P2Y₁₄ receptor using flow cytometry: pharmacological selectivity over the other member of P2Y receptors family, an exceptional high receptor affinity (K_i of 80 pM), and strikingly low nonspecific binding.⁷ However, its chemical synthesis suffered from a low yield, limiting its use as tracer in displacement assay. Thus, an improved synthetic route was developed and this enables quantification of antagonist affinity using a novel flow cytometry displacement assay of P2Y₁₄ receptor-expressing CHO cells.

In addition, we reported on the design, preparation, and biological evaluation of the agonist-based fluorescent probe **44** (MRS4183).⁸ Again, by exploiting the P2Y₁₄ receptor homology model, the first P2Y₁₄ agonist-based fluorescent probe has been

designed, based on the previously characterized P2Y₁₄ agonist UDP-glucuronic acid (**22**). The conjugation with the BODIPY fluorophore affords **44**, which retained P2Y₁₄R potency with an EC₅₀ value of 0.96 nM. It also effectively served as a tracer for microscopy and flow cytometry, displaying minimal nonspecific binding.⁸

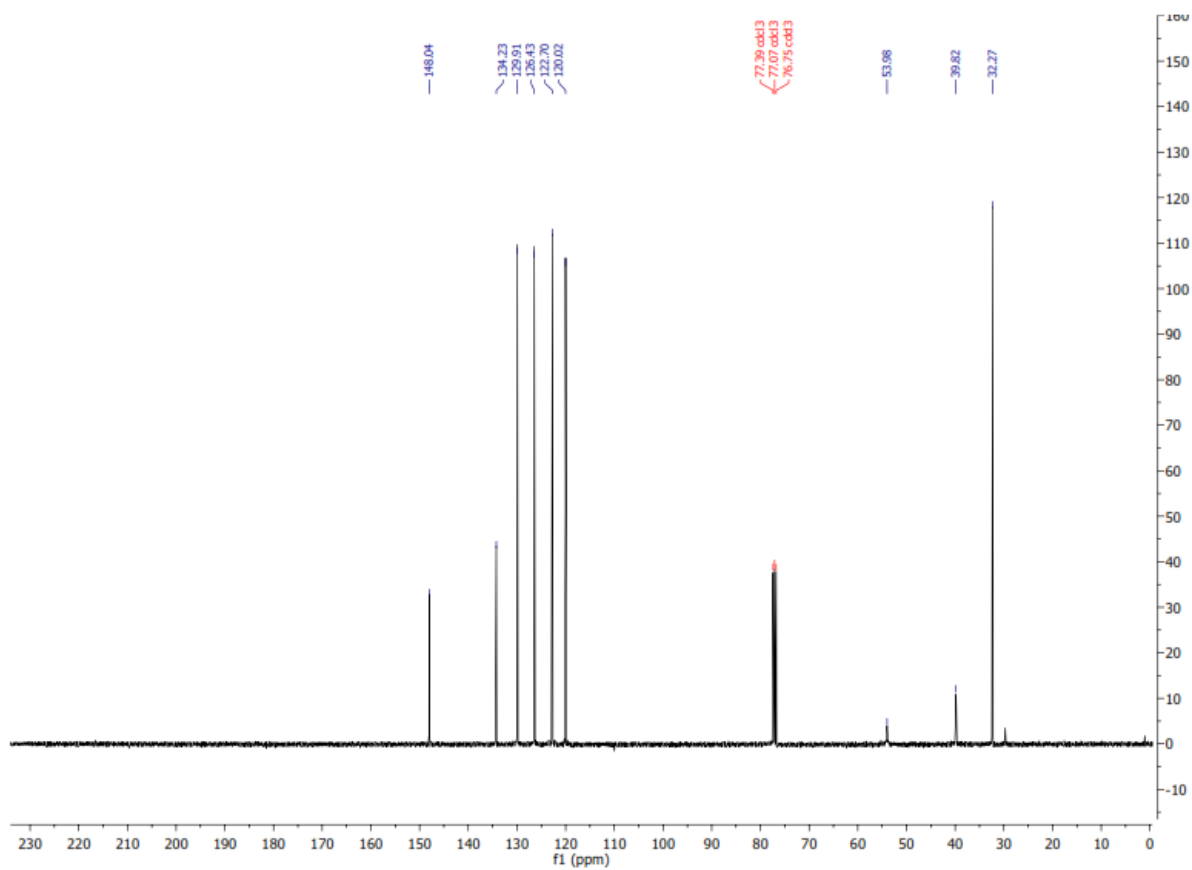
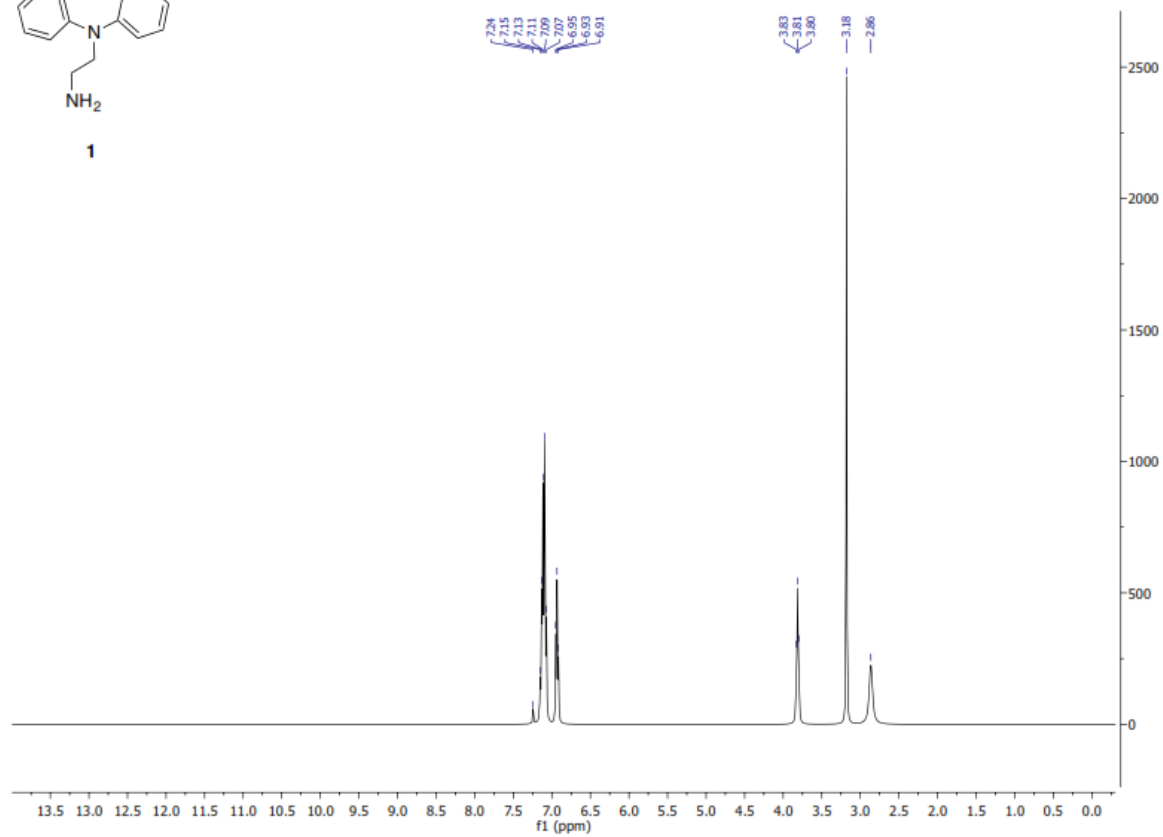
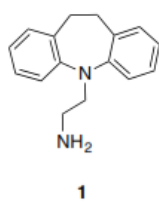
Furthermore, these promising results have already led to the development of a new series of P2Y₁₄R antagonists based on 3-(4-aryl-1H-1,2,3-triazol-1-yl)-biphenyl scaffold.^{7a, 9} Particularly, all the triazole derivatives **106-146** were evaluated in a novel flow cytometry competition assay using whole cells expressing P2Y₁₄ receptor and fluorescent antagonist **27** as a tracer. This led to the identification of the hit compound **107** (MRS4217), which displays an IC₅₀ of 32 nM.

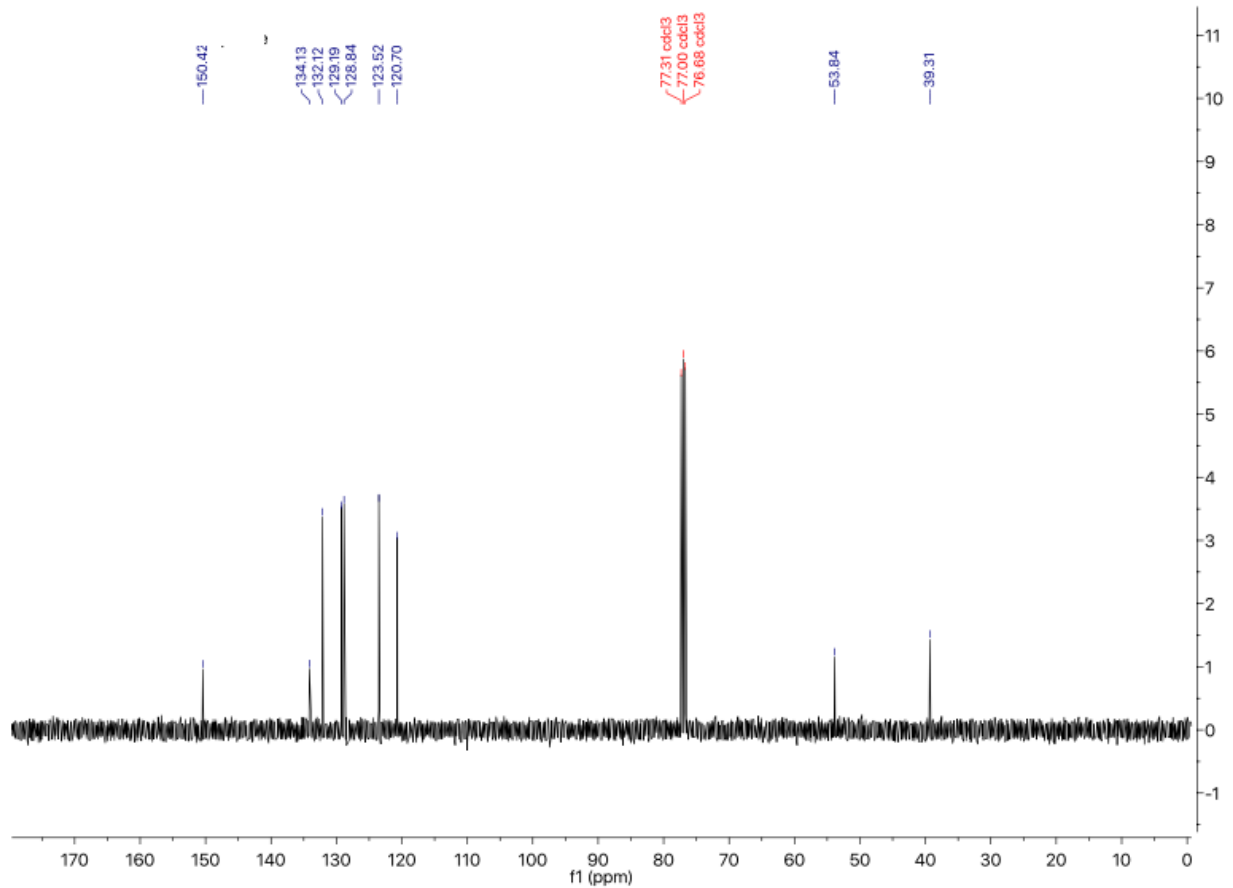
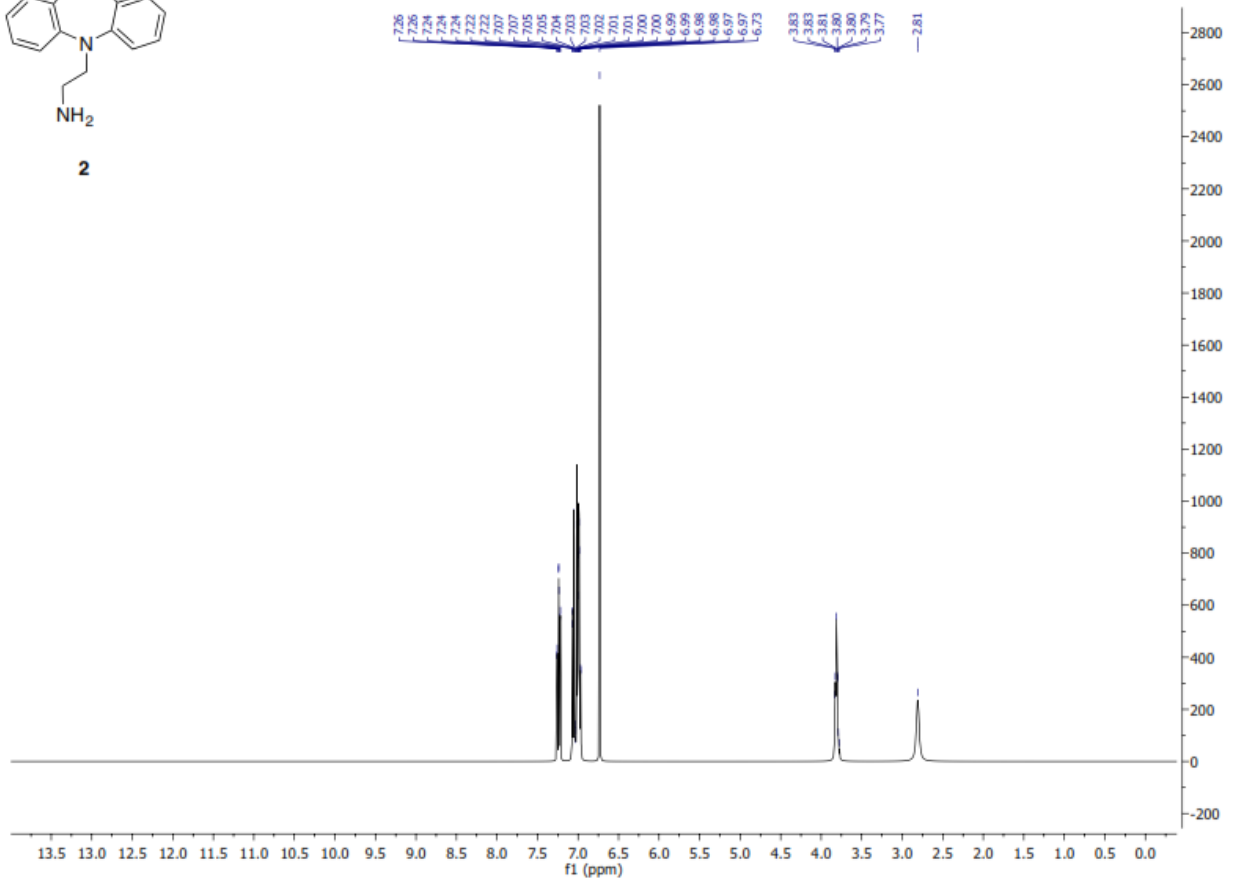
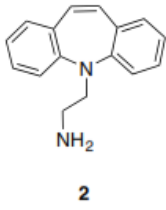
Collectively, all this results allowed expanding the SAR at this receptor, which still lacks chemical diversity in its ligands. Moreover, the synthesized probes could aid in unveiling the pharmacological potential of this receptor, and could inspire clinically useful drug candidates for inflammatory, endocrine and other pathological conditions.

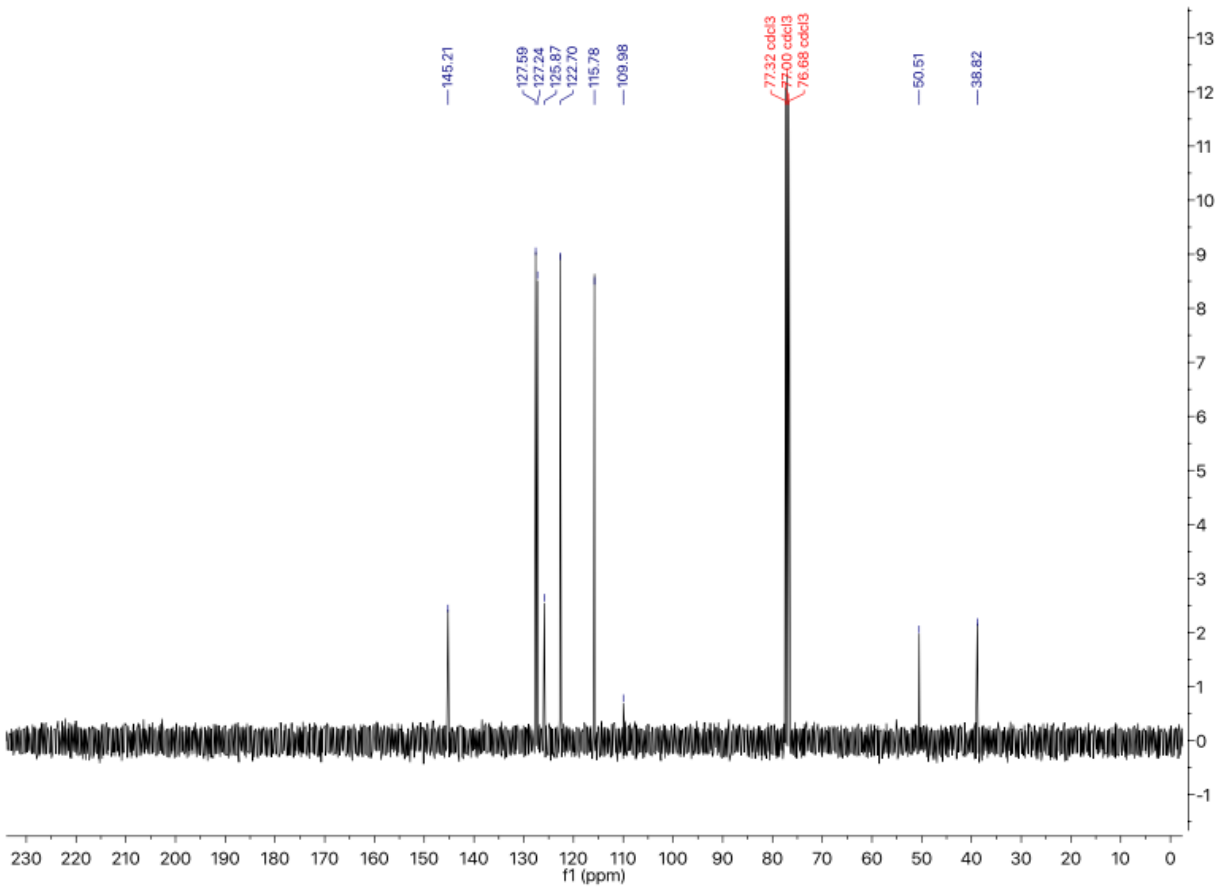
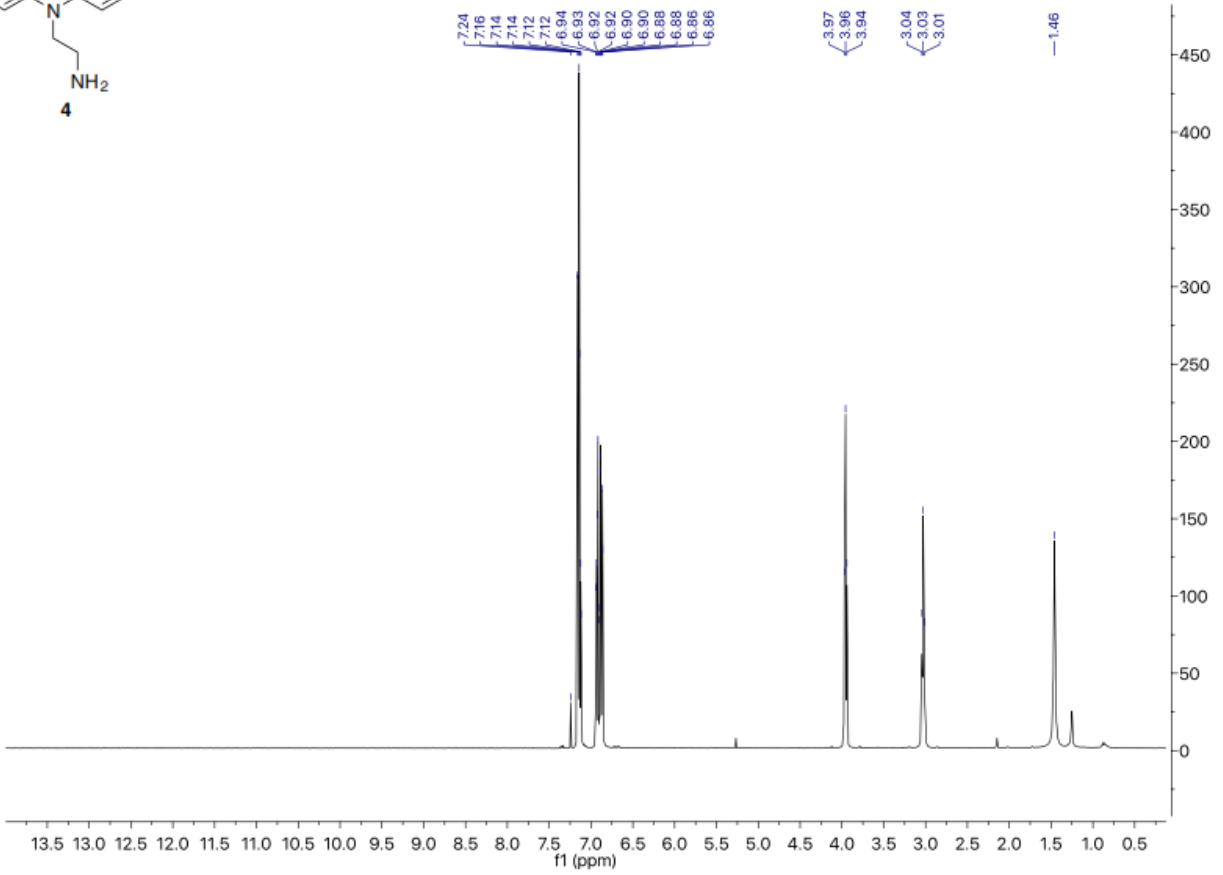
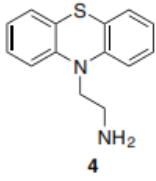
References

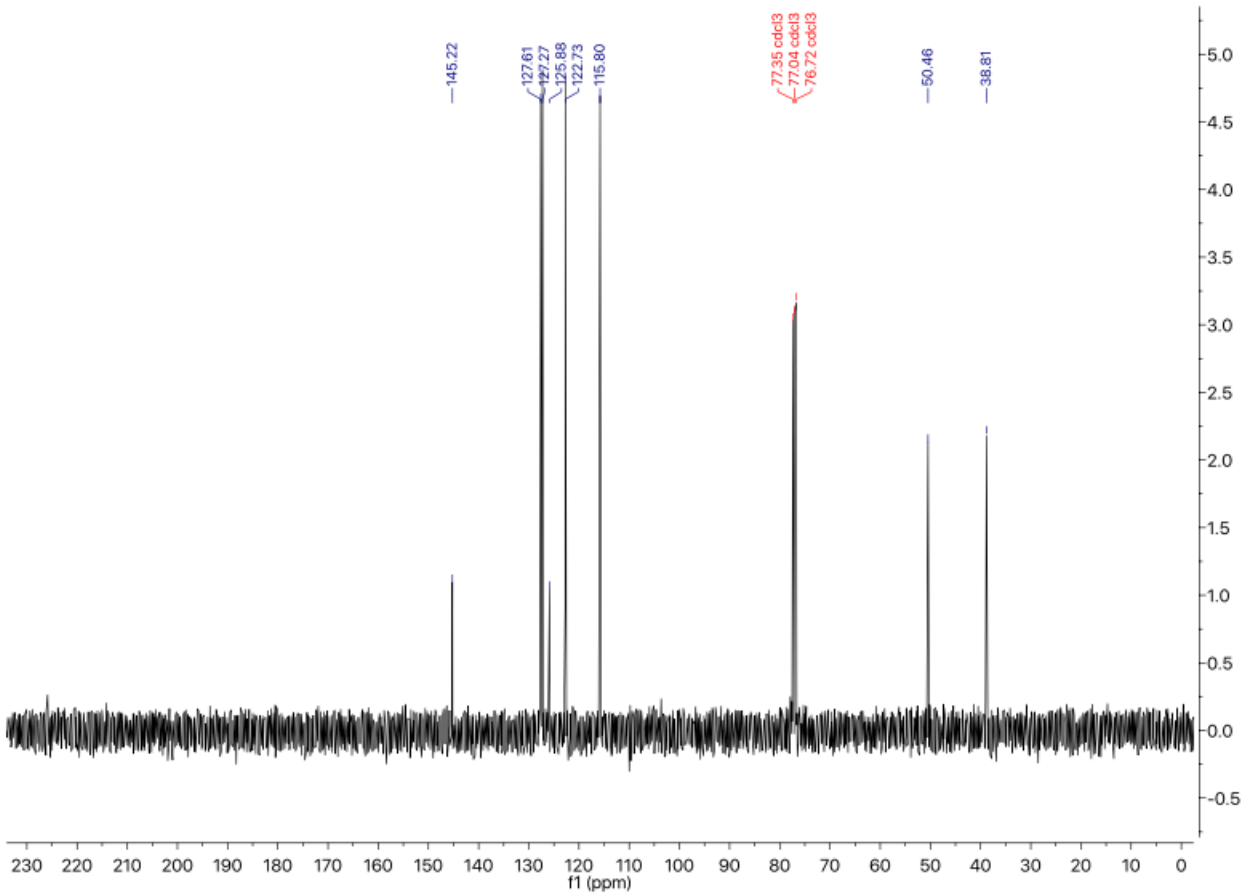
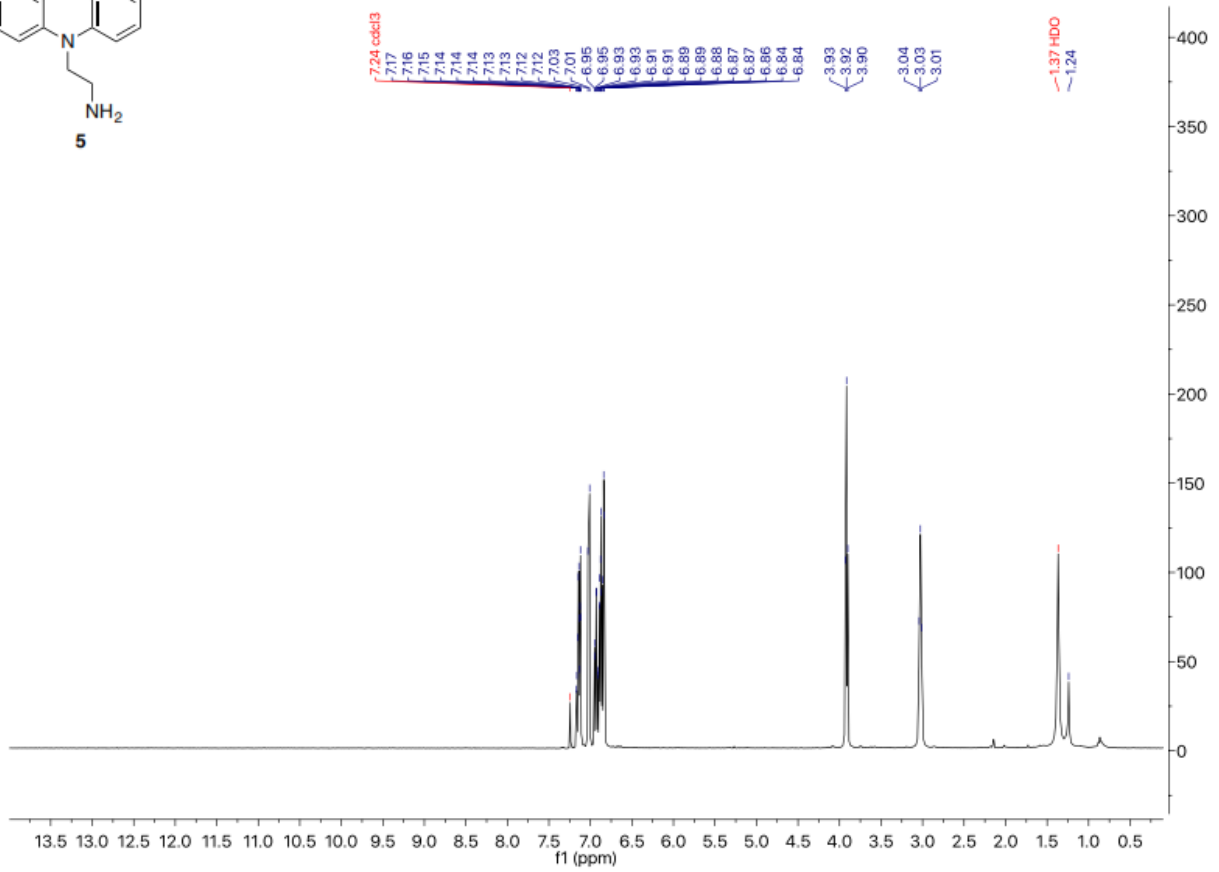
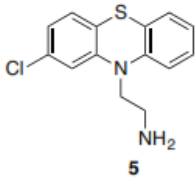
- [1] Arrowsmith, C. H.; Audia, J. E.; Austin, C.; Baell, J.; Bennett, J.; Blagg, J.; Bountra, C.; Brennan, P. E.; Brown, P. J.; Bunnage, M. E.; Buser-Doepner, C.; Campbell, R. M.; Carter, A. J.; Cohen, P.; Copeland, R. A.; Cravatt, B.; Dahlin, J. L.; Dhanak, D.; Edwards, A. M.; Frederiksen, M.; Frye, S. V.; Gray, N.; Grimshaw, C. E.; Hepworth, D.; Howe, T.; Huber, K. V.; Jin, J.; Knapp, S.; Kotz, J. D.; Kruger, R. G.; Lowe, D.; Mader, M. M.; Marsden, B.; Mueller-Fahrnow, A.; Muller, S.; O'Hagan, R. C.; Overington, J. P.; Owen, D. R.; Rosenberg, S. H.; Roth, B.; Ross, R.; Schapira, M.; Schreiber, S. L.; Shoichet, B.; Sundstrom, M.; Superti-Furga, G.; Taunton, J.; Toledo-Sherman, L.; Walpole, C.; Walters, M. A.; Willson, T. M.; Workman, P.; Young, R. N.; Zuercher, W. J. The promise and peril of chemical probes. *Nat Chem Biol* **2015**, *11* (8), 536-41.
- [2] Bunnage, M. E.; Chekler, E. L.; Jones, L. H. Target validation using chemical probes. *Nat Chem Biol* **2013**, *9* (4), 195-9.
- [3] Jacobson, K. A.; Boeynaems, J. M. P2Y nucleotide receptors: promise of therapeutic applications. *Drug Discov Today* **2010**, *15* (13-14), 570-8.
- [4] Brunschweiler, A.; Muller, C. E. P2 receptors activated by uracil nucleotides--an update. *Curr Med Chem* **2006**, *13* (3), 289-312.
- [5] Ma, Z.; Du, L.; Li, M. Toward fluorescent probes for G-protein-coupled receptors (GPCRs). *J Med Chem* **2014**, *57* (20), 8187-203.
- [6] Kobilka, B. The structural basis of G-protein-coupled receptor signaling (Nobel Lecture). *Angew Chem Int Ed Engl* **2013**, *52* (25), 6380-8.
- [7] (a) Junker, A.; Balasubramanian, R.; Ciancetta, A.; Uliassi, E.; Kiselev, E.; Martiriggiano, C.; Trujillo, K.; Mtchedlidze, G.; Birdwell, L.; Brown, K. A.; Harden, T. K.; Jacobson, K. A. Structure-Based Design of 3-(4-Aryl-1H-1,2,3-Triazol-1-yl)-Biphenyl Derivatives as P2Y₁₄ Receptor Antagonists. *J Med Chem under revision*; (b) Kiselev, E.; Barrett, M. O.; Katritch, V.; Paoletta, S.; Weitzer, C. D.; Brown, K. A.; Hammes, E.; Yin, A. L.; Zhao, Q.; Stevens, R. C.; Harden, T. K.; Jacobson, K. A. Exploring a 2-naphthoic acid template for the structure-based design of P2Y₁₄ receptor antagonist molecular probes. *ACS Chem Biol* **2014**, *9* (12), 2833-42.
- [8] Kiselev, E.; Balasubramanian, R.; Uliassi, E.; Brown, K. A.; Trujillo, K.; Katritch, V.; Hammes, E.; Stevens, R. C.; Harden, T. K.; Jacobson, K. A. Design, synthesis, pharmacological characterization of a fluorescent agonist of the P2Y₁₄ receptor. *Bioorg Med Chem Lett* **2015**, *25* (21), 4733-9.
- [9] Jacobson, K. A. J. A. U., E.; Kiselev, E. . Triazole derivatives as P2Y₁₄ receptor antagonists U.S. Patent Application No. 62/233,162 filed September 25, 2015.

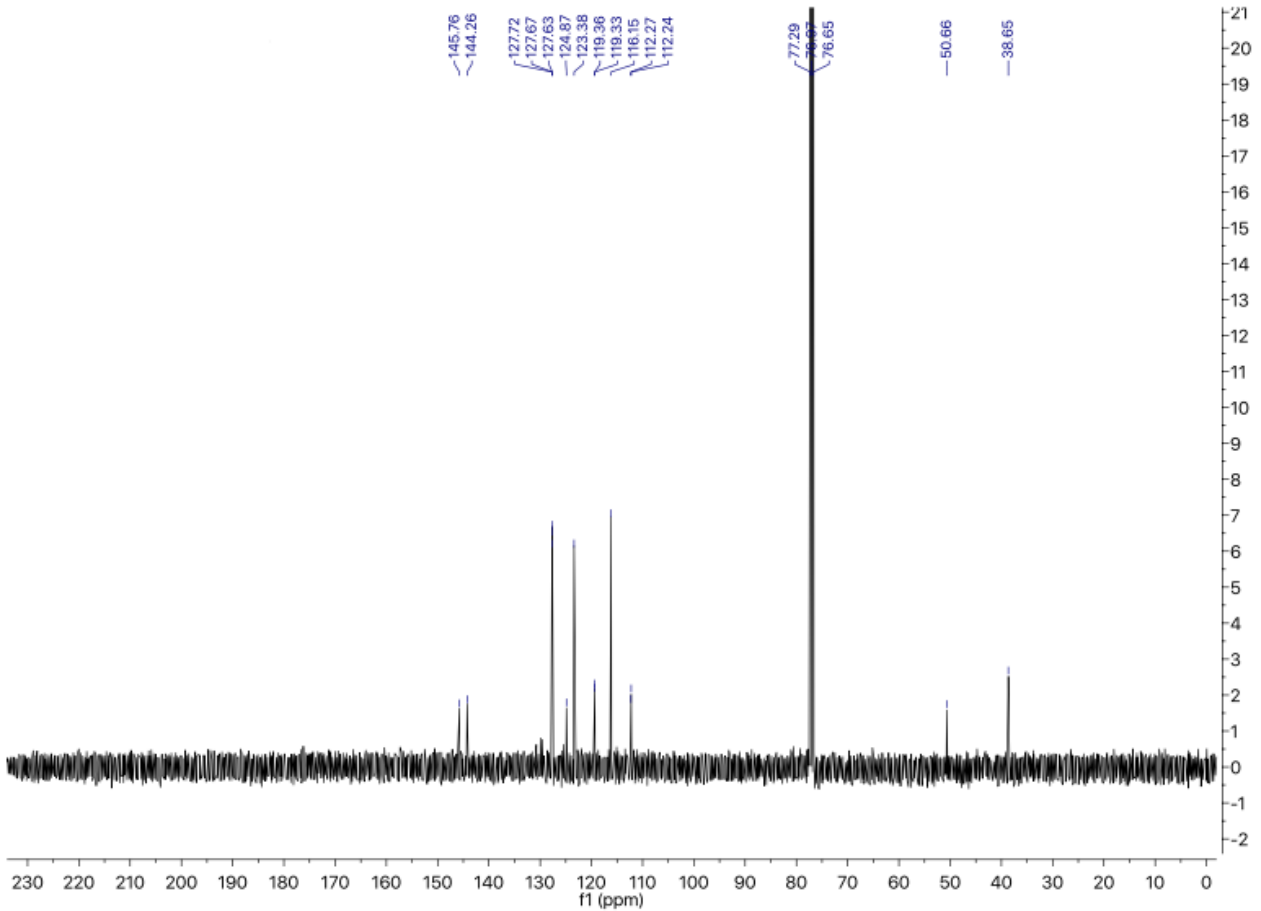
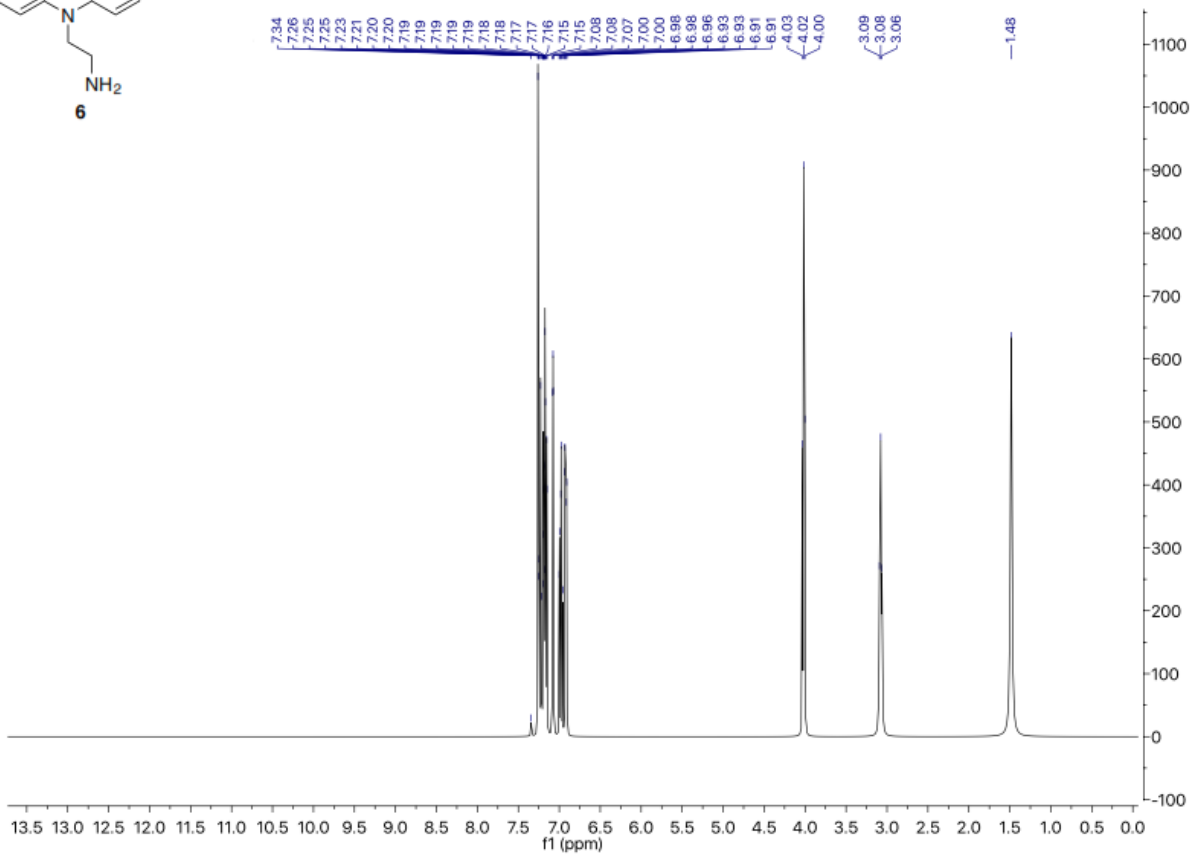
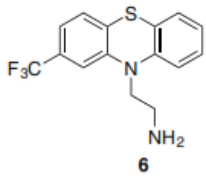
Appendix: Representative spectra

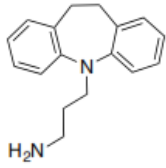




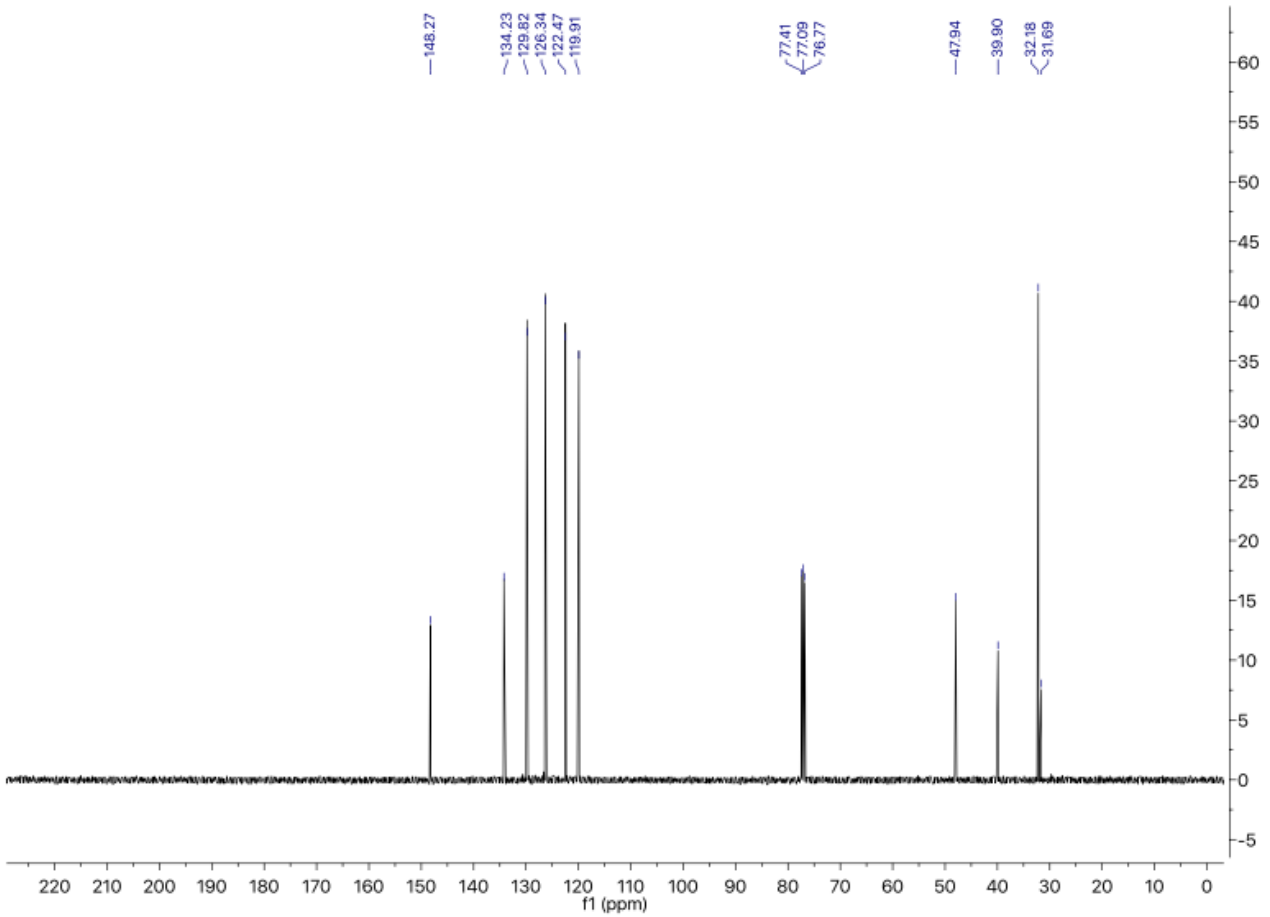
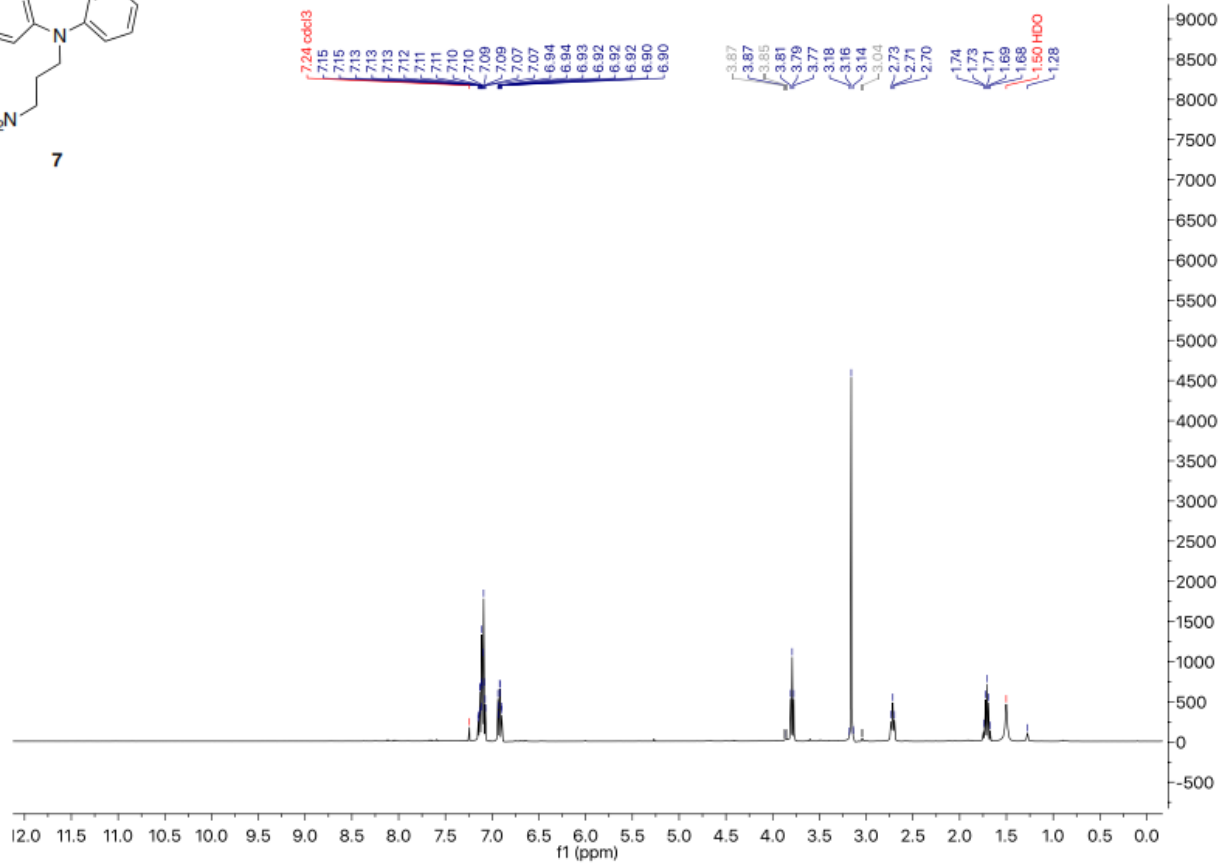


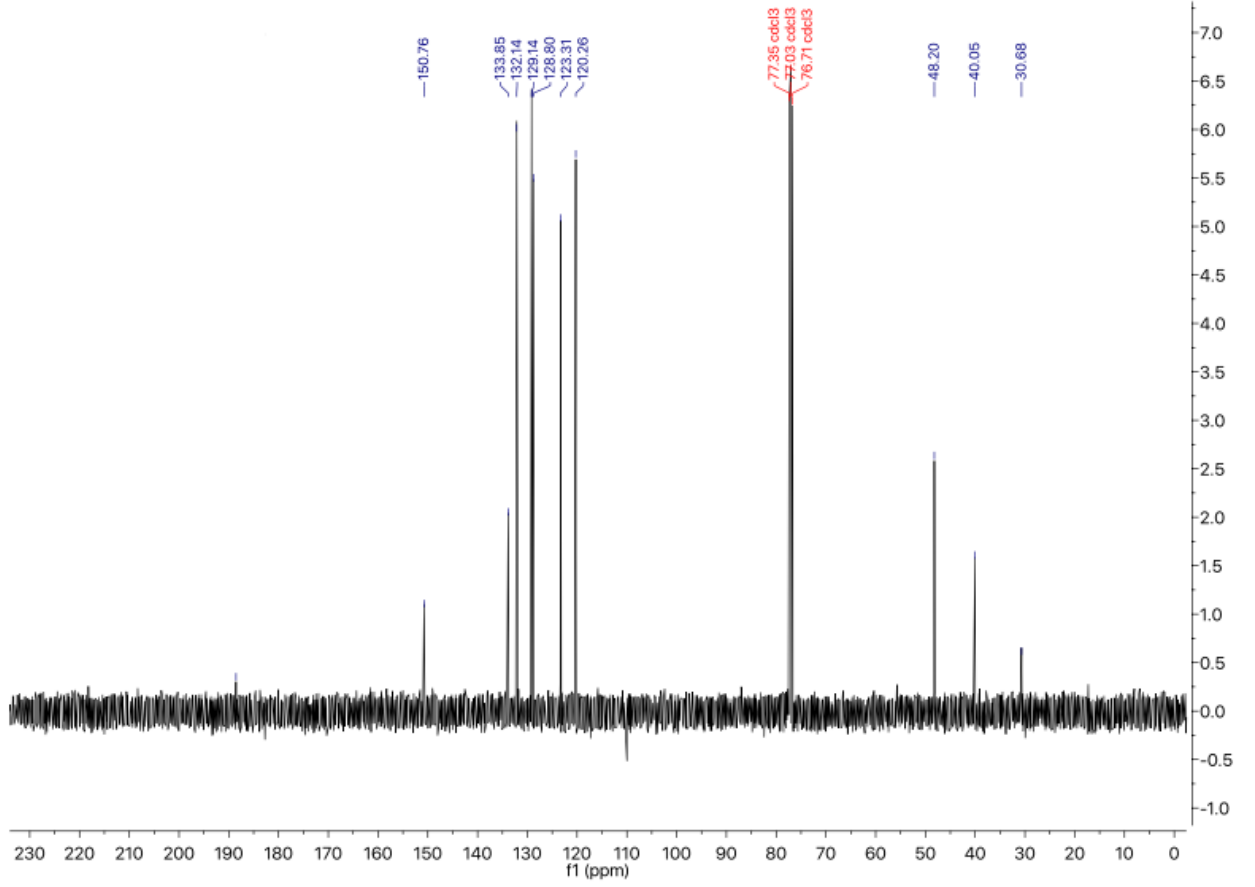
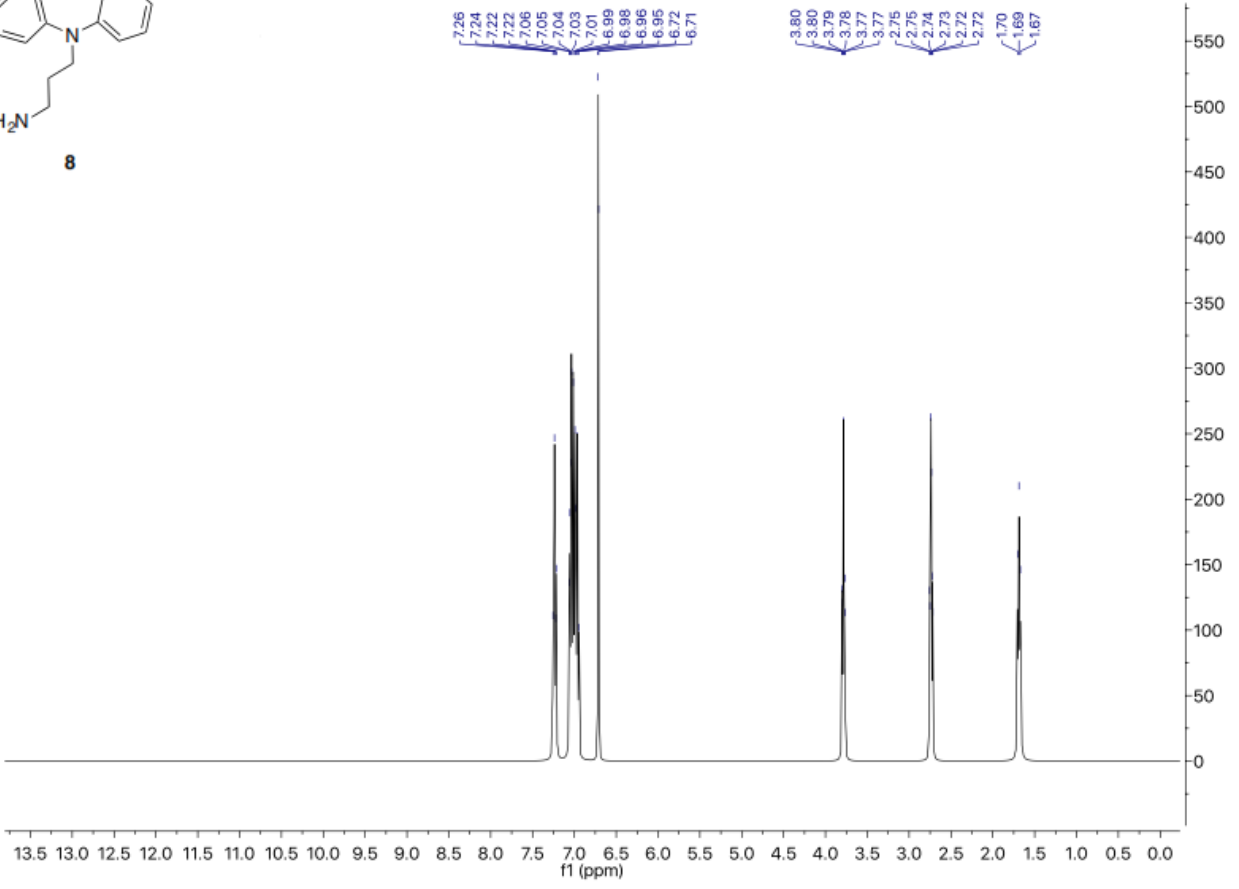
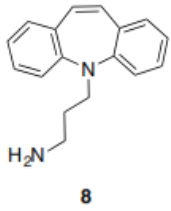


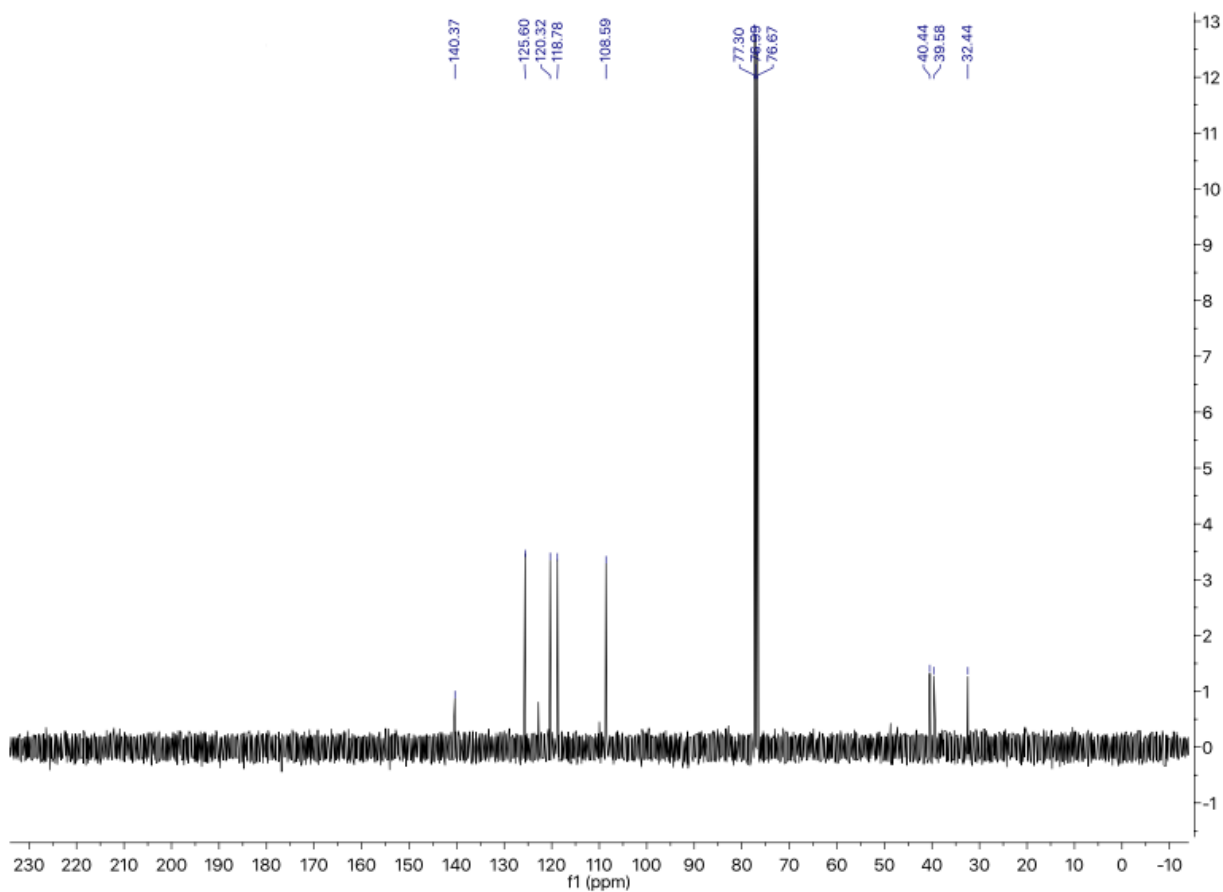
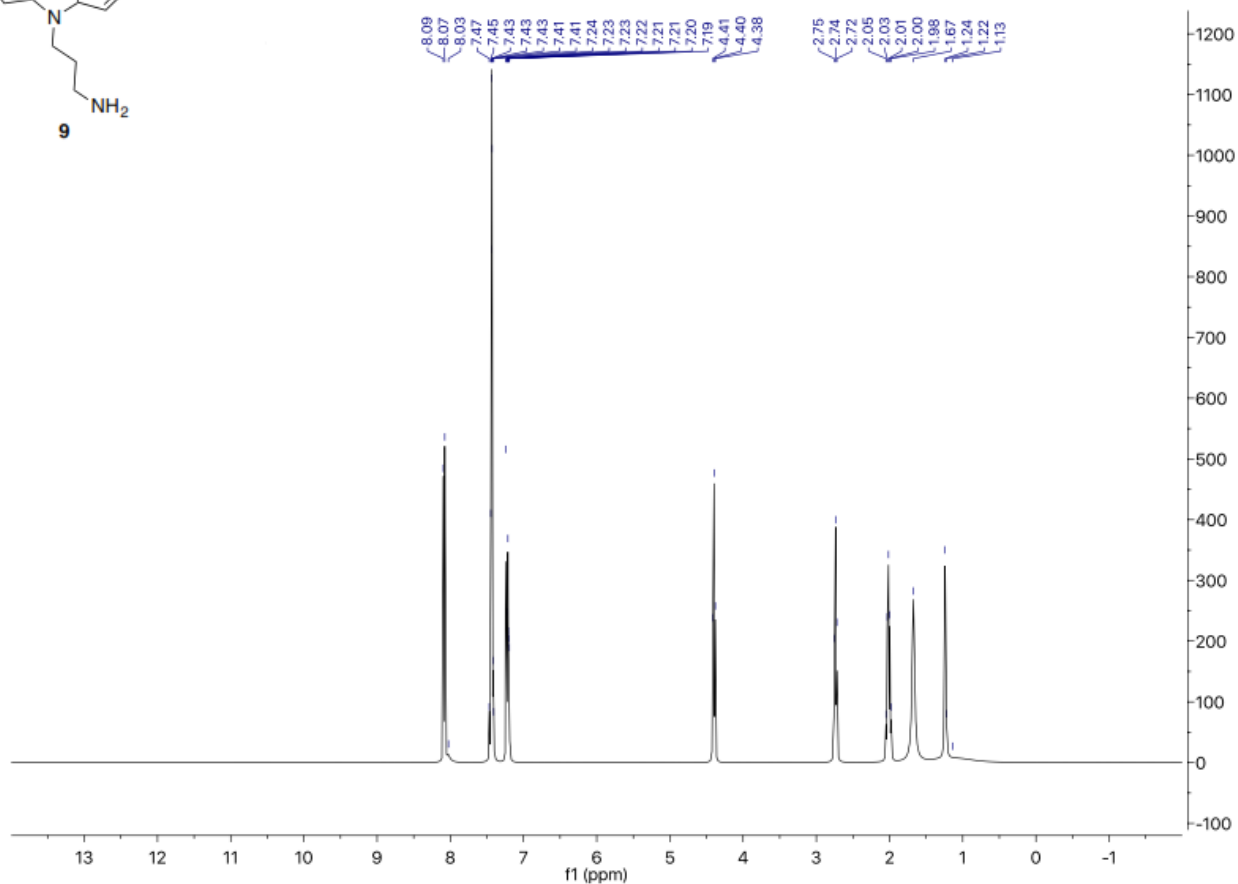
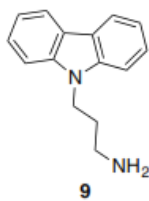


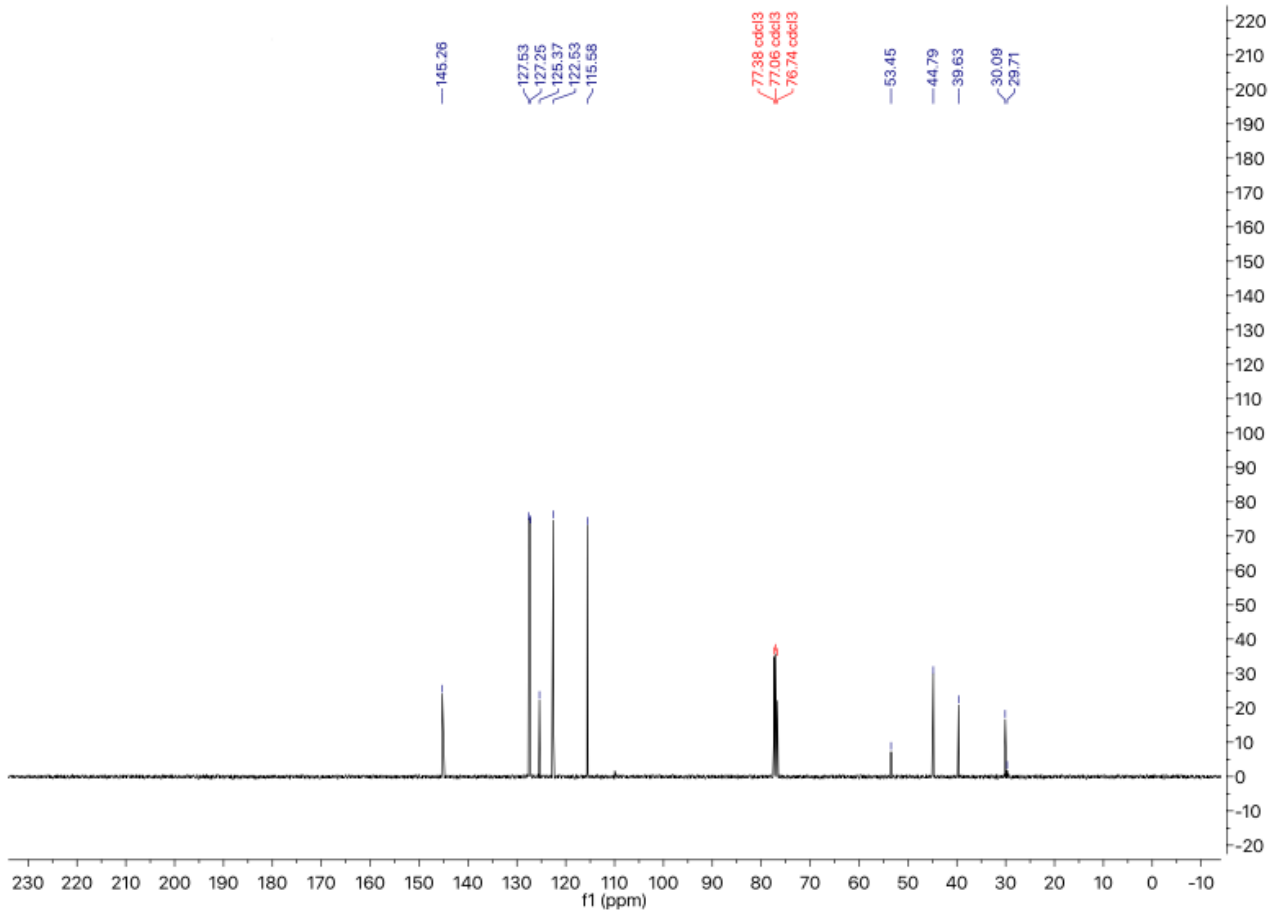
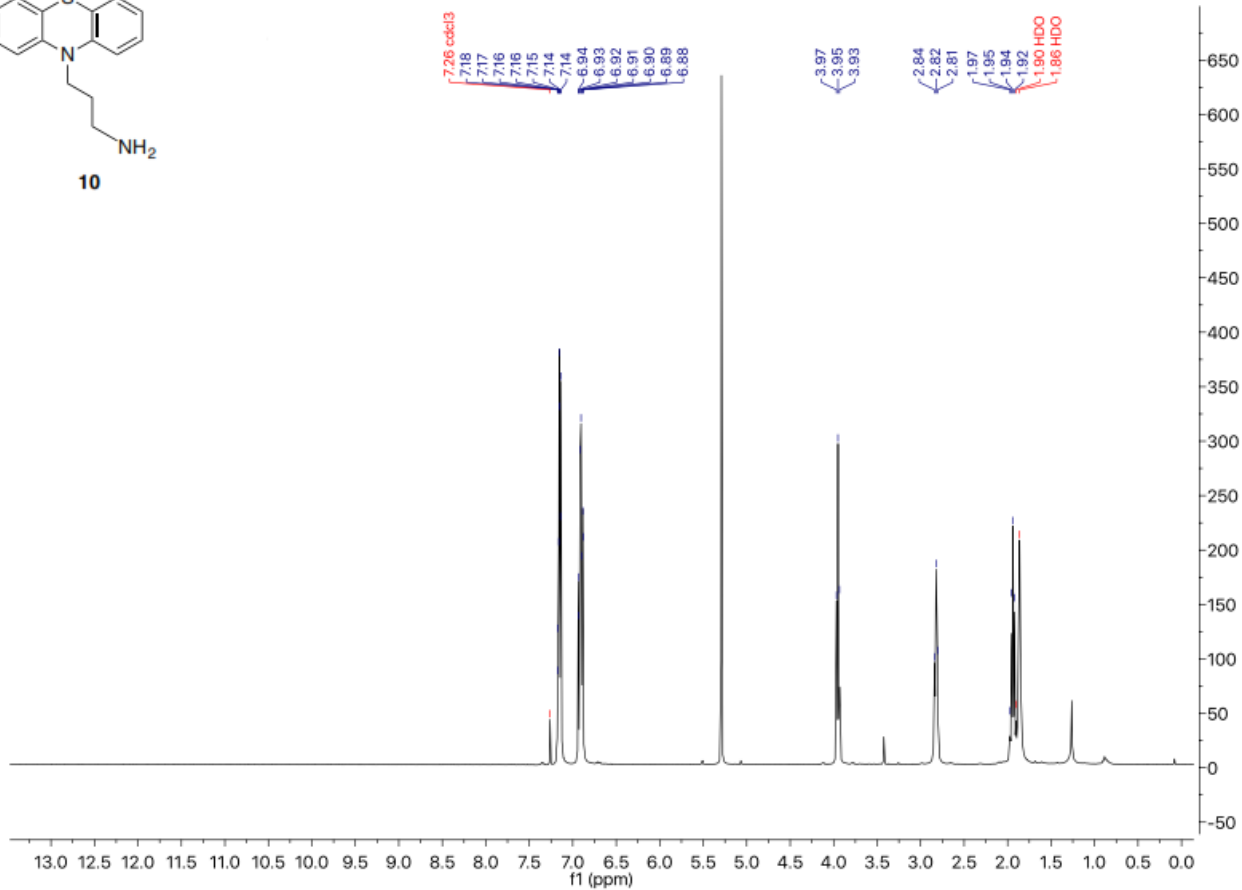
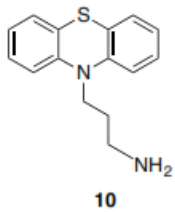


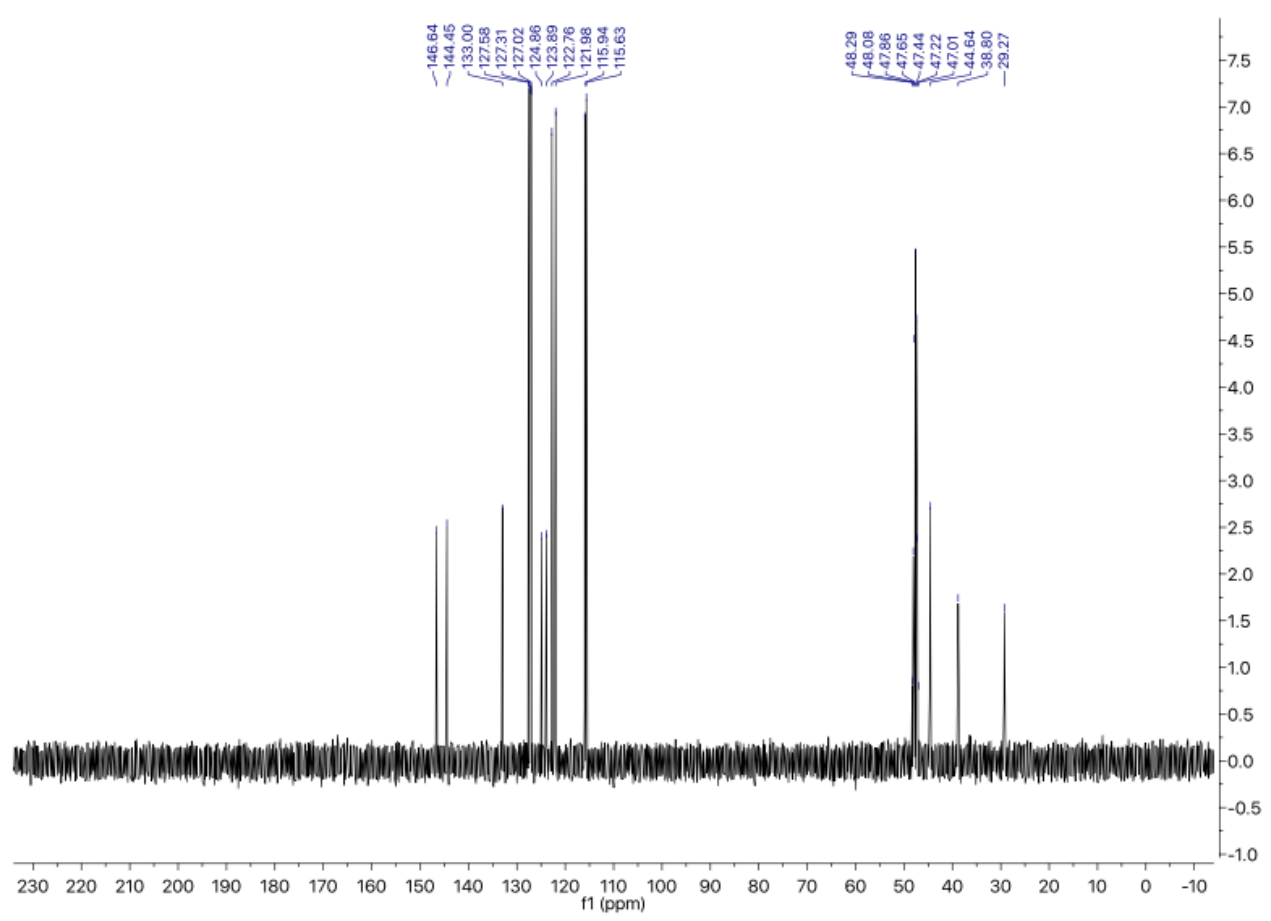
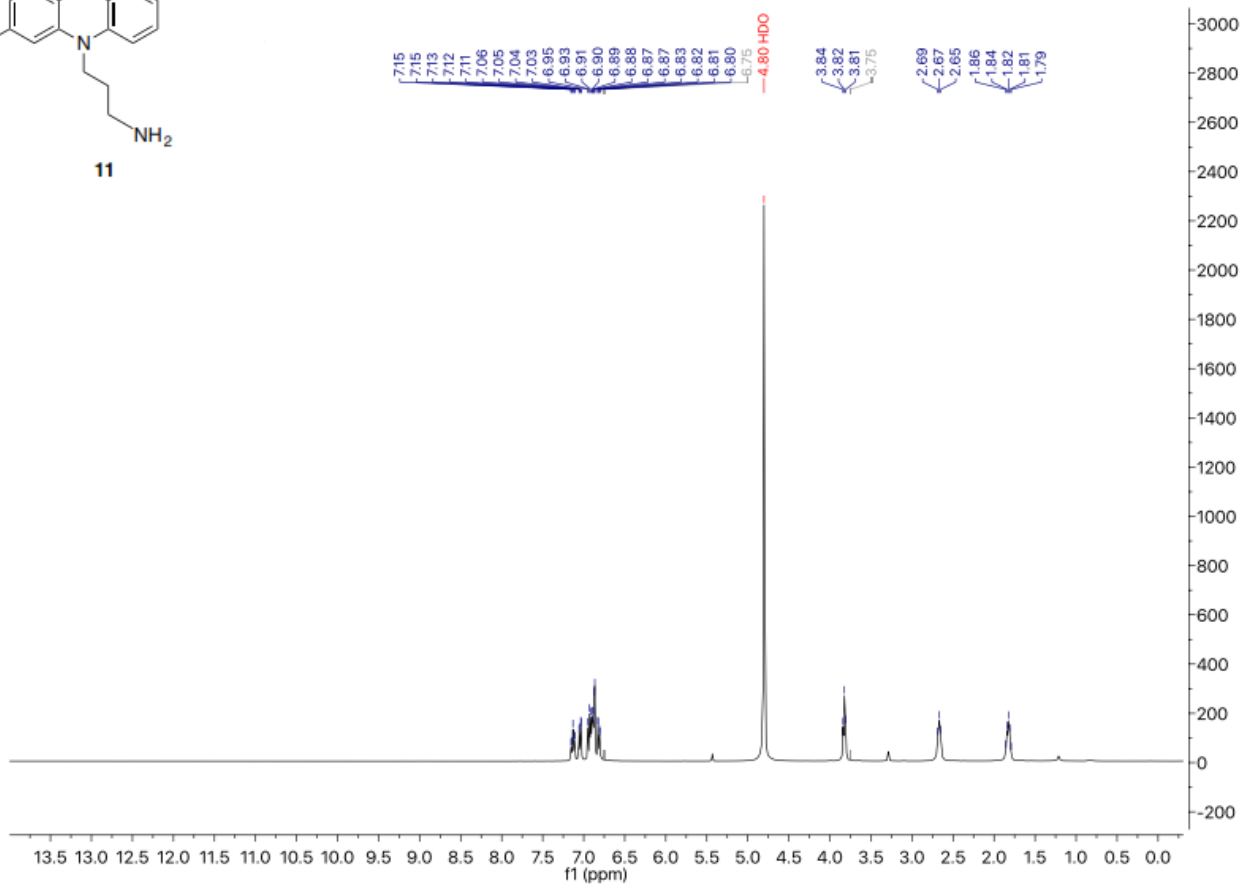
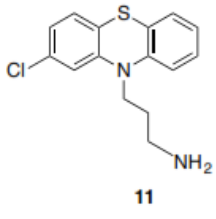
7

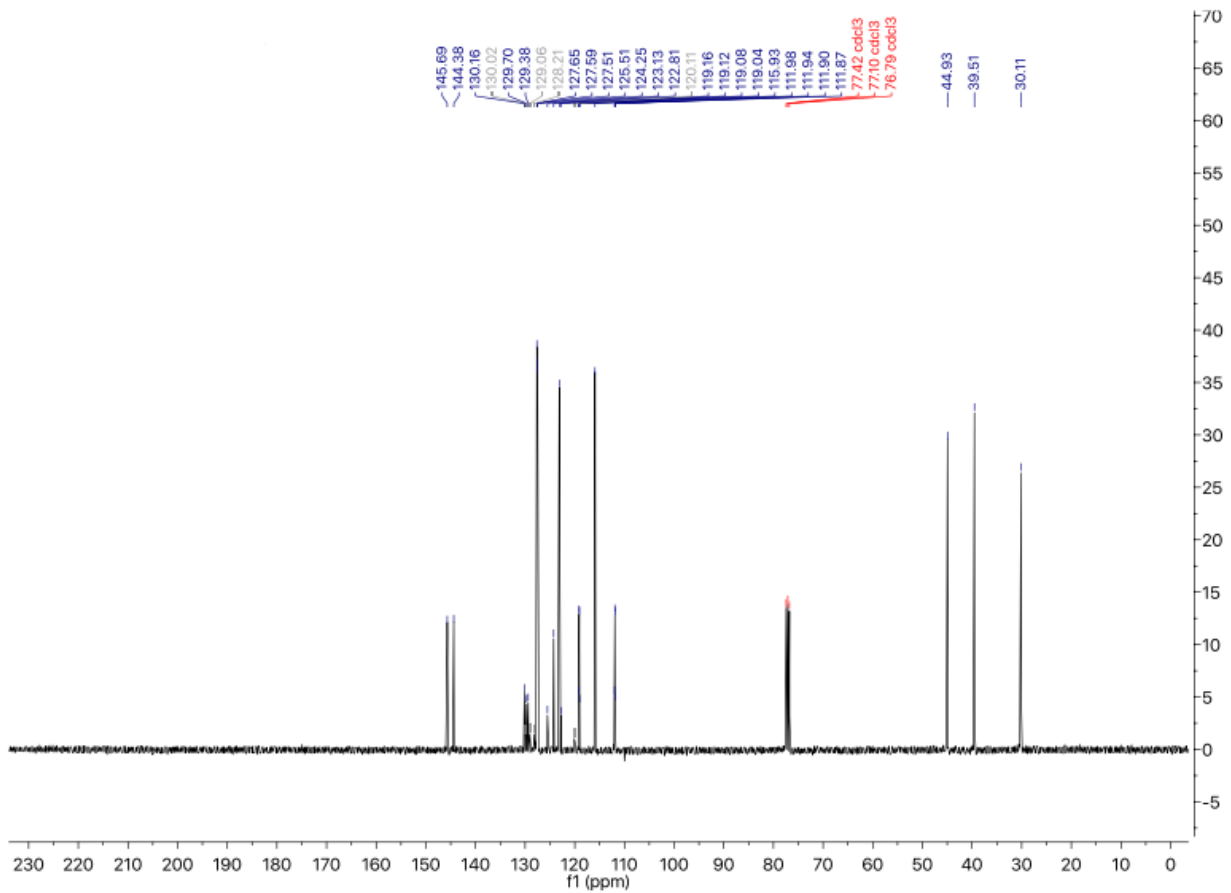
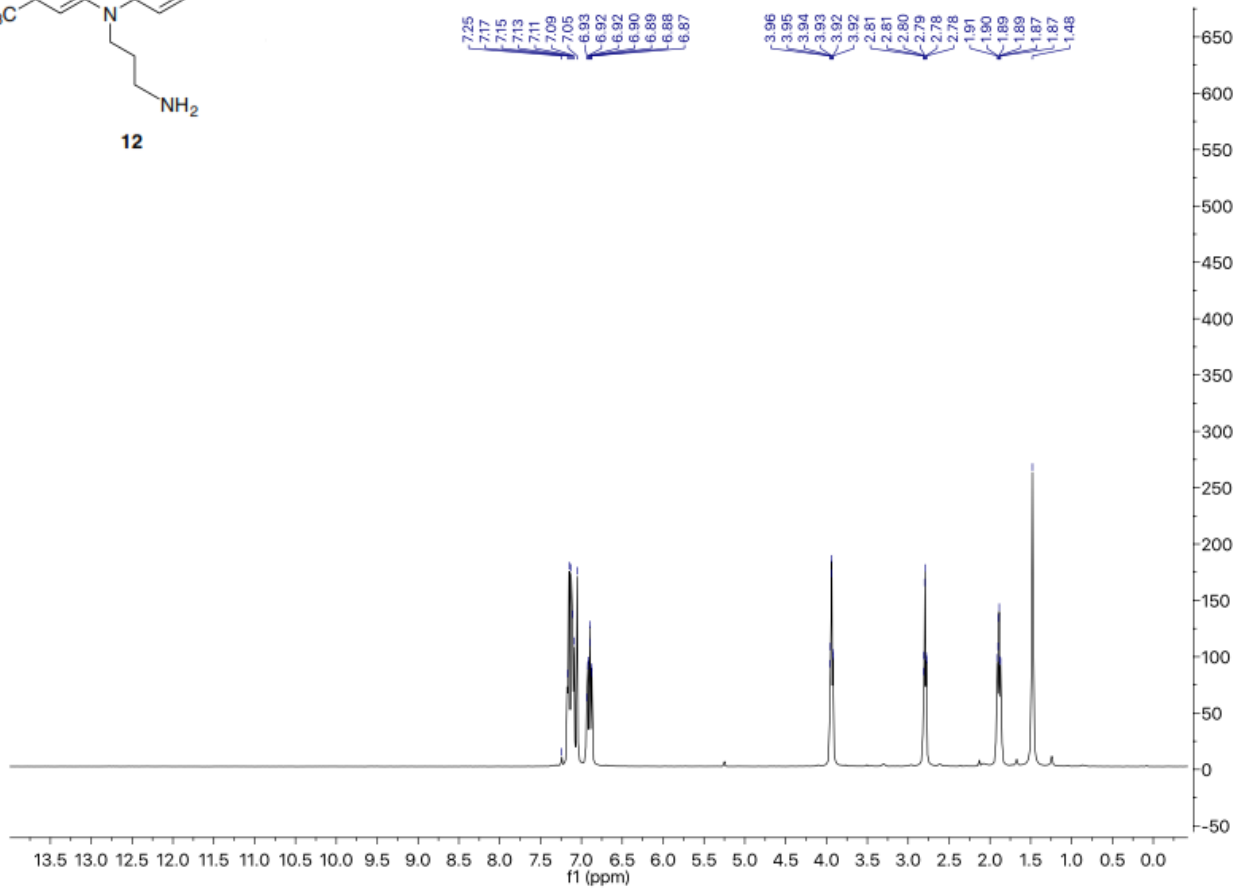
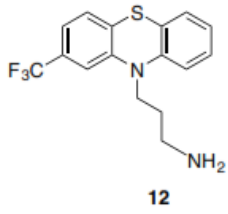


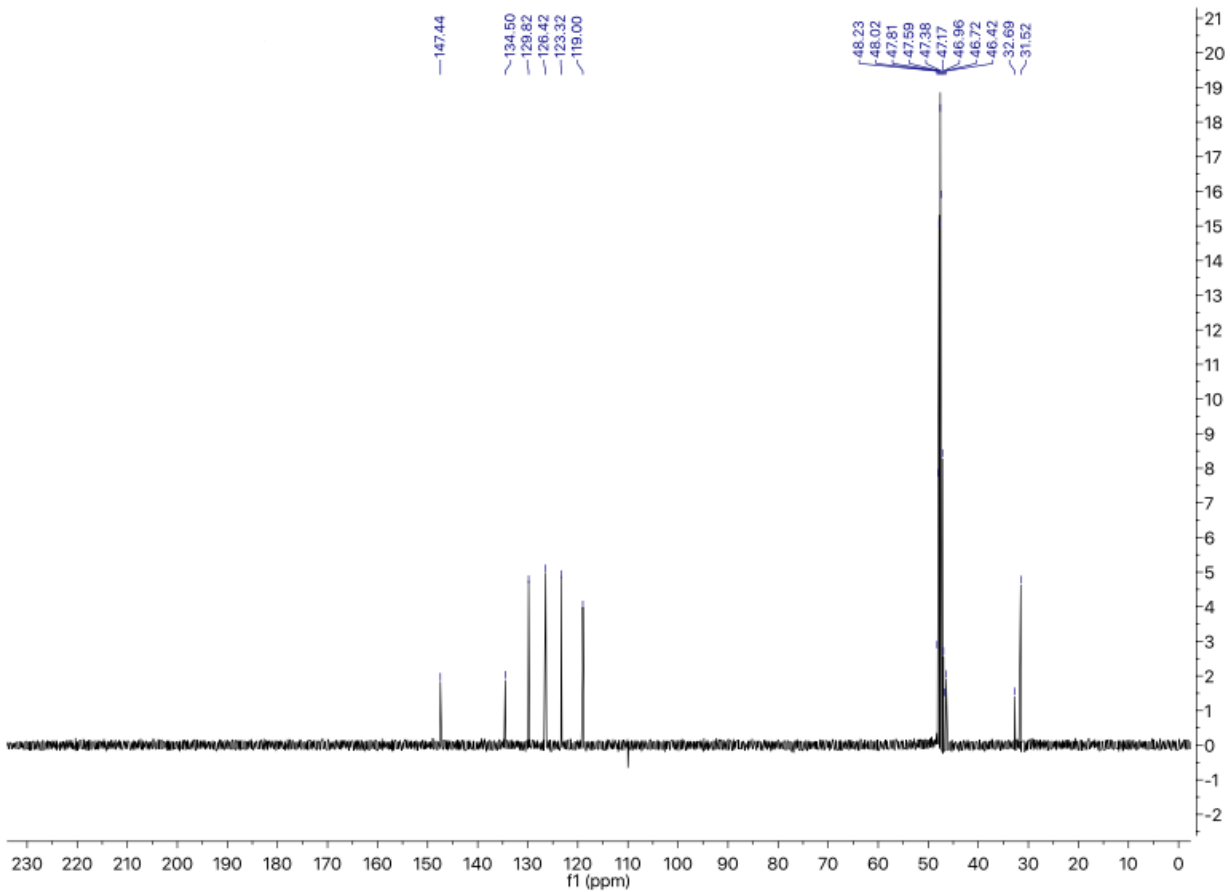
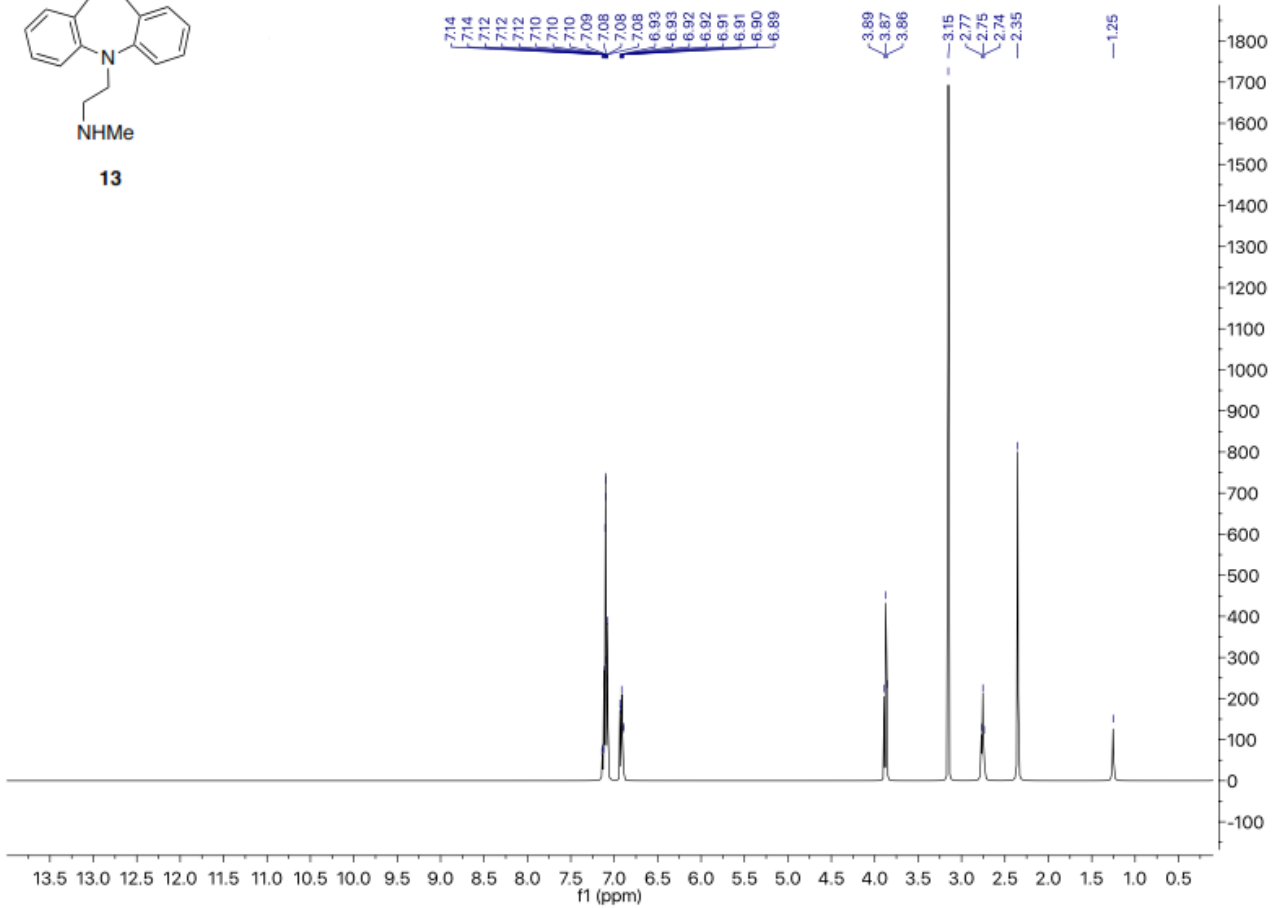
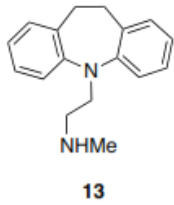


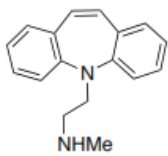




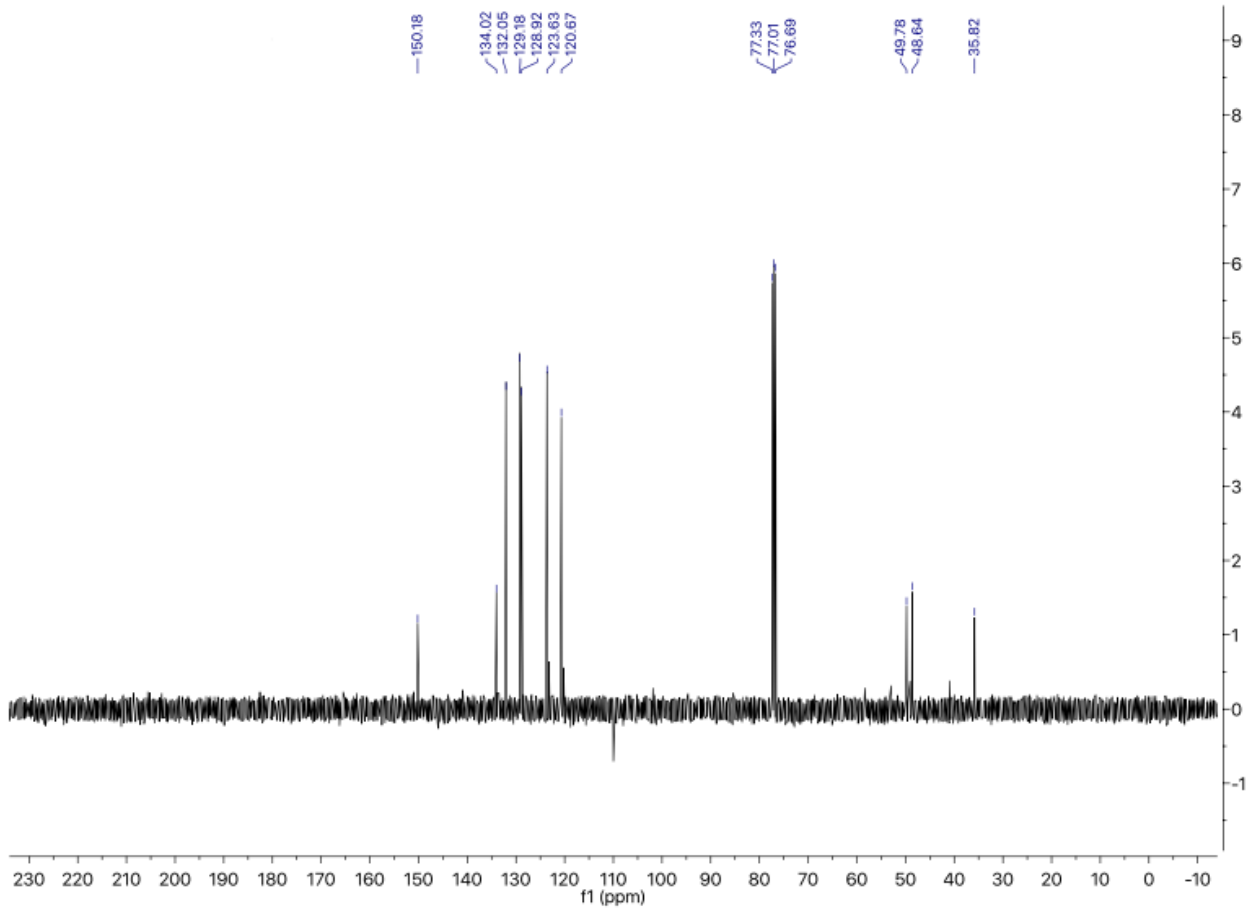
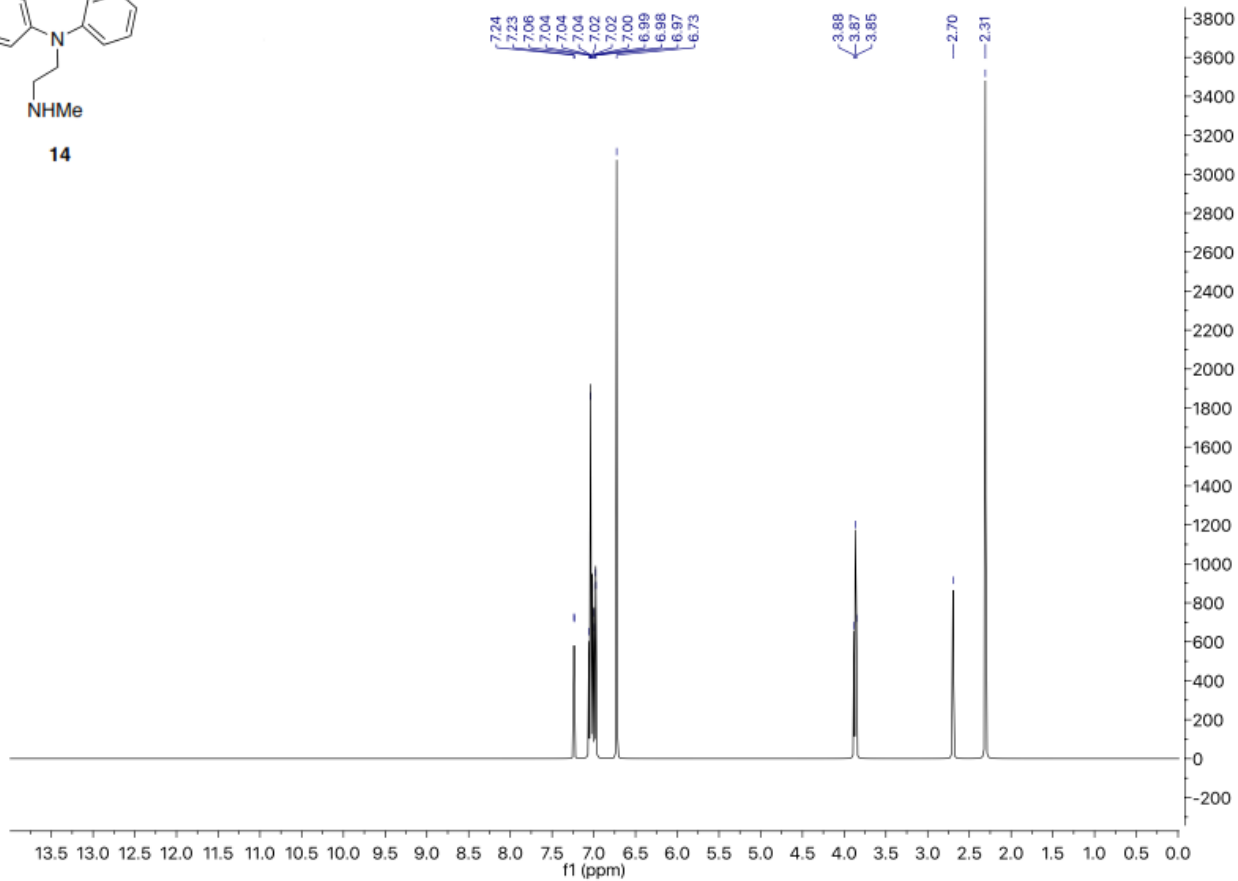


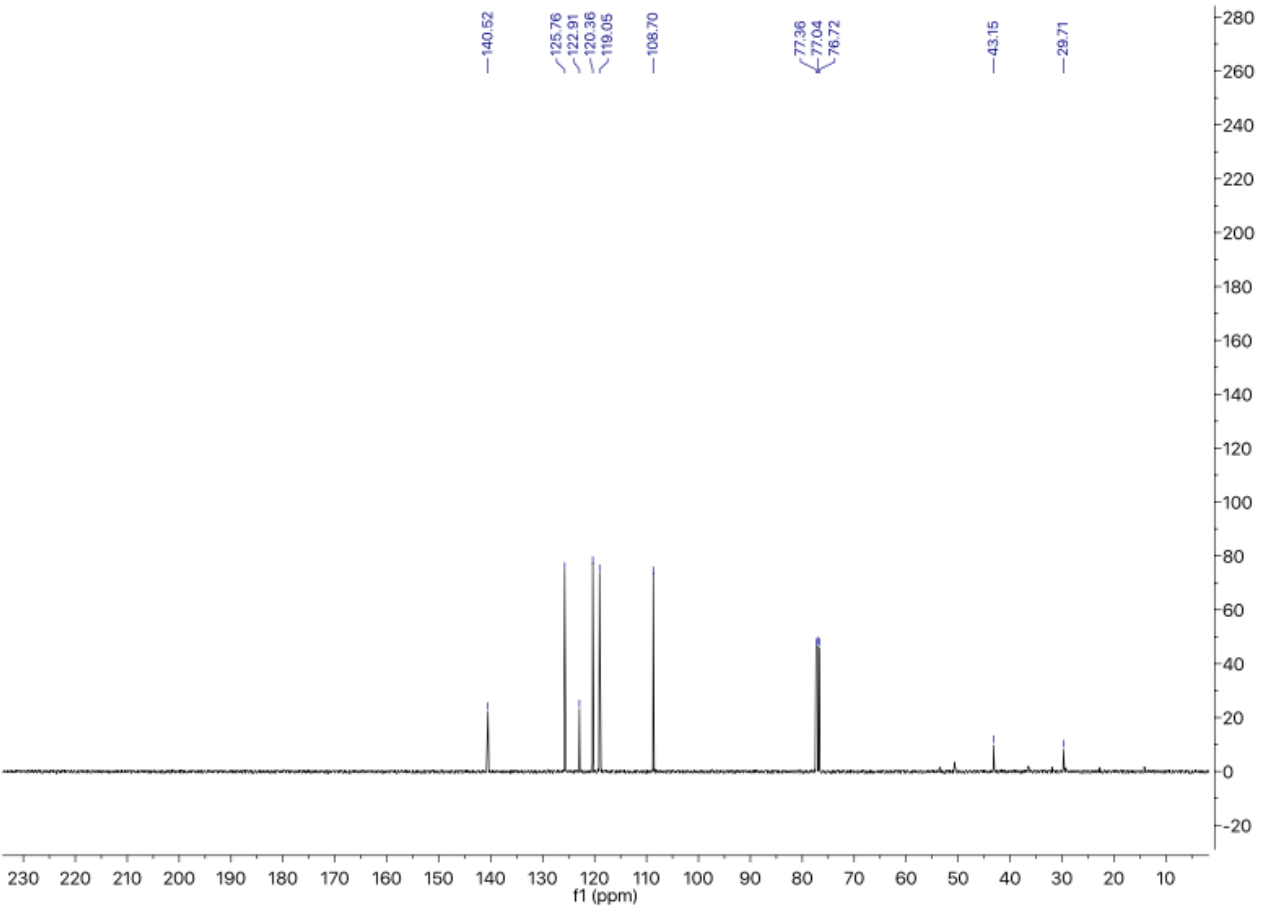
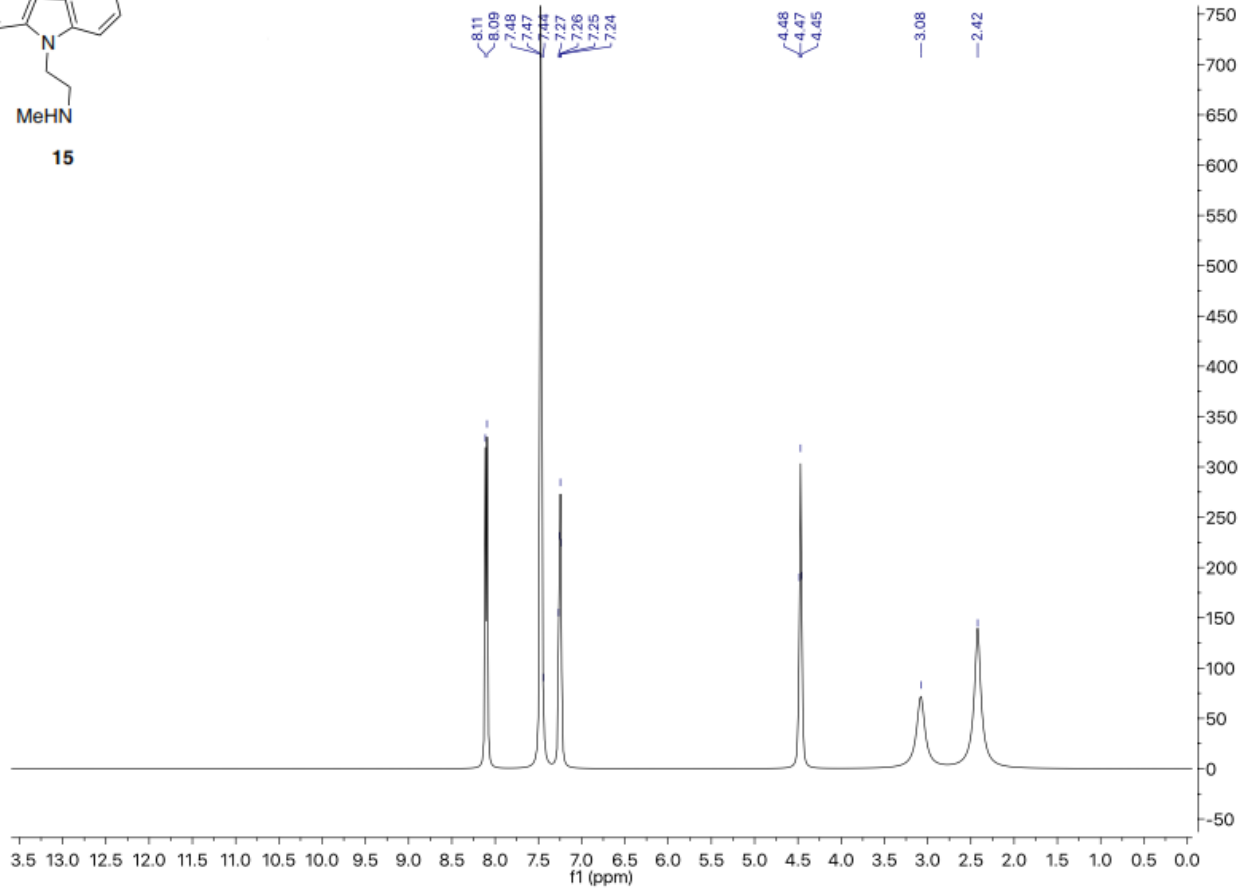
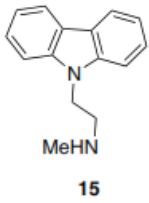


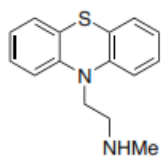




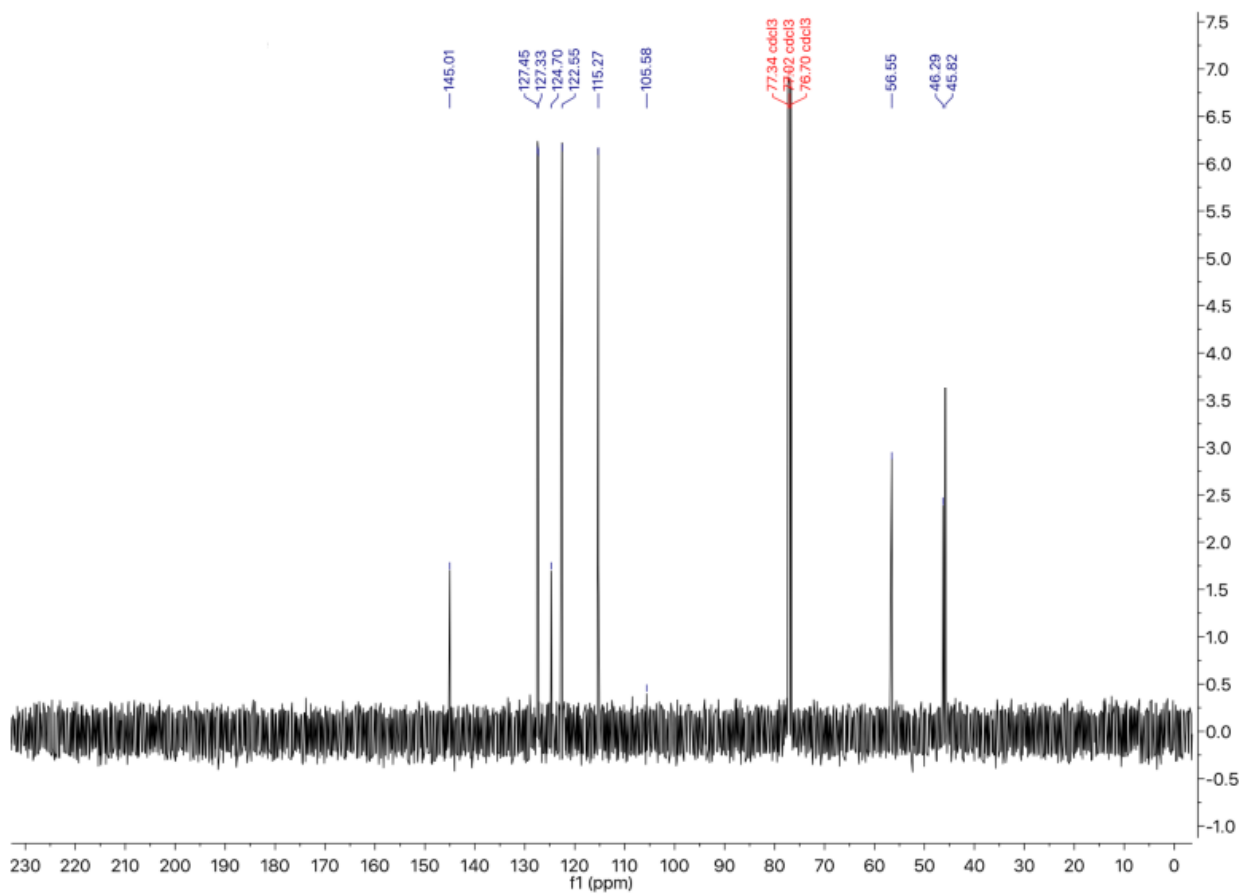
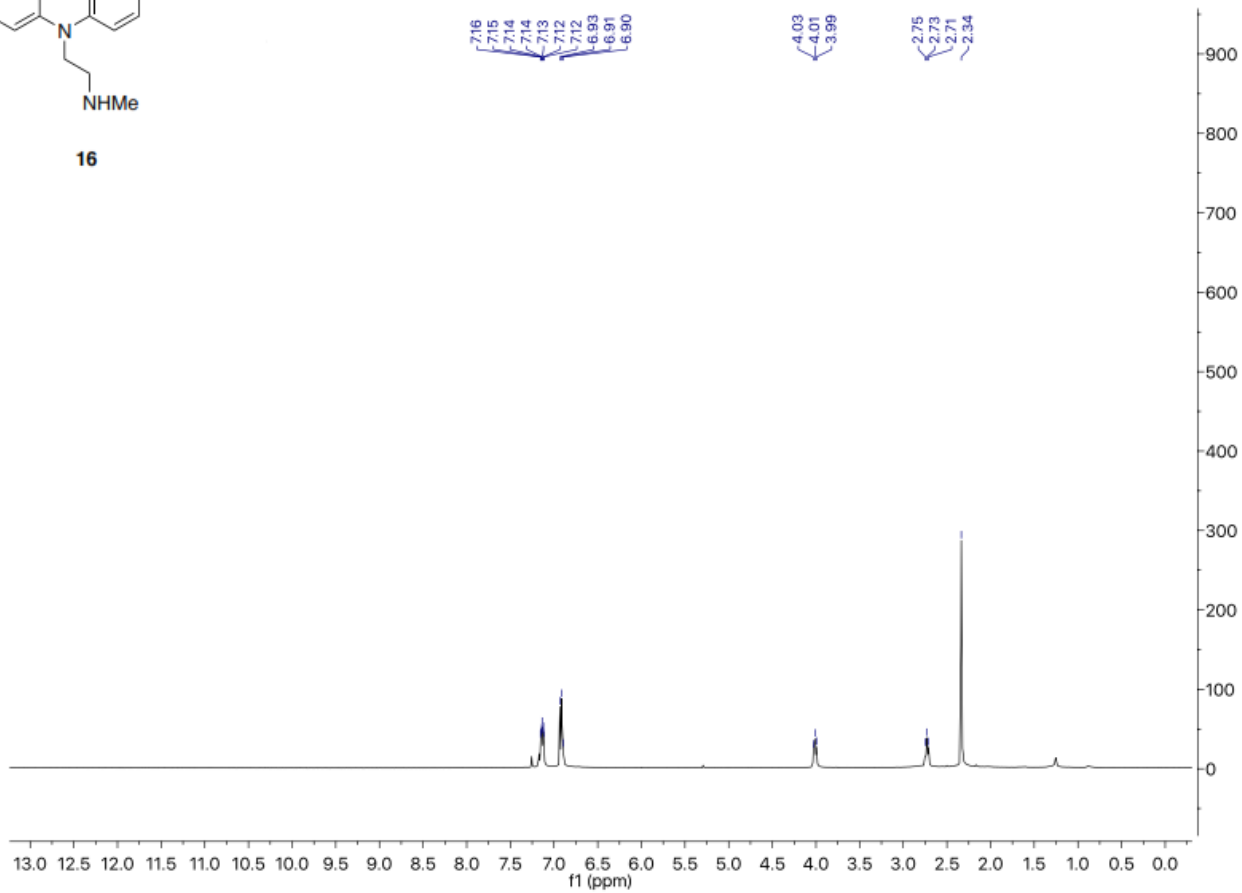
14

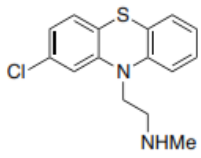




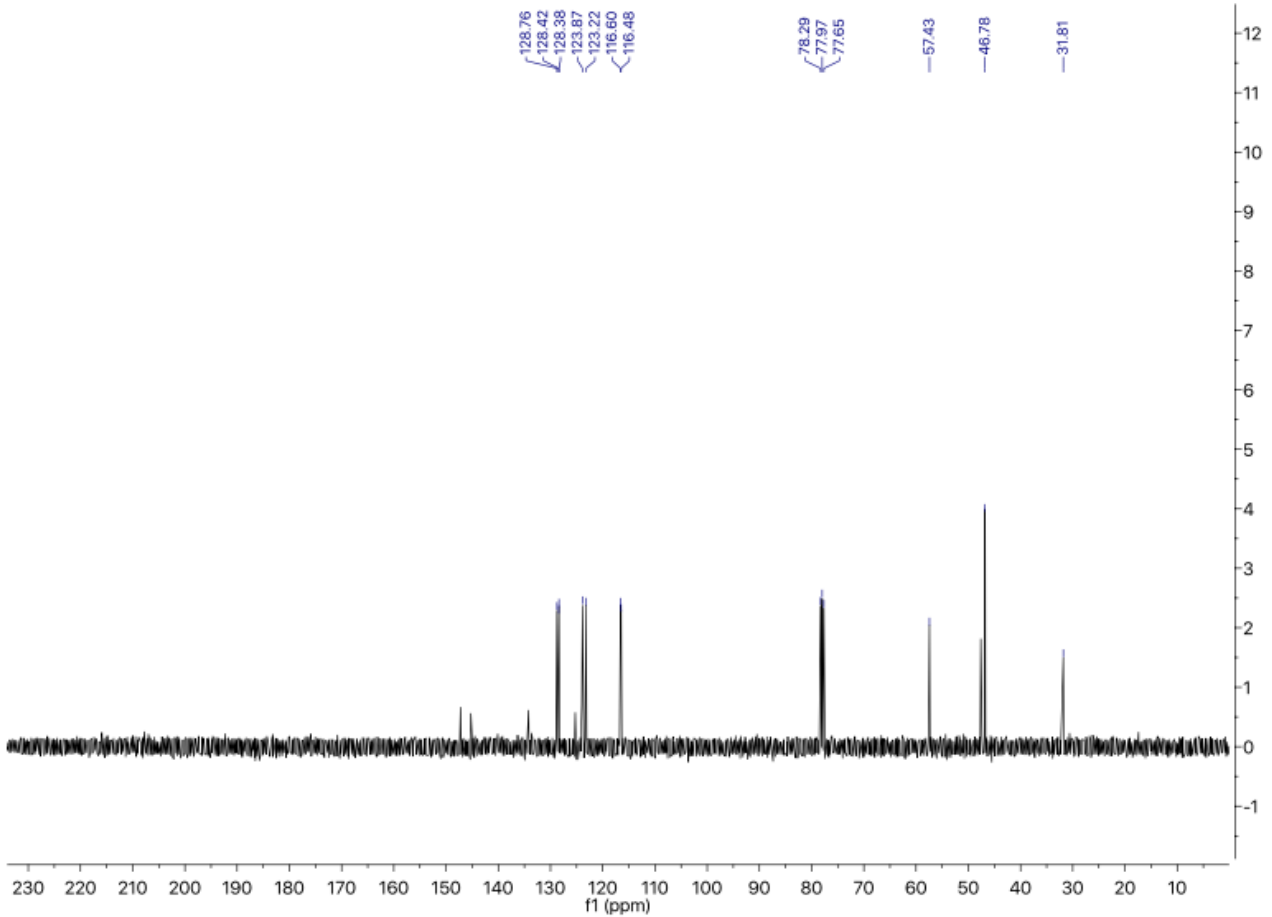
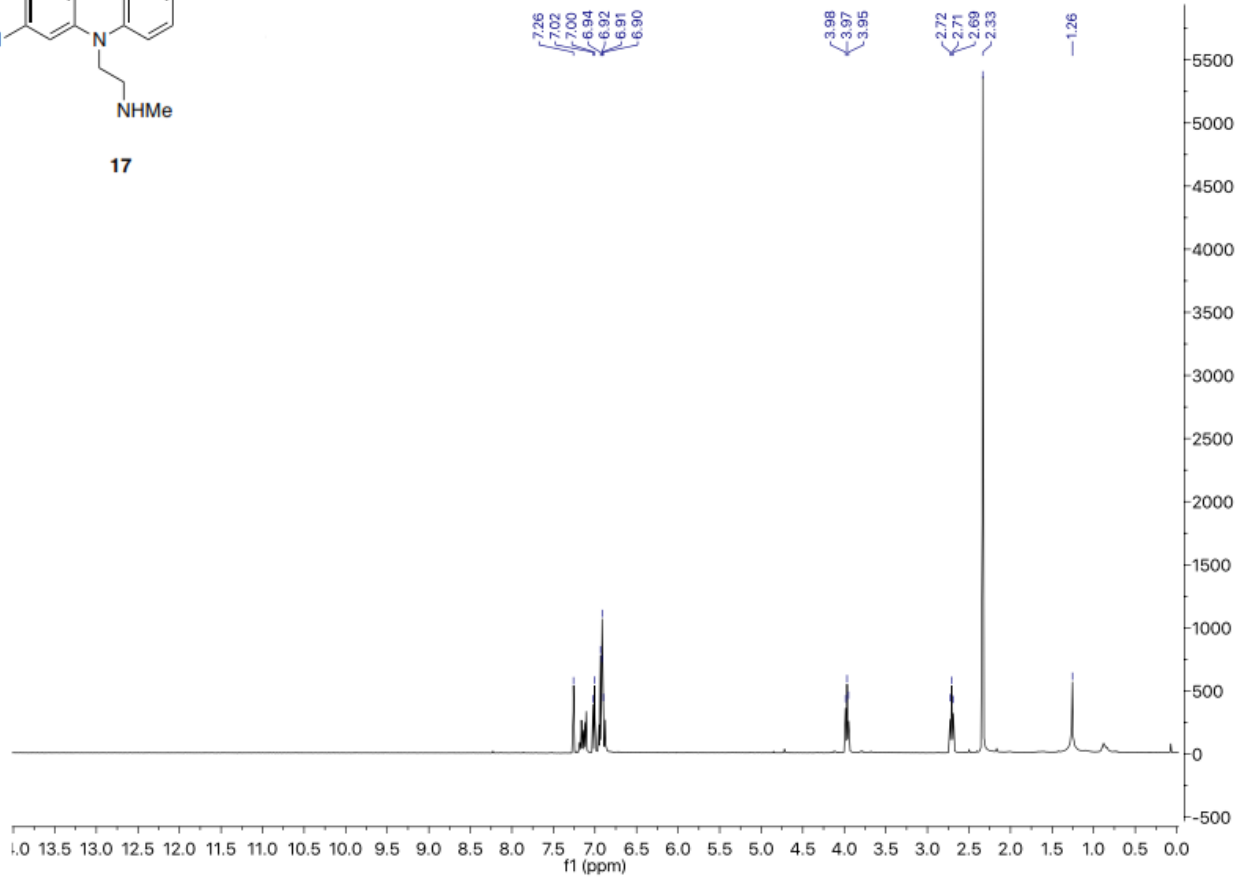


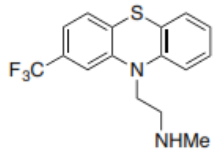
16



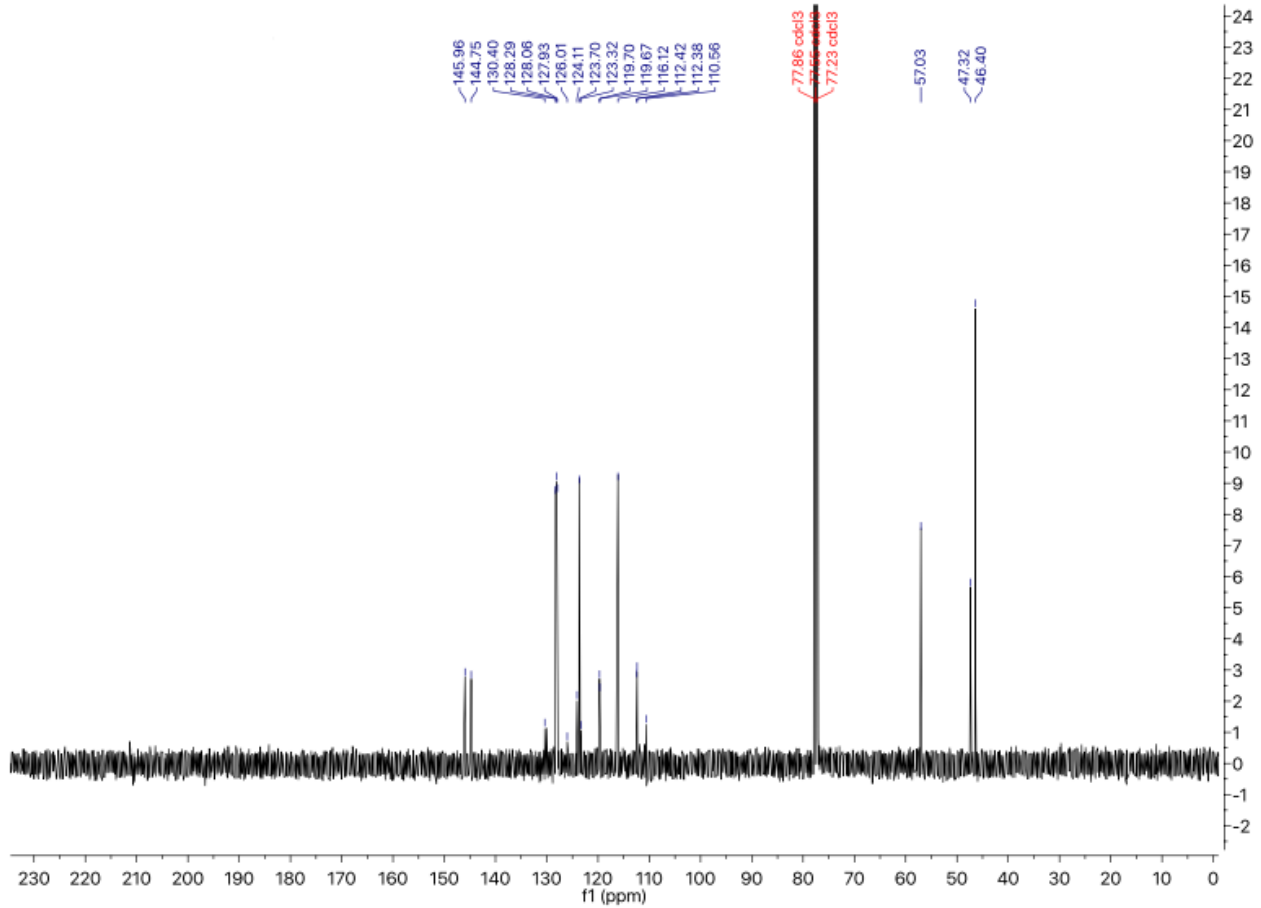
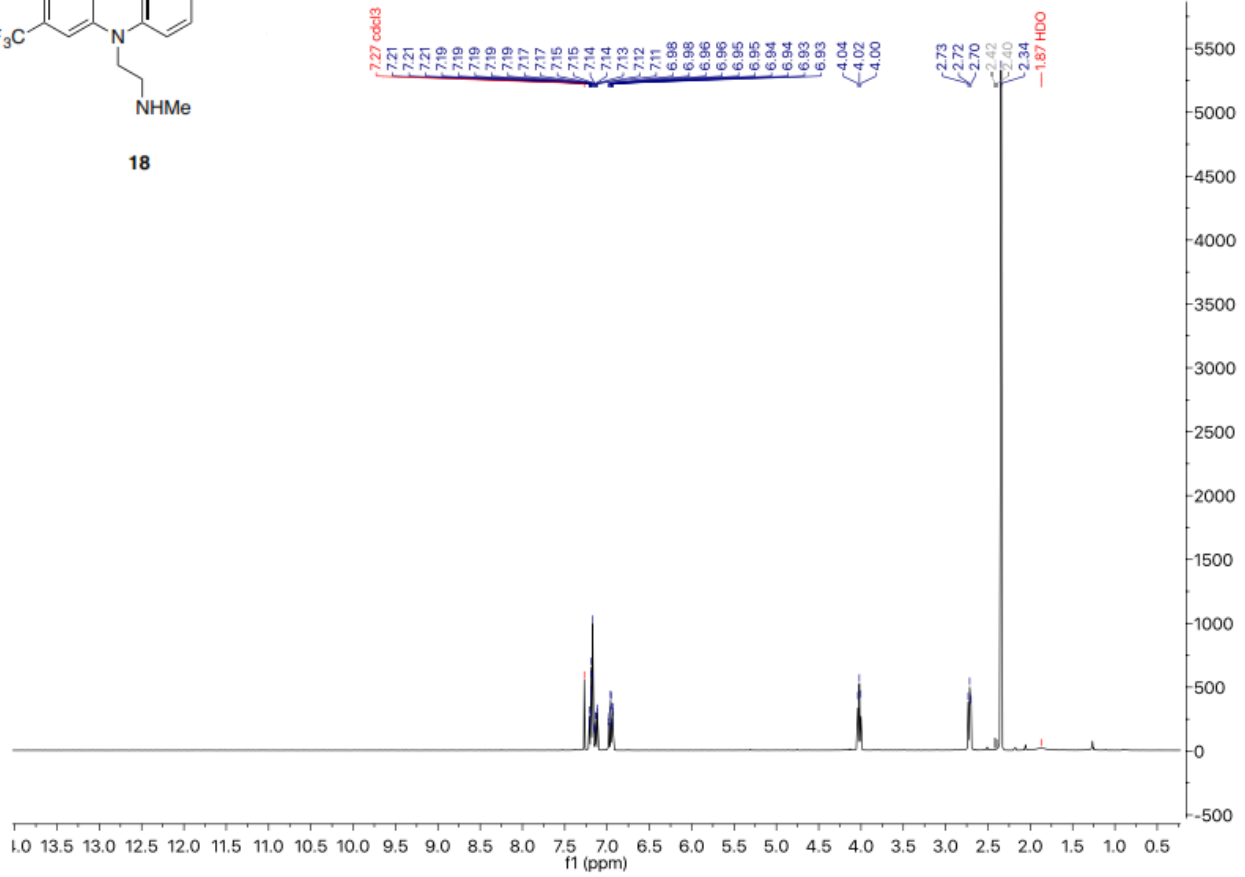


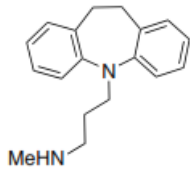
17



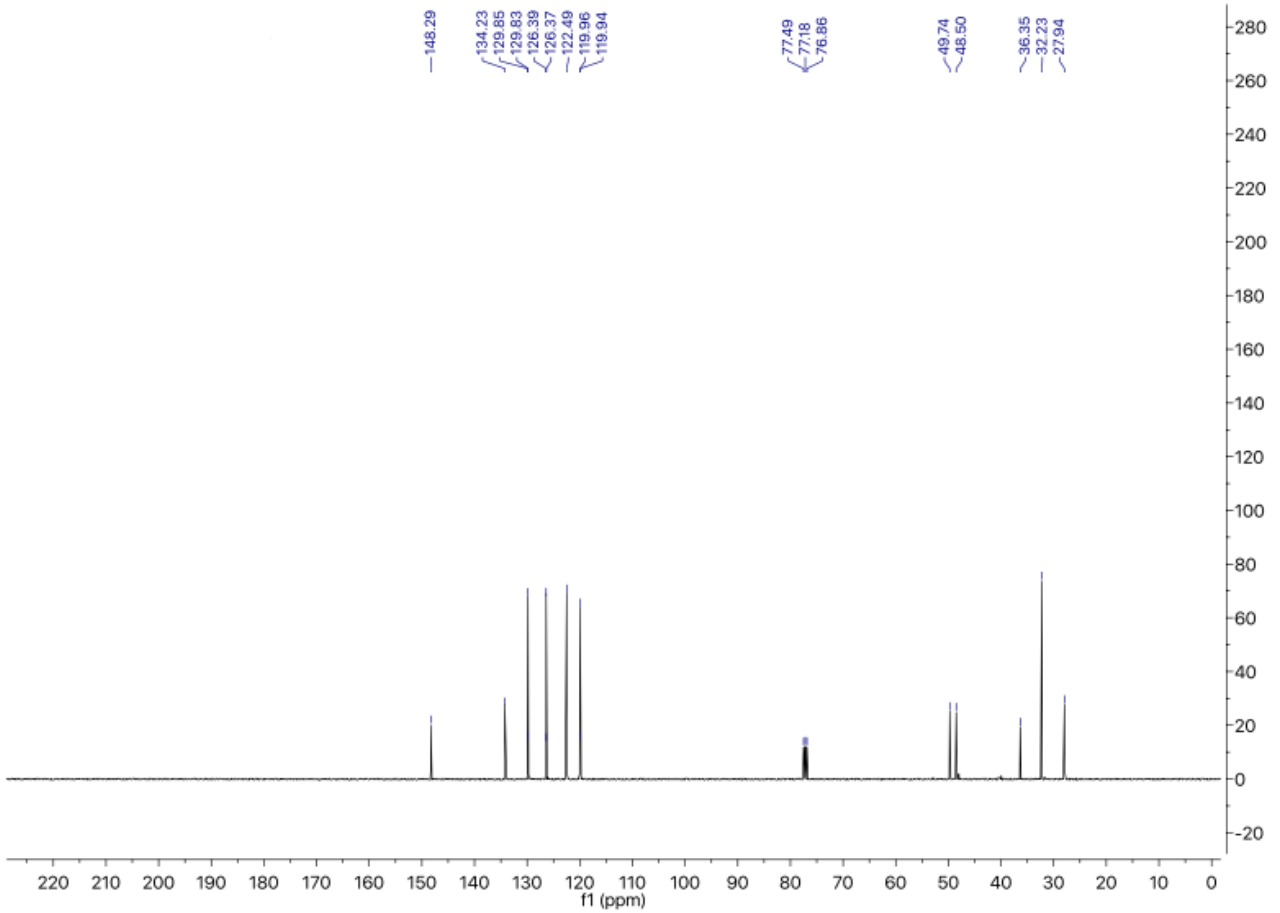
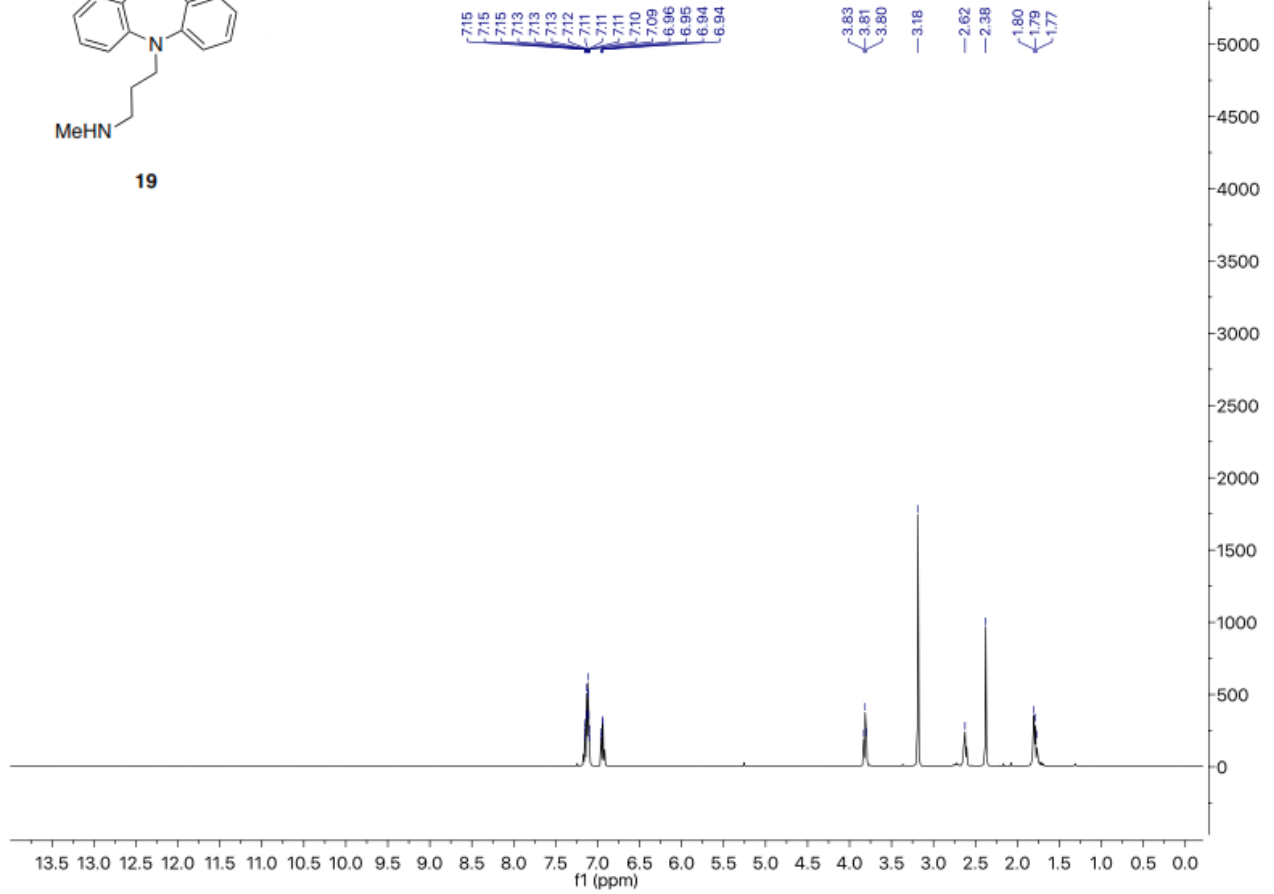


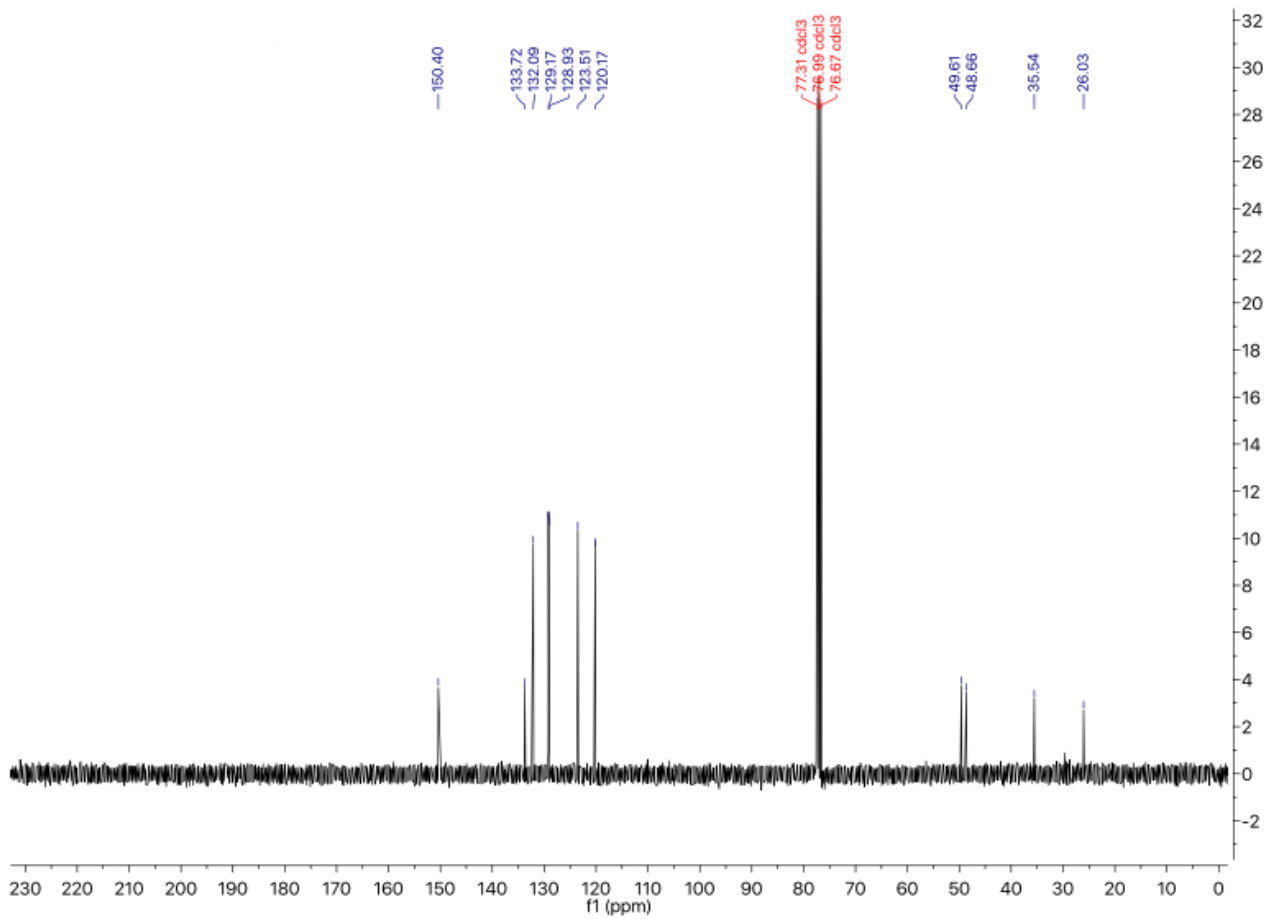
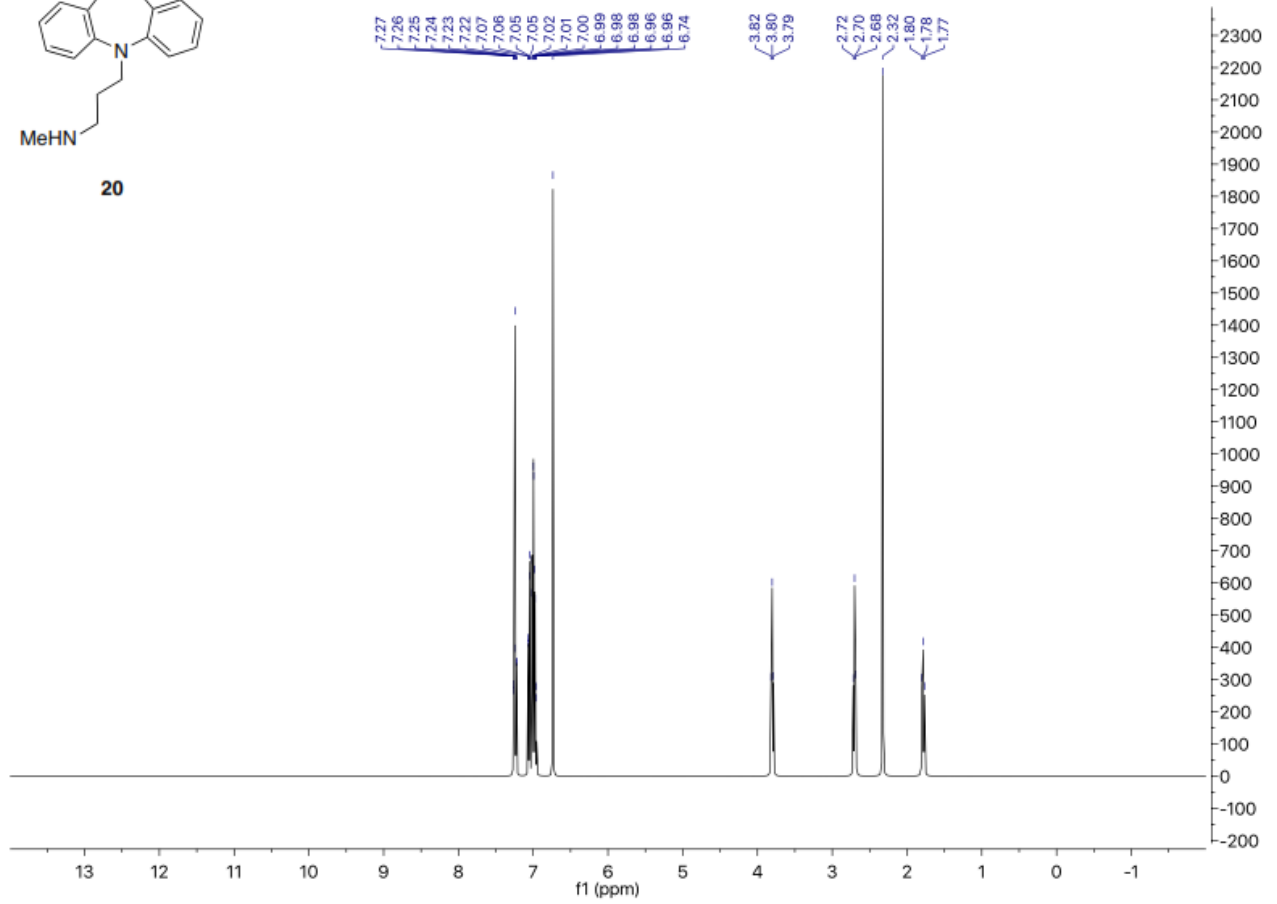
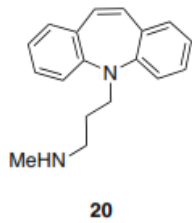
18

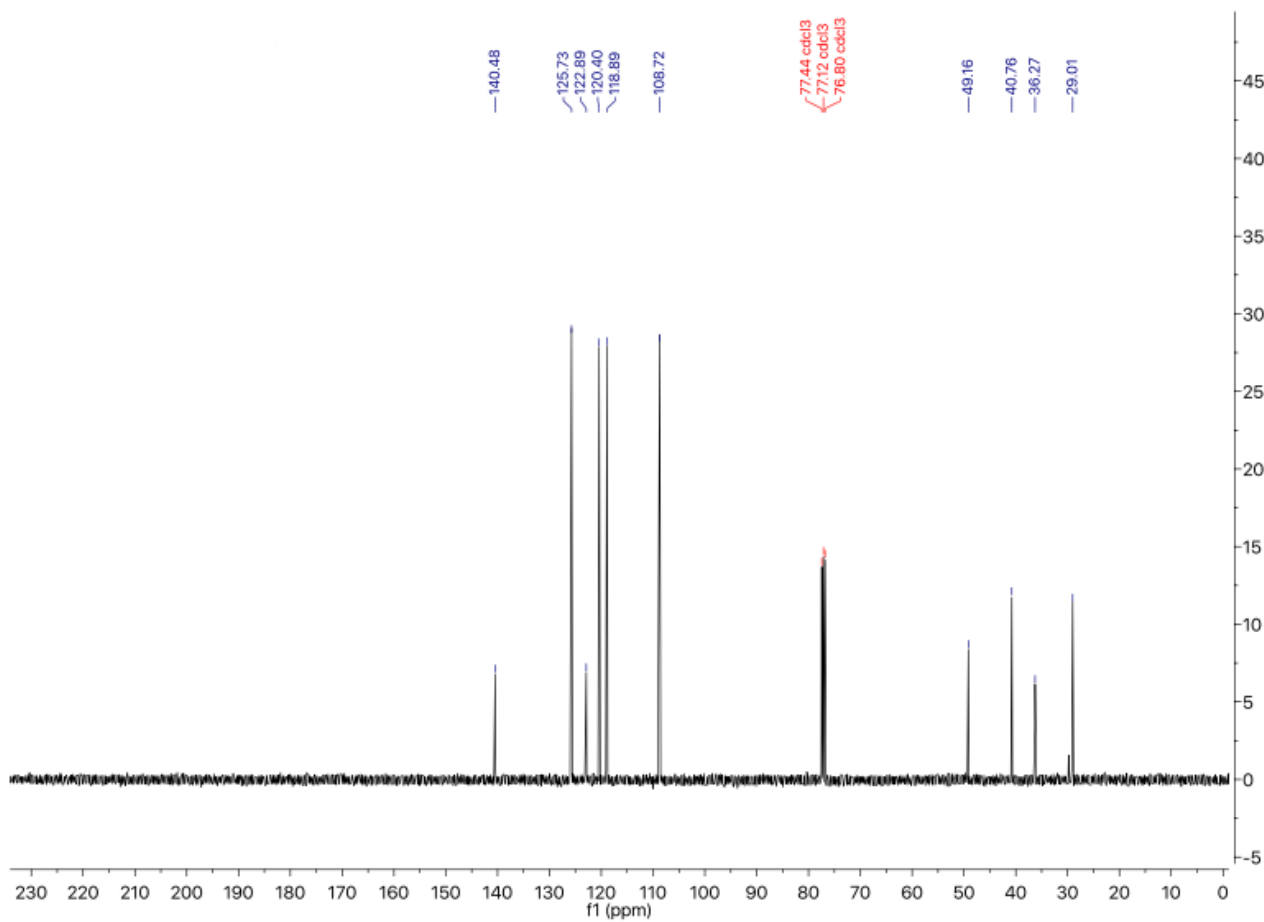
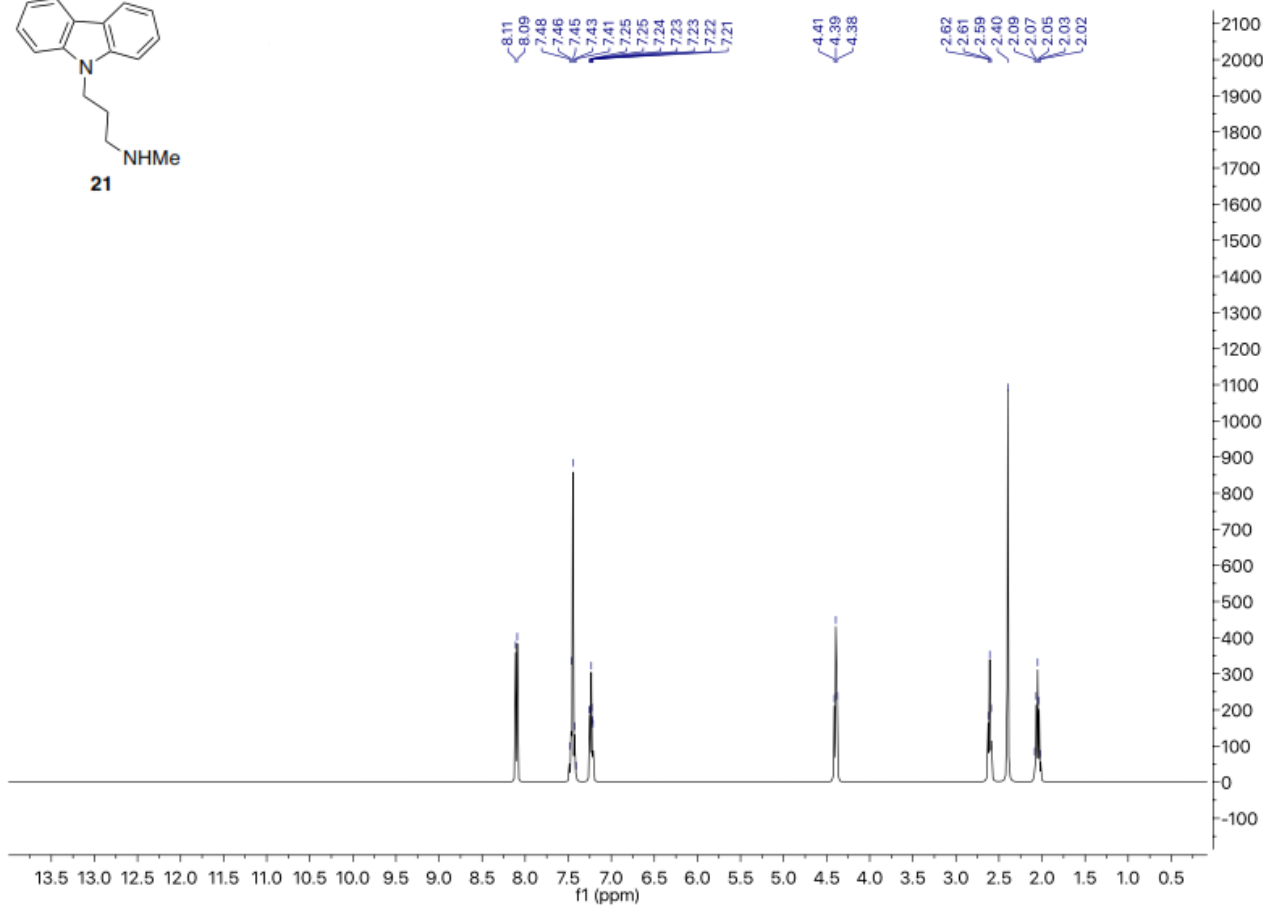
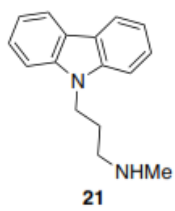


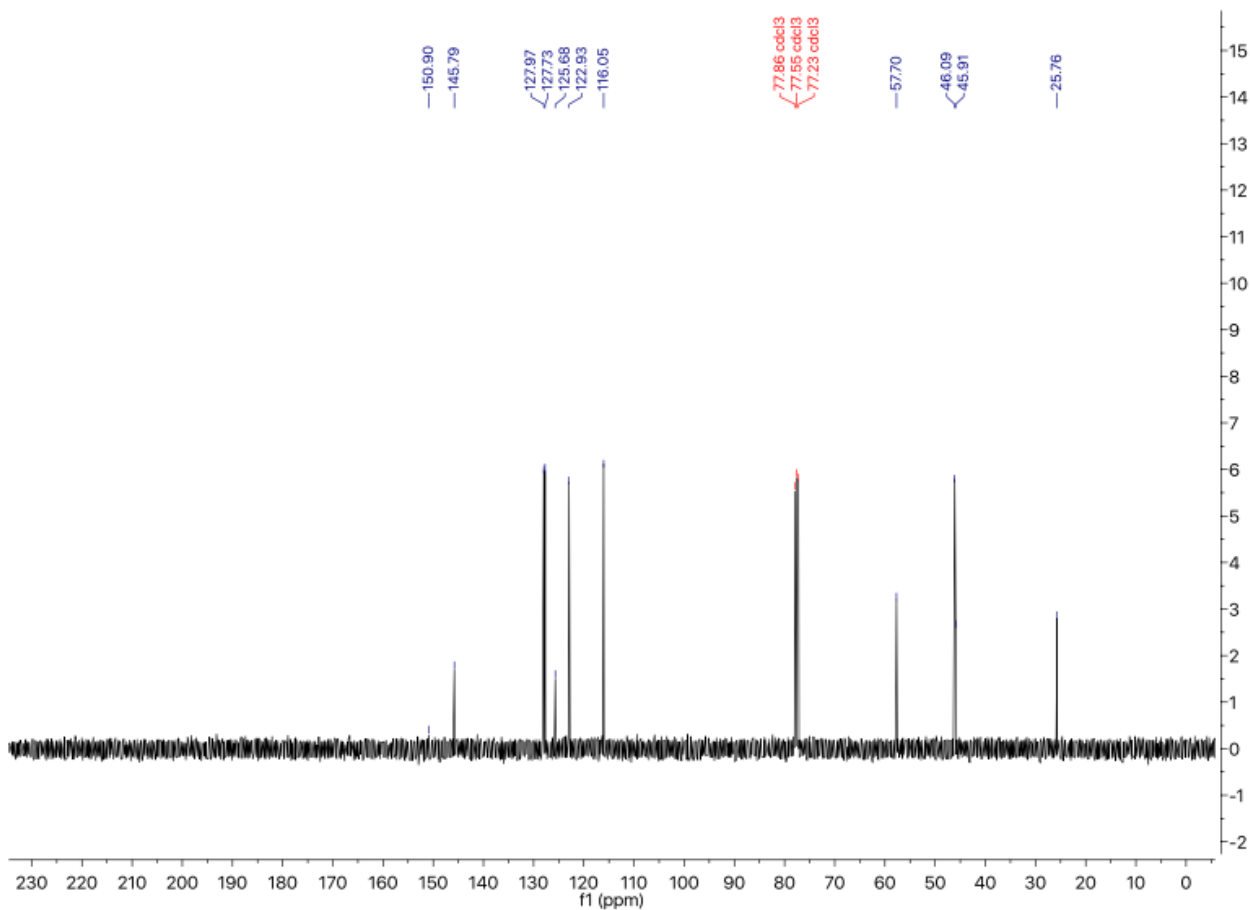
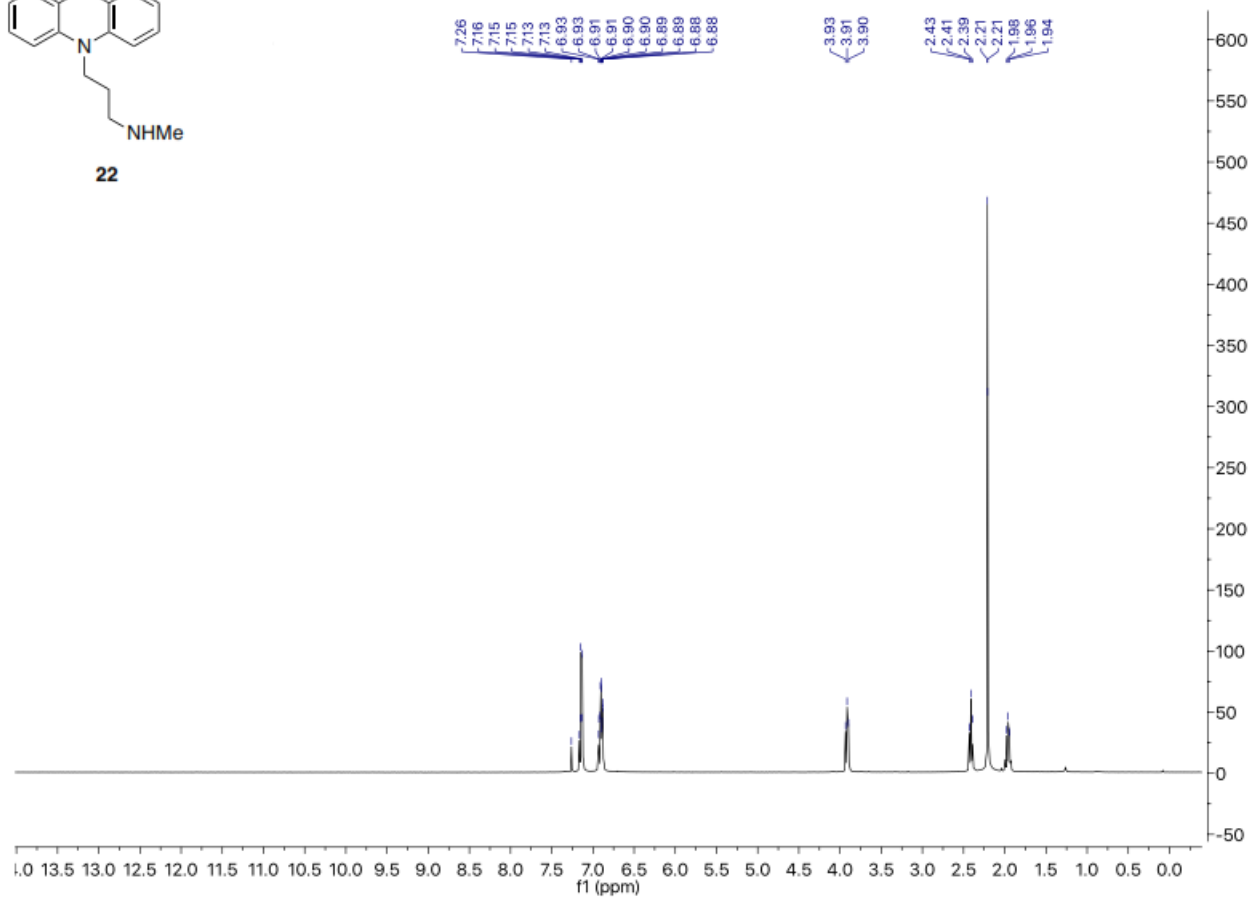
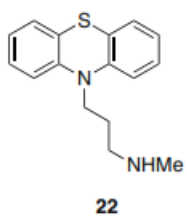


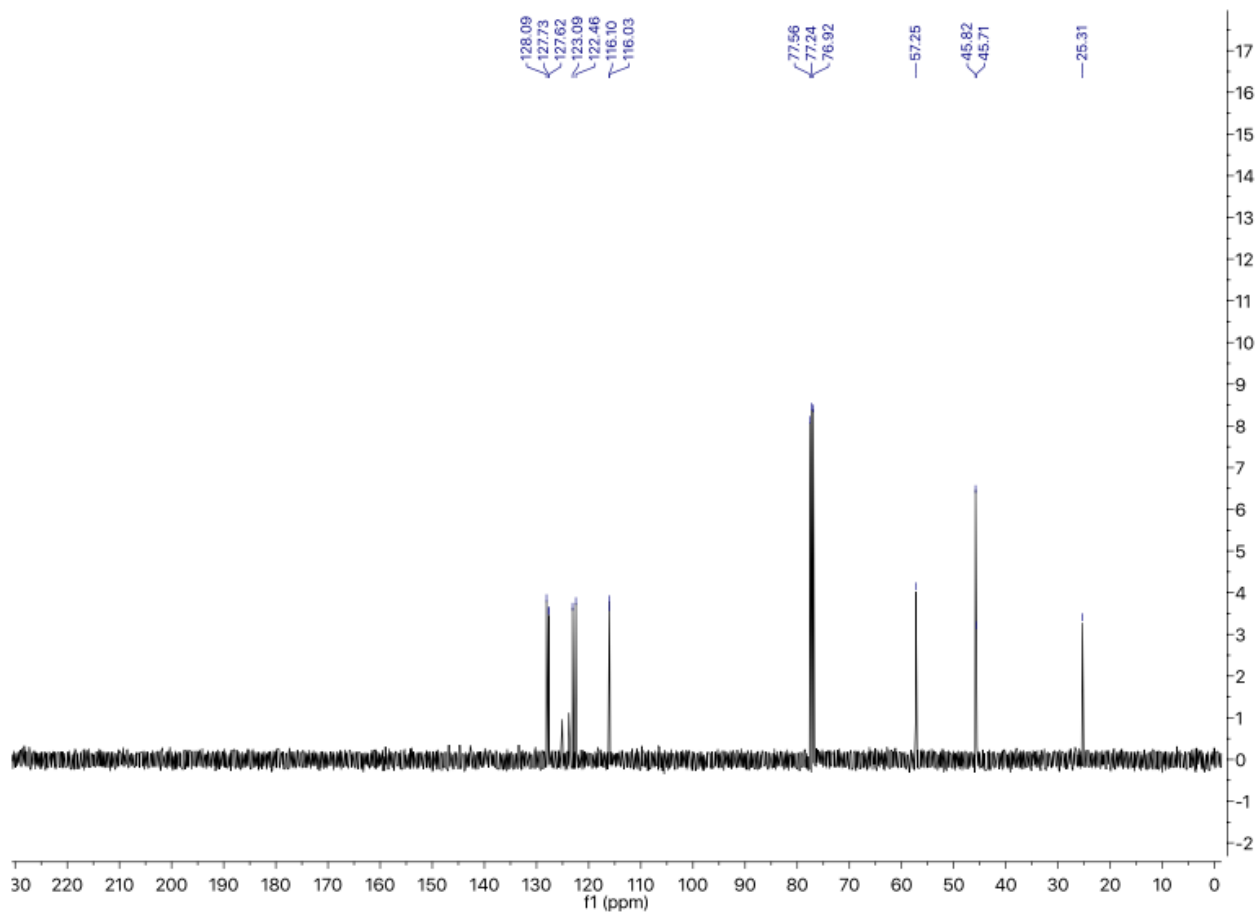
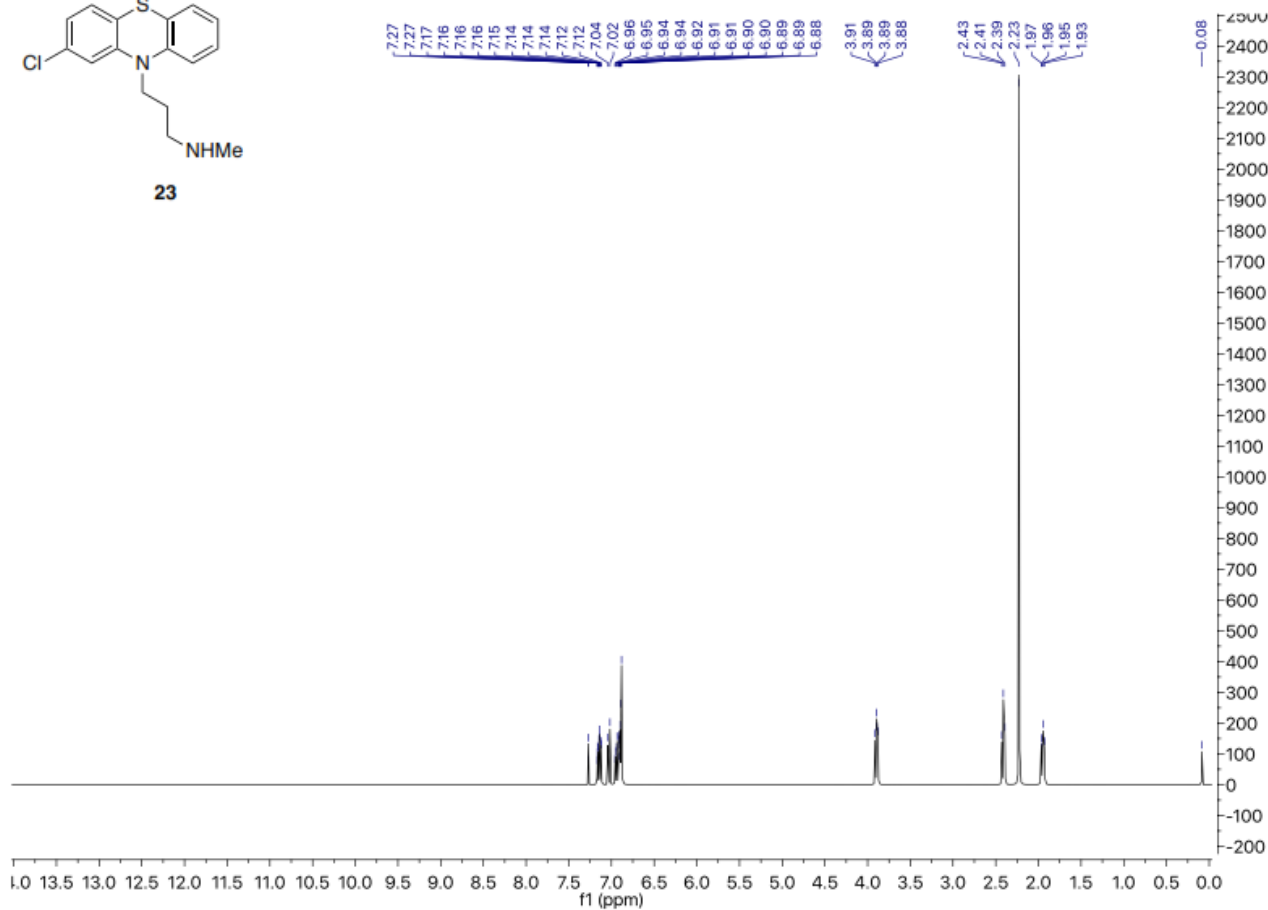
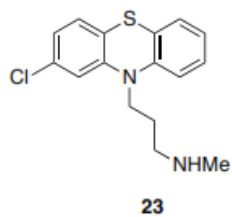
19

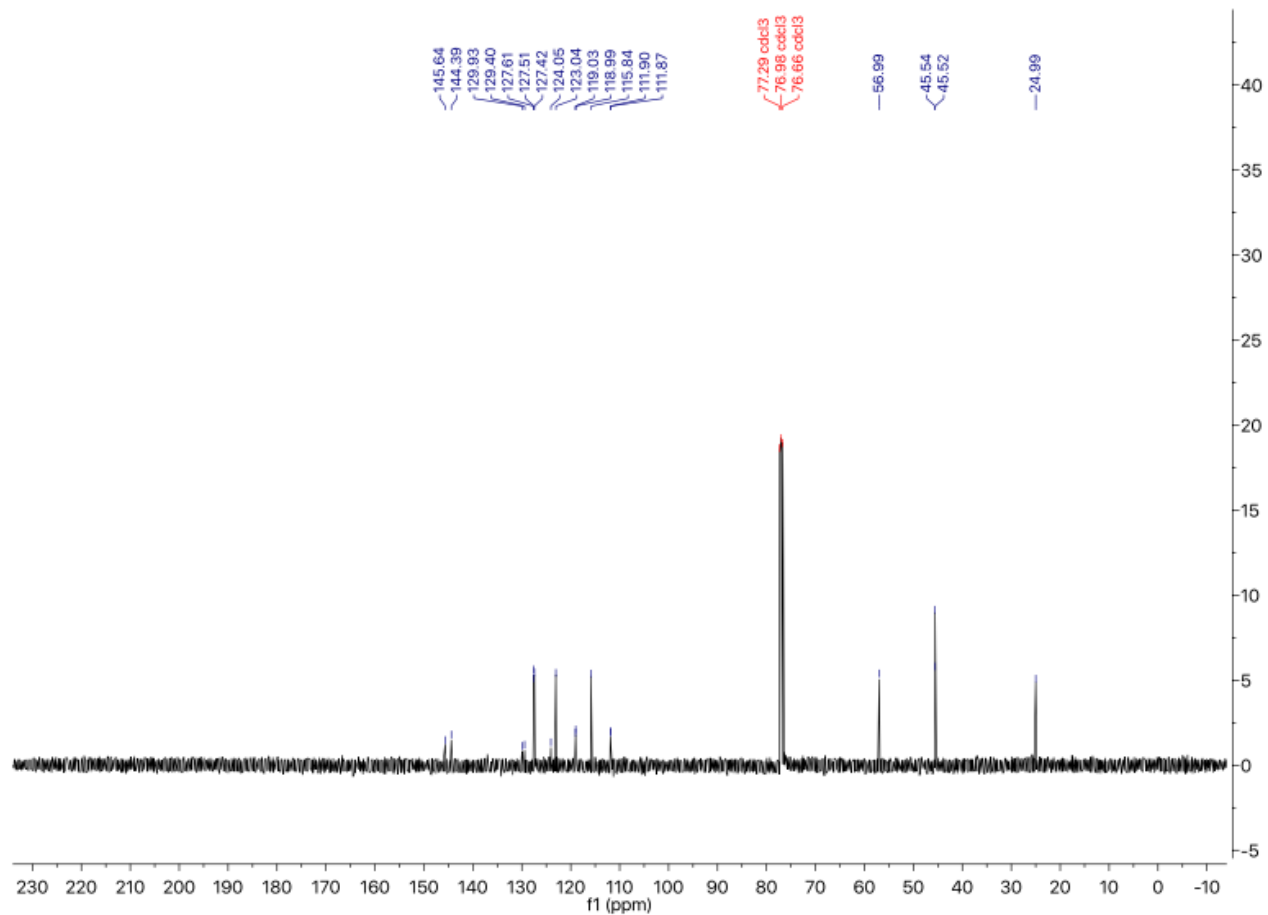
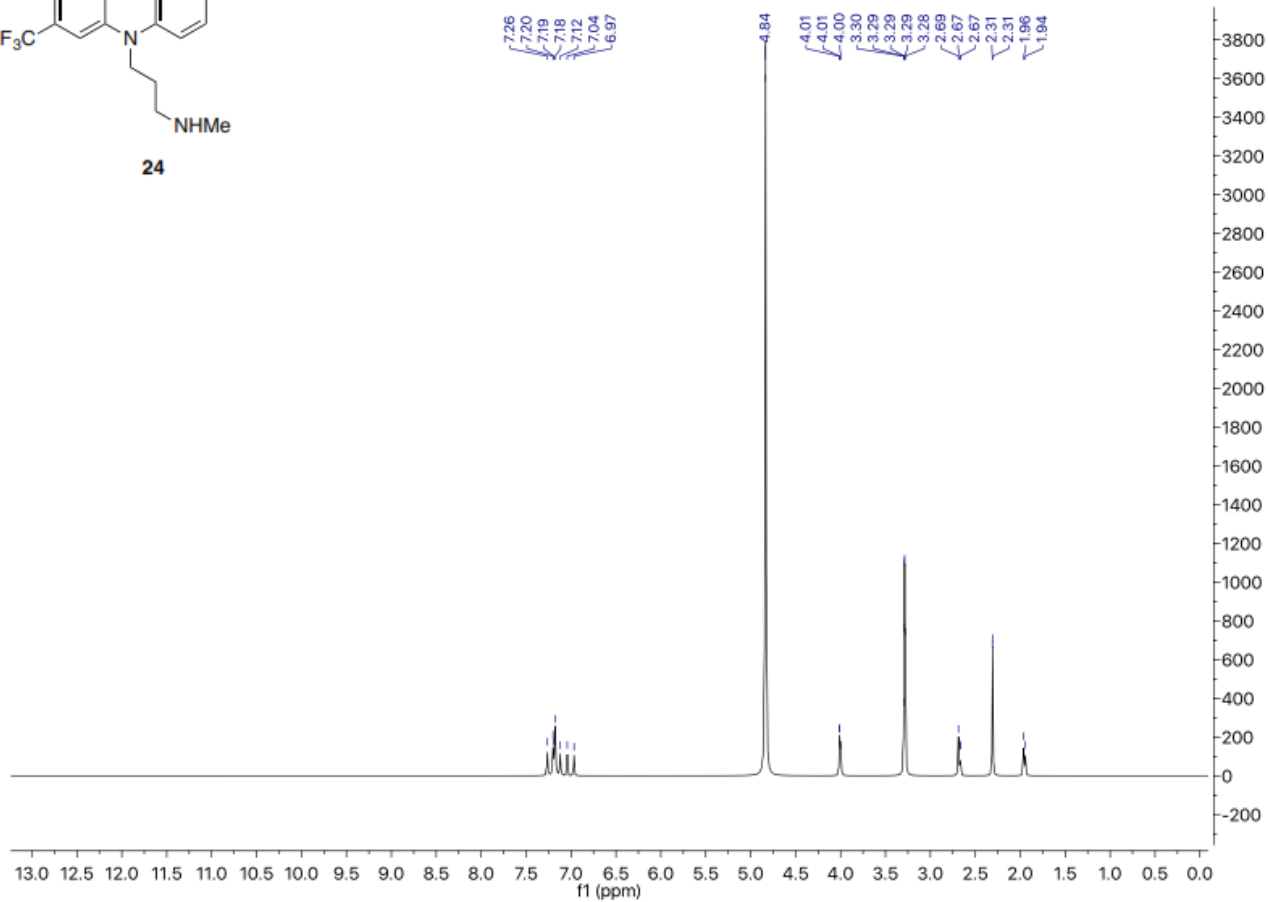
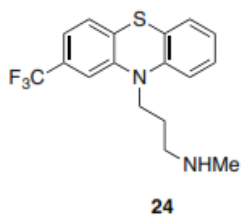


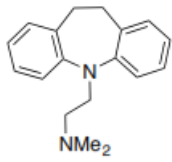




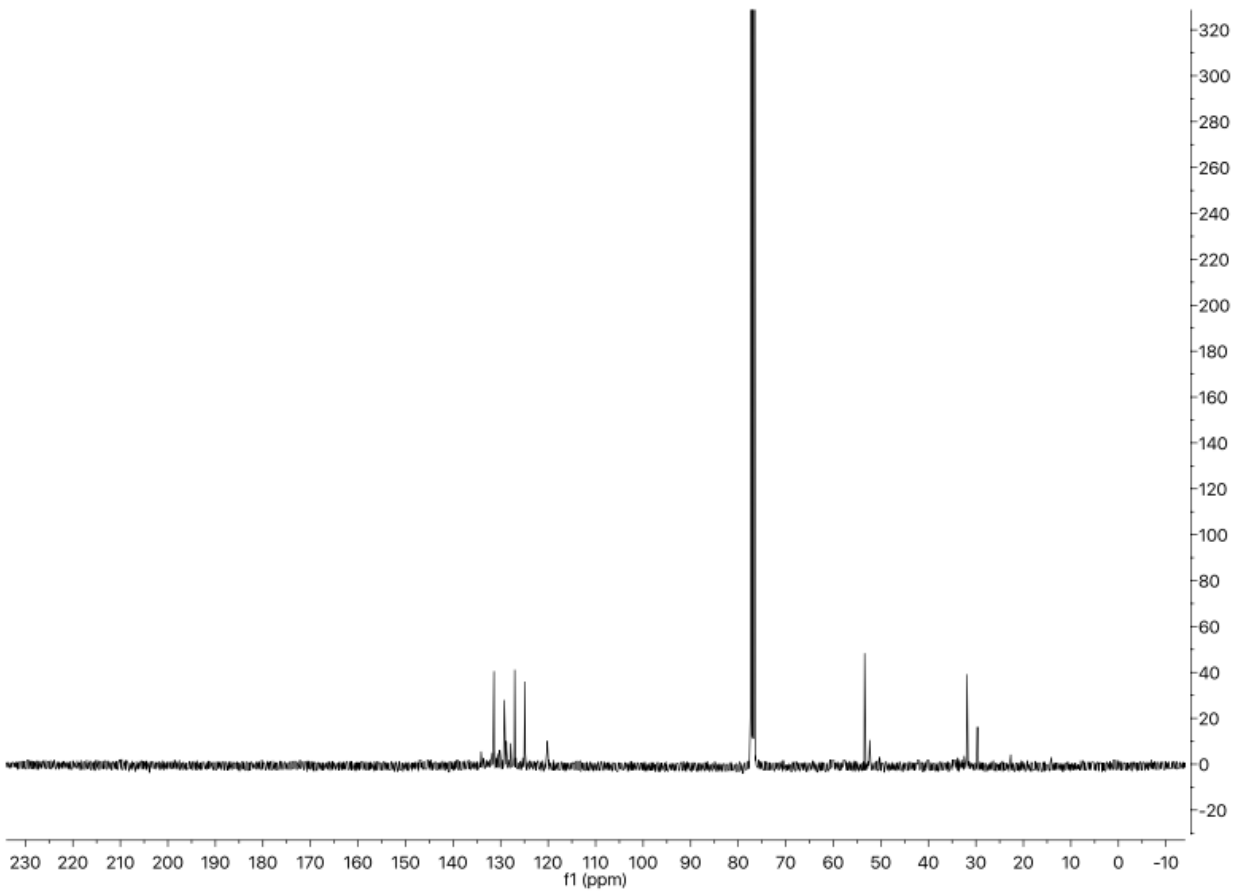
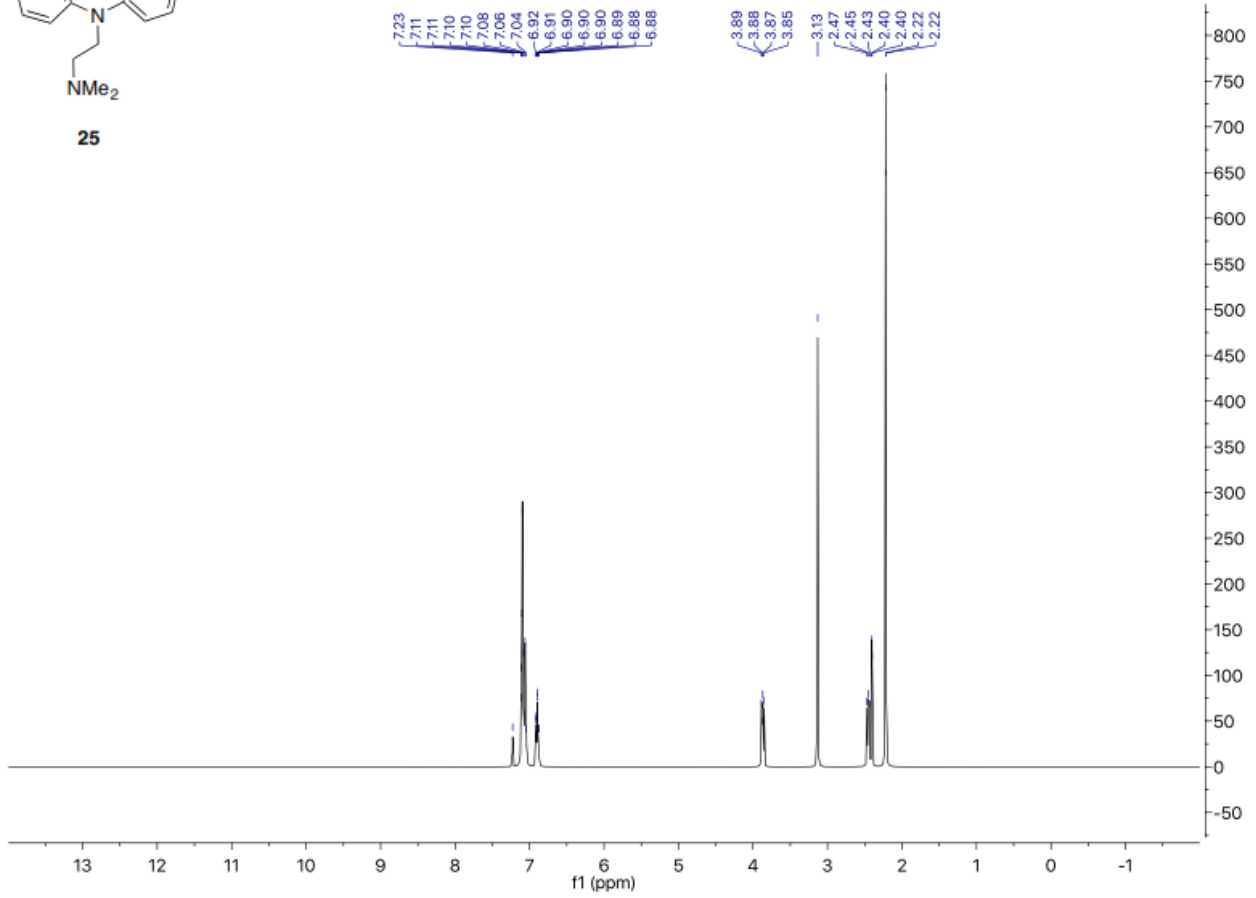


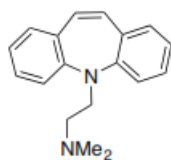




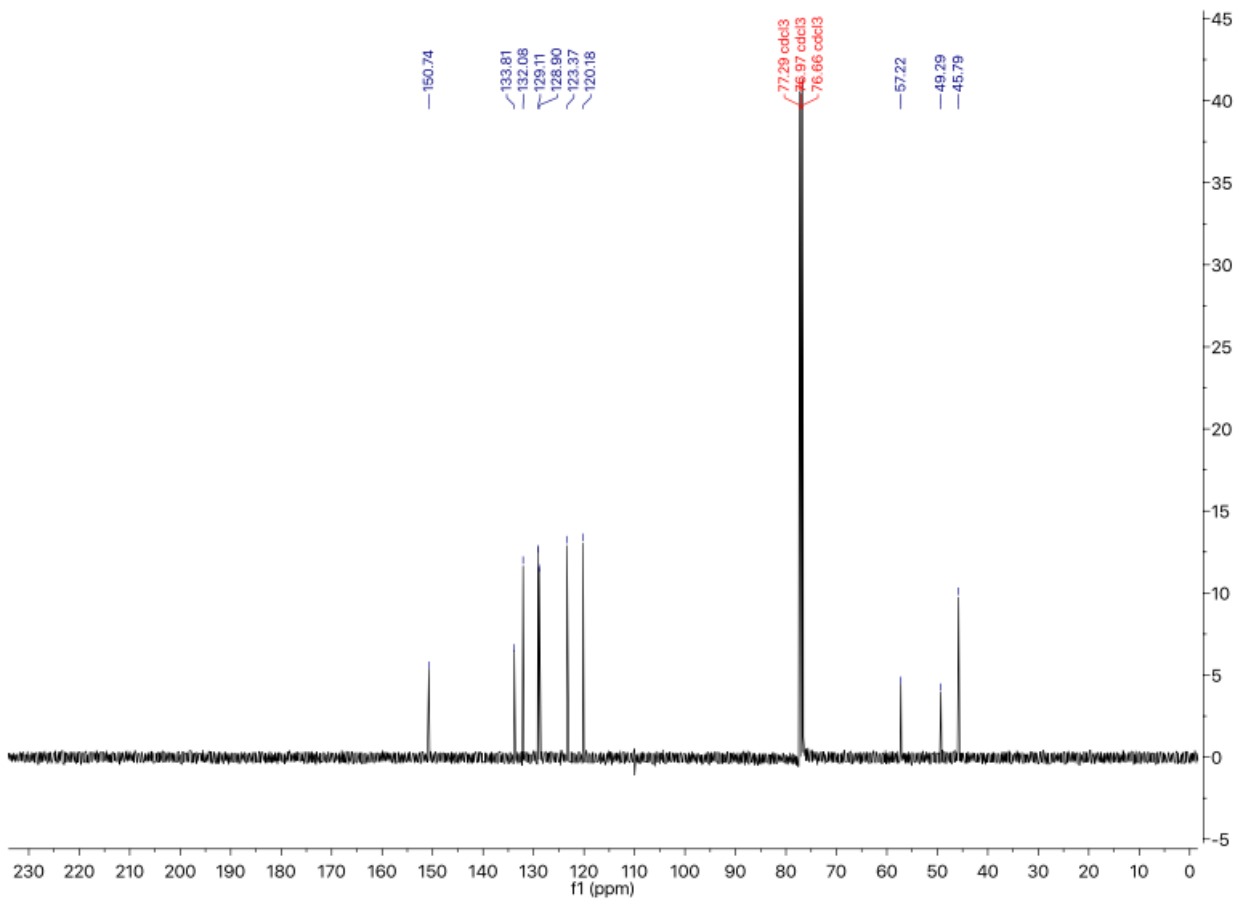
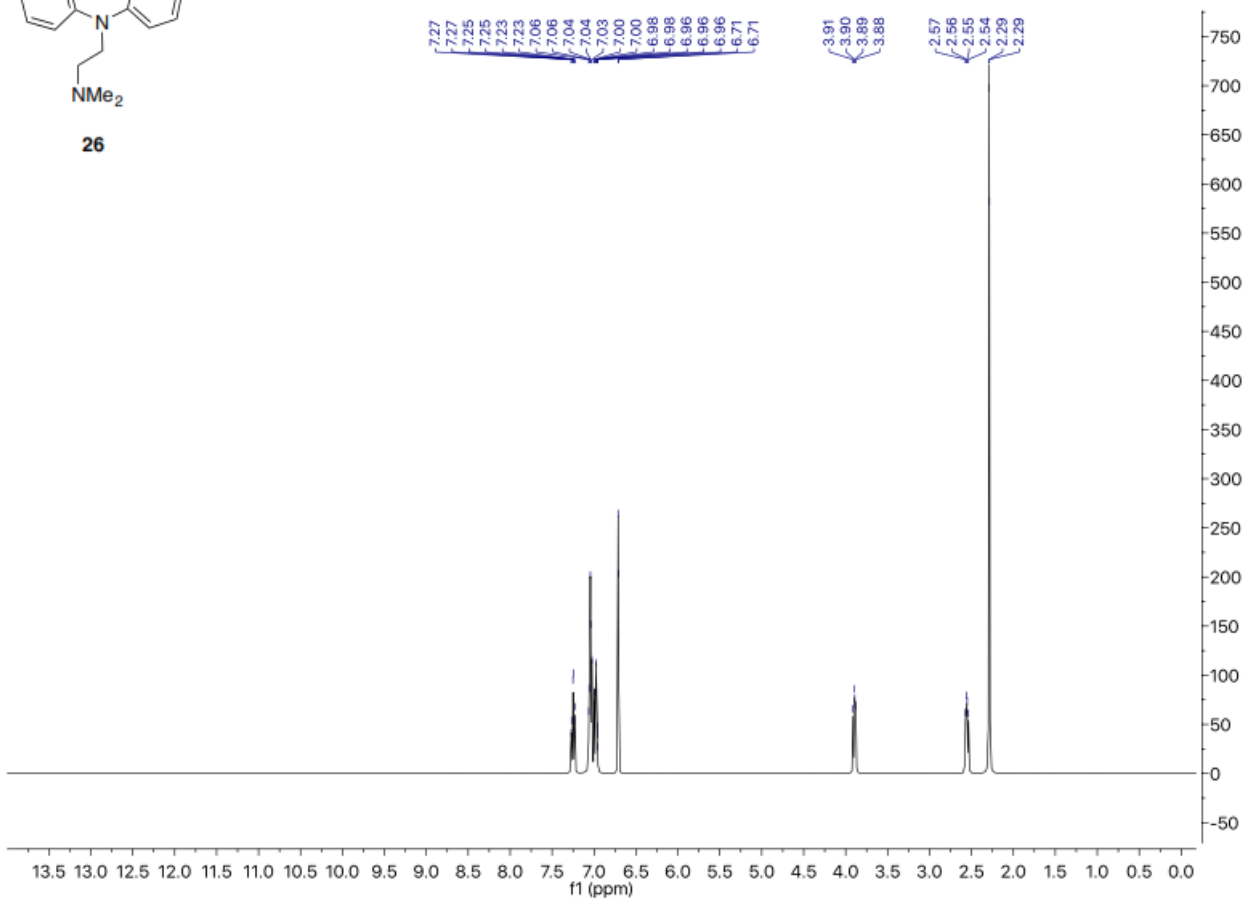


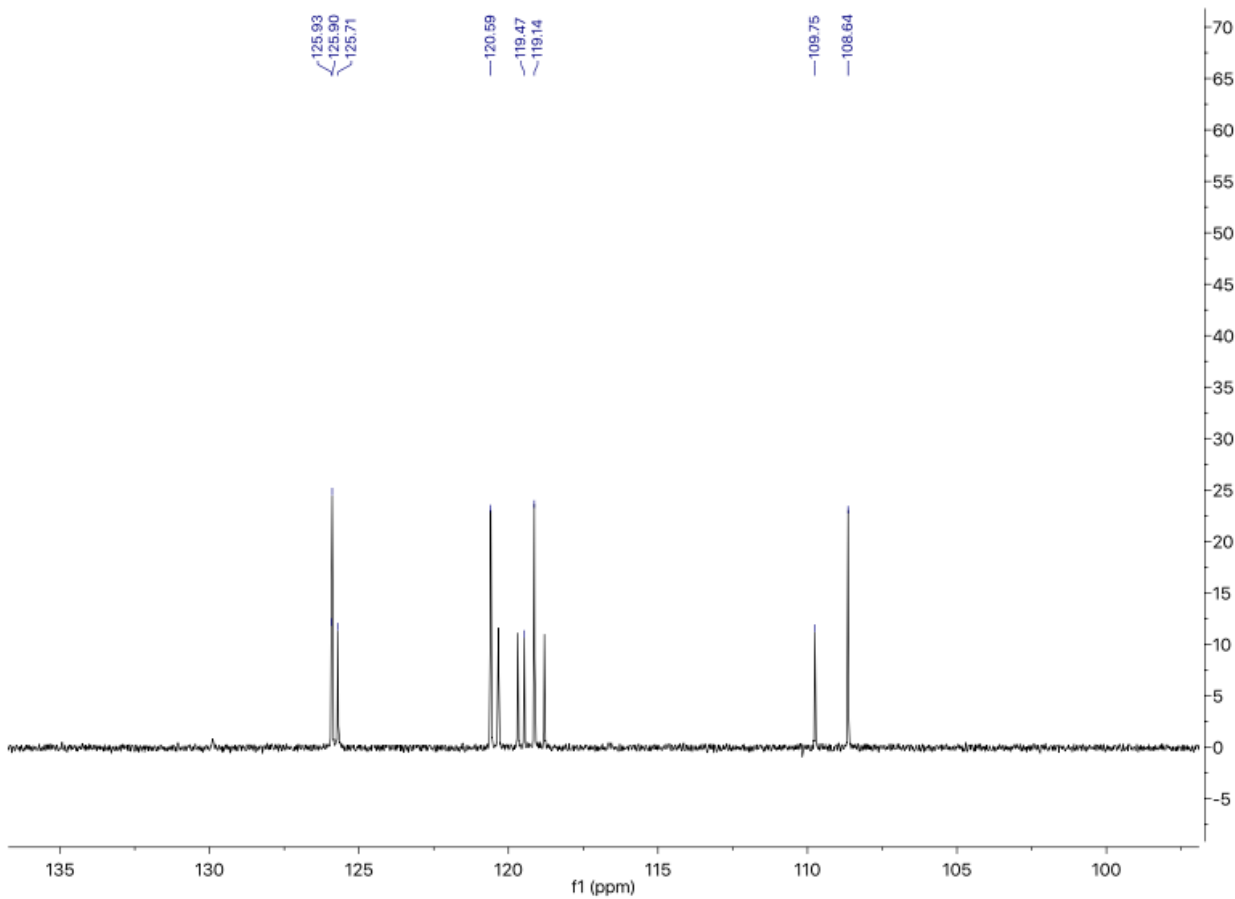
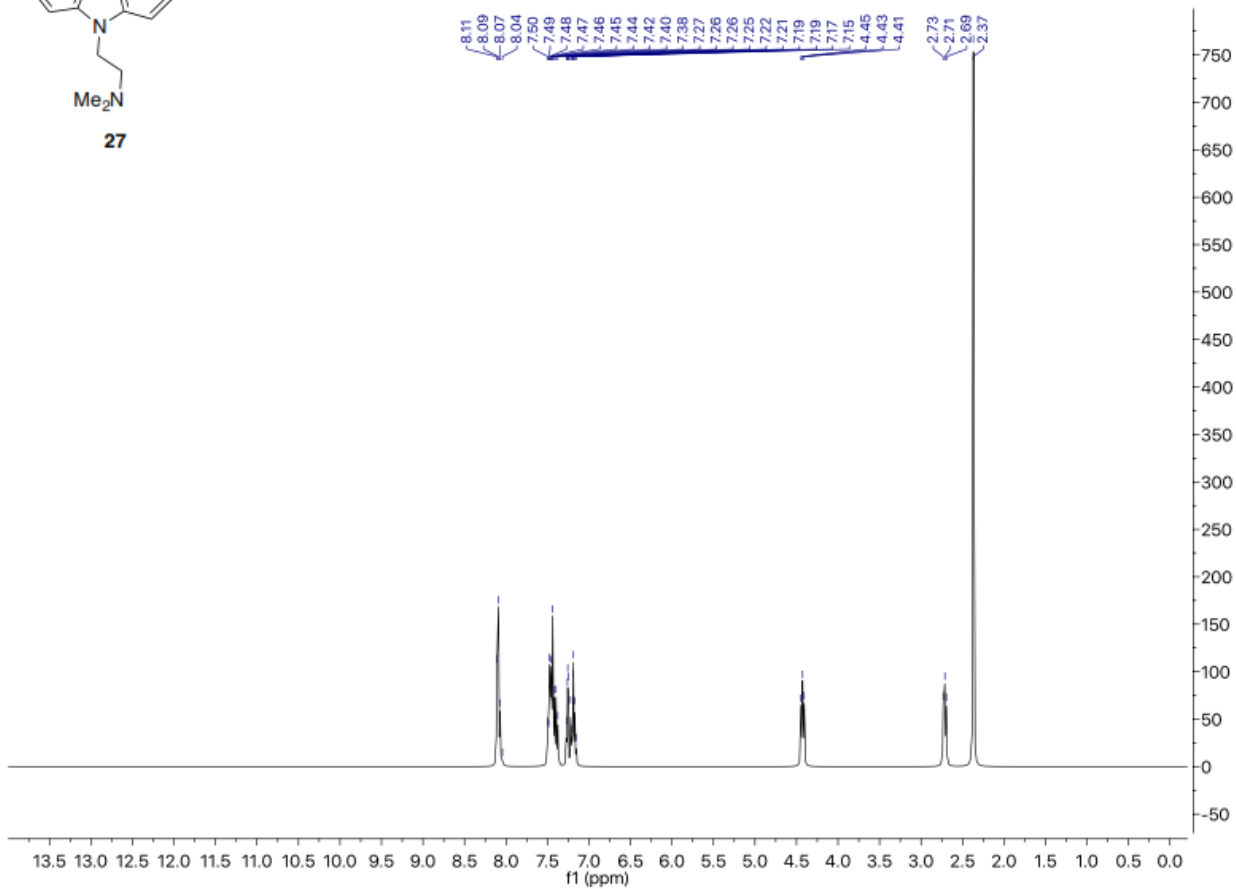
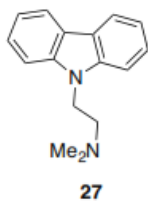
25

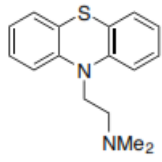




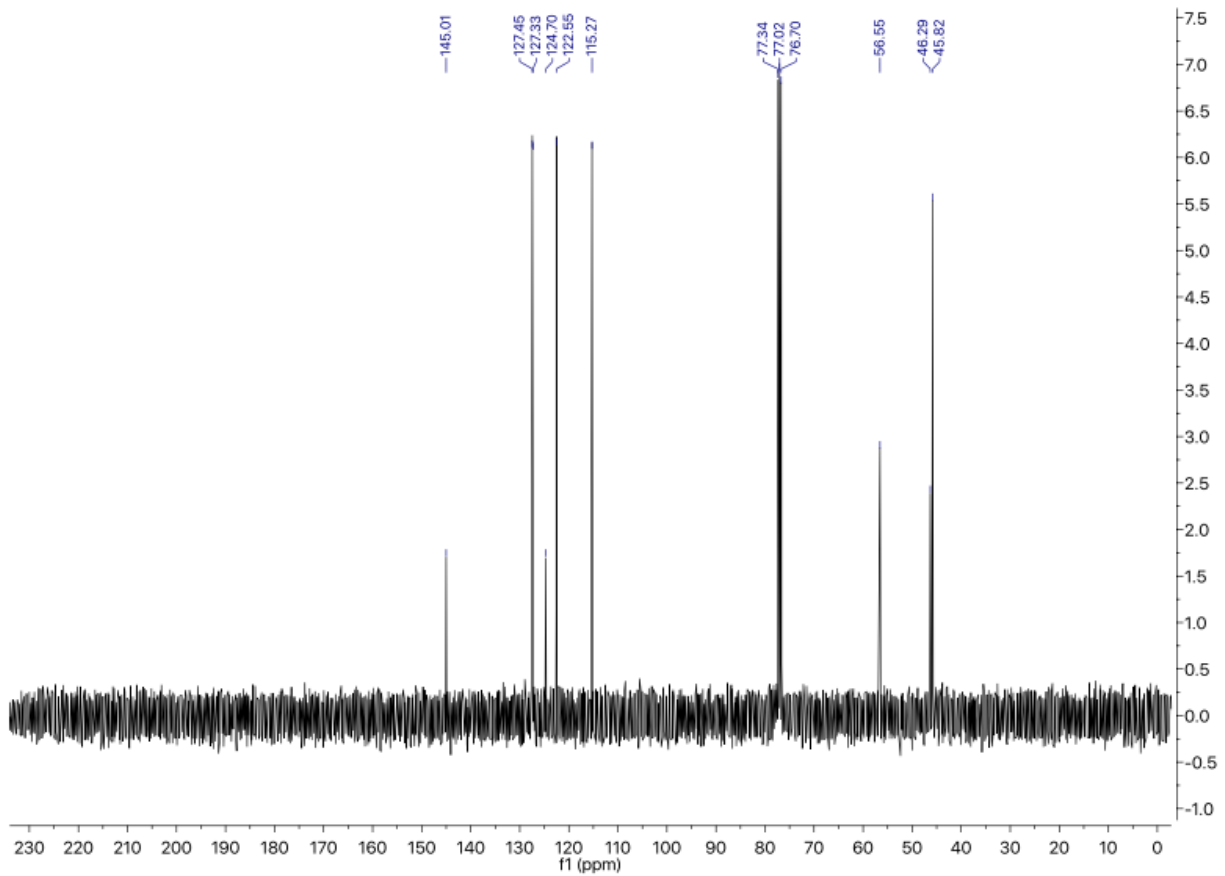
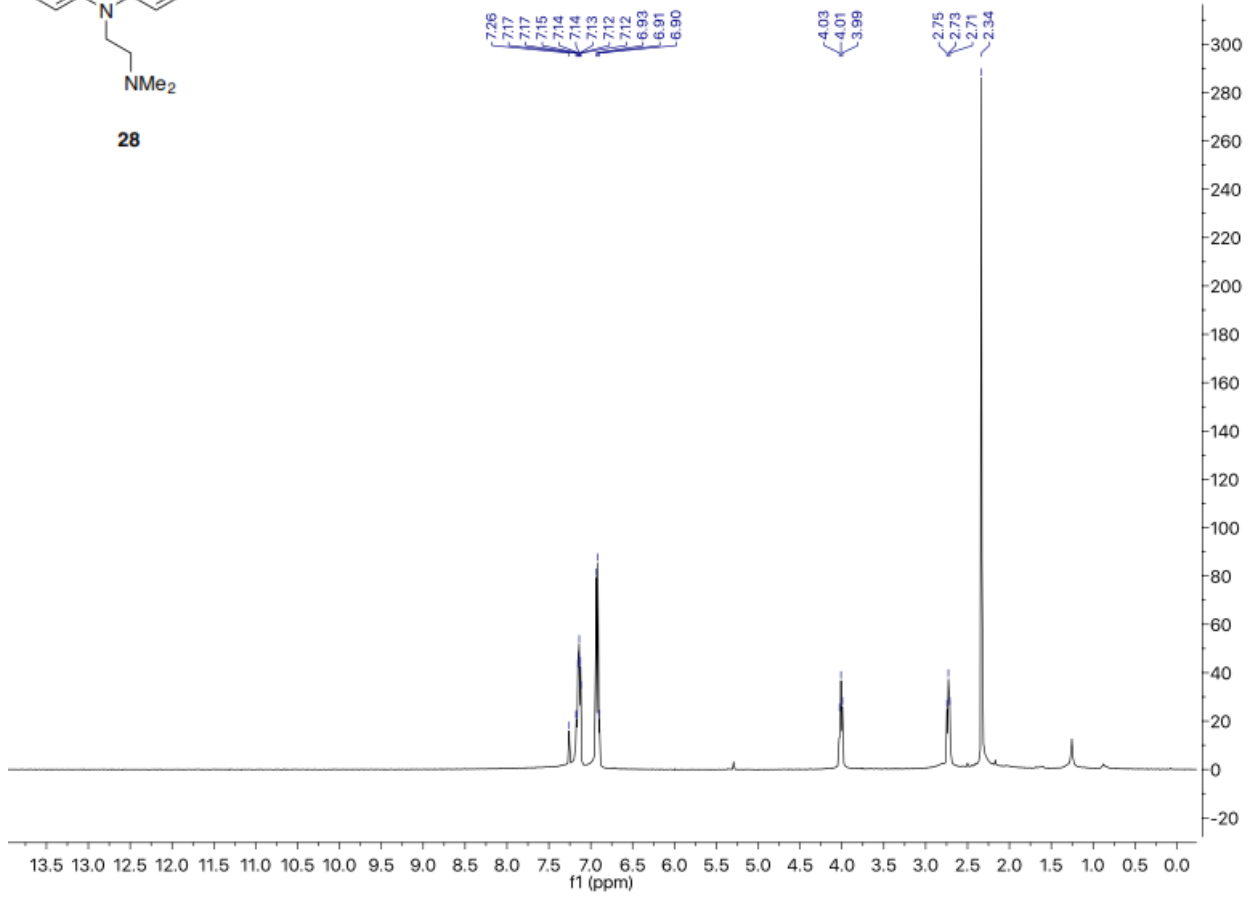
26

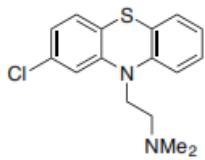




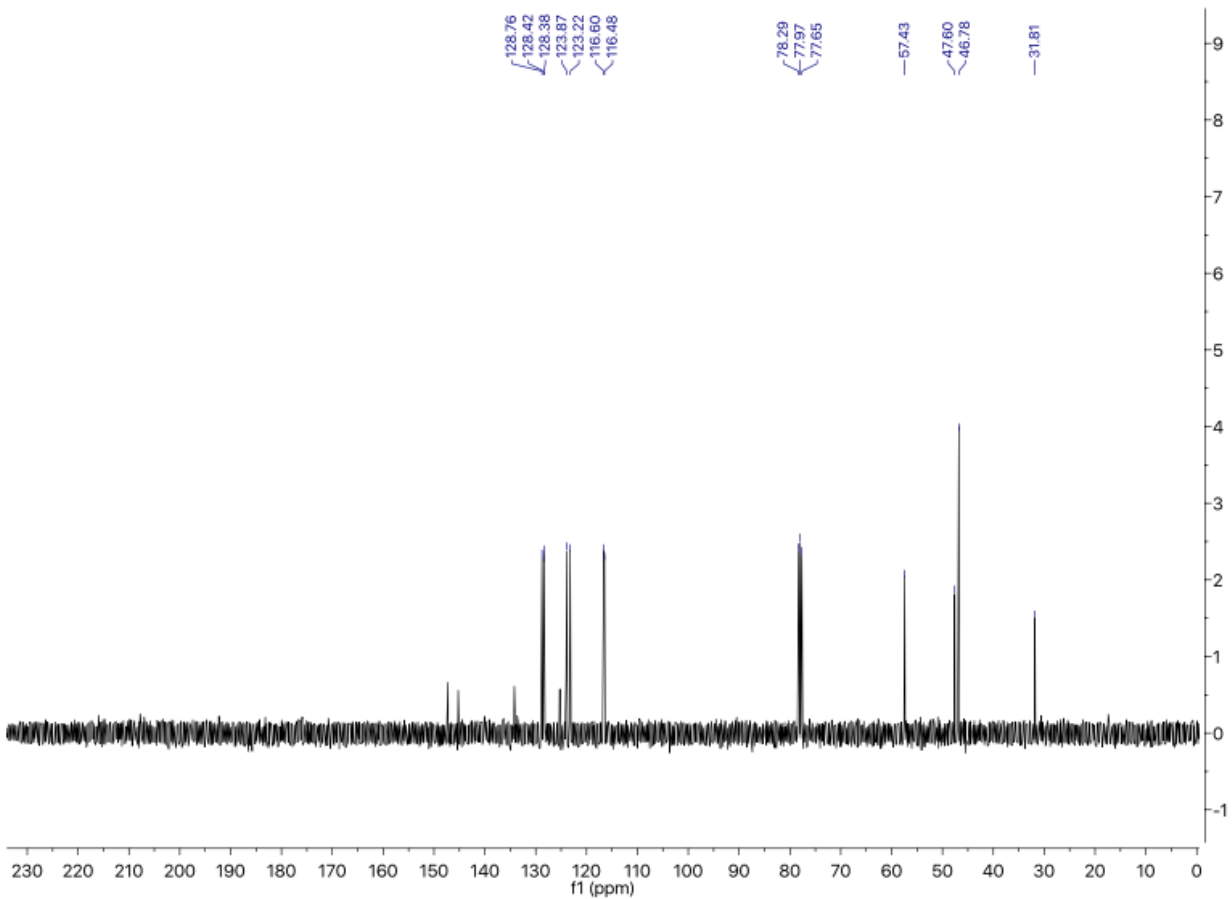
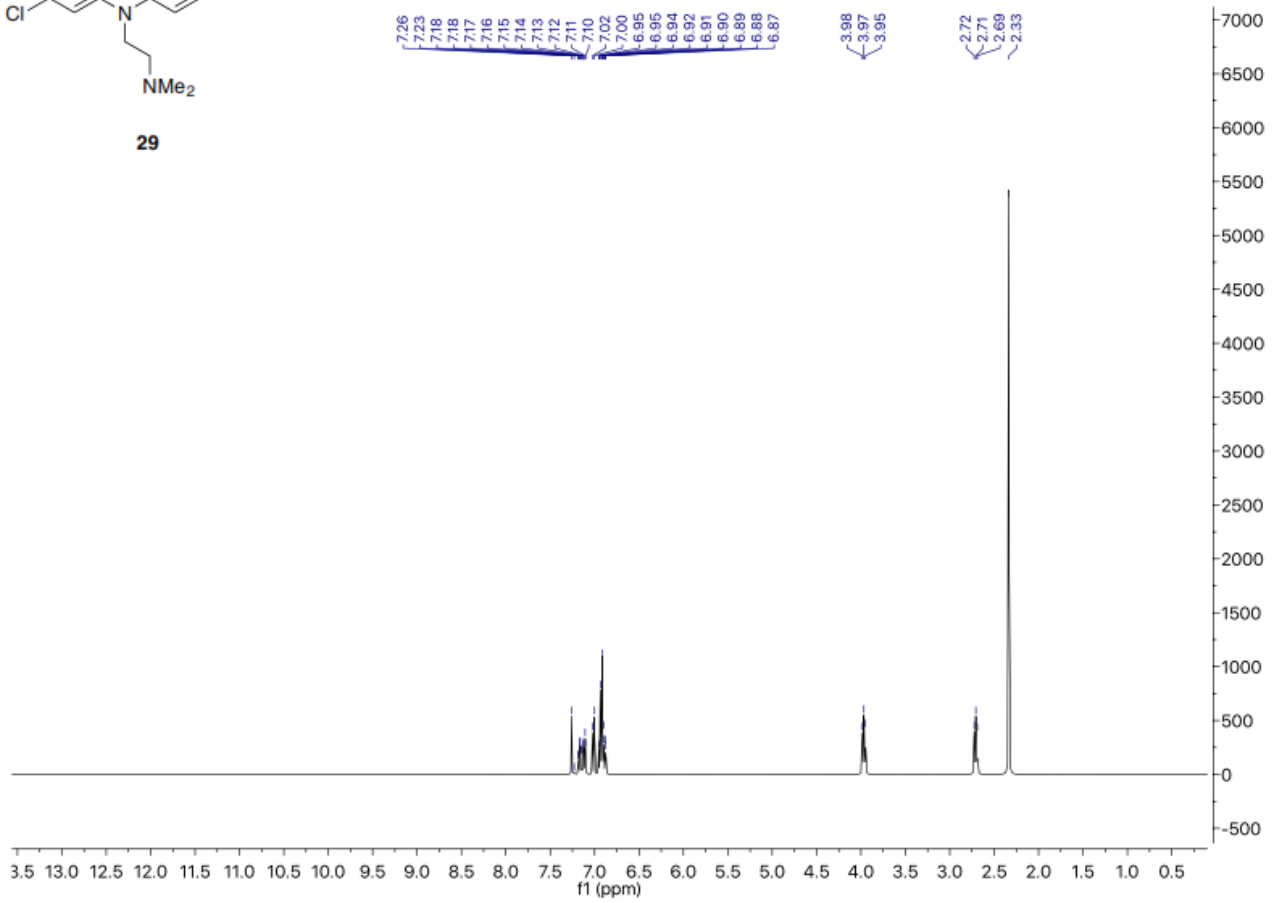


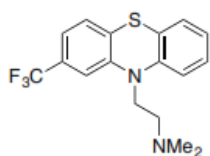
28



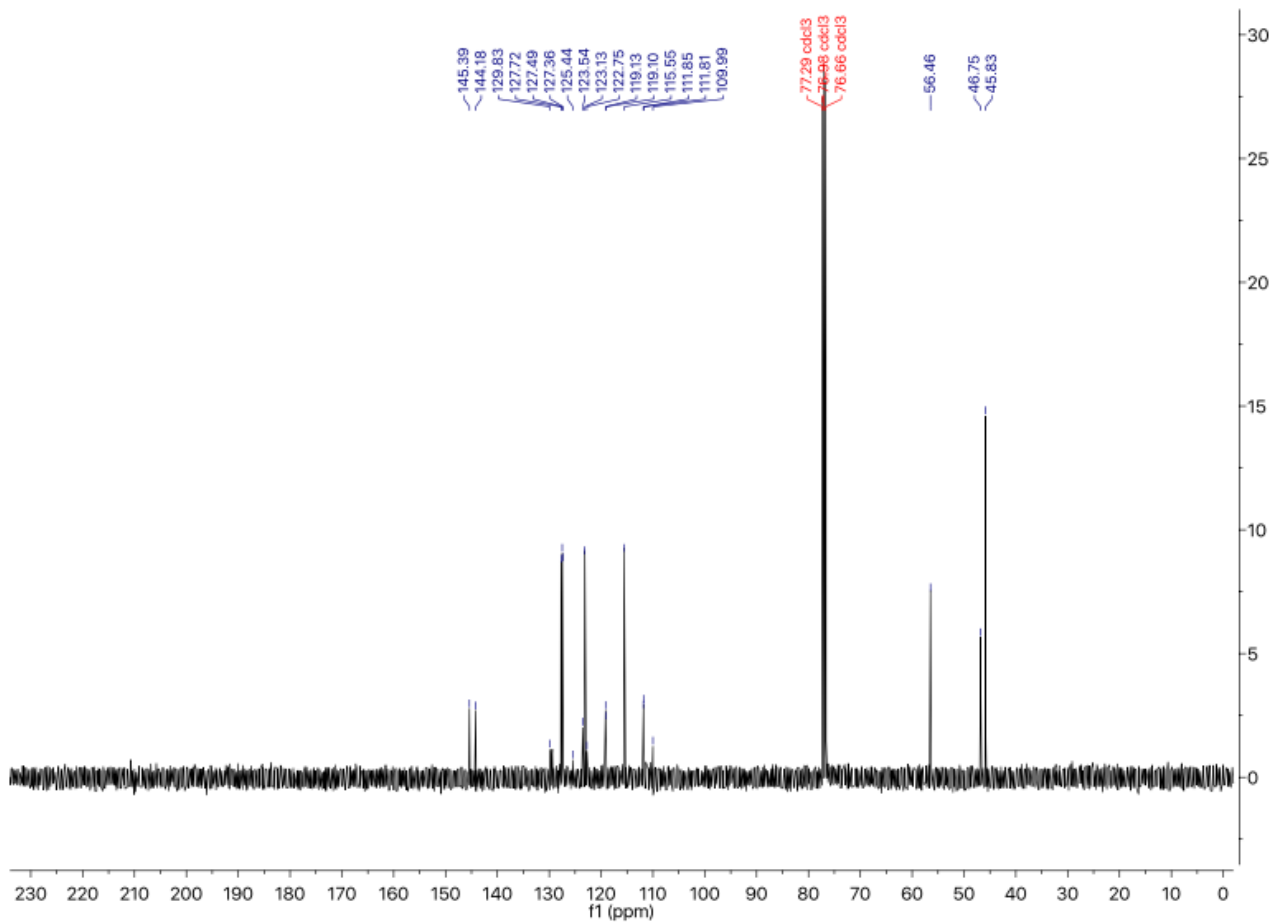
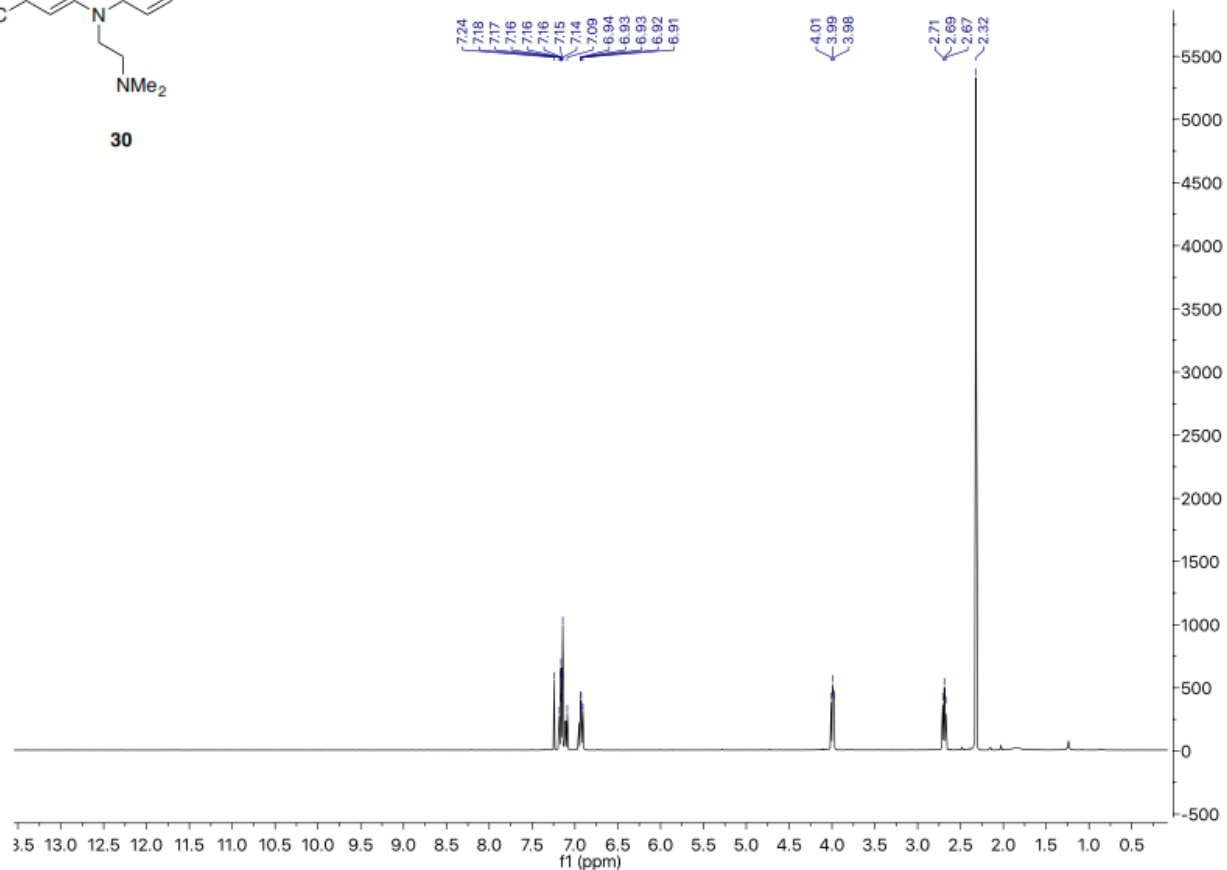


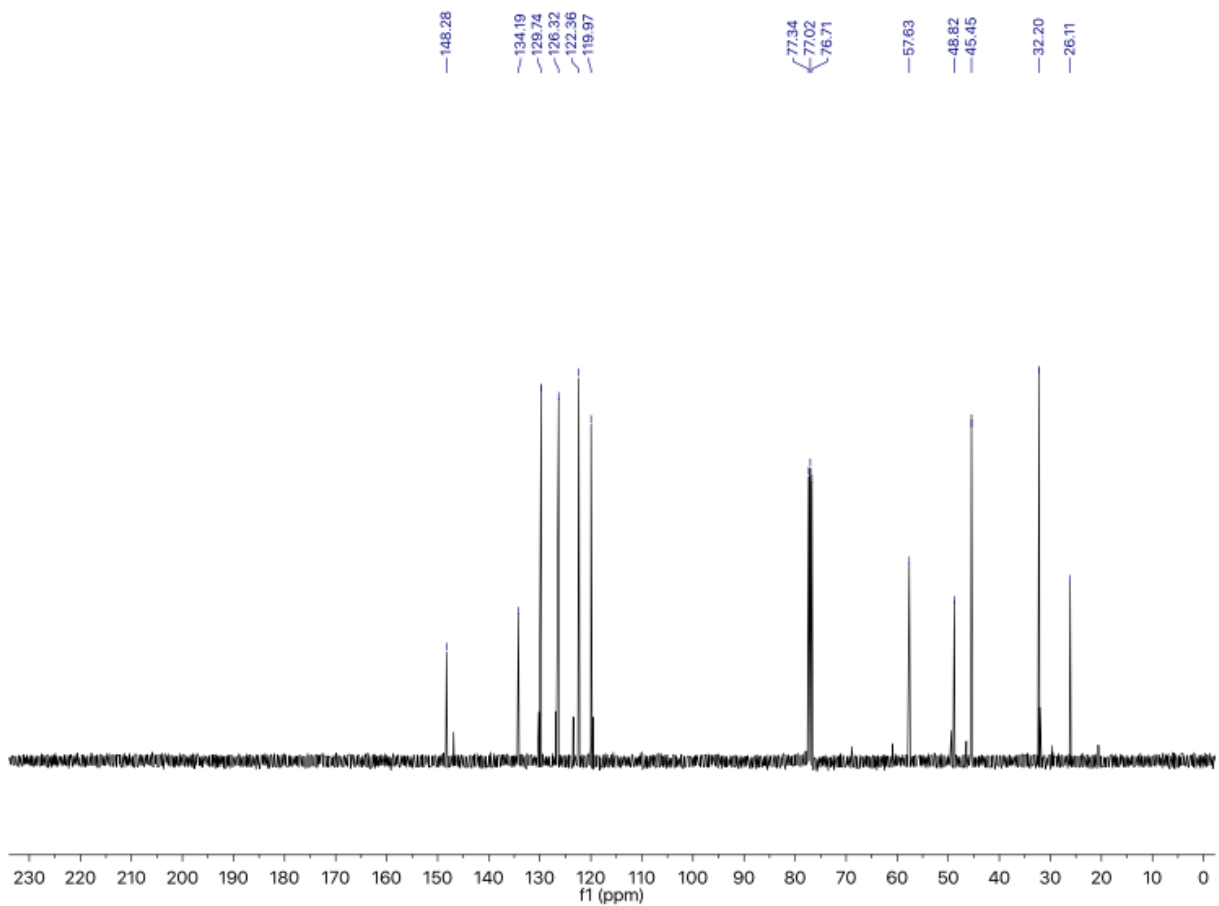
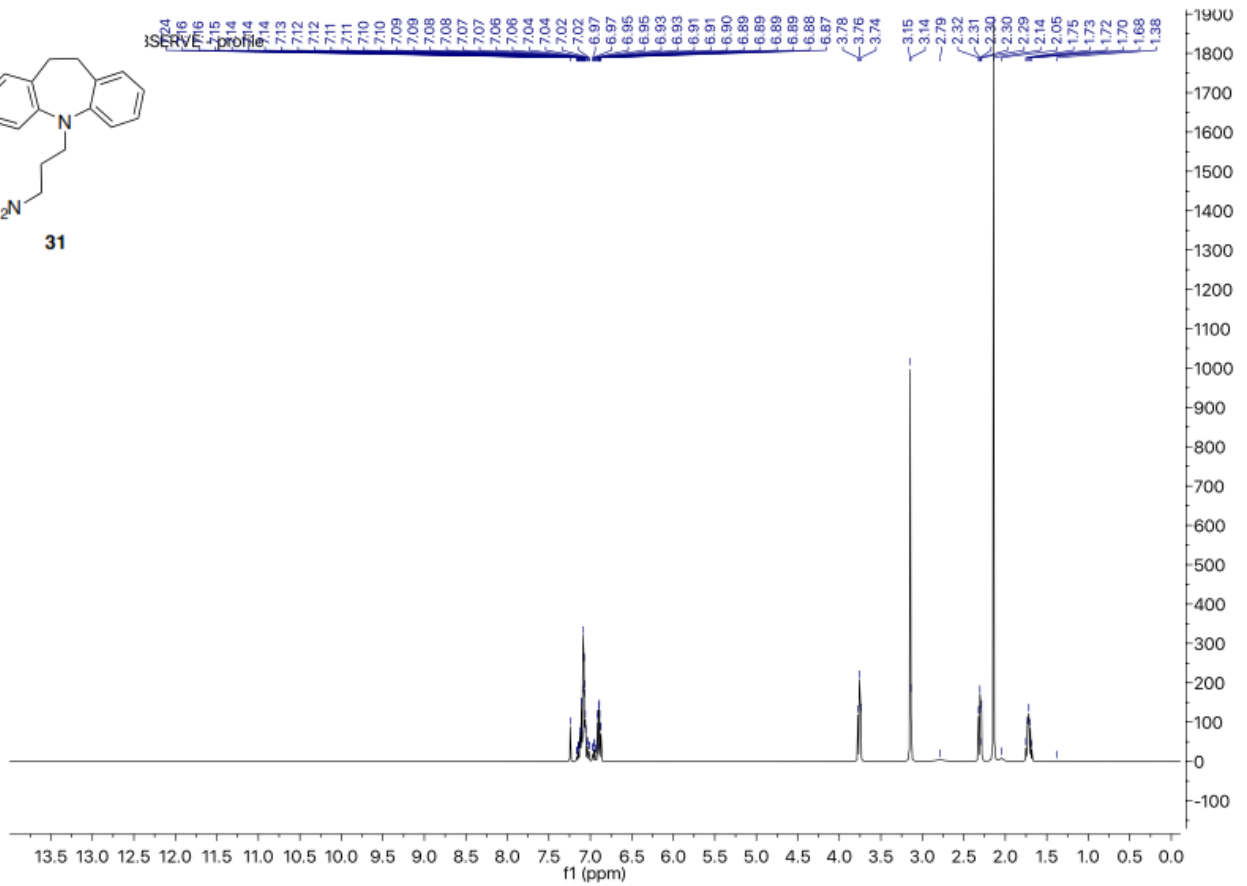
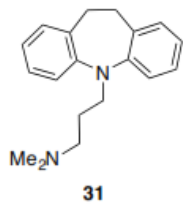
29

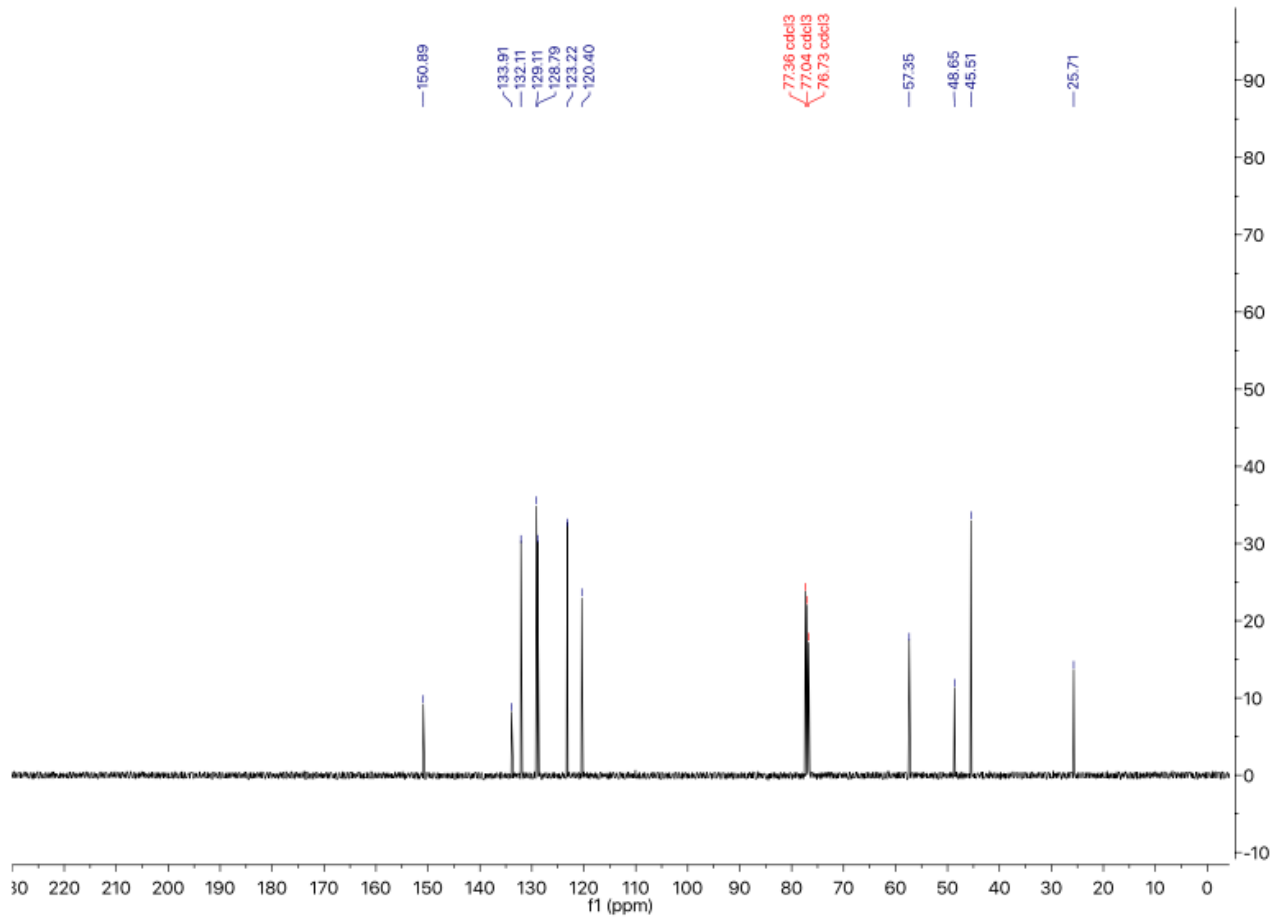
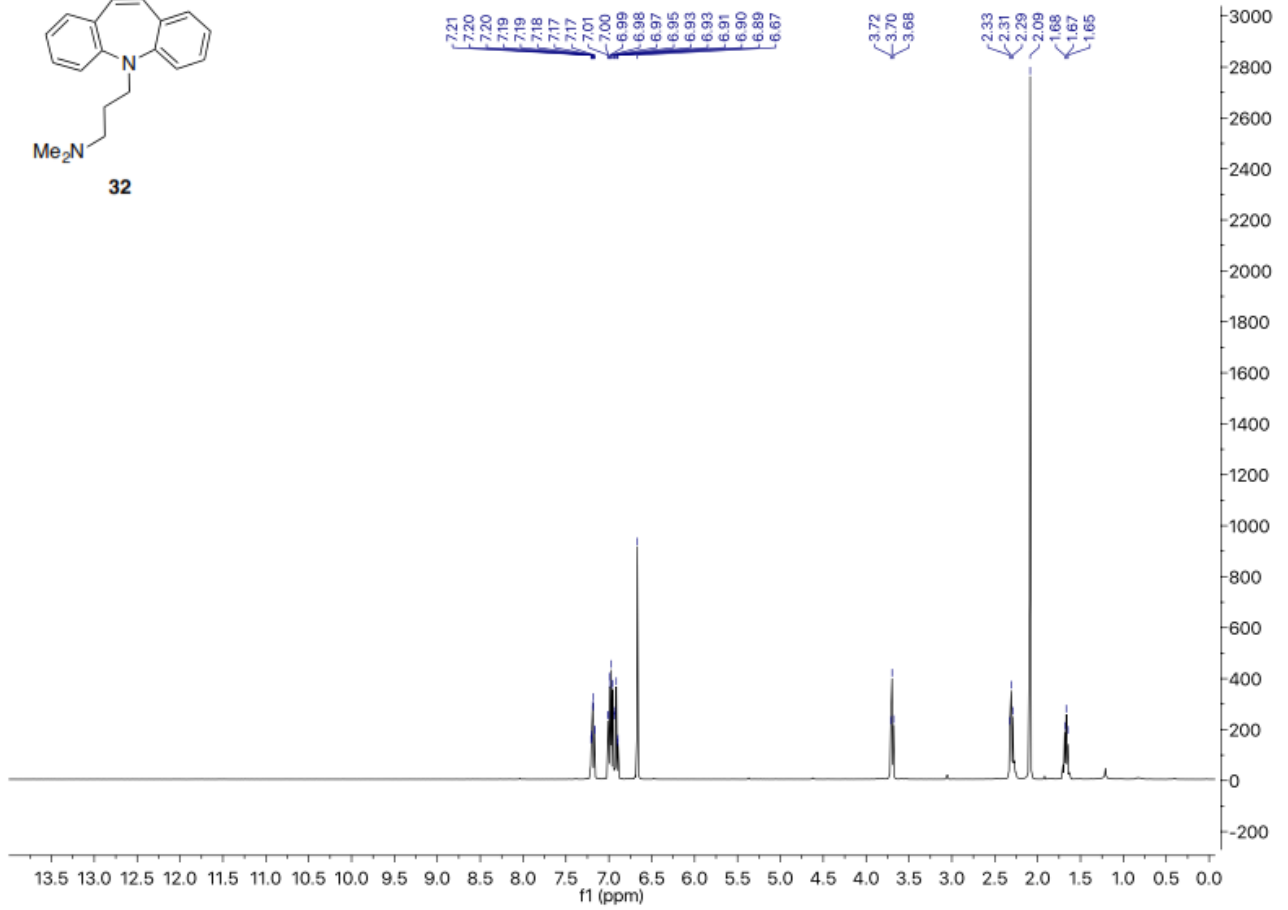
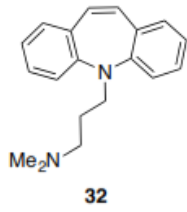


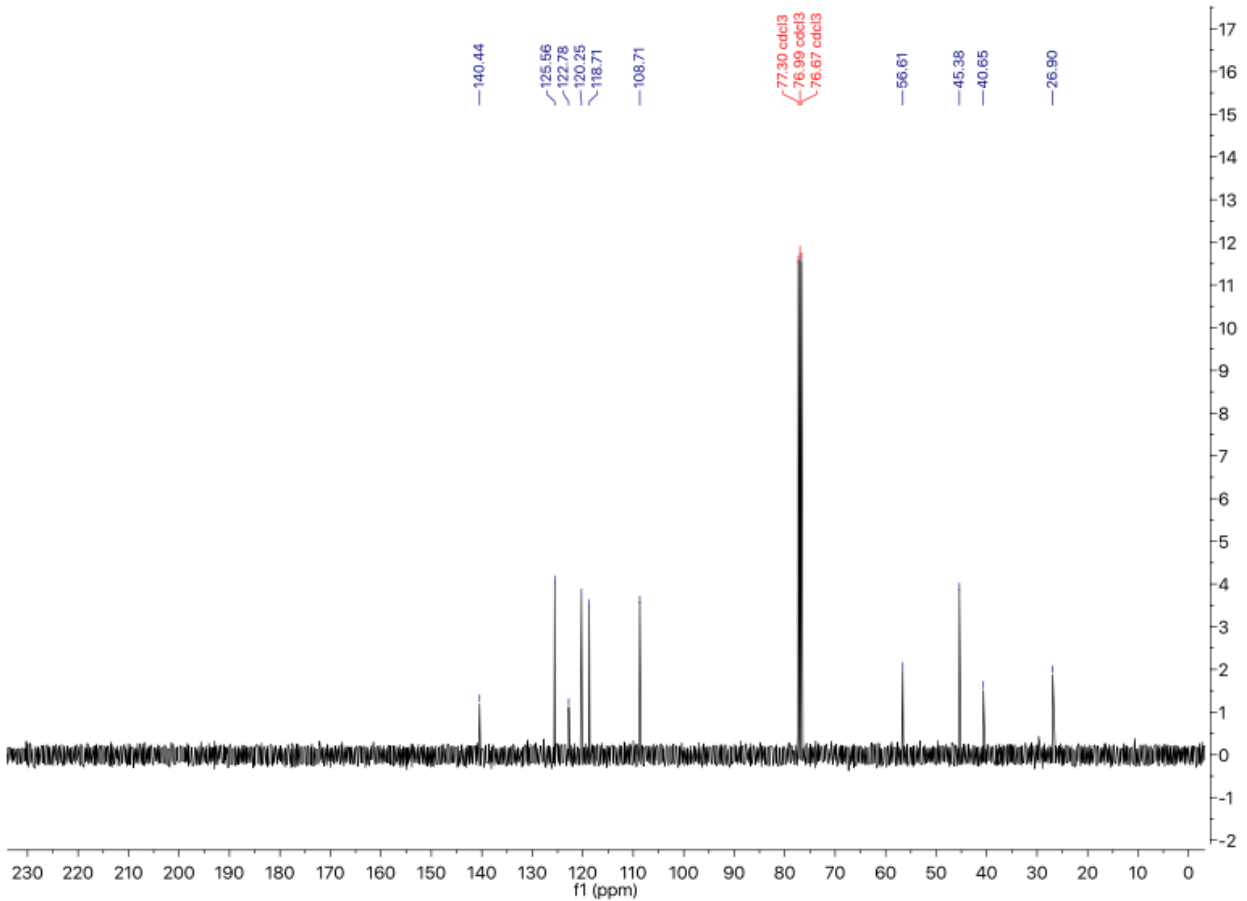
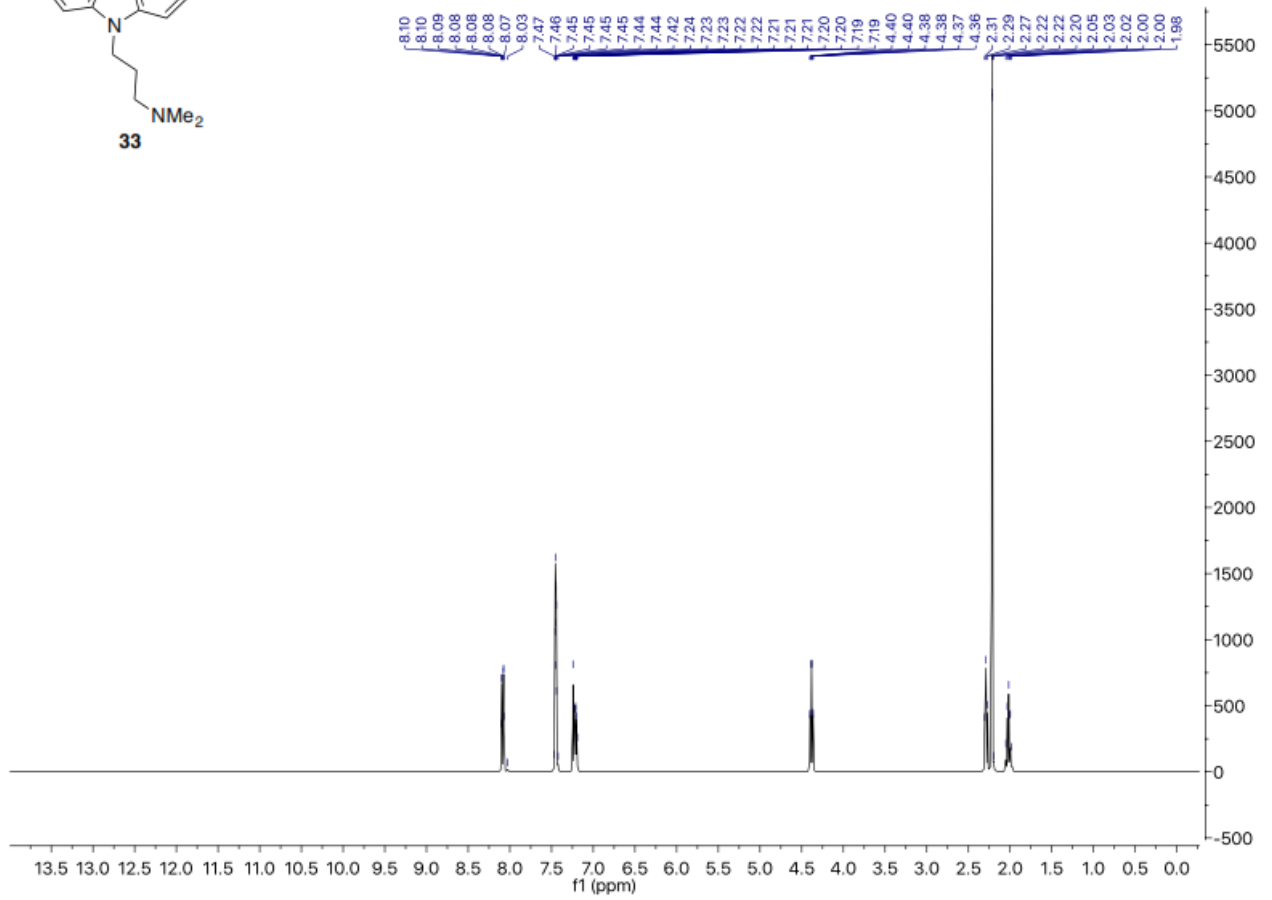
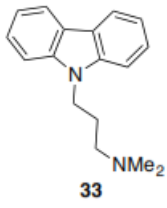


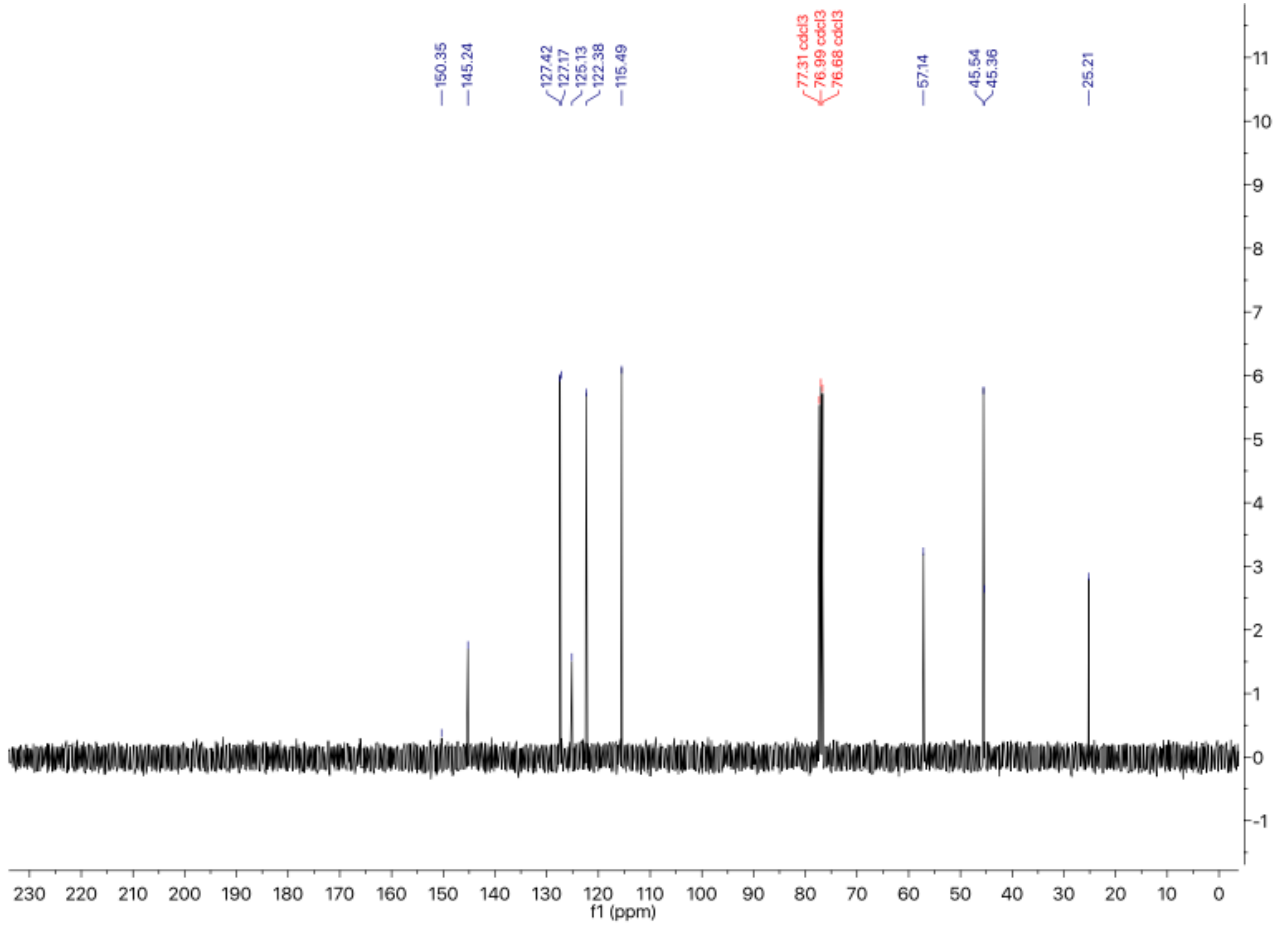
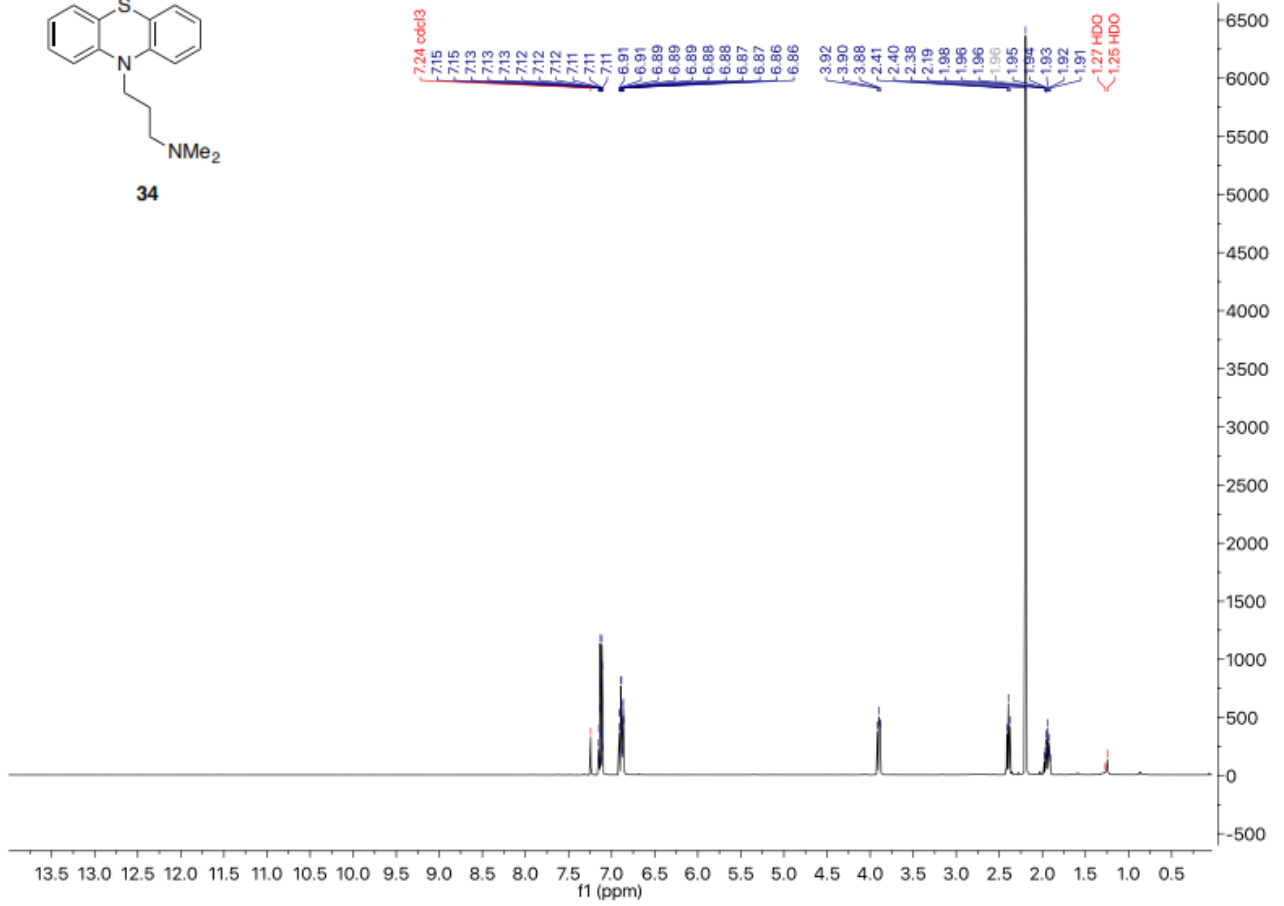
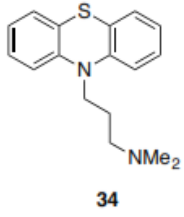
30

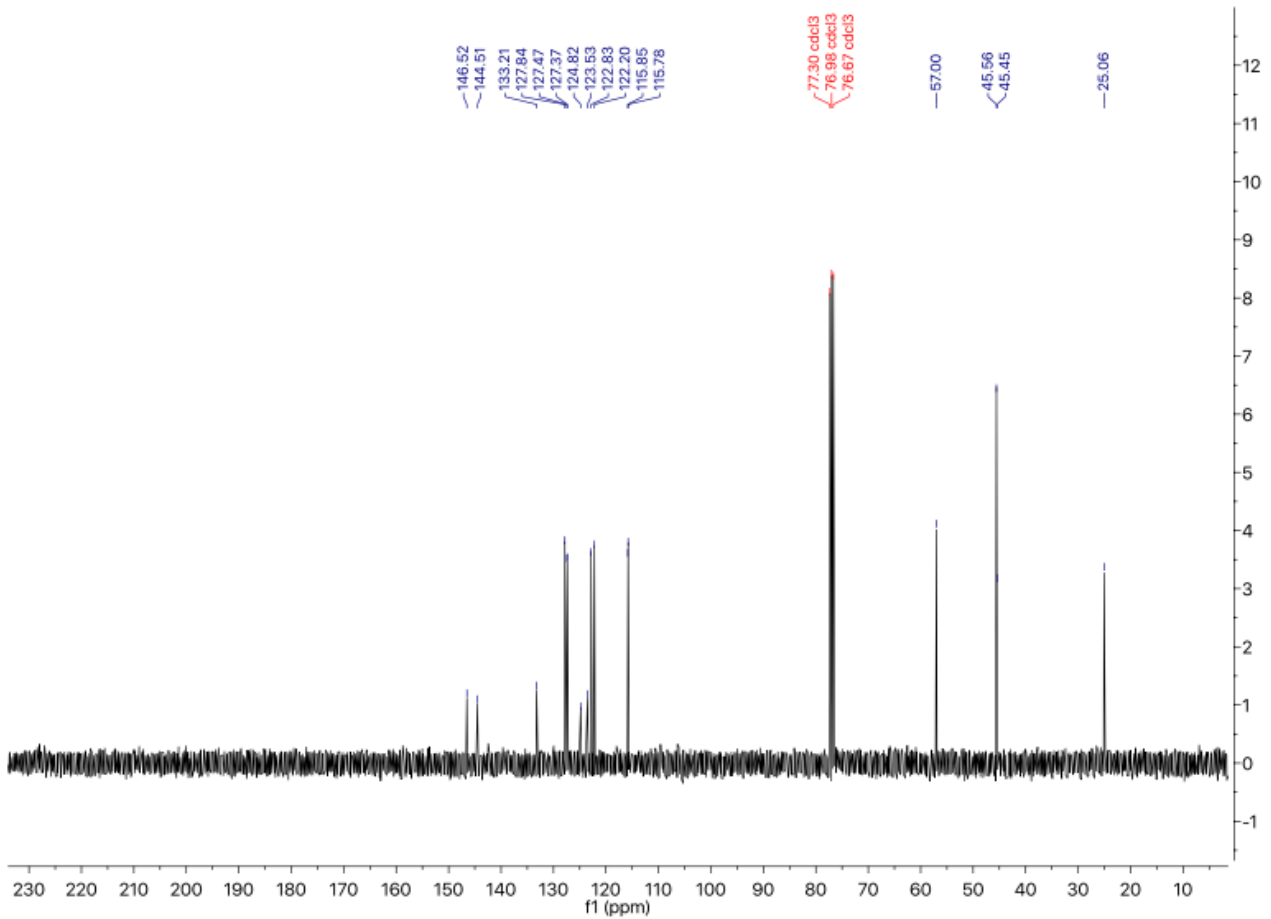
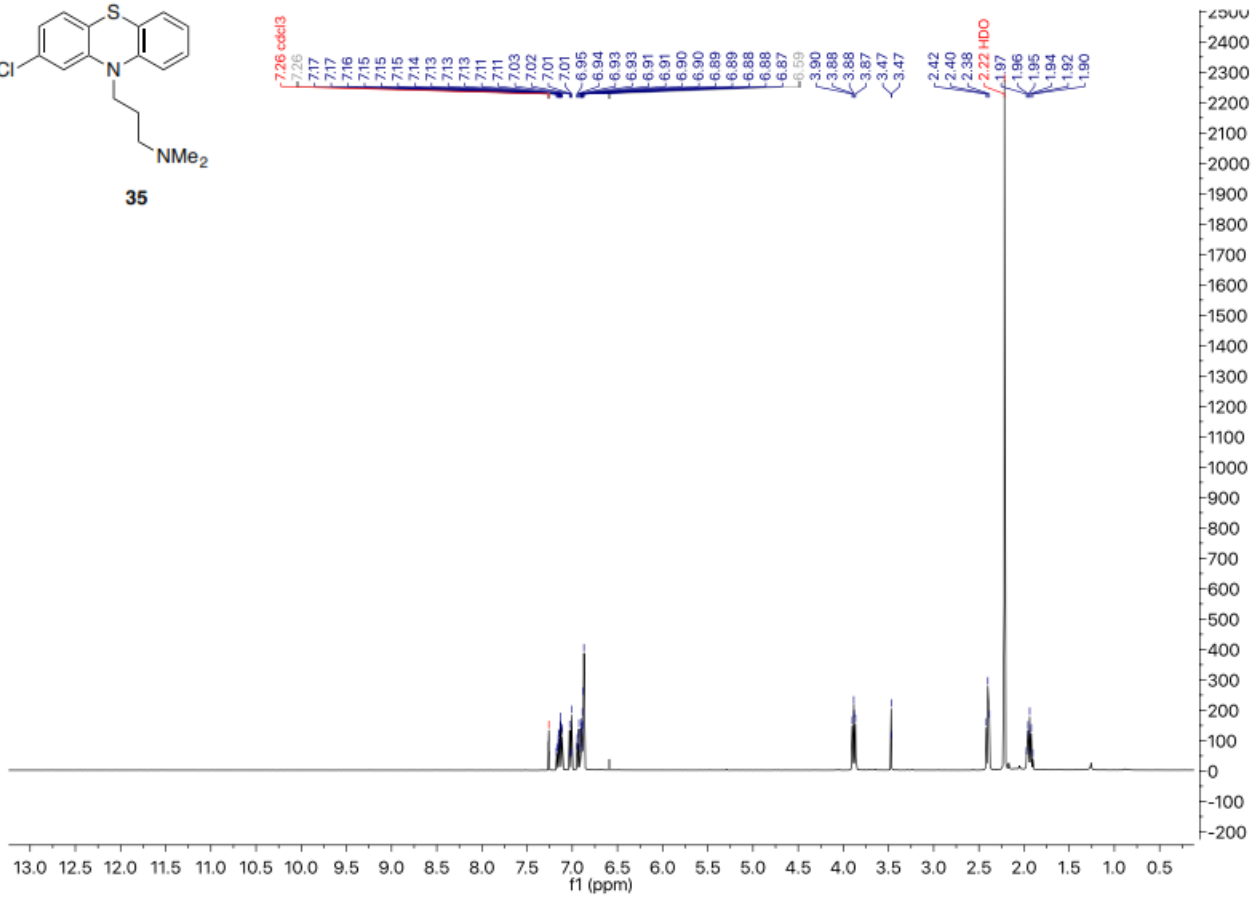
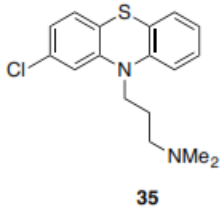


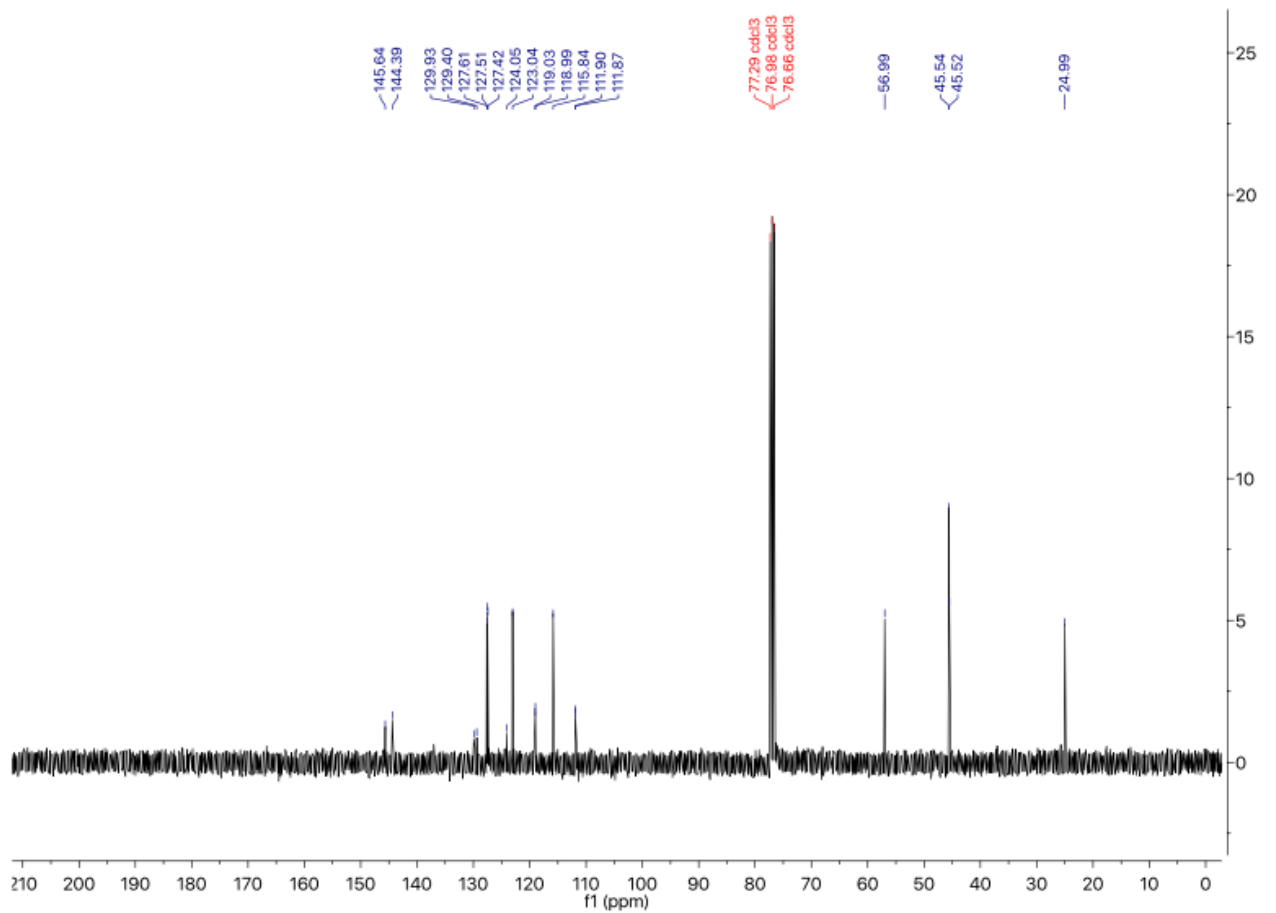
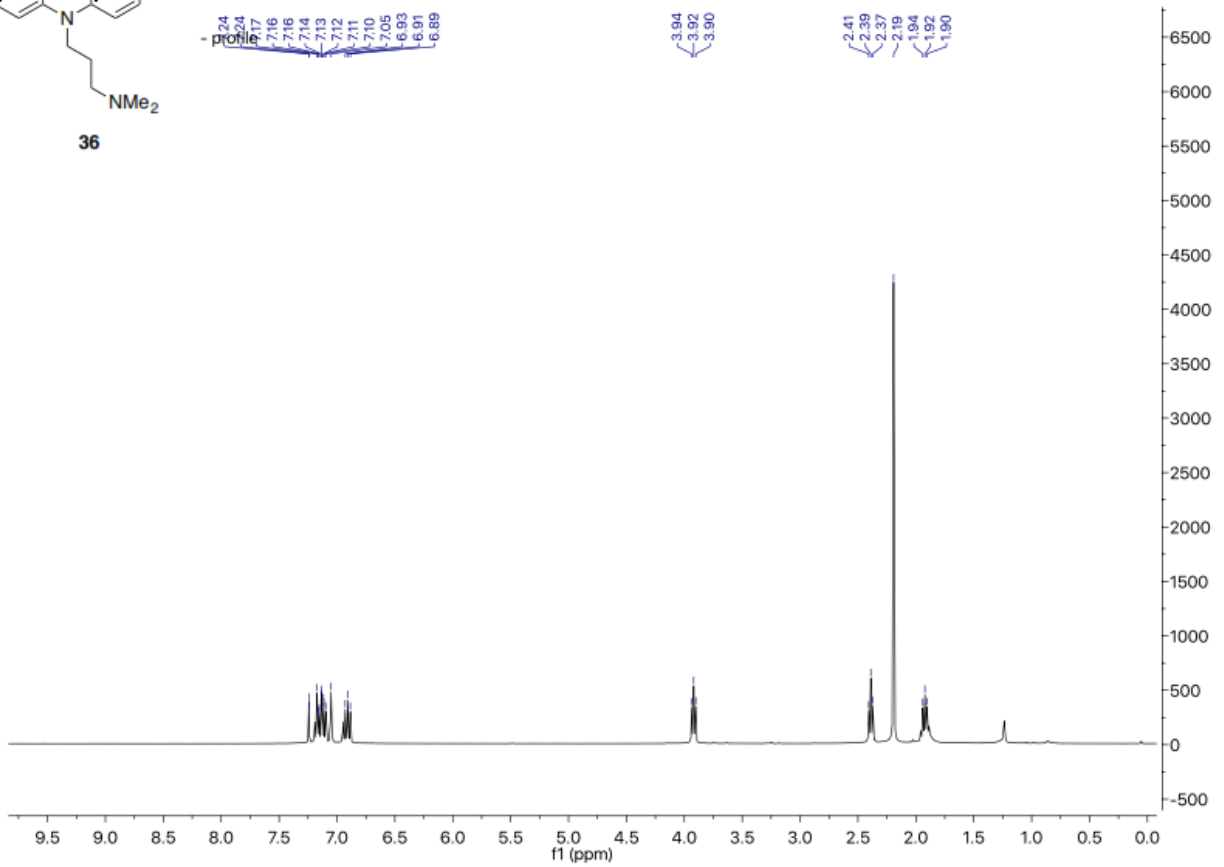
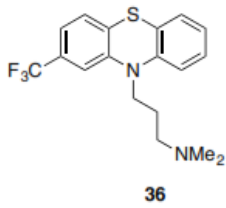


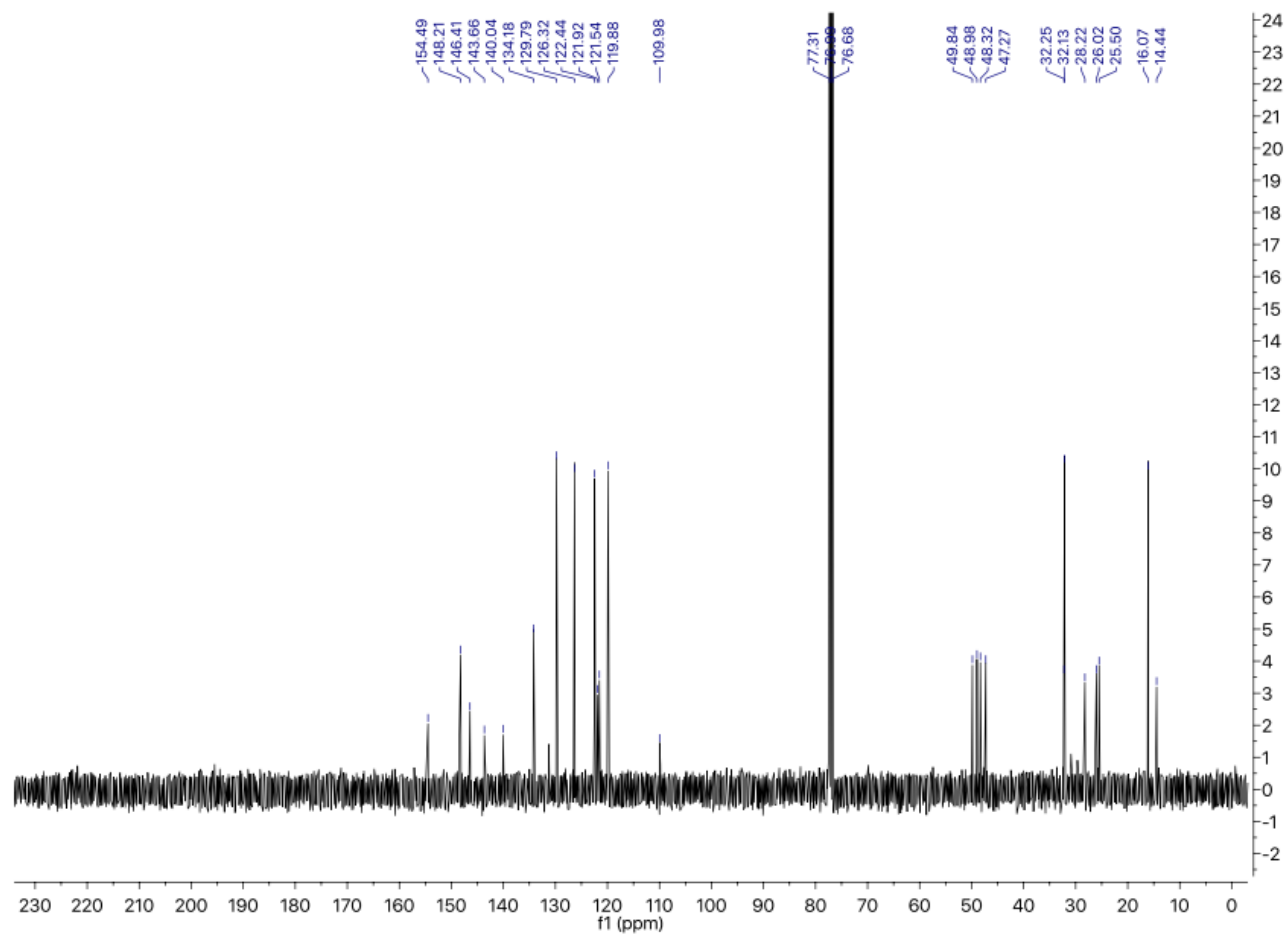
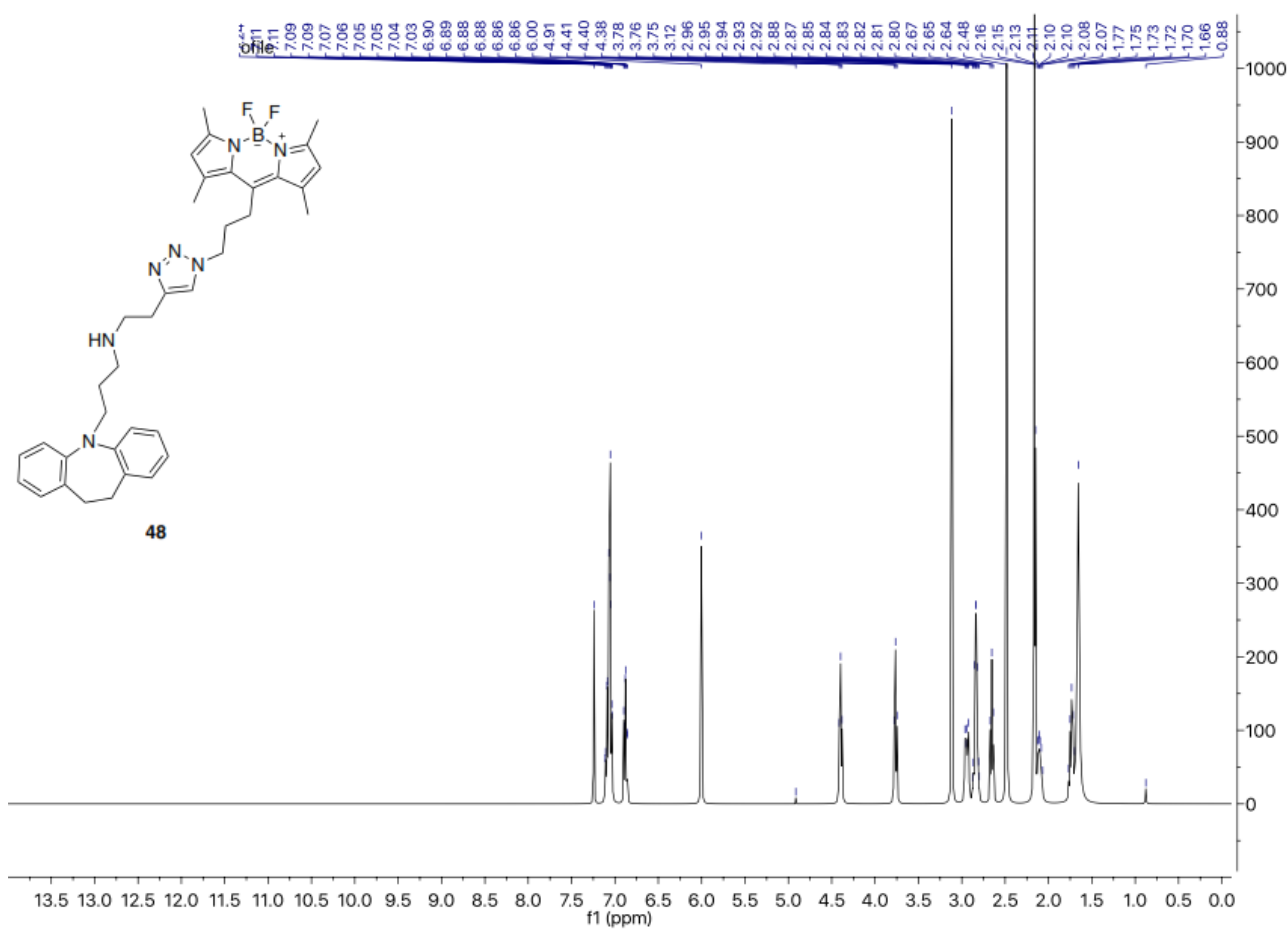


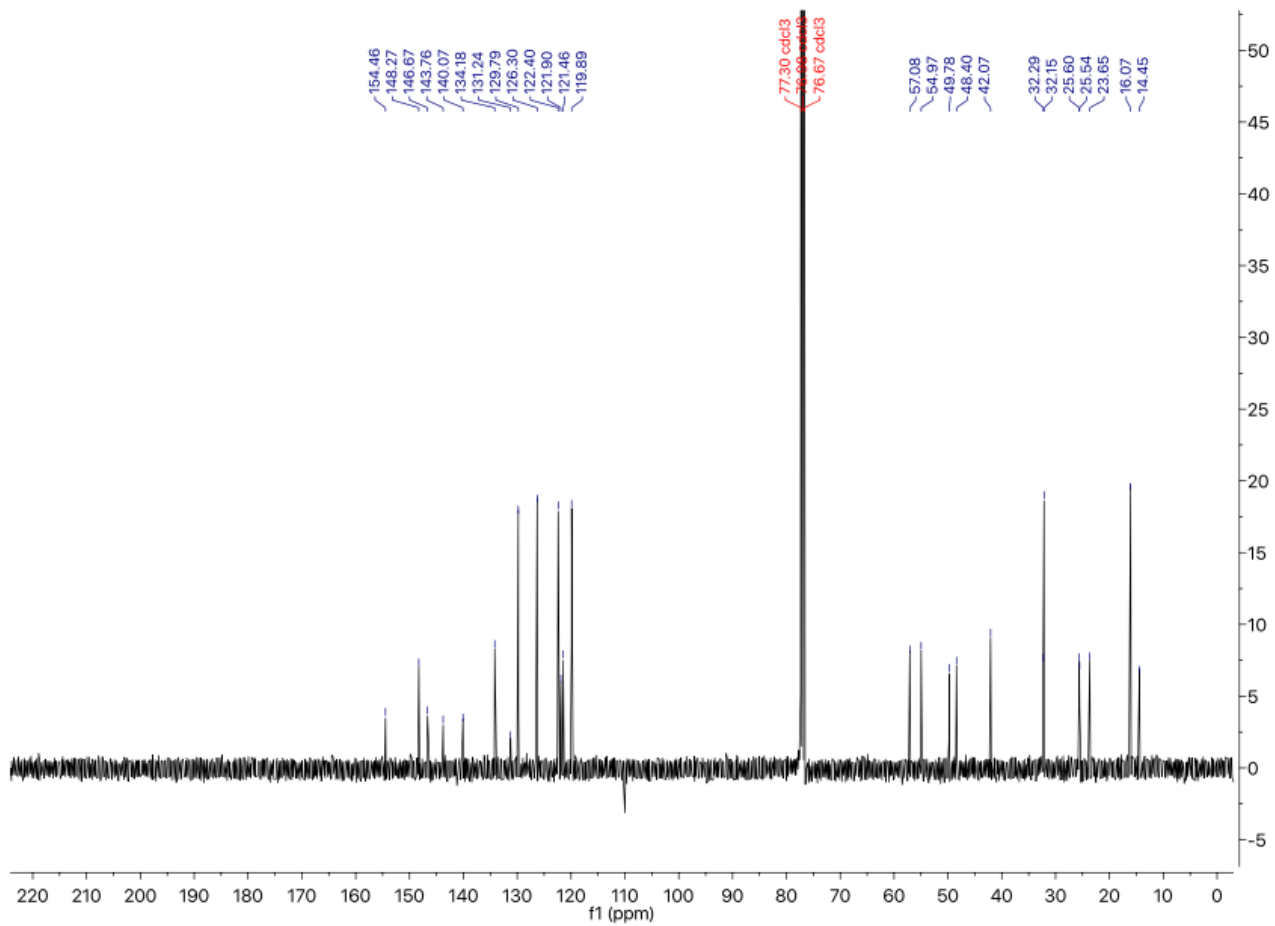
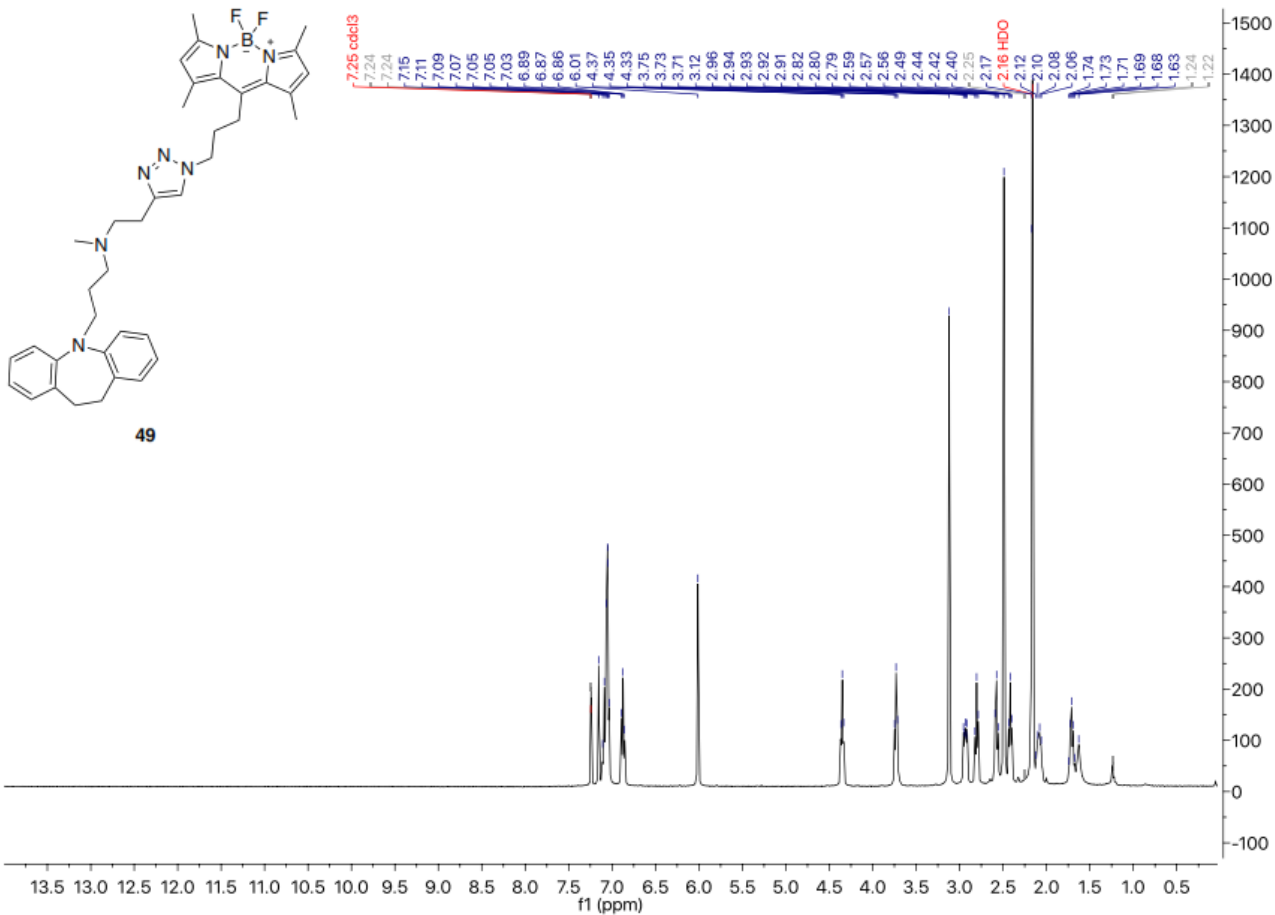


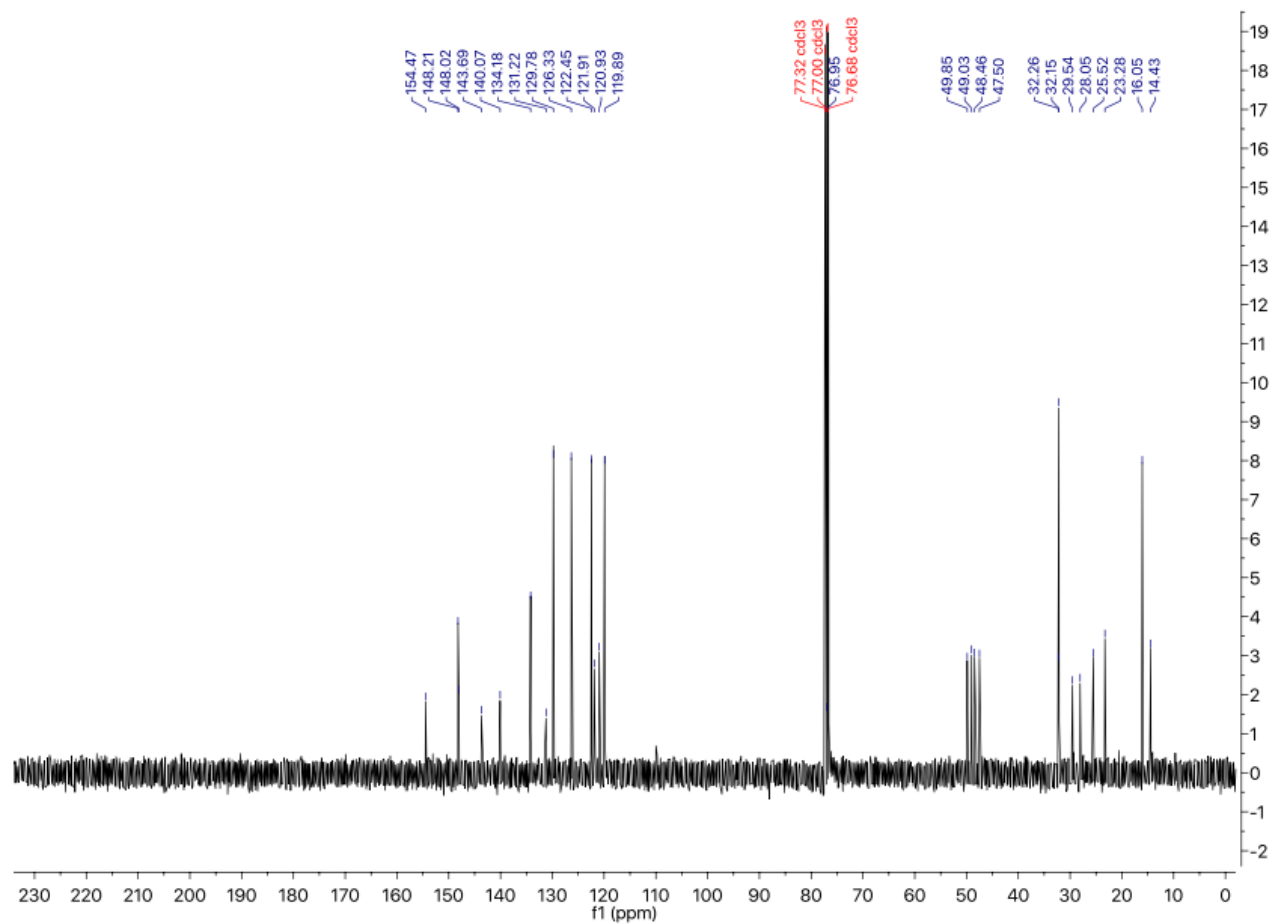
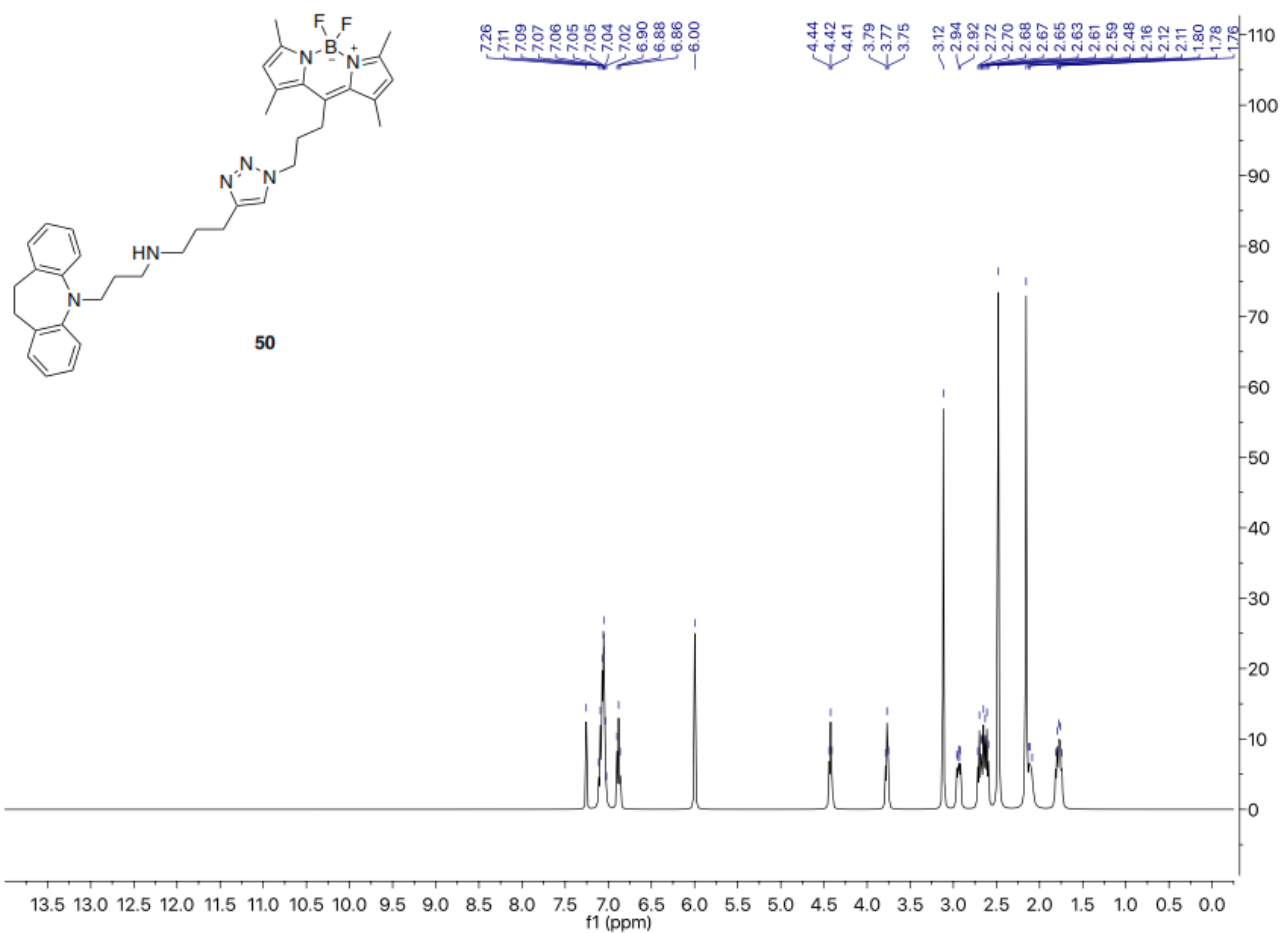


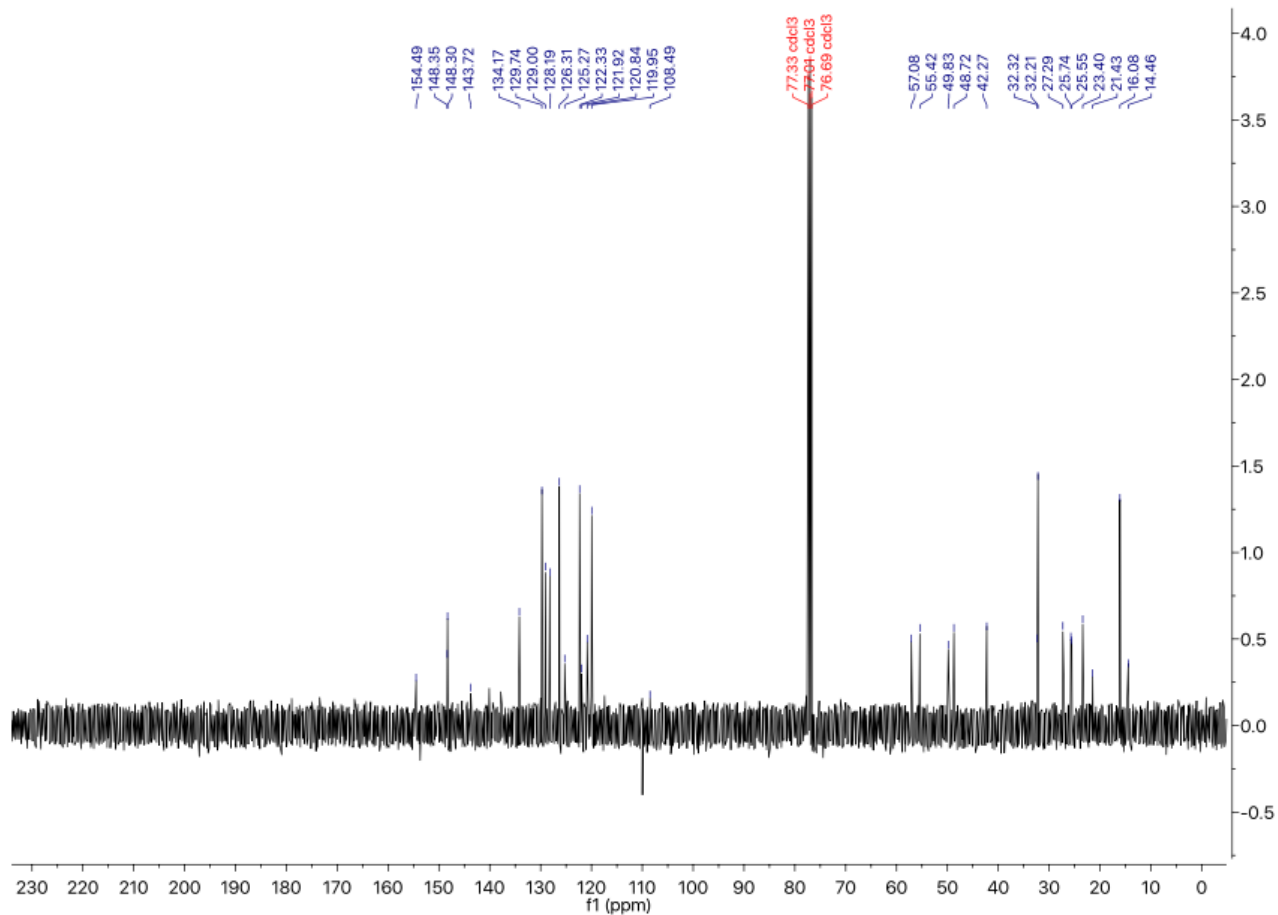
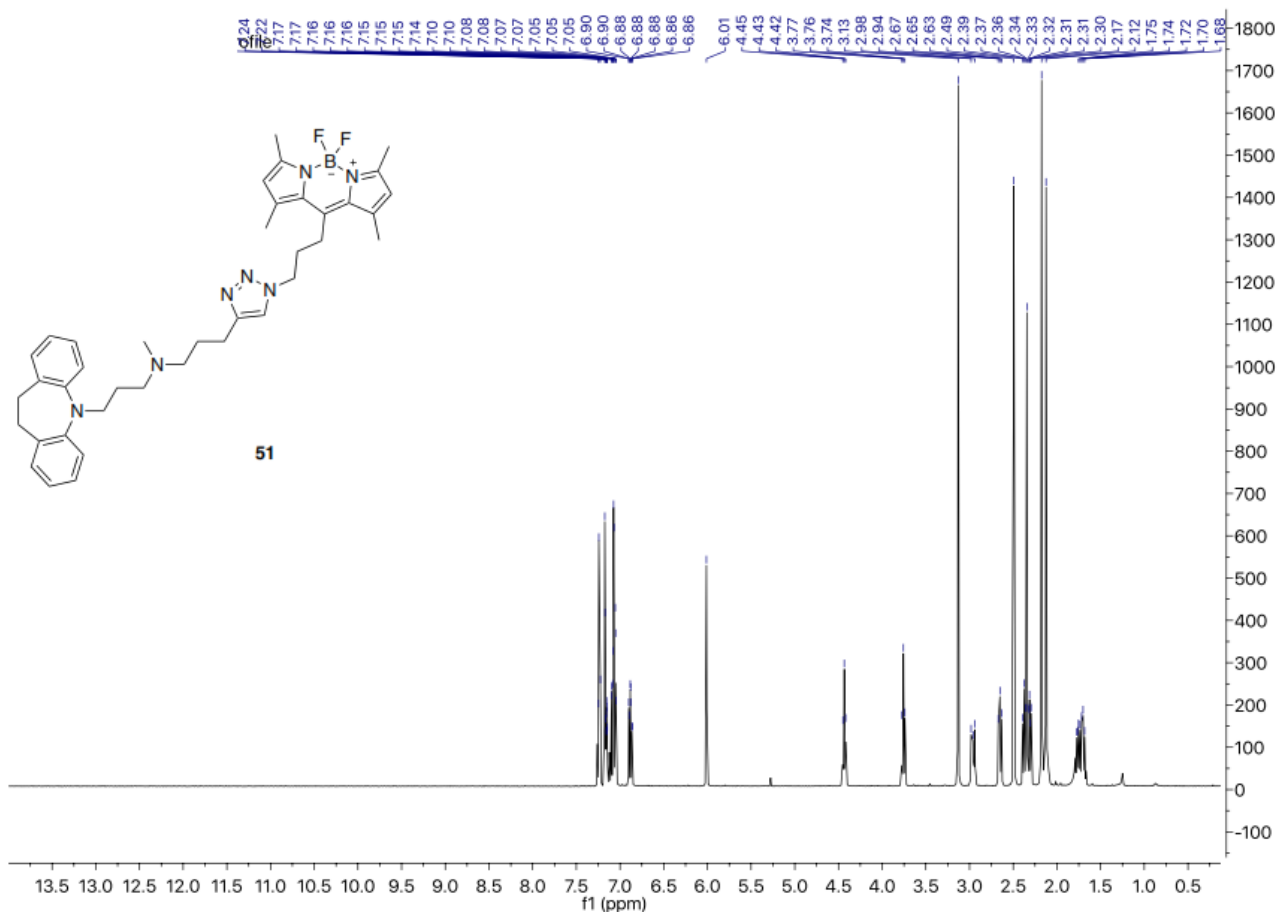




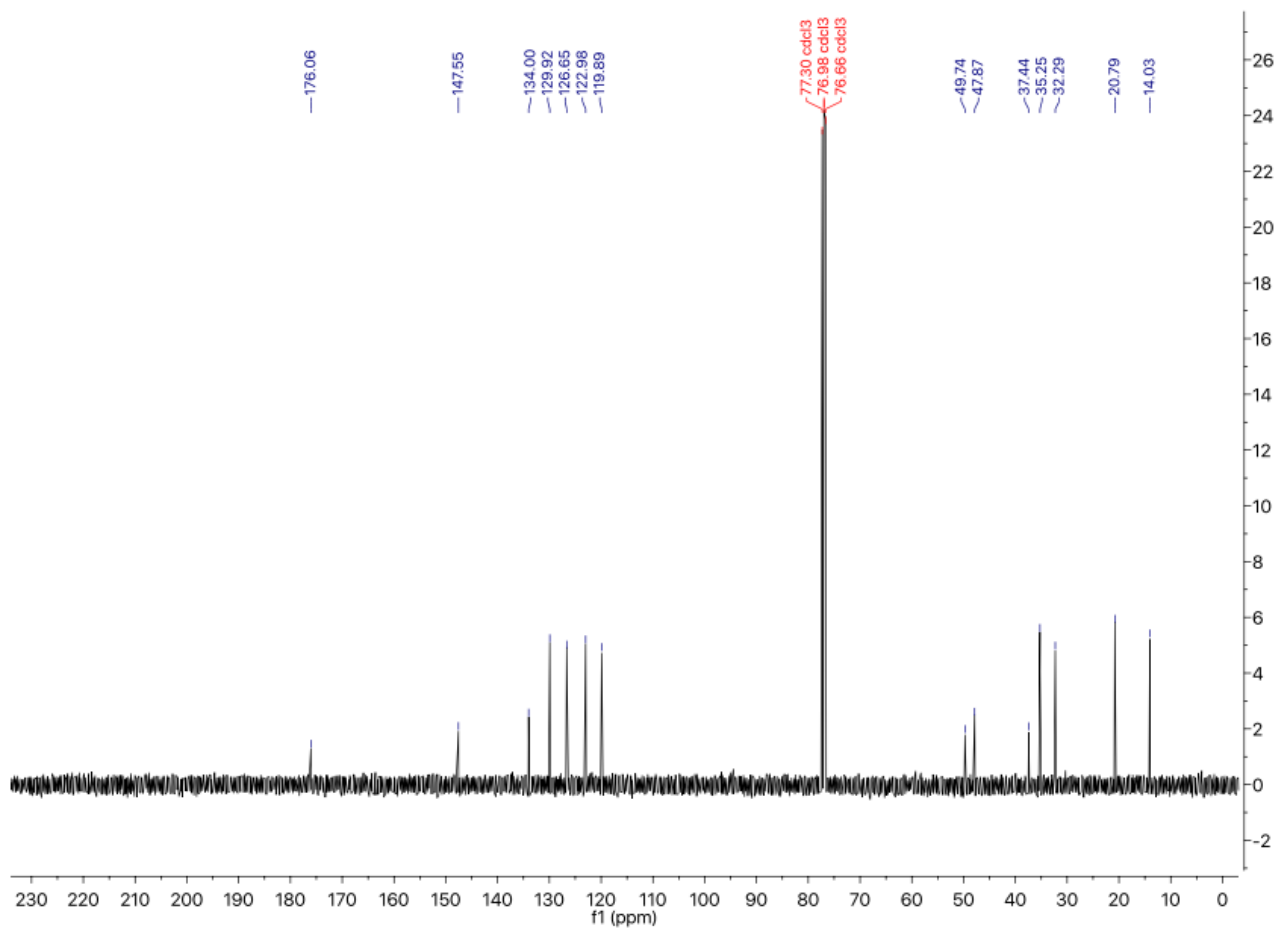
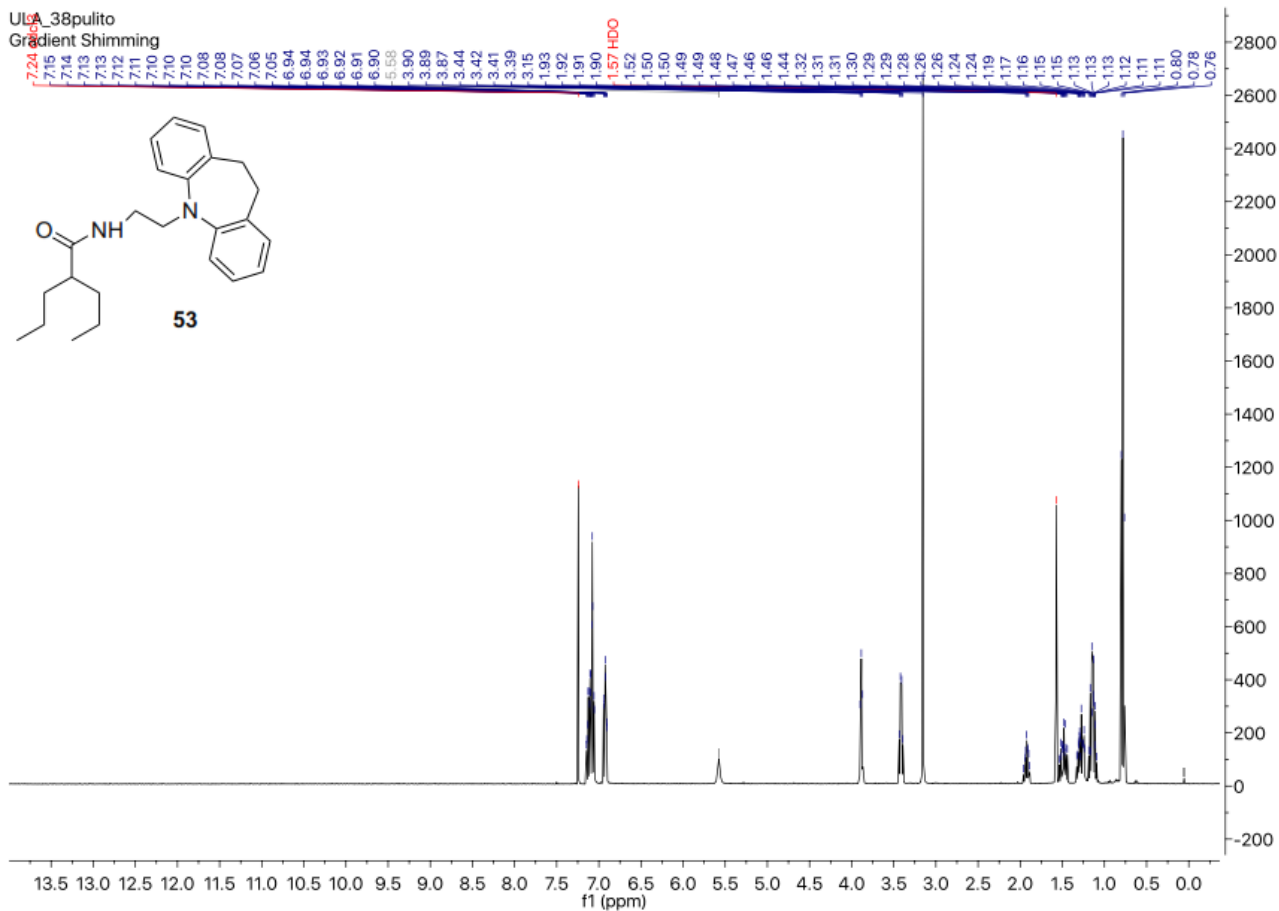
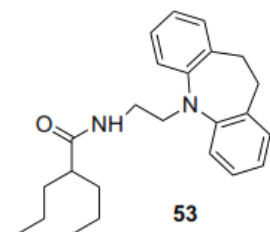


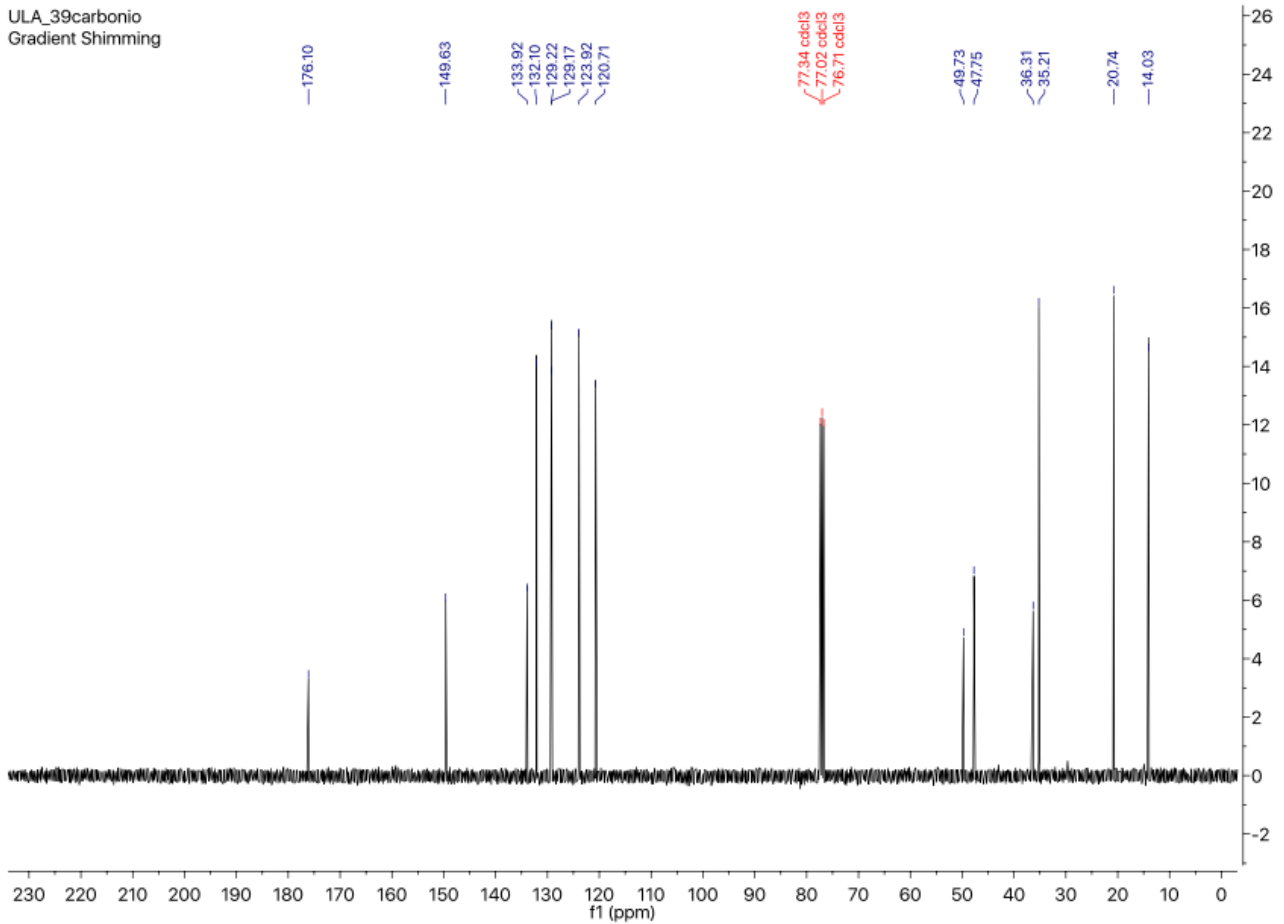
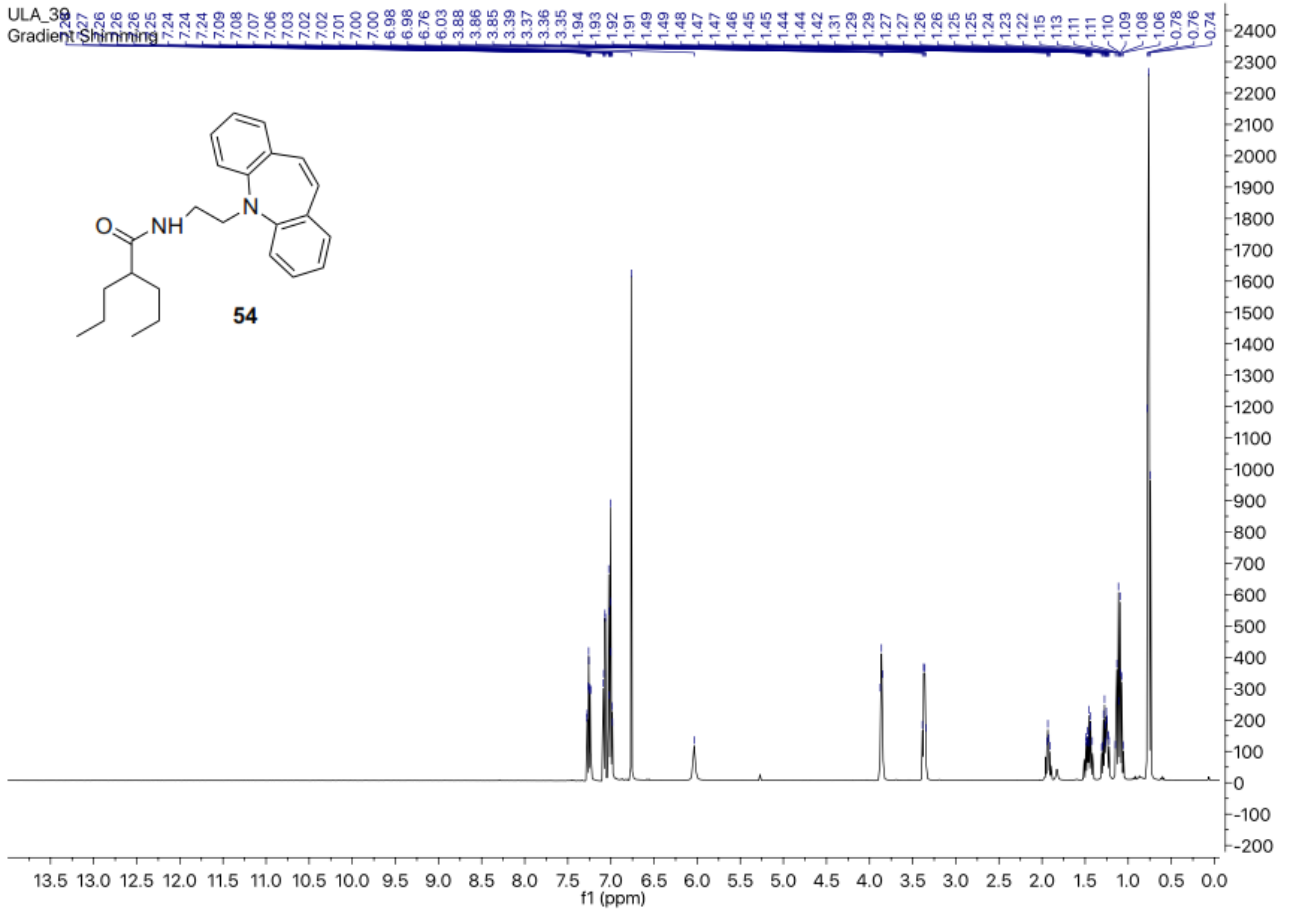




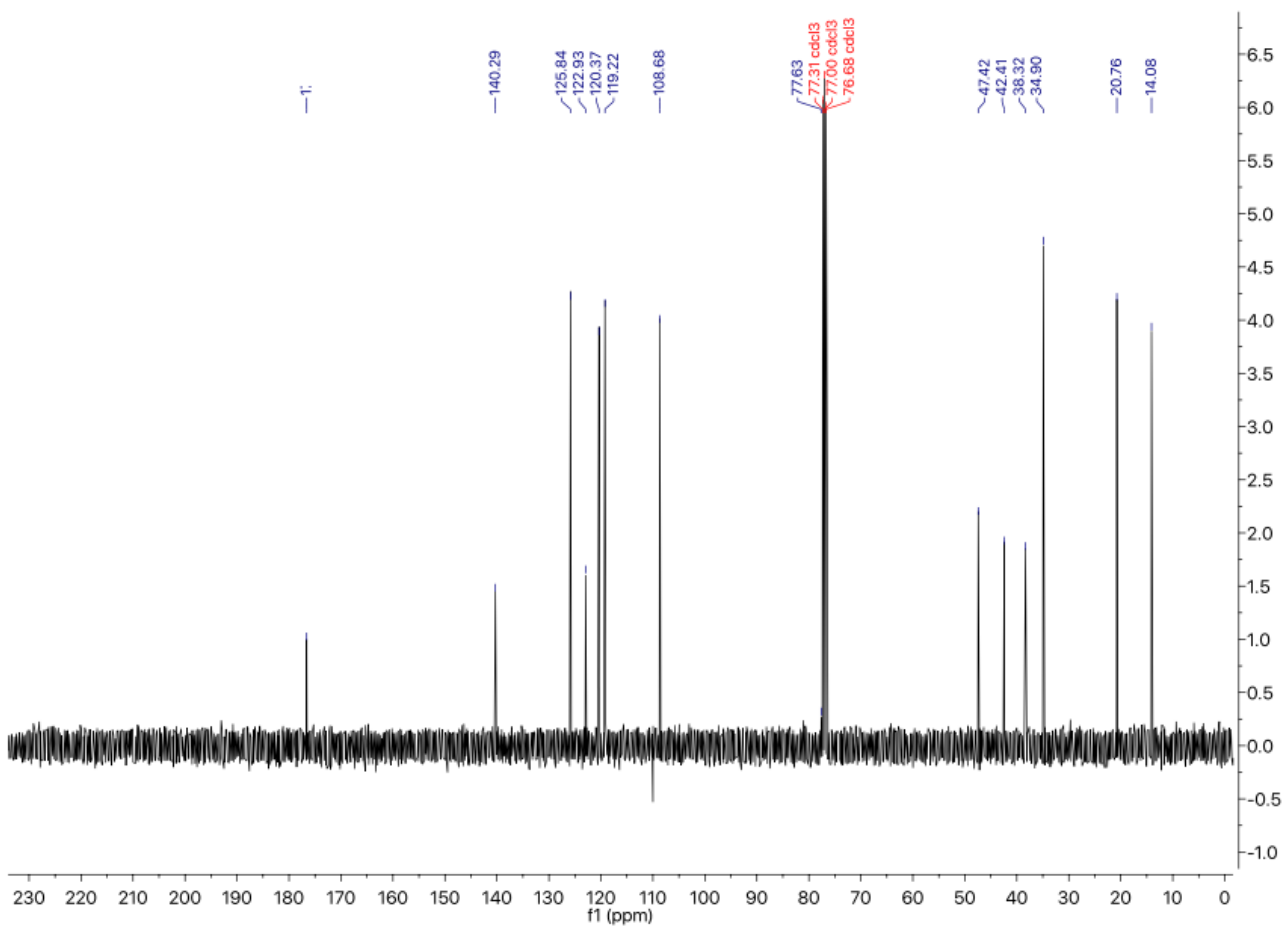
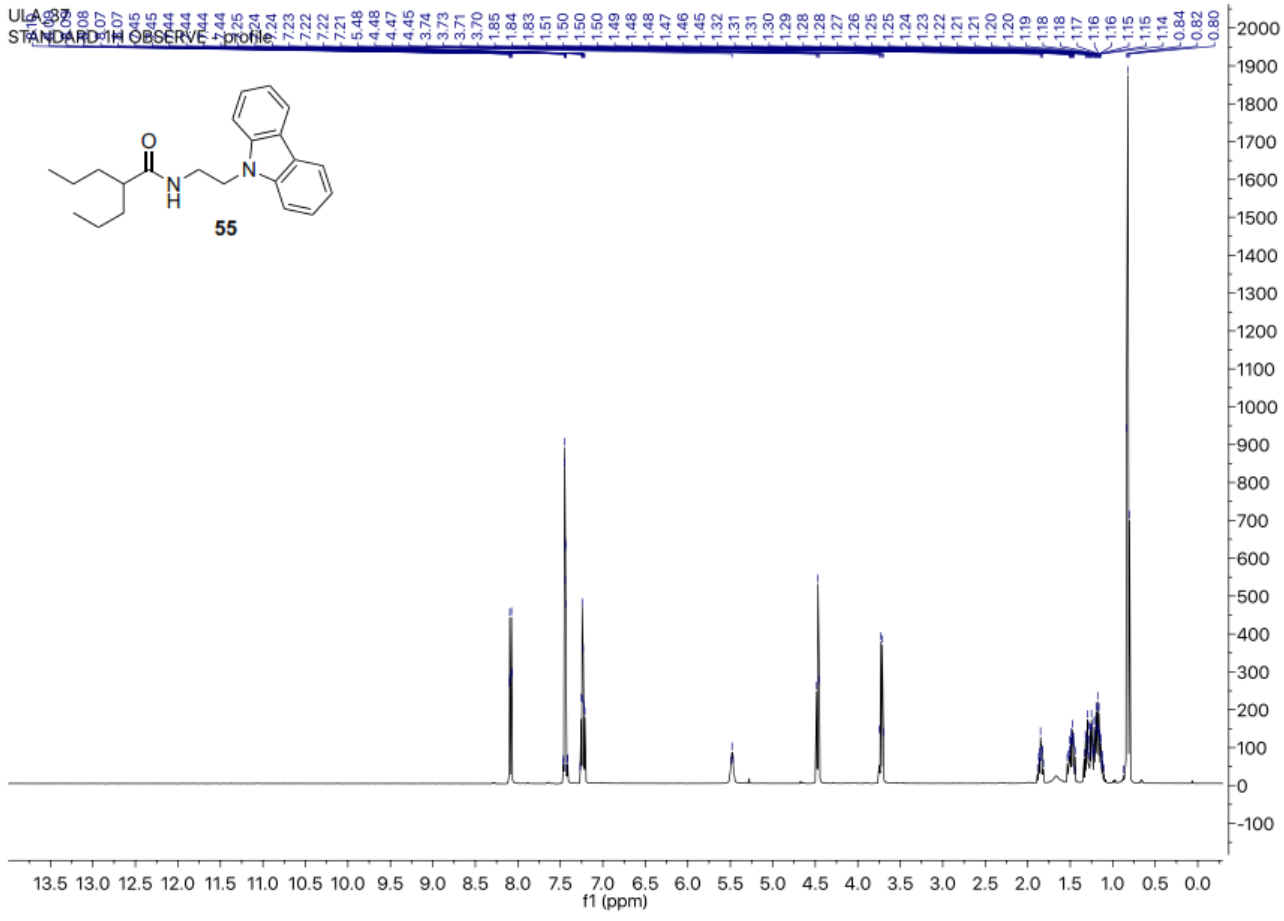
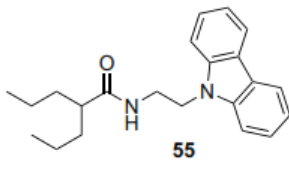


Ula_38pulito
Gradient Shimming

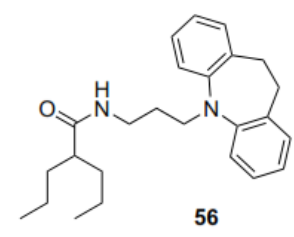
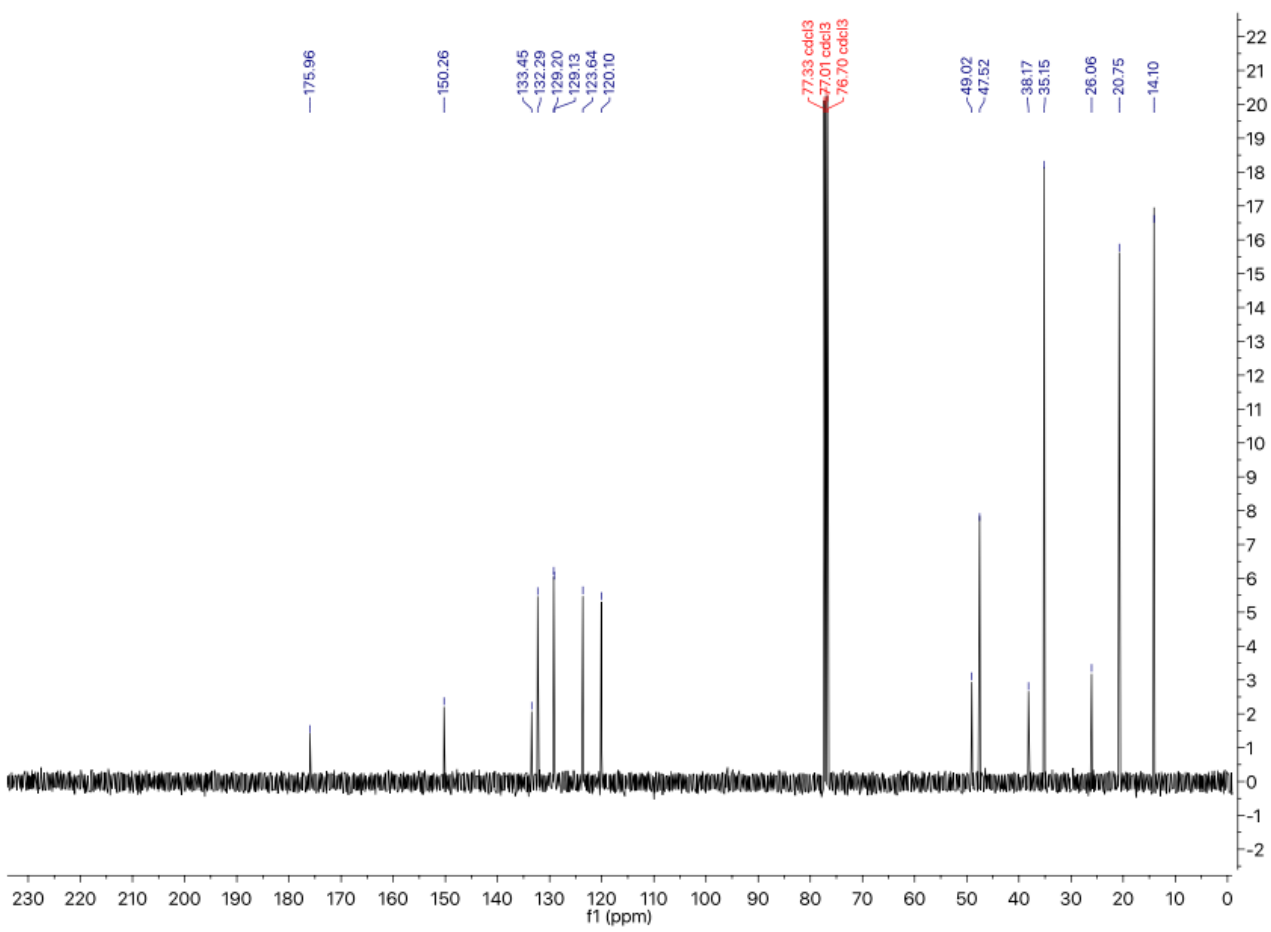
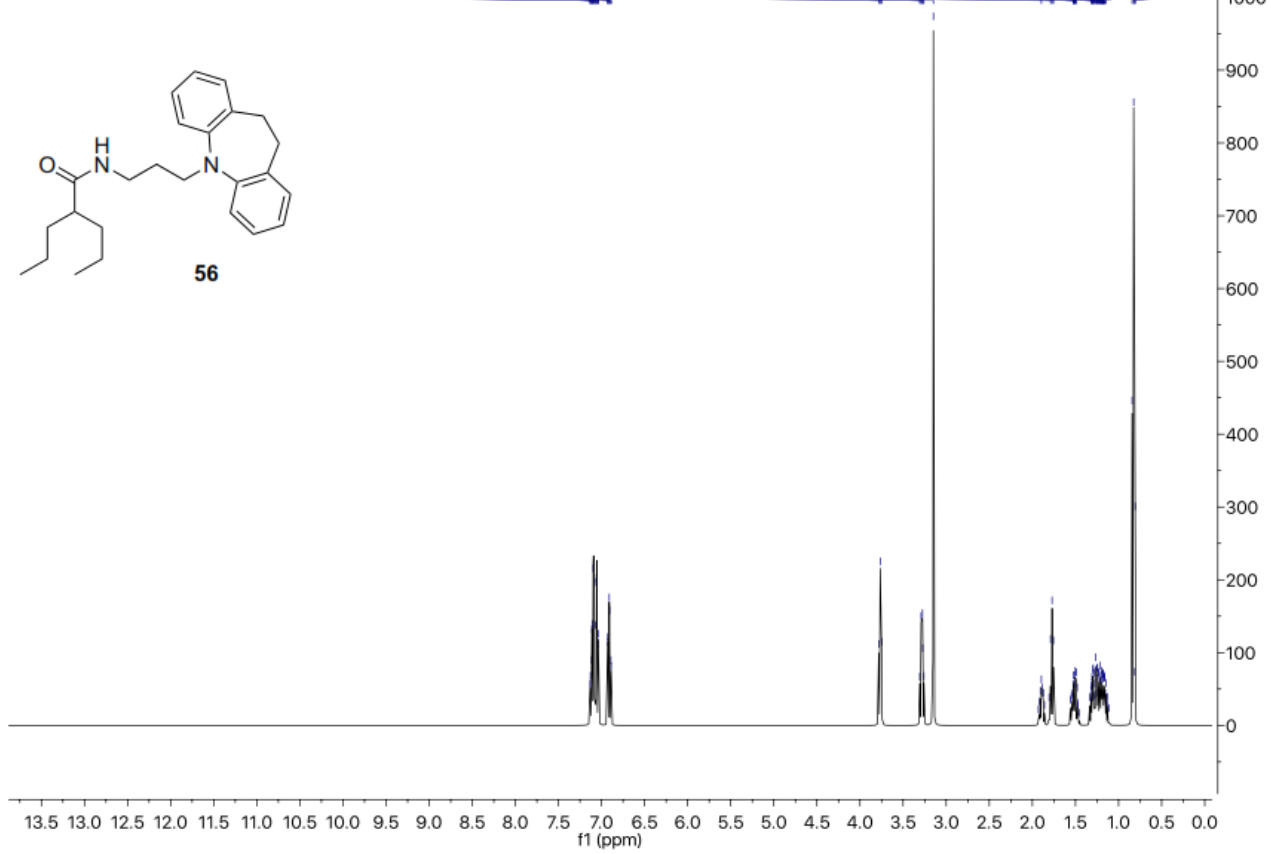




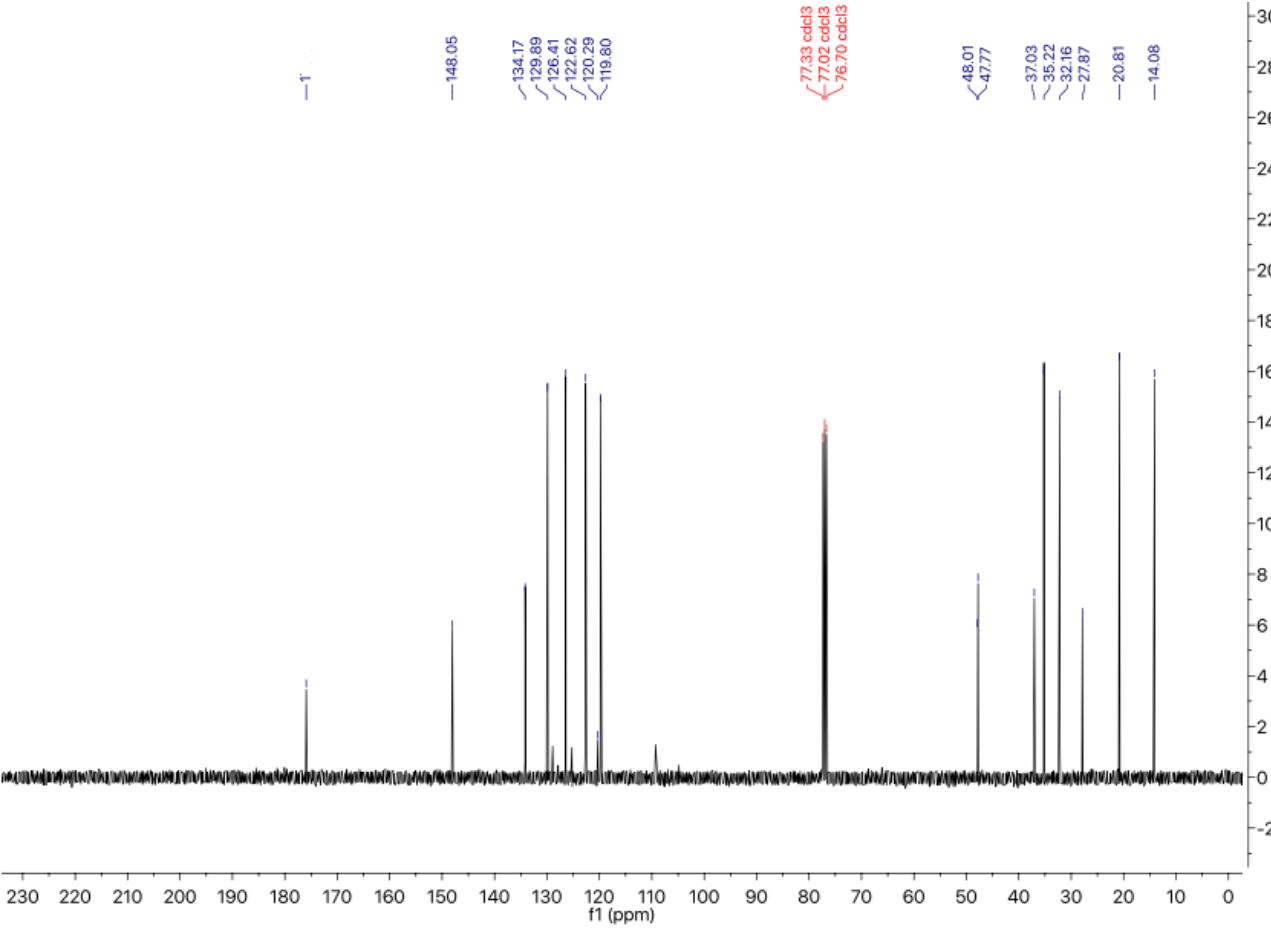
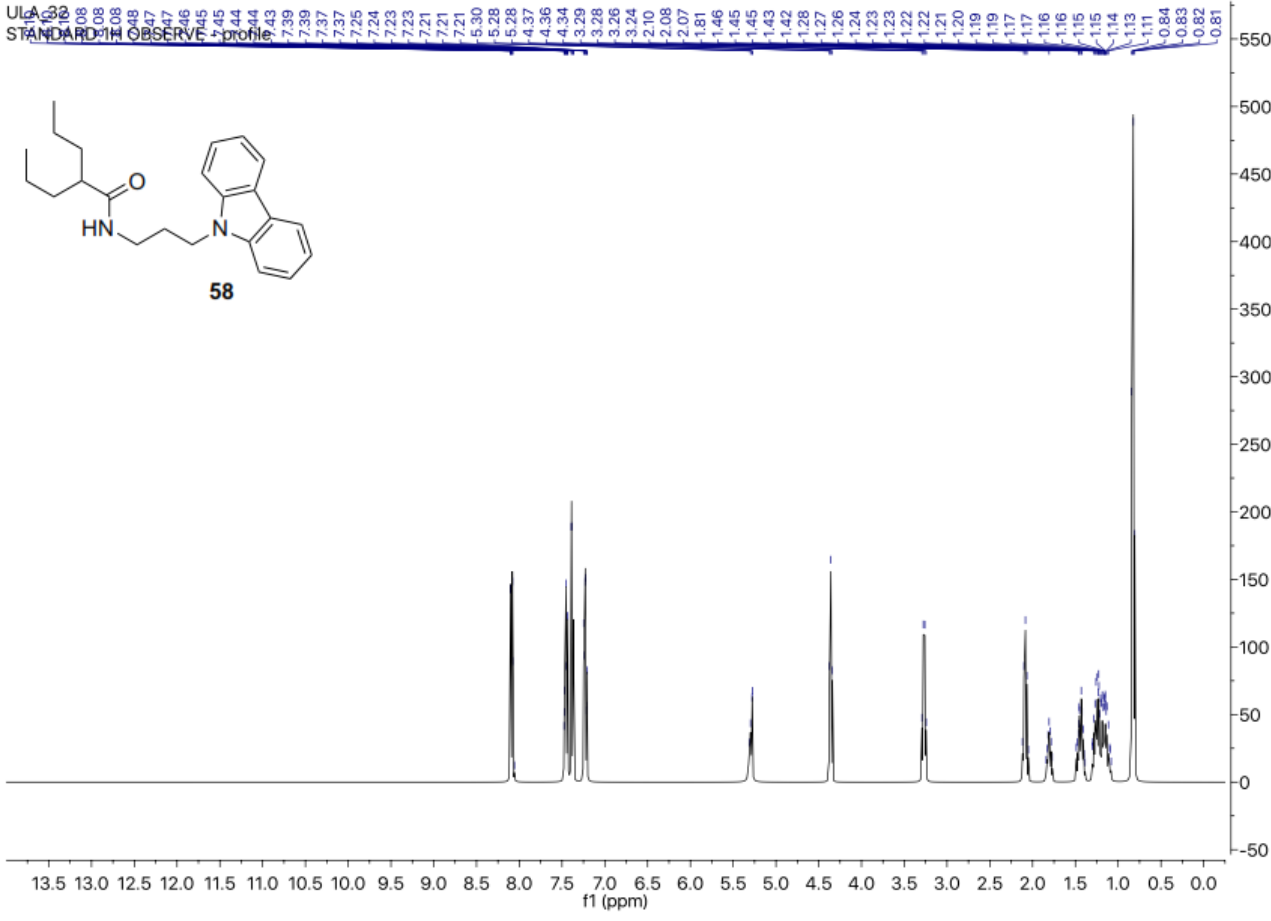
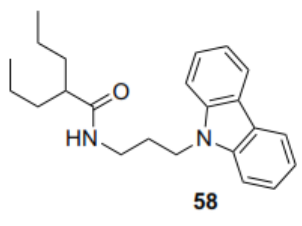
UIC-008
STANDARD-OBSERVE

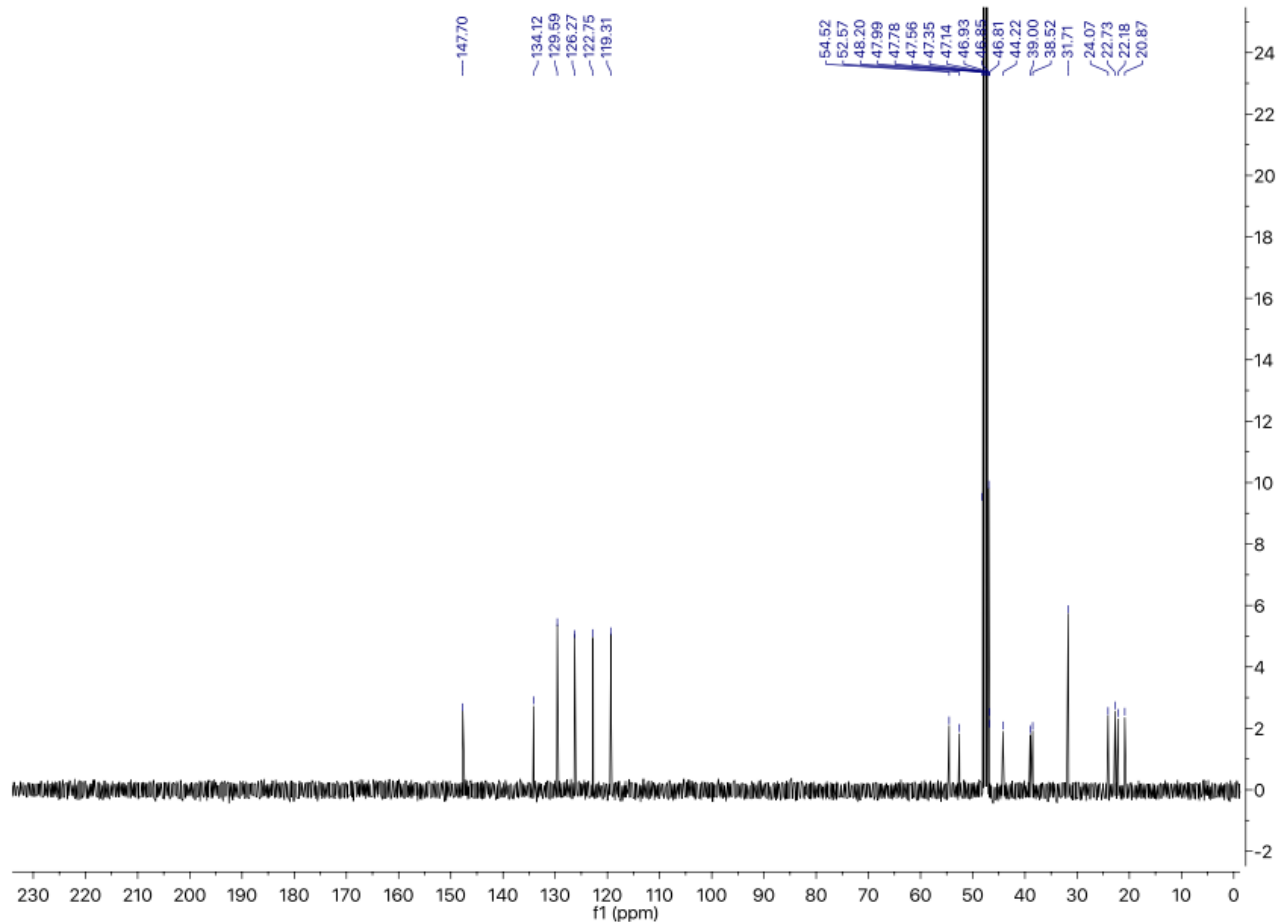
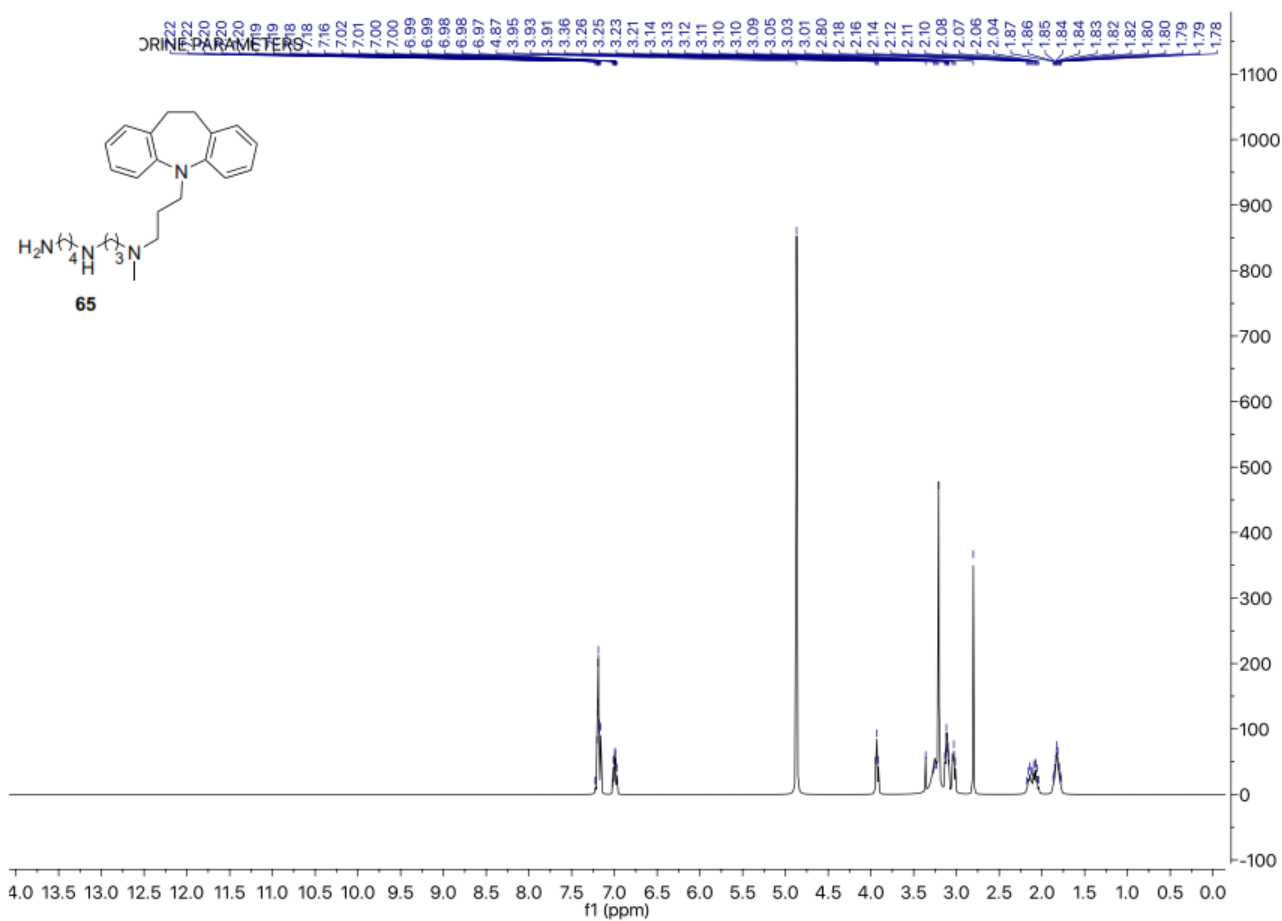


U1A_36
 STANDARD-1H OBSERVE profile

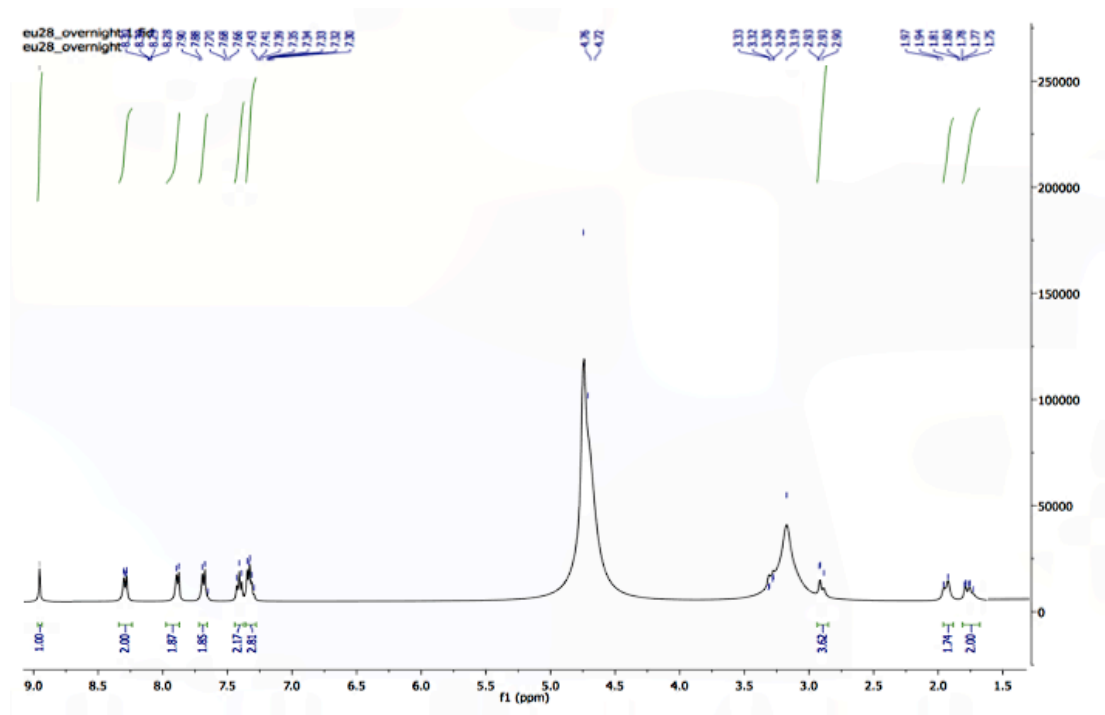


UPLC
STANDARD





Representative ^1H -NMR and high-resolution mass spectra of compound **106**



Elemental Composition Report

Single Mass Analysis

Tolerance = 10.0 mDa / DBE: min = -50.0, max = 500.0

Element prediction: Off

Number of isotope peaks used for i-FIT = 3

Monoisotopic Mass, Even Electron Ions

221 formula(e) evaluated with 5 results within limits (up to 19 closest results for each mass)

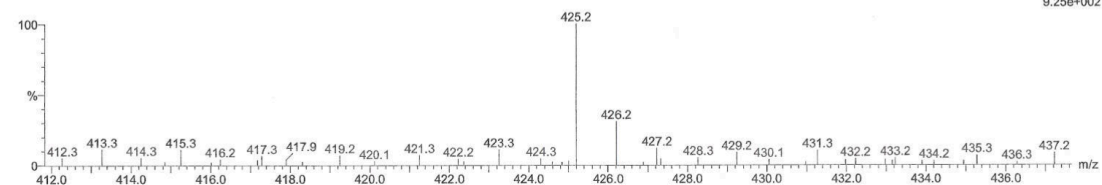
Elements Used:

C: 0-100 H: 0-200 N: 4-4 O: 0-30

21-Apr-2015

eu-21apr15-28-vial-2 267 (4.936) Cn (Cen,5, 50.00, Ar); Sm (SG, 3x5.00); Sb (12,5.00)

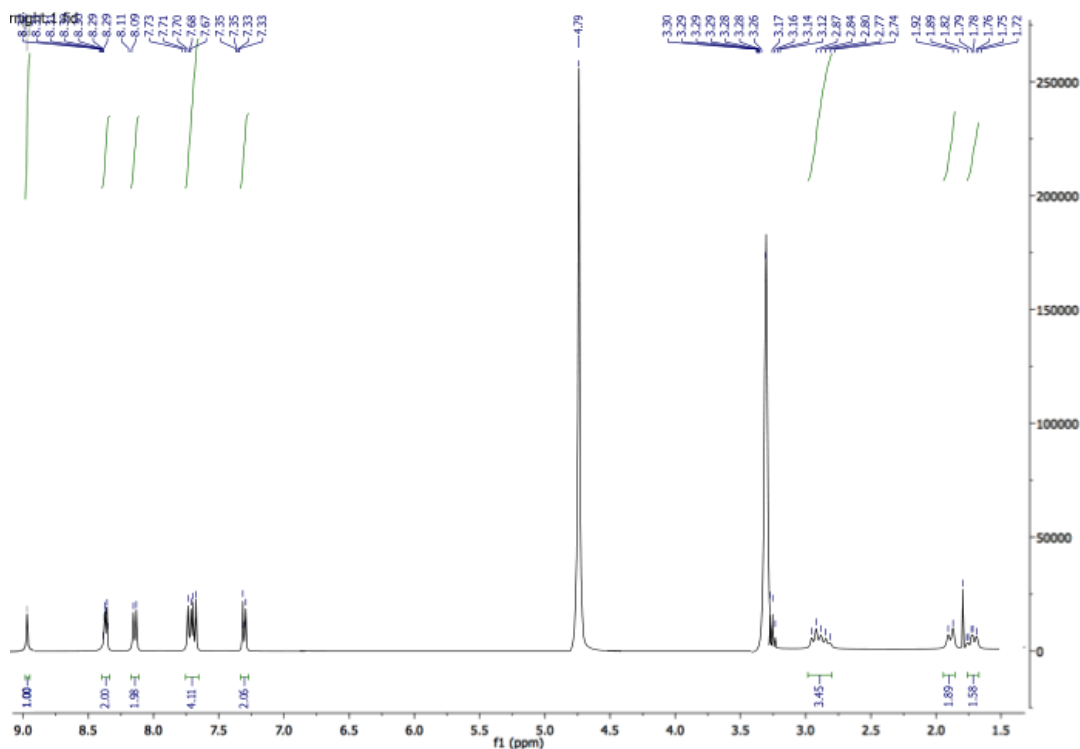
TOF MS ES+
9.25e+002



Minimum: -50.0
Maximum: 500.0

Mass	Calc. Mass	mDa	PPM	DBE	i-FIT	Formula
425.1980	425.1978	0.2	0.5	16.5	19.2	C26 H25 N4 O2
	425.2001	-2.1	-4.9	-14.5	132.1	C H37 N4 O20
	425.1942	3.8	8.9	-5.5	81.2	C8 H33 N4 O15
	425.2036	-5.6	-13.2	7.5	30.9	C19 H29 N4 O7
	425.1884	9.6	22.6	3.5	47.7	C15 H29 N4 O10

Representative ¹H-NMR and high-resolution mass spectra of compound 107



Elemental Composition Report

Single Mass Analysis

Tolerance = 10.0 mDa / DBE: min = -50.0, max = 500.0

Element prediction: Off

Number of isotope peaks used for i-FIT = 3

Monoisotopic Mass, Even Electron Ions

228 formula(e) evaluated with 5 results within limits (up to 19 closest results for each mass)

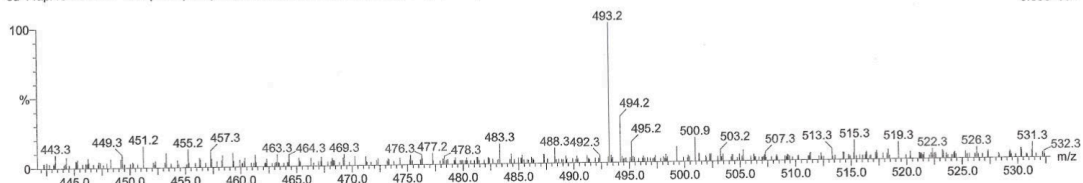
Elements Used:

C: 0-100 H: 0-200 N: 4-4 O: 0-30 F: 3-3

14-Apr-2015

eu-14apr15-mrs4127 323 (5.973) Cn (Cen,5, 50.00, Ar); Sm (SG, 3x5.00); Sb (12.5.00)

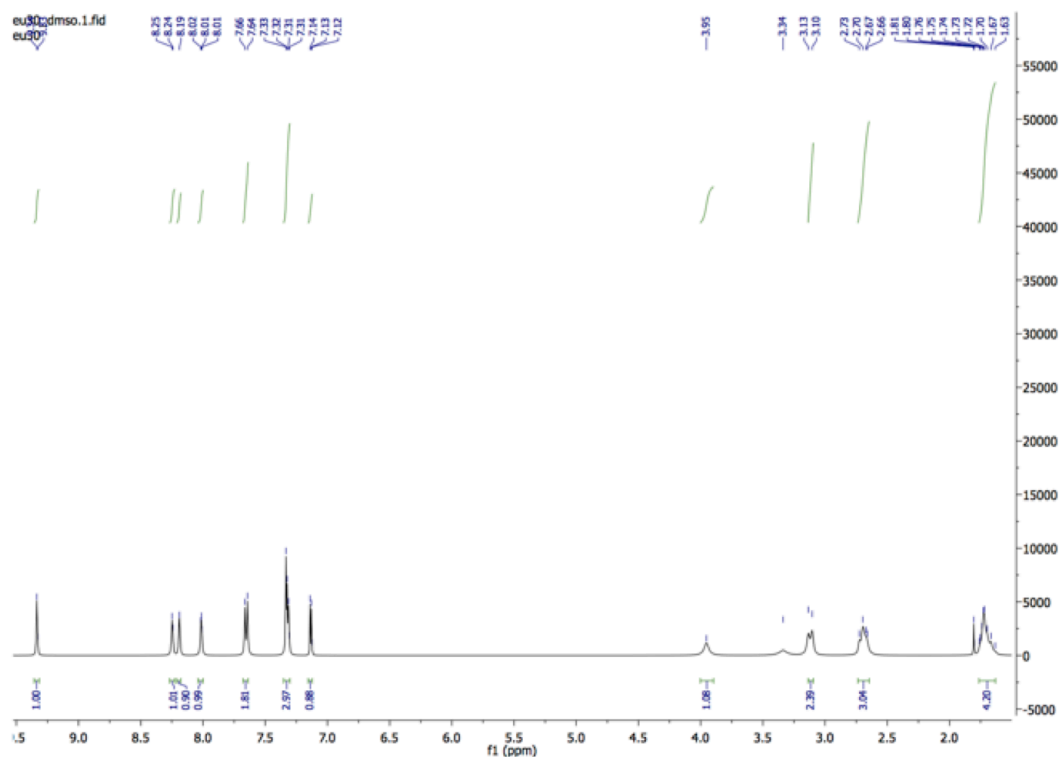
TOF MS ES+
6.69e+002



Minimum: -50.0
Maximum: 500.0

Mass	Calc. Mass	mDa	PPM	DBE	i-FIT	Formula
493.1854	493.1851	0.3	0.6	16.5	18.2	C27 H24 N4 O2 F3
	493.1875	-2.1	-4.3	-14.5	100.3	C2 H36 N4 O20 F3
	493.1816	3.8	7.7	-5.5	63.8	C9 H32 N4 O15 F3
	493.1910	-5.6	-11.4	7.5	28.0	C20 H28 N4 O7 F3
	493.1758	9.6	19.5	3.5	36.9	C16 H28 N4 O10 F3

Representative ¹H-NMR and high-resolution mass spectra of compound 116



Elemental Composition Report

Single Mass Analysis

Tolerance = 10.0 mDa / DBE: min = -50.0, max = 500.0
 Element prediction: Off
 Number of isotope peaks used for i-FIT = 3

Monoisotopic Mass, Even Electron Ions

197 formula(e) evaluated with 4 results within limits (up to 19 closest results for each mass)

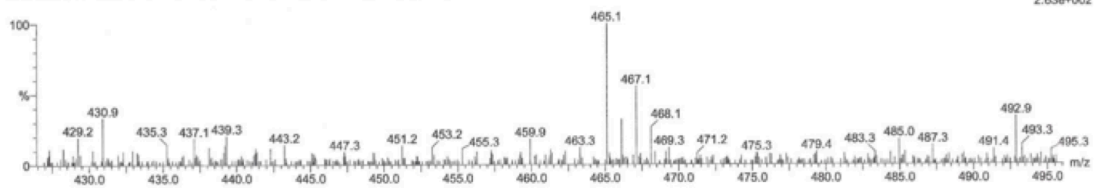
Elements Used:

C: 0-100 H: 0-200 N: 4-4 O: 0-30 S: 1-1 Cl: 1-1

29-Apr-2015

eu-29apr15-30 69 (1.276) Cn (Cen,5, 50.00, Ar); Sm (SG, 3x5.00); Sb (12.5.00)

TOF MS ES+
2.63e+002



Mass	Calc. Mass	mDa	PPM	DBE	i-FIT	Formula
465.1151	465.1152	-0.1	-0.2	15.5	61.7	C24 H22 N4 O2 32S 35Cl
	465.1117	3.4	7.3	-6.5	84.2	C6 H30 N4 O15 32S 35Cl
	465.1211	-6.0	-12.9	6.5	67.7	C17 H26 N4 O7 32S 35Cl
	465.1058	9.3	20.0	2.5	72.6	C13 H26 N4 O10 32S 35Cl

Elemental Composition Report

Single Mass Analysis

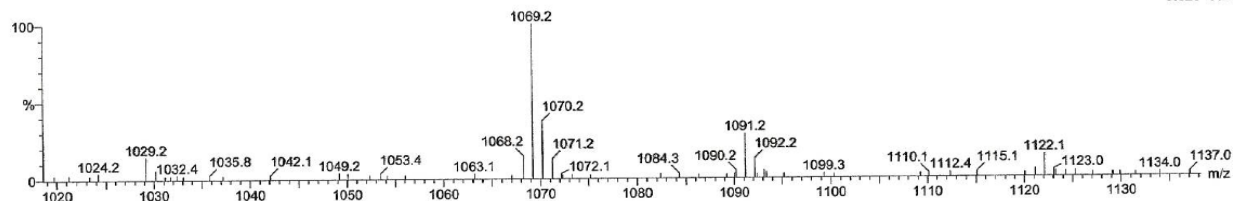
Tolerance = 10.0 mDa / DBE: min = -50.0, max = 500.0
 Element prediction: Off
 Number of isotope peaks used for i-FIT = 3

Monoisotopic Mass, Even Electron Ions
 473 formula(e) evaluated with 6 results within limits (up to 50 closest results for each mass)

Elements Used:
 C: 0-100 H: 0-200 N: 6-6 O: 0-30 S: 1-1 P: 2-2 F: 2-2 11B: 1-1

26-Jan-2015
 eu-26jan15-mrs-4183-neg 79 (1.461) Cn (Cen,5, 50.00, Ar); Sm (SG, 3x5.00); Sb (12.5.00); Sm (SG, 3x5.00); Cm (79-26x3.000)

TOF MS ES-
 9.62e+002



Minimum: -50.0
 Maximum: 500.0

Mass	Calc. Mass	mDa	PPM	DBE	i-FIT	Formula
1069.1721	1069.1711	1.0	0.9	23.5	21.5	C40 H42 N6 O20 S P2 F2 11B
	1069.1746	-2.5	-2.3	45.5	79.0	C58 H34 N6 O7 S P2 F2 11B
	1069.1687	3.4	3.2	54.5	106.5	C65 H30 N6 O2 S P2 F2 11B
	1069.1770	-4.9	-4.6	14.5	8.8	C33 H46 N6 O25 S P2 F2 11B
	1069.1652	6.9	6.5	32.5	41.3	C47 H38 N6 O15 S P2 F2 11B
	1069.1805	-8.4	-7.9	36.5	53.6	C51 H38 N6 O12 S P2 F2 11B

Figure S1. Fluorescent excitation spectrum of **44, MRS4183**, indicated a I_{\max} value at 590 nm (extinction coefficient for Bodipy-TR = $64,000 \text{ cm}^{-1}\text{M}^{-1}$, from www.lifetechnologies.com), as measured in solution ($6.25 \mu\text{M}$ in water) in a cuvette (path length = 1 cm) using a SpectraMax M5 reader (Molecular Devices, Sunnyvale, CA). Emission Wavelength for **11** was determined to be $616 \pm 4 \text{ nm}$.

